Short Course

on

Optimization Technology and Applications in High Frequency and Microwave Circuit Design

Copyright © 1994 Optimization Systems Associates Inc.

This document is for the exclusive use by the registered participants of the Short Course on Optimization Technology and Applications in High Frequency and Microwave Circuit Design. No part of this document or related computer programs may be copied, reproduced, disclosed or transcribed in any form into any machine without prior permission in writing from Optimization Systems Associates Inc. This title page and original cover may not be separated from the contents of this document.

LIABILITY AND WARRANTY

NEITHER OPTIMIZATION SYSTEMS ASSOCIATES INC. NOR ITS EMPLOYEES, OFFICERS, DIRECTORS OR ANY OTHER PERSON, COMPANY, AGENCY OR INSTITUTION: (1) MAKES ANY WARRANTY, EXPRESS OR IMPLIED AS TO ANY MATTER WHATSOEVER REGARDING THIS MATERIAL, INCLUDING BUT NOT LIMITED TO THE GENERALITY THEREOF, ALL IMPLIED WARRANTIES AND CONDITIONS OF MERCHANTABILITY AND FITNESS FOR A PARTICULAR PURPOSE, OR THOSE ARISING BY STATUTE OR OTHERWISE IN LAW OR FROM THE COURSE OF DEALING OR USAGE OF TRADE HAVE BEEN AND ARE HEREBY EXPRESSLY EXCLUDED; OR (2) ASSUMES ANY LEGAL RESPONSIBILITY WHATSOEVER FOR THE ACCURACY, COMPLETENESS OR USEFULNESS OF THIS MATERIAL; OR (3) REPRESENTS THAT ITS USE WOULD NOT INFRINGE UPON PRIVATELY OWNED RIGHTS OF THIRD PARTIES. IT IS EXPRESSLY UNDERSTOOD AND AGREED THAT ANY RISKS, LIABILITIES OR LOSSES ARISING OUT OF ANY USE, TRANSFER OR LEASE OF THIS MATERIAL WILL NOT BE ATTRIBUTED TO OPTIMIZATION SYSTEMS ASSOCIATES INC. OR ANY INDIVIDUAL ASSOCIATED WITH THE COMPANY. ACCURACY, COMPLETENESS OR USEFULNESS FOR ANY APPLICATION SHALL BE DETERMINED INDEPENDENTLY BY THE PARTY UNDERTAKING SUCH AN APPLICATION.

IN NO EVENT WHATSOEVER WILL OPTIMIZATION SYSTEMS ASSOCIATES INC., ITS EMPLOYEES, OFFICERS, DIRECTORS, OR AGENTS BE LIABLE FOR ANY DAMAGES, INCLUDING, BUT WITHOUT LIMITATION, DIRECT, INDIRECT, INCIDENTAL AND CONSEQUENTIAL DAMAGES AND DAMAGES FOR LOST DATA OR PROFITS, ARISING OUT OF THE USE OF OR INABILITY TO USE THIS MATERIAL.

Optimization Systems Associates Inc.
P.O. Box 8083, Dundas, Ontario
Canada L9H 5E7

Tel 905 628 8228
Fax 905 628 8225

Trademarks of Optimization Systems Associates Inc.

OSA90
OSA90/hope
Datapipe
Empipe
Spicepipe
HarPE
FAST
Space Mapping

Other Trademarks

HP is a trademark of Hewlett-Packard Company.
Sun and Sun Workstation are trademarks of Sun Microsystems, Inc.
SunOS is a trademark of Sun Microsystems, Inc.
UNIX is a registered trademark of AT&T.
em and xgeom are trademarks of Sonnet Software, Inc.
PostScript is a trademark of Adobe Systems Inc.

Table of Contents

REPRINTS

Reprint 9 J.W. Bandler, R.M. Biernacki and S.H. Chen, "Harmonic balance simulation and optimization of nonlinear circuits," (invited), *Proc. IEEE Int. Symp. Circuits and Systems* (San Diego, CA, May 1992), pp. 85-88.

Reprint 10 J.W. Bandler, R.M. Biernacki, Q. Cai, S.H. Chen, S. Ye and Q.J. Zhang, "Integrated physics-oriented statistical modeling, simulation and optimization," *IEEE Trans. Microwave Theory Tech.*, vol 40, 1992, pp. 1374-1400.

Reprint 11 J.W. Bandler, R.M. Biernacki, S.H. Chen, P.A. Grobelny and S. Ye, "Yield-driven electromagnetic optimization via multilevel multidimensional models," *IEEE Trans. Microwave Theory Tech.*, vol 41, 1993, pp. 2269-2278.

Reprint 12 J.W. Bandler, S.H. Chen, R.M. Biernacki, L. Gao, K. Madsen and H. Yu, "Huber optimization of circuits: a robust approach," *IEEE Trans. Microwave Theory Tech.*, vol. 41, 1993, pp. 2279-2287.

Reprint 13 J.W. Bandler, R.M. Biernacki, Q. Cai and S.H. Chen, "A robust physics-oriented statistical GaAs MESFET model," *Proc. European Gallium Arsenide Application Symposium* (Turin, Italy, April 1994), pp. 173-176.

Reprint 14 J.W. Bandler, R.M. Biernacki, S.H. Chen, P.A. Grobelny and R.H. Hemmers, "Exploitation of coarse grid for electromagnetic optimization," *IEEE Int. Microwave Symp. Digest* (San Diego, CA, May 1994), pp. 381-384.

Reprint 15 J.W. Bandler, R.M. Biernacki, Q. Cai and S.H. Chen, "A novel approach to statistical modeling using cumulative probability distribution fitting," *IEEE Int. Microwave Symp. Digest* (San Diego, CA, May 1994), pp. 385-388.

Reprint 16 J.W. Bandler, R.M. Biernacki, S.H. Chen, P.A. Grobelny, C. Moskowitz and S.H. Talisa, "Electromagnetic design of high-temperature superconducting microwave filters," *IEEE Int. Microwave Symp. Digest* (San Diego, CA, May 1994), pp. 993-996.

Reprint 17 J.W. Bandler, R.M. Biernacki, S.H. Chen and K. Madsen, "The Huber concept in device modeling, circuit diagnosis and design centering," *IEEE Int. Symp. Circuits and Systems* (London, England, May-June 1994), vol. 1, pp. 129-132.

Reprint 18 J.W. Bandler, R.M. Biernacki, S.H. Chen and P.A. Grobelny, "A CAD environment for performance and yield driven circuit design employing electromagnetic field simulators," *IEEE Int. Symp. Circuits and Systems* (London, England, May-June 1994), vol. 1, pp. 145-148.

Reprint 19 J.W. Bandler, R.M. Biernacki, Q. Cai and S.H. Chen, "Compression analysis of a high power BJT amplifier," *Third Int. Workshop on Integrated Nonlinear Microwave and Millimeterwave Circuits INMMC'94, Digest* (Duisburg, Germany, Oct. 1994).

Reprint 20 J.W. Bandler, R.M. Biernacki, S.H. Chen, D.G. Swanson, Jr., and S. Ye, "Microstrip filter design using direct EM field simulation," *IEEE Trans. Microwave Theory Tech.*, vol. 42, 1994, pp. 1353-1359.

TECHNICAL BRIEFS

HarPE Version 1.8 Technical Brief

OSA90/hope Version 3.0 Technical Brief

Empipe Version 2.0 Technical Brief

Chapter 1

Microwave Circuit Optimization Emphasizing Automated Direct EM Design and Modeling of Arbitrary Structures (Seminar)

Optimization Systems Associates Inc.

PIONEERS IN

yield and tolerance optimization

circuit performance optimization

parametric design centering

statistical device modeling

robust parameter extraction

harmonic balance simulation

physics based design

EM based design

large-scale optimization

benchmark CAD technology

software architecture for IC design

Areas of Expertise

RF/microwave circuit simulation, design and optimization

harmonic balance simulation techniques

robust and statistical modeling of active and passive devices

automated processing of DC, RF and spectrum data

device modeling, statistical estimation of production yield

powerful performance and yield optimization algorithms

manufacturing tolerance assignment and cost minimization

customized optimizers for large-scale problems

computer optimization of linear and nonlinear networks

algorithms for automated production alignment and tuning

software architectures for integrated approach to design

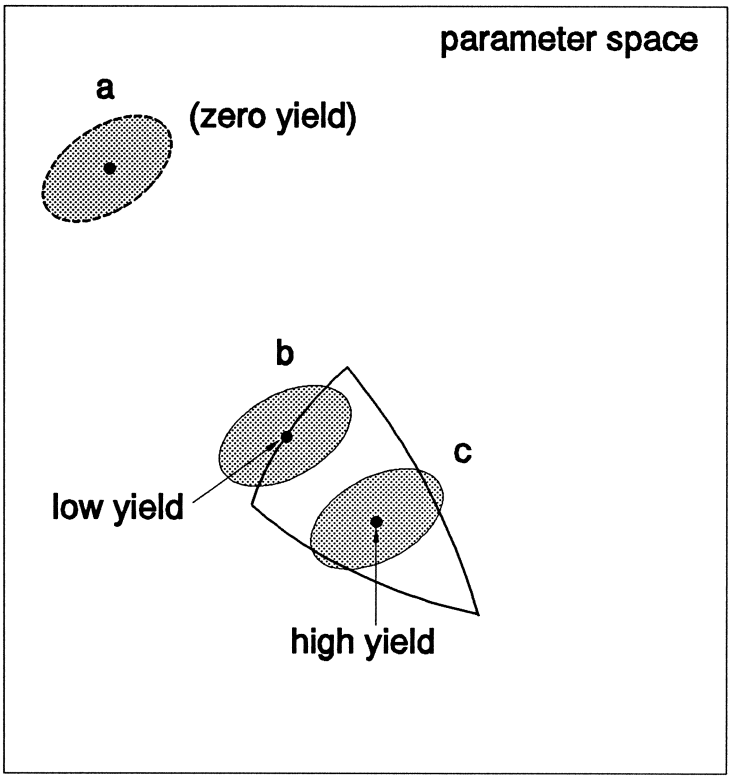

Yield interpretation in the parameter space

Milestones I

computerized Smith chart plots (1966)

performance-driven optimization (1968)

adjoint sensitivities (1970)

cost-driven worst-case design with optimized tolerances (1972)

centering, tolerance assignment integrated with tuning at the design stage (1974)

integrated approach to microwave design with tolerances and uncertainties (1975)

yield-driven optimization for general statistical distributions (1976)

new results for cascaded circuits (1978)

Milestones II

optimal tuning and alignment at the production stage (1980)

fault diagnosis and parameter extraction (1980)

world's fastest multiplexer optimizer (1984)

introduction of powerful minimax optimizers into commercial CAD/CAE products (1985)

large-scale microwave optimization (1986)

foundation of multi-circuit ℓ_1 modeling (1986)

world's first yield-driven design for Super-Compact® (1987)

computational enhancements of commercial CAD/CAE products (1988)

parameter extraction using novel large-scale concepts (1988)

Milestones III

nonlinear adjoint (harmonic balance) exact sensitivities (1988)

RoMPE™, world's first commercial product for FET parameter extraction featuring S-parameters and/or DC data (1988)

yield-driven design of nonlinear microwave circuits (1989)

FAST™, novel technique for high-speed nonlinear sensitivities (1989)

efficient large-signal FET parameter extraction using harmonics (1989)

HarPE™, world's first commercial product for harmonic balance driven FET parameter extraction (1989)

combined discrete/normal statistical modeling of active devices (1989)

Milestones IV

efficient quadratic approximation for statistical design (1989)

nonlinear circuit optimization with dynamically integrated physical device models (1990)

analytically unified DC/small-signal/large-signal circuit design (1990)

OSA90™, world's first friendly optimization engine for performance- and yield-driven design (1990)

Datapipe™ Technology, OSA90's interprocess communication system (1990)

OSA90/hope™, the microwave and RF harmonic optimization system (1991)

design optimization with external simulators, circuit-theoretic and field-theoretic (1991)

Milestones V

statistical modeling of GaAs MESFETs (1991)

gradient quadratic approximation for yield optimization (1991)

physics-based design and yield optimization of MMICs (1991)

Spicepipe™ connection of OSA90/hope™ with Zuberek's SPICE-PAC simulator (1992)

Empipe™ connection of OSA90/hope™ with Sonnet's *em*™ field simulator (1992)

predictable yield-driven circuit optimization (1992)

integrated physics-oriented statistical modeling, simulation and optimization (1992)

"*fulfills the requirement of microwave engineers to model and simulate nonlinear active and passive systems without having a thorough knowledge of analysis, and optimization methods*" - *MEE 1992*

Milestones VI

Datapipe™ connection of OSA90/hope™ with Hoefer's TLM electromagnetic field simulators (1993)

Datapipe™ connection of OSA90/hope™ with Nakhla/Zhang VLSI interconnect simulators (1993)

microstrip filter design using direct EM field simulation (1993)

yield-driven direct electromagnetic optimization (1993)

robustizing modeling and design using Huber functions (1993)

"CAD review: Non-linear CAD benchmark" by MEE (1993)

EM design of HTS microwave filters (1994)

CDF approach to statistical modeling (1994)

Space Mapping™ - a fundamental new theory for design with CPU intensive simulators (1994)

"CAD review: the 7 GHz doubler circuit" by MEE (1994)

optimization of structures with arbitrary geometry (1994)

OSA90/hope™ Version 3.0

general nonlinear circuit simulation and optimization
analytically unified DC, small-signal and large-signal
    harmonic balance analysis
statistical analysis and yield optimization
comprehensive optimization/nonlinear modeling
interconnects external simulators
    Empipe™ merges *em*™, even for arbitrary geometry!
    Spicepipe™ merges SPICE
Space Mapping breakthrough in EM optimization
3D visualization

HarPE™ Version 1.8

device characterization, simulation and optimization
FET, bipolar, HEMT, HBT, thermal modeling
parameter extraction
statistical modeling, Monte Carlo analysis
Huber optimization
cumulative probability distribution fitting

OSA90/hope™ Optimization

state-of-the-art gradient-based optimizers with a proven track record in electrical circuit and system optimization

- L1
- L2 (least squares)
- Huber
- minimax
- quasi-Newton
- conjugate gradient
- simplex
- random
- yield (design centering)

exact or approximate gradient

specification and goal definition

quadratic modeling of functions and gradients

sensitivity displays help the user to select the most crucial variables for optimization

Space Mapping™ for CPU intensive optimization

OSA90/hope™ Circuit Features

general nonlinear circuit simulation and optimization
physics-based yield optimization

analytically unified simulation:
DC/small-signal/large-signal harmonic balance

arbitrary topology
multitone, multisource excitations
nonlinear sources controlled by voltages and currents

symbolic subcircuit definition: linear and nonlinear
voltage and current labels (probes)

comprehensive device library
empirical microstrip models
em™ parameterized microstrip models
user-definable models

OSA90/hope™ Math Features

variable definition

expressions including conditional *if else* structures

extensive math library

vector and matrix operations

- multiplication
- transposition
- inverse
- LU factorization
- eigenvalues and eigenvectors
- solving linear equations

vector and matrix elements fully optimizable

Space Mapping™ functions

built-in transformations, including DFT, splines

operation control block

OSA90/hope™ Graphics

continuous, point, bar plots

parametric and multiple plots

histograms, run charts and scatter diagrams

sensitivity displays

waveforms

Smith chart and polar plots

3D visualization including scaling, rotating and smoothing

contours with trace of optimization variables

user-defined legends, colors, views

graphics zoom

HPGL and PostScript files

OSA90/hope™ Datapipe™

Datapipe™: predefined protocols for UNIX pipes

ready-to-use to facilitate high-speed data connections to and from the user's software; over networks

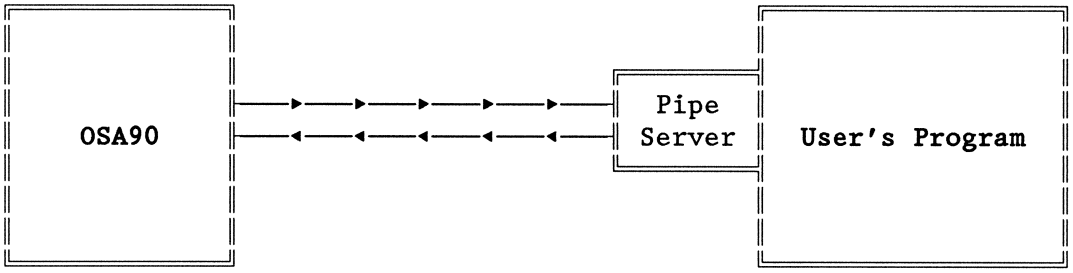

typical READ and WRITE statements are used to receive and send data

a small pipe server (about 350 lines) establishes the protocols; OSA provides the source code of the pipe server

maintains complete security of user's software: OSA does not need access to the user's source code

OSA90/hope™ Connections

Empipe™ merges ***em™***

from Sonnet Software, Inc.

for direct field-level optimizable microstrip designs
under circuit-level linear/nonlinear analysis

optimization of structures with arbitrary geometries

Spicepipe™ merges SPICE

for time-domain simulation, noise analysis, etc.
multidomain (frequency and time) specifications
nominal optimization
yield optimization

OSA90™ can call OSA90™

HarPE™ Version 1.8

characterize devices

extract parameters

simulation-driven
data-driven

build equivalent circuit models

build physics-based models

simulate and optimize

single device circuits at DC, small-signal and large-signal harmonic balance

statistically model devices

estimate Monte Carlo yield

cumulative probability distribution and histogram matching

HEMT models (*M. Golio, Motorola*)

Minimax Design Optimization

$$\underset{\phi}{\text{minimize}} \{ \max_{j} (e_j(\phi)) \}$$

where

ϕ the vector of optimization variables

$R_j(\phi)$ j=1,2,.. - the circuit responses (S parameters, return loss, insertion loss, etc.)

S_{uj}, $S_{\ell j}$ upper/lower specification on $R_j(\phi)$

the individual errors $e_j(\phi)$ are of the form

$$e_j(\phi) = R_j(\phi) - S_{uj}$$

or

$$e_j(\phi) = S_{\ell j} - R_j(\phi)$$

negative/positive error value indicates that the corresponding specification is satisfied/violated

effective minimax optimization requires a dedicated optimizer and accurate gradients of individual errors w.r.t. the optimization variables ϕ

Interconnection Between a Circuit Optimizer and a Numerical EM Simulator

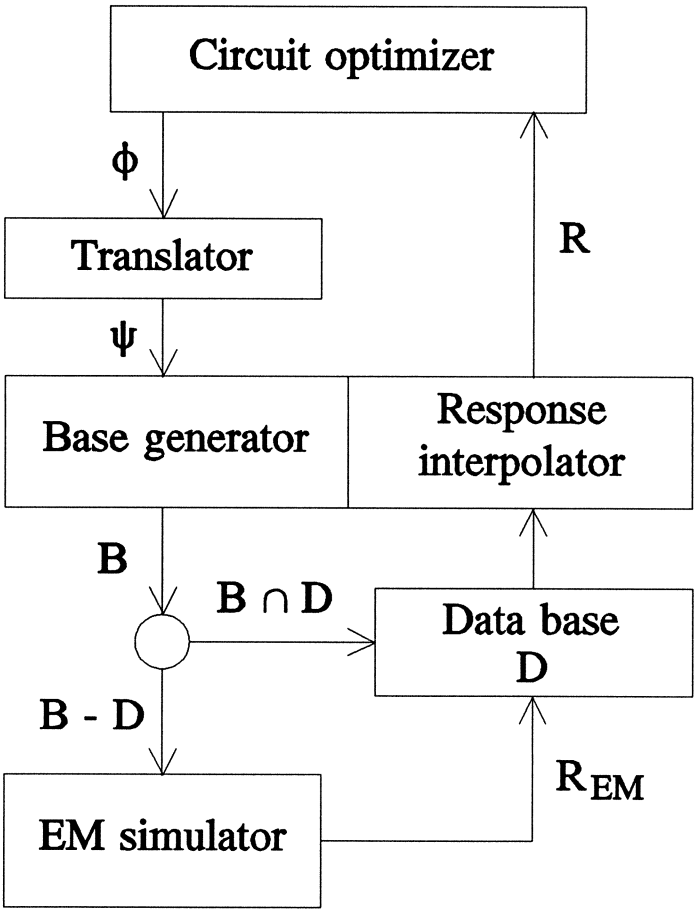

Conventional Double Stub Microstrip Structure

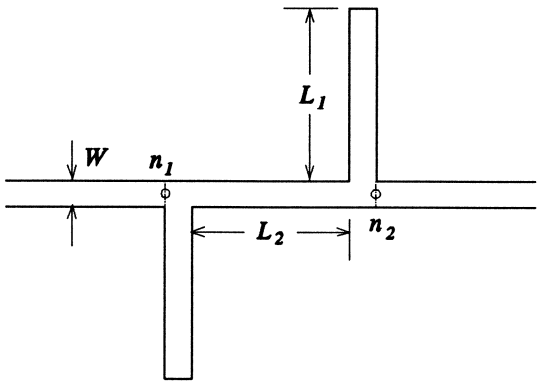

for band-stop filter applications

Double Folded Stub Microstrip Structure
(*Rautio, 1992*)

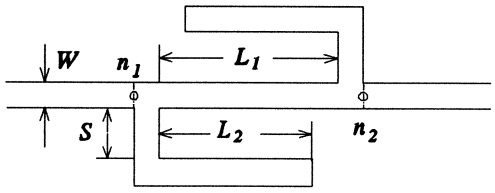

substantially reduces the filter area while achieving the same goal as the conventional double stub structure

can be described by 4 parameters: width, spacing and two lengths *W, S,* L_1 and L_2

Design of the Double Folded Microstrip Structure

minimax optimization to move the center frequency of the stop band from 15 GHz to 13 GHz

W fixed at 4.8 mils

L_1, L_2 and S - variables (designable parameters)

design specifications

$|S_{21}| > -3$ dB for $f < 9.5$ GHz and $f > 16.5$ GHz

$|S_{21}| < -30$ dB for 12 GHz $< f <$ 14 GHz

substrate thickness - 5 mils

relative dielectric constant - 9.9

em™ driven by the minimax gradient optimizer of OSA90/hope™ through Empipe™

optimization was carried out in two steps

(1) $\Delta x = \Delta y = 2.4$ mils

(2) the grid size was reduced to $\Delta x = \Delta y = 1.6$ mils for fine resolution

Minimax Optimization of the Double Folded Microstrip Structure

PARAMETER VALUES FOR THE DOUBLE FOLDED STUB BEFORE AND AFTER OPTIMIZATION

Parameter	Before optimization (mils)	After optimization (mils)
L_1	74.0	91.82
L_2	62.0	84.71
S	13.0	4.80

Results for the Double Folded Microstrip Structure

Before Optimization

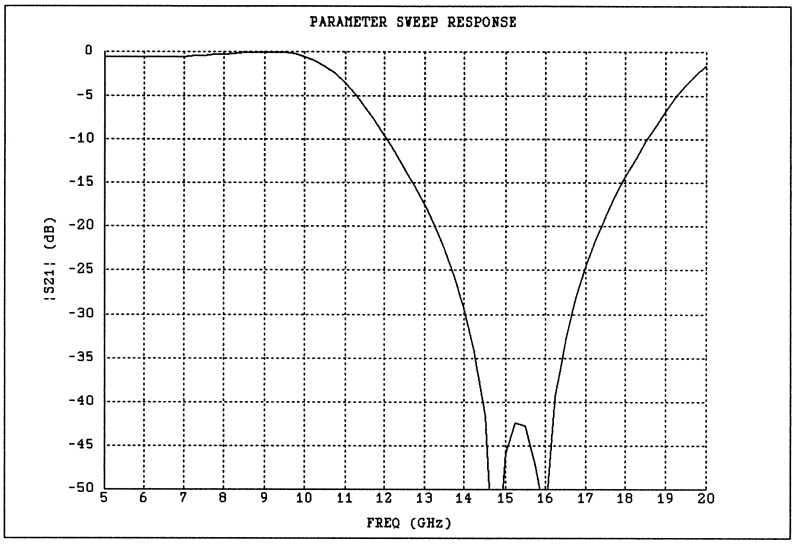

After Optimization

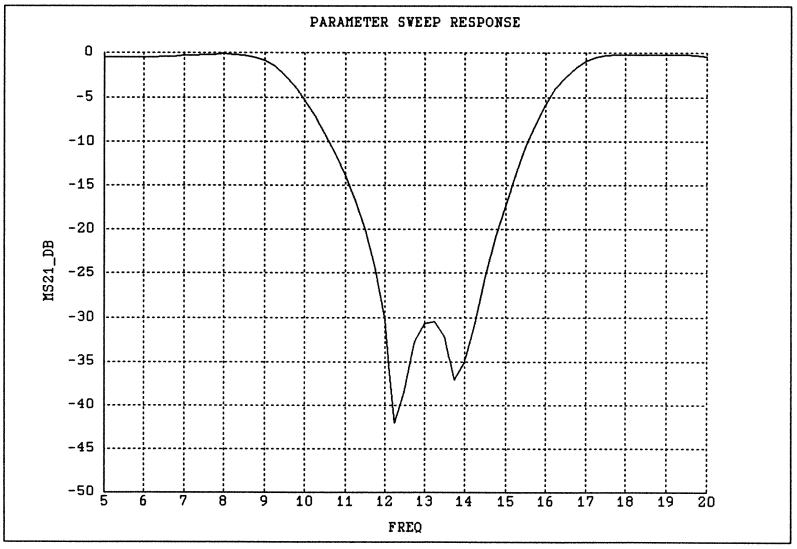

26-40 GHz Interdigital Microstrip Bandpass Filter

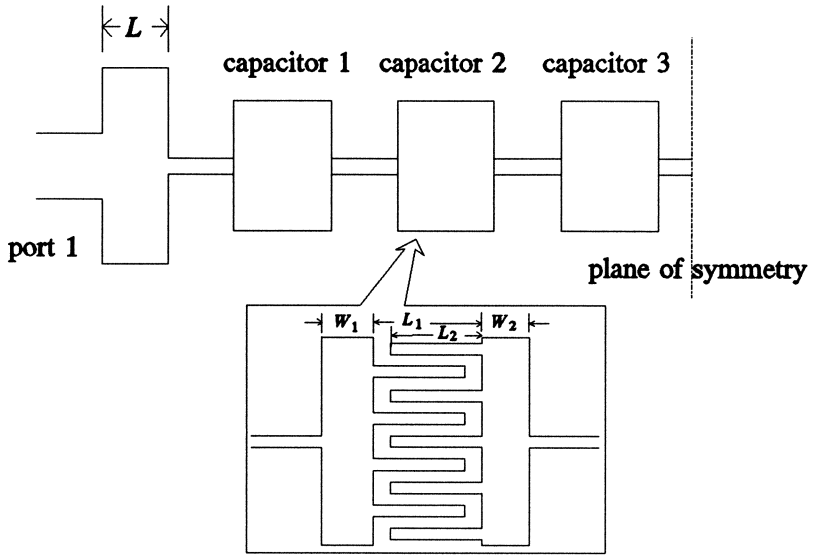

utilizes thin microstrip lines and interdigital capacitors to realize inductances and capacitances of a synthesized lumped ladder circuit

the original microstrip design was determined by matching the lumped prototype at the center frequency using *em*™

when the filter was simulated by *em*™ in the whole frequency range the results exhibited significant discrepancies w.r.t. the prototype

it necessitated manual adjustment and made a satisfactory design very difficult to achieve

Design of the 26-40 GHz Interdigital Microstrip Filter

a total of 13 designable parameters including the distance between the patches L_1, the finger length L_2 and two patch widths W_1 and W_2 for each of the three interdigital capacitors, and the length L of the end capacitor

the second half of the circuit, to the right of the plane of symmetry, is assumed identical to the first half, so it contains no additional variables

the transmission lines between the capacitors were fixed at the originally designed values

design specifications

$|S_{11}| < -20$ dB and $|S_{21}| > -0.04$ dB

for 26 GHz $< f <$ 40 GHz

substrate thickness - 10 mils

dielectric constant - 2.25

shielding height - 120 mils

em™ driven by the minimax gradient optimizer of OSA90/hope™ through Empipe™

Simulation of the 26-40 GHz Interdigital Capacitor Filter After Optimization

filter response after optimization

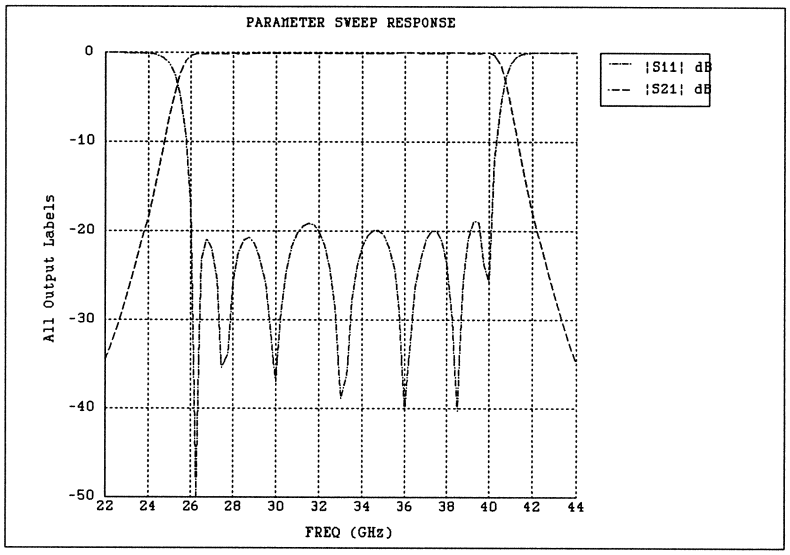

a typical minimax equal-ripple response of the filter was achieved after a series of consecutive optimizations with different subsets of optimization variables and frequency points

the resulting geometrical dimensions were finally rounded to 0.1 mil resolution

Measurements of the 26-40 GHz Interdigital Capacitor Filter - Return Loss After Optimization

measured and simulated $|S_{11}|$ of the filter after manufacturing

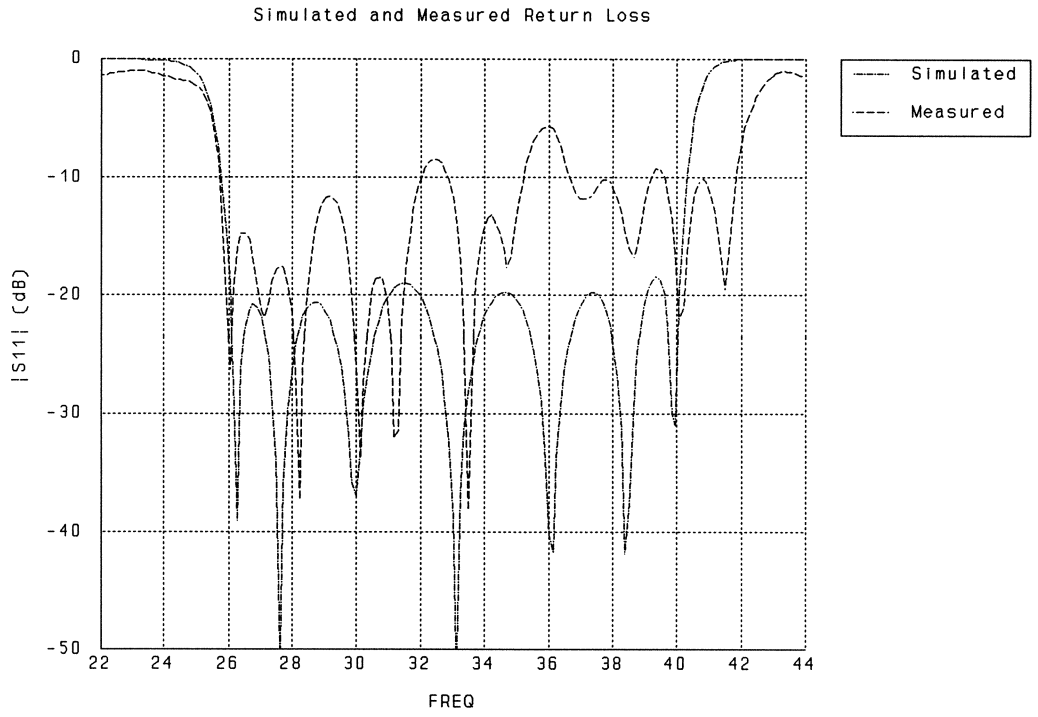

recent improvements in the field solver analysis of interdigital capacitors will improve the accuracy of the bandwidth prediction

Measurements of the 26-40 GHz Interdigital Capacitor Filter - Insertion Loss After Optimization

measured and simulated $|S_{21}|$ of the filter after manufacturing

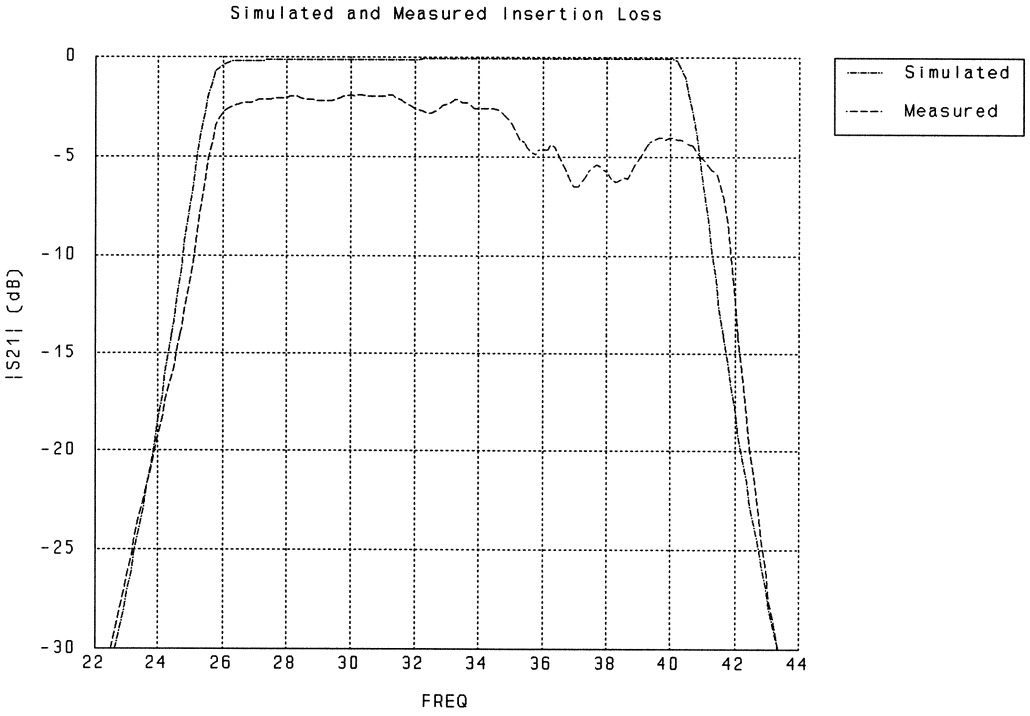

the insertion loss flatness will clearly improve after return loss has been tuned

Yield Optimization

the problem of yield optimization can be formulated as

$$\underset{\phi^0}{maximize} \{ Y(\phi^0) = \int_{R^n} I_a(\phi) f_\phi(\phi^0, \phi) d\phi \}$$

where

ϕ^0	nominal circuit parameters
ϕ	actual circuit outcome parameters
$Y(\phi^0)$	design yield
$f_\phi(\phi^0, \phi)$	probability density function of ϕ around ϕ^0
$I_a(\phi) = \begin{cases} 1 & if \quad \phi \in A \\ 0 & if \quad \phi \notin A \end{cases}$	
A	acceptability region

in practice, the integral is approximated using K Monte Carlo circuit outcomes ϕ^i and yield is estimated by

$$Y(\phi^0) \simeq \frac{1}{K} \left(\sum_{i=1}^{K} I_a(\phi^i) \right)$$

the outcomes ϕ^i are generated by a random number generator according to $f_\phi(\phi^0, \phi)$

Optimization of a Small-Signal Amplifier

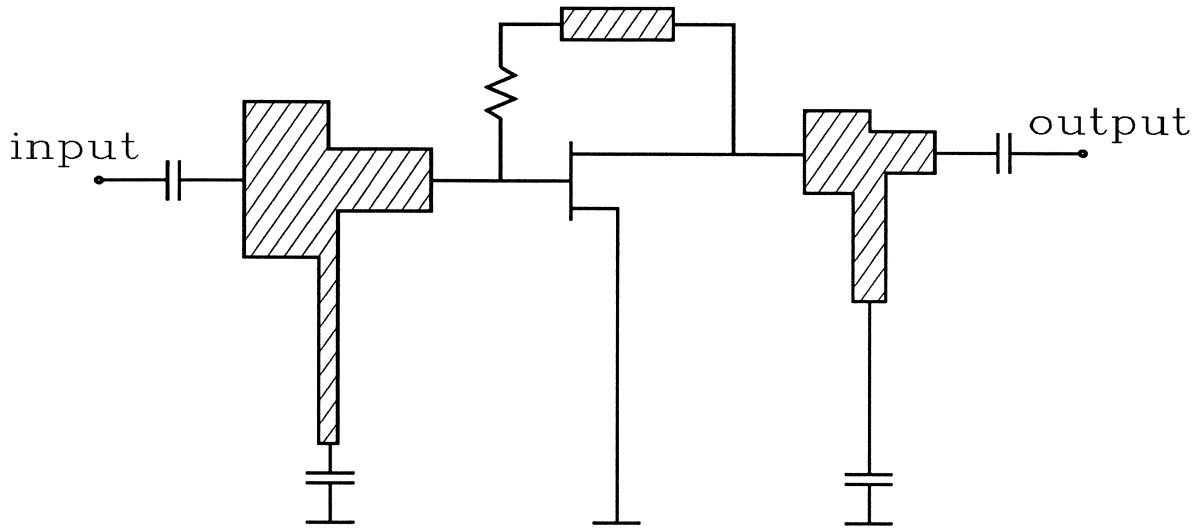

the specifications for yield optimization of the amplifier are

$$7\ \text{dB} \le |S_{21}| \le 8\ \text{dB} \qquad \text{for} \qquad 6\ \text{GHz} < f < 18\ \text{GHz}$$

the gate and drain circuit microstrip T-junctions and the feedback microstrip line are built on a 10 mil thick substrate with relative dielectric constant 9.9

the microstrip components of the amplifier are simulated using component level Q-models built from EM simulations

we used *em*™ from *Sonnet Software* for EM simulations

Optimization Variables

W_{g1}, L_{g1}, W_{g2}, L_{g2} of the gate circuit T-junction and W_{d1}, L_{d1}, W_{d2}, L_{d2} of the drain circuit T-junction are the optimization variables

W_{g3}, L_{g3}, W_{d3} and L_{d3} of the T-junctions, W and L of the feedback microstrip line, as well as the FET parameters are not optimized

parameters of the microstrip line (a) and the T-junctions (b)

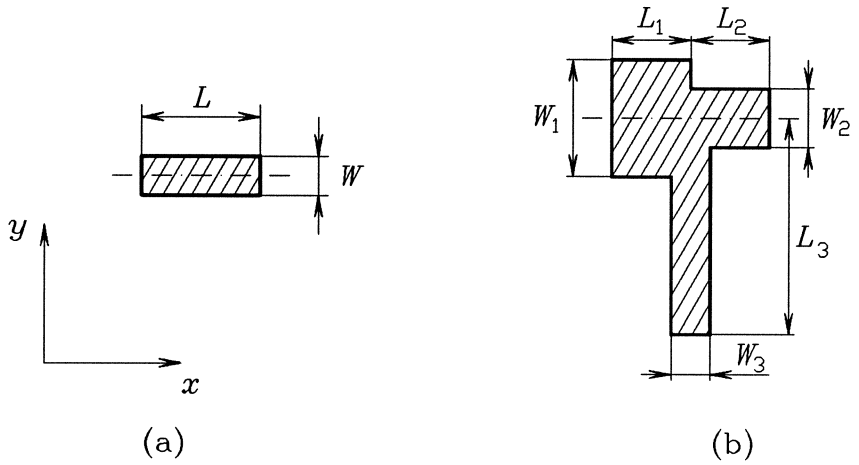

we assumed 0.5 mil tolerance and uniform distribution for all geometrical parameters of the microstrip components

the statistics of the small-signal FET model were extracted from measurement data

Small-Signal Amplifier Yield Before Optimization

the starting point for yield optimization was obtained by nominal minimax optimization using analytical/empirical microstrip component models

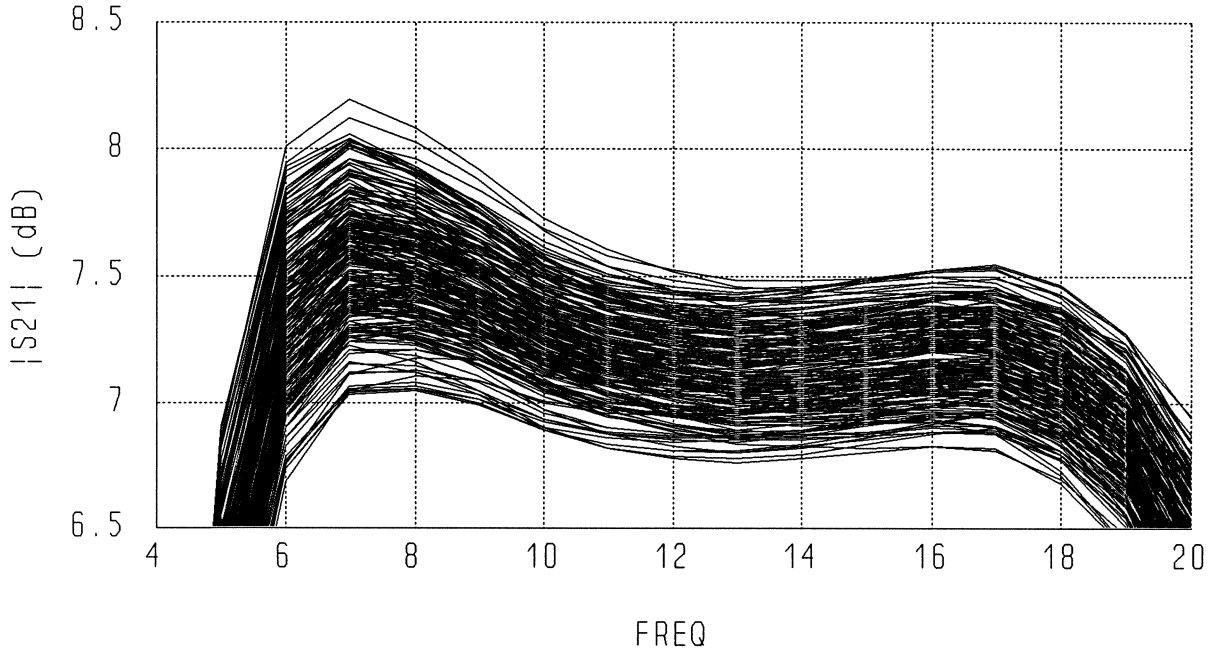

Monte Carlo simulation
- 250 outcomes
- 55% yield

Small-Signal Amplifier Yield After Optimization

the component level Q-models were used in yield optimization

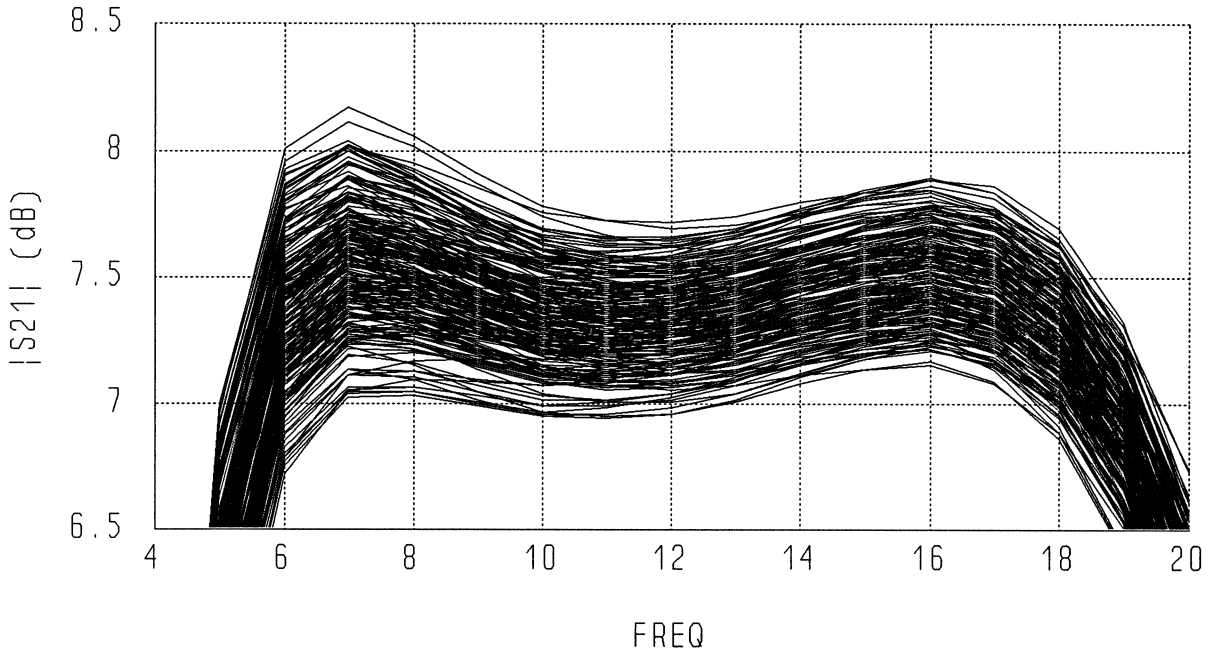

yield estimated by 250 Monte Carlo simulations increased to 82%

optimization was performed by OSA90/hope™ with Empipe™ driving *em*™

Optimization Results

MICROSTRIP PARAMETERS OF THE AMPLIFIER

Parameters	Nominal design	Centered design
W_{g1}	17.45	19.0
L_{g1}	35.54	34.53
W_{g2}	9.01	8.611
L_{g2}	30.97	32.0
W_{g3}	3.0*	3.0*
L_{g3}	107.0*	107.0*
W_{d1}	8.562	7.0
L_{d1}	4.668	6.0
W_{d2}	3.926	3.628
L_{d2}	9.902	11.0
W_{d3}	3.5*	3.5*
L_{d3}	50.0*	50.0*
W	2.0*	2.0*
L	10.0*	10.0*
Yield (250 outcomes)	55%	82%

* Parameters not optimized.
Dimensions of the parameters are in mils. 50 outcomes were used for yield optimization. 0.5 mil tolerance and uniform distribution were assumed for all the parameters.

Three-Section 3:1 Microstrip Impedance Transformer

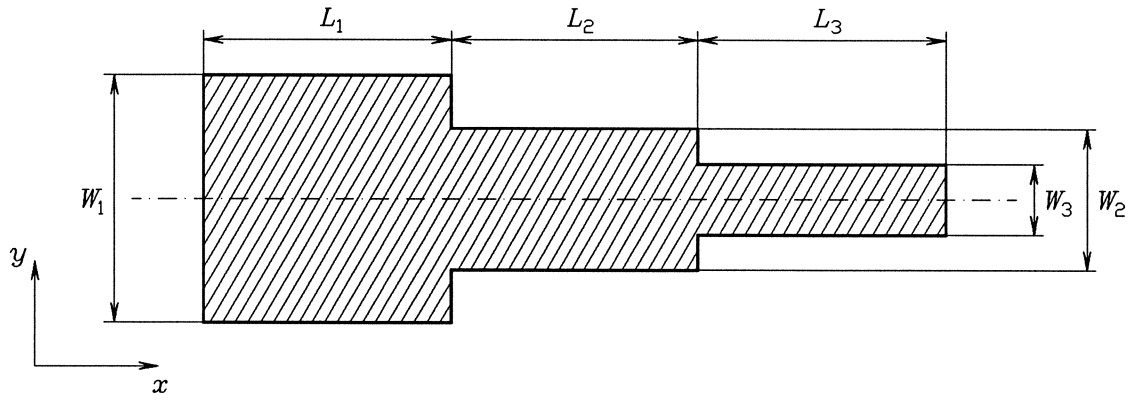

designed on a 0.635 mm thick substrate with relative dielectric constant of 9.7

the source and load impedances are 50 and 150 ohms

design specification set for the input reflection coefficient

$|S_{11}| \leq 0.12$, from 5 GHz to 15 GHz

normal distributions with 2% standard deviations assumed for W_1, W_2 and W_3 and 1% standard deviations assumed for L_1, L_2 and L_3

Three-Section Microstrip Transformer After Yield Optimization

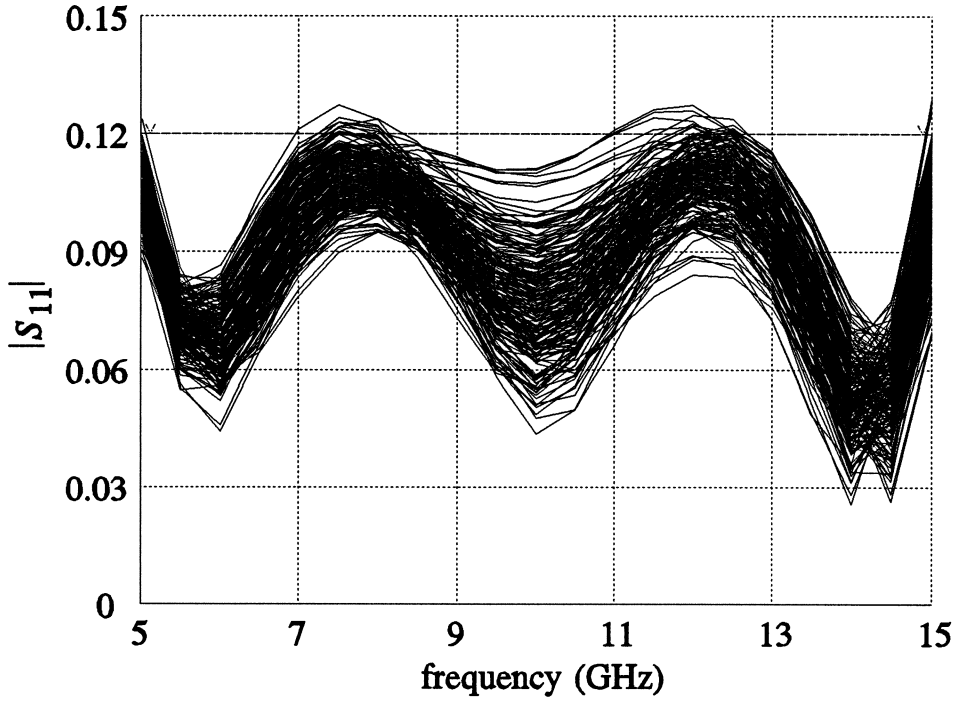

modulus of the reflection coefficient vs. frequency

optimization using single-level (component) Q-models

100 statistical outcomes used for yield optimization

yield is increased to 86%

Yield Sensitivity of the Microstrip Transformer

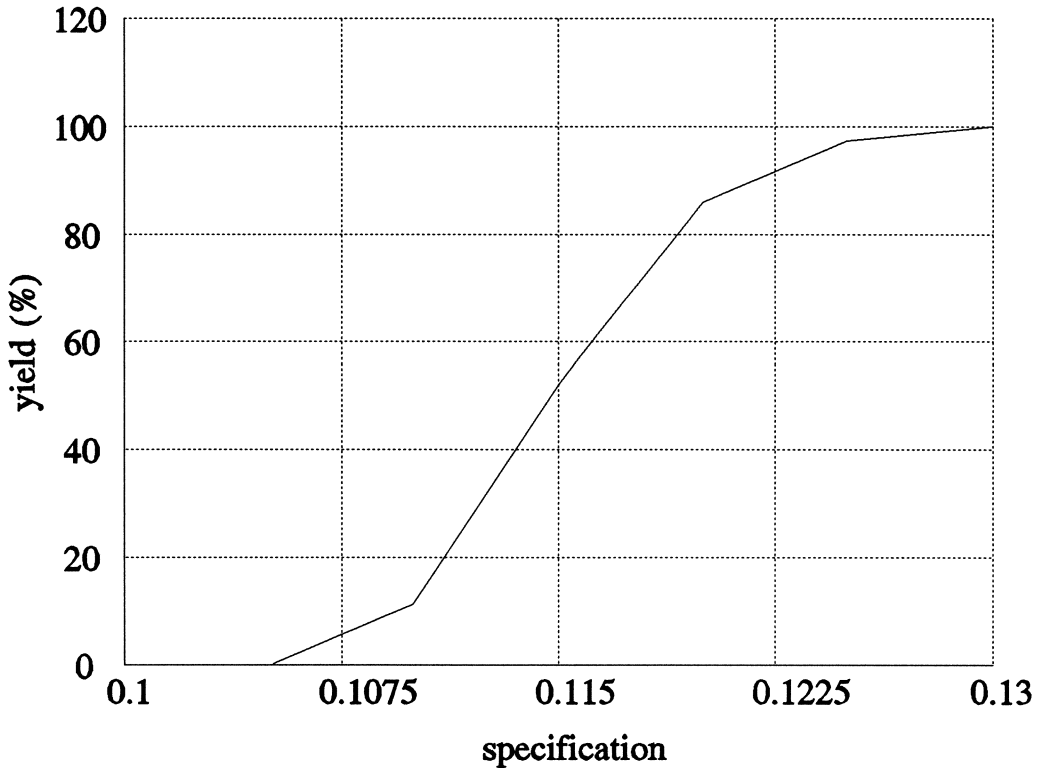

yield vs. specification on $|S_{11}|$

high sensitivity of yield w.r.t. the specification

yield varies from 0% to 100% over a very small range of the specification

yield estimated with 250 Monte Carlo outcomes

Yield Sensitivity of the Microstrip Transformer

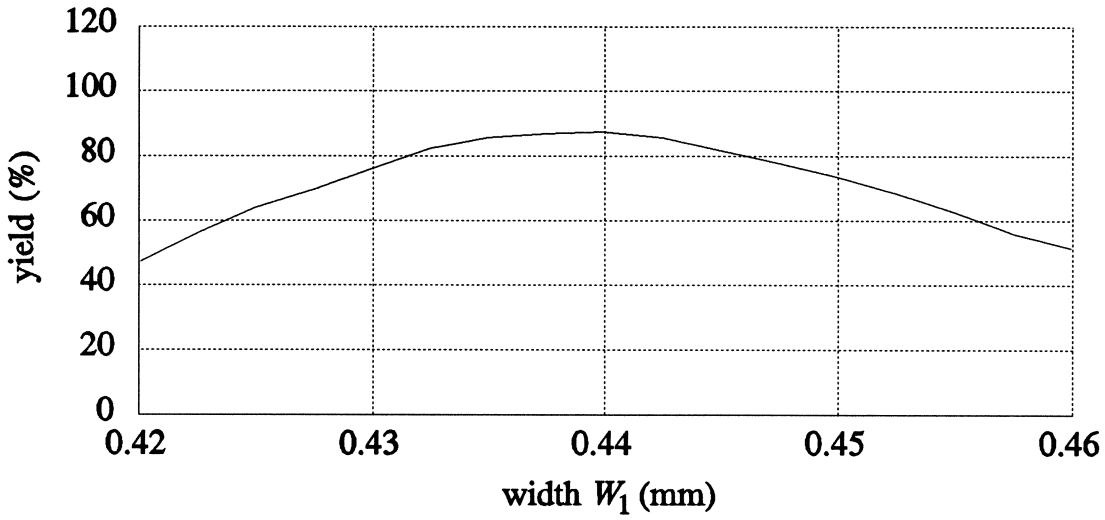

yield vs. W_1

relatively high sensitivity of yield w.r.t. W_1

yield estimated with 250 Monte Carlo outcomes

Yield Sensitivity of the Microstrip Transformer

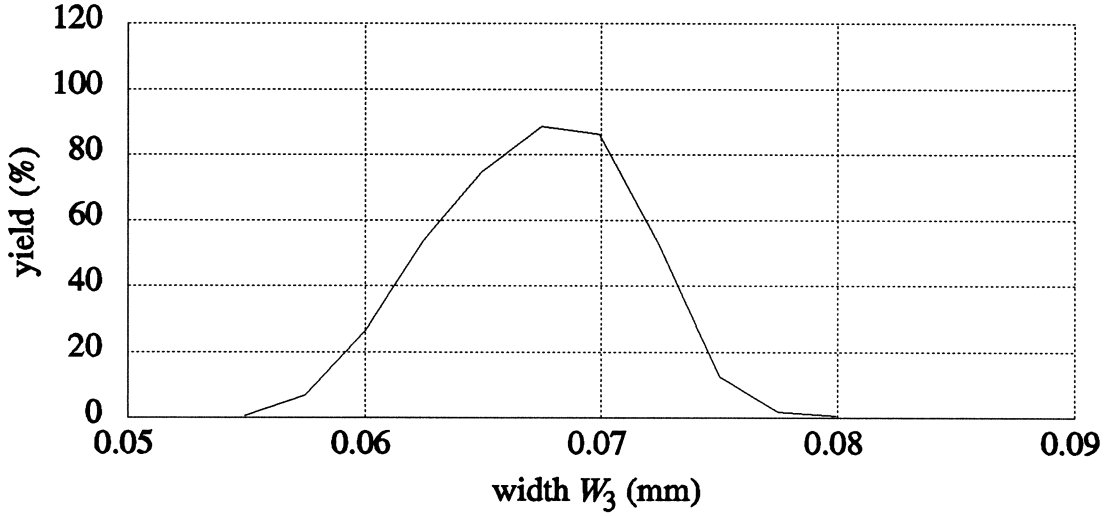

yield vs. W_3

high sensitivity of yield w.r.t. W_3

yield estimated with 250 Monte Carlo outcomes

Empipe™ (1992)

smart connection of OSA90/hope™ with Sonnet's *em*™ field simulator for interprocessing circuit/field/measurement data

a significant step towards the required integrated approach offering

simulation, modeling, parameter extraction
optimization, sensitivity analysis, statistical analysis
error analysis (probability of satisfying error specs)
automated processing of circuit/field/measurement data
fixed or optimizable geometries simulated by *em*™

recent applications include

EM microstrip filter design
yield-driven direct EM optimization
EM statistical sensitivity analyses
optimization of arbitrary geometries
Microwave Engineering Europe CAD Review of
7 GHz nonlinear frequency doubler

more relevant experimental validation applications to come!

Parameterized (Optimizable)
Microstrip Library of Empipe™

bend
cross junction
double patch capacitors
interdigital capacitors
line
mitered bend
open stub
overlay double patch capacitors
rectangular structure
spiral inductors
step junction
symmetrical and asymmetrical folded double stubs
symmetrical and asymmetrical gaps
symmetrical and asymmetrical double stubs
T junction

Electromagnetic Design of HTS Microwave Filters

available low-loss and narrow-bandwidth (0.5 - 3 %) filter banks are of very large size which in some satellite and airborne applications is intolerable

small conventional microstrip filters are too lossy for narrow-band applications

low-loss, narrow-bandwidth microstrip filters can be made using HTS technology with relatively inexpensive cooling

the dielectric constant of substrate materials used in HTS technology is too large to be accurately treated by traditional microwave circuit design software packages with analytical/empirical models

we employ electromagnetic field simulation which can provide results in good agreement with experimental data

high sensitivity requires a very fine grid in numerical EM simulations

The HTS Quarter-Wave Parallel Coupled-Line Filter

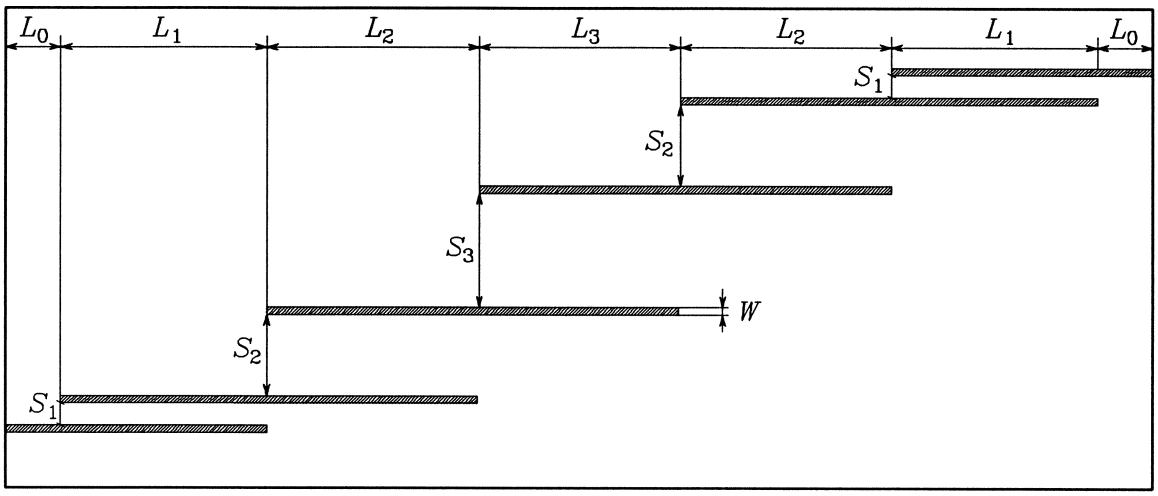

20 mil thick lanthanum aluminate substrate

the dielectric constant is 23.4

the *x* and *y* grid sizes for ***em*** simulations are 1.0 and 1.75 mil

100 elapsed minutes are needed for ***em*** analysis at a single frequency on a Sun SPARCstation 10

Design Specifications for the HTS Filter

$|S_{21}| < 0.05$ for $f < 3.967$ GHz and $f > 4.099$ GHz

$|S_{21}| > 0.95$ for $4.008 \text{ GHz} < f < 4.058$ GHz

narrow 1.2 % bandwidth

the lengths of the line sections: L_1, L_2 and L_3 and the gaps between the sections: S_1, S_2 and S_3 are the design parameters

the line width W is the same for all sections and is kept fixed

the length of the input and output lines L_0 is kept fixed

design carried out in cooperation with Westinghouse Science and Technology Center

Filter Design Using Traditional Simulators

we tested two commercial microwave CAD packages: OSA90/hope and Touchstone

Touchstone Results:

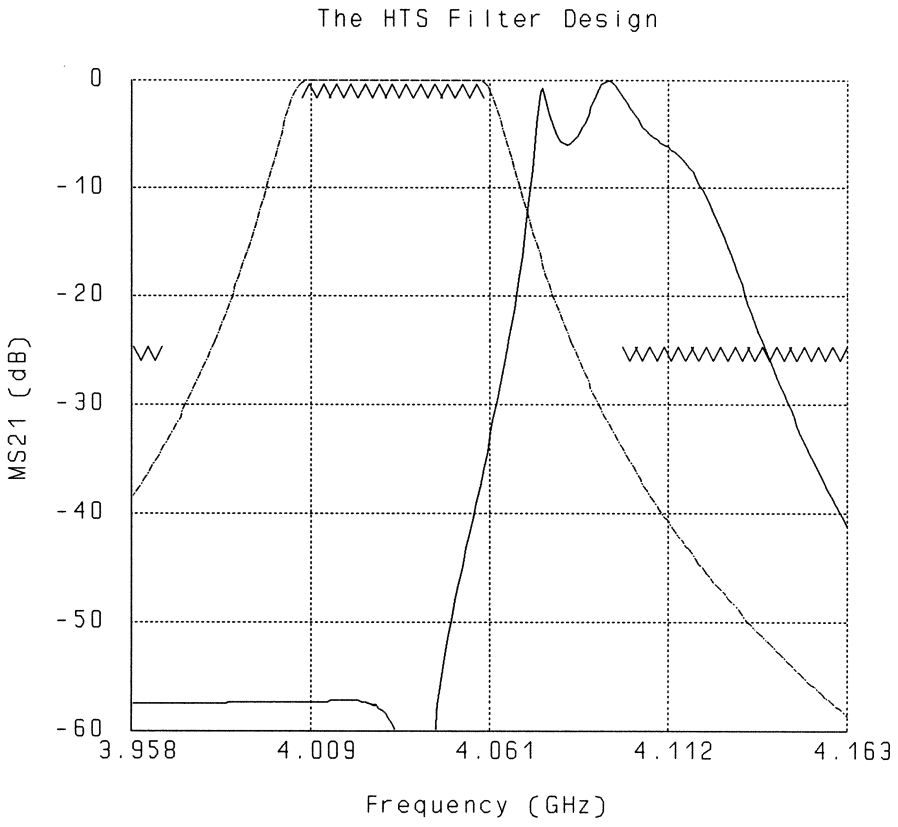

em simulation results differ significantly from Touchstone results and do not satisfy the specifications

The Space Mapping Technique

particularly attractive for designs involving CPU intensive simulators

it substantially decreases the number of necessary exact (EM) simulations

we create and iteratively refine a mapping from the EM simulator input space onto the parameter space of the model used by the optimizer

the initial mapping is found using a preselected set of k points in the EM input space

the set of corresponding points in the optimizer parameter space is determined by fitting the EM simulation results to the model used by the optimizer

HTS Filter Design Using Space Mapping Optimization

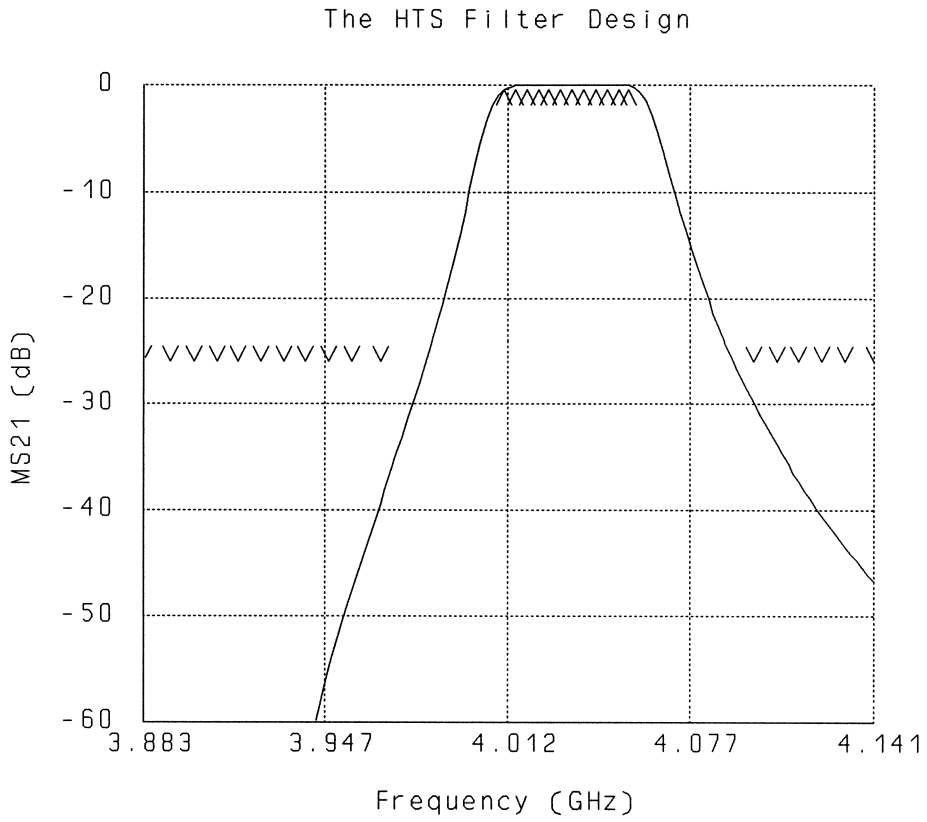

em interfaced to OSA90/hope through Empipe

all the processing needed to establish the mapping was performed within the OSA90/hope environment

a total of 13 *em* simulations was sufficient to establish the mapping

$|S_{21}|$ at the solution well exceeds the design specifications

Chapter 2

OSA90/hope Lab Manual Version 3.0

OSA90/hope™

Lab Manual

Version 3.0

August, 1994

Optimization Systems Associates Inc.

LIABILITY AND WARRANTY

NEITHER OPTIMIZATION SYSTEMS ASSOCIATES INC. NOR ITS EMPLOYEES, OFFICERS, DIRECTORS OR ANY OTHER PERSON, COMPANY, AGENCY OR INSTITUTION: (1) MAKES ANY WARRANTY, EXPRESS OR IMPLIED AS TO ANY MATTER WHATSOEVER REGARDING THIS MATERIAL, INCLUDING BUT NOT LIMITED TO THE GENERALITY THEREOF, ALL IMPLIED WARRANTIES AND CONDITIONS OF MERCHANTABILITY AND FITNESS FOR A PARTICULAR PURPOSE, OR THOSE ARISING BY STATUTE OR OTHERWISE IN LAW OR FROM THE COURSE OF DEALING OR USAGE OF TRADE HAVE BEEN AND ARE HEREBY EXPRESSLY EXCLUDED; OR (2) ASSUMES ANY LEGAL RESPONSIBILITY WHATSOEVER FOR THE ACCURACY, COMPLETENESS OR USEFULNESS OF THIS MATERIAL; OR (3) REPRESENTS THAT ITS USE WOULD NOT INFRINGE UPON PRIVATELY OWNED RIGHTS OF THIRD PARTIES. IT IS EXPRESSLY UNDERSTOOD AND AGREED THAT ANY RISKS, LIABILITIES OR LOSSES ARISING OUT OF ANY USE, TRANSFER OR LEASE OF THIS MATERIAL WILL NOT BE ATTRIBUTED TO OPTIMIZATION SYSTEMS ASSOCIATES INC. OR ANY INDIVIDUAL ASSOCIATED WITH THE COMPANY. ACCURACY, COMPLETENESS OR USEFULNESS FOR ANY APPLICATION SHALL BE DETERMINED INDEPENDENTLY BY THE PARTY UNDERTAKING SUCH AN APPLICATION.

IN NO EVENT WHATSOEVER WILL OPTIMIZATION SYSTEMS ASSOCIATES INC., ITS EMPLOYEES, OFFICERS, DIRECTORS, OR AGENTS BE LIABLE FOR ANY DAMAGES, INCLUDING, BUT WITHOUT LIMITATION, DIRECT, INDIRECT, INCIDENTAL AND CONSEQUENTIAL DAMAGES AND DAMAGES FOR LOST DATA OR PROFITS, ARISING OUT OF THE USE OF OR INABILITY TO USE THIS MATERIAL.

CONTENTS ARE SUBJECT TO CHANGE WITHOUT NOTICE.

Copyright

Copyright © 1994 Optimization Systems Associates Inc.

THIS DOCUMENTATION AND RELATED COMPUTER PROGRAM ARE THE PROPERTY OF OPTIMIZATION SYSTEMS ASSOCIATES INC. REPRODUCTION, DISCLOSURE OR TRANSCRIPTION OF ANY OF THIS MATERIAL IN ANY FORM INTO ANY MACHINE REQUIRES PRIOR PERMISSION IN WRITING FROM OPTIMIZATION SYSTEMS ASSOCIATES INC.

All Rights Reserved. OSA90/hope Lab Manual Version 3.0 first published in 1994.
Printed in Canada.

Optimization Systems Associates Inc.
P.O. Box 8083, Dundas, Ontario
Canada L9H 5E7

Tel 905 628 8228
Fax 905 628 8225

Trademarks of Optimization Systems Associates Inc.

OSA90
OSA90/hope
Datapipe
Empipe
Spicepipe
HarPE
FAST
Space Mapping

Other Trademarks

HP is a trademark of Hewlett-Packard Company.
Sun and Sun Workstation are trademarks of Sun Microsystems, Inc.
SunOS is a trademark of Sun Microsystems, Inc.
UNIX is a registered trademark of AT&T.
em and xgeom are trademarks of Sonnet Software, Inc.
PostScript is a trademark of Adobe Systems Inc.

Table of Contents

Lab 1 Simulation of an LC Transformer

Objectives

This lab is designed to help you set up linear circuit simulation using OSA90.

Circuit Diagram and Parameter Values

Consider the LC transformer circuit shown in Fig. L1. Use OSA90 to compute the branch currents, branch voltages and magnitude of the input reflection coefficient of the LC circuit. Use 21 uniformly spaced points in the frequency range 0.5 - 1.179 rad/s to obtain the reflection coefficient. Use frequency points 0.5 rad/s, 0.8 rad/s and 1.1 rad/s to obtain the requested voltages and currents. The parameter values are E = 3 V, R_1 = 3 Ω, R_2 = 1 Ω, L_1 = 1.041 H, C_2 = 0.979 F, L_3 = 2.341 H, C_4 = 0.781 F, L_5 = 2.937 H, C_6 = 0.347 F.

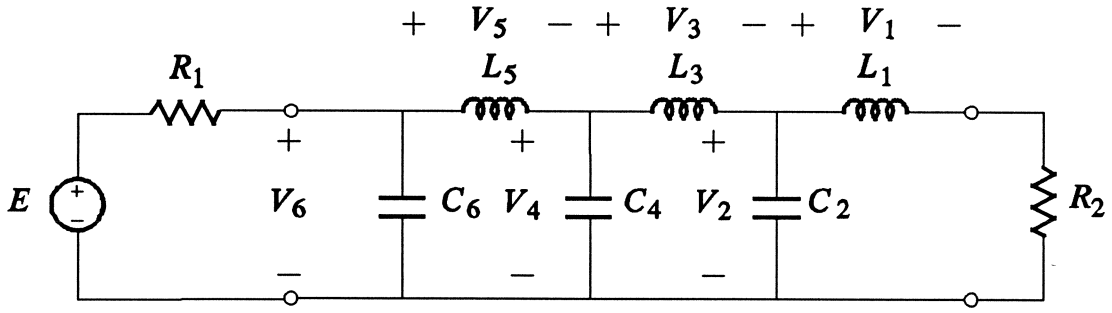

Fig. L1 A lumped element LC transformer.

Procedure

Create Your Circuit File

(1) Create a Control block to set the default unit system to Non_Microwave_Units (Manual Chapter 3, pages 3-24 to 3-25).

(2) Create a Model block to describe the circuit.

(a) Set the value of the angular frequency to 0.5 by assigning 0.5 to the label Omega.

(b) Define the elements R_2, L_1, L_3, L_5, C_2, C_4 and C_6 using the keywords RES, IND and CAP (Manual Chapter 6 - "Elements") and the topology of the circuit (Manual Chapter 6).

(c) Define the input port with the excitation (both the voltage E and the resistance R_1) (Manual Chapter 6 - "Ports"), e.g.,

```
PORT node1 node2 NAME=portname V=E R=R1;
```

(d) Define complex branch voltages V_1, V_2, V_3, V_4, and V_5 using Voltage Labels (Manual Chapter 6 -"Voltage Labels"). For example,

```
VLABEL node1 node0 NAME=V1;
```

Notice that this implies defining arrays: MV1[], PV1[], ..., MV5[], PV5[] where "M" stands for *magnitude* and "P" stands for *phase* of the complex voltages (Manual Chapter 6, page 6-31). In our case (linear circuit under sinusoidal excitation), only the fundamental components, namely, MV1[1], PV1[1], ..., MV5[1] and PV5[1], are nonzero.

(e) Complete the circuit description using the CIRCUIT statement (Manual Chapter 6 - "The Circuit Statement").

(f) You do not need to define the branch voltage V_6 by VLABEL, because it coincides with the input port. V_6 is automatically available as MV*portname*[1] and PV*portname*[1], where *portname* is the name of the input port you defined at Step 2(c).

(g) Use the MP2RI transformation (Manual Chapter 4 - "Built-In Transformations") to find the real and imaginary parts of the requested voltages. For example:

```
MP2RI(MV1[1], PV1[1], RV1, IV1);
```

where RV1 and IV1 are the real and imaginary parts of the voltage V_1. Apply Ohm's Law to compute the real and imaginary parts of the requested currents.

(h) Terminate your Model block with the "End" keyword.

(3) Define the Sweep block (Manual Chapter 9). Find the magnitude of the reflection coefficient MS11 and real and imaginary part of all branch voltages and currents over the specified range of frequency.

(a) AC simulation (Manual Chapter 9 - "Sweep Block"):

```
AC:  Omega: from 0.5 to 1.179 n=20, FREQ=(Omega/(2*PI)), RREF=3, MS11;
```

AC simulation computes the small-signal S parameters. MS11 is one of them, namely the modulus of S_{11}

(b) HB simulation (Manual Chapter 9 - "Sweep Block"):

```
HB:  Omega: 0.5 0.8 1.1 FREQ=(Omega/(2*PI)) RV1, IV1, ..., V6, IV6, RI1,
     II1, ..., RI6, II6;
```

HB simulation computes the branch voltages and currents.

(c) Terminate your Sweep block with the "End" keyword.

The Sweep block may have the following appearance.

```
Sweep
   AC:  Omega: from 0.5 to 1.179 n=20  FREQ=(Omega/(2*PI)), RREF=3OH, MS11;
   HB:  Omega: 0.5 0.8 1.1 FREQ=(Omega/(2*PI)), RV1, IV1, RV2, IV2, RV3,
        IV3, RV4, IV4, RV5, IV5, RV6, IV6, RI1, II1, RI2, II2, RI3, II3,
        RI4, II4, RI5, IV5, RI6, II6;
End
```

Perform Circuit Simulation

(1) Parse the circuit file by exiting the file editor (press <F7>).

(2) Press <D> to choose the "Display" option.

(3) Press <X> to choose the "Xsweep" option.

(4) Use the "Graphical" option to display the response diagrams (Manual Chapter 9 - "OSA90.Display Menu Option").

(5) Use the "Numerical" option to obtain the numerical outputs. To obtain all the responses, you need to toggle among the three sweep sets in the "Xsweep" menu.

Complete The Following Tables

You may find the Report Generation feature of OSA90 helpful in generating the tables. See the Appendix for details.

TABLE I REFLECTION COEFFICIENT

No.	ω (rad/s)	MS11= $\lvert \rho \rvert$
1	0.5	
2	0.8055	
3	1.179	

TABLE II BRANCH VOLTAGES*

No.	ω (rad/s)	V_1(V)	V_2(V)	V_3(V)	V_4(V)	V_5(V)	V_6(V)
1	0.5						
2	0.8						
3	1.1						

* The voltages should be presented in the form (Real(voltage), Imaginary(voltage)).

TABLE III BRANCH CURRENTS*

No.	ω (rad/s)	I_1(A)	I_2(A)	I_3(A)	I_4(A)	I_5(A)	I_6(A)
1	0.5						
2	0.8						
3	1.1						

* The currents should be presented in the form (Real(current), Imaginary(current)).

Appendix for Lab 1

Report Generation

The Report Generation feature in OSA90 helps the user create elegantly formatted numerical outputs directly from the OSA90 text editor.

For example, by adding the following Report block, a numerical report will be generated to help you in filling in the Tables I, II and III on the previous pages.

Report Block Template

```
Report

                  REAL PARTS OF BRANCH VOLTAGES
-------------------------------------------------------------------
    Omega    RV1       RV2       RV3       RV4       RV5       RV6
-------------------------------------------------------------------
${     $%3.1f$$Omega$Hz   $% -6.4f$$RV1$   $% -6.4f$$RV2$   $% -6.4f$$RV3$   $%
-6.4f$$RV4$  $% -6.4f$$RV5$  $% -6.4f$$RV6$}$
-------------------------------------------------------------------


               IMAGINARY PARTS OF BRANCH VOLTAGES
-------------------------------------------------------------------
    Omega    IV1       IV2       IV3       IV4       IV5       IV6
-------------------------------------------------------------------
${     $%3.1f$$Omega$Hz   $% -6.4f$$IV1$   $% -6.4f$$IV2$   $% -6.4f$$IV3$   $%
-6.4f$$IV4$  $% -6.4f$$IV5$  $% -6.4f$$IV6$}$
-------------------------------------------------------------------


                  REAL PARTS OF BRANCH CURRENTS
-------------------------------------------------------------------
    Omega    RI1       RI2       RI3       RI4       RI5       RI6
-------------------------------------------------------------------
${     $%3.1f$$Omega$Hz   $% -6.4f$$RI1$   $% -6.4f$$RI2$   $% -6.4f$$RI3$   $%
-6.4f$$RI4$  $% -6.4f$$RI5$  $% -6.4f$$RI6$}$
-------------------------------------------------------------------


               IMAGINARY PARTS OF BRANCH VOLTAGES
-------------------------------------------------------------------
    Omega    II1       II2       II3       II4       II5       II6
-------------------------------------------------------------------
${     $%3.1f$$Omega$Hz   $% -6.4f$$II1$   $% -6.4f$$II2$   $% -6.4f$$II3$   $%
-6.4f$$II4$  $% -6.4f$$II5$  $% -6.4f$$II6$}$
-------------------------------------------------------------------
```

```
MAGNITUDE OF THE REFLECTION COEFFICIENT
--------------------
    Omega   MS11
--------------------
${    $%5.3f$$Omega$Hz  $% -6.4f$$MS11$}$
--------------------

End
```

Please notice that it is not necessary to quit the OSA90 editor to generate the report. More details can be found about the report generation feature in the "New Features" chapter of the OSA90 manual.

The file "lab5.rpt" provides a template for the above report block. You can incorporate it into your circuit file using the mark and copy features of OSA90 (Manual Chapter 2 - "Block Operations").

Lab 2 Nonlinear Memoryless Circuits: DC and Time-Domain Simulation

Objectives

This lab is designed to familiarize you with DC and time-domain simulations of nonlinear memoryless circuits (i.e., containing no dynamic components such as capacitance or inductance) using the built-in simulators of OSA90. It is also intended to refresh your theoretical knowledge of frequency-domain representation of periodic signals (Fourier series).

Circuit Diagram and Parameter Values

A circuit with the diode bridge (full-wave rectifier) will be used throughout this lab. It is shown in Fig. L2.

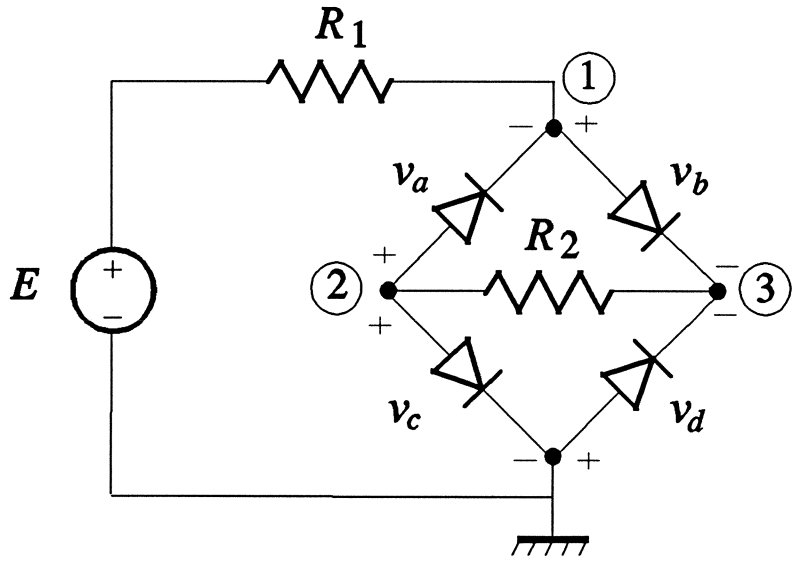

Fig. L2 A resistor-diode network.

The diodes are assumed memoryless, i.e., their capacitances are neglected. All diodes are identical and are fully described by the I-V characteristic given by the nonlinear equation

$$i_d = I_S[\exp(q v_d/(NkT)) - 1]$$

I_S, the saturation current, is such that the diodes are so called "10 mA" diodes: i_d is 10 mA for

v_d = 0.7 V (you will have to find the value of I_S). N, the emission coefficient, is 1, and T, the temperature, is 298°K. The parameters q and k in this equation are the electron charge and the Boltzmann constant, respectively. The expression kT/q is denoted by v_t and is called *thermal voltage*. Its value in this lab is constant and equals 25.67 mV. The aforementioned diode equation is implied when you define a diode within OSA90 using the keyword "DIODE". You can use the default values for all parameters except for I_S. Other parameters in the circuit are $R_1 = R_2 = 1$ kΩ, and various values for E.

Procedure

Preliminary Calculations

(1) Derive the expression to find the saturation current I_S for a "10 mA" diode.

The result is: I_S = _____A.

(2) Derive the expression to find the conductance of a linearized (companion) model of the diode at a given $v_d = V_D$. The result is: g_d = _____.

Create the OSA90 Input File

(1) Create the Model block. Describe the circuit elements and topology using "VSOURCE" (Manual Chapter 6 - "Circuit Models"), "RES" (Manual Chapter 8 - "Linear Elements"), and "DIODE" (Manual Chapter 7 - "Nonlinear Elements"). Define the nodal voltages v_1, v_2 and v_3 (with respect to ground) using Voltage Labels (Manual Chapter 6 - "Circuit Models"). Complete the circuit description using the CIRCUIT statement (Manual Chapter 6 - "Circuit Models"). Define all parameters either as constants or by labels.

(2) Create the Sweep block (Manual Chapter 9 - "Simulation"). Define the simulation type as "DC". Select E as the sweep parameter, initially with three values: 10 V, 1 V and -10 V. Define the responses to be simulated as the node voltages: v_1, v_2 and v_3.

(3) Show your input file to the instructor.

Simulation Experiment 1

(1) In the editor, you can click the left-hand mouse button to activate a pull-down menu. Parse the circuit file by selecting the option "Exit from editor" or by pressing the <F7> editor function key. Invoke the menu option "Display" by moving the cursor to highlight the option and click the left-hand mouse button or by pressing <D>. Select the "Xsweep" option by clicking the left-hand mouse button or by pressing <X>. Use the "Numerical" option to obtain the numerical output (Manual Chapter 9 - "Simulation"). Complete the following table.

TABLE I
VOLTAGE VALUES

E(V)	v_1(V)	v_2(V)	v_3(V)
10			
1			
—10			

(2) In the space below comment on the values of v_2 and v_3 at E = 10 V and E = —10 V.

(3) Show your results to the instructor.

Simulation Experiment 2

(1) Augment your input file to calculate the "output" voltage $V_{out} = v_3 - v_2$, and the conductance g_d of the linearized diode model for the diode denoted by the voltage v_b in Fig. L2. Resimulate the circuit and complete the following table.

TABLE II
OUTPUT VOLTAGE AND CONDUCTANCE

E(V)	V_{out}(V)	$g_d(1/\Omega)$
10		
1		
−10		

(2) In the space below comment on your result

(3) Show your results to the instructor.

Simulation Experiment 3

(1) Define a new sweep parameter t (time) and sweep it through 51 points (N = 50) in one period of the sinusoidal source voltage

$$E(t) = E_m \sin(2\pi f t)$$

where E_m = 10 V and f = 50 Hz. Define the source voltage as a function of the sweep parameter t using the foregoing expression. Set up your sweep definition to display V_{out} together with the source voltage $E(t)$. Note: Use repetitive DC simulations to obtain results. In the space below sketch the time domain waveforms generated by the program on the screen.

(3) Show your results to the instructor.

Harmonic Analysis of the Rectified Voltage

(1) Invoke "Numerical" display option for the results of time domain analysis performed in "Simulation Experiment 3". Select V_{out} for the output. Edit the numerical output by removing any text and the values of time points, leaving only the numerical values of V_{out}. Save the results in the file "waveform.inc".

(2) Create a new simple input file for OSA90 consisting of the Expression and Sweep blocks. Define an array with the time domain samples saved in the file "waveform.inc". Use the DFT_TF built-in transformation to generate the frequency domain spectrum of V_{out}. Use the RI2MP built-in transformation to generate the magnitude spectrum of V_{out}. Display the magnitude spectrum using the "OSA90.Display>Array" menu option. In the space below sketch the results generated by the program on the screen.

(3) Show your results to the instructor.

Lab 3 Performance-Driven Design of Nonlinear Circuits

Objectives

This lab is designed to familiarize you with performance-driven design of nonlinear circuits using the built-in optimizers and simulators of OSA90. It is also intended to show you how to formulate and optimize user-defined responses derived from the basic built-in responses of OSA90.

Circuit Diagram and Parameter Values

A simple, single-stage amplifier will be used throughout this lab. It is shown in Fig. L3.

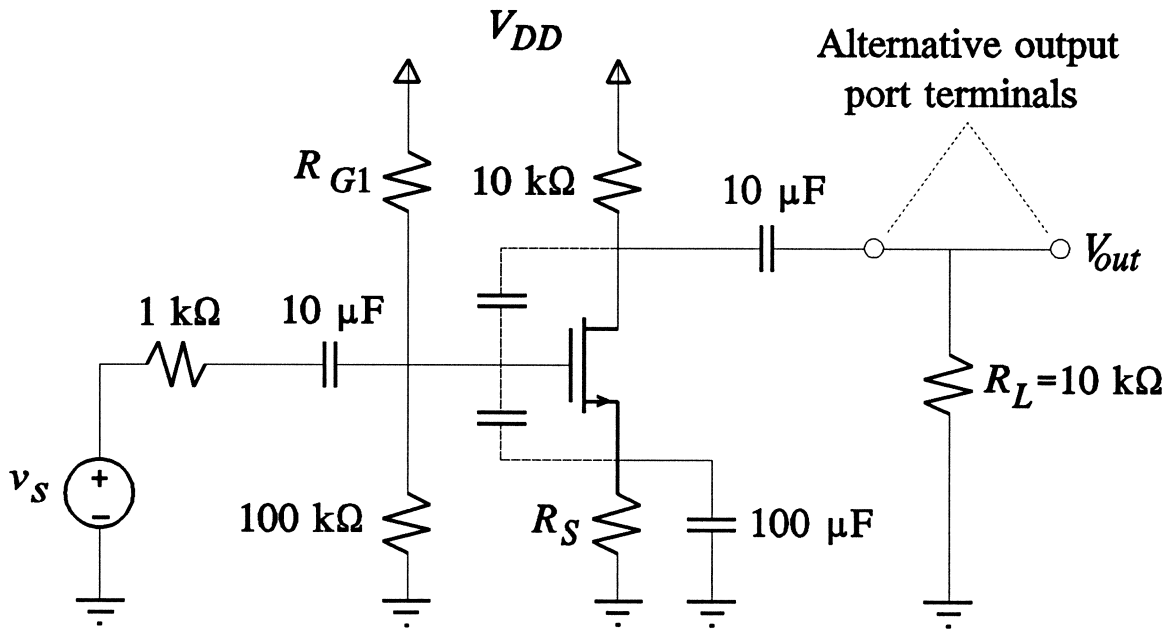

Fig. L3 A simple single-stage amplifier.

The amplifier is to be designed using a depletion type n-channel MOSFET with I_{DSS} = 4 mA and the pinch-off voltage V_P = —4 V. The parasitic capacitances of the FET are assumed as C_{gd} = 10 pF and C_{gs} = 0.1 μF. Other parasitic effects are neglected. The DC power supply is fixed at V_{DD} = 20 V. The resistances R_{G1}, R_S and the capacitance C_{gs} will be optimizable.

Procedure

Create the OSA90 Input File

(1) Define the Control block to use "Non_Microwave_Units".

(2) Create the Model block. Describe the circuit elements and topology using "RES", "CAP" and/or "PRC" (Manual Chapter 8 - "Linear Elements"), "FETM" (Manual Chapter 7 - "Nonlinear Elements"), "VSOURCE" (Manual Chapter 6 - "Circuit Models"), and "PORT" (Manual Chapter 6 - "Circuit Models"). Complete the circuit description using the CIRCUIT statement (Manual Chapter 6 - "Circuit Models"). The following hints should be helpful in setting up the circuit description.

   (a) Use two separate DC bias sources: one for the gate and the other for the drain. Define a label such as V_{DD} and apply it to both sources. This will have the same effect as defining one source only. The advantage is that you will be able to calculate and optimize the gate and drain currents.

   (b) Include the input source resistance in the "PORT" definition. Define the amplitude of the input voltage v_s through a label. This will allow you to sweep its value. The input source generates a sinusoidal voltage.

   (c) The load resistance R_L may or may not be included in the output "PORT" definition. For some experiments it might be advantageous to include R_L in the 2-port while for others it might be better to define it as the terminating impedance (see Fig. L3).

(3) Create the Sweep block (Manual Chapter 9 - "Simulation"). Initially define one sweep set with the simulation type of "DC". No sweep parameters will be needed, so only numerical output will be available. Define the currents I_G and I_D through the gate and drain DC bias sources as the responses to be simulated.

(4) Show your input file to the instructor.

Experiment 1: Design of the FET Biasing Circuit

(1) Assume the following values for the unknown resistances: R_{G1} = 100 kΩ and R_S = 1 kΩ, and perform DC simulation. Your results are

I_G = _____ μA and I_D = _____ mA

(2) Define R_{G1} and R_S as optimization variables. Create the Specification block (Manual Chapter 11 - "Optimization"). Define one specification set of "DC" simulation type with the gate and drain currents as the responses to be optimized. Optimize the biasing circuit to get $I_G < 17\mu A$ and I_D = 1 mA. Use the ℓ_1 optimizer. Your results are

R_{G1} = _____ kΩ and R_S = _____ kΩ

(3) Resimulate the circuit and save the input file. Now, your results are

I_G = _____ μA and I_D = _____ mA

(4) Define R_{G1} and R_S as the sweep parameters and specify the sweep range from 100 kΩ to 1000 kΩ with a step of 100 kΩ, and 1 kΩ to 10 kΩ with a step of 1 kΩ, respectively. Define I_G and I_D as the response labels. Use 3D visualization to display the simulated responses.

(5) Show your results to the instructor.

Experiment 2: Small-Signal Simulation of the Amplifier

(1) Augment your **Model** block of the input file to calculate the voltage gain $V_{gain} = V_{out}/V_s$ where V_{out} is the voltage across R_L. V_{gain} can be calculated from the S parameters in the following way. If you select the reference resistance for the calculation of S parameters as the input resistance $R_{ref} = R_{in}$ and if you include R_L in the 2-port (i.e., the amplifier - see Fig. L3) then the voltage gain can be expressed as

$$V_{gain} = S_{21} / (1 - S_{22})$$

Alternatively, if R_L is excluded from the 2-port then (again for $R_{ref} = R_{in}$)

$$V_{gain} = S_{21} / [(1 - S_{22}) + (1 + S_{22})R_{ref}/R_L]$$

You can implement either of the two formulas, but be careful how you define R_L. In any case, remember that the S parameters are complex numbers. Since only the magnitude of V_{gain} will be of interest, define V_{gain} as the absolute value of the corresponding expression.

(2) Define a new sweep set in the **Sweep** block. The simulation type should be "AC". Define the exponential frequency sweep from 10 Hz to 10 kHz, 3 points per decade (Manual Chapter 9 - "Simulation"). Define the exponential sweep steps with "NEXP". Define an appropriate "RREF" and specify V_{gain} as the response to be simulated.

(3) Produce a logarithmic scale for frequency by typing "LOG" for the "Zoom scale" option "N x-axis ticks" (Manual Chapter 9 - "Log-Scale Display"). Complete the following table.

TABLE I
RESULTS FOR EXPERIMENT 2

f(Hz)	10	100	1000	10000
V_{gain}(V)				

(3) Show your results to the instructor.

Experiment 3: Optimization of the Frequency Response

Your previous experiment indicates that the 3dB bandwidth does not extend to 10 kHz. It is known that the parasitic capacitances of the FET are responsible for the high-frequency drop of the response. The question to answer through this experiment is: What is the largest allowable value of the parasitic capacitance C_{gs} for the 3 dB bandwidth to be extended to 10 kHz?

(1) Designate C_{gs} as the optimization variable. Modify the Specification block by commenting out the existing "DC" specification set and creating a new "AC" specification set. Define only one specification at 10 kHz in the form "Vgain > ...". In determining the value for this specification, assume that the frequency response in the pass band does not change much when C_{gs} is varied. Do not forget to specify "RREF".

(2) Optimize the circuit using the ℓ_2 optimizer. Your result is

C_{gs} < _____ nF

(3) Resimulate the circuit and save the input file. Now, the frequency response is tabulated as follows.

TABLE II
RESULTS FOR EXPERIMENT 3

f(Hz)	10	100	1000	10000
V_{gain}(V)				

(4) Show your results to the instructor.

Experiment 4: Large-Signal Simulation of the Amplifier

(1) Define a new sweep set in the Sweep block. The simulation type should be "HB". Define the amplitude of the input source voltage as the sweep parameter and specify the sweep range from 0.2 V to 2 V with a step of 0.3 V. Set the frequency of the input source to 1 kHz. The output port must now include R_L, so it should be excluded from the 2-port. Define MVout and PVout as the response labels. Define a graphical view to display simultaneously two periods of the output voltage waveforms corresponding to all values of v_s.

(2) Simulate the circuit and, in the space below, sketch the output voltage waveforms.

(3) *Optional:* Define the output power spectrum in an array POUT[0:N_Spectra] (N_Spectra is a built-in label, which in our case defaults to 4). Create an expression for the harmonic distortion h which is defined as the square root of the ratio of the power at all higher harmonics (P2 + P3 + ...) to the power at the fundamental frequency (P1). Include Pout and h in the sweep set.

(4) *Optional:* Complete the following table.

TABLE III
RESULTS FOR EXPERIMENT 4

v_s(V)	MVout[1](V)	Pout[1](mW)	h(%)
0.2			
0.8			
1.4			
2.0			

(5) Show your results to the instructor.

Lab 4 Device Modeling from Experimental Data

Objectives

This lab is designed to familiarize you with device modeling using the built-in optimizers and simulators of OSA90. At the completion of this lab you should be able to better understand the concepts of different models: small-signal, large-signal, linear, bias-dependent and nonlinear, and to apply optimization for extracting model parameters from measurement data.

Measurement Setup and Device Data

A microwave Schottky barrier FET (MESFET) has been measured in the setup shown in Fig. L4a.

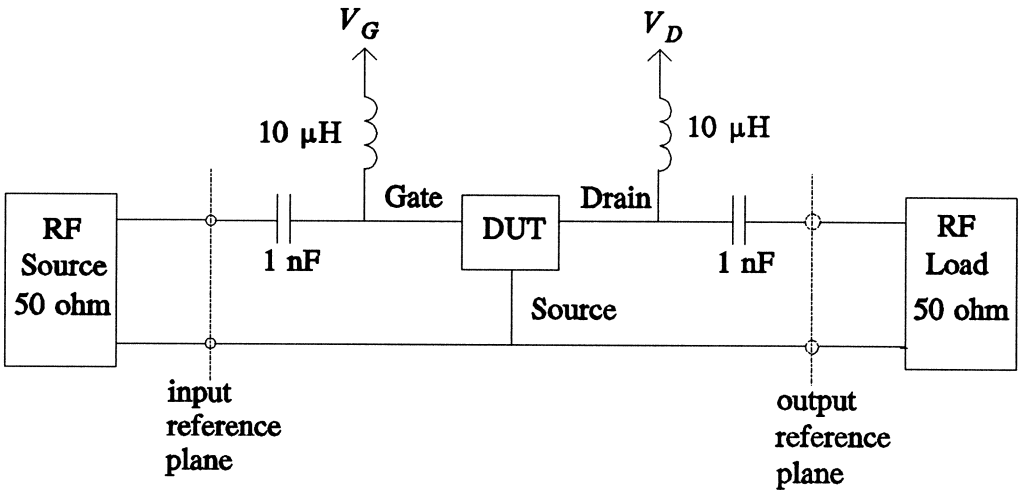

Fig. L4a MESFET measurement setup.

Measurements of S parameters with respect to 50 Ω were taken at the input and output reference planes for 17 frequencies in the range from 2 GHz to 18 GHz and for three values of the gate bias voltage V_G: 0, —1.74 and —3.1 volts. The drain bias voltage V_D was fixed at 4 V. The blocking capacitors of 1 nF and inductors of 10 μH were used to decouple the DC biasing circuit from the RF (or AC) circuit. The resulting S parameters are contained in an ASCII file generated by the

MicroCAT™ Test Executive system from Cascade Microtech. The file name is "cascade.dat" (see Appendix A).

Throughout this lab you will investigate two models for the FET. The first one is a simple small-signal model which may be suitable for simulating the FET around a specific operating point, determined and established separately. This model is shown in Fig. L4b. It consists of a voltage-controlled current source and four lumped, linear components. If the biasing of the FET is dropped out of the picture the resulting circuit is linear. The second model, shown in Fig. L4c, is a global, large-signal, nonlinear model which accounts for all nonlinearities, including biasing. In this lab you will use the Materka and Kacprzak built-in intrinsic nonlinear model (FETM) together with a built-in super-component "Extrinsic2", which consists of a number of linear elements connected internally in a predefined manner (Manual Chapters 7 and 8 - "Nonlinear Elements" and "Linear Elements").

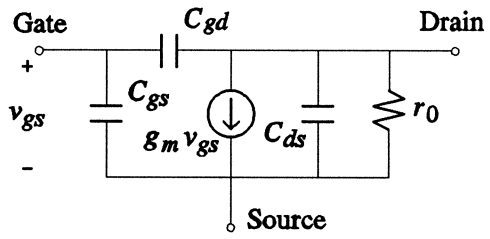

Fig. L4b A simple, small-signal FET model.

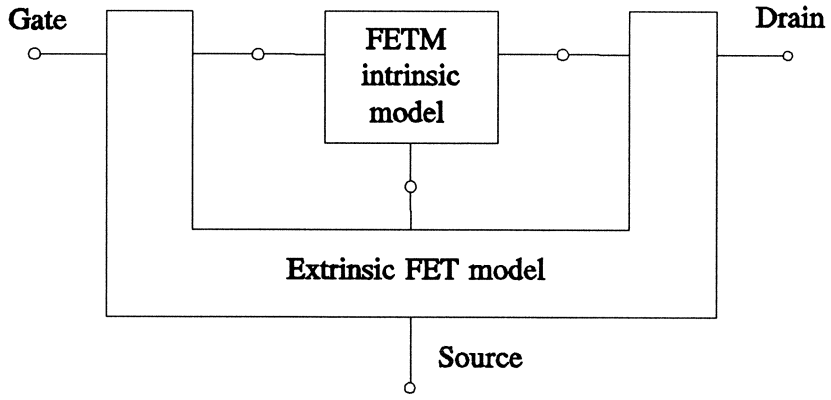

Fig. L4c Schematic diagram of a large-signal FET model.

Procedure

Experiment 1: Small-Signal FET Modeling

(1) Create the OSA90 Input File. It is recommended that you use default microwave units. Define the Model block. Describe the circuit of Fig. L4a with the model of Fig. L4b put in place of the device under test (DUT). Use "CAP" and "VCCS". You do not need to include the bias sources in this experiment, and you may exclude the blocking capacitors and inductors (if so, the overall circuit will simply reduce to that of Fig. L4b). Define the ports using "PORT" statements. Assume the following values for the model parameters.

$$C_{gs} = C_{gd} = C_{ds} = 1 \text{ pF}, \; g_m = 10 \text{ mA/V}, \; r_0 = 50 \; \Omega$$

All these parameters are to be optimizable. Be careful when you define the "VCCS". The orientation of the source in Fig. L4b is opposite to that in the Manual. Include r_0 in the definition of "VCCS". After completing the circuit description with the "CIRCUIT" statement, define the array "SP_SIM[8]" of simulated S parameters in the following order: Re(S_{11}), Im(S_{11}), Re(S_{21}), Im(S_{21}), Re(S_{12}), Im(S_{12}), Re(S_{22}), Im(S_{22}), which is the order of the data in each row in the file "cascade.dat".

(2) Define the array "SP_DATA[8]" and initialize it with the S parameters for $V_G = -1.74$ V at 2 GHz (copy the corresponding row, without the first number, from the data). Define the error functions in the array "SP_ERROR[8]" as the difference between the arrays "SP_SIM" and "SP_DATA". Close the Model block with the "End" statement.

(3) Define the Sweep block with one sweep set of the "AC" type to simulate the circuit at a single frequency of 2 GHz (only numerical output will be available). The responses of interest are "SP_SIM" and "SP_ERROR". Define the Specification block with one specification set of the "AC" type. Define a single specification of 0 for the whole array "SP_ERROR" at 2 GHz. Save your file.

(4) Perform simulation and then invoke the ℓ_1 optimizer. After optimization is completed, perform circuit simulation again, go to the file editor and save the back-annotated file under

a different name. Complete Table I.

TABLE I
S PARAMETERS

	S_{11}	S_{21}	S_{12}	S_{22}
Measurement Data				
Model Before Optimization				
Model After Optimization				

The extracted parameters of the model are

C_{gs} = _____pF, C_{gd} = _____pF, C_{ds} = _____pF, g_m = _____mA/V, r_0 = _____Ω.

(5) Show your results to the instructor.

Experiment 2: Checking the Validity of the Small-Signal FET Model

In this experiment you will investigate whether the model established in Experiment 1 is suitable for simulating device behaviour at a different operating point or in the whole frequency range.

(1) In the file saved after optimization performed in Experiment 1 replace the contents of the array "SP_DATA" with the S parameters for $V_G = -3.1$ V at 2 GHz (copy another row, without the first number, from the data). Repeat Step 4 of Experiment 1 without saving the resulting file. In the space below comment on the suitability of the model at different bias points.

(2) Retrieve the file saved after optimization performed in Experiment 1. Redefine your "SP_DATA" array to make it a two-dimensional array "SP_DATA[17,8]" and initialize it with the whole subset of the measurement data corresponding to $V_G = -1.74$ V. Do not forget to remove the first column of the data (frequencies). Define the new array "FREQs[17]" and initialize it with the frequencies at which the data was taken. If you use default microwave units enter the values in GHz but do not specify units (i.e., 2.0, 3.0, etc.). Now, the measurement data must be selected from the matrix "SP_DATA". You can do it by defining a frequency index "L", which will be swept, and selecting one row of the data for each specific value of "L" using the matrix function "ROW" (Manual Chapter 4 - "Array Function") to create a new array "SELECT_SP_DATA[8]". You will also need to redefine "SP_ERROR". Finally, extend the sweep and specification sets from a single frequency to all points by sweeping "L" from 1 to 17 and setting "FREQ" to the corresponding element of the array "FREQs". Repeat

Step 4 of Experiment 1. Save the files before and after optimization. In the space below comment on how the model fits the measurement data at 2 GHz and at all frequencies before and after optimization.

(3) Show your results to the instructor.

Experiment 3: Large-Signal FET Modeling

The preceding experiments indicate that a small-signal linear model is not capable of covering a large range of operating conditions, even for small-signal simulations. A linear model should at least have the parameter values that are bias-dependent (bias-dependent model). While such a model could be suitable for small-signal simulations under different bias conditions, only a true nonlinear model can be used as a global model. In this experiment you will use optimization to extract parameters of the Materka and Kacprzak model to fit simultaneously all measurement data.

(1) Retrieve either of the files used in Experiment 2, Step 2. Go to the secondary window of the editor by using the "Toggle file" command. Read in the file "lab4model.inc" (see Appendix B). Mark the whole contents of the file and copy it to the primary file. This is the model shown in Fig. L4c to be put in place of DUT in Fig. L4a and should replace the description of the small-signal model used in the preceding experiments. You may have to adjust the node numbers. You also need to include the blocking capacitors and inductors of Fig. L4a, and, using "VSOURCE", to define DC bias sources. When defining V_G, introduce a new array "VGS[3]" and a new bias index "K", which will be swept, and select the value of V_G using "VDC=VGS[K]". Adjust the number of rows of the matrix "SP_DATA" to accommodate all 51

lines of data from the file "cascade.dat". It is recommended that you edit that file (do not forget to delete the first column), save it under a different name such as "sp_data.inc" and use the "#include" directive in the input file. Now, to select the row of the data which corresponds to the Kth bias point and the Lth frequency you need the selector index "KL = (K - 1) * 17 + L". Finally, you need to define a double sweep in the Sweep and Specification blocks. Make "K" as the outer (first) sweep label and "L" as the inner (second) sweep label. Save your file and show it to the instructor.

(2) Perform simulation and view the error functions. Invoke the ℓ_1 optimizer. After optimization is completed, perform circuit simulation again, go to the file editor and save the back-annotated file under a different name. Again, view the error functions. Complete Table II with approximate values (orders of magnitude).

TABLE II
S-PARAMETER MATCHING ERRORS

	Average Error	Maximum Error
Model Before Optimization		
Model After Optimization		

(3) *Optional:* Define the parameter "NAME" for the drain bias source. Define the array "Ids_DATA[3]" and initialize it with the measured values of the current I_{ds} contained in the file "cascade.dat". Define the array "ID_ERROR" as the difference between the Kth element of "Ids_DATA" and the simulated DC current through the V_D source, multiplied by 50, the weighting factor for optimization. Include "ID_ERROR" in the Sweep and Specification blocks. Repeat Step 2 and comment on the result.

(4) *Optional:* Define a graphical view to display the fit of S_{21} for all frequencies and all bias conditions. Use continuous curves for displaying the simulated responses and "circles" to display measured data. You can define either a rectangular plot or polar plot. Sketch your results in the space below.

You can also generate an HPGL file for producing a hardcopy of the plot.

(5) Show your results to the instructor.

Appendix A for Lab 4

Data File "cascade.dat"

```
NOTE  FET S-parameter measurement for test with HarPE
NOTE  simulating the format by CASCADE MICROTECH
DATE  Nov 22, 1989
NOTE  the first bias
BIAS Vgs=0.0
BIAS Vds=4.0
BIAS Ids=0.177
S2RITABLE 17
 2.00E9     0.5952    -0.7405     -3.351      2.731    0.01574    0.02555     0.5699    -0.2847
 3.00E9     0.2782    -0.8682     -2.258      3.095    0.02697    0.02913      0.507    -0.3408
 4.00E9   0.003826    -0.8774     -1.332      3.088    0.03631    0.02841      0.448    -0.3896
 5.00E9    -0.2089    -0.8241    -0.6258      2.884    0.04307    0.02552     0.3927    -0.4319
 6.00E9     -0.367    -0.7442    -0.1137      2.599    0.04756    0.02184     0.3398    -0.4698
 7.00E9    -0.4831    -0.6561     0.2496      2.296    0.05027     0.0181     0.2879    -0.5043
 8.00E9    -0.5686    -0.5686     0.5039      2.002    0.05169    0.01465     0.2358    -0.5355
 9.00E9    -0.6318    -0.4851     0.6789      1.729    0.05217    0.01162     0.1829    -0.5634
10.00E9    -0.6788    -0.4068     0.7962      1.481    0.05197   0.009091      0.129    -0.5876
11.00E9    -0.7138    -0.3338     0.8709      1.258    0.05129   0.007052    0.07406    -0.6079
12.00E9    -0.7396    -0.2658      0.914       1.06     0.0503   0.005494    0.01827     -0.624
13.00E9    -0.7584    -0.2023     0.9333     0.8828     0.0491   0.004388   -0.03809    -0.6358
14.00E9    -0.7716    -0.1428     0.9347     0.7262    0.04779   0.003704   -0.09467    -0.6432
15.00E9    -0.7804   -0.08692     0.9226     0.5878    0.04644   0.003405    -0.1511    -0.6462
16.00E9    -0.7854   -0.03419     0.9002     0.4659    0.04512   0.003455     -0.207    -0.6448
17.00E9    -0.7874    0.01571     0.8703     0.3588    0.04386   0.003816    -0.2621    -0.6391
18.00E9    -0.7868    0.06306     0.8349     0.2652    0.04271    0.00445    -0.3159    -0.6294
ENDTABLE
NOTE  the second bias
BIAS Vgs=-1.74
BIAS Vds=4.0
BIAS Ids=0.08896
S2RITABLE 17
 2.00E9     0.7854    -0.5682     -2.667      1.616    0.01656     0.0352     0.5055    -0.2722
 3.00E9      0.577    -0.7439     -2.102      2.017    0.03109    0.04451     0.4452    -0.3342
 4.00E9     0.3559    -0.8389     -1.518      2.222    0.04608     0.0479     0.3823    -0.3876
 5.00E9     0.1491    -0.8697    -0.9818      2.265    0.05947    0.04668     0.3197    -0.4302
 6.00E9   -0.03086    -0.8564    -0.5255      2.195    0.07038    0.04242     0.2593    -0.4636
 7.00E9    -0.1815    -0.8155    -0.1548      2.058    0.07865    0.03644     0.2018    -0.4903
 8.00E9     -0.305    -0.7591     0.1372      1.885     0.0845    0.02968     0.1469    -0.5119
 9.00E9    -0.4053    -0.6947     0.3619      1.697    0.08829    0.02276    0.09385    -0.5294
10.00E9    -0.4864     -0.627     0.5311      1.507    0.09038    0.01605    0.04223    -0.5436
11.00E9    -0.5519    -0.5587     0.6554      1.322    0.09111   0.009802  -0.008427    -0.5546
12.00E9    -0.6049    -0.4915     0.7435      1.147    0.09076   0.004127   -0.05839    -0.5626
13.00E9    -0.6476    -0.4261     0.8028     0.9831    0.08957 -0.0009067    -0.1078    -0.5675
14.00E9    -0.6819    -0.3629     0.8389     0.8321    0.08775  -0.005273    -0.1567    -0.5695
15.00E9    -0.7093     -0.302     0.8566     0.6939    0.08546  -0.008975     -0.205    -0.5684
16.00E9    -0.7309    -0.2435     0.8596     0.5685    0.08284   -0.01203    -0.2527    -0.5643
17.00E9    -0.7476    -0.1873     0.8509     0.4553       0.08   -0.01447    -0.2995    -0.5571
18.00E9    -0.7601    -0.1332     0.8332     0.3539    0.07705   -0.01632    -0.3453    -0.5469
ENDTABLE
```

```
NOTE  the third bias point
BIAS Vgs=-3.1
BIAS Vds=4.0
BIAS Ids=0.0408
S2RITABLE 17
 2.00E9      0.835    -0.5042      -1.85      1.044    0.01928    0.04435     0.4908     -0.269
 3.00E9     0.6659    -0.6806     -1.509      1.335    0.03699    0.05763     0.4335     -0.333
 4.00E9     0.4752    -0.7942     -1.136      1.514    0.05638    0.06387     0.3715    -0.3904
 5.00E9     0.2856    -0.8521    -0.7732      1.587    0.07485    0.06398     0.3074    -0.4368
 6.00E9     0.1106    -0.8665    -0.4468      1.577    0.09087    0.05948     0.2439     -0.473
 7.00E9   -0.04368    -0.8502    -0.1682      1.511     0.1038    0.05193     0.1825    -0.5008
 8.00E9    -0.1762    -0.8135    0.06073      1.408     0.1136    0.04263     0.1235    -0.5221
 9.00E9    -0.2881    -0.7641     0.2435      1.285     0.1204    0.03251     0.0668    -0.5382
10.00E9     -0.382    -0.7073     0.3858      1.154     0.1247    0.02227    0.01213    -0.5501
11.00E9    -0.4604    -0.6467     0.4936       1.02     0.1268    0.01233   -0.04087    -0.5583
12.00E9    -0.5257    -0.5845     0.5727     0.8895     0.1272   0.002983   -0.09248    -0.5632
13.00E9    -0.5801     -0.522     0.6279      0.765     0.1261  -0.005595    -0.1429    -0.5649
14.00E9    -0.6251    -0.4603     0.6637      0.648     0.1239   -0.01331    -0.1922    -0.5636
15.00E9    -0.6624    -0.3997     0.6837     0.5396     0.1208   -0.02011    -0.2404    -0.5593
16.00E9     -0.693    -0.3405     0.6908     0.4402     0.1171     -0.026    -0.2875    -0.5521
17.00E9    -0.7179    -0.2829     0.6875     0.3497     0.1128   -0.03098    -0.3334    -0.5421
18.00E9    -0.7379     -0.227     0.6761     0.2681     0.1082   -0.03509     -0.378    -0.5294
ENDTABLE
```

Appendix B for Lab 4

Include File "lab4model.inc"

```
Extrinsic2  1 2 3 4 5
   RG: 0.0119   RD: 0.0006   RS: 0.33   CX: 1.5PF
   LG: ?0.1NH?
   LD: ?0.1NH?
   GDS: ?0.004?
   LS: ?0.1NH?
   CDS: ?0.1PF?;

FETM  1 2 3
   GAMMA: -0.1   KE: 0          SL: 0.2
   KG: -0.25     SS: 0          E: 2
   C10: 0.67PF   CF0: 0.023PF   KF: -0.12
   IG0: 5E-10    ALPHAG: 20     IB0: 8e-12
   ALPHAB: 1     VBC: 20        R10: 5.2
   KR: 0         K1: 1          C1S: 0.0048PF
   IDSS: ?0.2?
   VP0: ?-4?
   TAU: ?3PS?;
```

Lab 5 Statistical Design Centering

Objectives

This lab is intended to familiarize you with characterization of statistical variations of circuit parameters, Monte Carlo analysis and yield-driven design of nonlinear circuits using OSA90.

Procedure

Experiment 1: Monte Carlo Analysis of a Simple Voltage Divider

(1) Create the OSA90 input file for a simple voltage divider consisting of two resistors $R_1 = R_2 = 50\ \Omega$ connected in series. The input DC voltage source of 1 V is applied to both resistors and the output voltage is taken across R_2. Create the Model block using "VSOURCE", "RES", "VLABEL" and "CIRCUIT" statements. Define statistical variation of R_1 and R_2 using "UNIFORM" distribution (Manual Chapter 12 - "Uniform Distribution") within ±5% interval with respect to the nominal values ("TOL=5%"). Create the MonteCarlo block (Manual Chapter 12 - "MonteCarlo Block") with one sweep set of the DC type. Specify "N_outcomes = 100" and the output voltage as the response label.

(2) Invoke the OSA90.MonteCarlo menu option. After Monte Carlo analysis is finished view the Run Chart of the simulated output voltage. Select the numerical "Output form" in the Run Chart pop-up window. Create an array "OUTPUT[100]" to accommodate all outcomes of the MonteCarlo analysis.

Determine the minimum and maximum output voltages using "AMIN" and "AMAX" array function (Manual Chapter 4 - "Array Functions"). The spread of the output voltage is

min V_{out} = _____V, max V_{out} = _____V and variation of V_{out} = ± _____%

(3) Show your results to the instructor.

Experiment 2: Statistical Design Centering of a Small-Signal Amplifier (Fig. L5)

(1) Retrieve the input file generated during Experiment 3 of Lab 3 "Performance-Driven Design of Nonlinear Circuits". Assume that the nominal value of C_{gs} is 10 nF, which satisfies the specification V_{gain} > 3.5. Define statistical variations of "NORMAL" distribution (Manual Chapter 12 - "Normal Distribution") with the standard deviation of 5% ("SIGMA=5%") for all four resistors R_{G1}, R_{G2}, R_D and R_S, and for the capacitor C_{gs}. You should have 5 statistical variables altogether.

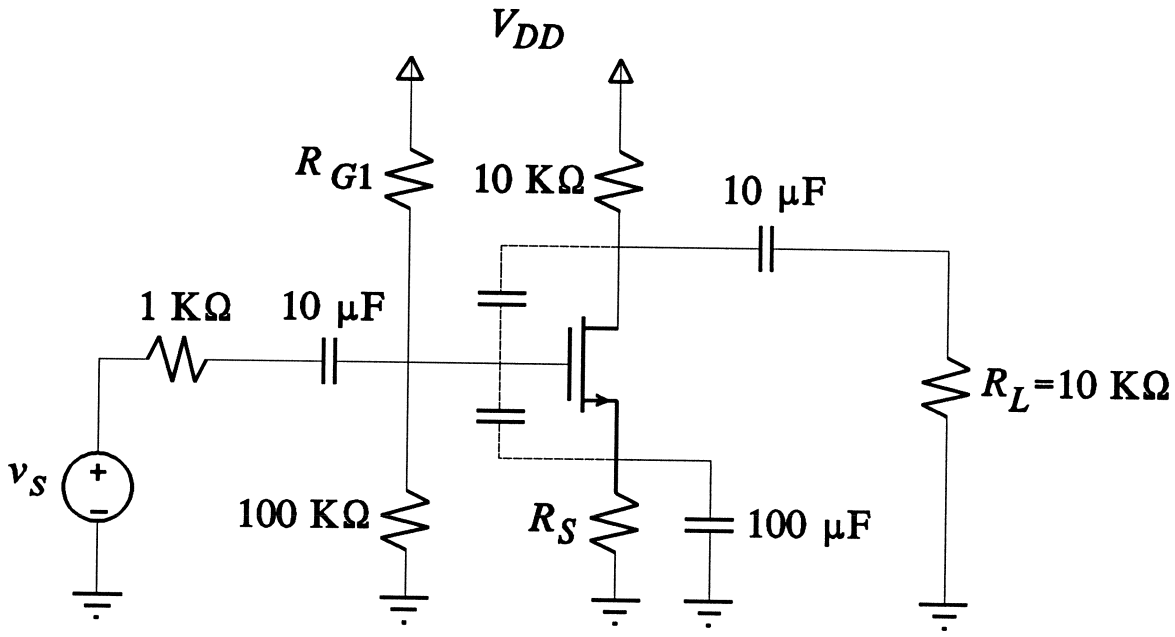

Fig. L5 A simple single-stage amplifier.

(2) Create the MonteCarlo block with one sweep set of the AC type by copying the existing sweep set from the Sweep block. Leave V_{gain} as the only response label. Use "N_outcomes = 100". Define design specifications V_{gain} > 3.5 and V_{gain} < 5 for yield estimation.

(3) Perform Monte Carlo analysis and invoke the OSA90.MonteCarlo.Xsweep menu option to simultaneously view all the responses corresponding to the 100 circuit outcomes generated according to the statistical distribution (statistical response). In the space below sketch the statistical response together with design specifications.

Initial yield = _____%

(4) Show your results to the instructor.

(5) Define the nominal values of R_{G1} and R_S as optimization variables. Modify the Specification block to define design specifications consistently with the MonteCarlo block (V_{gain} > 3.5 and V_{gain} < 5 for all 10 frequencies swept exponentially from 10 Hz to 10 kHz).

(6) Invoke the OSA90.Optimize menu option. Select "yield" as the optimizer. Once "yield" is selected, the pop-up window allows you to choose the number of outcomes to be involved in yield optimization. Select 50 outcomes. Accept defaults for all other options. Perform yield optimization. Then go back to the file editor and change the number of outcomes for Monte Carlo analysis to 300. Perform Monte Carlo analysis and view the statistical response. In the space below sketch the statistical response after yield optimization and report final yield and the values of optimization variables.

Yield after optimization = _____%

The values of the optimization variables after yield optimization are

R_{G1} = _____kΩ and R_S = _____kΩ

(7) Show your results to the instructor.

Lab 6 Simulation and Optimization Using Datapipe

Objectives

This lab is designed to familiarize students with simulation and optimization using the Datapipe.

Circuit Diagram and Parameter Values

Consider the LC transformer circuit shown in Fig. L6. Use OSA90 to carry out minimax optimization on the magnitude of the input reflection coefficient using all reactive components as optimization variables. Use 21 uniformly spaced points in the frequency range 0.5 - 1.179 (rad/s).

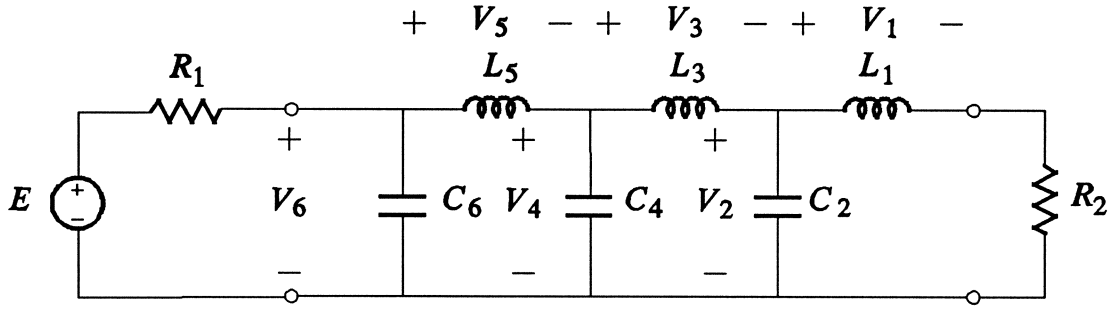

Fig. L6 A lumped element LC transformer.

The suggested starting point is

$$L_1 = C_2 = L_3 = C_4 = L_5 = C_6 = 1.$$

E = 3 V, R_1 = 3 Ω and R_2 =1 Ω. The solution, rounded to 3 decimal places, is

$$L_1 = 1.041$$

$$L_3 = 2.341$$

$$L_5 = 2.937$$

$$C_2 = 0.979$$

$$C_4 = 0.780$$

$$C_6 = 0.347$$

Procedure

Part I: Optimization Using the OSA90 Built-in Simulator

(1) Create the circuit file.

(a) Create a Model block to describe the circuit. Define the elements R_2, L_1, L_3, L_5, C_2, C_4 and C_6. Specify the parameters of L_1, L_3, L_5, C_2, C_4 and C_6 as optimization variables (Manual Chapter 6 - "Elements" and Chapter 4 - "Optimization Variables"). For example,

```
L1: ?1?;
IND n1 n2 L = L1;
```

or,

```
IND n1 n2 L = ?1?;
```

(b) Define the input port including both the voltage E and the resistance R_1 (Manual Chapter 6 - "Ports"):

```
PORT node1 node2 NAME=portname V=E R=R1;
```

(c) Complete the circuit description using the CIRCUIT statement (Manual Chapter 6 - "The Circuit Statement").

(d) Assign the initial value (0.5) to the label "Omega".

(e) Terminate the Model block with the "End" keyword.

(f) Define the Sweep block (Manual Chapter 9 - "Sweep Block"). This will enable OSA90 to display to magnitude of the reflection coefficient MS11 over the specified range of frequency, graphically or numerically (Manual Chapter 6 - "Small-Signal Responses" and Chapter 9 - "OSA90.Display Menu Option"):

```
Sweep
   AC: Omega: from 0.5 to 1.179 n=20, FREQ=(Omega/(2*PI)), RREF=3, MS11;
End
```

(g) Define the Specification block (Manual Chapter 10 - "Specification Block"). The goal for optimization is to minimize the magnitude of the reflection coefficient MS11 over the specified range of frequency.

```
Specification
   AC: Omega: from 0.5 to 1.179 n=20, FREQ=(Omega/(2*PI)), RREF=3,
       MS11=0;
End
```

(2) Save the circuit file you have created: press <F8>, enter the file name, and press <ENTER>.

(3) Perform minimax optimization.

(a) Exit the editor and parse the circuit file: press <F7>.

(b) Press <O> to choose the "Optimization" option.

(c) From the pop-up window, toggle to the "Optimizer" option and choose "Minimax". Change the "Number of iterations" option to "999".

(d) Press <ENTER> twice to start the optimization process.

(4) After the optimization is completed, press <F> to return to the circuit file. The optimizable parameters should have been updated with the minimax solution.

(5) Save the optimized circuit file for later comparison: press <F8>, enter a new file name and press <ENTER>.

DO NOT FORGET TO SAVE YOUR CURRENT FILE BEFORE THE NEXT STEP.

Part II: Simulation and Optimization via Datapipe

(1) Examine the C program listed in Appendix A. This simple C program is written for the simulation of the LC transformer. It also includes the Datapipe interface as outlined in the User's Manual Chapter 5. The disk file containing the C code is "lab6.c".

(2) Exit from OSA90. Compile the C program by the following command at the system prompt.

```
cc -o lab6 lab6.c -lm
```

"lab6" is the Datapipe child program (executable program). In the OSA90 input file you specify the Datapipe definition as illustrated in Appendix B.

(3) Perform minimax optimization within OSA90.

(a) Invoke OSA90 again at the system prompt by entering "osa90".

(b) Read in the circuit file you have prepared for Datapipe ("lab6.ckt").

(c) Exit the editor and parse the circuit file (press <F7>).

(d) Press <O> to choose the "Optimization" option.

(e) From the pop-up window, toggle to the "Optimizer" option and choose "Minimax". Change the "Number of iterations" option to "999".

(f) Press <ENTER> twice to start the optimization process.

(4) After the optimization is completed, press <F> to return to the circuit file. The optimizable parameters should have been updated with the minimax solution.

(5) Save the optimized circuit file: press <F8>, enter a new file name and press <ENTER>.

Complete the Following Tables

After you finish both Part I and Part II, please place the minimax solutions on the lines, designated as "Case A" in Tables I and II. Then try two additional cases, as indicated below, for minimax optimization and fill in the Tables with the corresponding results.

(1) Case B:

Starting point: solution to Case A.

Range of frequency: 11 uniformly spaced points in the range 0.5 - 1.0.

(2) Case C:

Starting point: original starting point.

Range of frequency: 11 uniformly spaced points in the range 0.5 - 1.0.

Use an upper specification of 0.04.

TABLE I MINIMAX SOLUTION FOR PART I

	L_1	L_3	L_5	C_2	C_4	C_6	max $\lvert\rho\rvert$
Case A							
Case B							
Case C							

"max $\lvert\rho\rvert$" is the maximum of the magnitudes of the reflection coefficients at the specified frequency points.

TABLE II MINIMAX SOLUTION FOR PART II

	L_1	L_3	L_5	C_2	C_4	C_6	max $\lvert\rho\rvert$
Case A							
Case B							
Case C							

"max $\lvert\rho\rvert$" is the maximum of the magnitudes of the reflection coefficients at the specified frequency points.

While filling in the tables you can find the Report Generation feature of OSA90 helpful. See Appendix C for details.

Appendix A for Lab 6: LC Transformer Simulator in C

```
#include <stdio.h>
#include <math.h>

   typedef struct { float real; float imag; }   COMPLEX;

   int trnsfmr ();
   COMPLEX ComplexAdd (),
           ComplexSub (),
           ComplexMul (),
           ComplexDiv ();
   float ComplexAbs ();

int trnsfmr ( Par, Omega, ReflectionCoef )
float Par[6], Omega, *ReflectionCoef;
{
   /* this subroutine calculates the lc transformer response at one
      frequency given by Omega.  The values of L1, C2, L3, C4, L5 and
      C6 are supplied in the array Par.  The response is the
      magnitude of the input reflection coefficient.
   */

   /* local variables */

   COMPLEX jOmegaPar[6], I0[6], V0[6], Iin, Vin, Iout, Vout,
           Is0, Rin, Zin;
   int i;

   for (i = 0; i < 6; i++) {
      jOmegaPar[i].real = 0.0;
      jOmegaPar[i].imag = Omega * Par[i];
   }

   Iout.real = Vout.real = 1.0;
   Iout.imag = Vout.imag = 0.0;

   I0[0] = Iout;
   V0[0] = ComplexMul(I0[0], jOmegaPar[0]);
   V0[1] = ComplexAdd(V0[0], Vout);
   I0[1] = ComplexMul(V0[1], jOmegaPar[1]);
   I0[2] = ComplexAdd(I0[1], I0[0]);
   V0[2] = ComplexMul(I0[2], jOmegaPar[2]);
   V0[3] = ComplexAdd(V0[2], V0[1]);
   I0[3] = ComplexMul(V0[3], jOmegaPar[3]);
   I0[4] = ComplexAdd(I0[3], I0[2]);
   V0[4] = ComplexMul(I0[4], jOmegaPar[4]);
   V0[5] = ComplexAdd(V0[4], V0[3]);
   I0[5] = ComplexMul(V0[5], jOmegaPar[5]);

   Iin = ComplexAdd(I0[5], I0[4]);
   Vin = V0[5];
```

```
   Rin.real = 3.0;
   Rin.imag = 0.0;

   Zin = ComplexDiv(Vin, Iin);
   *ReflectionCoef = ComplexAbs(ComplexDiv(ComplexSub(Zin, Rin),
                                           ComplexAdd(Zin, Rin)));

   return(0);
}

COMPLEX ComplexAdd ( a, b )
COMPLEX a, b;
{
   COMPLEX c;

   c.real = a.real + b.real;
   c.imag = a.imag + b.imag;

   return(c);
}

COMPLEX ComplexSub ( a, b )
COMPLEX a, b;
{
   COMPLEX c;

   c.real = a.real - b.real;
   c.imag = a.imag - b.imag;

   return(c);
}

COMPLEX ComplexMul ( a, b )
COMPLEX a, b;
{
   COMPLEX c;

   c.real = a.real * b.real - a.imag * b.imag;
   c.imag = a.imag * b.real + a.real * b.imag;

   return(c);
}

COMPLEX ComplexDiv ( a, b )
COMPLEX a, b;
{
   COMPLEX c, d;
   float det;

   det = b.real * b.real + b.imag * b.imag;

   d.real = b.real / det;
   d.imag = -b.imag / det;
```

```
   c = ComplexMul(a, d);

   return(c);
}

float ComplexAbs ( a )
COMPLEX a;
{
   float det;

   det = sqrt(a.real * a.real + a.imag * a.imag);

   return(det);
}
```

Appendix B for Lab 6: Templates for the Datapipe Connection

This template assumes that your C program calculates the reflection coefficient at a single frequency point. The frequency range is defined in the OSA90 circuit file and the child program is invoked repeatedly within the frequency loop. The advantage of this approach is that it allows you to define an arbitrary frequency range.

Circuit File Template

```
Expression
   L1 = ? 1 ?;
   C2 = ? 1 ?;
   L3 = ? 1 ?;
   C4 = ? 1 ?;
   L5 = ? 1 ?;
   C6 = ? 1 ?;

   Omega: 0.5;

   Datapipe: SIM FILE = "lab3_sim"
             N_INPUT = 7    INPUT = (L1, C2, L3, C4, L5, C6, Omega)
             N_OUTPUT = 1   OUTPUT = (Rout);
End

Sweep
   Omega: From 0.5 to 1.179 N=20 Rout;
End

Specification
   Omega: From 0.5 to 1.179 N=20 Rout=0;
End
```

Appendix C for Lab 6: Report Generation

The Report Generation feature of OSA90 facilitates postprocessing of OSA90 results. It allows the user to embed numerical outputs within an arbitrary text document.

In our case we can customize the OSA90 output so that it resembles Tables I and II as closely as possible. A possible Report block for our problem follows.

Report Block Template

```
Report
      Table I.  Minimax Solutions for Part I
-------------------------------------------------------------------------
           L1       L3       L5       C2       C4       C6       MS11
-------------------------------------------------------------------------

Case A     $%6.4f$$L1$   $%6.4f$$L3$   $%6.4f$$L5$   $%6.4f$$C2$   $%6.4f$$C4$
 $%6.4f$$C6$   $%6.4f$$max$

-------------------------------------------------------------------------
End
```

max indicates the maximum value of MS11.

The report block is included in the input file "lab6.ckt".

Chapter 3

OSA90/hope Version 2.5 Applications Illustrated

OSA90/hope™

Applications Illustrated

Version 2.5

May 1993

Optimization Systems Associates Inc.

LIABILITY AND WARRANTY

NEITHER OPTIMIZATION SYSTEMS ASSOCIATES INC. NOR ITS EMPLOYEES, OFFICERS, DIRECTORS OR ANY OTHER PERSON, COMPANY, AGENCY OR INSTITUTION: (1) MAKES ANY WARRANTY, EXPRESS OR IMPLIED AS TO ANY MATTER WHATSOEVER REGARDING THIS MATERIAL, INCLUDING BUT NOT LIMITED TO THE GENERALITY THEREOF, ALL IMPLIED WARRANTIES AND CONDITIONS OF MERCHANTABILITY AND FITNESS FOR A PARTICULAR PURPOSE, OR THOSE ARISING BY STATUTE OR OTHERWISE IN LAW OR FROM THE COURSE OF DEALING OR USAGE OF TRADE HAVE BEEN AND ARE HEREBY EXPRESSLY EXCLUDED; OR (2) ASSUMES ANY LEGAL RESPONSIBILITY WHATSOEVER FOR THE ACCURACY, COMPLETENESS OR USEFULNESS OF THIS MATERIAL; OR (3) REPRESENTS THAT ITS USE WOULD NOT INFRINGE UPON PRIVATELY OWNED RIGHTS OF THIRD PARTIES. IT IS EXPRESSLY UNDERSTOOD AND AGREED THAT ANY RISKS, LIABILITIES OR LOSSES ARISING OUT OF ANY USE, TRANSFER OR LEASE OF THIS MATERIAL WILL NOT BE ATTRIBUTED TO OPTIMIZATION SYSTEMS ASSOCIATES INC. OR ANY INDIVIDUAL ASSOCIATED WITH THE COMPANY. ACCURACY, COMPLETENESS OR USEFULNESS FOR ANY APPLICATION SHALL BE DETERMINED INDEPENDENTLY BY THE PARTY UNDERTAKING SUCH AN APPLICATION.

IN NO EVENT WHATSOEVER WILL OPTIMIZATION SYSTEMS ASSOCIATES INC., ITS EMPLOYEES, OFFICERS, DIRECTORS, OR AGENTS BE LIABLE FOR ANY DAMAGES, INCLUDING, BUT WITHOUT LIMITATION, DIRECT, INDIRECT, INCIDENTAL AND CONSEQUENTIAL DAMAGES AND DAMAGES FOR LOST DATA OR PROFITS, ARISING OUT OF THE USE OF OR INABILITY TO USE THIS MATERIAL.

CONTENTS ARE SUBJECT TO CHANGE WITHOUT NOTICE.

Copyright

Copyright © 1993 Optimization Systems Associates Inc.

THIS DOCUMENTATION AND RELATED COMPUTER PROGRAM ARE THE PROPERTY OF OPTIMIZATION SYSTEMS ASSOCIATES INC. REPRODUCTION, DISCLOSURE OR TRANSCRIPTION OF ANY OF THIS MATERIAL IN ANY FORM INTO ANY MACHINE REQUIRES PRIOR PERMISSION IN WRITING FROM OPTIMIZATION SYSTEMS ASSOCIATES INC.

All Rights Reserved. OSA90/hope Applications Illustrated Version 2.5 first published in 1993. Printed in Canada.

Optimization Systems Associates Inc.
P.O. Box 8083, Dundas, Ontario
Canada L9H 5E7

Tel 416 628 8228 (Before October 4, 1993)
905 628 8228 (After October 4, 1993)

Trademarks of Optimization Systems Associates Inc.

OSA90
OSA90/hope
Datapipe
HarPE
FAST

Applications Illustrated

TABLE 1 EXAMPLES CATEGORIZED BY APPLICATIONS

Application	Examples
Generic expressions and optimization	demo01 demo02 demo04 demo44 demo45 demo46 demo54 demo56
Matrices, vectors and interpolations	demo41 demo42 demo43 demo51 demo52
Datapipe connections	demo03 demo05 demo06 demo07 demo08 demo09 demo10 demo57 demo58
Nonlinear circuit harmonic balance simulation and optimization	demo11 demo14 demo21 demo22 demo23 demo38 demo39 demo40 demo47 demo49
Mixers and two-tone intermodulation	demo24 demo25 demo26 demo27 demo28
Small-signal circuit simulation and design optimization	demo12 demo13 demo19 demo20 demo33 demo34 demo48 demo50 demo53
Statistical analysis and yield optimization	demo10 demo35 demo36 demo37 demo55
Modeling and parameter extraction	demo14 demo15 demo16 demo17 demo18 demo31 demo32
Physics-based device simulation	demo29 demo30 demo48 demo60
Adjoint sensitivity analysis	demo59
Oscillator analysis and design	demo61 demo62

TABLE 2 DEMONSTRATION EXAMPLES

Page	Example	Highlights
1	demo01	Simple expressions, parameter sweep, and parametric display of circles.
2	demo02	Simple optimization example of matching two functions, ℓ_1 optimization.
4	demo03	Simulation and optimization of a transmission line transformer using an external simulator via Datapipe.
6	demo04	Minimax optimization of a generic mathematical problem.
7	demo05	Minimax optimization of the same problem as in demo04 but using an external program via Datapipe with the FUN protocol.
8	demo06	Time-domain transient analysis using an external simulator via Datapipe.
10	demo07	Solution of harmonic balance equations using ℓ_2 optimization with external simulators via Datapipe.
12	demo08	Solution of waveform balance equations using ℓ_2 optimization. The fact that the harmonic balance formulation in demo07 can be easily modified to the waveform balance formulation in this example demonstrates the flexibility of OSA90.
14	demo09	Minimax nominal optimization of a low-pass filter via Datapipe using the FDF protocol with gradients supplied by the external simulator.
16	demo10	Monte Carlo analysis and yield optimization of a low-pass filter using Datapipe, with quadratic modeling, starting from the solution of nominal optimization (demo09).
18	demo11	Harmonic balance simulation of a simple nonlinear FET circuit. The device is modeled by FETM extracted from *MGF1902* data.
21	demo12	Minimax optimization of a small-signal FET amplifier. The nonlinear FETR model is extracted from *NEC700* data.
24	demo13	Minimax optimization of a small-signal balanced amplifier. This example is similar to demo12, but two FETs are used in a balanced structure with Lange couplers.
29	demo14	Harmonic balance simulation of a simple FET circuit for estimating the second- and third-order harmonic intercept points. Also illustrated is the preprogrammed Curtice cubic symmetrical FET model using FETU1.
31	demo15	This example is similar to demo14 but illustrates the preprogrammed Curtice cubic asymmetrical FET model using the user-definable model FETU2.

TABLE 2 DEMONSTRATION EXAMPLES (cont'd)

Page	Example	Highlights
33	demo16	This example is adapted from demo12 to illustrate the preprogrammed Materka FET model using the user-definable model FETU2.
36	demo17	DC simulation of the preprogrammed Plessey FET model using the user-definable model FETU1. Also illustrated is how to display the match between simulated responses and measured data.
38	demo18	DC and small-signal AC simulation of the preprogrammed TOM FET model (TriQuint's Own Model) using the user-definable model FETU1. The match between simulated and measured *S* parameters are displayed on Smith Chart and polar plot.
42	demo19	Minimax optimization of a distributed (traveling wave) amplifier with 4 FETs. The FETs are modeled by FETR extracted from *NEC700* data. The design specifications include small-signal gain and input/output VSWRs from 1GHz to 9GHz. Large-signal power gain and 1-dB compression point are also calculated by harmonic balance simulation.
48	demo20	Minimax optimization of a broadband 2-20GHz distributed (traveling wave) amplifier with 3FETs. The FETs are modeled by FETR extracted from *NEC700* data. The small-signal gain and return loss are optimized. The large-signal power gain and 1-dB compression at different frequencies are calculated by harmonic balance simulation.
52	demo21	Harmonic balance simulation of a balanced amplifier with multi-harmonic excitations. The circuit is similar to demo13, but the FETs are modeled by a linearized equivalent circuit about the DC operating point. The input contains multi-harmonic components. Harmonic distortions at the output are simulated for different fundamental frequencies. Also illustrated is the use of imported data representing linear subcircuits.
56	demo22	Large-signal harmonic balance optimization of an X-band power amplifier. The 2400 μm FET are modeled by the Curtice cubic asymmetrical model. The gate bias voltage and matching circuits are optimized to increase output power and power-added efficiency.
60	demo23	Large-signal harmonic balance optimization of a Class-B X-band power amplifier. This example is similar to demo22 except that it is designed for Class-B instead of Class-A operation. The 2400 μm FET are modeled by the Curtice cubic asymmetrical model. The gate is biased near the pinch-off voltage. The matching circuits are optimized for maximum power-added efficiency.
64	demo24	A resistively matched single-ended diode mixer. Nonlinear two-tone simulation with LO = 1.5GHz, RF = 1.57GHz and IF = 0.07GHz.

TABLE 2 DEMONSTRATION EXAMPLES (cont'd)

Page	Example	Highlights
67	demo25	A singly-balanced diode mixer. Nonlinear two-tone simulation with LO = 3.75GHz, RF = 4GHz and IF = 0.25GHz. The conversion loss of the diode mixer is calculated versus sweep of the LO power.
70	demo26	Large-signal two-tone optimization of a broadband FET gate mixer. The FETR model is extracted from *NEC700* data. The mixer has a fixed LO frequency of 7GHz and broadband IF frequency from 0.1 - 1.5GHz. The gate bias voltage and input matching circuit are optimized to increase the transducer conversion gain.
73	demo27	Nonlinear two-tone simulation of a narrow-band FET gate mixer. The circuit topology is similar to the broadband mixer in demo26. This example assumes a fixed IF frequency of 1GHz. The conversion gain is calculated versus sweeps of the LO power and gate bias voltage.
77	demo28	Two-tone intermodulation analysis of a simple nonlinear FET circuit. The FET is modeled by FETM extracted from *MGF1902* data. The third-order IM products are calculated versus sweep of the input power.
80	demo29	DC simulation using FETT (physics-based Trew FET model).
82	demo30	DC simulation using FETT1 (FETT modified for uniform doping).
84	demo31	Example of using nonlinear controlled sources for user-created models.
86	demo32	Example of FET parameter extraction by fitting simulated model responses to measured *S* parameters.
91	demo33	Minimax optimization of a microstrip line 3:1 impedance transformer.
93	demo34	Simulation of microstrip filter.
95	demo35	Monte Carlo simulation of a single-stage feedback amplifier. The FET is represented by a statistical model extracted from measurements. Tolerances are included for the microstrip matching circuits and feedback line.
100	demo36	Illustration of the yield sensitivity feature using a small-signal amplifier.
103	demo37	Yield optimization of a nonlinear FET frequency doubler.
108	demo38	Harmonic balance simulation of an amplifier with square wave excitation.
111	demo39	Harmonic balance simulation of an amplifier with triangular wave excitation.
113	demo40	Harmonic balance simulation of an amplifier with pulse train excitations of different duty cycles.

TABLE 2 DEMONSTRATION EXAMPLES (cont'd)

Page	Example	Highlights
117	demo41	Illustration of the built-in cubic spline functions by an example of using cubic splines to interpolate a time-domain waveform response.
120	demo42	Illustration of the built-in 2D bicubic spline functions by an example of interpolating the DC drain current of a nonlinear FET circuit as a function of the gate and drain bias voltages.
122	demo43	Application of 2D bicubic spline interpolation to device modeling. A bias-dependent small-signal FET model is created using 2D bicubic splines.
127	demo44	Example of simple report generation.
129	demo45	Example of report generation for circuit simulation with parameter sweeps.
131	demo46	Report generation for displaying arrays and matrices in user-designed format.
133	demo47	DC and small-signal AC simulation with preprogrammed Raytheon-Statz FET model using FETU1.
137	demo48	DC and small-signal AC simulation of the physics-based bias-dependent small-signal FET model KTL.
141	demo49	Illustration of using a linear subcircuit as a port termination. A subcircuit consisting of a resistor and a capacitor in parallel is used as a complex load terminating the output port of a nonlinear FET circuit. Drain load lines at different input power levels and frequencies are shown.
144	demo50	Illustration of nested linear subcircuits to improve simulation efficiency.
146	demo51	Using the built-in matrix functions to define and solve the nodal equations of a linear resistive circuit.
148	demo52	Using the built-in matrix functions to define and solve the complex nodal equations of an RLC circuit.
150	demo53	Illustration of displaying FET drain load lines of an optimized small-signal amplifier.
153	demo54	Demonstration of Huber optimization. A sequence of Huber optimization with decreasing threshold values is shown to converge to the ℓ_1 solution.

TABLE 2 DEMONSTRATION EXAMPLES (cont'd)

Page	Example	Highlights
155	demo55	Monte Carlo analysis of a small-signal X-band amplifier. The FETs and the passive components are represented by physics-based models. The FET gate length, gate width, channel thickness and doping density as well as MIM capacitor metal plate areas and spiral inductor turns have been optimized for enhanced yield.
160	demo56	Testing the errors in inverting a nearly singular matrix. The Monte Carlo method is used to statistically perturb the matrix and the numerical errors at different perturbation levels are analyzed.
162	demo57	Illustration of using OSA90 as a child through Datapipe. A separate copy of OSA90 is called as a Datapipe child to compute the drain voltage and current of a nonlinear FET amplifier for displaying load lines.
165	demo58	Illustration of using OSA90 as a child through Datapipe. A separate copy of OSA90 is called as a Datapipe child to compute the large-signal power gain of a nonlinear FET circuit at different input power levels. The results are used by the parent OSA90 to calculate the 1-dB compression point versus frequency.
169	demo59	Illustration of using OSA90 for adjoint sensitivity calculations.
172	demo60	Implementation of a YIG resonator model published by J.A. Mezak and G.D. Vendelin.
174	demo61	Oscillator analysis using the OSCPORT element.
178	demo62	Oscillator design optimization using the OSCPORT element. The tuning capacitor of the FET oscillator is optimized to achieve free oscillator at the desired frequency of 15GHz.

demo01

Simple expressions, parameter sweep, and parametric display of circles.

Input File

```
!  Example  demo01.ckt
!  a simple example for OSA90
!  Xsweep displays X and Y as functions of Angle
!  Parametric plots of circles

Expression
   Angle: 0;    ! sweep label
   Center: 0;   ! center of the circles

   X: cos(Angle) + Center;   ! X coordinates of points on a circle
   Y: sin(Angle) - Center;   ! Y coordinates
end

Sweep
   Center: 0 1 2 3 4 5
   Angle: from 0 to (2 * PI) N=100  X  Y
   { Parametric  P=Angle  Center=ALL  Title="PARAMETRIC VIEW OF CIRCLES"
     X=X  X_title="cos(Angle) + Center"  Xmin=-4  Xmax=8  NXticks=12
     Y=Y  Y_Title="sin(Angle) - Center"  Ymin=-7  Ymax=2  NYTicks=9 };
end
```

Parametric Display of Circles

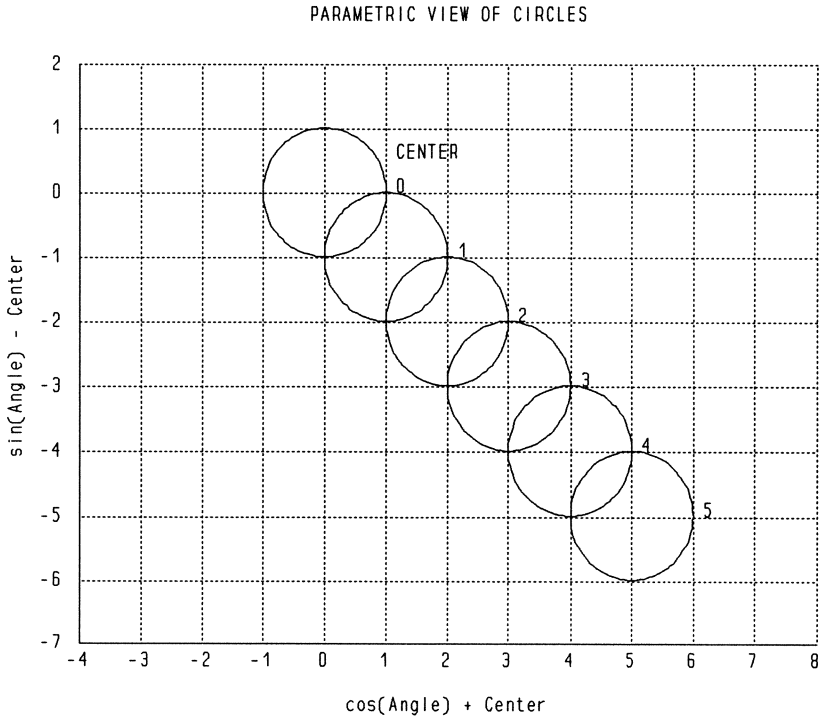

demo02

This simple example illustrates the definition of optimization variables, functions and goals.

Consider the function

$$Function = (x_1 t + x_2 t^2) \,/\, (1 + x_3 t + x_4 t^2)$$

We wish to optimize the coefficients x_1, x_2, x_3 and x_4 so that *Function* will match

$$Goal = \mathrm{sqrt}(t)$$

for t = 0, 0.02, 0.04, ..., 1.

ℓ_1 optimization is used.

Input File

```
!  Example  demo02.ckt
!  simple optimization example for OSA90
!  matching Goal(t)=sqrt(t) by a rational function Function(t)
!  in the interval [0  1] of t
!  the coefficients of Function(t) are optimized
!  by the L1 optimizer

Expression
   t: 0;       ! sweep label

   x1: ?10?;   ! coefficients of Function(t)
   x2: ?10?;
   x3: ?10?;
   x4: ?10?;

   Function: (x1 * t + x2 * t * t) / (1 + x3 * t + x4 * t * t);

   Goal: sqrt(t);

   Error = Function - Goal;
end

Sweep
   t: from 0 to 1 step=0.02  Function Goal Error
   {Xsweep  Y=Function.white & Goal.white.circle}
   {Xsweep  Y=Error  Ymin=-0.02 Ymax=0.02  NYTicks=8};
end

Specification
   t: from 0 to 1 step=0.02  Function = Goal;
end
```

Match Between Function and Goal After Optimization

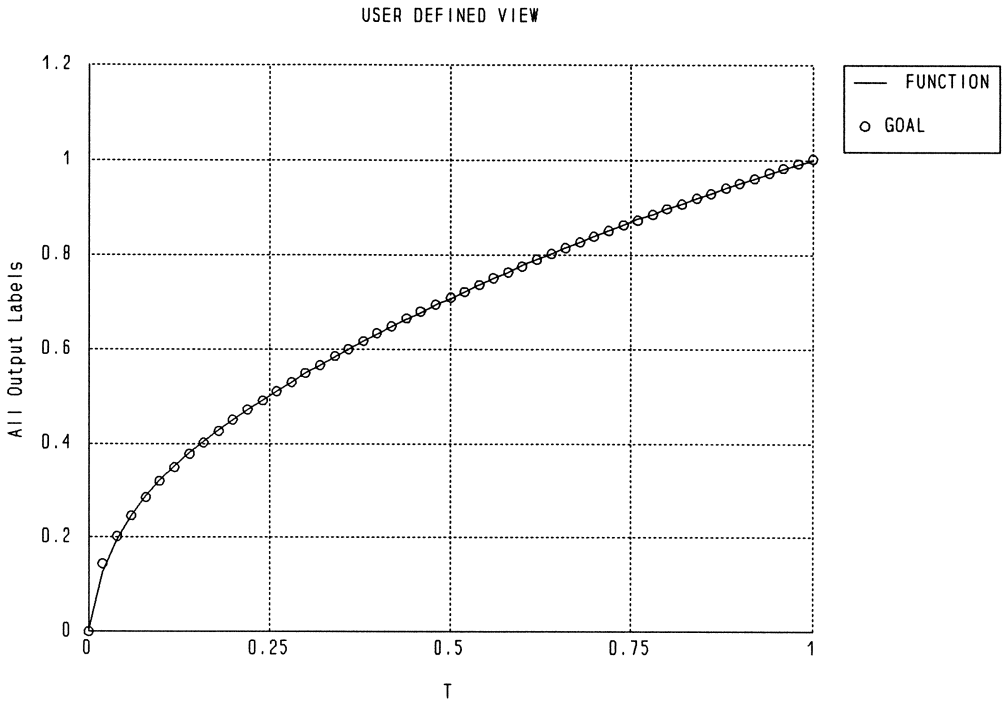

demo03

Simulation and minimax optimization of a three-section transmission line 10:1 transformer using an external simulator via Datapipe.

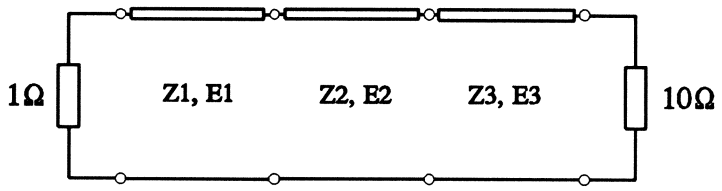

where Z1, Z2, Z3, E1, E2 and E3 are the characteristic impedances and electrical lengths of the transmission lines, respectively.

Input File

```
!  Example  demo03.ckt
!  Datapipe example for OSA90
!  using Datapipe to communicate with an external simulator "transfmr"
!  which simulates a three-section transmission line transformer
!
!  The child program "transfmr" can handle both "SIM" and "FDF" protocols
!  One of the inputs to the child is a flag indicating the protocol used
!  With the SIM protocol, the child returns the reflection coefficient
!  With the FDF protocol, the child also supplies the exact derivatives.

#define  SIM_protocol  0   ! flag to the child indicating the protocol
#define  FDF_protocol  1

Expression
   ! the vector of optimization variables X contains [E1 Z1 E2 Z2 E3 Z3]
   ! where Ei is the normalized length of the ith transmission line
   ! and Zi is the characteristic impedance of the ith transmission line
   X[6] = [?0.8?   ?1.5?   ?1.2?   ?3.0?   ?0.8?   ?6.0?];

   Datapipe: FDF  FILE="transfmr"  NAME=Transformer
                  N_INPUT=8  INPUT=(X, FREQ, FDF_protocol)
                  N_OUTPUT=1;

   Datapipe: SIM  FILE="transfmr"
                  N_INPUT=8  INPUT=(X, FREQ, SIM_protocol)
                  N_OUTPUT=1  OUTPUT=(Reflection_Coe);

   Return_Loss: if (Reflection_Coe > 0.01) (20 * log10(Reflection_Coe))
                else (-40);
end

Sweep
   FREQ: from 0.2 to 1.8 step=0.05  Reflection_Coe, Return_Loss;
end

Specification
   Datapipe:  FREQ: 0.5, 0.6, 0.7, 0.77, 0.9, 1.0, 1.1,
                    1.23, 1.3, 1.4, 1.5
              Transformer;
end

Control
   Optimizer=Minimax;
end
```

Transformer Reflection Coefficient After Minimax Optimization

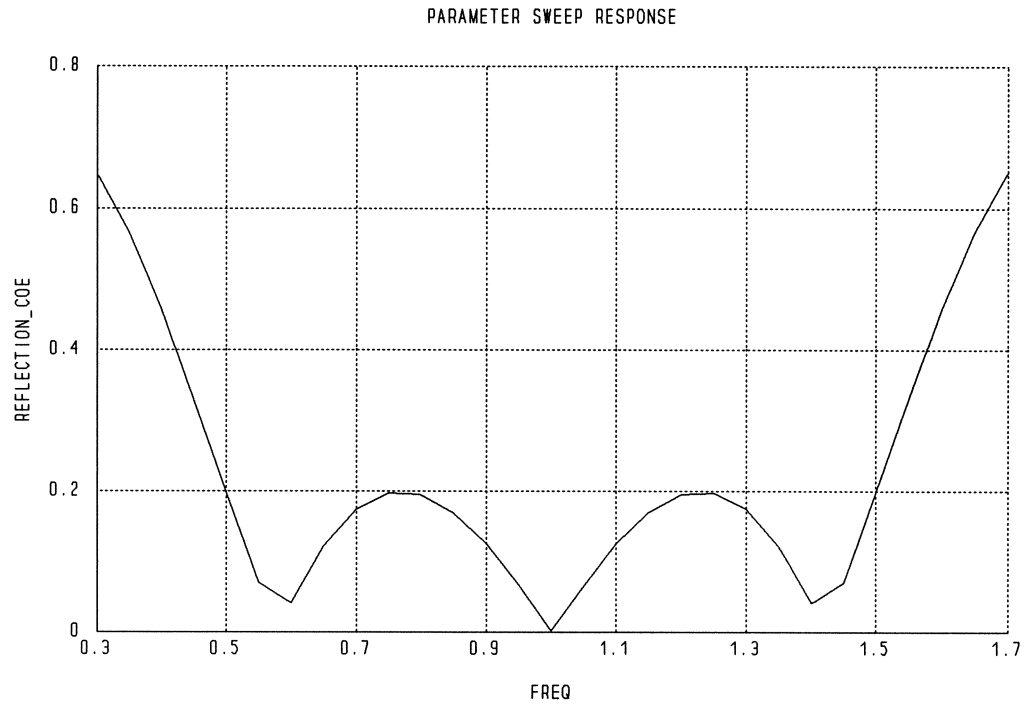

demo04

Minimax optimization of a generic mathematical problem:

$$\underset{x_1,x_2}{\text{minimize}} \quad \max \{ f_1, f_2, f_3 \}$$

where

$$f_1 = x_1^2 + x_2^2 - 1$$

$$f_2 = 3 - x_1^2 - x_2^2$$

$$f_3 = x_1 - x_2 + 3$$

Input File

```
! Example  demo04.ckt
! illustrate minimax optimization
! abstract problem of 2 variables and 3 functions
! the starting point is x1=-0.5 and x2=0.5
! the theorectical solution is x1=-1  x2=1

Expression
   x1: ?-0.5?;
   x2: ?0.5?;

   f1 = x1 * x1 + x2 * x2 - 1;
   f2 = 3 - x1 * x1 - x2 * x2;
   f3 = x1 - x2 + 3;
end

Specification
   f1  f2  f3;
end

Control
   Optimizer=Minimax;
end
```

demo05

Minimax optimization of the same problem as in demo04 but using an external program to calculate the function values via Datapipe with the FUN protocol.

$$\underset{x_1,x_2}{\text{minimize}} \quad \max \{ f_1, f_2, f_3 \}$$

where

$$f_1 = x_1^2 + x_2^2 - 1$$

$$f_2 = 3 - x_1^2 - x_2^2$$

$$f_3 = x_1 - x_2 + 3$$

During optimization the functions are evaluated by the Datapipe child program pipe_fun.

Input File

```
! Example  demo05.ckt
! minimax optimization using FUN Datapipe protocol
! the child program "pipe_fun" computes
!    f1 = x1*x1 + x2*x2 - 1
!    f2 = 3 - (x1*x1 + x2*x2)
!    f3 = x1 - x2 + 3.0
!
! this problem is the same as demo04
! the starting point is x1=-0.5 and x2=0.5
! the theoretical solution is x1=-1 and x2=1

Expression
   x1: ?-0.5?;
   x2: ?0.5?;

   Datapipe: FUN  FILE="pipe_fun"  NAME=ErrorFunctions
                  N_INPUT=2  INPUT=(x1, x2)
                  N_OUTPUT=3;
end

Specification
   Datapipe: ErrorFunctions;
end

Control
   Optimizer=Minimax;
end
```

demo06

Time-domain transient analysis of a feedback amplifier with tapered RC line (Vlach and Singhal, *Computer Methods for Circuit Analysis and Design*, p. 289) using an external simulator via Datapipe.

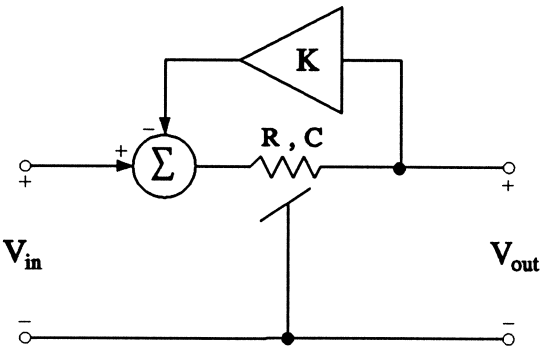

Input File

```
!  Example  demo06.ckt
!  simulation using SIM Datapipe protocol
!  the external program is a time-domain simulator
!  of a feedback amplifier with tapered RC lines

#define  Pulse_Excitation   -1   ! type of excitation, flag for the child
#define  Step_Excitation     0
#define  Linear_Excitation   1
#define  Square_Excitation   2
#define  Cubic_Excitation    3

Expression
   Excitation: Pulse_Excitation;

   Time: 0;
   LaplaceCode = 10;    ! code for numerical Laplace inversion
   K_Factor = 5;        ! gain of the amplifier

   Datapipe: SIM  FILE="feedback"
                  N_INPUT=4  INPUT=(Time, LaplaceCode, K_Factor, Excitation)
                  N_OUTPUT=2  OUTPUT=(Signal, Response);
end

Sweep
   Excitation: Pulse_Excitation, Step_Excitation, Linear_Excitation
               Square_Excitation, Cubic_Excitation
   Time: from 0.01 to 1 step=0.01
   Signal  Response;
end
```

Feedback Amplifier Pulse Response

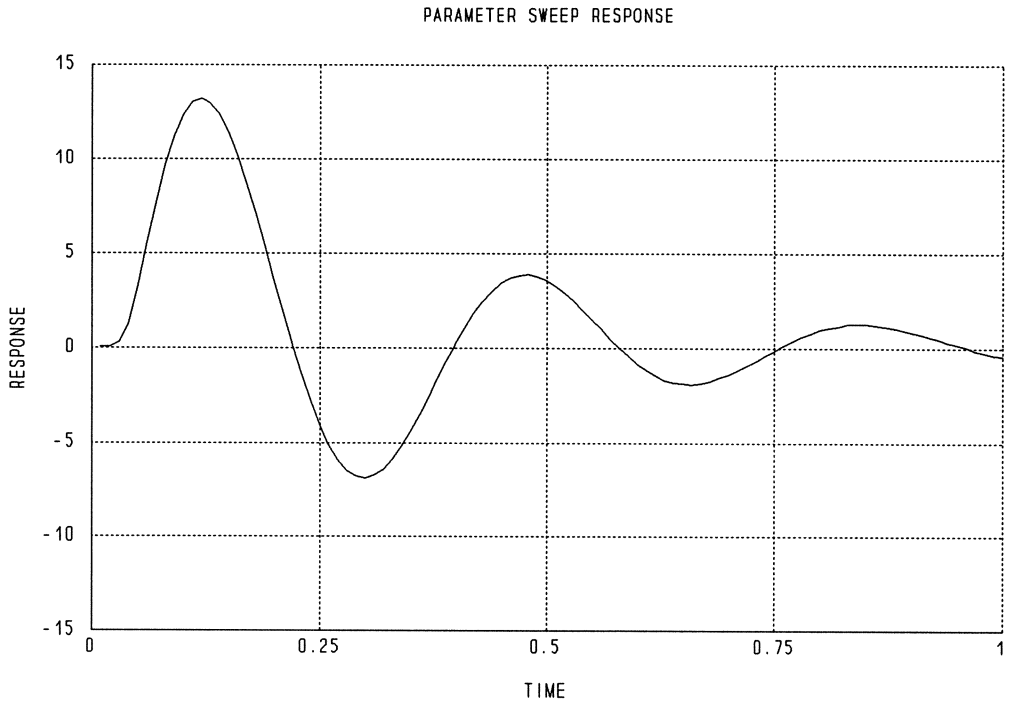

demo07

Solution of explicit harmonic balance equations using ℓ_2 optimization.

The circuit is split into linear and nonlinear subcircuits connected through two ports. The state variables are the frequency-domain spectra of the two port voltages: $\mathbf{V}_1$ and $\mathbf{V}_2$.

The linear subcircuit is simulated by the Datapipe child program p_linear which calculates the frequency-domain spectra of the two port currents: $\mathbf{I}_{1L}$ and $\mathbf{I}_{2L}$.

The nonlinear subcircuit (a FET) is simulated by the Datapipe child program p_device which calculates the time-domain currents and charges at the two connection ports. The results are transformed into the frequency domain using the built-in DFT_TF function. The frequency-domain spectra of the nonlinear currents and charges are denoted by $\mathbf{I}_{1N}$, $\mathbf{I}_{2N}$, $\mathbf{Q}_1$ and $\mathbf{Q}_2$, respectively.

The harmonic balance error functions are formulated as

$$\mathbf{Error1} = \mathbf{I}_{1L} + \mathbf{I}_{1N} + j\boldsymbol{\Omega}\,\mathbf{Q}_1$$

$$\mathbf{Error2} = \mathbf{I}_{2L} + \mathbf{I}_{2N} + j\boldsymbol{\Omega}\,\mathbf{Q}_2$$

where $\boldsymbol{\Omega}$ is a diagonal matrix containing the harmonic frequencies.

The harmonic balance solution is found by minimizing the ℓ_2 norm of the error functions.

Input File

```
!  Example  demo07.ckt
!  solution of harmonic balance equations using Datapipe
!  two child programs simulate the linear and nonlinear subcircuits
!  to simplify the illustration, the subcircuits' parameters and
!  the sources have fixed values
!  use L2 optimizer with accuracy set to 1.e-6

#define N_HARM      4  ! number of harmonics
#define N_T         9  ! number of time samples (2 * N_HARM + 1)
#define N_PORTS     2  ! number of nonlinear ports
#define N_STATES   20  ! number of frequency-domain state variables
                       ! 2 * N_PORTS * (N_HARM+1)

#define N_T_WAVEFORM  128   ! number of points for waveform display


Expression
   Omega: 2.0 * PI * FREQ;

   ! frequency-domain state variables
   V1_real[0:N_HARM] = [?-0.673?  ?0.5?  ?-1 0 1?  ?-1 0 1?  ?-1 0 1?];
   V1_imag[0:N_HARM] = [0  ?-5 0 5?  ?-1 0 1?  ?-1 0 1?  ?-1 0 1?];
   V2_real[0:N_HARM] = [?4?  ?-5 0 5?  ?-1 0 1?  ?-1 0 1?  ?-1 0 1?];
   V2_imag[0:N_HARM] = [0  ?-5 0 5?  ?-1 0 1?  ?-1 0 1?  ?-1 0 1?];

   ! simulate the linear subcircuit in the frequency domain
   Datapipe: SIM  FILE="p_linear"
      N_INPUT=(N_STATES + 3)
      INPUT=(N_PORTS, N_HARM, FREQ, V1_real, V1_imag, V2_real, V2_imag)
      N_OUTPUT=N_STATES
      OUTPUT=(I1L_real[0:N_HARM], I1L_imag[0:N_HARM],
```

```
            I2L_real[0:N_HARM], I2L_imag[0:N_HARM]);

   ! transform the voltages into the time domain
   V1_time[N_T] = DFT_FT(V1_real, V1_imag);
   V2_time[N_T] = DFT_FT(V2_real, V2_imag);

   ! simulate the nonlinear device (FET) in the time domain
   Datapipe: SIM  FILE="p_device"
      N_INPUT=(1 + N_PORTS * N_T)   INPUT=(N_T, V1_time, V2_time)
      N_OUTPUT=(2 * N_PORTS * N_T)
      OUTPUT=(I1N_time[N_T], I2N_time[N_T], Q1_time[N_T], Q2_time[N_T]);

   ! transform the device responses into the frequency domain
   DFT_TF(I1N_time, I1N_real[0:N_HARM], I1N_imag[0:N_HARM]);
   DFT_TF(I2N_time, I2N_real[0:N_HARM], I2N_imag[0:N_HARM]);
   DFT_TF(Q1_time, Q1_real[0:N_HARM], Q1_imag[0:N_HARM]);
   DFT_TF(Q2_time, Q2_real[0:N_HARM], Q2_imag[0:N_HARM]);

   ! construct the frequency-domain Harmonic Balance residual errors
   KS[0:N_HARM] = [0 1 2 3 4];
   K_Omega[0:N_HARM] = KS * Omega;

   Error1_real[0:N_HARM] = I1L_real + I1N_real - K_Omega * Q1_imag;
   Error1_imag[0:N_HARM] = I1L_imag + I1N_imag + K_Omega * Q1_real;
   Error2_real[0:N_HARM] = I2L_real + I2N_real - K_Omega * Q2_imag;
   Error2_imag[0:N_HARM] = I2L_imag + I2N_imag + K_Omega * Q2_real;

   ! calculate the voltage waveforms for display
   V1_waveform[N_T_WAVEFORM] = DFT_FT(V1_real, V1_imag);
   V2_waveform[N_T_WAVEFORM] = DFT_FT(V2_real, V2_imag);

   K: 1;  ! sweep parameter
end

Sweep
   Title="Voltage Waveform"
   FREQ: 6GHZ  K: from 1 to N_T_WAVEFORM step=1
   V1_waveform[K]  V2_waveform[K];
end

Spec
   FREQ: 6GHZ  Error1_real=0  Error1_imag=0;
   FREQ: 6GHZ  Error2_real=0  Error2_imag=0;
end

Control
   Optimizer=L2;
end
```

demo08

Solution of explicit waveform balance equations using ℓ_2 optimization. This example is identical to demo07 except that the nonlinear circuit equations are solved in the time domain by waveform balance instead of in the frequency domain by harmonic balance.

The fact that the harmonic balance formulation in demo07 can be readily modified to the waveform balance formulation in this example demonstrates the flexibility of OSA90.

Input File

```
!  Example  demo08.ckt
!  solution of waveform balance equations using Datapipe
!  modified from demo07 to demonstrate the flexibility of OSA90
!  two child programs simulate the linear and nonlinear subcircuits
!  to simplify the illustration, the subcircuits' parameters and
!  the sources have fixed values
!  use L2 optimizer with accuracy set to 1.e-6

#define N_HARM      4  ! number of harmonics
#define N_T         9  ! number of time samples (2 * N_HARM + 1)
#define N_PORTS     2  ! number of nonlinear ports
#define N_STATES   20  ! number of frequency-domain state variables
                       ! 2 * N_PORTS * (N_HARM+1)

#define N_T_WAVEFORM  128   ! number of points for waveform display


Expression
   Omega: 2.0 * PI * FREQ;

   ! frequency-domain state variables
   V1_real[0:N_HARM] = [?-0.673?  ?0.5?  ?-1 0 1?  ?-1 0 1?  ?-1 0 1?];
   V1_imag[0:N_HARM] = [0  ?-5 0 5?  ?-1 0 1?  ?-1 0 1?  ?-1 0 1?];
   V2_real[0:N_HARM] = [?4?  ?-5 0 5?  ?-1 0 1?  ?-1 0 1?  ?-1 0 1?];
   V2_imag[0:N_HARM] = [0  ?-5 0 5?  ?-1 0 1?  ?-1 0 1?  ?-1 0 1?];

   ! simulate the linear subcircuit in the frequency domain
   Datapipe: SIM  FILE="p_linear"
      N_INPUT=(N_STATES + 3)
      INPUT=(N_PORTS, N_HARM, FREQ, V1_real, V1_imag, V2_real, V2_imag)
      N_OUTPUT=N_STATES
      OUTPUT=(I1L_real[0:N_HARM], I1L_imag[0:N_HARM],
              I2L_real[0:N_HARM], I2L_imag[0:N_HARM]);

   ! transform the voltages into the time domain
   V1_time[N_T] = DFT_FT(V1_real, V1_imag);
   V2_time[N_T] = DFT_FT(V2_real, V2_imag);

   ! simulate the nonlinear device (FET) in the time domain
   Datapipe: SIM  FILE="p_device"
      N_INPUT=(1 + N_PORTS * N_T)   INPUT=(N_T, V1_time, V2_time)
      N_OUTPUT=(2 * N_PORTS * N_T)
      OUTPUT=(I1N_time[N_T], I2N_time[N_T],
              Q1_time[N_T], Q2_time[N_T]);

   ! transform the linear currents into the time domain
   I1L_time[N_T] = DFT_FT(I1L_real, I1L_imag);
   I2L_time[N_T] = DFT_FT(I2L_real, I2L_imag);

   ! we need to calculate the time-domain currents from the charges
   ! instead of doing differentiation in the time-domain
   ! we can transform the charges into the frequency domain
   DFT_TF(Q1_time, Q1_real[0:N_HARM], Q1_imag[0:N_HARM]);
   DFT_TF(Q2_time, Q2_real[0:N_HARM], Q2_imag[0:N_HARM]);
```

```
   ! time-domain differentiation can be realized in the frequency domain
   ! by simply multiplying the charges by -j*K*Omega
   KS[0:N_HARM] = [0 1 2 3 4];
   K_Omega[0:N_HARM] = KS * Omega;

   I1C_real[0:N_HARM] = -K_Omega * Q1_imag;
   I1C_imag[0:N_HARM] =  K_Omega * Q1_real;
   I2C_real[0:N_HARM] = -K_Omega * Q2_imag;
   I2C_imag[0:N_HARM] =  K_Omega * Q2_real;

   ! the results are then transformed back to the time domain
   I1C_time[N_T] = DFT_FT(I1C_real, I1C_imag);
   I2C_time[N_T] = DFT_FT(I2C_real, I2C_imag);

   ! construct the time-domain Waveform Balance residual errors
   Error1_time[N_T] = I1L_time + I1N_time + I1C_time;
   Error2_time[N_T] = I2L_time + I2N_time + I2C_time;

   ! calculate the voltage waveforms for display
   V1_waveform[N_T_WAVEFORM] = DFT_FT(V1_real, V1_imag);
   V2_waveform[N_T_WAVEFORM] = DFT_FT(V2_real, V2_imag);

   K: 1;  ! sweep parameter
end

Sweep
   Title="Voltage Waveform"
   FREQ: 6GHZ  K: from 1 to N_T_WAVEFORM step=1
   V1_waveform[K]  V2_waveform[K];
end

Spec
   FREQ: 6GHZ  Error1_time=0  Error2_time=0;
end

Control
   Optimizer=L2;
end
```

demo09

Minimax nominal optimization of an 11-element LC low-pass filter. The filter is simulated by the external program lcfilter via Datapipe. The child program lcfilter can also use the FDF protocol to provide analytical gradients for optimization.

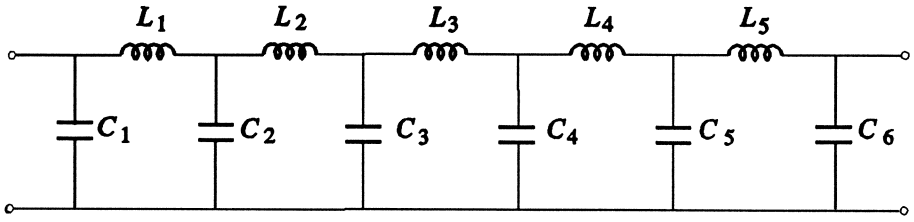

Input File

```
!  Example  demo09.ckt
!  optimization with external simulator and FDF via datapipe
!  11-element LC low-pass filter
!  This example takes advantage of user-supplied gradients
!  minimax optimization

! flags for calling the child program

#define  SIMULATION  0  ! SIM protocol, output insertion loss
#define  PASSBAND    1  ! FDF protocol, output Insertion_loss - SPEC
#define  STOPBAND    2  ! FDF protocol, output SPEC - Insertion_loss

Expression
   L1=?0.2NH?;
   L2=?0.2NH?;
   L3=?0.25NH?;
   L4=?0.25NH?;
   L5=?0.2NH?;
   C1=?0.2NF?;
   C2=?0.4NF?;
   C3=?0.4NF?;
   C4=?0.3NF?;
   C5=?0.3NF?;
   C6=?0.2NF?;

   X[11] = [C1, L1, C2, L2, C3, L3, C4, L4, C5, L5, C6];

   Omega = 2 * PI * FREQ;

   Passband_Spec: 0.32;  ! dB on Insertion_loss
   Stopband_Spec: 52;    ! dB on Insertion_loss

   Datapipe: FDF  FILE="lcfilter"  NAME=Passband_Error
                  N_INPUT=14  INPUT=(X, PASSBAND, Omega, Passband_Spec)
                  N_OUTPUT=1;

   Datapipe: FDF  FILE="lcfilter"  NAME=Stopband_Error
                  N_INPUT=14  INPUT=(X, STOPBAND, Omega, Stopband_Spec)
                  N_OUTPUT=1;

   Datapipe: SIM  FILE="lcfilter"
                  N_INPUT=13  INPUT=(X, SIMULATION, Omega)
                  N_OUTPUT=1  OUTPUT=(Insertion_loss);
end
```

```
Sweep
   FREQ: from 0.01GHZ to 1GHZ step 0.01GHZ
         from 1.025GHZ to 1.4GHZ step=0.025GHZ  Insertion_loss
      {Xsweep  Title="Passband Insertion Loss Of LC Filter"
       Y=Insertion_loss  Ymin=0  Ymax=0.5  NYTicks=5
       Xmin=0  Xmax=1 NXTicks=5}
      {Xsweep  Title="Insertion Loss Of LC Low-Pass Filter"
       Y=Insertion_loss  Xmin=0  Xmax=1.4  NXTicks=7};
end

Specification
   Datapipe:  FREQ: FROM 0.02GHZ TO 1GHZ STEP 0.02GHZ
              Passband_Error;
   Datapipe:  FREQ: 1.3GHZ  Stopband_Error;
end

Control
   Optimizer=Minimax;
end
```

Optimized Filter Passband Insertion Loss

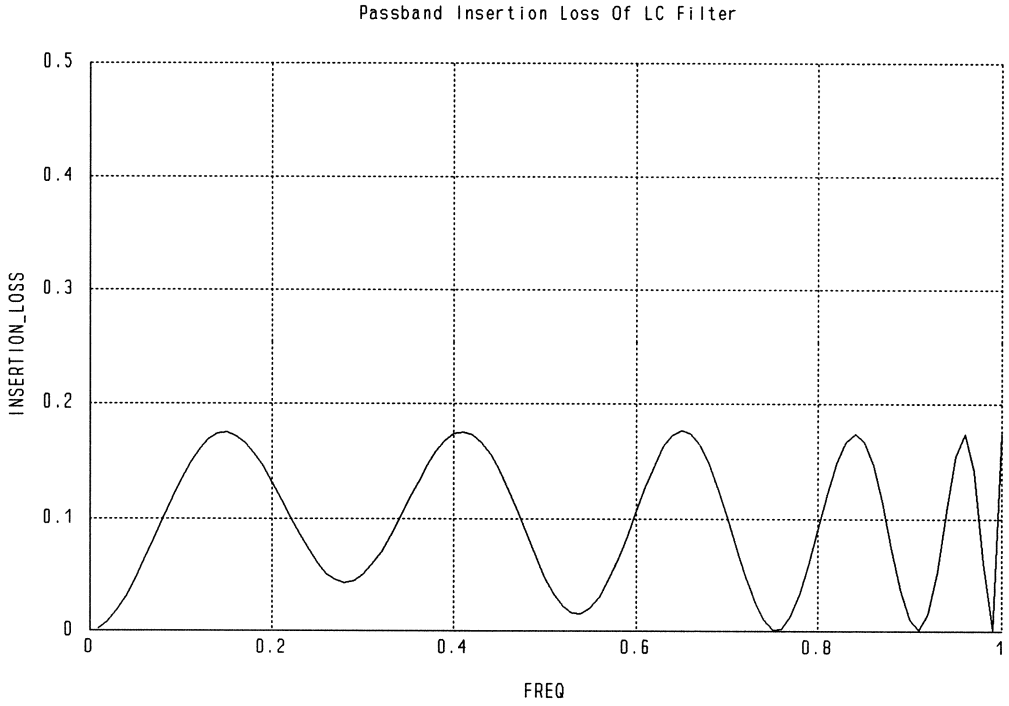

demo10

Monte Carlo analysis and yield optimization of an 11-element LC low-pass filter. This is the same filter as in demo09.

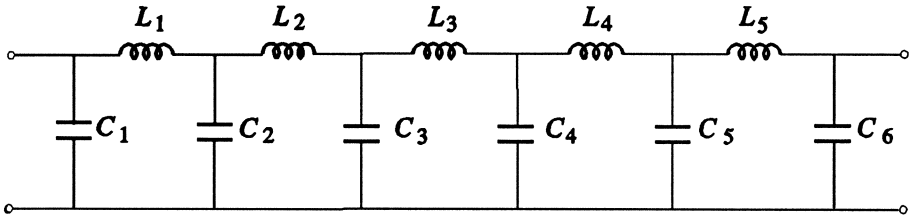

The filter is simulated by the external program lcfilter via Datapipe. The child program lcfilter can also use the FDF protocol to provide analytical gradients.

For yield optimization, the nominal minimax solution obtained for demo09 is used as the starting point, and quadratic models are employed for both the functions and gradients.

Input File

```
!  Example  demo10.ckt
!  yield optimization with external simulator via datapipe
!  11-element LC low-pass filter
!  starting point is the minimax nominal solution of demo09
!  use 50 outcomes in yield optimization with quadratic modeling

! flags for calling the child program

#define  SIMULATION  0  ! SIM protocol, output insertion loss
#define  PASSBAND    1  ! FDF protocol, output Insertion_loss - SPEC
#define  STOPBAND    2  ! FDF protocol, output SPEC - Insertion_loss

Expression
   L1=?0.220542NH? {Uniform TOL=1.5%};
   L2=?0.23407NH?  {Uniform TOL=1.5%};
   L3=?0.250419NH? {Uniform TOL=1.5%};
   L4=?0.268282NH? {Uniform TOL=1.5%};
   L5=?0.235821NH? {Uniform TOL=1.5%};
   C1=?0.216088NF? {Uniform TOL=1.5%};
   C2=?0.380065NF? {Uniform TOL=1.5%};
   C3=?0.396367NF? {Uniform TOL=1.5%};
   C4=?0.359655NF? {Uniform TOL=1.5%};
   C5=?0.338276NF? {Uniform TOL=1.5%};
   C6=?0.204885NF? {Uniform TOL=1.5%};

   X[11] = [C1, L1, C2, L2, C3, L3, C4, L4, C5, L5, C6];

   Omega = 2 * PI * FREQ;

   Passband_Spec: 0.32;  ! dB on Insertion_loss
   Stopband_Spec: 52;    ! dB on Insertion_loss

   Datapipe: FDF  FILE="lcfilter"  NAME=Passband_Error
                  N_INPUT=14  INPUT=(X, PASSBAND, Omega, Passband_Spec)
                  N_OUTPUT=1;

   Datapipe: FDF  FILE="lcfilter"  NAME=Stopband_Error
                  N_INPUT=14  INPUT=(X, STOPBAND, Omega, Stopband_Spec)
```

```
                N_OUTPUT=1;

   Datapipe: SIM  FILE="lcfilter"
                  N_INPUT=13  INPUT=(X, SIMULATION, Omega)
                  N_OUTPUT=1  OUTPUT=(Insertion_loss);
end

Sweep
   FREQ: from 0.01GHZ to 1GHZ step 0.01GHZ
         from 1.025GHZ to 1.4GHZ step=0.025GHZ  Insertion_loss
      {Xsweep  Title="Passband Insertion Loss Of LC Filter"
       Y=Insertion_loss  Ymin=0  Ymax=0.5  NYTicks=5
       Xmin=0  Xmax=1 NXTicks=5}
      {Xsweep  Title="Insertion Loss Of LC Low-Pass Filter"
       Y=Insertion_loss  Xmin=0  Xmax=1.4  NXTicks=7};
end

Specification
   Datapipe:  FREQ: FROM 0.02GHZ TO 1GHZ STEP 0.02GHZ
              Passband_Error;
   Datapipe:  FREQ: 1.3GHZ  Stopband_Error;
end

MonteCarlo
   N_outcomes=200
   FREQ: FROM 0.02GHZ TO 1GHZ STEP 0.02GHZ  Insertion_loss < Passband_Spec;

   FREQ: 1.3GHZ  Insertion_loss > Stopband_Spec;
end

Control
   Optimizer=Yield;
end
```

Statistical Response (Filter Passband Insertion Loss) After Yield Optimization

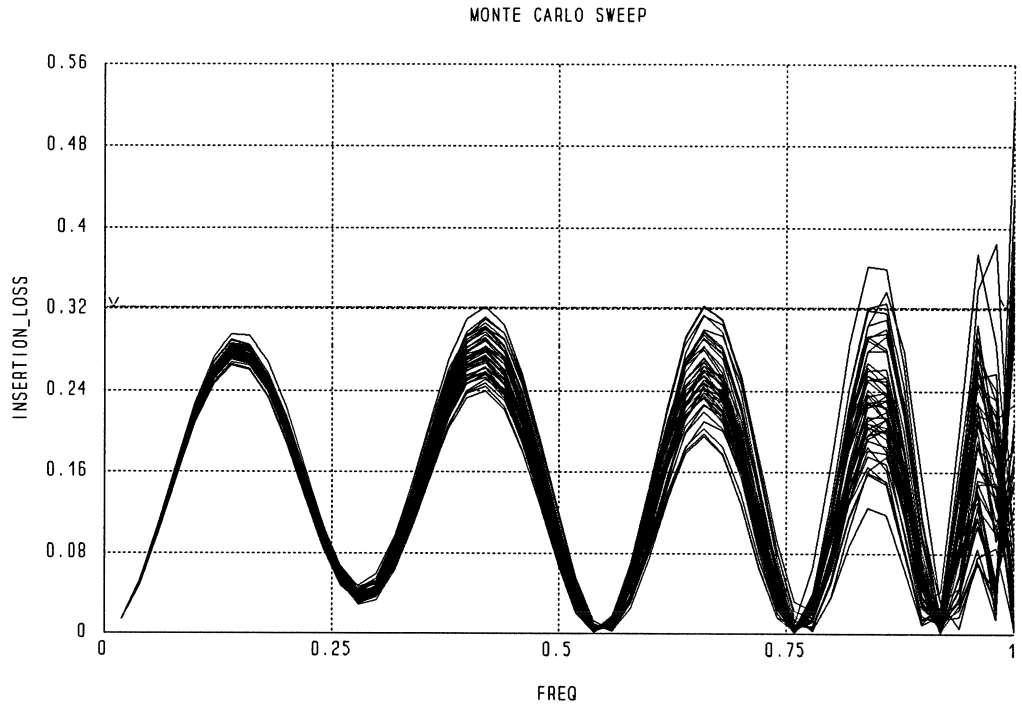

demo11

Harmonic balance simulation of a nonlinear FET circuit. The *MGF1902* FET is modeled using the built-in FETM.

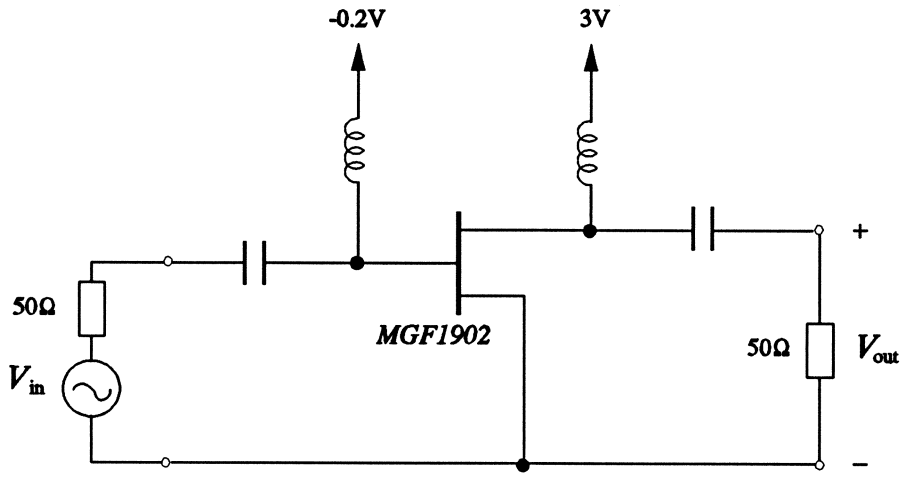

Input File

```
!  Example  demo11.ckt
!  demonstrate circuit simulation
!  harmonic balance analysis.  power sweep
!  the FET model for Mitsubishi MGF1902 is extracted by HarPE

Model
   CAP 1 2 C=1000pF;

   Extrinsic4  20 30 40 2 3
      RG=5          RD=0.2      RS=1.5     LS=0.0948NH
      LG=0.53633NH  LD=0.936NH  GDS=0.002  CDS=0.0278PF
      CDE=0.0682pF  CX=10pF;

   FETM  20 30 40
      E=1.4  SL=0.126  IB0=8e-12    ALPHAB=1     VBC=6
      GAMMA=-0.06356   K1=2         CF0=0.02PF   KF=-0.157
      IDSS=0.04716     VP0=-0.7338  R10=0.00343  C10=0.6294PF;

   CAP 2 0 C=0.184pF;  ! FET parasitic
   CAP 3 0 C=0.216pF;

   CAP 3 4 C=1000pF;

   Input_Power: 0;

   PORT 1 0  NAME=input P[1]=Input_Power;

   PORT 4 0 NAME=output;

   IND 2 200 L=1000nH;
   VSOURCE 200 0 NAME=gate VDC=-0.2;

   IND 3 300 L=1000nH;
   VSOURCE 300 0 NAME=drain VDC=3;
```

```
   CIRCUIT;

   Poutput[0:N_SPECTRA] = if (PWoutput > 0) (10 * log10(PWoutput) + 30);
end

Sweep
   HB: FREQ=2GHZ  Input_Power: from -12dBM to 6DBM step=3dBM
       MVoutput PVoutput Poutput[1] Poutput[2] Poutput[3]
       {Waveform  Spectrum=(MVoutput, PVoutput)."Voutput_T"
        Title="Power Sweep Output Voltage Waveforms"
        Input_Power=all  Tmin=0  Tmax=1  NT=100
        Ymin=-2.5  Ymax=2.5  NYticks=5}
       {Xsweep  Title="Output Power Spectra vs. Input Power Sweep"
        Y = Poutput[1] & Poutput[2] & Poutput[3]
        Y_Title = "Output Power Spectra"
        X_Title = "Available Input Power in dBm"
        Input_Power=all
        Ymin=-40  Ymax=20  NYticks=6  NXticks=6};
end
```

Output Voltage Waveforms at Different Input Power Levels

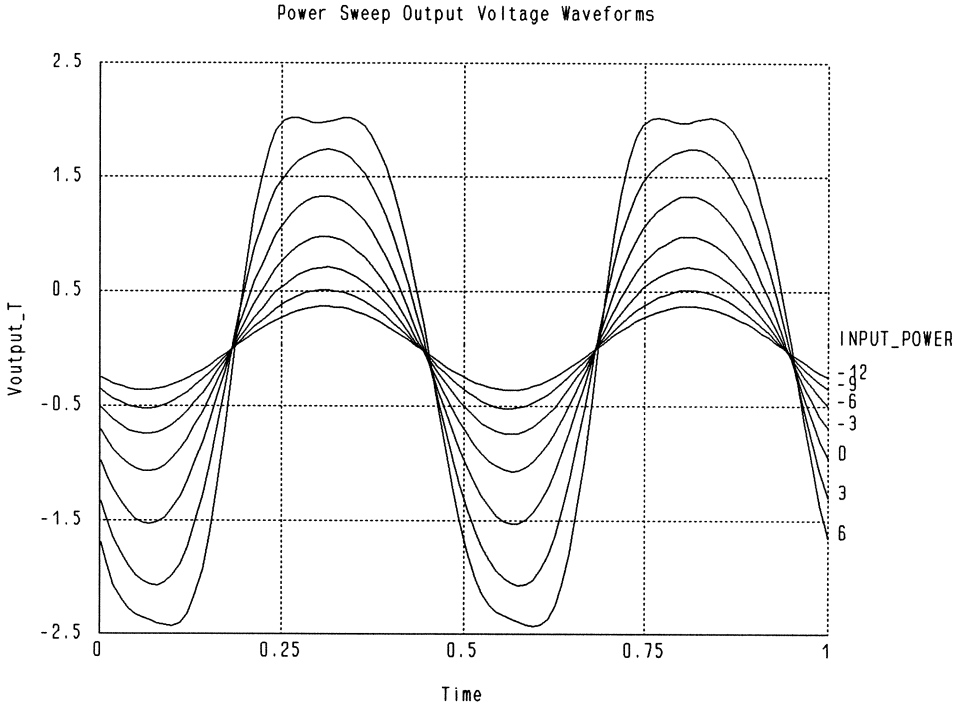

Output Power Spectrum versus Input Power Level

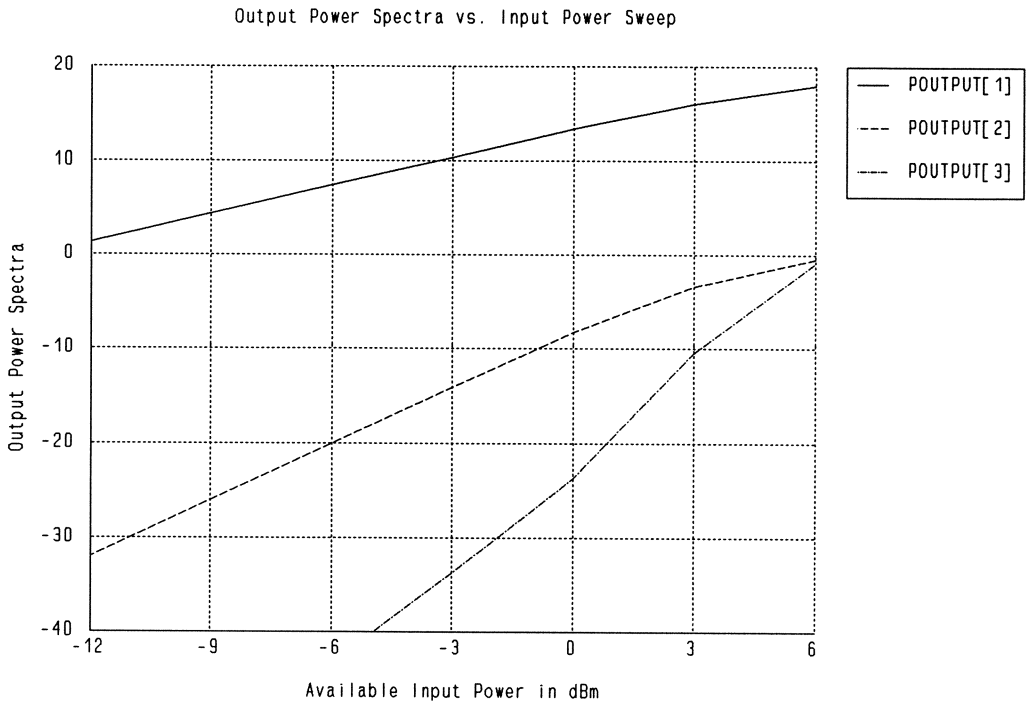

demo12

Minimax optimization of a small-signal amplifier. The nonlinear FETR model parameters are extracted by HarPE from *NEC700* data.

For small-signal analysis, OSA90 first solves the nonlinear DC circuit and then linearizes the nonlinear FET model at the DC operating point.

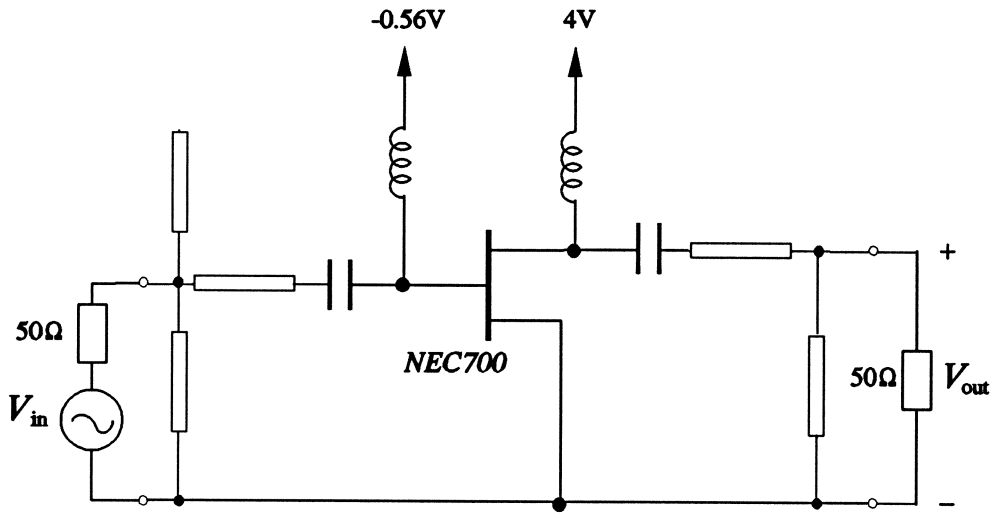

Input File

```
!  Example  demo12.ckt
!  Minimax optimization of small-signal amplifier
!  FETR model extracted by HarPE from NEC700 data
!  Large-signal compression is also simulated

Model
   ! optimize the electric lengths of two transmission lines

   TEM  @input  0  Z=70  E=?125?  F=18GHZ;
   TEM  @output 0  Z=50  E=?80?  F=18GHZ;

   TEM   @input @open1 0 @open2  Z=100 E=65 F=18GHZ;
   OPEN  @open1 @open2;

   TEM  @input @DC_block1  Z=100 E=25 F=18GHZ;

   ! FET model

   CAP @DC_block1 @FET_input  C=10NF;
   IND @Gate_bias @FET_input  L=100NH;

   Extrinsic2  @intrin1 @intrin2 @intrin3 @FET_input @FET_output
      RG=3.5   LG=0.0306NH  RD=0.5       LD=0.00792NH
      RS=4.73  LS=0.0451NH  GDS=0.00345  CDS=0.08738PF  CX=10PF;

   FETR  @intrin1 @intrin2 @intrin3
      IS=5E-15    N=1         FC=0.5          GMIN=1.0E-07
      VBI=0.8     VBR=20.0    ALPHA=2         THETA=0.003
      BETA=0.029  VT0=-1.637  LAMBDA=0.04978  TAU=2.8PS
```

```
      CGS0=0.4428PF  CGD0=0.1066PF;

   CAP @FET_output @DC_block2   C=10NF;
   IND @FET_output @Drain_bias  L=100NH;

   TEM  @DC_block2 @output  Z=100 E=15 F=18GHZ;

   VSOURCE  @Gate_bias  0  VDC=-0.56;
   VSOURCE  @Drain_bias 0  VDC=4;

   Pin: 5dBm;

   PORT  @input  0  P[1]=Pin;
   PORT  @output 0  NAME=OUT;

   CIRCUIT;

   MS21_DB: 20 * LOG10(MS21);

   upper_spec: if (FREQ >= 6GHZ & FREQ <= 18) (9) else (NAN);
   lower_spec: if (FREQ >= 6GHZ & FREQ <= 18) (7) else (NAN);

   Pout = 10 * log10(PWout[1]) + 30;
   Power_Gain = Pout - Pin;
end

Sweep
   AC:  FREQ: from 4GHZ to 20GHZ Step=1GHZ
        MS21_DB  lower_spec  upper_spec
        {Xsweep Title="Amplifier Small-Signal Gain"
         Y=MS21_DB.green & lower_spec.red & upper_spec.red
         Y_title="|S21| (dB)"  Ymin=0  NXticks=8};

   HB:  FREQ=8GHZ  Pin: from -9 to 3 step=3  from 4 to 9 step=1
        Pout, Power_Gain, MVout, PVout
        {Xsweep title="Amplifier 1dB Compression at 8GHZ"
         Y=Pout & Power_Gain  Ymin=0 Ymax=15 NYticks=15  NXticks=6}
        {WAVEFORM  title="Large-Signal Harmonic Distortion: Output Voltage"
         Spectrum=(MVout, PVout)."Vout_T"  Pin=5dBm
         Tmin=0 Tmax=0.25 NT=100  Ymin=-2 Ymax=2 NYticks=4  NXTicks=5};
end

Spec
   AC:  FREQ: from 6 to 18 Step=1
        MS21_DB > lower_spec   MS21_DB < upper_spec;
end

Control
   Optimizer=Minimax;
end
```

Small-Signal Amplifier Gain After Minimax Optimization

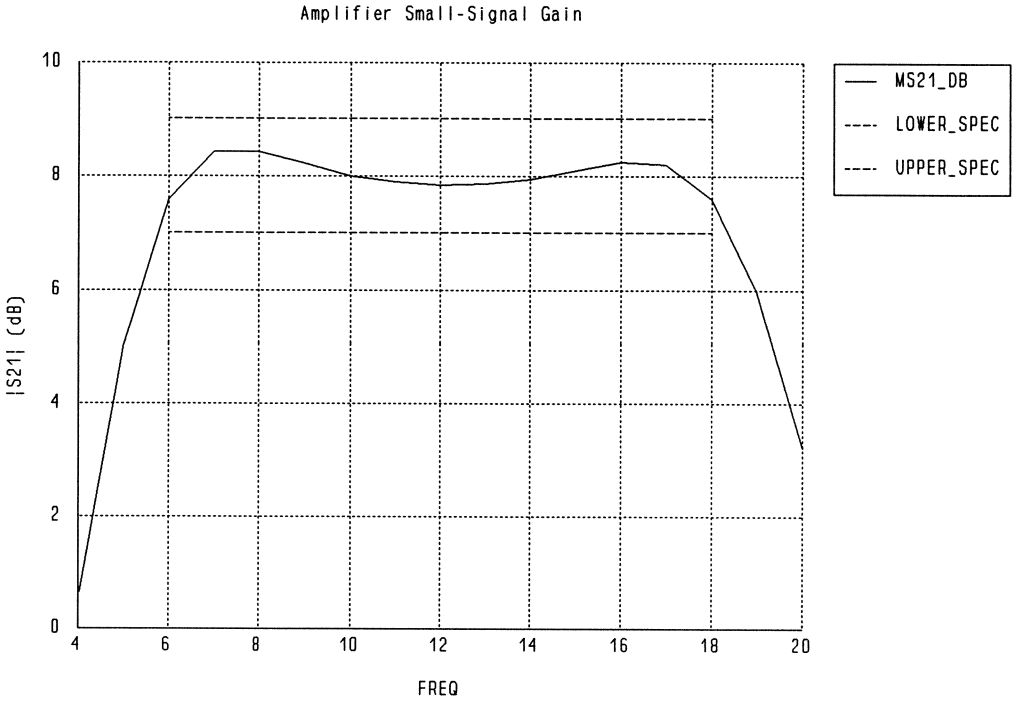

demo13

Minimax optimization of a small-signal balanced amplifier. This example uses the same design specifications as for demo12, but employs a balanced structure with 2 FETs and Lange couplers.

The nonlinear FETR model parameters are extracted by HarPE from *NEC700* data.

For small-signal analysis, OSA90 first solves the nonlinear DC circuit and then linearizes the nonlinear FET model at the DC operating point.

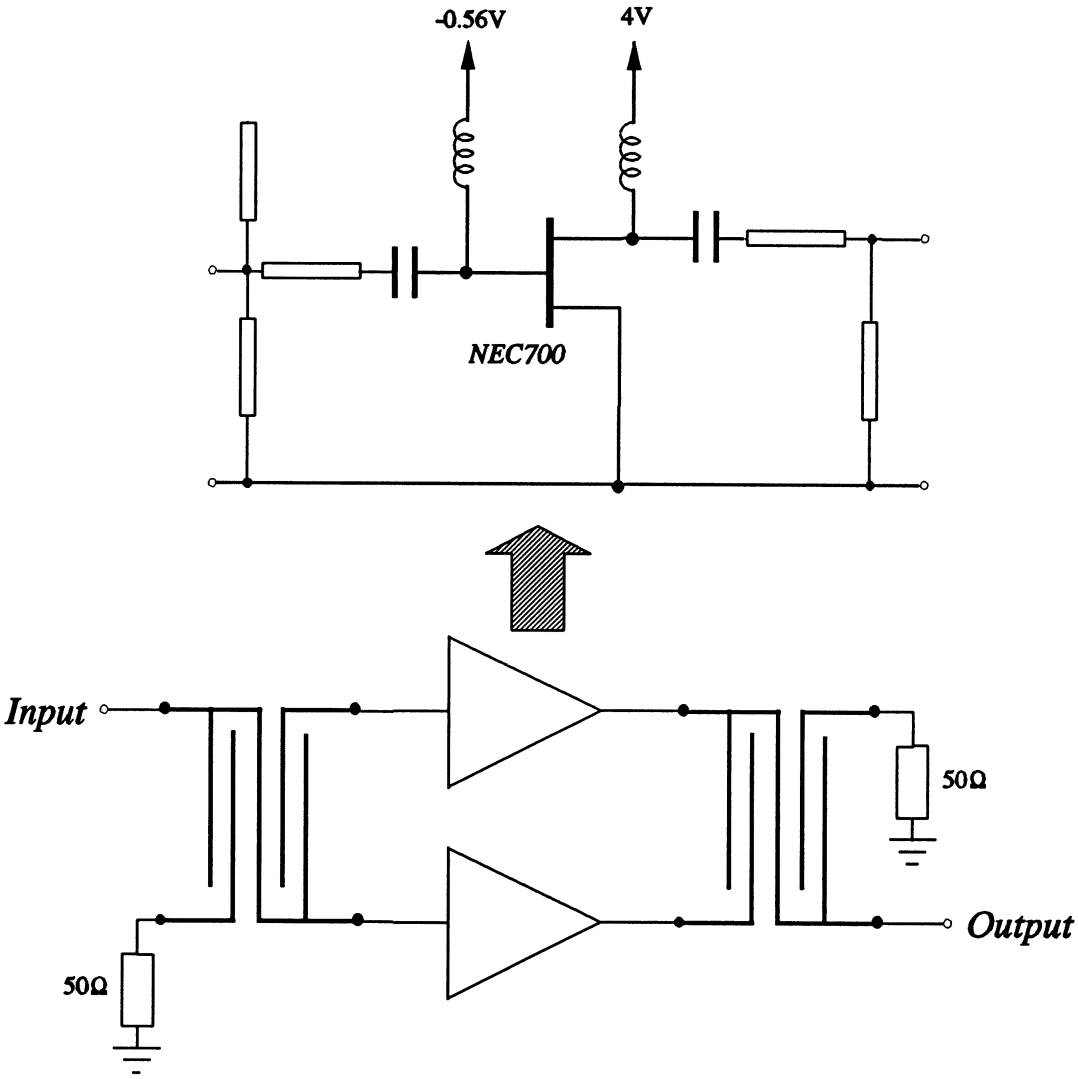

Input File

```
!  Example  demo13.ckt
!  Minimax optimization of small-signal balanced amplifier
!  the two amplifiers used in the balanced configuration are
!  originally optimized in demo12
!  FETR model extracted by HarPE from NEC700 data
!  Large-signal compression is also simulated

#define  Amplifier(input,output,$) {
   ! the electric lengths of two transmission lines are variables

   TEM   input  0  Z=70  E=X1  F=18GHZ;
   TEM   output 0  Z=50  E=X2  F=18GHZ;

   TEM   input @open1$ 0 @open2$  Z=100 E=65 F=18GHZ;
   OPEN  @open1$ @open2$;

   TEM   input @DC_block1$  Z=100 E=25 F=18GHZ;

   ! FET model

   CAP @DC_block1$ @FET_input$  C=10NF;
   IND @Gate_bias  @FET_input$  L=100NH;

   Extrinsic2  @gate$ @drain$ @source$ @FET_input$ @FET_output$
      RG=3.5   LG=0.0306NH  RD=0.5       LD=0.00792NH
      RS=4.73  LS=0.0451NH  GDS=0.00345  CDS=0.08738PF  CX=10PF;

   FETR  @gate$ @drain$ @source$
      IS=5E-15    N=1         FC=0.5          GMIN=1.0E-07
      VBI=0.8     VBR=20.0    ALPHA=2         THETA=0.003
      BETA=0.029  VT0=-1.637  LAMBDA=0.04978  TAU=2.8PS
      CGS0=0.4428PF  CGD0=0.1066PF;

   CAP  @FET_output$ @DC_block2$  C=10NF;
   IND  @FET_output$ @Drain_bias  L=100NH;

   TEM  @DC_block2$ output  Z=100 E=15 F=18GHZ;
}

Model
   MSUB  EPSR=9.9 H=25MIL T=0.2MIL ROC=2.44e-8 RHS=0;

   SUBCIRCUIT LANGE_COUPLER 1 2 3 4 0 {
      MLANG4 1 2 3 4  W=1.4MIL S=1MIL L=97MIL;
   };

   X1: ?128?;
   X2: ?61.7?;

   Amplifier(@amp1_in, @amp1_out, 1);
   Amplifier(@amp2_in, @amp2_out, 2);

   LANGE_COUPLER @input @amp2_in @load1 @amp1_in 0;
   LANGE_COUPLER @amp2_out @load2 @amp1_out @output 0;

   RES @load1 0  R=50;  ! matched terminations
   RES @load2 0  R=50;

   VSOURCE  @Gate_bias  0  VDC=-0.56;
   VSOURCE  @Drain_bias 0  VDC=4;

   Pin: 5dBm;

   PORT  @input  0  P[1]=Pin;
   PORT  @output 0  NAME=OUT;

   CIRCUIT;
```

```
   MS21_DB: 20 * LOG10(MS21);

   upper_spec: if (FREQ >= 6GHZ & FREQ <= 18) (9) else (NAN);
   lower_spec: if (FREQ >= 6GHZ & FREQ <= 18) (7) else (NAN);

   Pout = 10 * log10(PWout[1]) + 30;
   Power_Gain = Pout - Pin;
end

Sweep
   AC:  FREQ: from 4GHZ to 20GHZ Step=1GHZ
        MS21_DB  lower_spec  upper_spec
        {Xsweep Title="Amplifier Small-Signal Gain"
         Y=MS21_DB.green & lower_spec.red & upper_spec.red
         Y_title="|S21| (dB)"  Ymin=0  NXticks=8};

   HB:  FREQ=8GHZ  Pin: from -9 to 3 step=3  from 4 to 9 step=1
        Pout, Power_Gain, MVout, PVout
        {Xsweep title="Amplifier 1dB Compression at 8GHZ"
         Y=Pout & Power_Gain  Ymin=0 Ymax=16 NYticks=16  NXticks=6}
        {WAVEFORM  title="Large-Signal Harmonic Distortion: Output Voltage"
         Spectrum=(MVout, PVout)."Vout_T"  Pin=5dBm
         Tmin=0 Tmax=0.25 NT=100  Ymin=-2 Ymax=2 NYticks=4  NXTicks=5};
end

Spec
   AC:  FREQ: from 6 to 18 Step=1
        MS21_DB > lower_spec   MS21_DB < upper_spec;
end

Control
   Optimizer=Minimax;
end
```

Small-Signal Amplifier Gain After Minimax Optimization

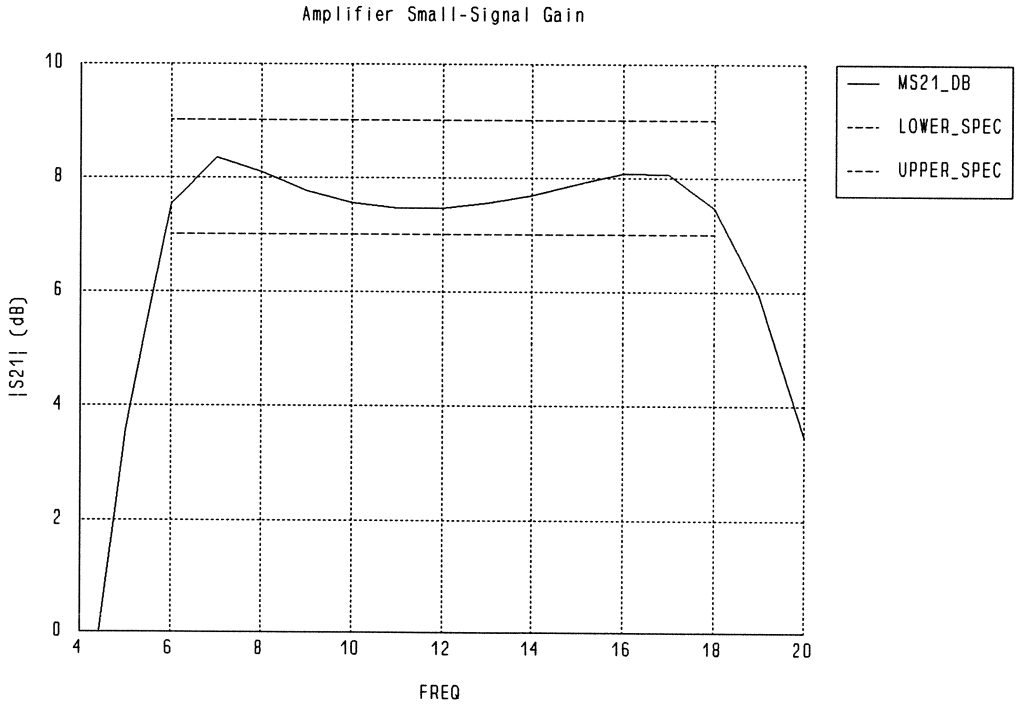

Balanced Amplifier Extends 1-dB Compression Point

Compared with the single FET amplifier in demo12, the balanced design in this example extends the 1-dB compression point under large-signal input.

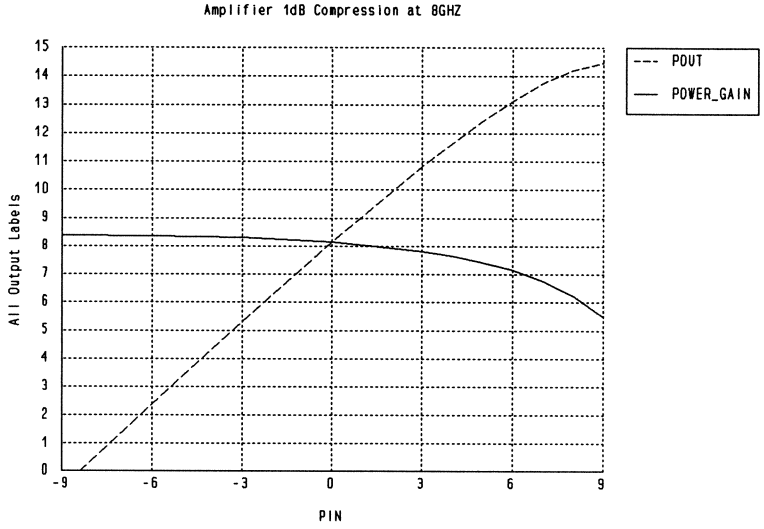

The 1-dB compression point for the single-FET amplifier of demo12 *is 12dBm output power (5dBm available input power) at 8GHz.*

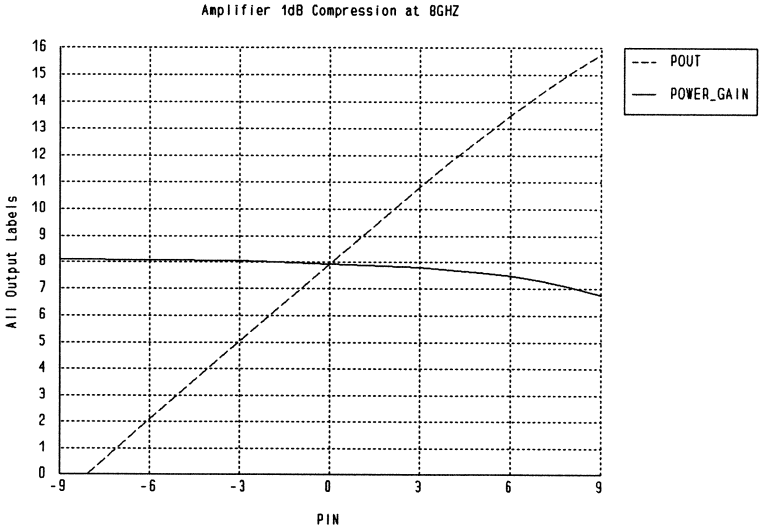

The balanced amplifier of demo13 *extends the 1-dB compression point by 3dB, to 15dBm output power (8dBm available input power).*

Output Voltage Waveforms

The higher 1-dB compression point achieved by the balanced amplifier means that, at a given input power level, the harmonic distortion at the output is reduced as compared with the single-FET amplifier.

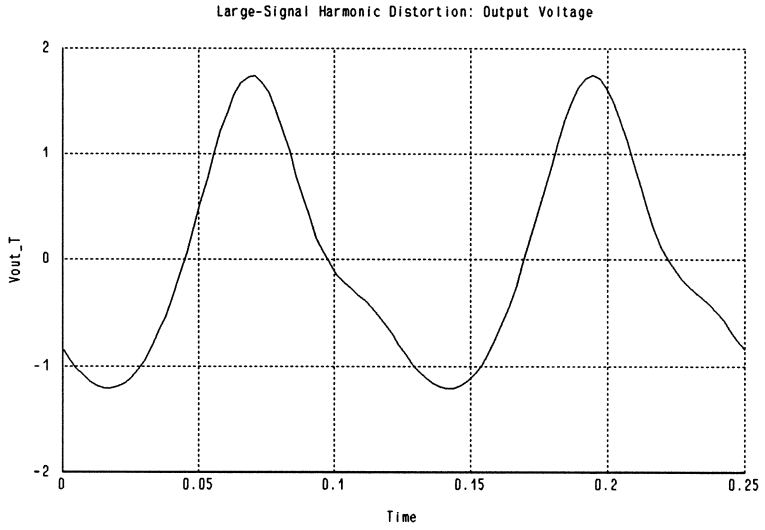

The output voltage waveform of the single-FET amplifier in demo12 *shows obvious harmonic distortion for 5dBm input power (1-dB compression point) at 8GHz.*

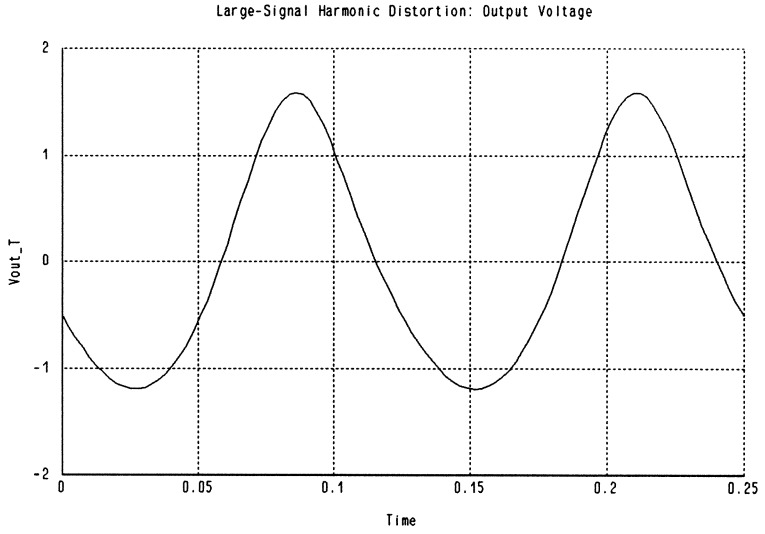

At the same 5dBm input power level, the output voltage harmonic distortion is reduced by the balanced structure in demo13.

demo14

Harmonic balance simulation of a simple FET circuit for estimating harmonic intercept points under large-signal excitation.

Also illustrated is the preprogrammed Curtice symmetrical model using the user-definable model FETU1. The model parameters are extracted by HarPE from measured power spectrum data (HarPE example demo02).

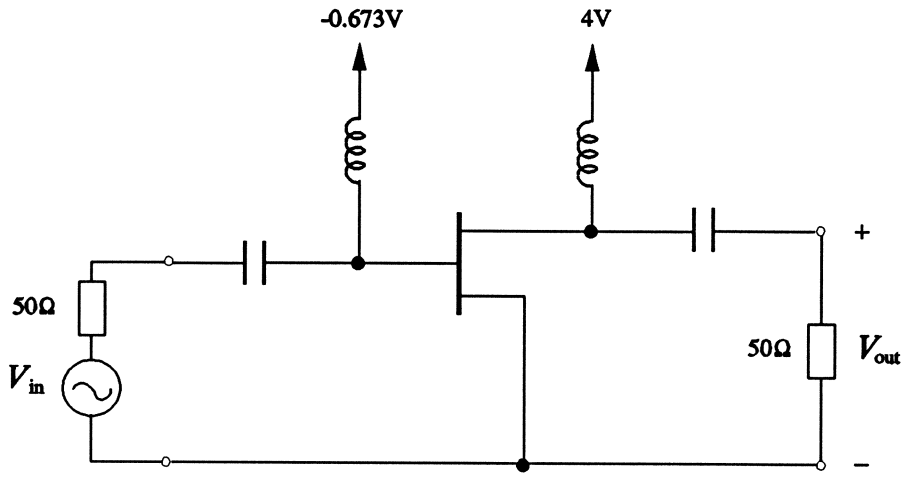

Input File

```
!  Example  demo14.ckt
!  harmonic balance analysis
!  check the harminic intercept points for the 2nd and 3rd harmonics
!  Preprogrammed Curtice cubic symmetrical FET model
!  using user-definable model FETU1
!  the formulas are in the file curtsym.inc

Model
   Extrinsic2    @gate @drain @source @ext_gate @ext_drain
      LG: 0.338NH     RG: 4.063    RD: 0.01
      LD: 0.254NH     RS: 2.49     LS: 0.08NH
      GDS: 0.2e-3     CX: 1.5PF    CDS: 0.1PF;

   ! user created FET model

   BETA: 0.03;       VDS0: 2;          IS0: 1e-14;    N: 1;
   CGS0: 0.545PF;    CGD0: 0.092PF;    FC: 0.77;      GMIN: 1.0E-07;
   VBI: 0.8;         VBR: 30;          K: 1.381;      Q: 16020;
   TEMP: 298;        A0: 0.06754;      A1: 0.05691;   A2: -5.396e-05;
   A3: -0.006768;    GAMMA: 7.143;

   VLABEL @gate @source  NAME=VGS_T;
   VLABEL @drain @source  NAME=VDS_T;
   VLABEL @gate @source  NAME=VGS_TAU  TAU=3PS;

   #include "curtsym.inc"    ! formulas of the Curtice symmetric model

   FETU1  @gate @drain @source
      IDS: IDS_MODEL
      IGS = (Diode_Current(VGS_T))
```

```
        IGD = (Diode_Current(VGD_T))
        QGS = (Charge(CGS0, VGS_T))
        QGD = (Charge(CGD0, VGD_T));

    IND @ext_gate @gate_bias L=100nH;
    VSOURCE @gate_bias @ground  NAME=gate  VDC=-0.673;

    IND @ext_drain @drain_bias L=100nH;
    VSOURCE @drain_bias @ground  NAME=drain  VDC=4;

    Power_Input: 0;

    CAP @ext_gate @input  C=10nF;
    PORT @input @ground  NAME=input_port  P[1]=Power_Input;

    CAP @ext_drain @output  C=10nF;
    PORT @output @ground  NAME=output_port;

    CIRCUIT;

   Power_Output[0:N_SPECTRA] = 10 * log10(PWoutput_port) + 30;
end

Sweep
   HB:  FREQ: 2GHZ  Power_Input: from -30DBM to 10DBM step=5DBM
        Power_Output[1]  Power_Output[2]  Power_Output[3];
end
```

Harmonic Intercept Points Can Be Estimated by Extrapolation

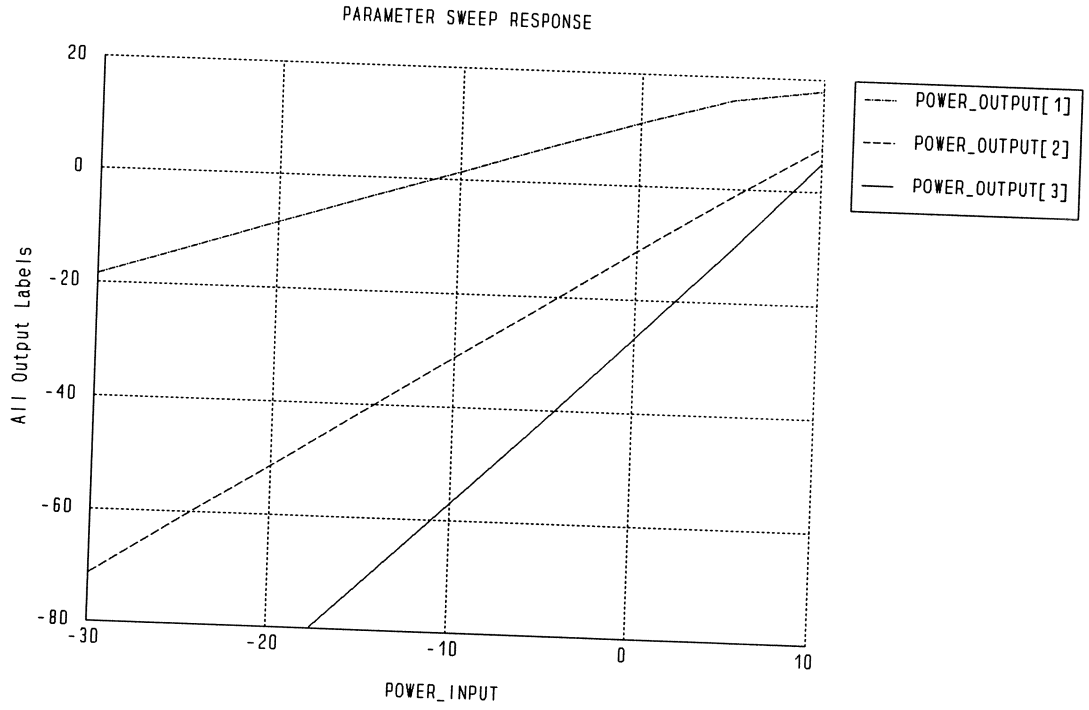

demo15

Harmonic balance simulation of a simple FET circuit for estimating harmonic intercept points under large-signal.

Also illustrated is the preprogrammed Curtice asymmetrical model using the user-definable model FETU2.

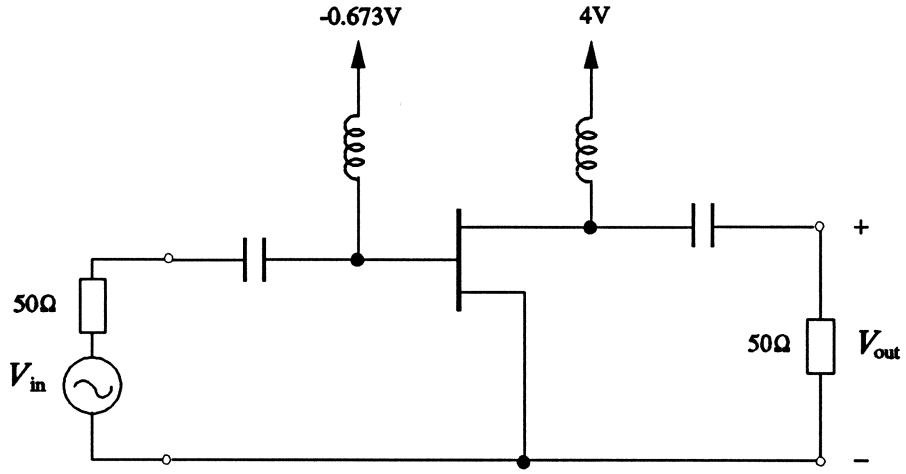

Input File

```
!  Example  demo15.ckt
!  harmonic balance analysis
!  check the harminic intercept points for the 2nd and 3rd harmonics
!  Preprogrammed Curtice cubic asymmetrical FET model
!  using user-definable model FETU2
!  the formulas are in the file curtasy.inc
!  similar to demo14 which uses the symmetrical model

Model
   Extrinsic2    @gate @drain @source @ext_gate @ext_drain
      LG: 0.338NH    RG: 3.063   RD: 0.01
      LD: 0.254NH    RS: 2.49    LS: 0.08NH
      GDS: 0.2e-3    CX: 1.5PF   CDS: 0.1PF;

   ! user created FET model

   BETA: 0.03;      VDS0: 2;         IS0: 1e-14;   N: 1;
   CGS0: 0.545PF;   CGD0: 0.092PF;   FC: 0.77;     GMIN: 1.0E-07;
   VBI: 0.8;        VBR: 30;         K: 1.381;     Q: 16020;
   TEMP: 298;       A0: 0.06754;     A1: 0.05691;  A2: -5.396e-05;
   A3: -0.006768;   GAMMA: 7.143;    RIN: 1;

   VLABEL @gate  @source    NAME=VGS_T;
   VLABEL @drain @source    NAME=VDS_T;
   VLABEL @gate  @internal  NAME=VGG_TAU  TAU=3PS;
   VLABEL @gate  @internal  NAME=VGG_T;

   #include "curtasy.inc"   ! model equations

   FETU2  @gate @drain @source @internal
          IDS  = IDS_MODEL
```

```
            IRIN = IRIN_MODEL
            IGG  = (Diode_Current(VGG_T))
            IDG  = (-Diode_Current(VGD_T))
            QGG  = (Charge(CGS0, VGG_T))
            QDG  = (-Charge(CGD0, VGD_T));

    IND @ext_gate @gate_bias L=100nH;
    VSOURCE @gate_bias @ground  NAME=gate  VDC=-0.673;

    IND @ext_drain @drain_bias L=100nH;
    VSOURCE @drain_bias @ground  NAME=drain  VDC=4;

    Power_Input: 0;

    CAP @ext_gate @input  C=10nF;
    PORT @input @ground  NAME=input_port  P[1]=Power_Input;

    CAP @ext_drain @output  C=10nF;
    PORT @output @ground  NAME=output_port;

    CIRCUIT;

   Power_Output[0:N_SPECTRA] = 10 * log10(PWoutput_port) + 30;
end

Sweep
   HB:  FREQ: 2GHZ  Power_Input: from -30DBM to 10DBM step=5DBM
        Power_Output[1]  Power_Output[2]  Power_Output[3];
end
```

Harmonic Intercept Points Can Be Estimated by Extrapolation

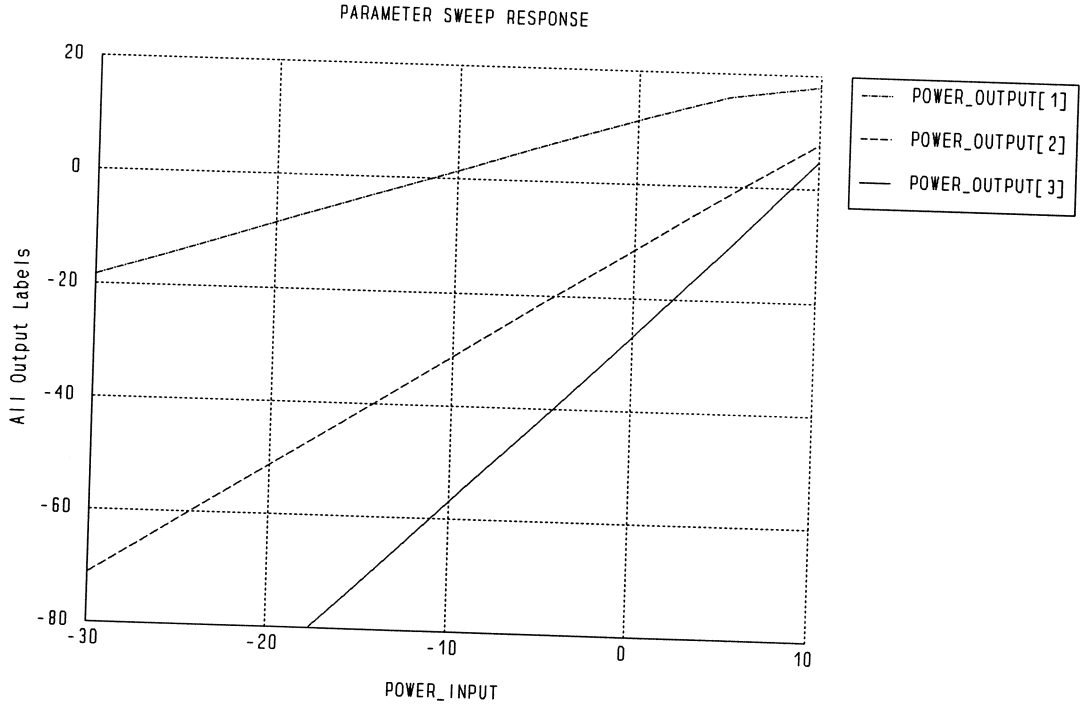

demo16

Illustration of the preprogrammed Materka FET model. This example is identical to demo12 except that the built-in FETR model is replaced by the user-definable FETU2 model. The preprogrammed Materka model equations are supplied in the file "materka.inc".

Minimax optimization is performed to design the 6-18GHz small-signal amplifier.

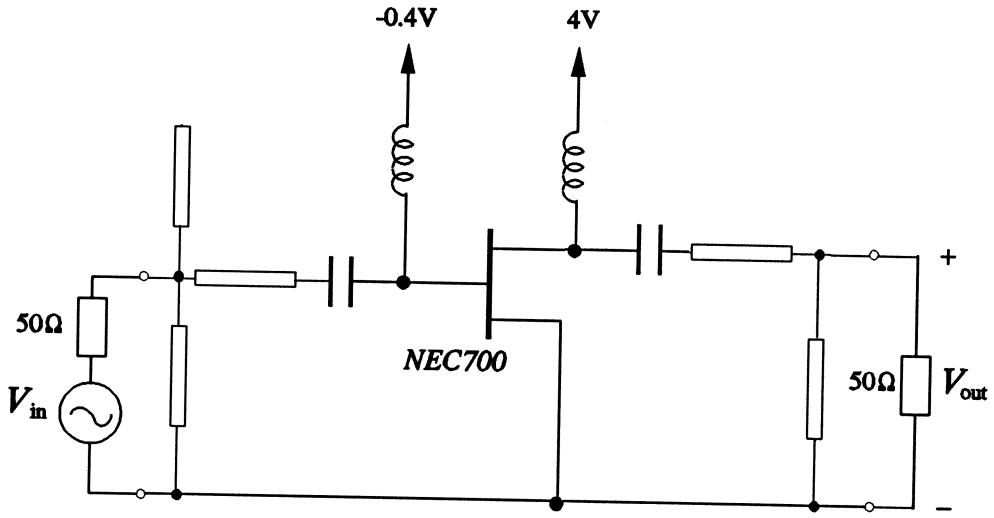

Input File

```
!  Example  demo16.ckt
!  adapted from demo12 to illustrate preprogrammed Materka FET model
!  using user-definable FETU2.
!  The model equations are in the file materka.inc
!  Minimax optimization of small-signal amplifier

Model
   ! optimize the electric lengths of two transmission lines

   TEM  @input  0  Z=70  E=?125?  F=18GHZ;
   TEM  @output 0  Z=50  E=?80?  F=18GHZ;

   TEM   @input @open1 0 @open2  Z=100 E=65 F=18GHZ;
   OPEN  @open1 @open2;

   TEM  @input @DC_block1  Z=100 E=22.5 F=18GHZ;

   ! FET model

   CAP @DC_block1 @FET_input  C=10NF;
   IND @Gate_bias @FET_input  L=100NH;

   Extrinsic2  @gate @drain @source @FET_input @FET_output
      RG=3.66   RD=2          LG=0.0432NH  LD=0.0795NH
      RS=3.24   LS=0.0578NH  GDS=0.00269  CDS=0.08388PF  CX=10pF;

   GAMMA=-0.05;   E=2;           KE=0;          SL=0.2;
   SS=0;          IG0=5E-10;     ALPHAG=20;     IB0=8e-12;
   ALPHAB=1;      VBC=20;        KR=0;          K1=1;
   C1S=0.0048PF;  CF0=0.026PF;   KF=-0.12;      IDSS=0.063;
```

```
    VP0=-1.5;      R10=0.0117;   C10=0.3598PF;  KG=0;

    VLABEL @gate @source  NAME=VGS_T;
    VLABEL @drain @source  NAME=VDS_T;
    VLABEL @gate @internal  NAME=VGG_TAU  TAU=2PS;
    VLABEL @gate @internal  NAME=VGG_T;

    #include "materka.inc";    ! model equations

    FETU2  @gate @drain @source @internal
           IGG: IGG_MODEL  IDS: IDS_MODEL
           IDG: IDG_MODEL  IRIN: IRIN_MODEL
           QGG: QGG_MODEL  QDG: QDG_MODEL;

    CAP @FET_output @DC_block2   C=10NF;
    IND @FET_output @Drain_bias  L=100NH;

    TEM  @DC_block2 @output  Z=100 E=15 F=18GHZ;

    VSOURCE  @Gate_bias  0  VDC=-0.4;
    VSOURCE  @Drain_bias 0  VDC=4;

    PORT  @input  0  P[1]=9DBM;
    PORT  @output 0  NAME=OUT;

    CIRCUIT;

    MS21_DB: 20 * LOG10(MS21);

    upper_spec: if (FREQ >= 6GHZ & FREQ <= 18) (8.25) else (NAN);
    lower_spec: if (FREQ >= 6GHZ & FREQ <= 18) (7) else (NAN);
end

Sweep
   AC:  FREQ: from 4GHZ to 20GHZ Step=1GHZ
        MS21_DB  lower_spec  upper_spec
        {Xsweep Title="Amplifier Small-Signal Gain"
         Y=MS21_DB.green & lower_spec.red & upper_spec.red
         Y_title="|S21| (dB)"  Ymin=0  NXticks=8};

   HB:  FREQ: 8GHZ  PVout, MVout
        {WAVEFORM  title="Large-Signal Harmonic Distortion: Output Voltage"
         Spectrum=(MVout, PVout)."Vout_T"
         Tmin=0 Tmax=0.25 NT=100  Ymin=-3 Ymax=3 NYticks=6  NXTicks=5};
end

Spec
   AC:  FREQ: from 6 to 18 Step=1
        MS21_DB > lower_spec   MS21_DB < upper_spec;
end

Control
   Optimizer=Minimax;
end
```

Small-Signal Amplifier Gain After Minimax Optimization

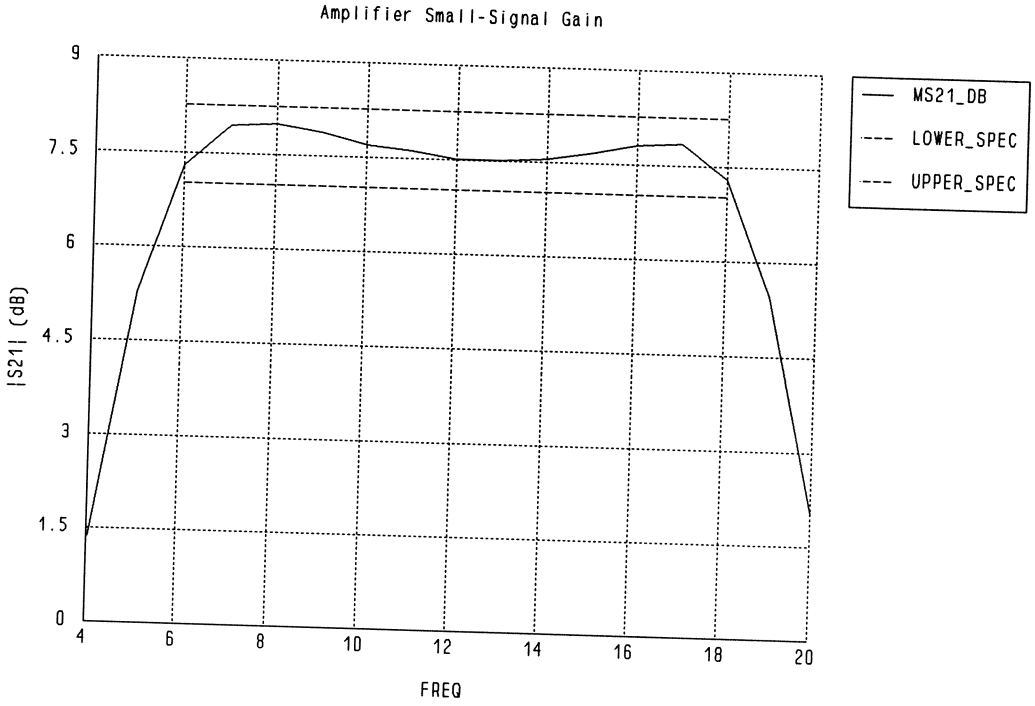

demo17

Illustration of the preprogrammed Plessey FET model.

The Plessey FET model (a modified version of the Raytheon-Statz model) is preprogrammed using the user-definable FETU1 model. The model equations are supplied in the include file "plessey.inc".

The model parameters are extracted by HarPE from DC measurements.

Input File

```
! Example  demo17.ckt
! illustrate preprogrammed Plessey model using user-definable FETU1

Model
   ! DC measurement data for  VDS = 0, 1, 2, 3, 5, 8, 10, 12

   VGS[5] = [-2  -1.5  -1  -0.5  0];
   IDS[5,8] = [0.0  0.0  0.0  0.1  0.5  3.7  8.0 12.4
               0.0  3.1  4.2  5.2  7.4 14.0 18.5 23.0
               0.1 15.7 17.5 18.8 21.2 27.3 31.1 35.0
               0.1 33.3 35.5 36.7 38.4 42.3 44.7 47.4
               0.2 53.6 56.8 57.5 57.9 58.5 59.0 59.9];

   ! Plessey model parameters

   THETA: ?0.320652?;
   VTO: ?-1.81628?;
   LAMBDA: ?-0.0829165?;
   ALPHA: ?2.51312?;
   GDST: ?0.0053694?;
   B: ?0.0304724?;
   BETA: ?0.0322512?;
   ISS: 5E-15;
   N: 1;
   FC: 0.5;
   GMIN: 1.0E-07;
   VBI: 0.8;
   VBR: 20.0;
   TAU: 3PS;
   CGS0: 0.488PF;
   CGD0: 0.0968PF;

   VLABEL 1 3  NAME=VGS_T;
   VLABEL 1 3  NAME=VGS_TAU TAU=TAU;
   VLABEL 2 3  NAME=VDS_T;

   #include "plessey.inc"

   Extrinsic1 1 2 3 4 5
      RS: 3       RD: 3.5      RG: 0.5
      LG: 0.39NH  LD: 0.337NH  LS: 0.1NH
      CDS: 0.0989PF;

   FETU1  1 2 3
      IDS=IDS_MODEL  IGS=IGS_MODEL   IGD=IGD_MODEL
      QGS=QGS_MODEL  QGD=QGD_MODEL;

   I: 1;
   VDS: 0;

   VSOURCE 4 0  NAME=GATE  VDC=VGS[I];
   VSOURCE 5 0  NAME=DRAIN  VDC=VDS;
```

```
    CIRCUIT;

    ID_mA: IDRAIN_DC * 1000.0;

    ! check if we have data for a given value of VDS

    VDS_map[0:12] = [1 2 3 4 0 5 0 0 6 0 7 0 8];
    VDS_int = floor(VDS);
    VDS_index: if (VDS >= 0 & VDS <= 12 & VDS = VDS_int) (VDS_map[VDS_int]);

   ID_data: if (VDS_index) (IDS[I,VDS_index]) else (NAN);
end

Sweep
   DC: I: from 1 to 5 step=1
       VDS: from 0 to 2 step=0.2  from 3 to 12 step=1
       ID_mA  ID_data
       {Xsweep  Title="Plessey Model Fitting DC Measurement"
        X=VDS I=all NXticks=6 Y_title="ID (mA)"
        Y=ID_mA.green & ID_data.white.circle  Ymin=0 Ymax=70 NYTicks=7};
end
```

Preprogrammed Plessey Model Fitting Measured DC Data

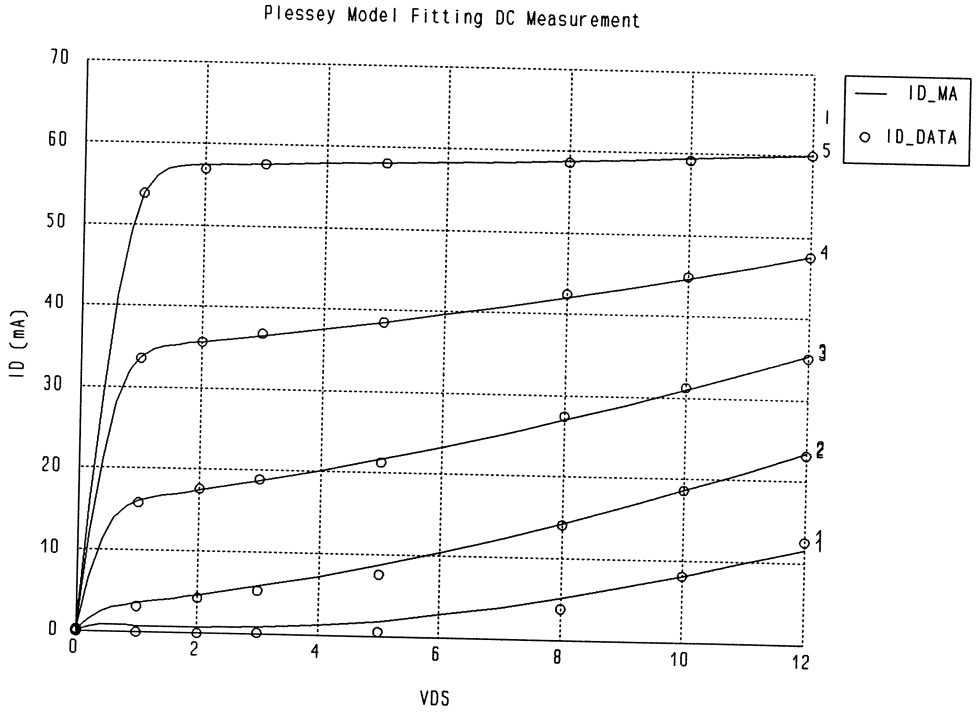

demo18

Illustration of the preprogrammed TriQuint's TOM FET model.

The TOM model (a modified version of the Raytheon-Statz model) is preprogrammed using the user-definable FETU1 model. The model equations are supplied in the include file "tom.inc".

The model parameters are extracted by HarPE from *S*-parameter measurements.

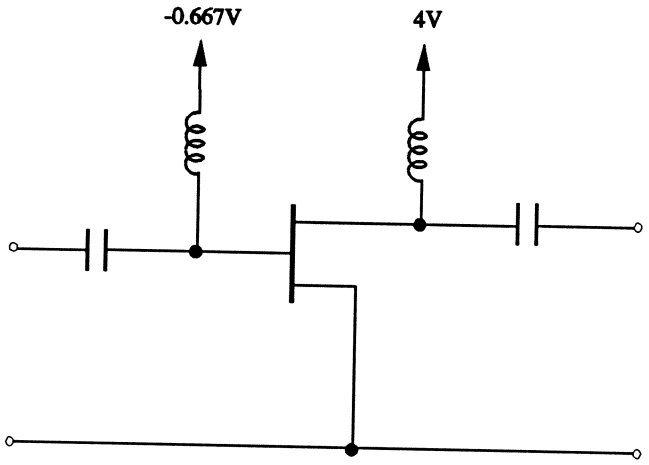

Input File

```
!  Example  demo18.ckt
!  illustrate preprogrammed TOM model (TriQuint's Own Model)
!  using user-definable FETU1

Model
   ! TOM model parameters

   VTO: ?-1.73739?;
   ALPHA: 2;
   BETA: ?0.0387839?;
   DELTA: ?0.12335?;
   GAMMA: ?0.0439447?;
   ISS: 5E-15;
   N: 1;
   FC: 0.5;
   GMIN: 1.0E-07;
   VBI: 0.8;
   VBR: 20.0;
   TAU: ?4.58553PS?;
   CGS0: ?0.708439PF?;
   CGD0: ?0.0970303PF?;

   VLABEL 1 3  NAME=VGS_T;
   VLABEL 1 3  NAME=VGS_TAU TAU=TAU;
   VLABEL 2 3  NAME=VDS_T;

   #include "tom.inc";
```

```
    Extrinsic2   1 2 3 4 5
       CX: 20PF    RG: 4     RD: 0.05
       LG: ?0.317556NH?
       LD: ?0.189109NH?
       RS: ?4.89522?
       LS: ?0.087396NH?
       GDS: ?0.00201215?
       CDS: ?0.100811PF?;

    FETU1  1 2 3
       IDS=IDS_MODEL  IGS=IGS_MODEL    IGD=IGD_MODEL
       QGS=QGS_MODEL  QGD=QGD_MODEL;

    VG: -0.667;
    VD: 4;

    CAP 4 40 C=10nF;
    CAP 5 50 C=10nF;
    IND 4 41 L=1mH;
    IND 5 51 L=1mH;

    VSOURCE 41 0  NAME=GATE  VDC=VG;
    VSOURCE 51 0  NAME=DRAIN  VDC=VD;

    PORT 40 0;
    PORT 50 0;

    CIRCUIT;

    ID_mA: IDRAIN_DC * 1000.0;
end

Sweep
   DC: VG: from -1 to 0 step=0.2  VD: from 0 to 6 step=0.3
       ID_mA;

   AC: FREQ: from 1GHZ to 20GHZ step=1GHZ  K=(FREQ/1GHZ)
       MS PS MS11_data PS11_data MS21_data PS21_data
             MS12_data PS12_data MS22_data PS22_data
       {Smith title="TOM Model Fitting Measured S11 & S22"
        MP=(MS11,PS11)."S11".green & (MS22,PS22)."S22".yellow &
           (MS11_data,PS11_data)."S11_data".green.circle &
           (MS22_data,PS22_data)."S22_data".yellow.circle}
       {Polar title="TOM Model Fitting Measured S21"
        MP=(MS21,PS21)."S21" &
           (MS21_data,PS21_data)."S21_data".circle}
       {Polar title="TOM Model Fitting Measured S12"
        MP=(MS12,PS12)."S12" &
           (MS12_data,PS12_data)."S12_data".circle};
end

Expression
   ! measured data: MS11 PS11 MS21 PS21 MS12 PS12 MS22 PS22, 1GHZ - 20GHZ

   Data[20,8] = [
      .983  -20.2   4.5734   163.5    .0187    80.2    .675   -8.7
      .945  -38.1   4.2792   148.5    .0344    70.4    .659  -17.1
      .898  -53.4   3.9170   135.0    .0459    63.3    .642  -21.5
      .830  -68.4   3.6557   122.4    .0574    56.4    .623  -28.4
      .787  -83.2   3.4163   111.1    .0657    52.4    .592  -32.0
      .723  -97.8   3.2070   100.0    .0734    47.4    .568  -37.1
      .683 -112.8   3.0142    90.0    .0791    44.4    .534  -40.7
      .638 -128.7   2.8536    79.4    .0846    40.9    .497  -46.3
      .609 -143.9   2.6537    70.1    .0891    38.8    .465  -51.1
      .598 -159.5   2.5056    60.6    .0935    36.7    .423  -57.3
      .597 -172.7   2.3270    51.5    .0960    35.0    .390  -65.5
      .601  174.7   2.1758    43.3    .1024    34.0    .362  -75.3
      .614  165.1   2.0045    35.0    .1063    33.4    .351  -84.4
      .627  157.2   1.8696    28.6    .1134    32.5    .329  -97.2
      .622  151.0   1.7376    20.6    .1216    31.7    .367 -106.5
      .625  146.2   1.6303    15.8    .1331    31.9    .349 -113.8
```

```
      .611  141.6   1.5467     9.2    .1456    32.0    .401 -120.8
      .596  138.0   1.4606     5.0    .1644    31.9    .396 -121.7
      .582  132.6   1.4213     -.7    .1852    32.2    .425 -126.9
      .554  127.7   1.3582    -4.8    .2130    30.0    .418 -127.7];

   K: 1;

   MS11_data = data[K,1];
   MS21_data = data[K,3];
   MS12_data = data[K,5];
   MS22_data = data[K,7];
   PS11_data = data[K,2];
   PS21_data = data[K,4];
   PS12_data = data[K,6];
   PS22_data = data[K,8];
end
```

TOM Model Fitting Measured S-Parameters

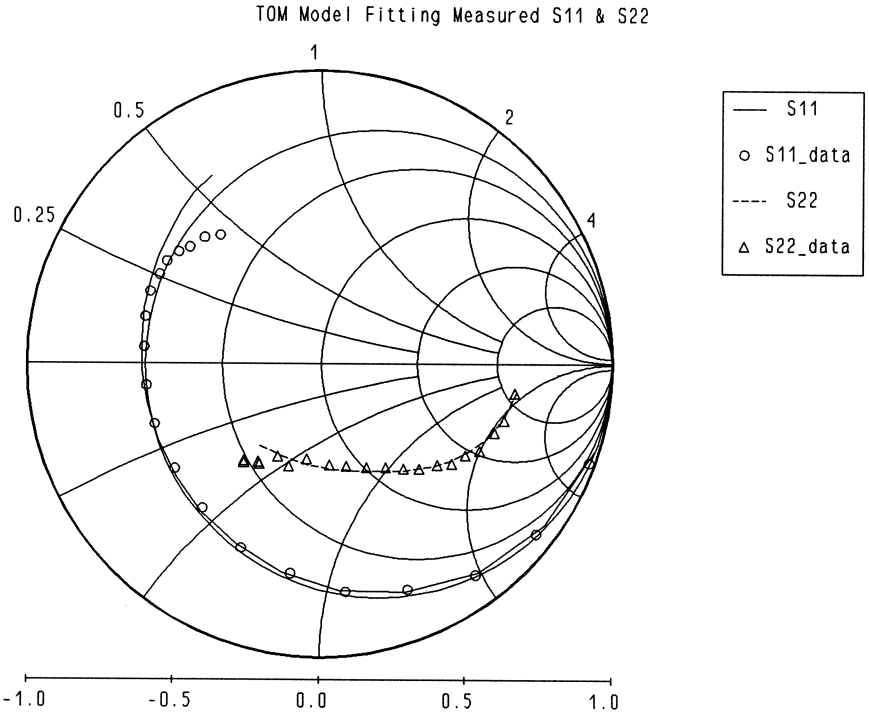

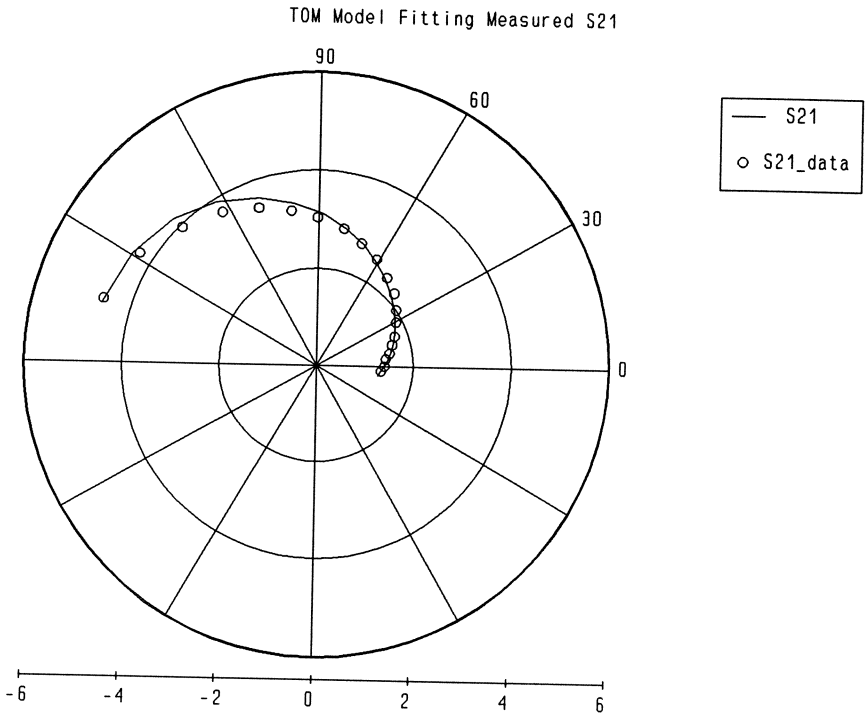
TOM Model Fitting Measured S21
90
60
30
0
S21
S21_data
-6
-4
-2
0
2
4
6

demo19

Minimax optimization of a distributed (traveling wave) amplifier with 4 FETs. The FETs are represented by nonlinear FETR models. The model parameters are extracted by HarPE from *NEC700* data.

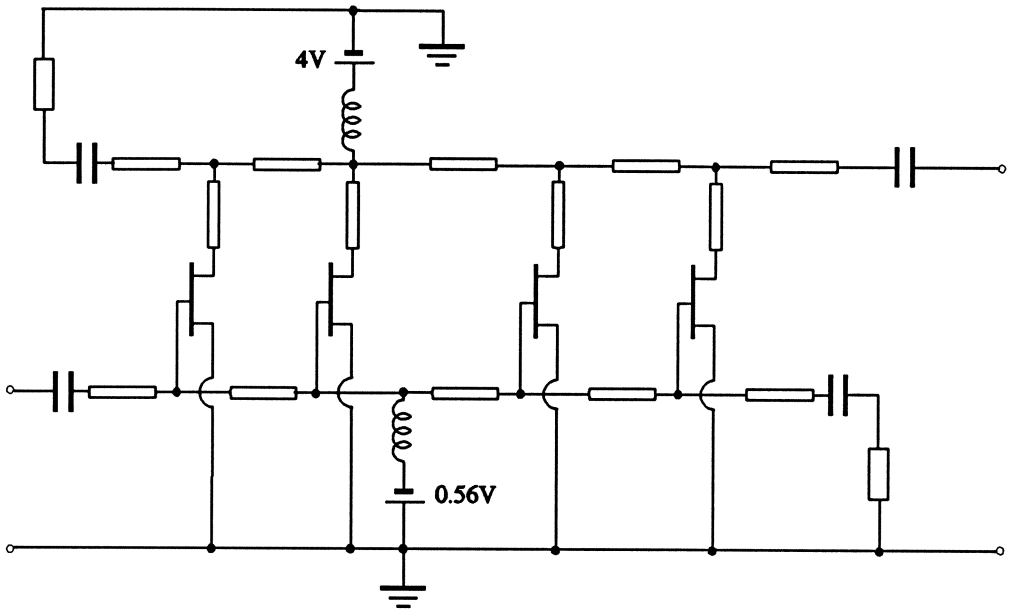

The design specifications are

12dB ≤ small-signal gain ≤ 13dB

input VSWR ≤ 1.5

output VSWR ≤ 1.5

from 1GHz to 9GHz.

These specifications can be implemented directly by defining gain in dB and VSWR as user-defined responses. However, in the input file equivalent specifications on MS21, MS11 and MS22 are used. This is because MS21, MS11 and MS22 are better scaled than gain in dB and VSWR.

Input File

```
!  Example  demo19.ckt
!  optimization of a distributed (traveling wave) amplifier
!  the FETR model is extracted by HarPE from NEC700 data
!  1GHz - 9GHz, 12dB < gain < 13dB, VSWR < 1.5:1

#define FET($) {
   Extrinsic2  @g$ @d$ @s$ @gate$ @drain$
      RG=3.5   LG=0.0306NH  RD=0.5       LD=0.00792NH
      RS=4.73  LS=0.0451NH  GDS=0.00345  CDS=0.08738PF  CX=10PF;

   FETR  @g$ @d$ @s$
      IS=5E-15    N=1         FC=0.5          GMIN=1.0E-07
      VBI=0.8     VBR=20.0    ALPHA=2         THETA=0.003
      BETA=0.029  VTO=-1.637  LAMBDA=0.04978  TAU=2.8PS
      CGSO=0.4428PF  CGDO=0.1066PF;
}

Model
   FET(1);
   FET(2);
   FET(3);
   FET(4);

   IND @gate2  @gate_bias   L=100nH;
   IND @drain2 @drain_bias  L=100nH;

   VSOURCE @gate_bias  0  VDC=-0.56;
   VSOURCE @drain_bias 0  VDC=4;

   Pin: 0;

   PORT 10  0  P=Pin;
   CAP  10 20  C=10nF;

   ! gate lines

   XE1: ?50?;
   XE2: ?75?;
   XE3: ?50?;

   TEM  20     @gate1  Z=90 E=?15? F=9;
   TEM  @gate1 @gate2  Z=90 E=XE1 F=9;
   TEM  @gate2 @gate3  Z=70 E=XE2 F=9;
   TEM  @gate3 @gate4  Z=80 E=XE3 F=9;
   TEM  @gate4 30      Z=90 E=?25? F=9;

   SRC 30 0  C=10nF  R=?50?;

   XE4: ?25?;
   TEM  @drain1 1  Z=85 E=XE4 F=9;
   TEM  @drain2 2  Z=85 E=XE4 F=9;
   TEM  @drain3 3  Z=85 E=XE4 F=9;
   TEM  @drain4 4  Z=85 E=XE4 F=9;

   ! drain lines

   SRC 40 0  C=10nF  R=?75?;

   TEM  40  1  Z=90 E=?45? F=9;
   TEM   1  2  Z=90 E=XE1 F=9;
   TEM   2  3  Z=70 E=XE2 F=9;
   TEM   3  4  Z=80 E=XE3 F=9;
   TEM   4 50  Z=75 E=?5? F=9;

  CAP  50 60  C=10nF;
  PORT 60  0  NAME=out;

  CIRCUIT;
```

```
   MS21_DB = 20 * log10(MS21);
   MS11_DB = -20 * log10(MS11);
   MS22_DB = -20 * log10(MS22);
   VSWR1 = if (MS11 < 0.8) ((1 + MS11)/(1 - MS11)) else (NAN);
   VSWR2 = if (MS22 < 0.8) ((1 + MS22)/(1 - MS22)) else (NAN);

   Pout[0:N_SPECTRA] = if (PWout > 0) (10 * log10(PWout) + 30) else (NAN);
   Power_Gain = Pout[1] - Pin;
end

Sweep
   AC: FREQ: from 1 to 9GHZ step=0.25GHZ  MS21_DB VSWR1 VSWR2
       {Xsweep title="Distributed Amplifier Small-Signal Gain"
        NXticks=8  Y=MS21_DB Ymin=8 Ymax=15 NYticks=7}
       {Xsweep title="Distributed Amplifier VSWR"
        NXticks=8  Y=VSWR1 & VSWR2 Ymin=0 Ymax=3 NYticks=6};

   HB: FREQ=5GHZ  Pin: from -9dBM to 9DBM step=3DBM  Pout Power_Gain
       {Xsweep title="Distributed Amplifier Large-Signal Responses at 5GHz"
        NXticks=6  Y=Pout[1] & Power_Gain Ymin=3 Ymax=20 NYticks=17};
end

spec
   AC: FREQ: from 1 to 9 step=1
       MS21 > 4    ! 12dB
       MS21 < 4.5  ! 13dB
       MS11 < 0.2  ! VSWR 1.5:1
       MS22 < 0.2;
end

Control
   Optimizer=minimax;
end
```

Distributed Amplifier Small-Signal Gain Before and After Optimization

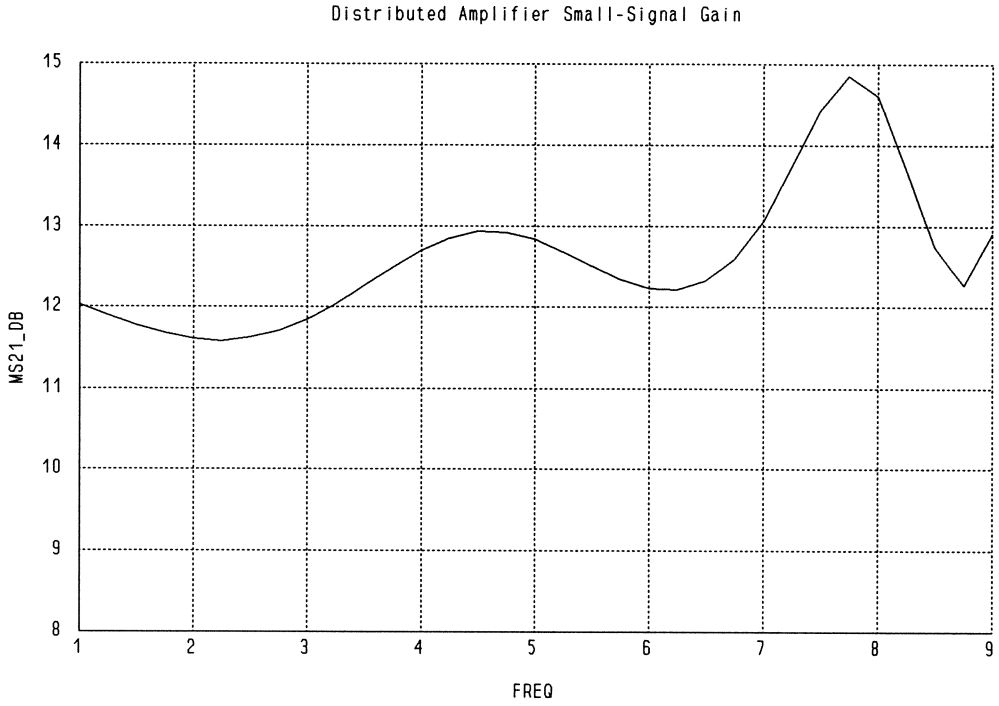

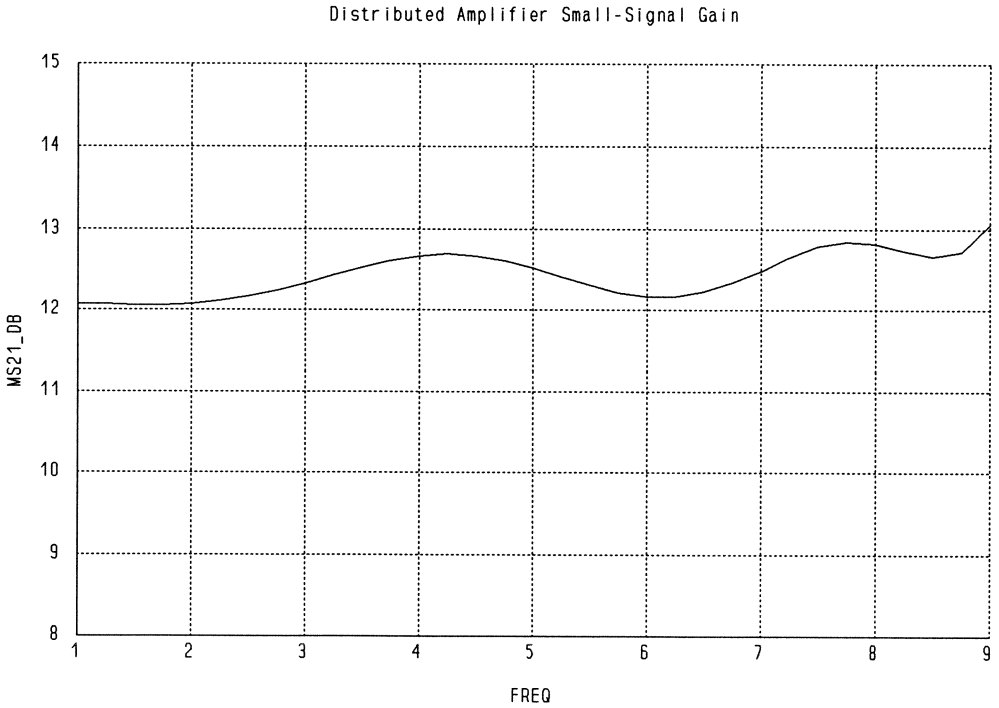

Distributed Amplifier VSWRs Before and After Optimization

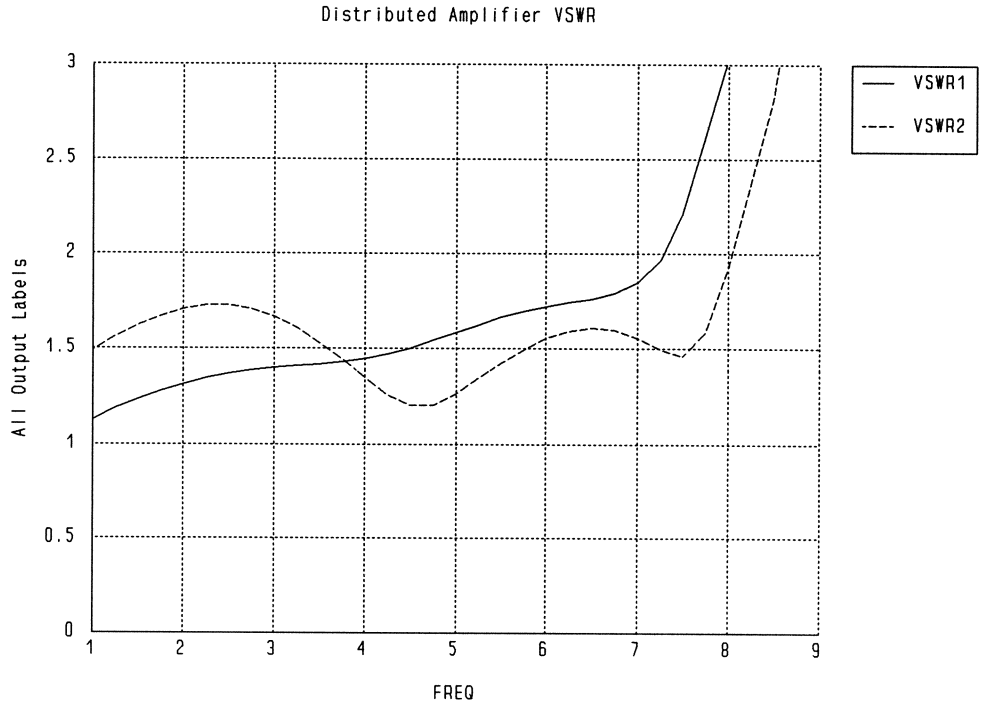

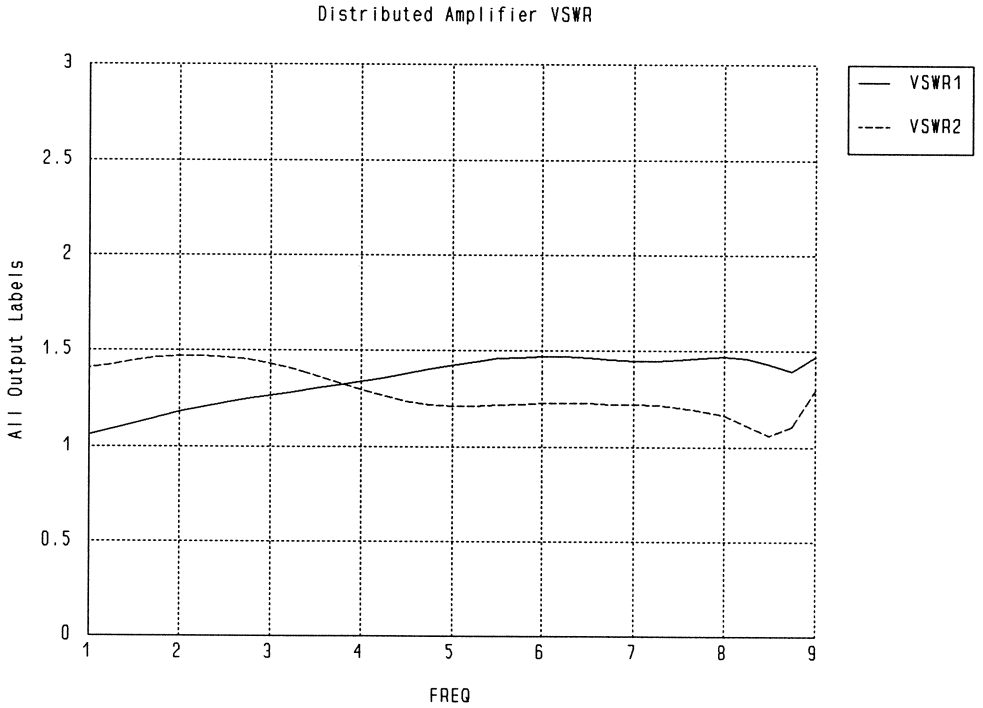

Distributed Amplifier Large-Signal Responses

The following figure shows the large-signal power gain and fundamental output power of the distributed amplifier as calculated by harmonic balance simulation.

The power gain at 5GHz is 12.5dB when the input power level is low, which is identical to the result from small-signal simulation.

The 1-dB compression point is 18.5dBm output power (7dBm available input power).

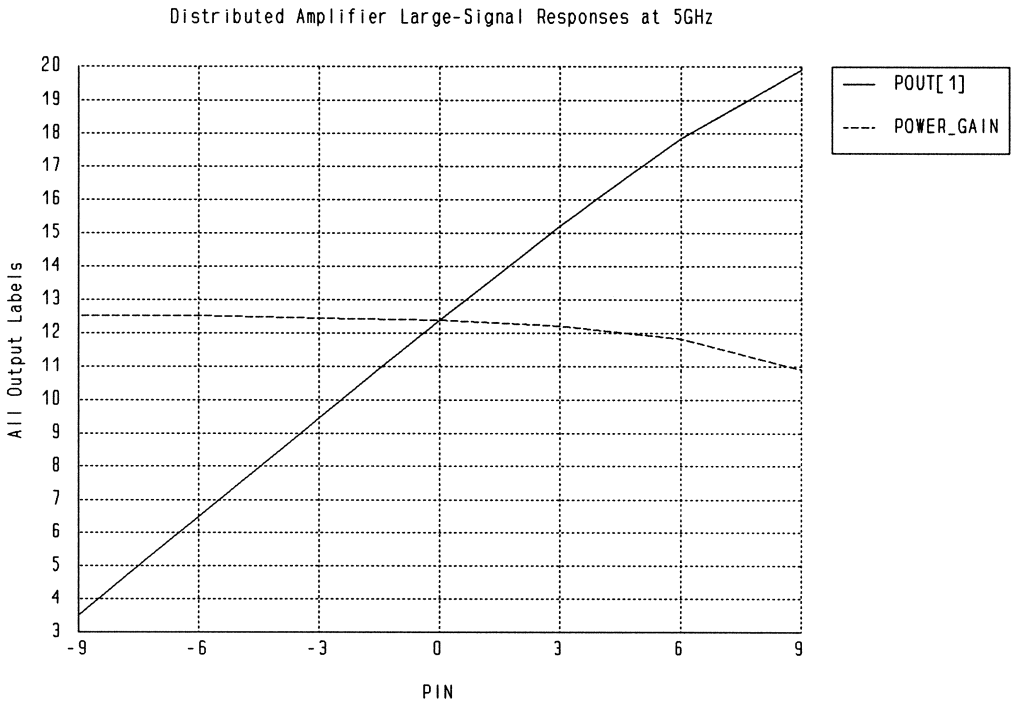

demo20

Minimax optimization of a broadband 2-20GHz distributed (traveling wave) amplifier with 3 FETs. The FETs are represented by the nonlinear FETR model extracted by HarPE from *NEC700* data.

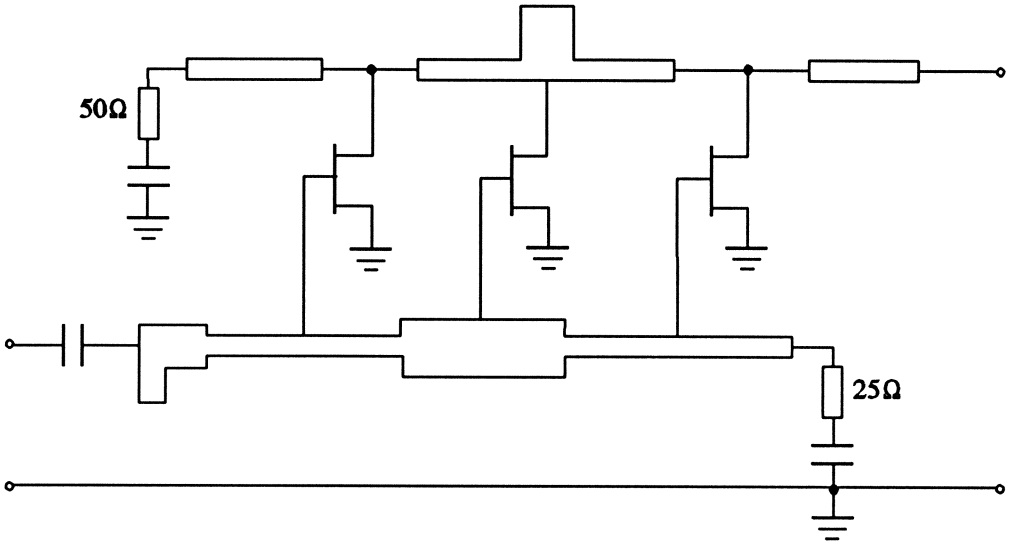

Input File

```
!  Example  demo20.ckt
!  broadband distributed (traveling wave) amplifier
!  2 - 20GHz.  minimax optimization.
!  the FETR model is extracted by HarPE from NEC700 data

#define FET(n1, n2, $) {
   Extrinsic2  20$ 30$ 40$ n1 n2
      RG=3.5   LG=0.0306NH  RD=0.5       LD=0.00792NH
      RS=4.73  LS=0.0451NH  GDS=0.00345  CDS=0.08738PF  CX=10PF;

   FETR  20$ 30$ 40$
      IS=5E-15    N=1         FC=0.5          GMIN=1.0E-07
      VBI=0.8     VBR=20.0    ALPHA=2         THETA=0.003
      BETA=0.029  VT0=-1.637  LAMBDA=0.04978  TAU=2.8PS
      CGS0=0.4428PF  CGD0=0.1066PF;

   IND n1 200 L=1000nH;
   IND n2 300 L=1000nH;
}

Model
   Pin: 0;

   MSUB  EPSR=3.9 H=0.254mm T=0.006mm ROC=2E-8;

   L1: ?0.54mm?;
   W1: ?1.25mm?;
   L2: ?0.36mm?;
   W2: ?0.59mm?;
```

```
   PORT   2  0     P=Pin;

   CAP    2  3     C=10pF;
   MTEE   3  4  5  W1=W1 W2=W1 W3=W2;
   MSL    4  6     L=L1 W=W1;
   MOPEN  5        L=L2 W=W2;

   L3: ?0.43mm?;
   W3: ?0.2mm?;
   L4: ?0.46mm?;
   W4: ?0.37mm?;

   MSTEP   6  7  W1=W1 W2=W3;
   MSL     7  8  L=L3 W=W3;
   MSL     8 10  L=L3 W=W3;
   MSTEP  10 11  W1=W3 W2=W4;
   MSL    11 12  L=L4 W=W4;
   MSL    12 13  L=L4 W=W4;
   MSTEP  13 14  W1=W4 W2=W3;
   MSL    14 15  L=L3 W=W3;
   MSL    15 17  L=L3 W=W3;

   RES    17 18  R=25;
   CAP    18  0  C=10pF;

   CAP    20  0  C=10pF;
   RES    20 21  R=500;

   L6: ?0.1mm?;
   W6: ?0.05mm?;
   L7: ?0.88mm?;
   L8: ?0.66mm?;
   W8: ?0.59mm?;

   MSL    21 23     L=L6 W=W6;
   MSL    23 24     L=L7 W=W6;
   MTEE   24 25 26  W1=W6 W2=W6 W3=W8;
   MOPEN  26        L=L8 W=W8;
   MSL    25 28     L=L7 W=W6;
   MSL    28 29     L=L6 W=W6;

   FET( 8,23,1);
   FET(12,25,2);
   FET(15,28,3);

   CAP   29 30  C=10pF;
   PORT  30  0  NAME=out;

   VG: -0.56;
   VD: 4;
   VSOURCE 200 0 NAME=gate VDC=VG;
   VSOURCE 300 0 NAME=drain VDC=VD;

   CIRCUIT;

   MS21_DB = 20 * log10(MS21);
   MS11_DB = -20 * log10(MS11);
   MS22_DB = -20 * log10(MS22);

   Pout[0:N_SPECTRA] = if (PWout > 0) (10 * log10(PWout) + 30) else (NAN);
   Power_Gain = Pout[1] - Pin;
end

Sweep
   AC: FREQ: from 2 to 20 step=1 MS21_DB MS11_DB MS22_DB;

   HB: FREQ=10GHz  Pin: from -9dBm to 15dBm step=3dBm  Pout
       {Xsweep title="Output Power Spectrum at 10GHz"
        Y=Pout[1].green & Pout[2].red & Pout[3].yellow & Pout[4].pink
        NXticks=8  Ymin=-40 Ymax=30 NYticks=7};
```

```
   HB: FREQ: 2GHz, 10GHz, 18GHz, 20GHz
       Pin: from -9dBm to 15dBm step=3dBm  Pout[1] Power_Gain
       {Xsweep title="Large-Signal Power Gain"
        Y=Power_Gain  FREQ=all  NXticks=8  Ymin=3 Ymax=9 NYticks=6};
end

spec
   AC: FREQ: from 2 to 20 step=1
       MS21 > 2.5   ! 8dB
       MS11 < 0.3
       MS22 < 0.3;
end

Control
   Optimizer = minimax;
end
```

Broadband Distributed Amplifier Small-Signal Gain After Minimax Optimization

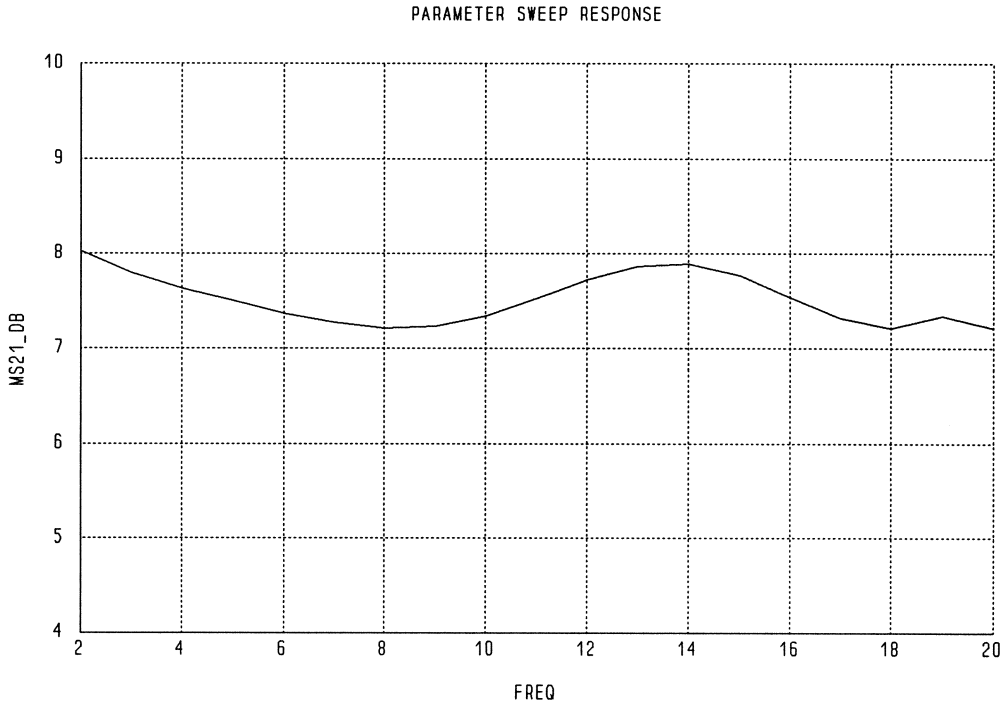

Output Power Spectrum versus Input Power at 10GHz

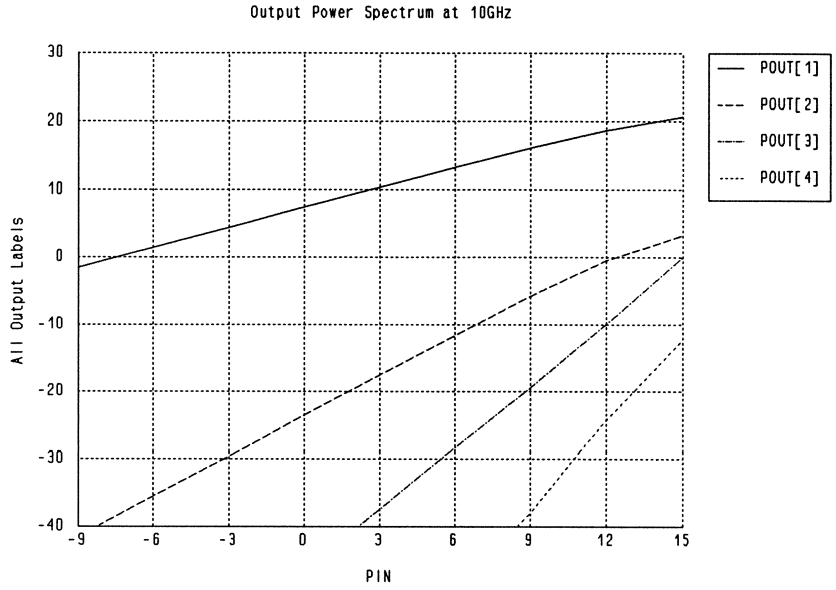

Large-Signal Power Gain at 2GHz, 10GHZ, 18GHz and 20GHz

The large-signal power gain is between 7dB and 8dB across a broad range of frequencies and input power levels. The 1-dB compression point is about 13dBm input power (19dBm - 20dBm output power) from 2 to 18GHz. At 20GHz, the 1-dB compression point drops by about 3dB.

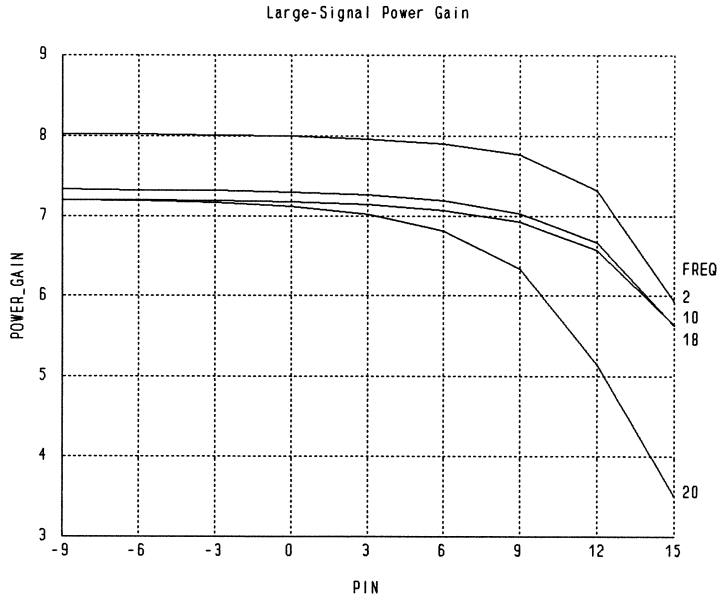

demo21

Simulation of a balanced amplifier under multi-harmonic excitations. This is very similar to demo13 with the following differences.

(1) The FETs are represented by the nonlinear FETR model in demo13 but in this example they are represented by a linear model, namely, FETR linearized about the DC operating point.

(2) To illustrate the use of imported data for linear subcircuits, the Lange couplers used in demo13 are replaced by coupled lines, which are represented by imported *Y* parameters.

(3) Multi-harmonic excitations are used, i.e., the input contains higher harmonic components.

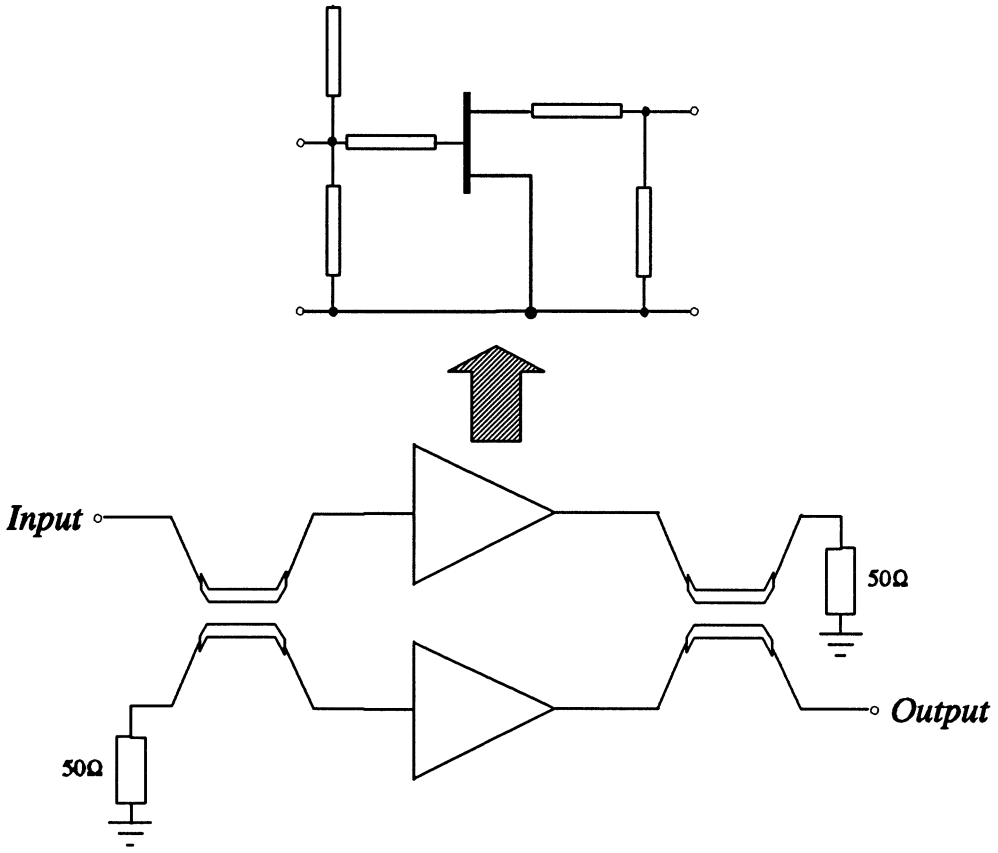

Input File

```
!  Example  demo21.ckt
!  illustrate the use of import data to represent a linear subcircuit
!  a small-signal balanced amplifier based on demo13 except:
!  (1) in demo13 the FET is represented by the nonlinear FETR model
!      in this example the FET is represented by a linear model which
!      is FETR linearized about the DC operating point
!  (2) the lange couplers in demo13 are replaced by coupled lines
!      which are represented by imported Y parameters
!  (3) the input includes multi-harmonic excitations

Import
#include "cpln0330.dat"   ! import Y parameters for the coupled line
End

! define subcircuits by macros

#define  CoupledLine(n1, n2, n3, n4)   DATAPORT n1 n2 n3 n4 DATA=CPLN0330

#define  Amplifier(input,output,$) {
   TEM   input  0  Z=70  E=119  F=18GHZ;
   TEM   output 0  Z=50  E=60   F=18GHZ;

   TEM   input @open1$ 0 @open2$  Z=100 E=65 F=18GHZ;
   OPEN  @open1$ @open2$;

   TEM   input @FET_input$  Z=100 E=25 F=18GHZ;

   ! FET model

   Extrinsic2  @gate$ @drain$ @source$ @FET_input$ @FET_output$
      RG=3.5   LG=0.0306NH  RD=0.5      LD=0.00792NH
      RS=4.73  LS=0.0451NH  GDS=0.0047  CDS=0.08738PF  CX=10PF;

   CAP  @gate$ @source$  C=0.3231PF;

   VCCS  @gate$ @drain$ @source$ @source$  T=2.8PS  M=-0.06429;

   CAP  @gate$ @drain$   C=0.04PF;

   TEM  @FET_output$ output  Z=100 E=15 F=18GHZ;
}

Model
   Amplifier(@amp1_in, @amp1_out, 1);
   Amplifier(@amp2_in, @amp2_out, 2);

   CoupledLine(@input, @amp2_in, @load1, @amp1_in);     ! input coupled line
   CoupledLine(@amp2_out, @load2, @amp1_out, @output);  ! output coupled line

   RES @load1 0  R=50;  ! matched terminations
   RES @load2 0  R=50;

   PORT  @input  0  V[1]=1 V[2]=1 V[3]=1;
   PORT  @output 0  NAME=out;

   CIRCUIT;

   MS21_DB: 20 * LOG10(MS21);

   MVsource[0:3] = [0 1 1 1];
   PVsource[0:3] = 0;
end

Sweep
   AC:  FREQ: from 4GHZ to 20GHZ Step=1GHZ  MS21_DB;

   HB:  FREQ: 6GHZ 7GHZ   MVsource PVsource MVout PVout
        {Waveform title="Output Voltage vs. Input Voltage"
```

```
        Spectrum=(MVsource,PVsource)."Vsource_T" & (MVout,PVout)."Vout_T"
        FREQ=6GHZ  Tmin=0  Tmax=0.2  NT=100  NXticks=4
        Ymin=-4  Ymax=4  NYticks=8}
       {Waveform title="Output Voltage vs. Input Voltage"
        Spectrum=(MVsource,PVsource)."Vsource_T" & (MVout,PVout)."Vout_T"
        FREQ=7GHZ  Tmin=0  Tmax=0.2  NT=100  NXticks=4
        Ymin=-4  Ymax=4  NYticks=8};
end
```

Amplifier Gain

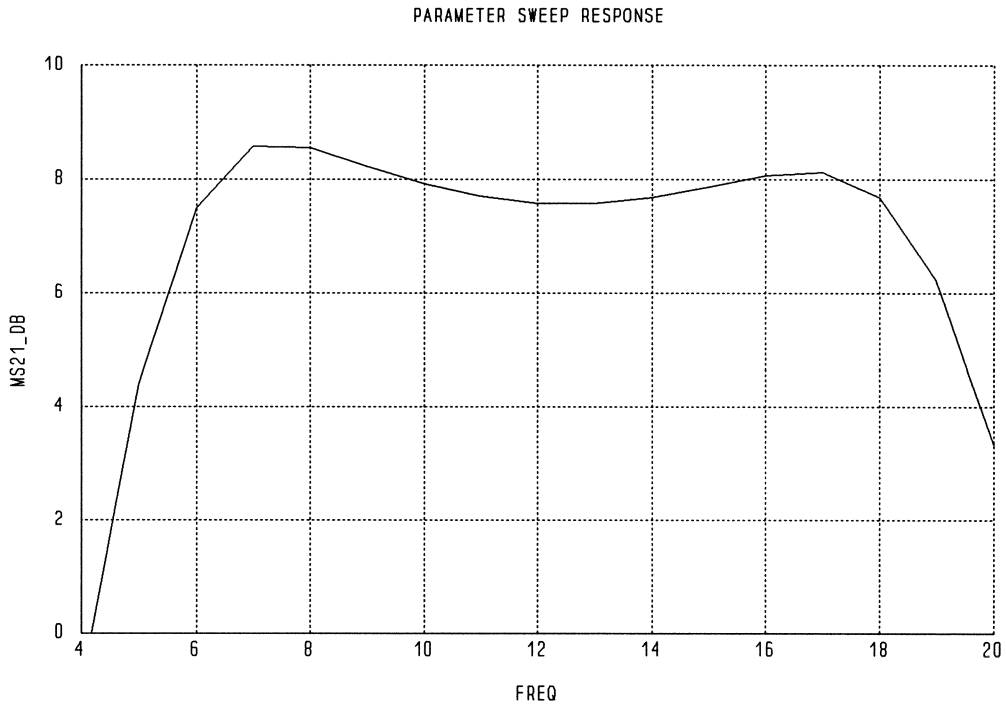

Multi-Harmonic Excitations

The AC source consists of three harmonic components of equal magnitudes:

$$V_{source} = \cos(\omega t) + \cos(2\omega t) + \cos(3\omega t)$$

We consider two different fundamental frequencies, namely 6GHz and 7GHz.

For the fundamental frequency of 6GHz, all three harmonics are within the passband of the amplifier (6GHz - 18GHz). Since the amplifier has a relatively constant gain within the passband, ideally the harmonic components of the output should have equal magnitudes (the FET model used is linear, hence there is no harmonic distortion due to nonlinearity).

For the fundamental frequency of 7GHz, the third harmonic frequency is outside the passband of the amplifier and therefore we can expect significant distortions in the output.

These observations are confirmed by the simulation results shown in the following figures.

Output Waveform for Fundamental Frequency = 6GHz

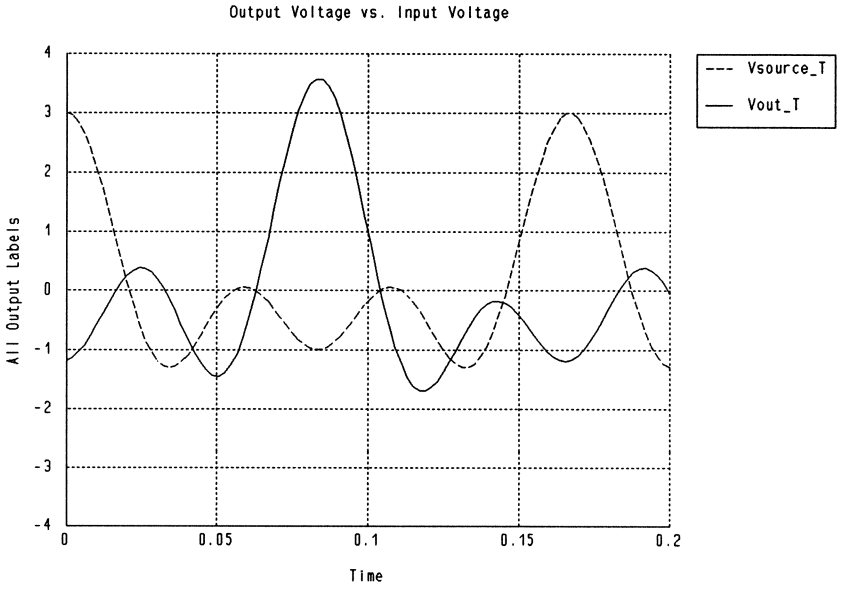

Output Waveform for Fundamental Frequency = 7GHz

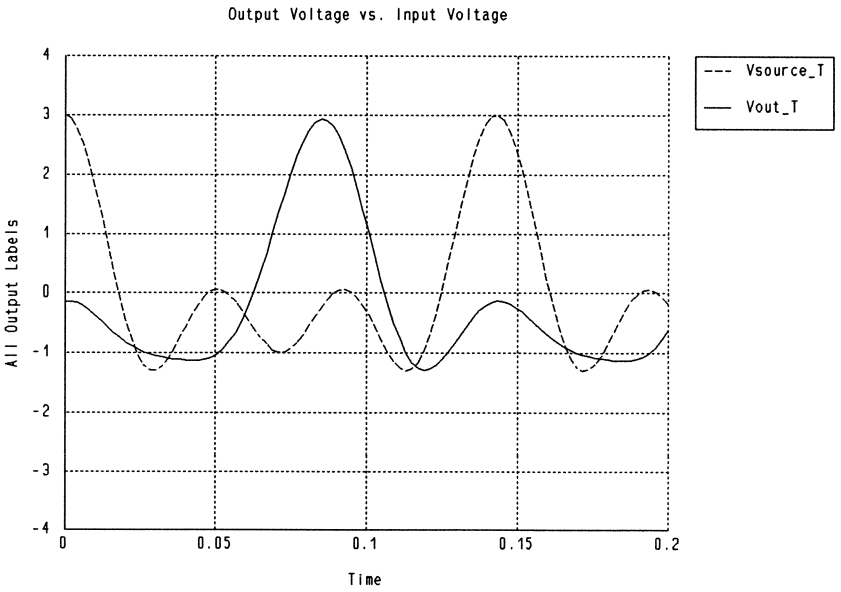

demo22

Large-signal optimization of an X-band power amplifier. We followed the general strategy for power amplifier design described by Stephen A. Maas in *Nonlinear Microwave Circuits*, Chapter 9.

The FETCA model is based on the 2400 μm FET described by Stephen Maas in the same reference.

The gate bias voltage and matching circuits are optimized to increase output power and power-added efficiency at 10GHz around the 1-dB compression point.

This example optimizes a Class-A amplifier. See demo23 for a Class-B design.

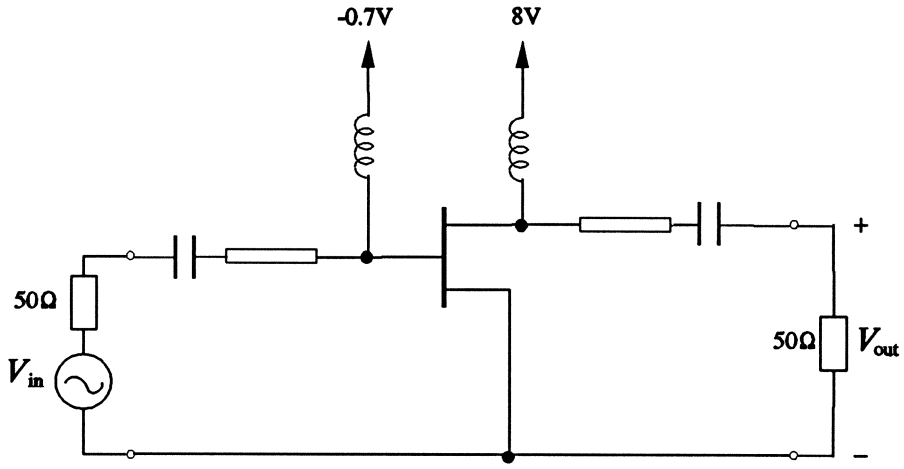

Input File

```
!  Example  demo22.ckt
!  Large-signal optimization of a X-band FET power amplifier.
!  The 2400um FET model is based on Stephen A. Maas: "Nonlinear microwave
!  circuits", chapter 9.
!  Optimize the gate bias and matching circuits to increase output power
!  and power-added efficiency at 10GHz around 1-dB compression.
!  This is a Class-A amplifier, see demo23 for a Class B design.

Model
   Pin: 20;
   VG: ?-0.7?;
   VD: 8;

   PORT   1 0   NAME=input P=Pin;

   CAP    1 2   C=1000pF;

   TEM    2 3   Z=?15? E=?120? F=10;

   IND       3 4   L=1000nH;
   VSOURCE   4 0   NAME=gate VDC=VG;
```

```
   EXTRINSIC1  20 30 40 3 5  RG=1 RD=1 RS=0.7 CDS=0.6pF LS=5pH;

   FETCA  20 30 40
      A0=0.5304  A1=0.2595  A2=-0.0542  A3=-0.0305  VBI=0.7
      BETA=0.01  VDS0=8     FC=0.7      RIN=1       GAMMA=1
      IS=0       GMIN=0     CGS0=4pF    CGD0=0.2pF;

   IND      5 6  L=1000nH;
   VSOURCE  6 0  NAME=drain VDC=VD;

   TEM   5 7  Z=?15? E=?120? F=10;

   CAP   7 8 C=1000pF;

   PORT  8 0 NAME=out;

   CIRCUIT;

   Pout[0:N_SPECTRA] = if (PWout > 0) (10 * log10(PWout) + 30) else (NAN);
   Power_Gain = Pout[1] - Pin;
   Pdc = MIdrain[0] * VD;
   PAE0 = (PWout[1] - 10^(0.1 * Pin - 3)) / Pdc;
   PAE = 100 * PAE0;
   E_DC_RF = 100 * PWout[1] / Pdc;
end

Sweep
   HB: FREQ=10  Pin: from 13 to 23 step=1
       Pout PAE Pdc Power_Gain E_DC_RF MVout PVout
       {Xsweep title="Amplifier Output Power"
        NXticks=10  Y=Pout[1]  Ymin=25 Ymax=31 NYticks=6}
       {Xsweep title="Amplifier Output Power and Power-Added Efficiency"
        NXticks=10  Y=Pout[1] & PAE  Ymin=25 Ymax=40 NYticks=15}
       {Xsweep title="Output Power Spectrum vs. Input Power"
        NXticks=10  Y=Pout[1] & Pout[2] & Pout[3] & Pout[4]
        Ymin=-20 Ymax=40 NYticks=6}
       {Waveform title="Power Amplifier Output Voltage Waveform"
        Spectrum=(MVout,PVout)."Vout_T"  Pin=all
        Tmin=0 Tmax=0.2 NT=150  Ymin=-12 Ymax=12 NYticks=4};
end

Spec
   HB: FREQ=10  Pin=18  PWout[1] > 0.8  PAE0 > 0.38;
end

Control
   Optimizer=Quasi_Newton;
end
```

Power Amplifier Output Power

The 1dB-compression point is about 28dBm output power. At 1-dB compression, the power gain is 12dB, the fundamental output power is 630mW with 40mW available input power.

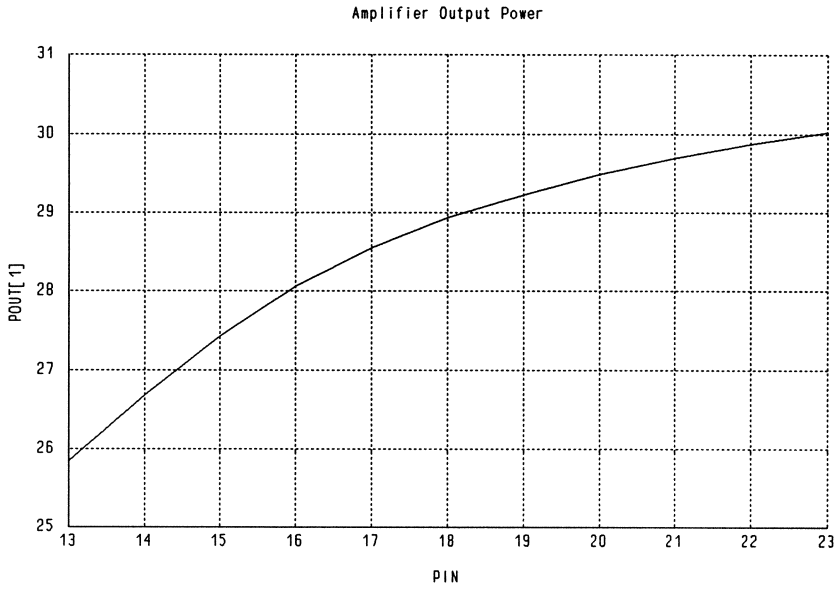

Output Power Spectrum

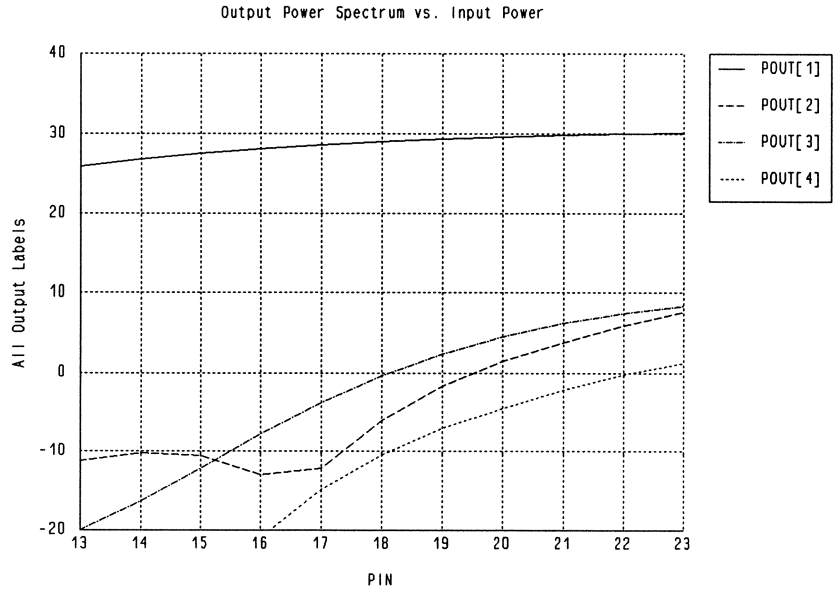

Power-Added Efficiency and Saturated Output Power

The power-added efficiency is defined as

$$\eta_a = (P_{out,1} - P_{in}) / P_{dc}$$

where $P_{out,1}$ represents the fundamental output power, P_{in} represents the available input power and P_{dc} represents the dc power provided by the bias sources.

For the power amplifier in this example, the power-added efficiency at 1-dB compression is 31%. The maximum power-added efficiency is 39% and the saturated output power (i.e., the output power corresponding to the maximum power-added efficiency) is 29.7dBm (slightly less than 1W).

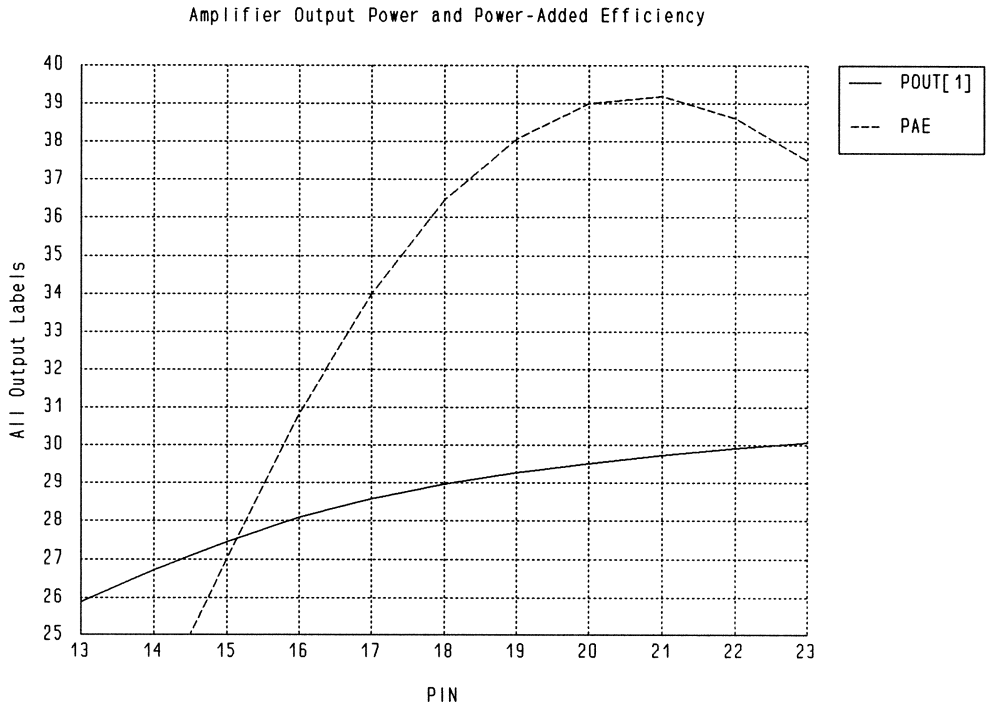

demo23

Large-signal optimization of a Class-B X-band power amplifier. We followed the general strategy for power amplifier design described by Stephen A. Maas in *Nonlinear Microwave Circuits*, Chapter 9.

The FETCA model is based on the 2400 μm FET described by Stephen Maas in the same reference.

This example is similar to demo22 except that demo22 is a Class-A amplifier and this example optimizes a Class-B design. Class-B amplifiers can achieve a higher efficiency than Class-A amplifiers.

The FET gate is biased near the pinch-off voltage for Class-B operation. The matching circuits are optimized for maximum power-added efficiency.

Because Class-B operation generates greater harmonic distortion, a low-pass filter is added to the output.

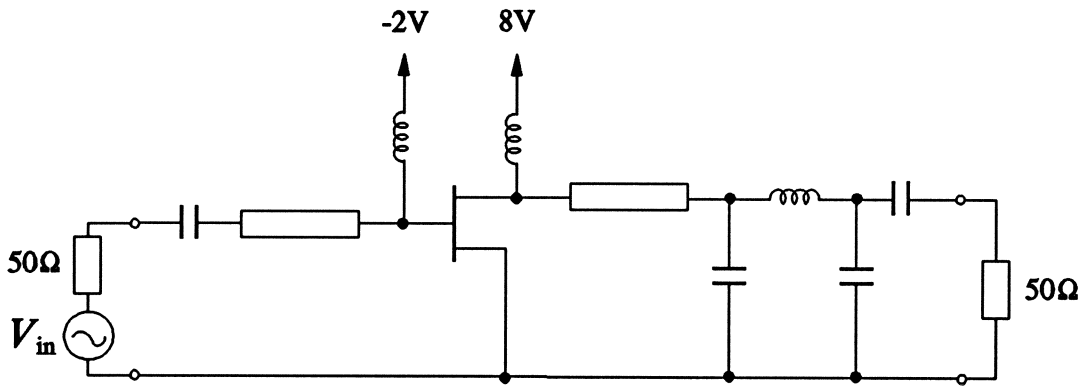

Input File

```
!  Example  demo23.ckt
!  Large-signal optimization of a X-band Class-B FET power amplifier.
!  This is similar to demo22 except that the amplifier is designed for
!  Class-B instead of Class-A operation.  Class-B has higher efficiency
!  but lower gain.  The gate is biased near the pinch-off voltage.
!  The matching circuits are optimized for maximum power-added efficiency.
!  Because Class-B operation generates greater harmonic distortion,
!  a 10GHz low-pass filter is added at the output.
!  The 2400um FET model is based on Stephen A. Maas: "Nonlinear microwave
!  circuits", chapter 9.

Model
   Pin: 20;
   VG: -2;
   VD: 8;

   PORT  1 0  NAME=input P=Pin;
```

```
   CAP   1 2  C=1000pF;

   TEM   2 3  Z=?10.7272? E=?119.297? F=10;

   IND      3 4  L=1000nH;
   VSOURCE  4 0  NAME=gate VDC=VG;

   EXTRINSIC1  20 300 40 3 5  RG=1 RD=1 RS=0.7 CDS=0.6pF LS=5pH;

   ILABEL  300 30  NAME=Id;  ! excluding the current through CDS

   FETCA  20 30 40
      A0=0.5304  A1=0.2595  A2=-0.0542  A3=-0.0305  VBI=0.7
      BETA=0.01  VDS0=8     FC=0.7      RIN=1       GAMMA=1
      IS=0       GMIN=0     CGS0=4pF    CGD0=0.2pF;

   IND      5 6  L=1000nH;
   VSOURCE  6 0  NAME=drain VDC=VD;

   TEM   5 7  Z=?19.0918? E=?131.946? F=10;

   CAP   7 0  C=0.475PF;   ! low-pass filter
   IND   7 8  L=0.7NH;
   CAP   8 0  C=0.625PF;

   CAP   7 9 C=1000pF;

   PORT  9 0 NAME=out;

   CIRCUIT;

   Pout[0:N_SPECTRA] = if (PWout > 0) (10 * log10(PWout) + 30) else (NAN);
   Power_Gain = Pout[1] - Pin;
   Pdc = MIdrain[0] * VD;
   PAE = 100 * (PWout[1] - 10^(0.1 * Pin - 3)) / Pdc;
   E_DC_RF = 100 * PWout[1] / Pdc;
end

Sweep
   HB: FREQ=10  Pin: from 15 to 25 step=1
       Pout PAE Pdc Power_Gain E_DC_RF MId PId MVout PVout
       {Xsweep title="Amplifier Output Power"  NXticks=10
        Y=Pout[1]  Ymin=23 Ymax=30 NYticks=7}
       {Xsweep title="Amplifier Output Power and Power-Added Efficiency"
        NXticks=10  Y=Pout[1] & PAE  Ymin=20 Ymax=50 NYticks=6}
       {Xsweep title="Amplifier dc-RF and Power-Added Efficiencies"
        NXticks=10  Y=PAE & E_DC_RF  Ymin=30 Ymax=65 NYticks=7}
       {Xsweep title="Output Power Spectrum vs. Input Power"
        NXticks=10  Y=Pout[1] & Pout[2] & Pout[3] & Pout[4]
        Ymin=-50 Ymax=40 NYticks=9}
       {Waveform title="FET Drain Current in Class-B Operation"
        Spectrum=(MId,PId)."Id_T"  Pin=18
        Tmin=0 Tmax=0.2 NT=150  Ymin=-0.1 Ymax=0.5 NYticks=6}
       {Waveform title="Power Amplifier Output Voltage Waveform"
        Spectrum=(MVout,PVout)."Vout_T"  Pin=all
        Tmin=0 Tmax=0.2 NT=150  Ymin=-12 Ymax=12 NYticks=4};
end

Spec
   HB: FREQ=10  Pin: 21 22 23  PAE > 45;
end

Control
   Optimizer=Quasi_Newton;
end
```

Class-B Amplifier Power-Added Efficiency

The power-added efficiency is defined as

$$\eta_a = (P_{out,1} - P_{in}) / P_{dc}$$

where $P_{out,1}$ represents the fundamental output power, P_{in} represents the available input power and P_{dc} represents the dc power provided by the bias sources.

It is well-known that Class-B amplifiers can achieve a higher efficiency than Class-A amplifiers. The following figure shows that the optimized Class-B design in this example has a power-added efficiency better than 40% over a wide range of input power levels. The maximum power-added efficiency is close to 45%. In comparison, the maximum power-added efficiency of the Class-A amplifier in demo22 is only 39%.

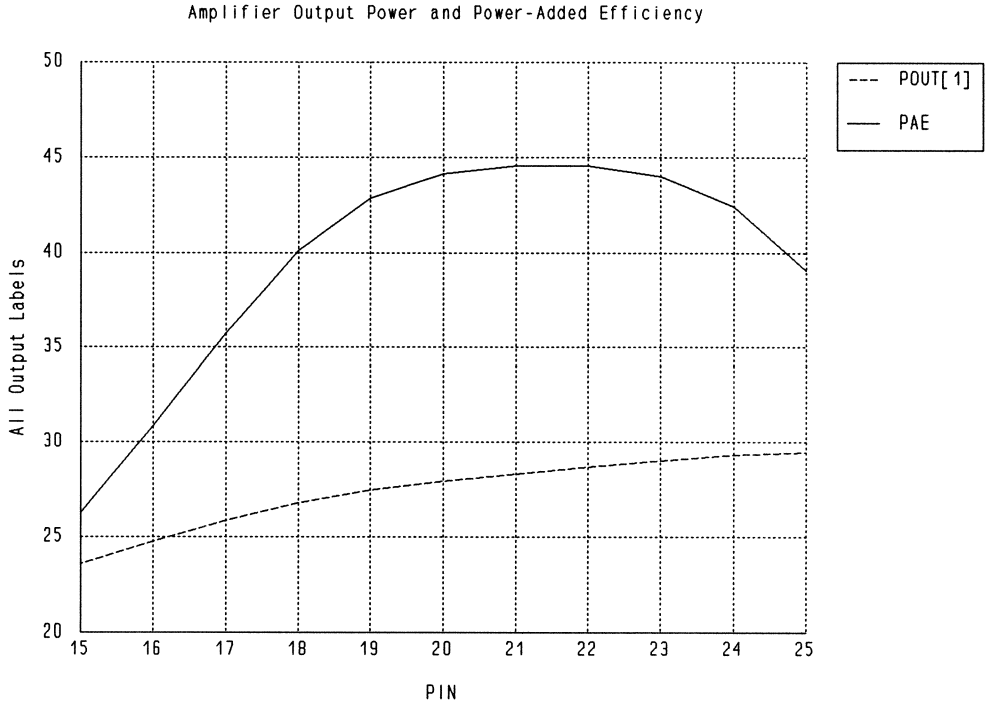

Amplifier Output Power

The price for the high efficiency in Class-B operation is a lower gain as compared with Class-A operation. The power gain at 1-dB compression for the amplifier in this example is about 8dB, which is 4dB lower than the Class-A design in demo22.

The lower gain means that a stronger input drive is needed. For instance, to achieve the 1-dB compression output power of 630mW, 100mW of available input power is required (to achieve the same output power level, demo22 requires only 40mW of available input power).

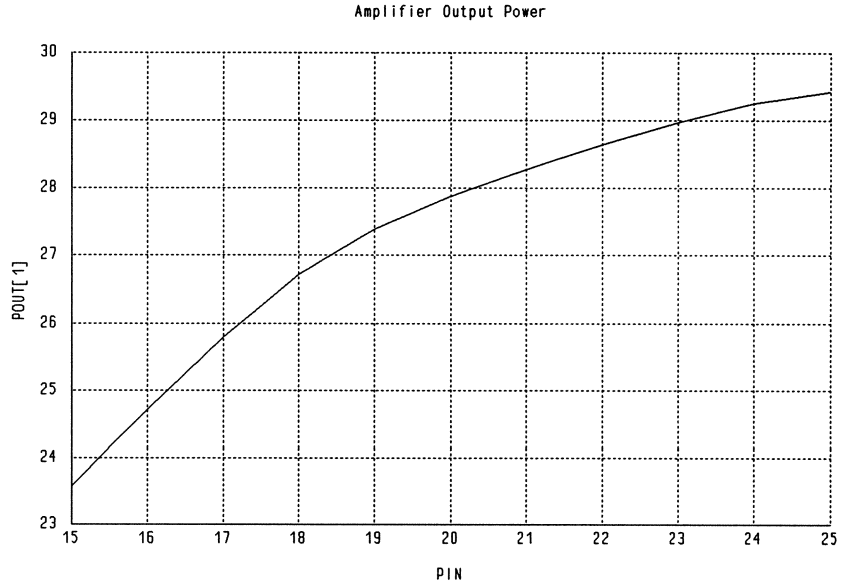

FET Drain Current in Class-B Operation

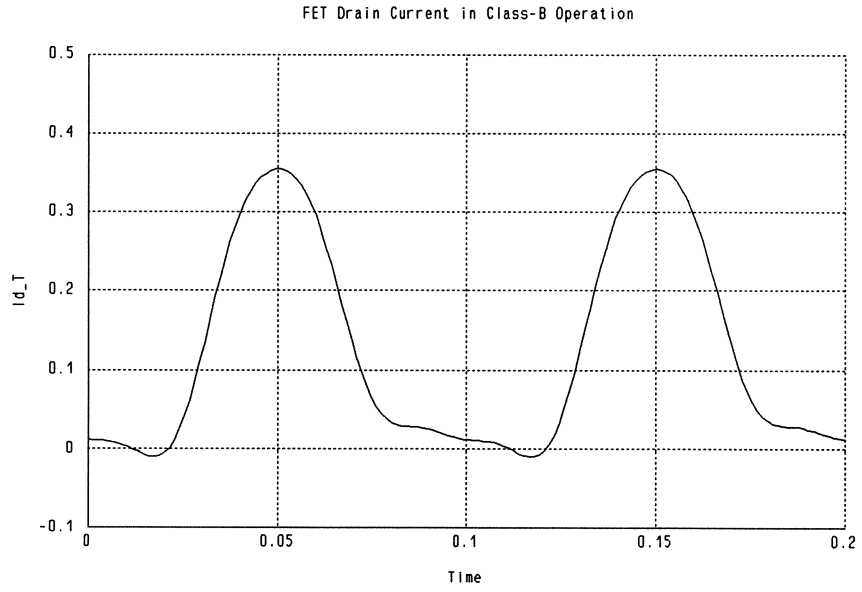

demo24

Nonlinear two-tone simulation of a resistively matched single-ended diode mixer. The diode is represented by the built-in nonlinear DIODE model.

The local oscillator (LO) power level is -5dBm at 1.5GHz, the RF input power level is -20dBm at 1.57GHz, and the intermediate frequency (IF) is 70MHz.

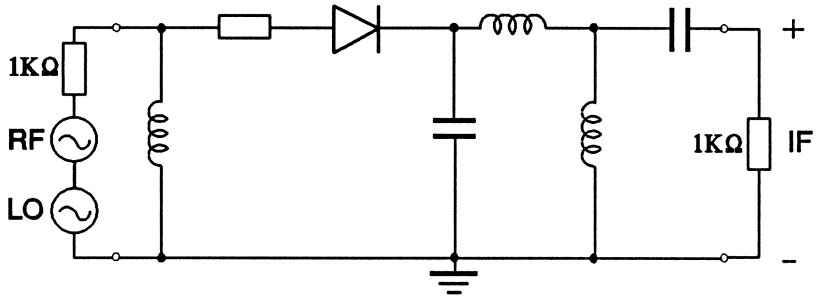

Input File

```
! Example  demo24.ckt
! A resistively matched single-ended mixer

Model
   IND  1 0  L=1.8uH;

   RES    1 2  R=10;  ! resistance in diode model
   DIODE  2 3  IS=1.e-14  N=1  TEMP=295  VJ=0.9  CJ0=0.001pF;

   CAP  3 0  C=2.8pF;
   IND  3 4  L=1uH;
   IND  4 0  L=20uH;

   Power_LO: -5DBM;
   Power_RF: -20DBM;

   PORT  1 0  NAME=in R=1KOH  P=Power_LO  P2=Power_RF;

   CAP   4 6  C=100nF;
   PORT  6 0  NAME=out R=1KOH;

   CIRCUIT  MIXER;

   Pout[0:N_SPECTRA] = if (PWout > 0) (10 * log10(PWout) + 30) else (NAN);

   K: 1;
end

Sweep
   HB: FREQ=1.5GHZ  FREQ2=1.57GHZ
       MVout, PVout
       {Waveform title="Output Voltage Waveform"
        Spectrum=(MVout,PVout)."Vout"
        Tmin=0 Tmax=28 NT=256 NXticks=4
        Ymin=-0.08 Ymax=0.08 NYticks=4};

   HB: FREQ=1.5GHZ  FREQ2=1.57GHZ  K: from 0 to N_SPECTRA step=1
       Pout[K], Spectral_Freq[K]
```

```
        {Parametric title="Output Power Spectrum"
         X=Spectral_Freq[K] X_title="Frequency (GHz)"  Xmax=2 NXticks=4
         Y=Pout[K].bar Y_title="Pout (dBm)"  Ymin=-100 Ymax=-20 NYticks=4};
end
```

Mixer IF Output Voltage Waveform

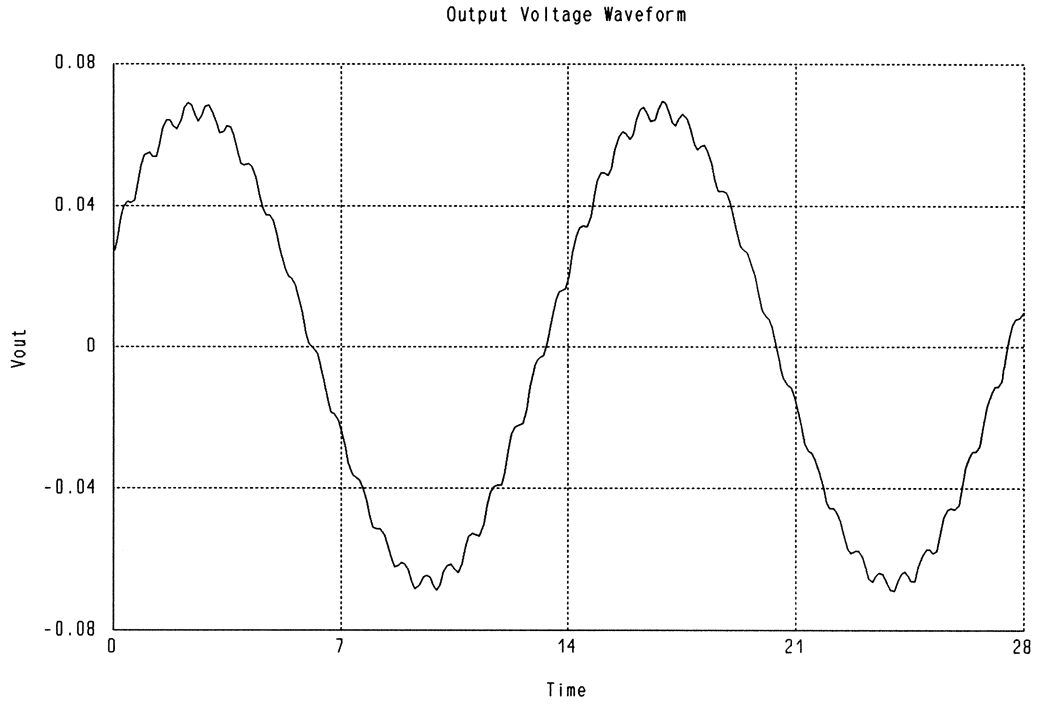

Mixer IF Output Power Spectrum

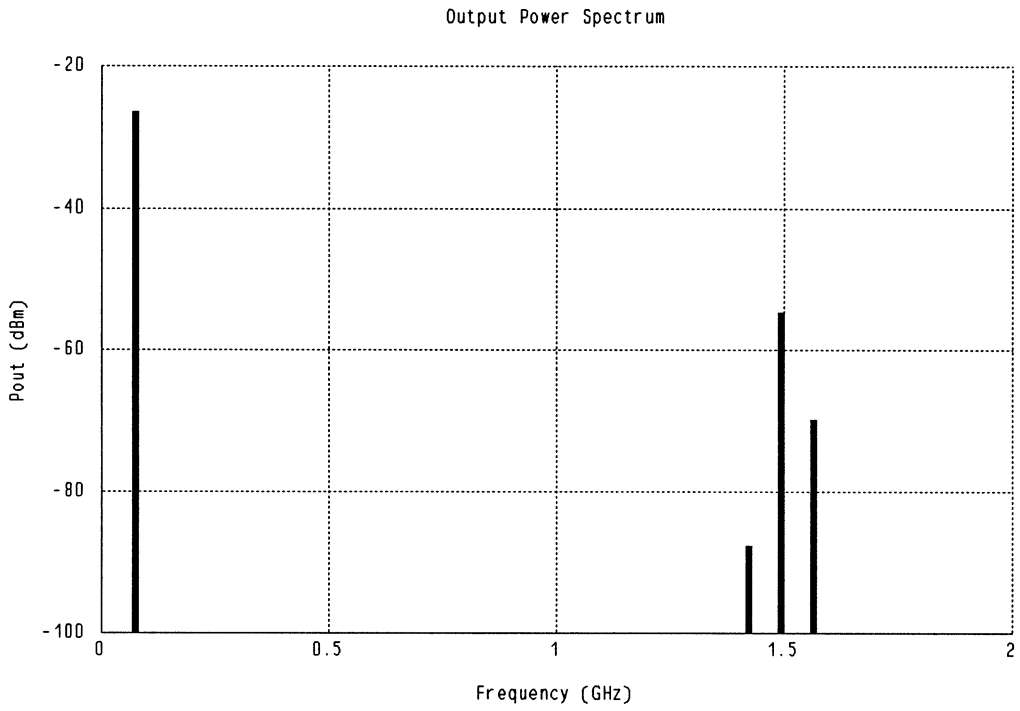

demo25

Nonlinear two-tone simulation of a singly balanced diode mixer. The two diodes are represented by the built-in nonlinear DIODE model.

The local oscillator (LO) frequency is 3.75GHz, the RF frequency is 4GHz and the intermediate frequency (IF) is 0.25GHz.

The conversion loss of the diode mixer is calculated versus a sweep of the LO power level. The IF output voltage waveform and output power spectrum are also analyzed.

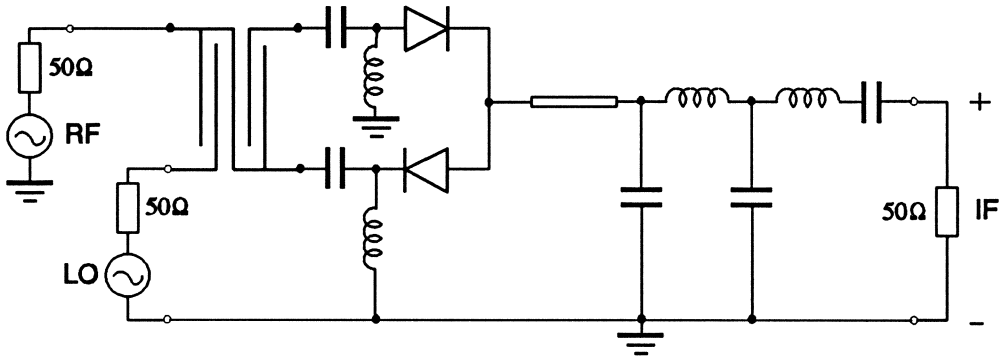

Input File

```
!  Example  demo25.ckt
!  singly balanced diode mixer
!  LO frequency 3.75GHZ
!  RF frequency 4GHZ
!  IF frequency 0.25GHZ

Model
   MSUB  EPSR=6  H=50MIL  T=1MIL  ROC=2.44e-8  RHS=0;
   MLANG4  1 2 3 4  W=7.2MIL  S=3.8MIL  L=400MIL;

   CAP  2 5  C=1.9PF;
   IND  5 0  L=1.7NH;

   CAP  4 6  C=1.9PF;
   IND  6 0  L=1.7NH;

   RES    5 7  R=10;
   DIODE  7 8  IS=1.0e-14  VB=-15  IB0=1.e-3  VJ=1;

   RES    8 9  R=10;
   DIODE  9 6  IS=1.0e-14  VB=-15  IB0=1.e-3  VJ=1;

   MSL   8 10  W=72MIL  L=46MIL;
   CAP  10  0  C=19PF;
   IND  10 11  L=28NH;
   CAP  11  0  C=25PF;
   IND  11 12  L=16NH;
   CAP  12 20  C=50PF;

   Power_LO: 12;
   Power_RF: -10dBm;
```

```
   PORT  1 0  P2=Power_RF;
   PORT  3 0  P =Power_LO;
   PORT 20 0  NAME=IF_out;

   CIRCUIT  HARM=4  INTMOD;

   Power_IF[0:N_SPECTRA] = if (PWIF_out < 1.E-15) (-120)
                           else (10 * log10(PWIF_out) + 30);

   K: 0;

   Conversion_Loss = Power_RF - Power_IF[1];
end

Sweep
   HB:  FREQ=3.75 FREQ2=4  Power_LO: from 6 to 12 step=1  Conversion_Loss;

   HB:  FREQ=3.75 FREQ2=4  Power_LO: from 6 to 12 step=3  MVIF_out PVIF_out
        {Waveform title="IF Output Voltage Waveform"
         SPECTRUM=(MVIF_out, PVIF_out)."IF Output Voltage"
         Power_LO=all Tmin=0 Tmax=4 NT=150 NXticks=4
         Ymin=-0.05 Ymax=0.05 NYticks=4};

   HB:  FREQ=3.75 FREQ2=4  K: from 0 to N_SPECTRA step=1
        Spectral_Freq[K] Power_IF[K]
        {Parametric title="IF Output Power Spectrum"
         X=Spectral_Freq[K]  X_title="Spectral Frequency (GHz)"
         Y=Power_IF[K].bar   Y_title="IF Output Power (dBm)"
         Xmin=0 Xmax=10 NXticks=10  Ymin=-120 Ymax=0 NYticks=6};
end
```

Diode Mixer Conversion Loss versus LO Power Level

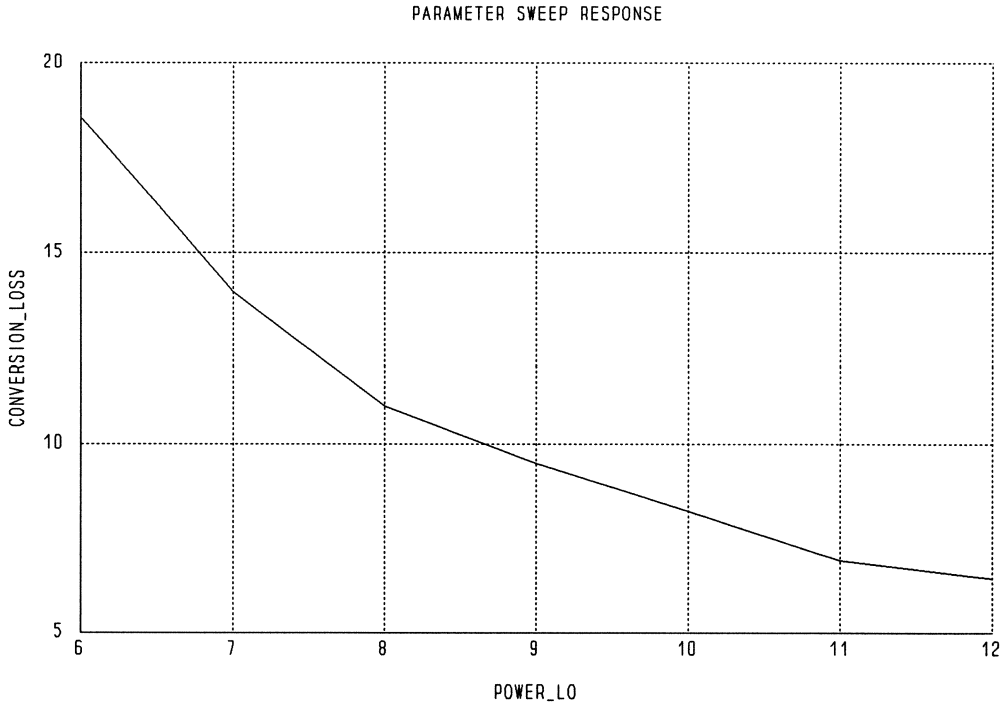

Mixer Output Power Spectrum (LO Power = 12dBm)

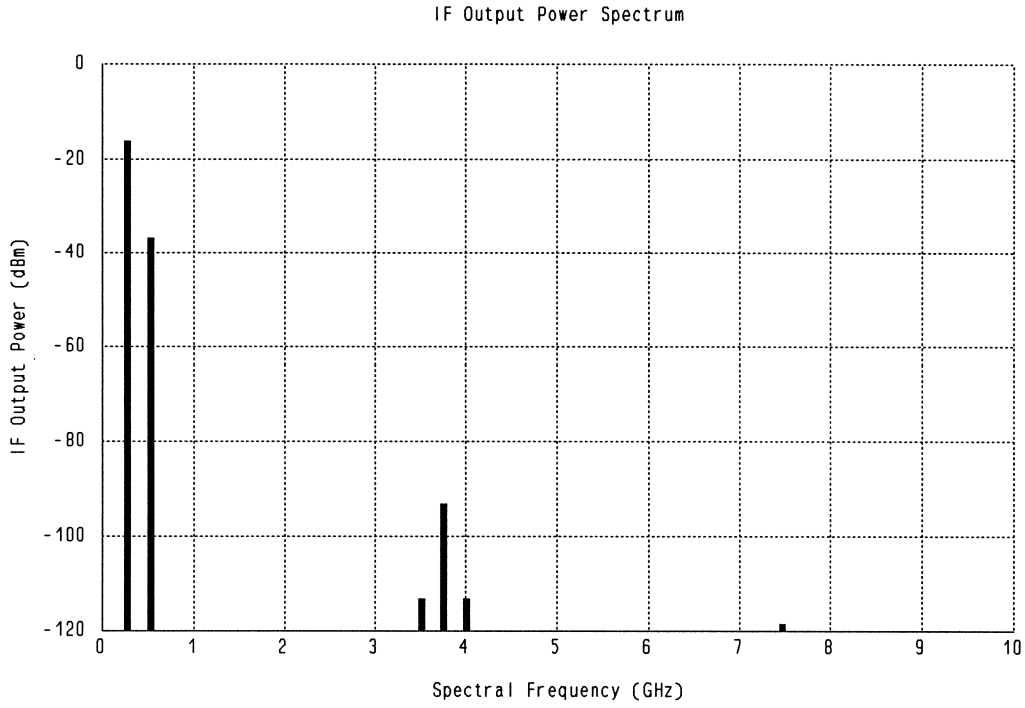

Mixer IF Output Voltage Waveform at Different LO Power Levels

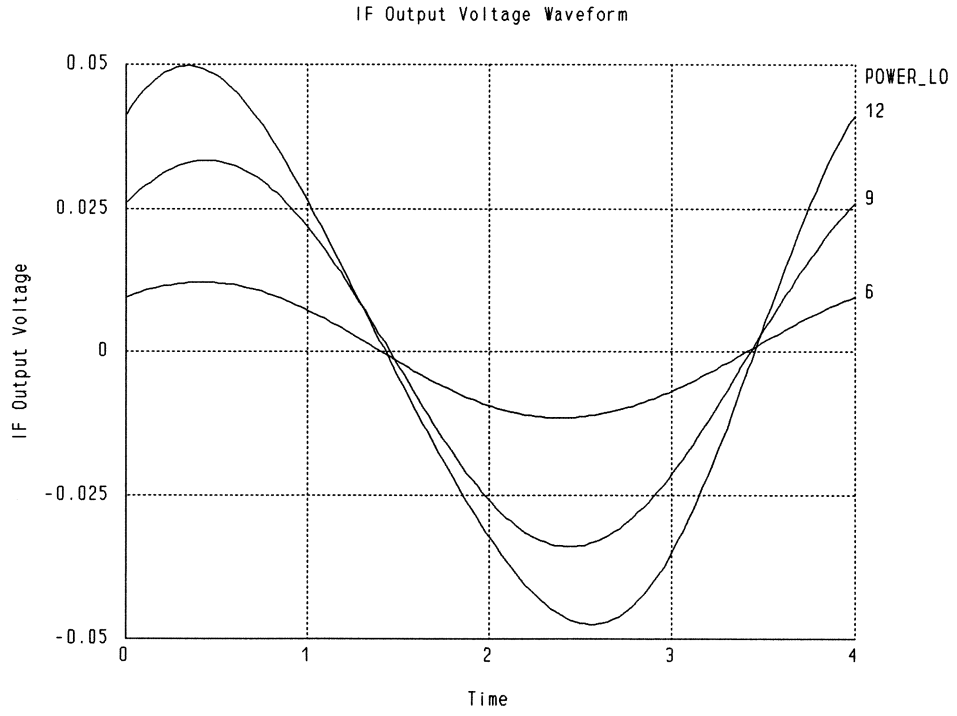

demo26

Large-signal two-tone optimization of a broadband FET gate mixer. The FET is modeled by the FETR model extracted by HarPE from *NEC700* data.

The main advantage of FET mixers over diode mixers is that we can obtain transducer conversion gain instead of conversion loss.

This example is loosely based on the example given by V. Rizzoli *et al.* in "State-of-the-art harmonic-balance simulation of forced nonlinear microwave circuits by the piecewise technique", *IEEE Trans. Microwave Theory Tech.*, vol. 40, pp. 12-28, 1992.

The FET gate mixer has a fixed LO frequency of 7GHz and broadband IF frequency from 0.1GHz to 1.5GHz.

The gate bias voltage and input matching circuit are optimized for high conversion gain over the frequency band.

In comparison, demo27 is a narrow-band FET mixer for which the conversion gain is maximized for a single IF frequency.

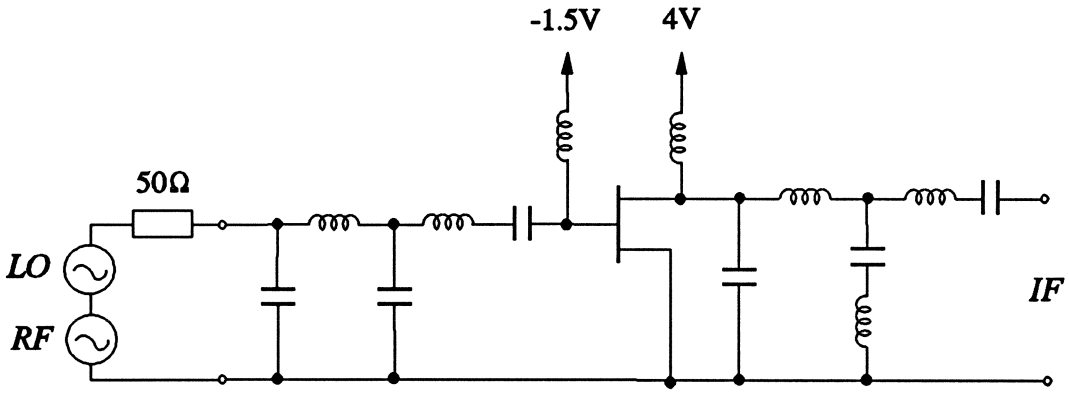

Input File

```
!  Example  demo26.ckt
!  Broadband FET gate mixer, fixed LO 7GHz, IF 0.1GHz - 1.5GHz.
!  The FETR model for NEC700 is extracted by HarPE.
!  The gate bias voltage and input matching circuit are optimized

Model
   IF_FREQ: 0.1GHz;
   P_LO: 6dBm;
   P_RF: -12dBm;

   PORT  1 0  P=P_LO  P2=P_RF;

   CAP  1 0  C=?0.28pF?;   ! input matching circuit
   IND  1 2  L=?0.1nH?;
```

```
   CAP  2 0  C=?0.25pF?;
   IND  2 3  L=?1.9nH?;

   CAP  3 4  C=50pF;

   IND      4 200  L=100nH;
   VSOURCE  200 0  VDC=?-1.5?;   ! gate biased near pinch-off

   Extrinsic2  10 20 30 4 5
      RG=3.5   LG=0.0306NH  RD=0.5       LD=0.00792NH
      RS=4.73  LS=0.0451NH  GDS=0.00345  CDS=0.08738PF  CX=10PF;

   FETR  10 20 30
      IS=5E-15    N=1         FC=0.5          GMIN=1.0E-07
      VBI=0.8     VBR=20.0    ALPHA=2         THETA=0.003
      BETA=0.029  VTO=-1.637  LAMBDA=0.04978  TAU=2.8PS
      CGS0=0.4428PF  CGD0=0.1066PF;

   IND      5 300  L=100NH;
   VSOURCE  300 0  VDC=4;

   CAP  5 0  C=1.284pF;  ! output IF low-pass filter
   IND  5 6  L=6.235nH;
   CAP  6 8  C=2.493pF;  ! resonant series L-C to short-circuit LO
   IND  8 0  L=0.207nH;
   IND  6 9  L=3.267nH;

   CAP  9 400  C=50pF;
   PORT 400 0  NAME=out;

   Circuit MIXER;

   Pout[0:N_SPECTRA] = if (PWout > 0) (10 * log10(PWout) + 30) else (NAN);
   Conversion_Gain = Pout[1] - P_RF;

   Return_Loss = -20 * log10(MS11);
end

sweep
   HB: IF_FREQ: from 0.1 to 1.5 step=0.2  FREQ=7GHZ FREQ2=(FREQ + IF_FREQ)
       Conversion_Gain Pout;

   HB: IF_FREQ: 0.1 0.5  FREQ=7GHZ FREQ2=(FREQ + IF_FREQ)  MVout PVout
       {Waveform  Spectrum=(MVout,PVout)."Vout_T"  IF_FREQ=all
        Tmin=0 Tmax=10 NT=150  Ymin=-0.4 Ymax=0.4 NYTicks=4};

   AC: FREQ: from 7GHZ to 8.5GHZ step=0.1GHz Return_Loss;
end

Spec
   HB: IF_FREQ: from 0.1 to 1.5 step=0.2  FREQ=7GHZ FREQ2=(FREQ + IF_FREQ)
       Conversion_Gain > 7;
end

Control
   Optimizer=Minimax;
end
```

Broadband FET Gate Mixer Transducer Conversion Gain versus IF Frequency

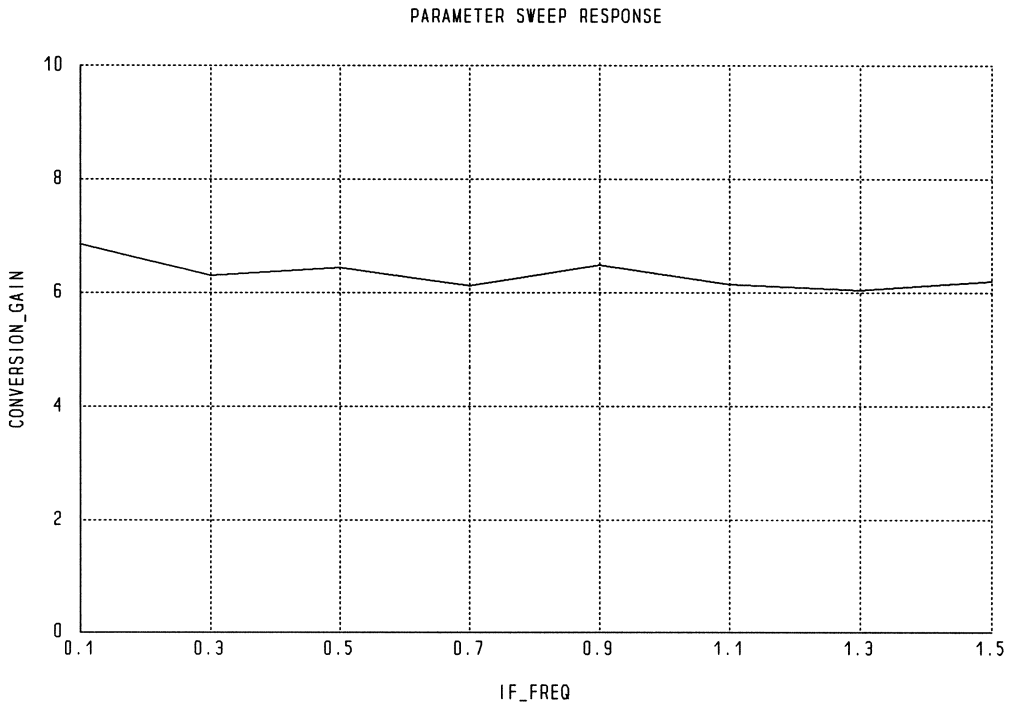

Mixer IF Output Voltage Waveforms at Two Different IF Frequencies

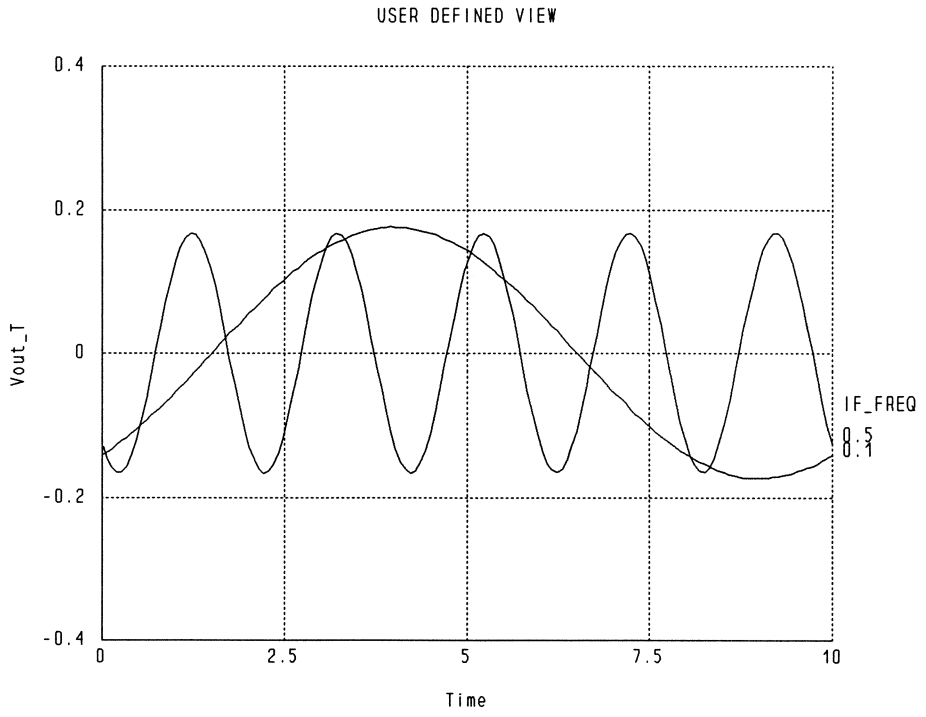

demo27

Nonlinear two-tone simulation of a narrow-band FET gate mixer. The FET is represented by the built-in FETR model extracted by HarPE from *NEC700* data.

This example has a similar topology as the broadband FET mixer in demo26. But this is a narrow-band design with fixed LO and RF frequencies of 7GHz and 8GHz, respectively.

Within the narrow band, we can obtain a higher conversion gain than that of the broadband design. The input matching circuit is tuned for maximum power extraction at the given RF frequency of 8GHz. The output matching circuit is design not only to serve as a low-pass IF filter but also to provide a high drain load at the IF frequency to increase the conversion gain.

We sweep the LO power and gate bias voltage to see their influence on the conversion gain.

A general strategy for FET mixer design is outlined by Stephen A. Maas in *Nonlinear Microwave Circuits*, Chapter 11.

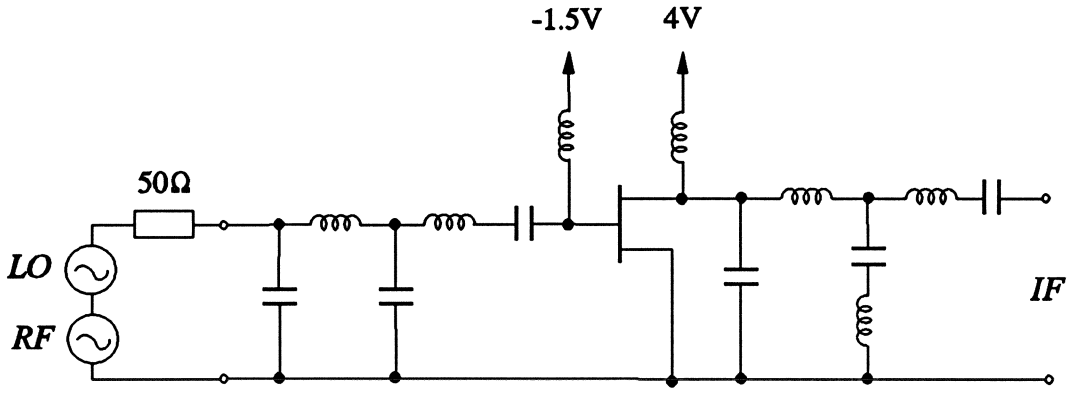

Input File

```
!  Example  demo27.ckt
!  narrow-band FET mixer, LO 7GHz, RF 8GHz, IF 1GHz.
!  The FETR model for NEC700 is extracted by HarPE.
!  This is very similar to demo26 except that demo26 is a broadband
!  design for IF from 0.1GHz to 1.5GHz.  Because this mixer is
!  narrow-band, we can design the input matching circuit for maximum
!  power extraction for a specific RF frequency.  We design the output
!  low-pass IF filter to serve as a matching circuit also, for high
!  drain load resistance at a single IF frequency.
!  The gate bias voltage is optimized for maximum conversion gain.

Model
   P_LO: 6;
   P_RF: -12dBm;
   VBIAS: -1.05;

   PORT  1 0  P=P_LO P2=P_RF;
```

```
   CAP  1 0  C=0.4196pF;   ! inpput matching circuit
   IND  1 2  L=0.0964nH;
   CAP  2 0  C=0.3385pF;
   IND  2 3  L=1.7679nH;

   CAP   3 4  C=50pF;

   IND      4 200  L=100nH;
   VSOURCE  200 0  VDC=VBIAS;   ! gate biased near pinch-off

   Extrinsic2  10 20 30 4 5
      RG=3.5   LG=0.0306NH  RD=0.5       LD=0.00792NH
      RS=4.73  LS=0.0451NH  GDS=0.00345  CDS=0.08738PF  CX=10PF;

   FETR  10 20 30
      IS=5E-15    N=1         FC=0.5          GMIN=1.0E-07
      VBI=0.8     VBR=20.0    ALPHA=2         THETA=0.003
      BETA=0.029  VTO=-1.637  LAMBDA=0.04978  TAU=2.8PS
      CGSO=0.4428PF  CGDO=0.1066PF;

   IND      5 300  L=100NH;
   CAP      300 0  C=50pF;
   VSOURCE  300 0  VDC=4;

   CAP  5 0  C=1.247pF;  ! output IF matching circuit and low-pass filter
   IND  5 6  L=14.43nH;  ! narrow-band for 1GHz
   CAP  6 8  C=1.963pF;
   IND  8 0  L=0.2633nH;
   IND  6 9  L=4.657nH;

   CAP  9 400  C=50pF;
   PORT 400 0  NAME=out;

   Circuit MIXER;

   Pout[0:N_SPECTRA] = if (PWout > 0) (10 * log10(PWout) + 30) else (NAN);
   Conversion_Gain = Pout[1] - P_RF;

   Ptotal = SUM(PWout);
   Spectral_Purity = 10 * log10(PWout[1] / (Ptotal - PWout[1]));

   Return_Loss = -20 * log10(MS11);
end

sweep
   HB: FREQ=7GHZ FREQ2=8GHZ  P_LO: from -9 to 9 step=3 from 10 to 12 step=1
       Conversion_Gain Spectral_Purity;

   HB: FREQ=7GHZ FREQ2=8GHZ  P_RF: -12 -9 -6 -3   Pout MVout PVout
       {Waveform  Spectrum=(MVout,PVout)."Vout_T"  P_RF=all
        Tmin=0 Tmax=2 NT=100  Ymin=-0.8 Ymax=0.8 NYTicks=4};

   HB: FREQ=7GHZ FREQ2=8GHZ
       VBIAS: -1.5 -1.3 -1.2 -1.15 -1.1 -1.075 -1.05 -1.025 -1 -0.95 -0.9 -0.8
       Conversion_Gain;

   AC: FREQ: 7GHZ 8GHZ  Return_Loss;
end
```

FET Mixer Conversion Gain versus LO Power Level

The following figure shows the FET mixer transducer conversion gain versus the LO power level with a gate bias voltage of -1.05V and -12dBm of RF available power.

At 6dBm LO power level, the conversion gain is greater than 9dB, about 3dB higher than that of the broadband mixer in demo26 under the same LO drive.

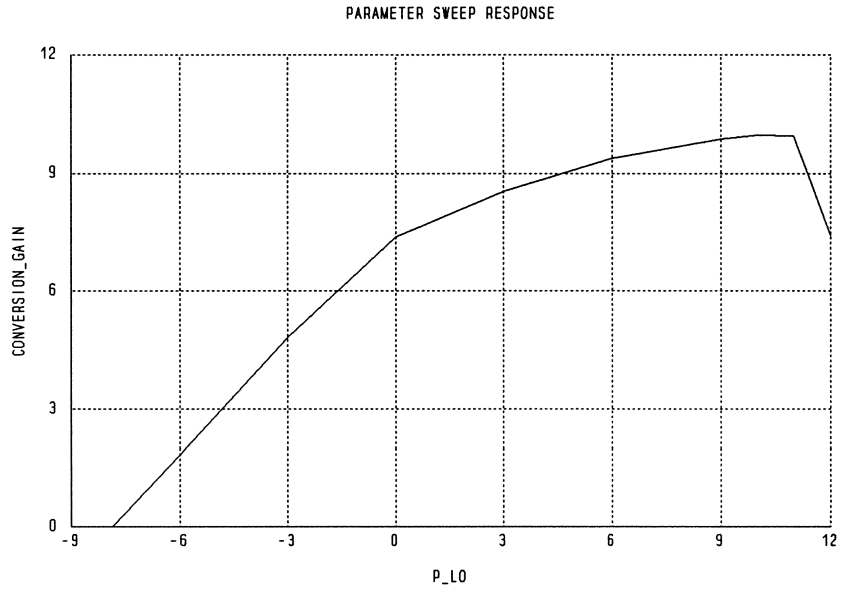

FET Mixer Conversion Gain versus Gate Bias Voltage

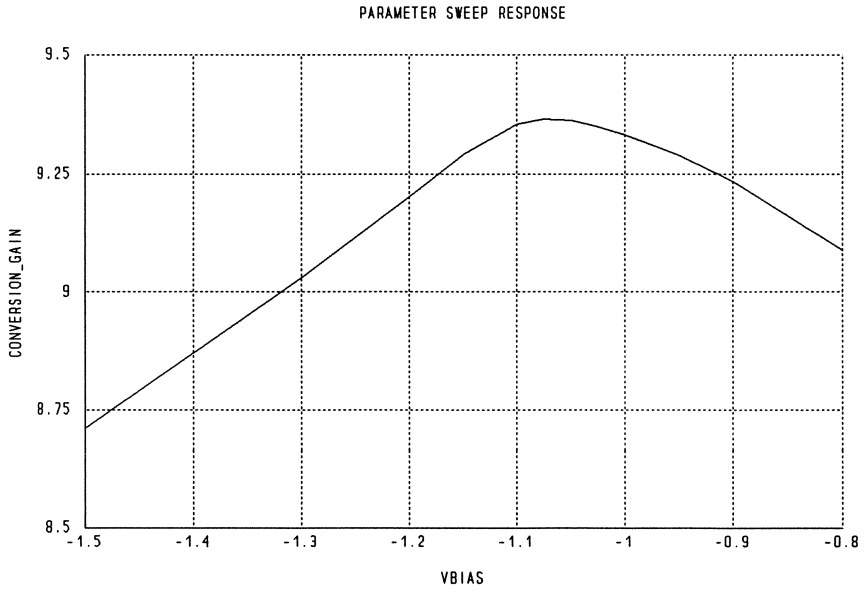

FET Mixer IF Output Voltage Waveforms at Different RF Power Levels

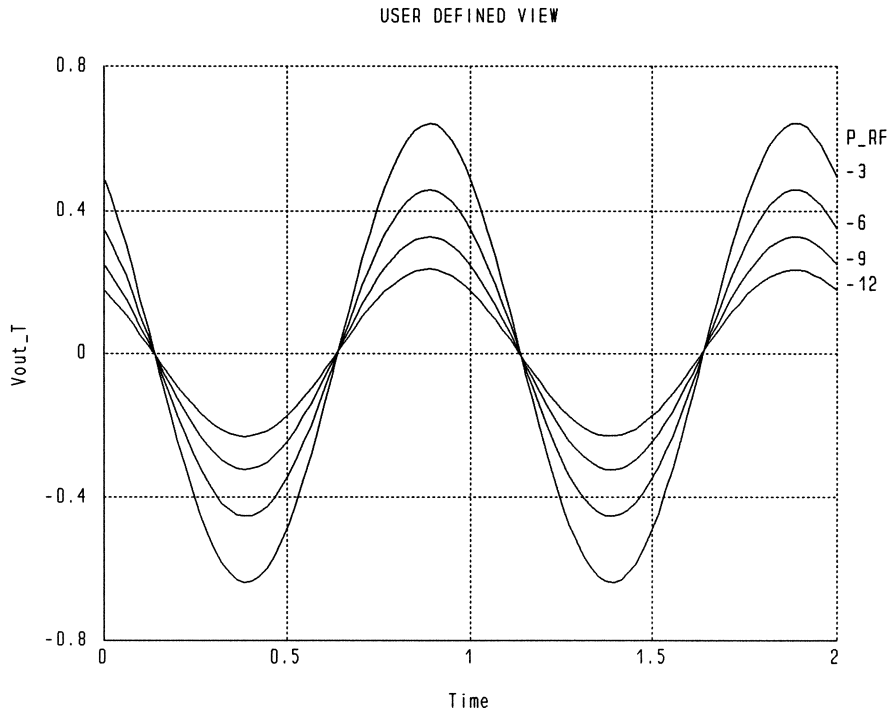

demo28

Two-tone intermodulation analysis of a simple nonlinear FET circuit. The FETM model parameters are extracted by HarPE from *MGF1902* data.

The two input tones are 1GHz and 1.01GHz, respectively, and have the same power level. The input power level is swept from -15dBm to 6dBm.

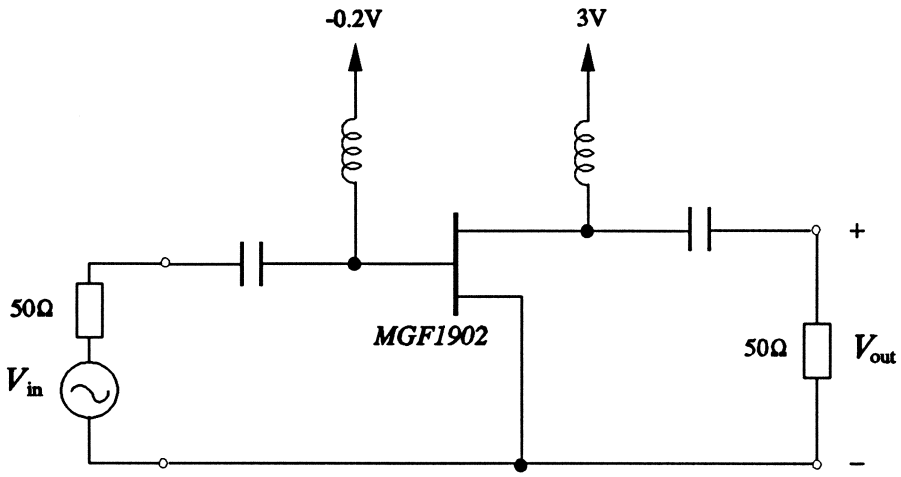

Input File

```
!  Example  demo28.ckt
!  third-order intermodulation product intercept point analysis
!  two-tone intermodulation analysis
!  the FET model for Mitsubishi MGF1902 is extracted by HarPE

Model
   CAP 1 2 C=1000pF;

   Extrinsic4  20 30 40 2 3
      RG=5          RD=0.2      RS=1.5     LS=0.0948NH
      LG=0.53633NH  LD=0.936NH  GDS=0.002  CDS=0.0278PF
      CDE=0.0682pF  CX=10pF;

   FETM  20 30 40
      E=1.4  SL=0.126  IB0=8e-12    ALPHAB=1     VBC=6
      GAMMA=-0.06356   K1=2         CF0=0.02PF   KF=-0.157
      IDSS=0.04716     VP0=-0.7338  R10=0.00343  C10=0.6294PF;

   CAP 2 0 C=0.184pF;  ! FET parasitic
   CAP 3 0 C=0.216pF;

   CAP 3 4 C=1000pF;

   Power: 0;

   PORT 1 0  P=Power P2=Power;

   PORT 4 0 NAME=out;

   IND 2 200 L=1000nH;
```

```
   VSOURCE 200 0  VDC=-0.2;

   IND 3 300 L=1000nH;
   VSOURCE 300 0  VDC=3;

   CIRCUIT  INTMOD;

   Pout[0:N_SPECTRA] = if (PWout > 0) (10 * log10(PWout) + 30);

   K10: Spectral_Index(FREQ,1,0);
   K01: Spectral_Index(FREQ,0,1);
   K21: Spectral_Index(FREQ,2,-1);
   K12: Spectral_Index(FREQ,-1,2);

   Pout_K[4] = [Pout[K21] Pout[K10] Pout[K01] Pout[K12]];
   FREQ_K[4] = [Spectral_Freq[K21] Spectral_Freq[K10]
                Spectral_Freq[K01] Spectral_Freq[K12]];

   K: 1;
end

Sweep
   HB: FREQ=1GHZ  FREQ2=1.01  Power: from -15dBm to 6dBm step=3dBm
       K: 1 2 3 4   Pout_K[K]  FREQ_K[K]
       {Xsweep title="Third-Order Intermodulation Intercept Point Analysis"
        X=Power  K=all  NXTicks=3  X_title="Input Power (dBm)"
        Y=Pout_K[K]  Ymin=-80 Ymax=20 NYTicks=5  Y_title="Pout (dBm)"}
       {Parametric  title="Output Power Spectrum"  P=K  Power=all
        X=FREQ_K[K]  Xmin=0.96 Xmax=1.05 NXticks=9  X_title="Frequency (GHz)"
        Y=Pout_K[K].bar & Pout_K[K]  Ymin=-40 Ymax=20 NYticks=6  Y_title="Pout (dBm)"};
end
```

Fundamental Output Power and Third-Order IM Products

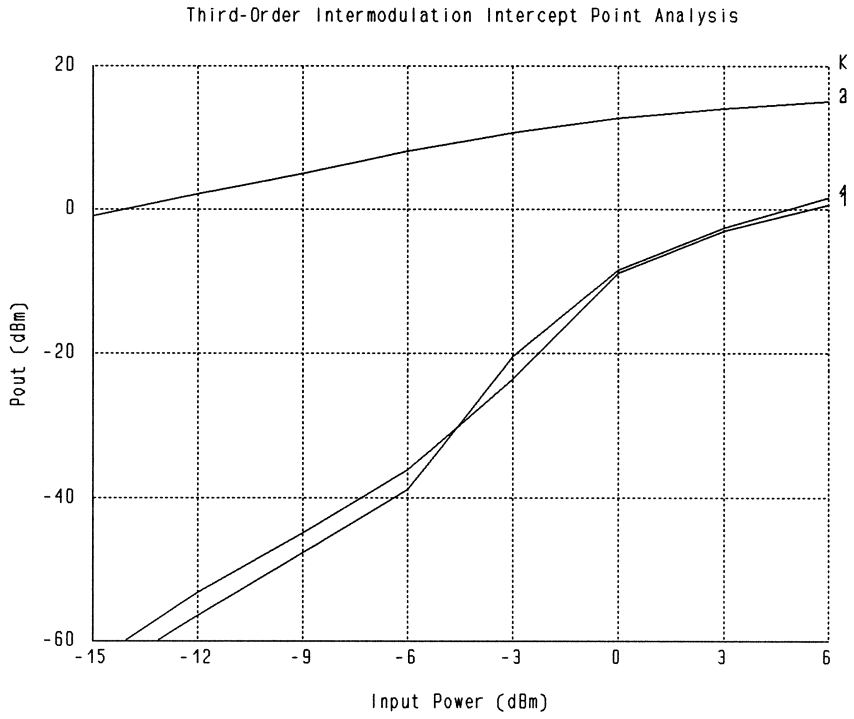

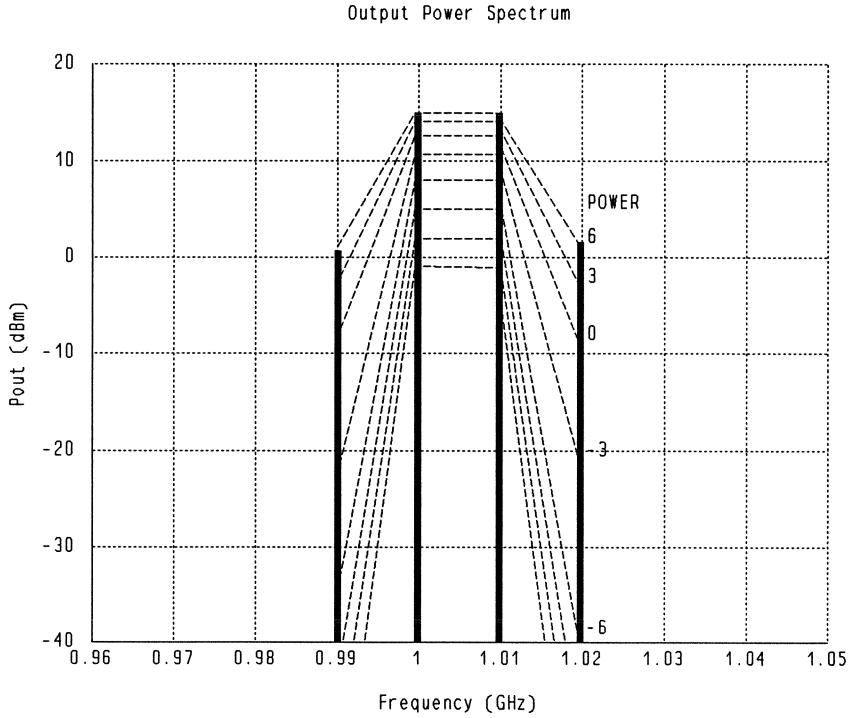

demo29

DC simulation of a single FET using the physics-based model FETT.

Input File

```
!  Example  demo29.ckt
!  DC simulation of the Trew Model (physics-based)

Model
   !  parasitics

   SRL  @int_gate   @gate     R=0.573  L=0.05NH;
   SRL  @int_drain  @drain    R=1.83   L=0.05NH;
   SRL  @int_source @ground   R=0.62   L=0.02NH;

   !  Trew FETT model

   FETT  @int_gate @int_drain @int_source
      L: 0.42UM     A: 0.35UM      W: 1MM
      ND: 2.1E23    EPSR: 12.5     EC: 3.75E5    VS: 1.5E-4
      VBI: 0.6      U0: 4.0E-10    D: 1.0E-12    LAMBDA: 0.01UM
      TAU: 3PS      Y0: 7.5E-8     YNOM: 9.3E-8  ALPHA: 0.2326;

   VG: 0;
   VD: 0;

   VSOURCE @gate @ground  NAME=GateBias  VDC=VG;
   VSOURCE @drain @ground  NAME=DrainBias  VDC=VD;

   CIRCUIT;

   IDS_mA: 1000 * IDrainBias_DC;
end

Sweep
   DC: VG: from -5 to 0 step=1
       VD: from 0 to 4 step=0.2 4.5  IDS_mA
       {Xsweep  Title="DC Drain Current Simulated Using FETT"
        X=VD VG=ALL Y=IDS_mA  Ymin=0  Ymax=450  NYTicks=9  NXTicks=9};
end
```

DC IV Characteristics Calculated Using FETT

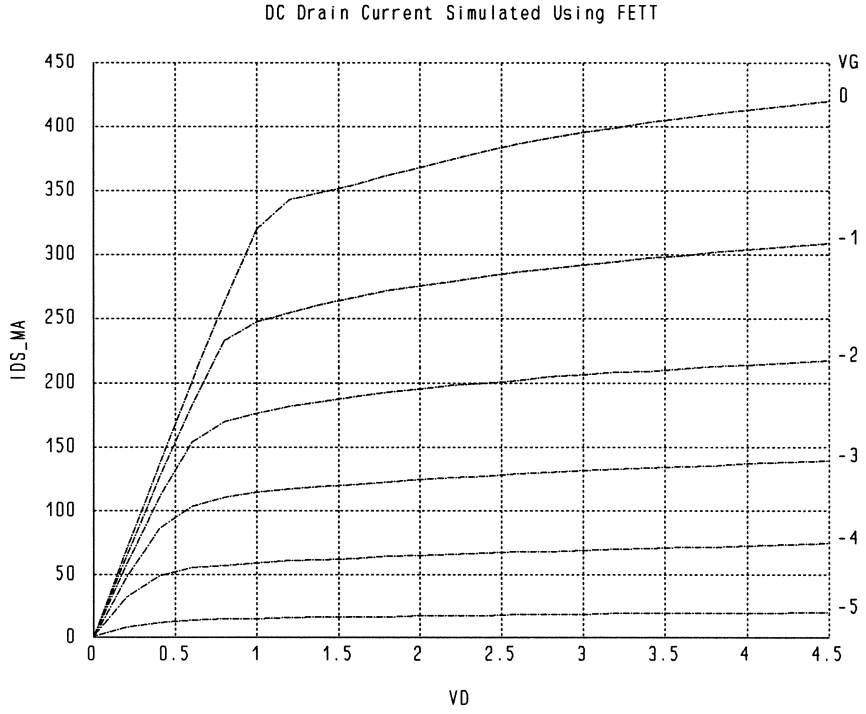

demo30

DC simulation of a single FET using the physics-based model FETT1 (a modified version of FETT for uniform doping).

Input File

```
! Example  demo30.ckt
! DC simulation of the modified Trew model (physics-based) FETT1

Model
   ! parasitics

   SRL  @int_gate   @gate     R=0.573  L=0.05NH;
   SRL  @int_drain  @drain    R=1.83   L=0.05NH;
   SRL  @int_source @ground   R=0.62   L=0.02NH;

   ! Trew FETT model

   FETT1  @int_gate @int_drain @int_source
      L: 0.42UM     A: 0.35UM      W: 1MM
      ND: 7.5E22    EPSR: 12.5     EC: 3.75E5    VS: 1.5E-4
      VBI: 0.6      U0: 4.0E-10    D: 1.0E-12    LAMBDA: 0.01UM
      TAU: 3PS      ALPHA: 0.2326;

   VG: 0;
   VD: 0;

   VSOURCE @gate @ground NAME=gate VDC=VG;
   VSOURCE @drain @ground NAME=drain VDC=VD;

   CIRCUIT;

   ID_mA = Idrain_DC * 1000;
end

Sweep
   DC: VG: from -5 to 0 step=1
       VD: from 0 to 4 step=0.2 4.5  ID_mA
       {Xsweep  Title="DC Drain Current Simulated Using FETT1"
        X=VD VG=ALL  Y=ID_mA Ymin=0 Ymax=450 NYTicks=9  NXTicks=9};
end
```

DC IV Characteristics Calculated Using FETT1

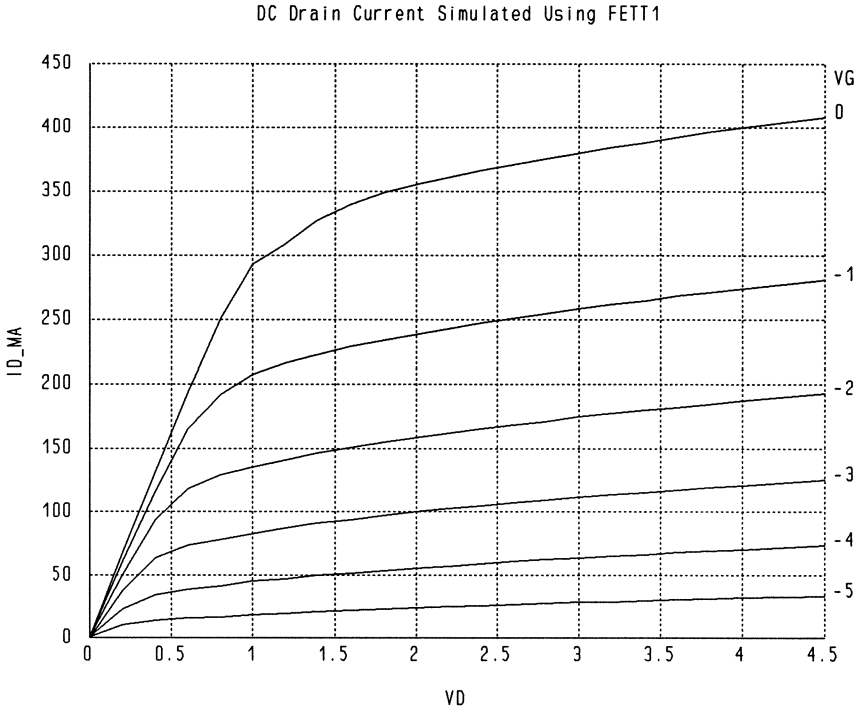

demo31

Illustration of a user-created nonlinear device model using the nonlinear controlled current source NLCCS. The Plessey FET model is created using NLCCS (demo17 illustrates the Plessey model using FETU1).

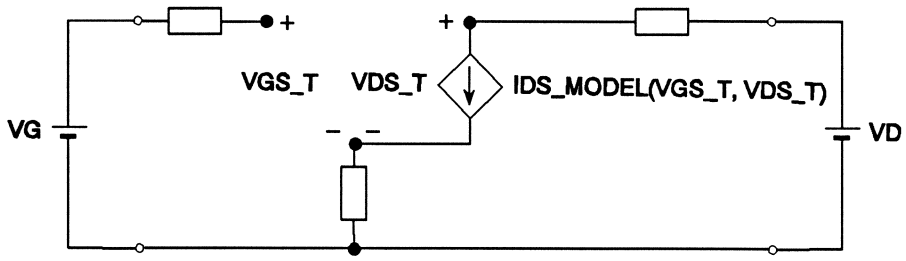

Input File

```
!  Example  demo31.ckt
!  demonstrate nonlinear controlled sources
!  Plessey model created using NLCCS

Model
   ! DC measurement data for  VDS = 0, 1, 2, 3, 5, 8, 10, 12

   VGS[5] = [-2  -1.5  -1  -0.5  0];
   IDS[5,8] = [0.0  0.0  0.0  0.1  0.5  3.7  8.0 12.4
               0.0  3.1  4.2  5.2  7.4 14.0 18.5 23.0
               0.1 15.7 17.5 18.8 21.2 27.3 31.1 35.0
               0.1 33.3 35.5 36.7 38.4 42.3 44.7 47.4
               0.2 53.6 56.8 57.5 57.9 58.5 59.0 59.9];

   ! Plessey model parameters

   THETA: ?0.320652?;
   VT0: ?-1.81628?;
   LAMBDA: ?-0.0829165?;
   ALPHA: ?2.51312?;
   GDST: ?0.0053694?;
   B: ?0.0304724?;
   BETA: ?0.0322512?;

   VLABEL  @gate  @source  NAME=VGS_T;
   VLABEL  @drain @source  NAME=VDS_T;

   xx0 = VGS_T - VT0;
   xx1 = (BETA * xx0 * xx0) / (1 + THETA * xx0);
   xx2 = 1 + LAMBDA * VDS_T;
   xx3 = (1 - VGS_T / (VT0 * (1 + B * VDS_T))) * GDST;
   IDS_MODEL = (xx1 * xx2 + xx3 * VDS_T) * tanh(ALPHA * VDS_T);

   NLCCS  @drain @source  I=IDS_MODEL;

   RES  @gate0  @gate   R=0.5;
   RES  @drain0 @drain  R=3.5;
   RES  @source 0       R=3;

   I: 1;
   VDS: 0;
```

```
   VSOURCE  @gate0  0  VDC=VGS[I];
   VSOURCE  @drain0 0  NAME=DS  VDC=VDS;

   CIRCUIT;

   ID_mA: IDS_DC * 1000.0;

   ! check if we have data for a given value of VDS

   VDS_map[0:12] = [1 2 3 4 0 5 0 0 6 0 7 0 8];
   VDS_int = floor(VDS);
   VDS_index: if (VDS >= 0 & VDS <= 12 & VDS = VDS_int) (VDS_map[VDS_int]);

   ID_data: if (VDS_index) (IDS[I,VDS_index]) else (NAN);
end

Sweep
   DC: I: from 1 to 5 step=1
       VDS: from 0 to 2 step=0.2  from 3 to 12 step=1
       ID_mA  ID_data
       {Xsweep  Title="Plessey Model Fitting DC Measurement"
        X=VDS I=all NXticks=6 Y_title="ID (mA)"
        Y=ID_mA.green & ID_data.white.circle  Ymin=0 Ymax=70 NYTicks=7};
end
```

Plessey Model Defined Using NLCCS Fitting Measured DC Data

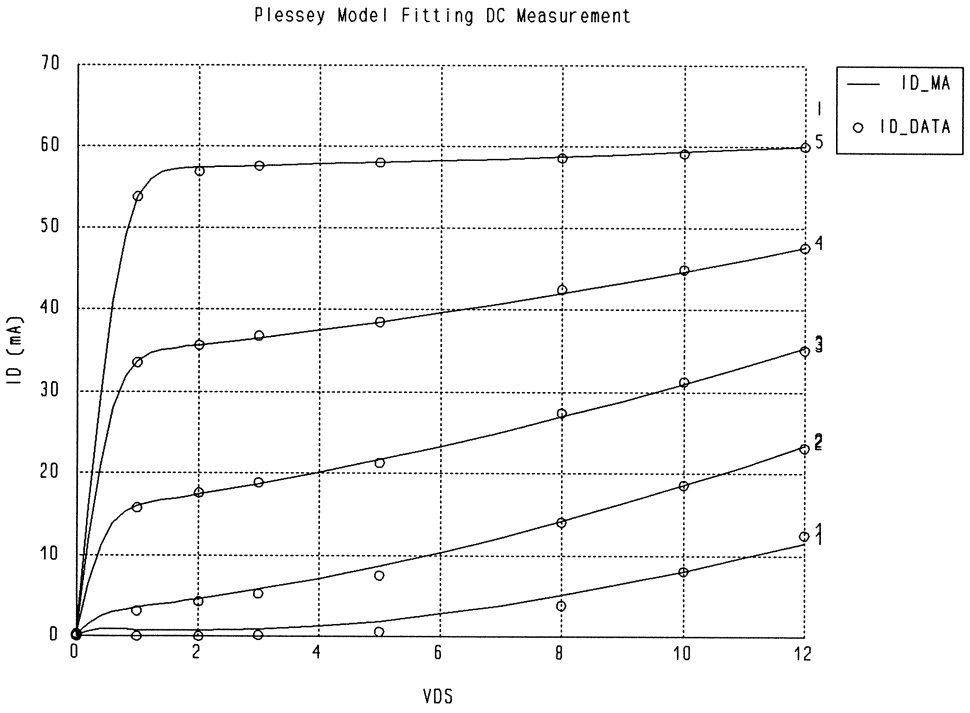

demo32

Illustration of using OSA90 for parameter extraction.

The parameters of the Materka FET model FETM are extracted by ℓ_1 optimization from measured S parameters. Compared with HarPE, OSA90 offers greater flexibility in the definition of device models. On the other hand, straightforward parameter extraction of a single nonlinear device can usually be done faster using HarPE, since it is specialized for this purpose.

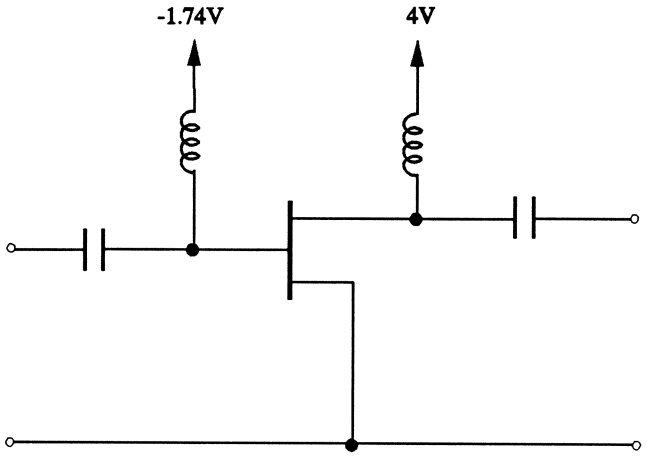

Input File

```
! Example  demo32.ckt
! illustrate parameter extraction: fitting measured S-parameters
! also illustrate Smith chart and polar plot Views
! model used: built-in FETM (Materka and Kacprzak model)
! not as efficient as OSA's HarPE for parameter extraction

Model
   #define N_FREQS  17

   Freqs[N_FREQS] = [2 3 4 5 6 7 8 9 10 11 12 13 14 15 16 17 18];

   ! measured data

   MS11_data[N_FREQS] =
      [0.9585 0.9457 0.9004 0.8847 0.8597 0.8375 0.8262 0.8144
       0.8145 0.8080 0.8023 0.7920 0.8003 0.7885 0.7926 0.7871 0.7972];

   PS11_data[N_FREQS] =
      [-36.75 -54.12 -67.99 -82.22 -92.49 -104.76 -111.74 -122.27 -128.60
       -134.73 -141.64 -146.83 -153.41 -159.07 -162.96 -167.84 -169.40];

   MS21_data[N_FREQS] =
      [3.1389 2.8906 2.7296 2.4969 2.2895 2.0371 1.8851 1.7462 1.6536
       1.4918 1.4118 1.3213 1.2339 1.1325 1.0965 0.9808 0.9671];

   PS21_data[N_FREQS] =
      [150.53 135.84 125.90 111.25 103.05 91.36 86.36 75.87 66.69 64.58
       53.94 49.51 42.40 33.85 32.61 21.65 20.98];
```

```
   MS12_data[N_FREQS] =
      [0.0408 0.0567 0.0688 0.0787 0.0836 0.0868 0.0873 0.0896 0.0951
       0.0906 0.0942 0.0896 0.0905 0.0856 0.0857 0.0811 0.0799];

   PS12_data[N_FREQS] =
      [66.80 56.58 47.29 37.94 32.18 21.53 20.33 12.49 9.33 7.99
       0.67 0.20 -5.70 -8.18 -9.30 -13.31 -14.38];

   MS22_data[N_FREQS] =
      [0.5439 0.5303 0.5204 0.5232 0.5309 0.5177 0.5312 0.5321 0.5543
       0.5553 0.5692 0.5759 0.5958 0.6067 0.6098 0.6270 0.6318];

   PS22_data[N_FREQS] =
      [-23.91 -36.95 -45.35 -55.70 -62.18 -71.76 -76.63 -84.21 -88.84
       -92.92 -99.86 -102.41 -109.06 -114.76 -115.86 -121.67 -120.02];

   Extrinsic2  1 2 3 4 5
      LG: 0.1NH   RG: 0.0119   RD: 0.0006
      LD: 0.1NH   RS: 0.33     CX: 10PF
      GDS: ?0.004?
      LS: ?0.1NH?
      CDS: ?0.1PF?;

   FETM  1 2 3
      GAMMA: -0.1   KE: 0        SL: 0.2
      KG: -0.25     TAU: 3PS     SS: 0
      IG0: 5E-10    ALPHAG: 20   IB0: 8e-12
      ALPHAB: 1     VBC: 20      R10: 5.2
      KR: 0         K1: 1        C1S: 0.0048PF
      IDSS: ?0.2?
      VP0: ?-4?
      E: ?2?
      C10: ?0.67PF?
      CF0: ?0.023PF?
      KF: ?-0.12?;

   CAP 4 6 C=10pF;
   PORT 6 0;

   CAP 5 7 C=10pF;
   PORT 7 0;

   IND 4 8 L=20nH;
   VSOURCE 8 0  VDC=-1.74V;

   IND 5 9 L=20nH;
   VSOURCE 9 0  VDC=4V;

   CIRCUIT;

   MP2RI(MS11_data, PS11_data, RS11_data[N_FREQS], IS11_data[N_FREQS]);
   MP2RI(MS21_data, PS21_data, RS21_data[N_FREQS], IS21_data[N_FREQS]);
   MP2RI(MS12_data, PS12_data, RS12_data[N_FREQS], IS12_data[N_FREQS]);
   MP2RI(MS22_data, PS22_data, RS22_data[N_FREQS], IS22_data[N_FREQS]);

   K: 1;
end

Sweep
   AC: K: from 1 to N_FREQS step=1
       FREQ = Freqs[K]
       RS11, IS11, RS11_data[K], IS11_data[K]
       RS21, IS21, RS21_data[K], IS21_data[K]
       RS12, IS12, RS12_data[K], IS12_data[K]
       RS22, IS22, RS22_data[K], IS22_data[K], FREQ
       {Parametric title="Match Between Simulated and Measured S11 and S22"
        X=FREQ  x_title="Frequency in GHz"
        y_title="Real[S11], Imag[S11], Real[S22] and Imag[S22]"
        y=RS11.green & RS11_data[k].green.circle &
          IS11.yellow & IS11_data[k].yellow.triangle &
          RS22.red & RS22_data[k].red.square &
```

```
          IS22.cream & IS22_data[k].cream.X
         Ymin=-1 Ymax=1 NYTicks=4}
        {Parametric title="Match Between Simulated and Measured S21"
         X=FREQ  x_title="Frequency in GHz"
         y_title="Real[S21] and Imag[S21]"
         y=RS21.green & RS21_data[k].green.circle &
           IS21.yellow & IS21_data[k].yellow.triangle
         Ymin=-4 Ymax=3 NYTicks=7 }
        {Parametric title="Match Between Simulated and Measured S12"
         X=FREQ  x_title="Frequency in GHz"
         y_title="Real[S12] and Imag[S12]"
         y=RS12.green & RS12_data[k].green.circle &
           IS12.yellow & IS12_data[k].yellow.triangle
         Ymin=-0.05 Ymax=0.1 NYTicks=3}
        {Smith title="Match Between Simulated and Measured S11 and S22"
         RI=(RS11,IS11)."S11".green &
            (RS11_data[k],IS11_data[k])."S11_data".green.circle &
            (RS22,IS22)."S22".red &
            (RS22_data[k],IS22_data[k])."S22_data".red.triangle}
        {Polar title="Match Between Simulated and Measured S21"
         RI=(RS21,IS21)."S21" &
            (RS21_data[k],IS21_data[k])."S21_data".circle}
        {Polar title="Match Between Simulated and Measured S12"
         RI=(RS12,IS12)."S12" &
            (RS12_data[k],IS12_data[k])."S12_data".circle};
end

Specification
   AC: K: from 1 to N_FREQS step=1
       FREQ = Freqs[K]
       RS11 = RS11_data[K]
       IS11 = IS11_data[K]
       RS21 = RS21_data[K]  W=0.5
       IS21 = IS21_data[K]  W=0.5
       RS12 = RS12_data[K]  W=10
       IS12 = IS12_data[K]  W=10
       RS22 = RS22_data[K]
       IS22 = IS22_data[K];
end
```

Match Between Simulated and Measured S Parameters After Optimization

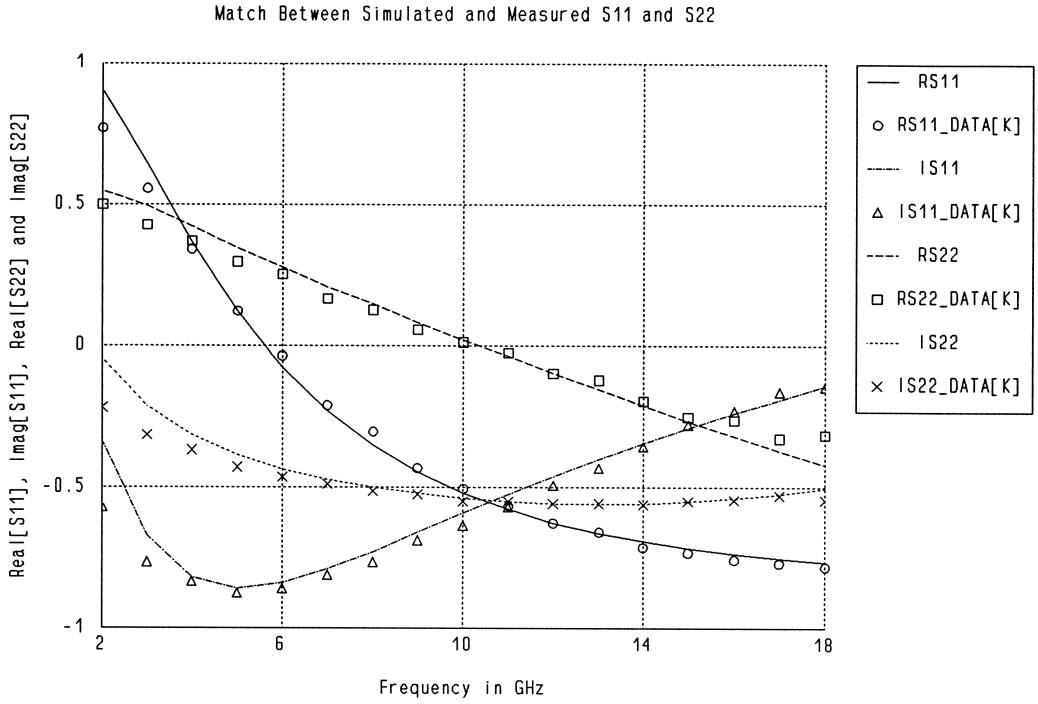

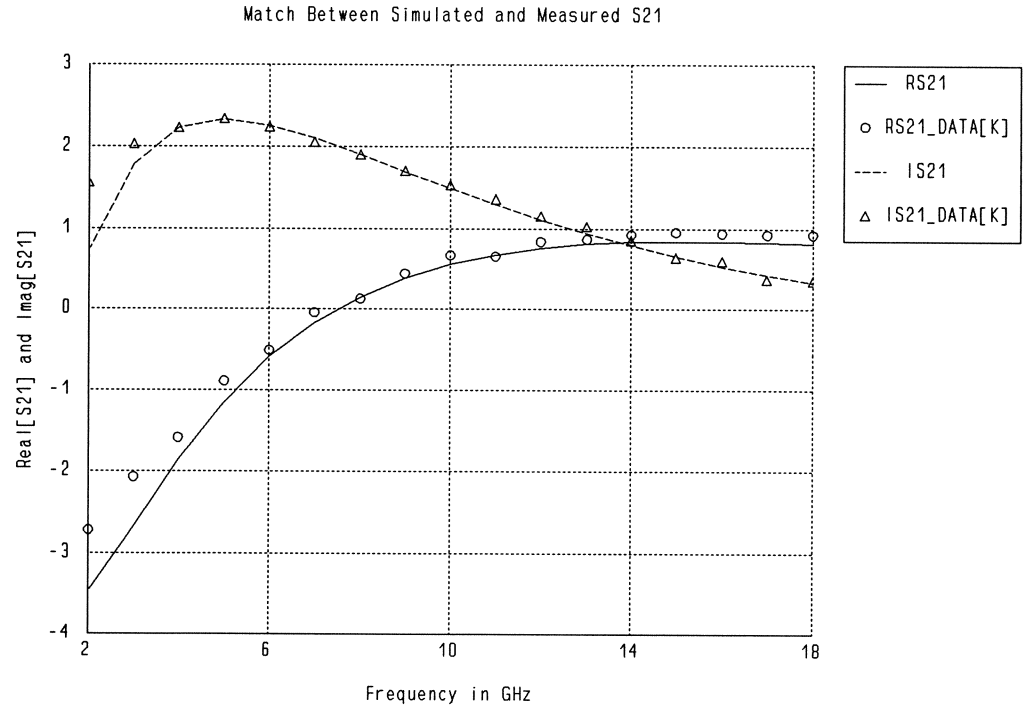

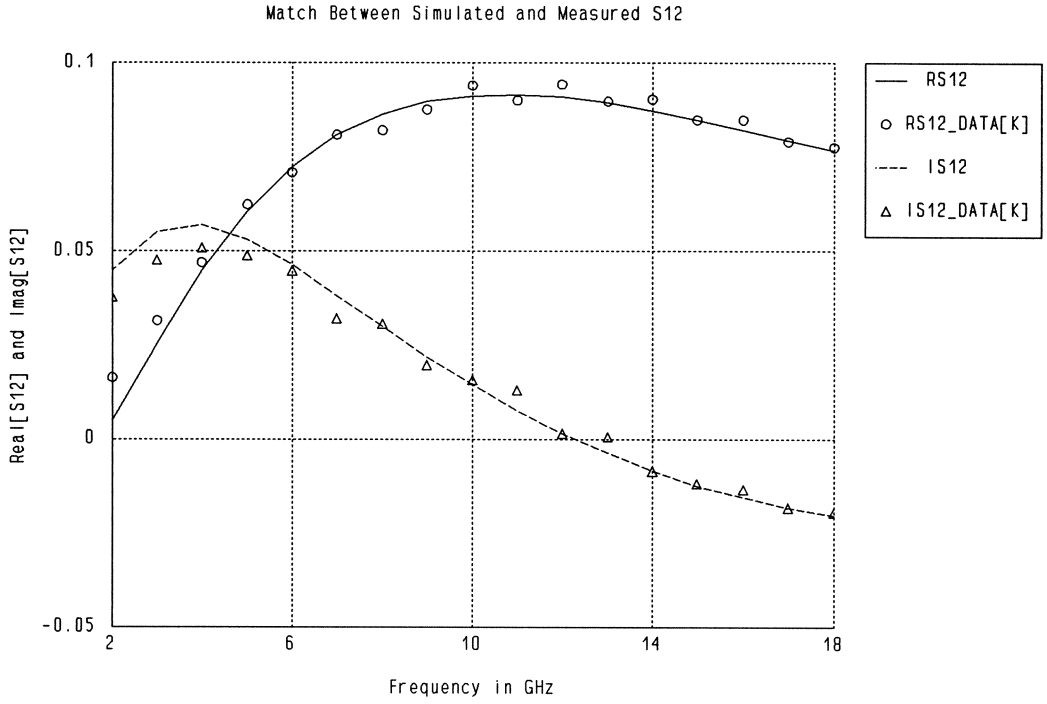
Match Between Simulated and Measured S12
0.1
0.05
0
-0.05
Real[S12] and Imag[S12]
2
6
10
14
18
Frequency in GHz
RS12
RS12_DATA[K]
IS12
IS12_DATA[K]

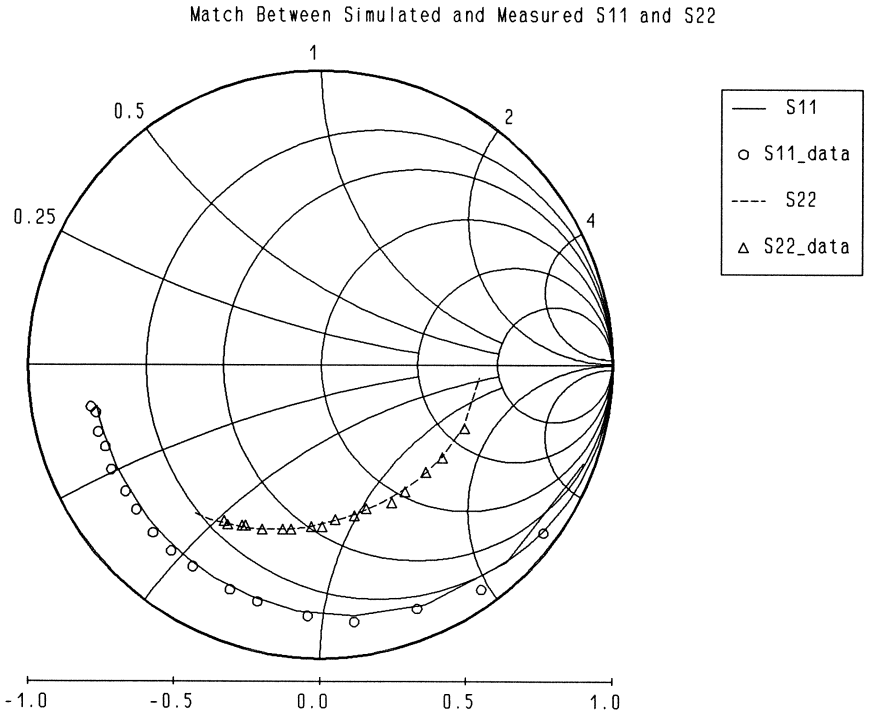
Match Between Simulated and Measured S11 and S22
1
0.5
2
0.25
4
-1.0
-0.5
0.0
0.5
1.0
S11
S11_data
S22
S22_data

demo33

Minimax optimization of a microstrip line 3:1 impedance transformer.

The design goal is to match a 50OH input impedance to a 150OH load. The input reflection coefficient is minimized over the frequency range from 5GHz to 15GHz.

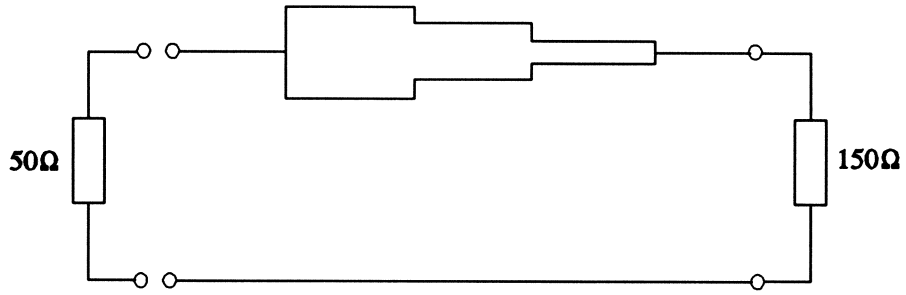

Input File

```
!  Example  demo33.ckt
!  minimax optimization of a microstrip impedance transformer
!  minimize the reflection coefficient, Z0=50, ZL=150, 5GHz to 15GHz

Model
   H    = 0.635MM;
   L_MM = 1MM;
   W10  = ?1?;
   W1   = W10 * H;
   W20  = ?0.4?;
   W2   = W20 * H;
   W30  = ?0.2?;
   W3   = W30 * H;
   L0   = 3;
   L1   = L0 * L_MM;
   L2   = L0 * L_MM;
   L3   = L0 * L_MM;
   Z0   = 50;
   ZL   = 150;

   MSUB  EPSR=9.7 H=0.635MM T=0 TAND=0 ROC=0 RHS=0;
   MSL     1 2  W=W1  L=L1 ;
   MSTEP   2 3  W1=W1 W2=W2;
   MSL     3 4  W=W2  L=L2 ;
   MSTEP   4 5  W1=W2 W2=W3;
   MSL     5 6  W=W3  L=L3 ;

   RES     6 0  R=ZL;

   PORT    1 0;

   CIRCUIT;
End

Sweep
   AC: FREQ: from 2GHZ to 18GHZ step=0.25GHZ  MS11;
End

Spec
   AC: FREQ: from 5GHZ to 15GHZ step=1GHZ  MS11;
```

```
End

Control
   Optimizer=Minimax;
end
```

Transformer Reflection Coefficient After Minimax Optimization

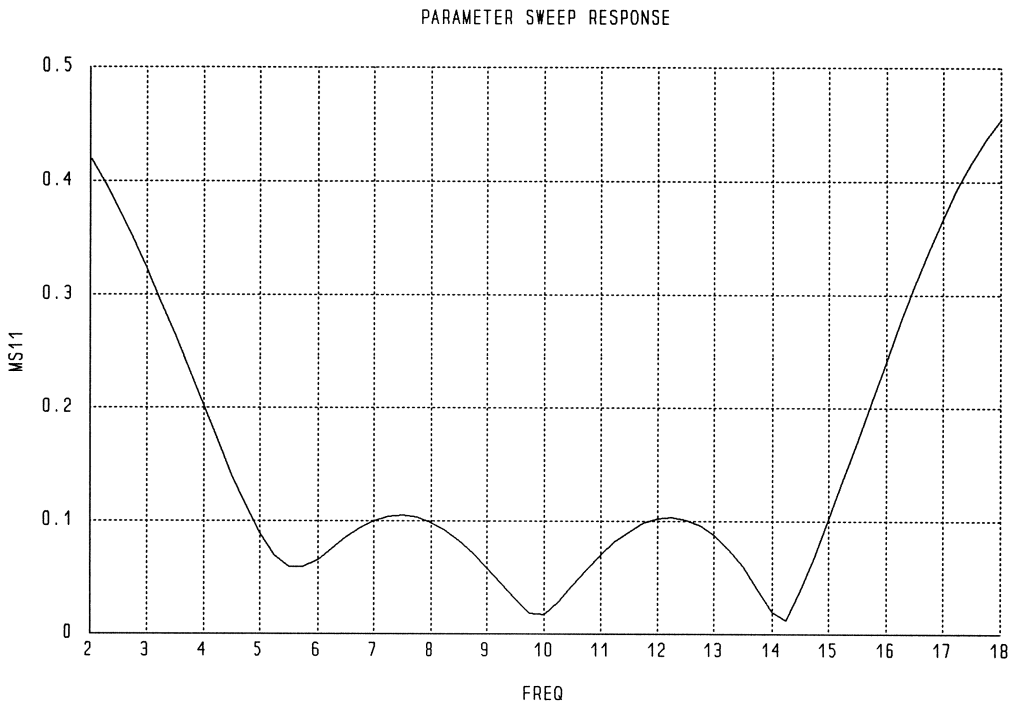

demo34

Small-signal simulation of a microstrip filter. The microstrip structure is published in *Radio and Electronics Eng.*, vol. 50, 1980, pp. 54-58.

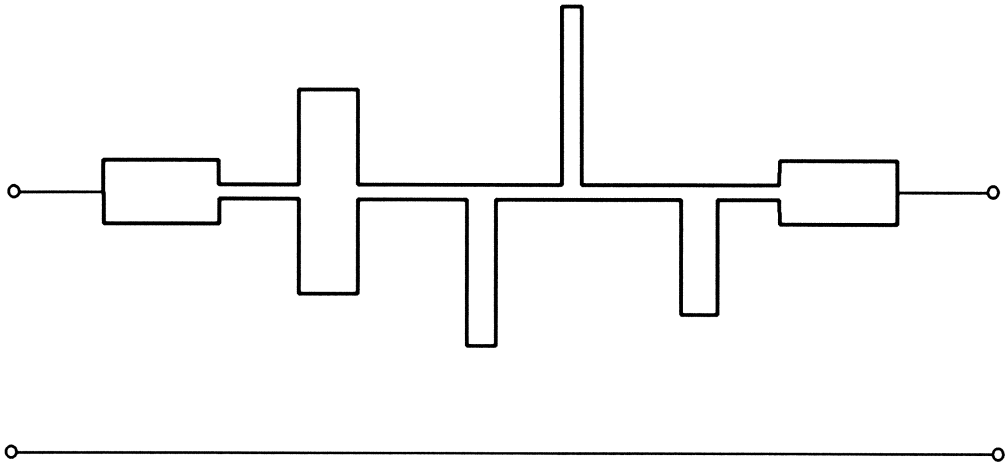

Input File

```
!  Example  demo34.ckt
!  microstrip filter example for OSA90
!  the diagram of the structure can be found in
!  Fig. 7 of The Radio and Electronics Eng., vol. 50,
!  no. 1/2, 1980, pp. 54-58

Model

   W10 = 4.76mm;
   W20 = 0.67mm;

   WA = 0.67E-3;
   WB = 0.67E-3;
   WS = 4.44E-3;
   H0 = 1.56E-3;
   ER = 2.32;
   MSUB EPSR=2.32 H=1.56mm T=0.006mm TAND=0.0002 RHS=0.0 ROC=0.0172E-6;
   MSL    1  2  L=4mm      W=W10;
   MStep  2 20             W1=W10 W2=W20;
   MSL    20 3  L=6.94mm   W=W20;
   MCROSS 3 30 4 5 W1=WA W2=WS W3=WB;
   MOPEN  30    L=9.78mm W=4.44mm;
   MOPEN  5     L=9.78mm W=4.44mm;
   MSL    4 6   L=8.48mm    W=W20;
   MTEE   6 7 8            W1=W20 W2=W20 W3=1.85mm;
   MOPEN  8     L=16.7mm   W=1.85mm;
   MSL    7 9   L=6.0mm    W=W20;
   MTEE 9 10 11            W1=W20 W2=W20 W3=W20;
   MOPEN  11    L=17.81mm W=W20;
   MSL    10 12 L=6.7mm    W=W20;
   MTEE 12 13 14           W1=W20 W2=W20 W3=2.77mm;
   MOPEN  14    L=14.54mm W=2.77mm;
   MSL    13 15 L=4.67mm   W=W20;
```

```
   MSTEP  15 16           W1=W20 W2=W10;
   MSL    16 17 L=4mm     W=W10;

   PORT 1 0 NAME=p1;
   PORT 17 0 NAME=p2;

   CIRCUIT;

end

Sweep
! S-parameter simulation
   AC: FREQ: from 0.1GHZ to 8GHZ step=0.05ghz
       MS11 PS11 MS12 PS12
       MS21 PS21 MS22 PS22
end
```

Microstrip Filter Response

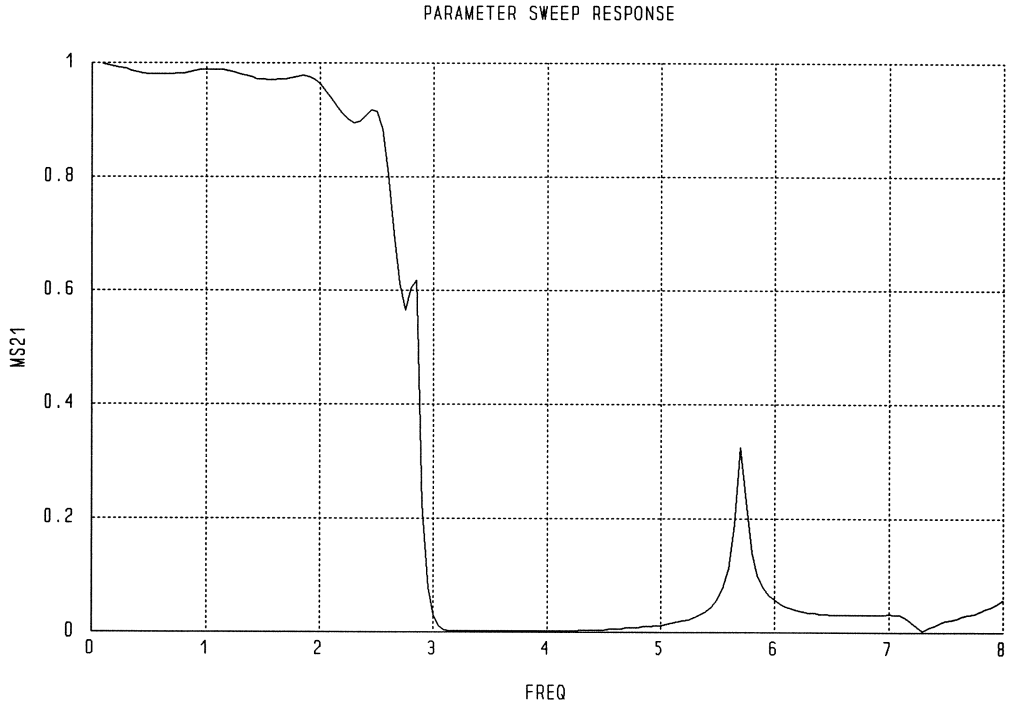

demo35

Monte Carlo analysis of a single-stage feedback amplifier.

The FET is represented by a small-signal linear equivalent circuit. The FET parameter statistics are extracted from Plessey measurements.

The matching circuits and drain to gate feedback are realized by microstrip line structures. A 0.5MIL tolerance (uniform distribution) is assumed for all goemetrical dimensions of the microstrip lines.

Yield is estimated by Monte Carlo simulation with 250 outcomes w.r.t. the specification of $7\text{dB} \leq |S_{21}| \leq 8\text{dB}$, from 6GHz to 18GHz.

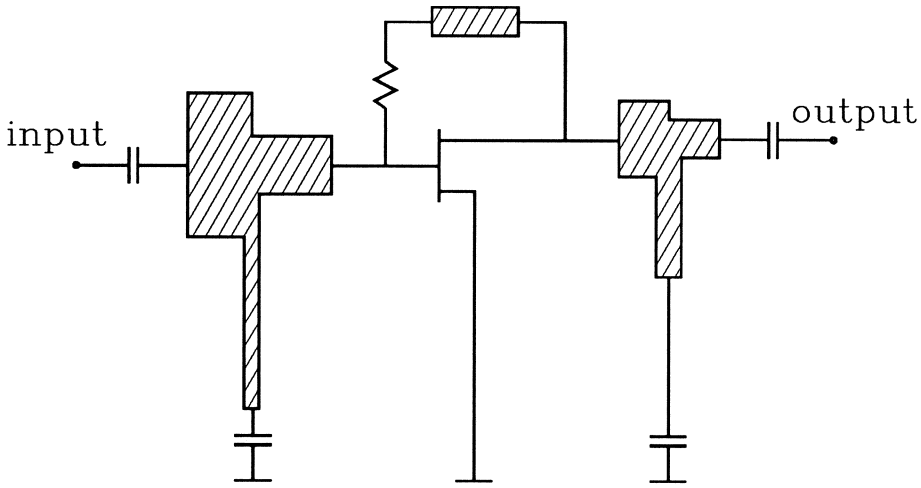

Input File

```
!  Example  demo35.ckt
!  Monte Carlo analysis of a microstrip feedback amplifier.
!  The nominal design satisfies 7dB <= MS21 <= 8dB, 6GHz - 18GHz.
!  The FET is represented by a small-signal linear equivalent circuit.
!  The model parameter statistics are extracted from Plessey measurements.

Model
   MSUB  EPSR=9.9 H=10MIL T=0.15MIL ROC=0.0 RHS=0;

   tol: 0.5MIL;

   PORT  1 0;
   CAP   1 2  C=10pF;

   ! input matching structure

   Wg1: 17MIL   {Uniform tol=tol};
   Lg1: 37.4MIL {Uniform tol=tol};
   Wg2: 8MIL    {Uniform tol=tol};
   Lg2: 29.2MIL {Uniform tol=tol};
   Wg3: 3MIL    {Uniform tol=tol};
   Lg3: 113MIL  {Uniform tol=tol};
```

```
   MSL   2 3    W=Wg1 L=Lg1;
   MTEE  3 4 5  W1=Wg1 W2=Wg2 W3=Wg3;
   MSL   4 6    W=Wg2 L=Lg2;
   MSL   5 7    W=Wg3 L=Lg3;
   CAP   7 0    C=10pF;

   FET_STATISTICAL_MODEL(6,8);

   ! feed back microstrip line

   Wfb: 2MIL  {Uniform tol=tol};
   Lfb: 10MIL {Uniform tol=tol};

   RES  6 9  R=1.6KOH;
   MSL  9 8  W=Wfb L=Lfb;

   ! output matching structure

   Wd1: 8.5MIL {Uniform tol=tol};
   Ld1: 4.5MIL {Uniform tol=tol};
   Wd2: 4MIL   {Uniform tol=tol};
   Ld2: 10MIL  {Uniform tol=tol};
   Wd3: 3.5MIL {Uniform tol=tol};
   Ld3: 50MIL  {Uniform tol=tol};

   MSL    8 10     W=Wd1 L=Ld1;
   MTEE  10 11 12  W1=Wd1 W2=Wd2 W3=Wd3;
   MSL   11 13     W=Wd2 L=Ld2;
   MSL   12 14     W=Wd3 L=Ld3;
   CAP   14  0     C=10pF;

   CAP   13 15  C=10pF;
   PORT  15 0;

   CIRCUIT;

   MS21_dB = 20 * log10(MS21);
end

Sweep
   AC: FREQ: from 4GHz to 20GHz step=0.5GHz  MS21_dB
       {Xsweep Y=MS21_DB NXticks=8  Ymin=5 Ymax=9 NYTicks=4};
end

MonteCarlo
   AC: FREQ: from 6GHz to 18GHz step=1GHz
       MS21_DB > 7  MS21_DB < 8
       N_OUTCOMES=250;

   AC: FREQ: from 4GHz to 20GHz step=1GHz  MS21_DB;
End

#define FET_STATISTICAL_MODEL(n1,n2) {
   RG: 2.03466 {Normal Sigma=3% Correlation=CORMAT[1] DDF= 12 10 13 22 22 9 4 3 2 3};
   RD: 3.42131 {Normal Sigma=8% Correlation=CORMAT[2] DDF= 5 3 5 4 7 8 7 8 6 47};
   RS1:3.75428 {Normal Sigma=6% Correlation=CORMAT[3] DDF= 14 13 5 6 9 4 13 12 13 11};
   LS: 0.0810829NH {Normal Sigma=7% Correlation=CORMAT[4] DDF= 7 12 19 9 4 2 4 13 25 5};
   GDS:0.00598346 {Normal Sigma=1% Correlation=CORMAT[5] DDF= 2 4 13 18 18 12 11 10 10 2};
   CDS:0.0697762PF {Normal Sigma=1% Correlation=CORMAT[6] DDF= 4 10 10 14 15 23 7 6 7 4};
   gm0:  -0.0712678 {Normal Sigma=2% Correlation=CORMAT[7] DDF= 6 4 6 10 13 15 14 13 11 8};
   TAU:  1.90932PS {Normal Sigma=2% Correlation=CORMAT[8] DDF= 6 13 15 26 20 12 4 2 0 2};
   CGD0: 0.0260632PF {Normal Sigma=2% Correlation=CORMAT[9] DDF= 2 4 8 9 9 23 21 14 5 5};
   CGS0: 0.303187PF {Normal Sigma=1.5% Correlation=CORMAT[10] DDF= 5 6 11 15 13 18 14 6 6 6};

   EXTRINSIC2  @gate @drain @source n1 n2
      LS: ls    RG: rg     RD: rd    RS: rs1
      GDS: gds  CX: 2.0PF  CDS: cds;

   CAP  @gate @source C=Cgs0;
   CAP  @gate @drain  C=Cgd0;
   VCCS @gate @drain @source @source T=Tau M=gm0;
```

```
}

STATISTICS
  CORRELATION: CORMAT DIMENSION=10 FORMAT=FULL;
         1   -0.3121   -0.5869    0.5244    0.1914   -0.1805   -0.4473  -0.05673   -0.0971   -0.2548
   -0.3121         1    0.7279   -0.7479   0.07056     0.411    0.3914  -0.04698    -0.206    0.2474
   -0.5869    0.7279         1   -0.8461  -0.06628    0.4825    0.6637   -0.2376   -0.1262    0.1974
    0.5244   -0.7479   -0.8461         1    0.0162   -0.7326   -0.5204   0.02553    0.3676   -0.3084
    0.1914   0.07056  -0.06628    0.0162         1    0.1504   -0.5752   -0.2991    -0.171    0.3561
   -0.1805     0.411    0.4825   -0.7326    0.1504         1    0.1765    0.0295   -0.6786    0.1946
   -0.4473    0.3914    0.6637   -0.5204   -0.5752    0.1765         1   -0.1781    0.0863   -0.3412
  -0.05673  -0.04698   -0.2376   0.02553   -0.2991    0.0295   -0.1781         1   -0.2122    0.2624
   -0.0971    -0.206   -0.1262    0.3676    -0.171   -0.6786    0.0863   -0.2122         1   -0.2904
   -0.2548    0.2474    0.1974   -0.3084    0.3561    0.1946   -0.3412    0.2624   -0.2904         1
END
```

Amplifier Nominal Gain Response

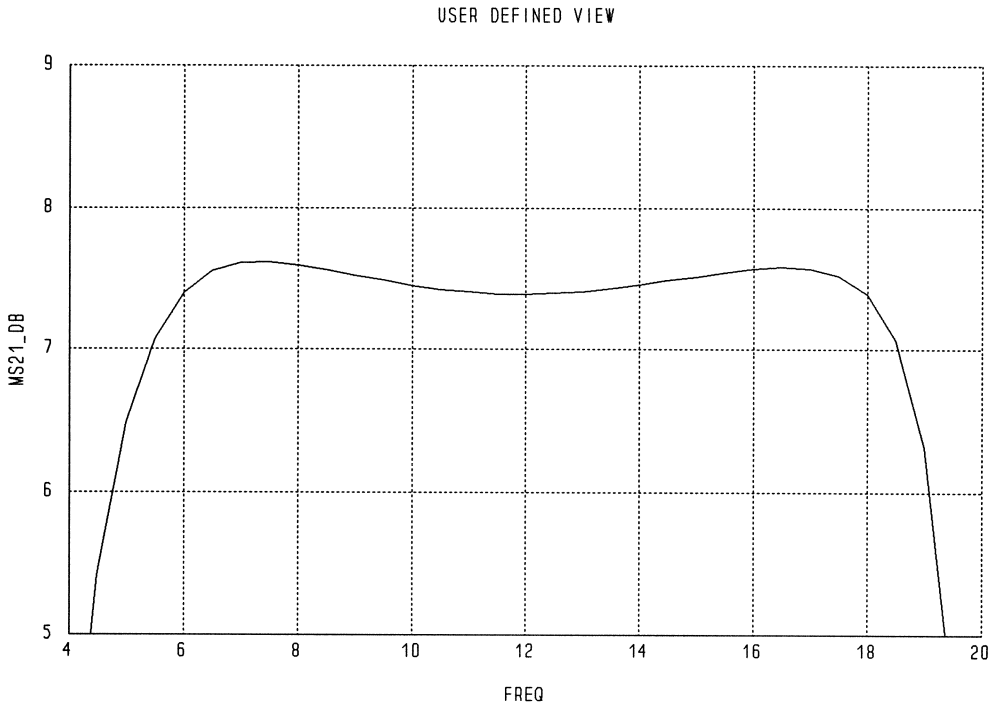

Amplifier Gain from Monte Carlo Simulation with 250 Outcomes

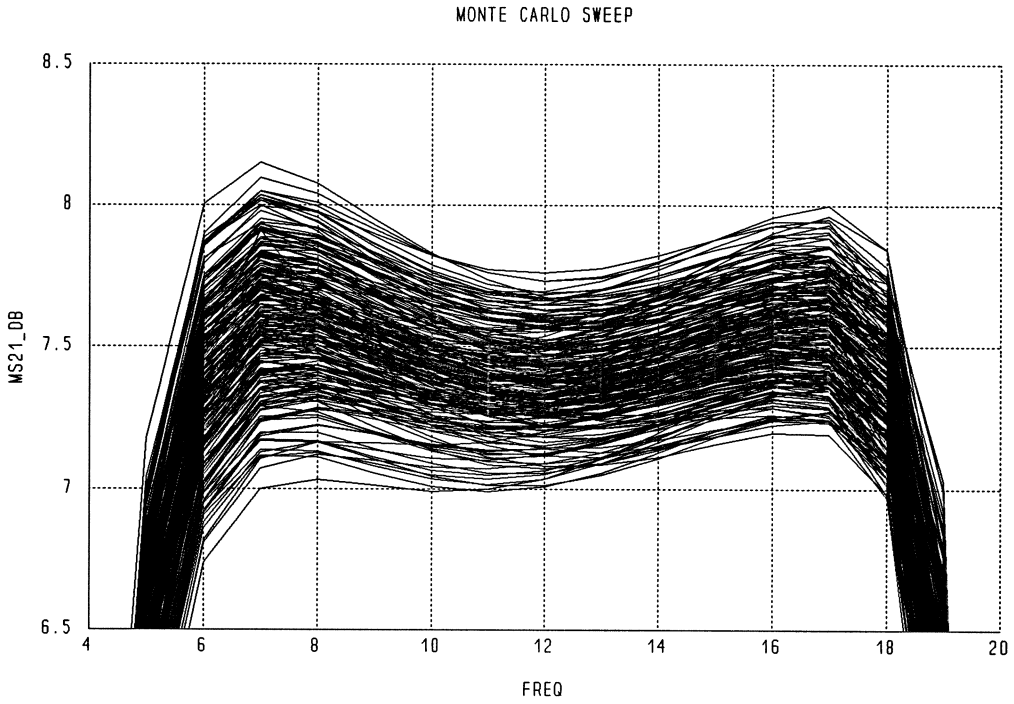

Histogram of the Maximum Errors of Monte Carlo Outcomes

The design specification for the amplifier in this example is 7dB ≤ $|S_{21}|$ ≤ 8dB, from 6GHz to 18GHz. We can define a set of error functions w.r.t. the specification, as

$$e_i = 7 - |S_{21}(f_i)|, \quad i = 1, 2, ..., 13,$$

$$e_j = |S_{21}(f_i)| - 8, \quad j = 13 + i,$$

where

$$f_i = 6 + i - 1$$

represents frequency in GHz.

For each Monte Carlo outcome, we can calculate the maximum error

$$e_{max} = \max_{1 \le i \le 26} \{ e_i \}.$$

The sign of e_{max} indicates the acceptability of the outcome: $e_{max} > 0$ for an unacceptable outcome (specification violated) or $e_{max} \le 0$ for an acceptable outcome.

A histogram of e_{max} depicts graphically the percentage of acceptable outcomes (i.e., yield) and the distribution of outcomes in terms of how much they satisfy or violate the design specification(s).

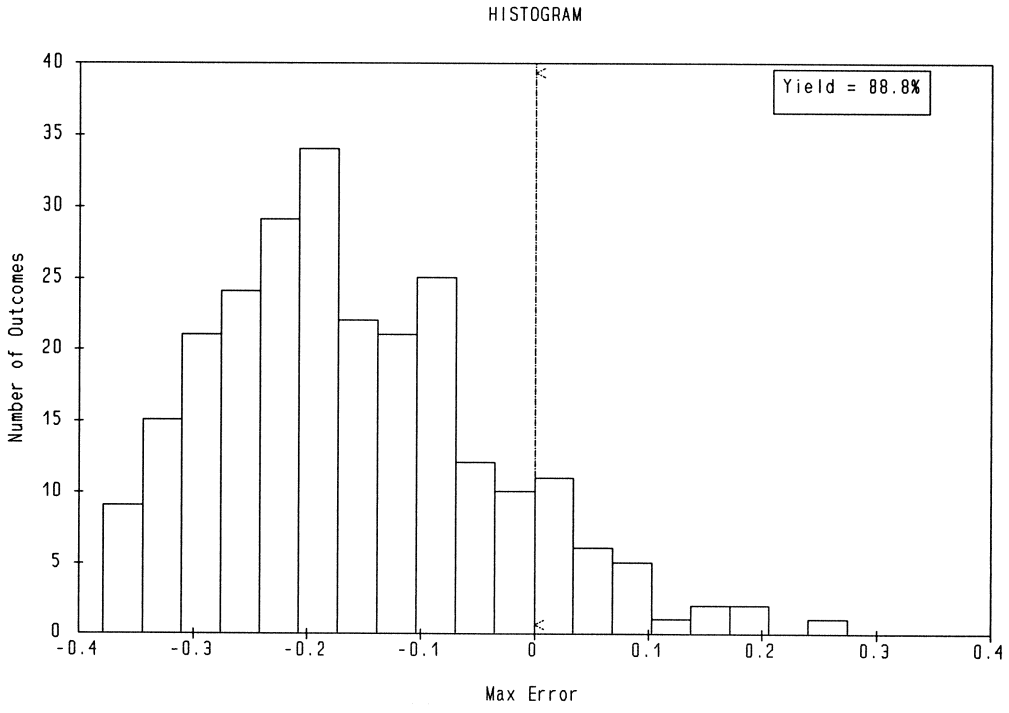

demo36

Illustration of the yield sensitivity feature.

The circuit is a small-signal amplifier. The bipolar transistor is represented by measured *S* parameters. The circuit parameter statistics are modeled by uniform and normal distributions.

The yield sensitivities w.r.t. frequency and w.r.t. a circuit parameter are estimated by Monte Carlo simulation.

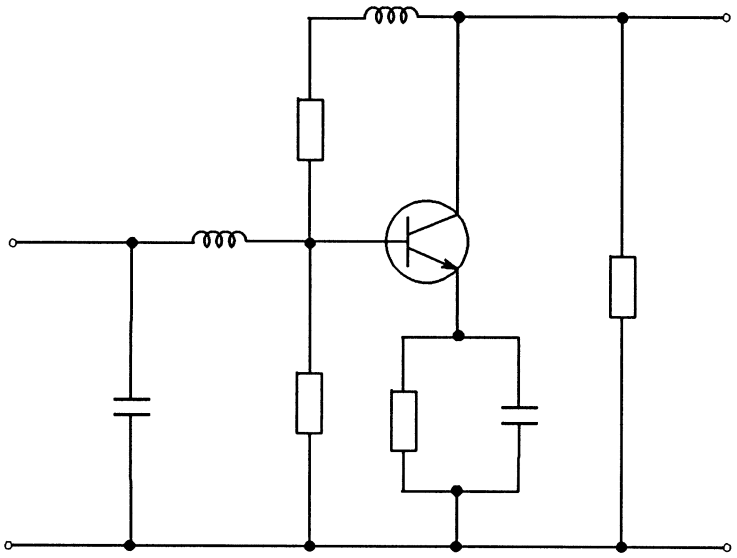

Input File

```
! Example  demo36.ckt
! illustrates yield sensitivity display

Model
   X: 24nH;

   CAP 1 0  C=4pF {NORMAL SIGMA=5%};
   IND 1 2  L=7.7nH {UNIFORM TOL=15%};
   RES 2 0  R=550;

   DATAPORT 2 3 4  Data=Transistor_Data;

   PRC 4 0  R=5 {NORMAL SIGMA=5%}
            C=14.5pF;
   SRL 2 3  R=154 {NORMAL SIGMA=10%}
            L=X;
   RES 3 0  R=300;

   PORT 1 0  NAME=input;
   PORT 3 0  NAME=output;

   Circuit;
```

```
   Input_Return_Loss = 20 * log10(MS11);
   Output_Return_Loss = 20 * log10(MS22);
   Gain = 20 * log10(MS21);
End

MonteCarlo
   AC: X: from 20nh to 28nh step=0.5nh
       FREQ: 10MHz  from 250MHz to 1GHz step=250MHz
       Input_Return_Loss < -8
       Output_Return_Loss < -8
       Gain > 9  Gain < 10
       N_Outcomes = 100;
end

Import
   Parameter  NAME=Transistor_Data;
   Format FREQ(MHz)  S2MP;
     10  0.42   -40  35    170  0.005  80  0.9   -10
    250  0.50   -75  21    145  0.02   65  0.7   -18
    500  0.58  -120   9.4  121  0.04   40  0.52  -28
    750  0.48  -153   6.2  109  0.04   45  0.49  -29
   1000  0.58  -144   4.5  102  0.05   49  0.46  -30
End
```

Yield Sensitivity w.r.t. Circuit Parameter X

The following figure shows the yield versus the value of X, which is an inductance (see the input file).

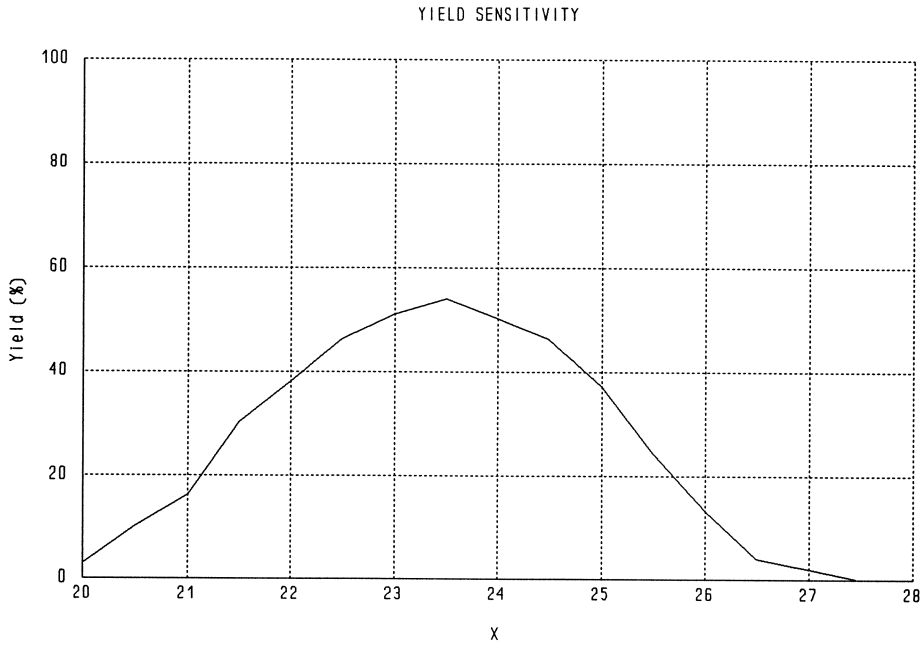

Marginal Yield at Different Values of X and at Different Frequencies

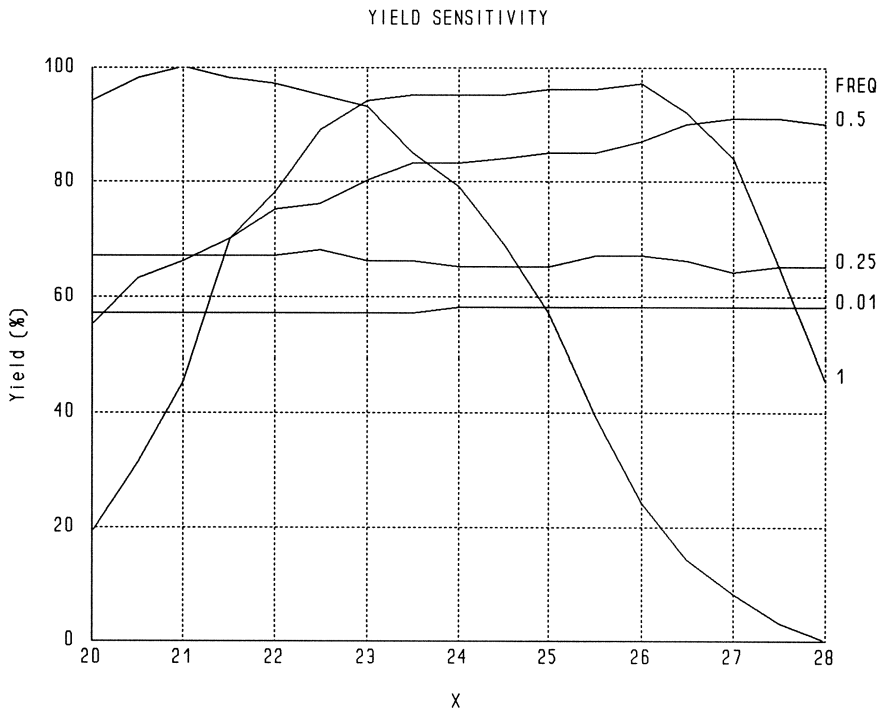

This display shows the marginal yield for different combinations of X and frequency values. For instance, it shows that for X=21, the most critical frequency is 1GHz (corresponding to the lowest marginal yield). For X=22, the most critical frequency is 0.01GHz.

demo37

Nonlinear yield optimization of a frequency doubler. The FET is represented by the built-in FETM model.

The design specifications are conversion gain > 2.5dB and spectral purity > 19dB at 5GHz and 3dBm input power.

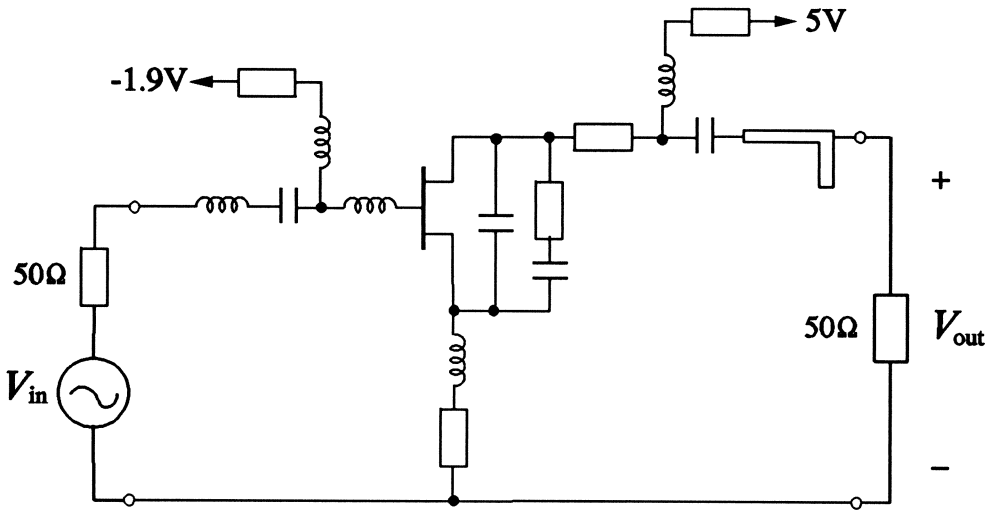

Input File

```
!  Example  demo37.ckt
!  Nonlinear yield optimization of a frequency doubler
!  using one-sided L1 yield optimization
!  50 outcomes without quadratic modeling

Model
   RDS = 440 {Normal Sigma=14% Correlation=FET[5]};

   MSUB H=0.635E-3 EPSR=9.8 T=6.E-6 ROC=3.846153E-8 RHS=0.15E-6;

   Extrinsic2  1 2 3 4 5
      GDS: (1.0 / RDS)
      CX: 1.15PF {Normal Sigma=3%}
      RD: 2.153 {Normal Sigma=3%}
      LG: 0.16NH {Normal Sigma=5% Correlation=FET[1]}
      RG: 0.0001 {Normal Sigma=5% Correlation=FET[2]}
      RS: 1.144 {Normal Sigma=5% Correlation=FET[3]}
      LS: 0.07NH {Normal Sigma=5% Correlation=FET[4]}
      CDS: 0.12PF {Normal Sigma=4.5% Correlation=FET[6]};

   FETM  1 2 3
      KE: 0      VBC: 0      KR: 1.111      K1: 1.282      KF: 1.282
      IDSS: 0.06 {Normal Sigma=5% Correlation=FET[7]}
      VP0: -1.906 {Normal Sigma=0.65%}
      GAMMA: -1.5E-2 {Normal Sigma=0.65%}
      E: 1.8 {Normal Sigma=0.65%}
      SL: 0.0676 {Normal Sigma=0.65%}
      KG: 1.1 {Normal Sigma=0.65%}
      TAU: 7PS {Normal Sigma=6% Correlation=FET[8]}
```

```
      SS: 1.666E-3 {Normal Sigma=0.65%}
      IG0: 0.713E-5 {Normal Sigma=3%}
      ALPHAG: 38.64 {Normal Sigma=3%}
      IB0: -0.713E-5 {Normal Sigma=3%}
      ALPHAB: -38.64 {Normal Sigma=3%}
      R10: 3.5 {Normal Sigma=8% Correlation=FET[9]}
      C10: 0.42PF {Normal Sigma=4.16% Correlation=FET[10]}
      CF0: 0.02PF {Normal Sigma=6.64% Correlation=FET[11]};

   ! input network

   IND  11 12  L=?5.462NH? {UNIFORM TOL=3%};
   CAP  12  4  C=20PF {UNIFORM TOL=5%};

   ! output network

   CAP  5 13  C=20PF {UNIFORM TOL=5%};
   MSL  13 14  L=?0.0014828? {UNIFORM TOL=3%}  W=0.1E-3 {UNIFORM TOL=5%};
   DATAPORT  15 14 16  DATA=TJUNCTION;
   MSL  15 17  L=?0.0057705? {UNIFORM TOL=3%}  W=0.635E-3 {UNIFORM TOL=5%};
   OPEN  17 0;

   ! bias

   SRL  4 10  R=10 L=15NH {UNIFORM TOL=5%};
   SRL  5 20  R=10 L=15NH {UNIFORM TOL=5%};

   VSOURCE 10 0  VDC=-1.9;
   VSOURCE 20 0  VDC=5;

   PIN: 3dBm;

   PORT  11 0  P[1]=PIN  R=50 {UNIFORM TOL=5%};
   PORT  16 0  NAME=out  R=50 {UNIFORM TOL=5%};

   CIRCUIT;

   Vs: sqrt(400 * 10^((Pin - 30)/10));
   MVs[0:N_SPECTRA] = [0 Vs 0 0 0];
   PVs[0:N_SPECTRA] = 0;

   POUT[0:4] = if (PWout > 0) (10.0 * log10(PWout) + 30.0) else (NAN);

   Conversion_Gain = POUT[2] - PIN;
   Spectral_Purity = 10 * LOG10(PWout[2]/(PWout[1]+PWout[3]+PWout[4]));
end

Sweep
   HB: FREQ=5GHZ  Pout MVout PVout MVs PVs
       {Waveform  Title="Frequency Doubler Source and Output Voltage Waveforms"
        Spectrum=(MVs, PVs)."VS_T" & (MVout, PVout)."Vout_T"
        Tmin=0 Tmax=0.2 NT=150  Ymin=-1 Ymax=1 NYTicks=4}
end

Spec
   HB: FREQ=5GHZ  Conversion_Gain > 2.5  Spectral_Purity > 19;
end

Control
   Optimizer=Yield;
end

MonteCarlo
   HB: N_outcomes=500  FREQ=5GHZ  Conversion_Gain > 2.5  Spectral_Purity > 19;
end

Importdata
   Parameter NAME=TJUNCTION;
   Format FREQ RY11(/KOH) IY11(/KOH) RY21(/KOH) IY21(/KOH) RY31(/KOH) IY31(/KOH)
               RY12(/KOH) IY12(/KOH) RY22(/KOH) IY22(/KOH) RY32(/KOH) IY32(/KOH)
               RY13(/KOH) IY13(/KOH) RY23(/KOH) IY23(/KOH) RY33(/KOH) IY33(/KOH);
```

```
#include "tjunctn.dat"
end

Statistics

   Correlation: FET DIMENSION=11 FORMAT=FULL;

   1.00 -0.01 -0.16  0.11 -0.22 -0.20  0.15  0.06  0.15  0.25  0.04
  -0.01  1.00 -0.04  0.53 -0.14 -0.08  0.03  0.27 -0.35  0.21 -0.04
  -0.16 -0.04  1.00 -0.28  0.02  0.06 -0.09 -0.16  0.12 -0.24  0.26
   0.11  0.53 -0.28  1.00  0.11 -0.26  0.53  0.41 -0.52  0.78 -0.12
  -0.22 -0.14  0.02  0.11  1.00 -0.44  0.03  0.04 -0.54  0.02 -0.14
  -0.20 -0.08  0.06 -0.26 -0.44  1.00 -0.13 -0.14  0.23 -0.24 -0.04
   0.15  0.03 -0.09  0.53  0.03 -0.13  1.00 -0.08 -0.26  0.78  0.38
   0.06  0.27 -0.16  0.41  0.04 -0.14 -0.08  1.00 -0.19  0.27 -0.46
   0.15 -0.35  0.12 -0.52 -0.54  0.23 -0.26 -0.19  1.00 -0.35  0.05
   0.25  0.21 -0.24  0.78  0.02 -0.24  0.78  0.27 -0.35  1.00  0.15
   0.04 -0.04  0.26 -0.12 -0.14 -0.04  0.38 -0.46  0.05  0.15  1.00
end
```

Frequency Doubler Output Power Spectrum After Optimization

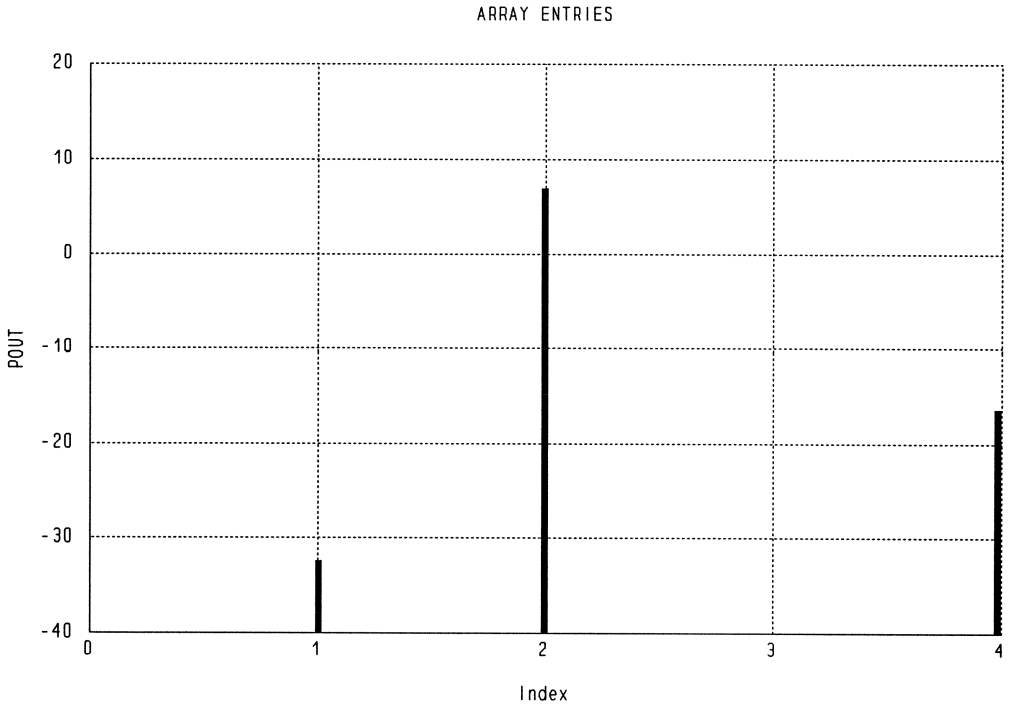

Frequency Doubler Source and Output Voltage Waveforms

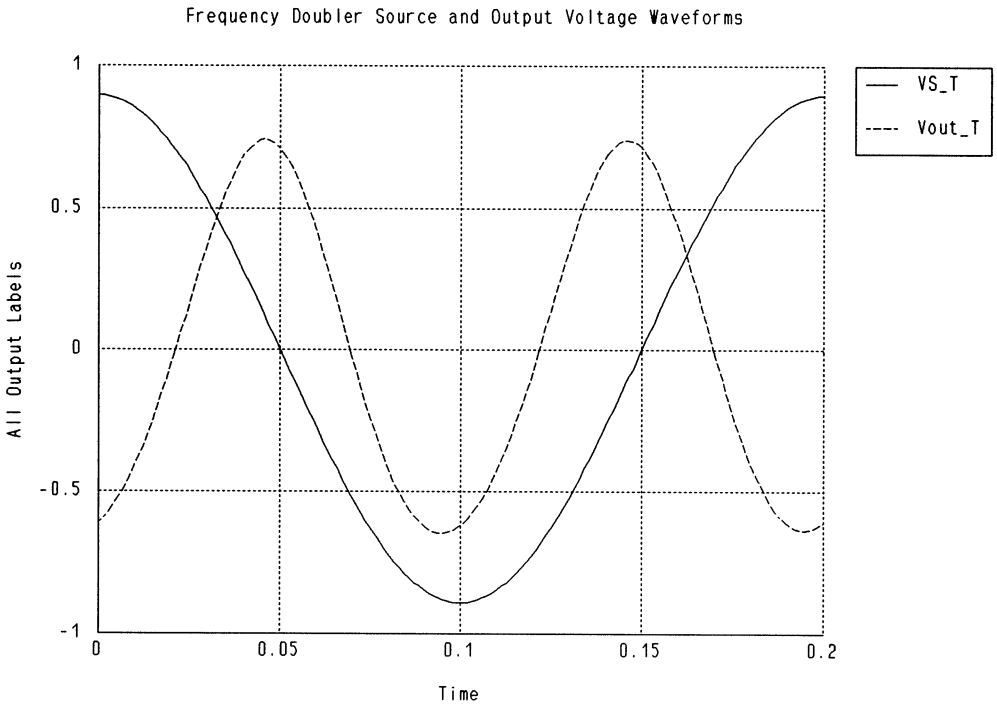

Histograms of Doubler Spectral Purity Before and After Yield Optimization

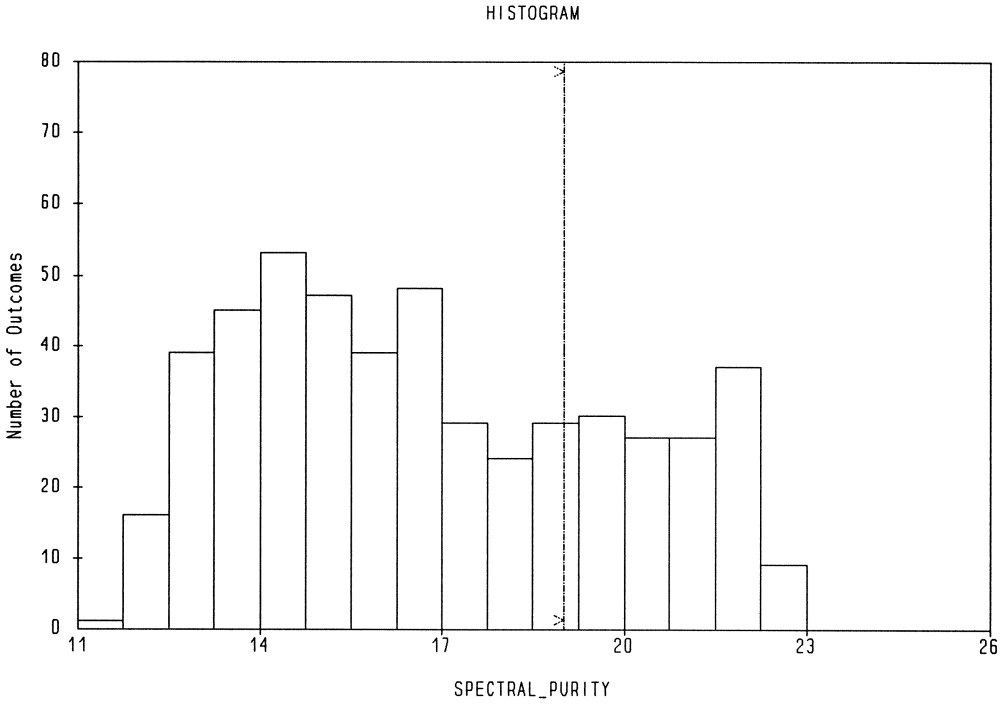

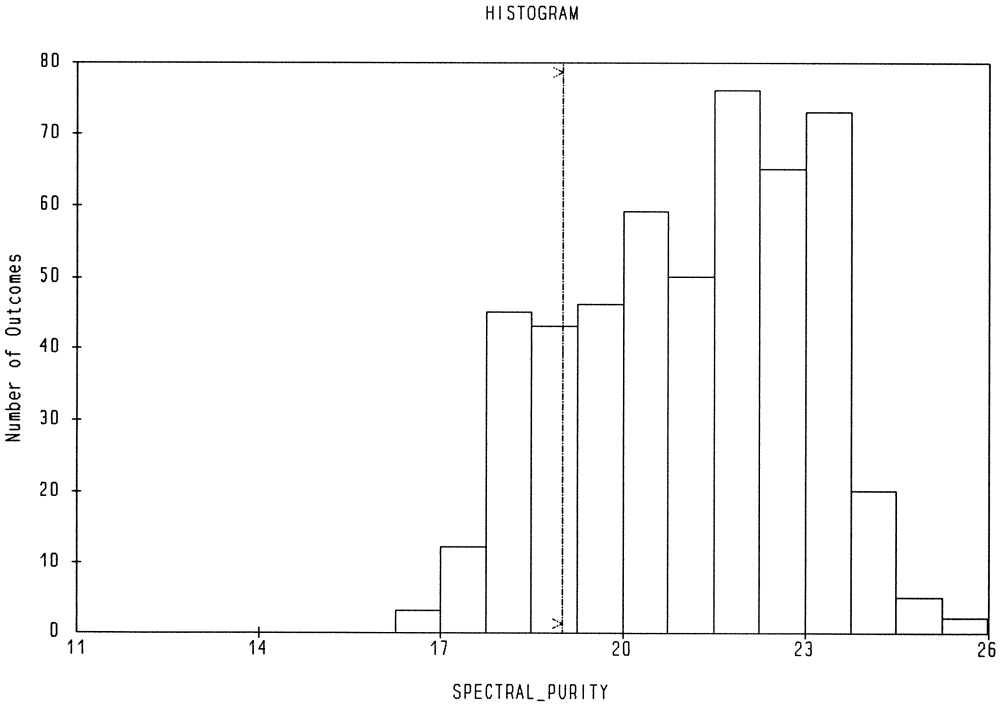

demo38

Simulation of a nonlinear circuit under square wave (pulse train) excitation. The circuit is a single-FET amplifier (identical to the circuit in demo11). The *MGF1902* FET is modeled by the built-in nonlinear FETM model.

The square wave input is approximated by Fourier series to the 15th harmonic, i.e., by a series of harmonically related voltage sources. The amplitudes of the Fourier coefficients are weighted by Lanczos factors to smooth out overshoot near the rise and fall of the pulse (Gibb's phenomenon).

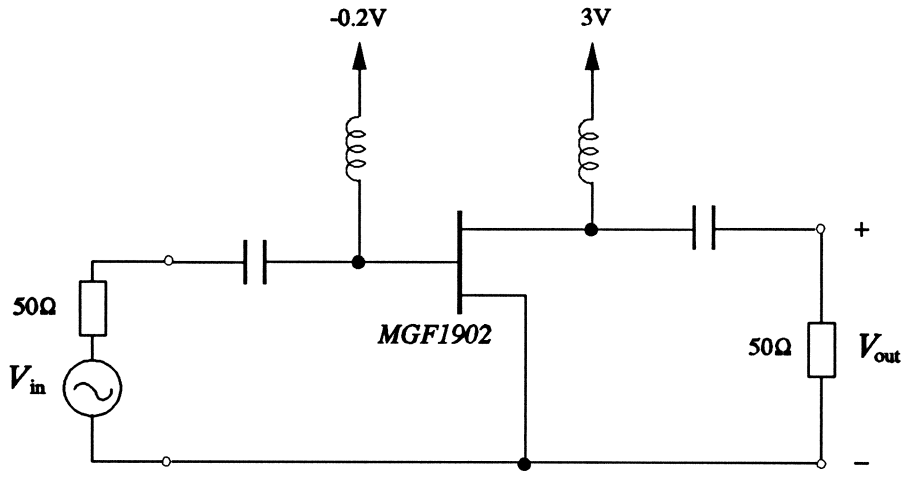

Input File

```
!  Example  demo38.ckt
!  nonlinear circuit excited by square waves
!  also see demo40 for more general pulse train inputs

Model
   ! Fourier coefficients of square waves with Lanczos's smoothing

   Vpeak: 0.5;
   N = 16;
   w = PI / N;
   Va = Vpeak * 2 / PI;

   V1  = Va * sin(     w) / w;
   V3  = Va * sin( 3 * w) / (  9 * w);
   V5  = Va * sin( 5 * w) / ( 25 * w);
   V7  = Va * sin( 7 * w) / ( 49 * w);
   V9  = Va * sin( 9 * w) / ( 81 * w);
   V11 = Va * sin(11 * w) / (121 * w);
   V13 = Va * sin(13 * w) / (169 * w);
   V15 = Va * sin(15 * w) / (225 * w);

   CAP 1 2 C=1000pF;

   Extrinsic4  20 30 40 2 3
      RG=5          RD=0.2      RS=1.5     LS=0.0948NH
      LG=0.53633NH  LD=0.936NH  GDS=0.002  CDS=0.0278PF
```

```
      CDE=0.0682pF  CX=10pF;

   FETM  20 30 40
      E=1.4  SL=0.126  IB0=8e-12    ALPHAB=1     VBC=6
      GAMMA=-0.06356   K1=2         CF0=0.02PF   KF=-0.157
      IDSS=0.04716     VP0=-0.7338  R10=0.00343  C10=0.6294PF;

   CAP 2 0 C=0.184pF;  ! FET parasitic
   CAP 3 0 C=0.216pF;

   CAP 3 4 C=1000pF;

   PORT 1 0 V[1]=V1 V[3]=V3 V[5]=V5 V[7]=V7 V[9]=V9
            V[11]=V11 V[13]=V13 V[15]=V15
            PHASE[1]=90 PHASE[3]=90 PHASE[5]=90 PHASE[7]=90
            PHASE[9]=90 PHASE[11]=90 PHASE[13]=90 PHASE[15]=90;

   PORT 4 0 NAME=output;

   IND 2 200 L=1000nH;
   VSOURCE 200 0  VDC=-0.2;

   IND 3 300 L=1000nH;
   VSOURCE 300 0  VDC=3;

   CIRCUIT  HARM=15;

   MVsource[0:15] = [0 V1 0 V3 0 V5 0 V7 0 V9 0 V11 0 V13 0 V15];
   PVsource[0:15] = 90;
end

Sweep
   HB: FREQ: 1GHZ 2GHz  HARM=15  MVoutput PVoutput MVsource PVsource
       {Waveform  Title="Nonlinear Circuit Under Square Excitation"
        Spectrum=(MVoutput, PVoutput)."Voutput_T".Green &
                 (MVsource, PVsource)."Vsource_T".Red
        FREQ=1GHZ  Comments="Freq = 1GHz"
        Tmin=0 Tmax=2 NT=200 NXticks=4 Ymin=-1 Ymax=1 NYticks=4}
       {Waveform  Title="Nonlinear Circuit Under Square Excitation"
        Spectrum=(MVoutput, PVoutput)."Voutput_T".Green &
                 (MVsource, PVsource)."Vsource_T".Red
        FREQ=2GHZ  Comments="Freq = 2GHz"
        Tmin=0 Tmax=1 NT=200 NXticks=4 Ymin=-1 Ymax=1 NYticks=4};
end
```

Source and Output Voltage Waveforms at 1GHz and 2GHz

By comparing the following two figures, we can see that the output distortion increases significantly when the fundamental frequency is increased from 1GHz to 2GHz.

The reason is quite simple. The highest harmonic frequency considered in simulation (the 15th harmonic) increases from 15GHz to 30GHz as the fundamental frequency is increased from 1GHz to 2GHz. Because the *MGF1902* FET's performance deteriorates substantially above 12GHz, the output distortion worsens as the fundamental frequency gets higher.

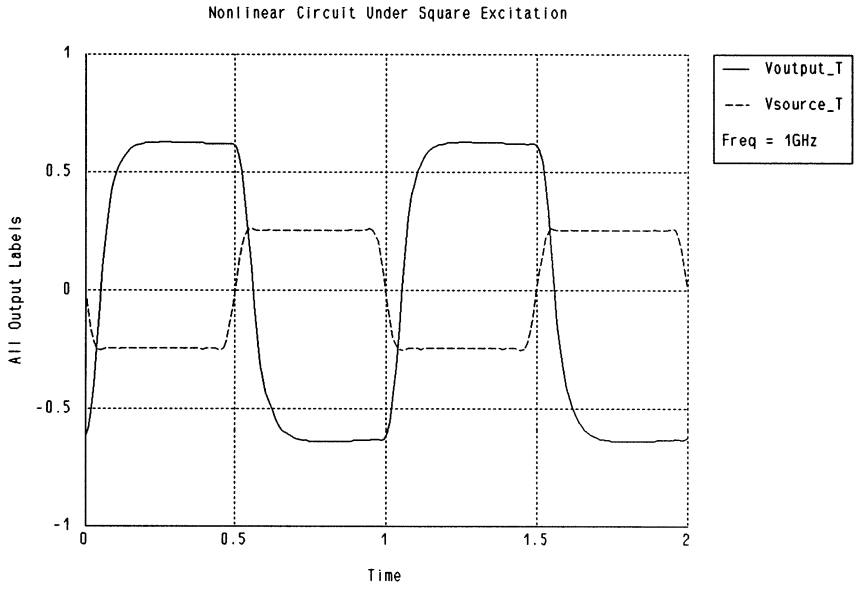

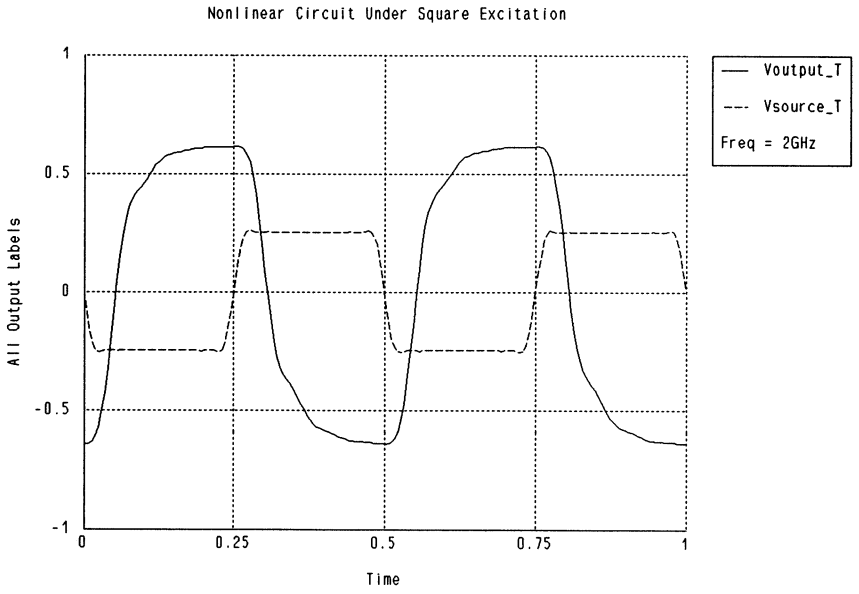

demo39

Simulation of a nonlinear circuit under triangular wave (pulse train) excitation. The circuit is a single-FET amplifier (identical to the circuit in demo11). The *MGF1902* FET is modeled by the built-in nonlinear FETM model.

The triangular wave input is approximated by Fourier series to the 9th harmonic, i.e., by a series of harmonically related voltage sources.

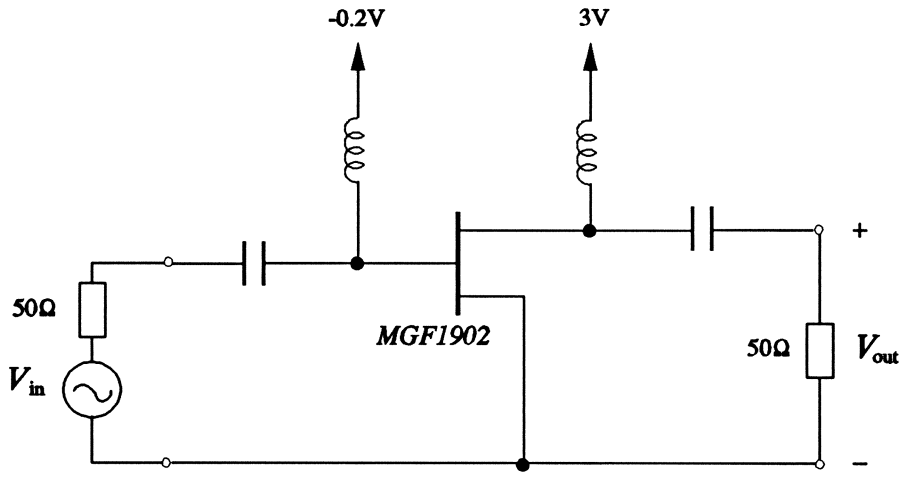

Input File

```
!  Example  demo39.ckt
!  nonlinear circuit excited by triangular waves

Model
   CAP 1 2 C=1000pF;

   Extrinsic4  20 30 40 2 3
      RG=5          RD=0.2      RS=1.5      LS=0.0948NH
      LG=0.53633NH  LD=0.936NH  GDS=0.002   CDS=0.0278PF
      CDE=0.0682pF  CX=10pF;

   FETM  20 30 40
      E=1.4  SL=0.126  IB0=8e-12    ALPHAB=1     VBC=6
      GAMMA=-0.06356   K1=2         CF0=0.02PF   KF=-0.157
      IDSS=0.04716     VP0=-0.7338  R10=0.00343  C10=0.6294PF;

   CAP 2 0 C=0.184pF;  ! FET parasitic
   CAP 3 0 C=0.216pF;

   CAP 3 4 C=1000pF;

   Psource: -3;
   Vs1 = sqrt(400 * 10^((Psource - 30)/10));
   Vs3 = Vs1 / 9;
   Vs5 = Vs1 / 25;
   Vs7 = Vs1 / 49;
   Vs9 = Vs1 / 81;

   PORT 1 0  V[1]=Vs1 V[3]=Vs3 V[5]=Vs5 V[7]=Vs7 V[9]=Vs9;
```

```
   PORT 4 0  NAME=output;

   IND 2 200 L=1000nH;
   VSOURCE 200 0  VDC=-0.2;

   IND 3 300 L=1000nH;
   VSOURCE 300 0  VDC=3;

   CIRCUIT  HARM=9;

   MVs[0:N_SPECTRA] = [0 Vs1 0 Vs3 0 Vs5 0 Vs7 0 Vs9];
   PVs[0:N_SPECTRA] = 0;
end

Sweep
   HB: FREQ=1GHZ  HARM=9  Psource: from -6 to 3 step=3
       MVoutput PVoutput MVs PVs
       {Waveform  Title="Nonlinear Circuit Under Triangular Excitation"
        Psource=all  Spectrum=(MVoutput, PVoutput)."Voutput_T".Green
        Tmin=0 Tmax=2 NT=200 NXticks=4 Ymin=-3 Ymax=3 NYticks=6}
       {Waveform  Title="Nonlinear Circuit Under Triangular Excitation"
        Spectrum=(MVoutput, PVoutput)."Voutput_T".Green &
                 (MVs, PVs)."Vsource_T".Red
        Psource=-6  Comments="Psource = -6dBm"
        Tmin=0 Tmax=2 NT=200 NXticks=4 Ymin=-1 Ymax=1 NYticks=4};
end
```

Output Voltage Waveforms at Different Input Power Levels

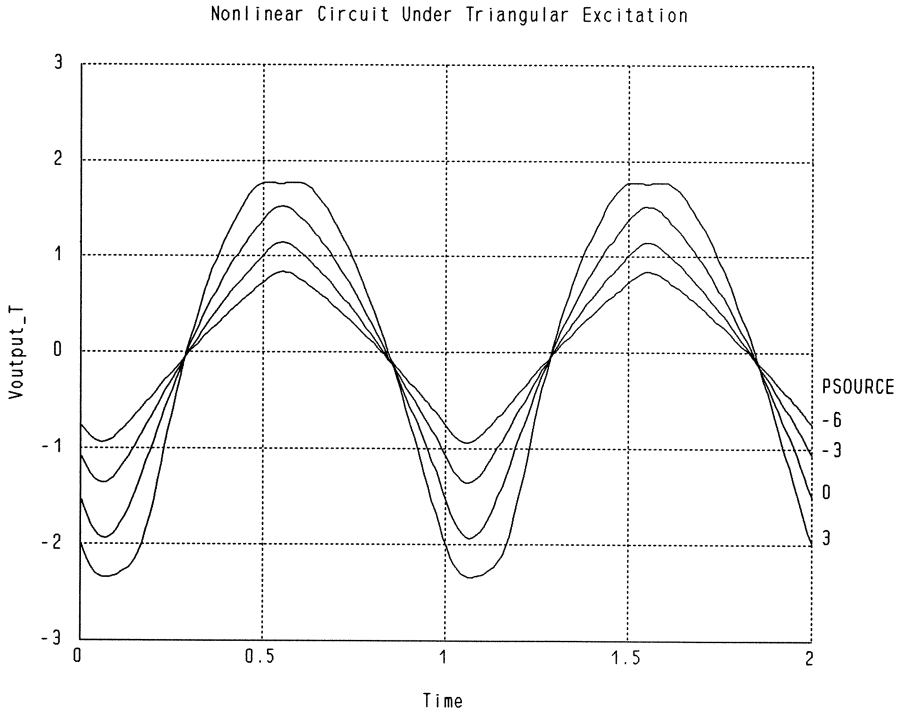

demo40

Simulation of a nonlinear circuit under pulse train excitation. The circuit is a single-FET amplifier (identical to the circuit in demo11). The *MGF1902* FET is modeled by the built-in nonlinear FETM model.

The pulse train input is approximated by Fourier series to the 16th harmonic, i.e., by a series of harmonically related voltage sources. The amplitudes of the Fourier coefficients are weighted by Lanczos factors to smooth out overshoot near the rise and fall of the pulse (Gibb's phenomenon).

Three different duty cyles of the pulse train input are considered, namely 25%, 50% and 75%. A 50% duty cyle would produce identical results as demo38 (square wave).

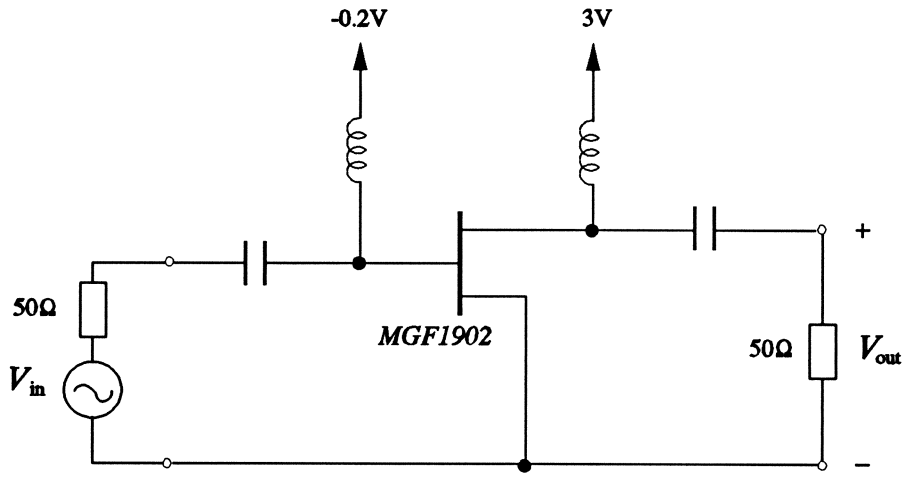

Input File

```
!  Example  demo40.ckt
!  nonlinear circuit excited by pulse trains with different duty cycles

Model
   CAP 1 2 C=1000pF;

   Extrinsic4  20 30 40 2 3
      RG=5          RD=0.2      RS=1.5     LS=0.0948NH
      LG=0.53633NH  LD=0.936NH  GDS=0.002  CDS=0.0278PF
      CDE=0.0682pF  CX=10pF;

   FETM  20 30 40
      E=1.4  SL=0.126  IB0=8e-12    ALPHAB=1     VBC=6
      GAMMA=-0.06356   K1=2         CF0=0.02PF   KF=-0.157
      IDSS=0.04716     VP0=-0.7338  R10=0.00343  C10=0.6294PF;

   CAP 2 0 C=0.184pF;  ! FET parasitic
   CAP 3 0 C=0.216pF;

   CAP 3 4 C=1000pF;

   PORT 1 0 V[1]=V1 V[2]=V2 V[3]=V3 V[4]=V4 V[5]=V5
```

```
            V[6]=V6 V[7]=V7 V[8]=V8 V[9]=V9 V[10]=V10
            V[11]=V11 V[12]=V12 V[13]=V13 V[14]=V14
            V[15]=V15 V[16]=V16  VDC=V0
            PHASE[1]=P1 PHASE[2]=P2 PHASE[3]=P3 PHASE[4]=P4
            PHASE[5]=P5 PHASE[6]=P6 PHASE[7]=P7 PHASE[8]=P8
            PHASE[9]=P9 PHASE[10]=P10 PHASE[11]=P11 PHASE[12]=P12
            PHASE[13]=P13 PHASE[14]=P14 PHASE[15]=P15 PHASE[16]=P16;

   PORT 4 0 NAME=output;

   IND 2 200 L=1000nH;
   VSOURCE 200 0  VDC=-0.2;

   IND 3 300 L=1000nH;
   VSOURCE 300 0  VDC=3;

   CIRCUIT  HARM=16;

   MVsource[0:16] = [V0 V1 V2 V3 V4 V5 V6 V7 V8 V9 V10 V11 V12 V13 V14 V15 V16];
   PVsource[0:16] = [0  P1 P2 P3 P4 P5 P6 P7 P8 P9 P10 P11 P12 P13 P14 P15 P16];
end

Sweep
   HB: FREQ=1GHZ  HARM=16  DutyCycle: 0.25 0.5 0.75
       MVoutput PVoutput MVsource PVsource
       {Waveform  Title="Nonlinear Circuit with Pulse Train Input"
        Spectrum=(MVoutput, PVoutput)."Voutput_T".Green &
                 (MVsource, PVsource)."Vsource_T".Red
        DutyCycle=0.25  Comments="Duty Cycle = 25%"
        Tmin=0 Tmax=2 NT=200 NXticks=4 Ymin=-3 Ymax=2 NYticks=5}
       {Waveform  Title="Nonlinear Circuit with Pulse Train Input"
        Spectrum=(MVoutput, PVoutput)."Voutput_T".Green &
                 (MVsource, PVsource)."Vsource_T".Red
        DutyCycle=0.5  Comments="Duty Cycle = 50%"
        Tmin=0 Tmax=2 NT=200 NXticks=4 Ymin=-2 Ymax=2 NYticks=8}
       {Waveform  Title="Nonlinear Circuit with Pulse Train Input"
        Spectrum=(MVoutput, PVoutput)."Voutput_T".Green &
                 (MVsource, PVsource)."Vsource_T".Red
        DutyCycle=0.75  Comments="Duty Cycle = 75%"
        Tmin=0 Tmax=2 NT=200 NXticks=4 Ymin=-2 Ymax=2 NYticks=8};
end

Expression
   Vpeak = 0.5;
   DutyCycle: 0.5;

   W = DutyCycle * 2 * PI;
   Va = Vpeak / PI;
   RadToDeg = 180 / PI;

   ! define the Fourier coef. of the pulse train

   a1 = sin(w);
   b1 = 1 - cos(w);
   a2 = sin(2*w);
   b2 = 1 - cos(2*w);
   a3 = sin(3*w);
   b3 = 1 - cos(3*w);
   a4 = sin(4*w);
   b4 = 1 - cos(4*w);
   a5 = sin(5*w);
   b5 = 1 - cos(5*w);
   a6 = sin(6*w);
   b6 = 1 - cos(6*w);
   a7 = sin(7*w);
   b7 = 1 - cos(7*w);
   a8 = sin(8*w);
   b8 = 1 - cos(8*w);
   a9 = sin(9*w);
   b9 = 1 - cos(9*w);
   a10 = sin(10*w);
```

```
    b10 = 1 - cos(10*w);
    a11 = sin(11*w);
    b11 = 1 - cos(11*w);
    a12 = sin(12*w);
    b12 = 1 - cos(12*w);
    a13 = sin(13*w);
    b13 = 1 - cos(13*w);
    a14 = sin(14*w);
    b14 = 1 - cos(14*w);
    a15 = sin(15*w);
    b15 = 1 - cos(15*w);
    a16 = sin(16*w);
    b16 = 1 - cos(16*w);

    v0 = Vpeak * DutyCycle;

    Y1 = Va * sqrt(a1 * a1 + b1 * b1);
    p1 = atan2(-b1, a1) * RadToDeg;
    Y2 = Va * sqrt(a2 * a2 + b2 * b2) / 2;
    p2 = atan2(-b2, a2) * RadToDeg;
    Y3 = Va * sqrt(a3 * a3 + b3 * b3) / 3;
    p3 = atan2(-b3, a3) * RadToDeg;
    Y4 = Va * sqrt(a4 * a4 + b4 * b4) / 4;
    p4 = atan2(-b4, a4) * RadToDeg;
    Y5 = Va * sqrt(a5 * a5 + b5 * b5) / 5;
    p5 = atan2(-b5, a5) * RadToDeg;
    Y6 = Va * sqrt(a6 * a6 + b6 * b6) / 6;
    p6 = atan2(-b6, a6) * RadToDeg;
    Y7 = Va * sqrt(a7 * a7 + b7 * b7) / 7;
    p7 = atan2(-b7, a7) * RadToDeg;
    Y8 = Va * sqrt(a8 * a8 + b8 * b8) / 8;
    p8 = atan2(-b8, a8) * RadToDeg;
    Y9 = Va * sqrt(a9 * a9 + b9 * b9) / 9;
    p9 = atan2(-b9, a9) * RadToDeg;
    Y10 = Va * sqrt(a10 * a10 + b10 * b10) / 10;
    p10 = atan2(-b10, a10) * RadToDeg;
    Y11 = Va * sqrt(a11 * a11 + b11 * b11) / 11;
    p11 = atan2(-b11, a11) * RadToDeg;
    Y12 = Va * sqrt(a12 * a12 + b12 * b12) / 12;
    p12 = atan2(-b12, a12) * RadToDeg;
    Y13 = Va * sqrt(a13 * a13 + b13 * b13) / 13;
    p13 = atan2(-b13, a13) * RadToDeg;
    Y14 = Va * sqrt(a14 * a14 + b14 * b14) / 14;
    p14 = atan2(-b14, a14) * RadToDeg;
    Y15 = Va * sqrt(a15 * a15 + b15 * b15) / 15;
    p15 = atan2(-b15, a15) * RadToDeg;
    Y16 = Va * sqrt(a16 * a16 + b16 * b16) / 16;
    p16 = atan2(-b16, a16) * RadToDeg;

    ! Lanczos factor for smoothing out Gibb's phenomenon

    N = 16;
    w2 = PI / N;

    V1  = Y1  * sin(   w2) / w2;
    V2  = Y2  * sin( 2*w2) / (2 * w2);
    V3  = Y3  * sin( 3*w2) / (3 * w2);
    V4  = Y4  * sin( 4*w2) / (4 * w2);
    V5  = Y5  * sin( 5*w2) / (5 * w2);
    V6  = Y6  * sin( 6*w2) / (6 * w2);
    V7  = Y7  * sin( 7*w2) / (7 * w2);
    V8  = Y8  * sin( 8*w2) / (8 * w2);
    V9  = Y9  * sin( 9*w2) / (9 * w2);
    V10 = Y10 * sin(10*w2) / (10 * w2);
    V11 = Y11 * sin(11*w2) / (11 * w2);
    V12 = Y12 * sin(12*w2) / (12 * w2);
    V13 = Y13 * sin(13*w2) / (13 * w2);
    V14 = Y14 * sin(14*w2) / (14 * w2);
    V15 = Y15 * sin(15*w2) / (15 * w2);
    V16 = Y16 * sin(16*w2) / (16 * w2);
end
```

Source and Output Voltage Waveforms for 25% Duty Cycle

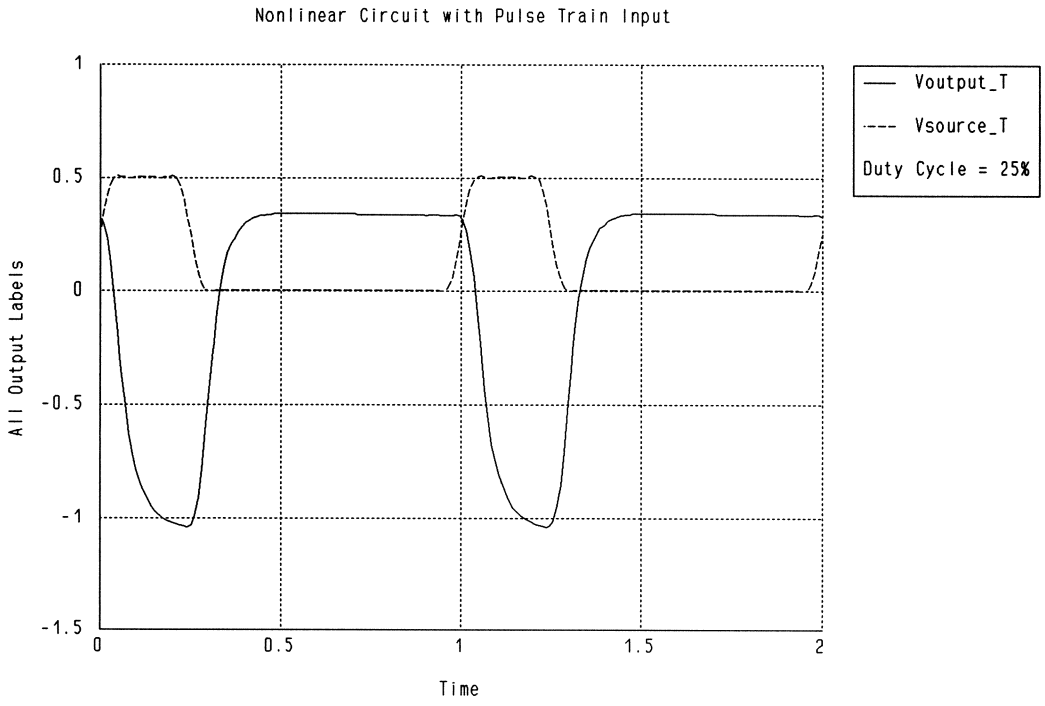

demo41

Illustration of the built-in cubic spline interpolation functions SPLINE() and SPLINT().

SPLINE() is used to establish cubic spline coefficients from data. Typically the data contains values of a function $f(x)$ sampled at some discrete points of x. Then, SPLINT() can be used to interpolate $f(x)$ at arbitrary values of x.

In this example, $f(x)$ is a time-domain waveform and x is time. The waveform is sampled at 11 time points and from this data the cubic spline coefficients are calculated using SPLINE(). Then, SPLINT() is used to reconstruct the waveform at 100 time points. The result is compared with the original waveform (by circuit simulation) and with the result from linear interpolation.

Input File

```
! Example  demo41.ckt
! Illustrates the built-in cubic spline interpolation functions
! A circuit response curve (waveform) is sampled at 11 points and
! the data is used to calculate the cubic spline coefficients.
! Cubic spline interpolation is then used to reconstruct the waveform
! at 100 time points.  The result is compared to circuit simulation
! as well as a linear interpolation model.

Expression
   time_sample[11] = [0 0.05 0.1 0.15 0.2 0.25 0.3 0.35 0.4 0.45 0.5];

   waveform_sample[11] = [-2.168 -2.434 -1.611   0.1499  1.48   1.705
                          1.74   1.575  0.5597 -0.9961 -2.168];

   coef[11] = SPLINE(time_sample, waveform_sample);

   t: 0;
   spline_model = SPLINT(t, coef, time_sample, waveform_sample);

   K1: floor(t * 20) + 1;
   K2: ceil(t * 20) + 1;

   t1 = time_sample[K1];
   t2 = time_sample[K2];
   y1 = waveform_sample[K1];
   y2 = waveform_sample[K2];

   linear_model: if (K1 = K2) (y1) else (y1 + (y2 - y1) * (t - t1) / (t2 - t1));
end

Model
   CAP 1 2 C=1000pF;

   Extrinsic2  20 30 40 2 3
      RG=3.5   LG=0.0306NH  RD=0.5       LD=0.00792NH
      RS=4.73  LS=0.0451NH  GDS=0.00345  CDS=0.08738PF  CX=10PF;

   FETR  20 30 40
      IS=5E-15    N=1          FC=0.5          GMIN=1.0E-07
      VBI=0.8     VBR=20.0     ALPHA=2         THETA=0.003
      BETA=0.029  VT0=-1.637   LAMBDA=0.04978  TAU=2.8PS
      CGS0=0.4428PF  CGD0=0.1066PF;

   CAP 3 4 C=1000pF;

   PORT 1 0  P=6dBm;
```

```
   PORT 4 0  NAME=out;

   IND     2 200  L=1000nH;
   VSOURCE 200 0  VDC=-0.56;

   IND     3 300  L=1000nH;
   VSOURCE 300 0  VDC=4;

   CIRCUIT;

   MP2RI(MVout, PVout, RVout[0:N_SPECTRA], IVout[0:N_SPECTRA]);

   circuit_model = DFT_FT(RVout, IVout, Spectral_Freq, t);
end

Sweep
   HB: FREQ=2GHZ  t: from 0 to 0.5 step=0.005
       circuit_model  spline_model  linear_model
       {Xsweep  Y=circuit_model & spline_model & linear_model
        NXticks=5  Ymin=-3 Ymax=2 NYticks=5}
       {Xsweep  Y=circuit_model & spline_model & linear_model
        Xmin=0.2 Xmax=0.35 NXticks=3  Ymin=1.4 Ymax=1.8 NYticks=4};
end
```

Cubic Spline Compared with Exact Simulation and Linear Interpolation

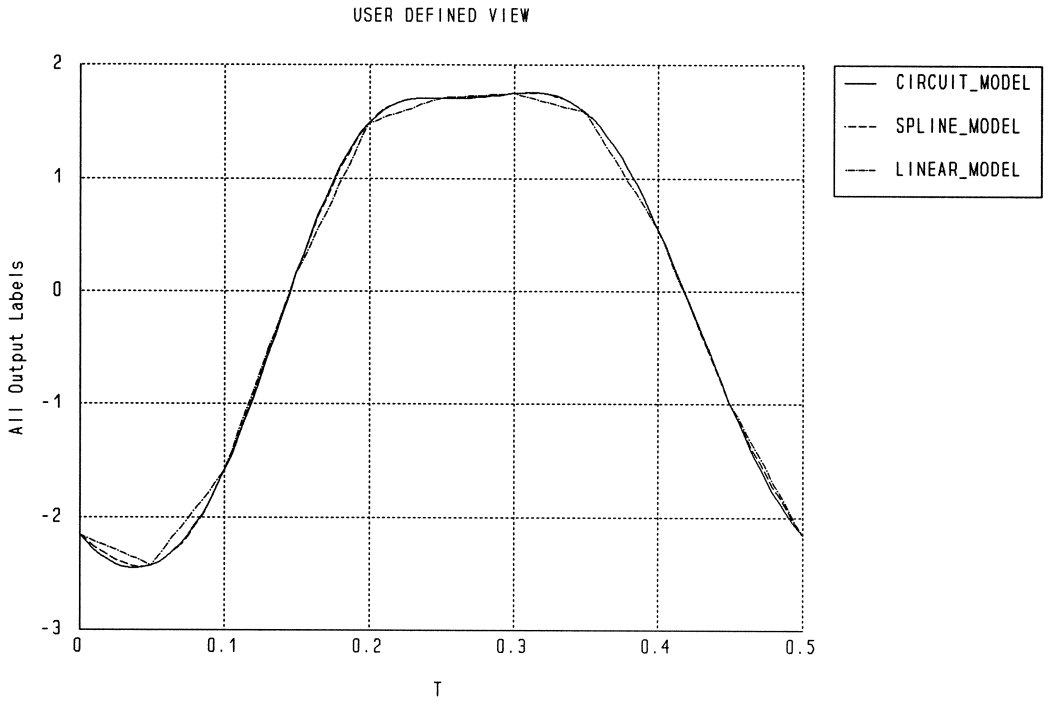

Enlarged Portion for Detail

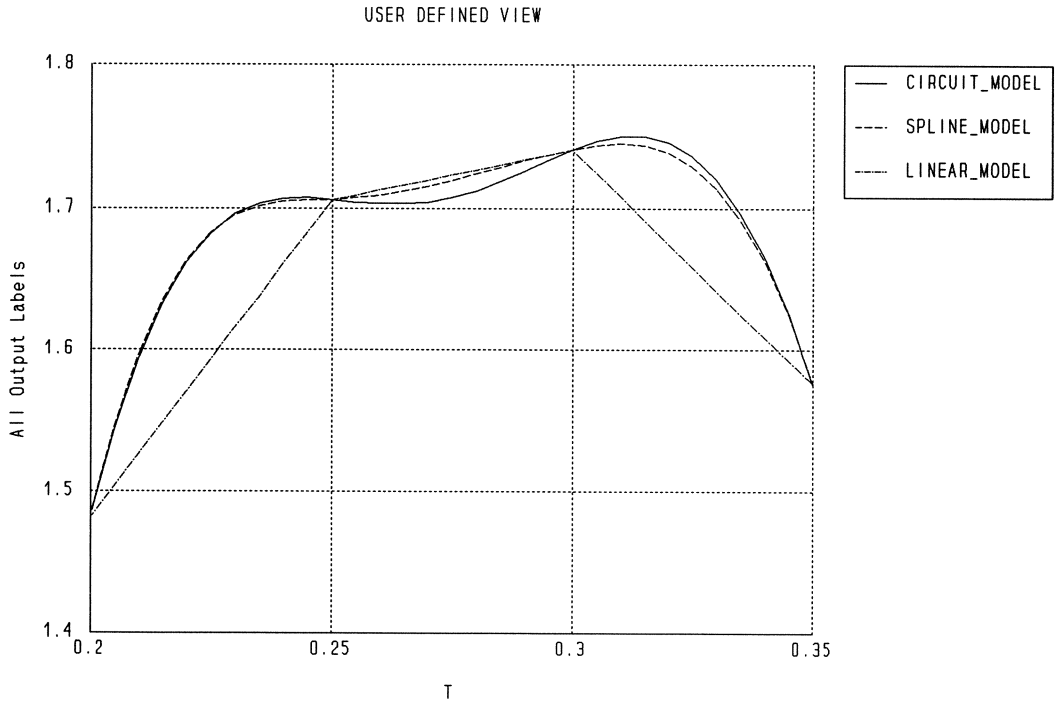

demo42

Illustration of the built-in 2D bicubic spline interpolation functions SPLINE2D() and SPLINT2D().

SPLINE2D() is used to establish bicubic spline coefficients from data. Typically the data contains values of a function $f(x,y)$ sampled on a 2-dimensional grid formed by discrete points of (x,y). Then, SPLINT2D() can be used to interpolate $f(x,y)$ at arbitrary values of x and y.

In this example, $f(x,y)$ is the DC drain current of a nonlinear FET circuit, where x and y are the gate and drain bias voltages, respectively. The DC drain current is sampled at a 4×9 grid and from this data the bicubic spline coefficients are calculated using SPLINE2D(). Then, SPLINT2D() is used to reconstruct the DC IV curve at 7×15 bias points (i.e., double the density of the grid for the sampled data). The result is compared with exact circuit simulation.

Input File

```
! Example  demo42.ckt
! Illustrates 2D bicubic spline interpolation
! The DC drain current of a nonlinear FET circuit is sampled
! at different bias points (a 4 x 9 grid).
! The data is used to construct 2D bicubic splines which
! are then used to interpolate the drain current at 7 x 15
! bias points.  The result is compared to circuit simulation.

Expression
   VG_data[4] = [ -1.2  -0.8  -0.4  0 ];
   VD_data[9] = [ 0  0.5  1  1.5  2  3  4  5  6 ];

   ID_data[4,9] = [
      0 3.593 4.969 5.278 5.387 5.603 5.817 6.029 6.239
      0 11.67 16.41 17.59 17.93 18.58 19.23 19.87 20.5
      0 22.2 32.26 35.22 35.9 37.12 38.32 39.49 40.65
      0 33.37 50.69 56.85 58.11 59.97 61.79 63.57 65.3
   ];

   Coef[4,9] = SPLINE2D(VG_data, VD_data, ID_data);

   VG: 0;
   VD: 0;

   spline_model = SPLINT2D(VG, VD, Coef, VG_data, VD_data, ID_data);
end

Model
   Extrinsic1  20 30 40 2 3
      RG=3.5   RD=0.5  RS=4.73;

   FETR  20 30 40
      IS=5E-15  VBI=0.8  GMIN=1.0E-07  ALPHA=2     THETA=0.003
      VBR=20.0  N=1      VTO=-1.637    BETA=0.029  LAMBDA=0.04978;

   VSOURCE  2 0  VDC=VG;
   VSOURCE  3 0  NAME=drain  VDC=VD;

   CIRCUIT;

   Circuit_model: IDRAIN_DC * 1000.0;
end
```

```
Sweep
   DC: VG: from -1.2 to 0 step=0.2  VD: from 0 to 2 step=0.2 from 3 to 6 step=1
       spline_model Circuit_model
       {Xsweep VG=all  Ymin=0 Ymax=70 NYticks=7
        Y=spline_model.green & Circuit_model.green.circle};
end
```

Comparison of 2D Bicubic Spline Interpolation and Exact Circuit Simulation

The following figure shows an excellent match between the results from 2D bicubic spline interpolation and from circuit simulation. Note that only about a quarter of the points shown were used as data in establishing the bicubic spline coefficients.

For instance, the figures shows 7 different values of the gate bias voltage. Only 4 of the values, namely -1.2, -0.8, -0.4 and 0, were included in the data for computing the spline coefficients by SPLINE2D(). Also, for each of these gate bias voltage, only half of the drain bias voltage values shown were included in the data.

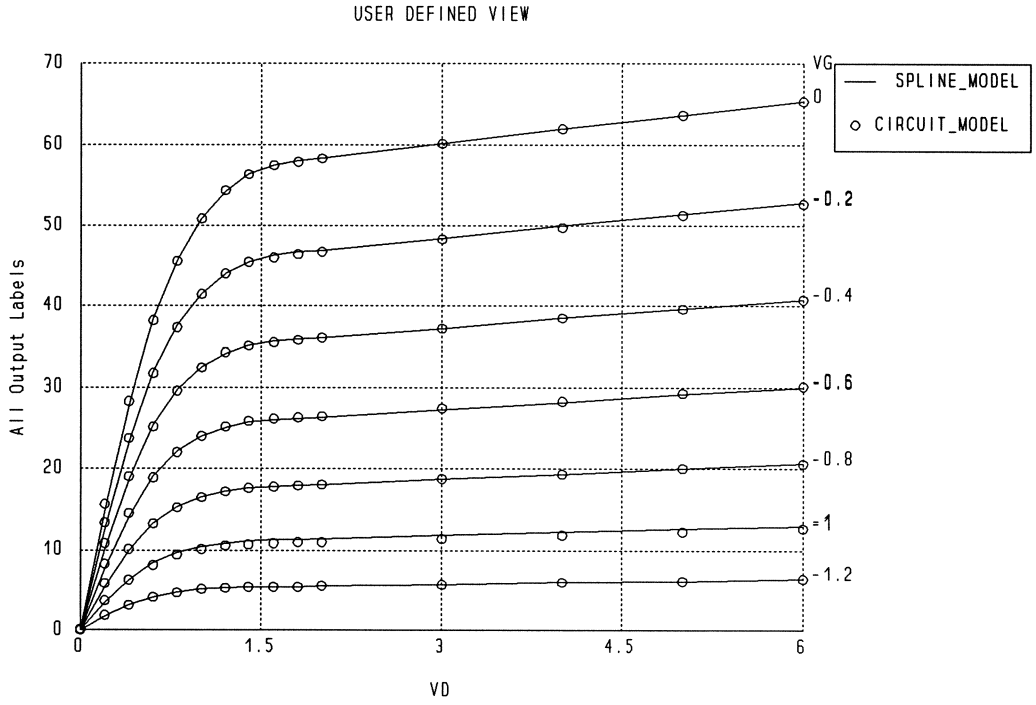

demo43

FET modeling using the built-in 2D bicubic spline interpolation functions SPLINE2D() and SPLINT2D().

SPLINE2D() is used to establish bicubic spline coefficients from data. Typically the data contains values of a function $f(x,y)$ sampled on a 2-dimensional grid formed by discrete points of (x,y). Then, SPLINT2D() can be used to interpolate $f(x,y)$ at arbitrary values of x and y.

This example applies 2D bicubic splines to a bias-dependent small-signal FET model. We consider four model parameters, namely g_m, C_{gs}, C_{gd} and G_{ds}, as functions of the bias voltages V_g and V_d. The values of $g_m(V_g,V_d)$, $C_{gs}(V_g,V_d)$, $C_{gd}(V_g,V_d)$ and $G_{ds}(V_g,V_d)$ are derived from a nonlinear FET model at 6×13 bias points. From each of these parameters a 2D bicubic spline model is establised using SPLINE2D(). Then, SPLINT2D() is used to evaluate g_m, C_{gs}, C_{gd} and G_{ds} at arbitrary bias points, thus form a bias-dependent small-signal FET model.

To validate the model, S parameters calculated from the bias-dependent small-signal model are compared with those calculated using the nonlinear FET model (i.e., the nonlinear FET model from which the sample of g_m, C_{gs}, C_{gd} and G_{ds} values are derived).

Input File

```
!  Example demo43.ckt
!  Use 2D bicubic spline interpolation for small-signal modeling
!  The small-signal parameters gm, Cgs, Cgd and Gds are sampled
!  at 6 x 13 bias points.  For each of the parameters a 2D bicubic
!  spline model is constructed.  The 2D spline models are then used
!  to form a bias-dependent small-signal linear FET model.
!  This interpolation model is then compared with a nonlinear FET
!  model.

Expression
   Vg_data[6] = [ -1.5  -1.2  -0.9  -0.6  -0.3  0 ];

   Vd_data[13] = [ 0.0  0.1  0.2  0.4  0.6  0.8  1
                   1.3  1.6  2.0  2.5  3.0  4.0 ];

   gm_data[6,13] = [
      0.0      0.0       0.0      0.0      0.0      0.0      0.0
      0.0      0.0       0.0      0.0      0.0      0.0
      0.0      0.004162  0.0078   0.01366  0.01789  0.02076  0.02256
      0.02387  0.02442   0.02505  0.02585  0.02664  0.02822
      0.0      0.00775   0.01456  0.02565  0.03377  0.03939  0.04299
      0.0457   0.04678   0.04796  0.04942  0.05088  0.05379
      0.0      0.01048   0.01986  0.03548  0.04727  0.05569  0.06129
      0.06571  0.06743   0.06908  0.07113  0.07317  0.07722
      0.0      0.01232   0.02359  0.04295  0.05817  0.06951  0.07738
      0.08398  0.08661   0.08869  0.09127  0.09382  0.09888
      0.0      0.01336   0.02588  0.04815  0.06644  0.08069  0.0911
      0.1005   0.1045    0.107    0.11     0.1131   0.119
   ];

   cgs_data[6,13] = [
      0.3539  0.3539  0.3539  0.3539  0.3539  0.3539  0.3539
      0.3539  0.3539  0.3539  0.3539  0.3539  0.3539
      0.3795  0.3793  0.3791  0.3788  0.3786  0.3784  0.3783
      0.3783  0.3782  0.3782  0.3782  0.3781  0.3781
```

```
      0.4116  0.4106  0.4097  0.4083  0.4073  0.4067  0.4063
      0.406   0.4059  0.4057  0.4056  0.4054  0.4051
      0.4536  0.4508  0.4484  0.4447  0.4421  0.4404  0.4392
      0.4383  0.438   0.4377  0.4373  0.4369  0.4362
      0.5117  0.5055  0.5002  0.492   0.4862  0.4822  0.4796
      0.4774  0.4766  0.476   0.4752  0.4744  0.4729
      0.6     0.5867  0.5755  0.5582  0.5459  0.5373  0.5316
      0.5267  0.5247  0.5235  0.522   0.5206  0.5178
   ];

   cgd_data[6,13] = [
      5.898  5.774  5.657  5.443  5.252  5.08   4.924
      4.714  4.529  4.313  4.082  3.885  3.563
      6.325  6.172  6.03   5.774  5.547  5.345  5.164
      4.924  4.714  4.472  4.216  4.0    3.652
      6.86   6.667  6.489  6.173  5.898  5.657  5.444
      5.165  4.924  4.65   4.365  4.126  3.747
      7.559  7.304  7.072  6.668  6.326  6.032  5.775
      5.445  5.165  4.852  4.53   4.265  3.85
      8.528  8.166  7.847  7.306  6.863  6.492  6.175
      5.776  5.446  5.082  4.716  4.419  3.962
      10.00  9.431  8.948  8.171  7.565  7.077  6.672
      6.177  5.777  5.348  4.926  4.59   4.084
   ];

   gds_data[6,13] = [
      0.0      0.0      0.0      0.0      0.0      0.0      0.0
      0.0      0.0      0.0      0.0      0.0      0.0
      0.6834   0.5972   0.5182   0.3797   0.265    0.1726   0.102
      0.03775  0.0239   0.02385  0.02378  0.02371  0.02358
      2.731    2.374    2.053    1.5      1.052    0.6925   0.4169
      0.1576   0.0883   0.08794  0.0875   0.08706  0.0862
      6.139    5.343    4.628    3.407    2.418    1.624    1.006
      0.3974   0.1851   0.1841   0.1828   0.1816   0.1792
      10.9     9.543    8.314    6.204    4.481    3.084    1.976
      0.8325   0.3283   0.3067   0.3041   0.3017   0.2969
      17.02    15.02    13.19    10.02    7.387    5.222    3.472
      1.577    0.5851   0.4518   0.4475   0.4433   0.4353
   ];

   Coef_gm[6,13] = SPLINE2D(Vg_data, Vd_data, Gm_data);
   Coef_cgs[6,13] = SPLINE2D(Vg_data, Vd_data, cgs_data);
   Coef_cgd[6,13] = SPLINE2D(Vg_data, Vd_data, cgd_data);
   Coef_gds[6,13] = SPLINE2D(Vg_data, Vd_data, gds_data);

   K: 1;
   VGS[3]: [ -0.4  -0.7  -1.3 ];
   VDS[3]: [  0.5   3.5   6.0 ];

   VG: 0;
   VD: 0;

   gm_spline = SPLINT2D(VG, VD, Coef_gm, Vg_data, Vd_data, Gm_data);
   cgs_spline = SPLINT2D(VG, VD, Coef_gm, Vg_data, Vd_data, cgs_data);
   cgd_spline = SPLINT2D(VG, VD, Coef_gm, Vg_data, Vd_data, cgd_data);
   gds_spline = SPLINT2D(VG, VD, Coef_gm, Vg_data, Vd_data, gds_data);
end

Model
   Extrinsic2   1 2 3 4 5
      CX: 10PF   RG: 4       RD: 0.05
      LG: 0.3NH  LD: 0.2NH   RS: 3.75
      LS: 0.1NH  GDS: 0.004  CDS: 0.1PF;

   VCCS 1 2 3 3  M=-gm_spline T=4pS;

   CAP 1 3 C=(cgs_spline * 1pF);
   CAP 1 2 C=(cgd_spline * 0.01pF);
   RES 2 3 R=(100 / gds_spline);

   IND 4 0 L=50NH;
```

```
   IND 5 0 L=50NH;

   CAP 4 8 C=1NF;
   CAP 5 9 C=1NF;

   PORT  8 0;
   PORT  9 0;

   Extrinsic2   11 12 13 14 15
      CX: 10PF   RG: 4       RD: 0.05
      LG: 0.3NH  LD: 0.2NH   RS: 3.75
      LS: 0.1NH  GDS: 0.004  CDS: 0.1PF;

   FETR  11 12 13
      IS: 5E-15    N: 1         FC: 0.5    GMIN: 1.0E-07
      VBI: 0.8     VBR: 20.0    ALPHA: 2   THETA: 0.003
      BETA: 0.038  VTO: -1.5    LAMBDA: 0.0765
      TAU: 4PS     CGSO: 0.6PF  CGDO: 0.1PF;

   IND 14 16 L=50NH;
   IND 15 17 L=50NH;

   CAP 14 18 C=1NF;
   CAP 15 19 C=1NF;

   VSOURCE 16 0  VDC=VG;
   VSOURCE 17 0  VDC=VD;

   PORT 18 0;
   PORT 19 0;

   Circuit;

   MSS[8] = [MS11 MS22 MS33 MS44 MS12 MS21 MS34 MS43];
   PSS[8] = [PS11 PS22 PS33 PS44 PS12 PS21 PS34 PS43];

   RSS[8] = [RS11 RS22 RS33 RS44 RS12 RS21 RS34 RS43];
   ISS[8] = [IS11 IS22 IS33 IS44 IS12 IS21 IS34 IS43];
end

Sweep
   AC: K: from 1 to 3 step=1  FREQ: from 2 to 18 step=1
       VG=VGS[K]  VD=VDS[K]  MSS  PSS  RSS  ISS
       {Smith MP=(MS11,PS11)."S11_spline".green &
                 (MS33,PS33)."S11_circuit".yellow.circle  K=all}
       {Smith MP=(MS22,PS22)."S22_spline".green &
                 (MS44,PS44)."S22_circuit".yellow.circle  K=all}
       {Polar MP=(MS21,PS21)."S21_spline".green &
                 (MS43,PS43)."S21_circuit".yellow.circle  K=all}
       {Polar MP=(MS12,PS12)."S12_spline".green &
                 (MS34,PS34)."S12_circuit".yellow.circle  K=all}
       {Xsweep K=all Y=RS11.green & RS33.green.circle &
                     IS11.yellow & IS33.yellow.circle}
       {Xsweep K=all Y=RS22.green & RS44.green.circle &
                     IS22.yellow & IS44.yellow.circle}
       {Xsweep K=all Y=RS21.green & RS43.green.circle &
                     IS21.yellow & IS43.yellow.circle}
       {Xsweep K=all Y=RS12.green & RS34.green.circle &
                     IS12.yellow & IS34.yellow.circle};

   AC: FREQ: from 2 to 18 step=1  VG=0.5  VD=-0.5
       MSS  PSS  RSS  ISS
       {Smith MP=(MS11,PS11)."S11_spline".green &
                 (MS33,PS33)."S11_circuit".green.circle &
                 (MS22,PS22)."S22_spline".yellow &
                 (MS44,PS44)."S22_circuit".yellow.circle}
       {Polar MP=(MS21,PS21)."S21_spline".green &
                 (MS43,PS43)."S21_circuit".yellow.circle}
       {Polar MP=(MS12,PS12)."S12_spline".green &
                 (MS34,PS34)."S12_circuit".yellow.circle}
       {Xsweep Y=RS11.green & RS33.green.circle &
```

```
                IS11.yellow & IS33.yellow.circle}
        {Xsweep Y=RS22.green & RS44.green.circle &
                IS22.yellow & IS44.yellow.circle}
        {Xsweep Y=RS21.green & RS43.green.circle &
                IS21.yellow & IS43.yellow.circle}
        {Xsweep Y=RS12.green & RS34.green.circle &
                IS12.yellow & IS34.yellow.circle};
end
```

Match of S11 by Spline/Small-Signal FET Model and Nonlinear FET Model

The following figure shows the match of S_{11} as calculated by the bicubic spline/small-signal FET model and by the nonlinear FETR model. S_{11} is shown in rectangular form, namely as RS11 and IS11.

The match is shown for three different bias points, namely

V_g = -0.4V, V_d = 0.5,
V_g = -0.7V, V_d = 3.5,
V_g = -1.3V, V_d = 6.0.

Note that none of these bias points is included in the data used for establishing the spline coefficients. In other words, at these bias points, the bias-dependent small-signal model parameters are obtained by interpolation. The excellent match of the S parameters verifies the accuracy of the bicubic spline model.

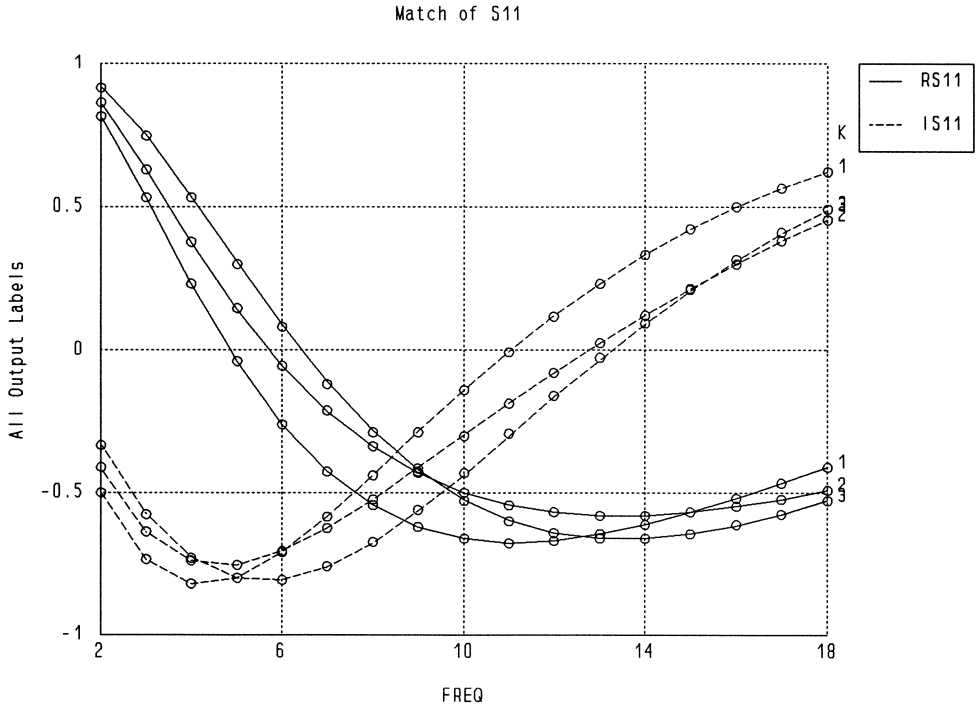

Match of S21 by Spline/Small-Signal FET Model and Nonlinear FET Model

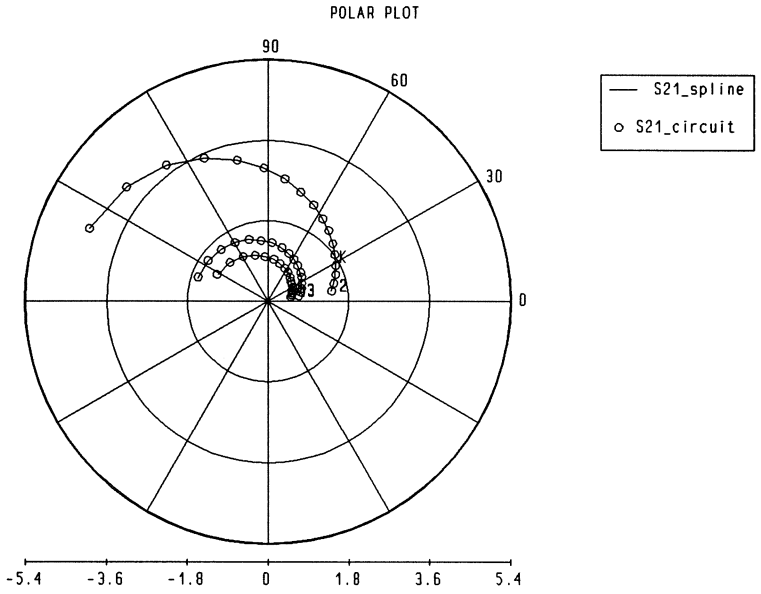

Cubic Spline May Not Be Accurate for Extrapolation

In general, cubic splines should be used only for interpolation. In some cases extrapolation may produce good results, e.g., the preceding figures include the bias point V_d = 6V which is outside the sample grid, yet the result obtained by extrapolation seems to be accurate. The following figure, however, shows gross errors generated by extrapolation to the bias point V_g = 0.5V and V_d = -0.5V.

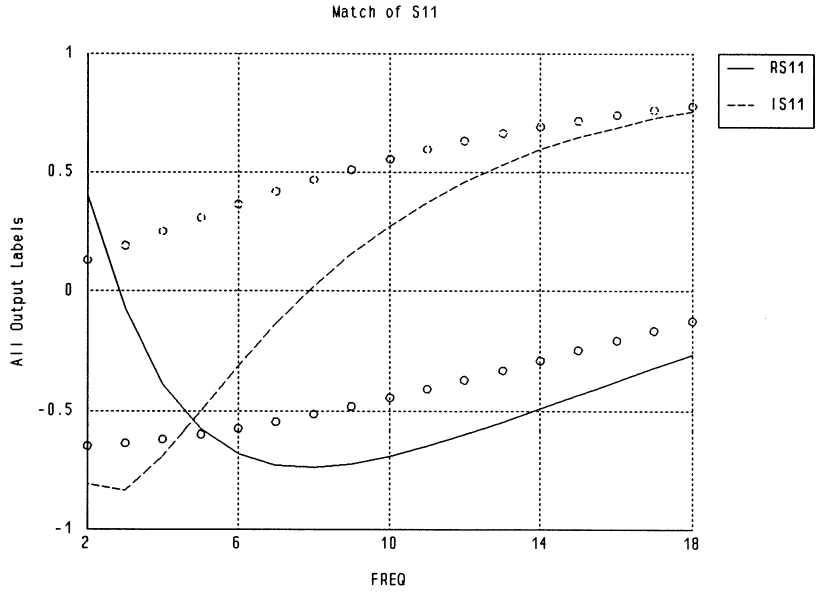

demo44

Illustration of simple report generation.

Input File

```
!  Example  demo44.ckt
!  Illustrate simple report generation

Expression
   x1: ?-0.5?;
   x2: ?0.5?;

   f1 = x1 * x1 + x2 * x2 - 1;
   f2 = 3 - x1 * x1 - x2 * x2;
   f3 = x1 - x2 + 3;

   fmax = max(f1, f2, f3);
end

Sweep
   f1 f2 f3 fmax;
end

Report
   We have two variables and three functions.

     Optimization Variables
     ----------------------
       x1  $x1$
       x2  $x2$
     ----------------------

     Function Values
     ----------------------
       f1  $f1$
       f2  $f2$
       f3  $f3$
     ----------------------

   We are supposed to use minimax optimization,
   and the minimax objective is given by

   fmax = max($f1$, $f2$, $f3$) = $fmax$.
end

Specification
   f1  f2  f3;
end

Control
   Optimizer=Minimax;
end
```

Report Generated

```
We have two variables and three functions.

  Optimization Variables
  ----------------------
    x1  -0.5
    x2  0.5
  ----------------------

  Function Values
  ----------------------
    f1  -0.5
    f2  2.5
    f3  2
  ----------------------

We are supposed to use minimax optimization,
and the minimax objective is given by

fmax = max(-0.5, 2.5, 2) = 2.5.
```

demo45

Illustration of report generation with parameter sweeps.

Input File

```
!  Example  demo45.ckt
!  Illustrate report generation for tabulating simulation results

Model
   VG: 0;
   VD: 0;

   PORT  1 0;
   CAP   1 2  C=10NF;

   IND      2 3  L=100NH;
   VSOURCE  3 0  VDC=VG;

   Extrinsic1  4 5 6 2 7
      RG=3.5  RD=2  RS=4  LG=0.03NH  LD=0.07NH  LS=0.1NH  CDS=0.08pF;

   FETM  4 5 6
      GAMMA=-0.1  E=2       SL=0.2  KG=-0.25  IG0=5E-10  ALPHAG=20
      IB0=8e-12   ALPHAB=1  VBC=20  KR=0      K1=1       CF0=0.03pF
      KF=-0.12    IDSS=0.3  VP0=-3  TAU=2ps   R10=0.01   C10=0.5pF;

   IND      7 8  L=100NH;
   VSOURCE  8 0  NAME=DRAIN  VDC=VD;

   CAP   7 9  C=10NF;
   PORT  9 0;

   CIRCUIT;

   gain = 20 * log10(MS21);
   ID_mA = Idrain_DC * 1000;
end

Sweep
   AC: FREQ: from 4GHZ to 10GHZ step=1GHZ  VG=-2  VD=3V  gain  MS11  PS21;

   DC: VG=-1  VD: 0 1 2 3 4  ID_mA;

   AC: FREQ: from 4GHZ to 10GHZ step=1GHZ  VG=-1  VD=2V  gain  MS11  PS21;
end

Report
            Circuit Simulation Results: Small-Signal AC
   ------------------------------------------------------------------------
     Frequency  Gate Bias   Drain Bias     |S11|      gain    phase of S21
   ------------------------------------------------------------------------
${
    $%4g$ $FREQ$GHz  $VG$volts    $VD$volts   $%7.4f$ $MS11$ $%6.2f%$ $gain$dB $%6.1f$ $PS21$degrees
}$
   ------------------------------------------------------------------------



          Circuit Simulation Results: DC
   -----------------------------------------
${ $%g$    VG=$VG$   VD=$VD$  $%5.2f$ DC drain current=$Id_mA$mA }$
   -----------------------------------------
end
```

Report Generated

Circuit Simulation Results: Small-Signal AC

Frequency	Gate Bias	Drain Bias	|S11|	gain	phase of S21
4GHz	-2volts	3volts	0.8707	11.19dB	137.2degrees
5GHz	-2volts	3volts	0.8199	10.54dB	127.4degrees
6GHz	-2volts	3volts	0.7730	9.88dB	119.2degrees
7GHz	-2volts	3volts	0.7333	9.24dB	112.0degrees
8GHz	-2volts	3volts	0.6948	8.59dB	105.2degrees
9GHz	-2volts	3volts	0.6633	7.96dB	99.0degrees
10GHz	-2volts	3volts	0.6389	7.43dB	93.4degrees
4GHz	-1volts	2volts	0.8901	9.34dB	139.2degrees
5GHz	-1volts	2volts	0.8458	8.76dB	129.9degrees
6GHz	-1volts	2volts	0.8037	8.16dB	121.8degrees
7GHz	-1volts	2volts	0.7671	7.57dB	114.8degrees
8GHz	-1volts	2volts	0.7315	6.99dB	108.1degrees
9GHz	-1volts	2volts	0.7018	6.41dB	102.0degrees
10GHz	-1volts	2volts	0.6776	5.92dB	96.5degrees

Circuit Simulation Results: DC

VG=-1	VD=0	DC drain current= 0.00mA
VG=-1	VD=1	DC drain current=59.07mA
VG=-1	VD=2	DC drain current=88.02mA
VG=-1	VD=3	DC drain current=96.80mA
VG=-1	VD=4	DC drain current=100.71mA

demo46

Illustration of report generation for displaying arrays and matrices in user-designed format.

Input File

```
!  Example  demo46.ckt
!  Illustrate report generation for arrays and matrices

Expression
   Matrix[3,3] =
      [ 7.3 1.9 2.8
        3.7 8.2 4.6
        5.5 6.4 9.1 ];

   Vector[3] = [ 4.35 6.69 8.76 ];

   Mat_Vec[3] = product(Matrix, Vector);

   Inverse_Matrix[3,3] = Inverse(Matrix);
   sol3[3] = product(Inverse_Matrix, Vector);
end

Report
$%9.4f$
   Consider a 3x3 matrix:

   A =  [$matrix$ ]

   and a vector:

   B =  [$vector$ ]

   The product of the matrix and the vector is

   A * B =  [$mat_vec % 1$ ]

   The inverse of the matrix A is

   C = inverse(A) =  [$inverse_matrix$ ]

   The solution of the linear system

   A * D = B

   can be obtained from the product of the inverse
   matrix and the right-hand-side vector:

   D = C * B =  [$sol3 % 1$ ]
end
```

Report Generated

```
Consider a 3x3 matrix:

A =  [   7.3000    1.9000    2.8000
         3.7000    8.2000    4.6000
         5.5000    6.4000    9.1000 ]

and a vector:

B =  [   4.3500    6.6900    8.7600 ]

The product of the matrix and the vector is

A * B =  [  68.9940
          111.2490
          146.4570 ]

The inverse of the matrix A is

C = inverse(A) =  [   0.1779    0.0025   -0.0560
                     -0.0330    0.2010   -0.0914
                     -0.0844   -0.1428    0.2080 ]

The solution of the linear system

A * D = B

can be obtained from the product of the inverse
matrix and the right-hand-side vector:

D = C * B =  [   0.3000
                 0.4000
                 0.5000 ]
```

demo47

Illustration of the preprogrammed Raytheon-Statz FET model.

This is the same model as the built-in FETR. This example illustrates how to program the model equations using expressions and FETU1. The preprogrammed equations are supplied in the include file "statz.inc".

This example can be used as a template for creating a custom modified version of the Raytheon-Statz model.

The model parameters are extracted by HarPE from *S*-parameter measurements.

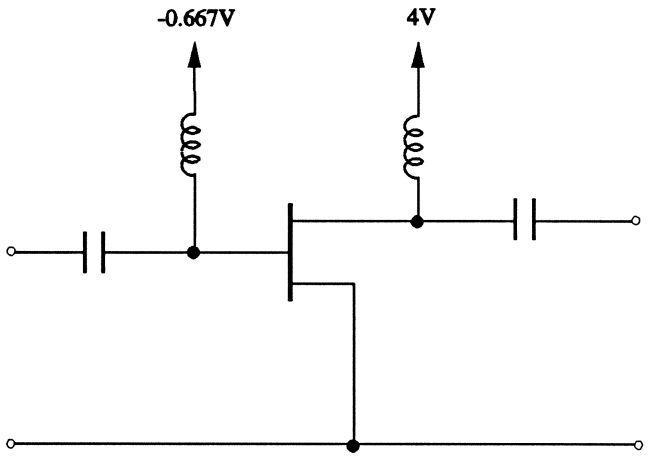

Input File

```
!  Example  demo47.ckt
!  Illustrate preprogrammed Raytheon-Statz model using FETU1.
!  Show match to measured S parameters and DC IV curves

Model
   ! Raytheon-Statz model parameters

   ISS: 5E-15;
   N: 1;
   FC: 0.5;
   GMIN: 1.0E-07;
   VBI: 0.8;
   VBR: 20.0;
   ALPHA: 2;
   THETA: 0.003;
   BETA: ?0.0367905?;
   VT0: ?-1.61391?;
   LAMBDA: ?0.0824712?;
   TAU: ?4.54375PS?;
   CGS0: ?0.699982PF?;
   CGD0: ?0.0969199PF?;

   VLABEL 1 3  NAME=VGS_T;
   VLABEL 1 3  NAME=VGS_TAU TAU=TAU;
   VLABEL 2 3  NAME=VDS_T;
```

```
   #include "statz.inc";

   Extrinsic2   1 2 3 4 5
      CX: 20PF    RG: 4     RD: 0.05
      LG: ?0.316701NH?
      LD: ?0.196607NH?
      RS: ?4.8994?
      LS: ?0.0880644NH?
      GDS: ?0.00310382?
      CDS: ?0.0991592PF?;

   FETU1  1 2 3
      IDS=IDS_MODEL  IGS=IGS_MODEL    IGD=IGD_MODEL
      QGS=QGS_MODEL  QGD=QGD_MODEL;

   VG: -0.667;
   VD: 4;

   CAP 4 40 C=10nF;
   CAP 5 50 C=10nF;
   IND 4 41 L=1mH;
   IND 5 51 L=1mH;

   VSOURCE 41 0  VDC=VG;
   VSOURCE 51 0  NAME=DRAIN  VDC=VD;

   PORT 40 0;
   PORT 50 0;

   CIRCUIT;

   ID_mA: IDRAIN_DC * 1000.0;
end

Sweep
   DC: VG: from -1 to 0 step=0.2  VD: from 0 to 6 step=0.3  ID_mA;

   AC: FREQ: from 1GHZ to 20GHZ step=1GHZ  K=(FREQ/1GHZ)
       MS PS MS11_data PS11_data MS21_data PS21_data
             MS12_data PS12_data MS22_data PS22_data
       {Smith MP=(MS11_data,PS11_data)."S11_data".green.circle &
                 (MS22_data,PS22_data)."S22_data".yellow.circle &
                 (MS11,PS11)."S11".green & (MS22,PS22)."S22".yellow}
       {Polar MP=(MS21,PS21)."S21" & (MS21_data,PS21_data)."S21_data".circle}
       {Polar MP=(MS12,PS12)."S12" & (MS12_data,PS12_data)."S12_data".circle};
end

Expression
   ! measured data: taken from spar_2.dat for HarPE
   ! MS11 PS11 MS21 PS21 MS12 PS12 MS22 PS22, 1GHZ - 20GHZ

   Data[20,8] = [
      .983  -20.2   4.5734   163.5    .0187    80.2    .675   -8.7
      .945  -38.1   4.2792   148.5    .0344    70.4    .659  -17.1
      .898  -53.4   3.9170   135.0    .0459    63.3    .642  -21.5
      .830  -68.4   3.6557   122.4    .0574    56.4    .623  -28.4
      .787  -83.2   3.4163   111.1    .0657    52.4    .592  -32.0
      .723  -97.8   3.2070   100.0    .0734    47.4    .568  -37.1
      .683 -112.8   3.0142    90.0    .0791    44.4    .534  -40.7
      .638 -128.7   2.8536    79.4    .0846    40.9    .497  -46.3
      .609 -143.9   2.6537    70.1    .0891    38.8    .465  -51.1
      .598 -159.5   2.5056    60.6    .0935    36.7    .423  -57.3
      .597 -172.7   2.3270    51.5    .0960    35.0    .390  -65.5
      .601  174.7   2.1758    43.3    .1024    34.0    .362  -75.3
      .614  165.1   2.0045    35.0    .1063    33.4    .351  -84.4
      .627  157.2   1.8696    28.6    .1134    32.5    .329  -97.2
      .622  151.0   1.7376    20.6    .1216    31.7    .367 -106.5
      .625  146.2   1.6303    15.8    .1331    31.9    .349 -113.8
      .611  141.6   1.5467     9.2    .1456    32.0    .401 -120.8
      .596  138.0   1.4606     5.0    .1644    31.9    .396 -121.7
      .582  132.6   1.4213     -.7    .1852    32.2    .425 -126.9
```

```
      .554  127.7   1.3582    -4.8    .2130    30.0    .418 -127.7];

   K: 1;

   MS11_data = data[K,1];
   MS21_data = data[K,3];
   MS12_data = data[K,5];
   MS22_data = data[K,7];
   PS11_data = data[K,2];
   PS21_data = data[K,4];
   PS12_data = data[K,6];
   PS22_data = data[K,8];
end
```

Match Between Simulated and Measured S11 and S22

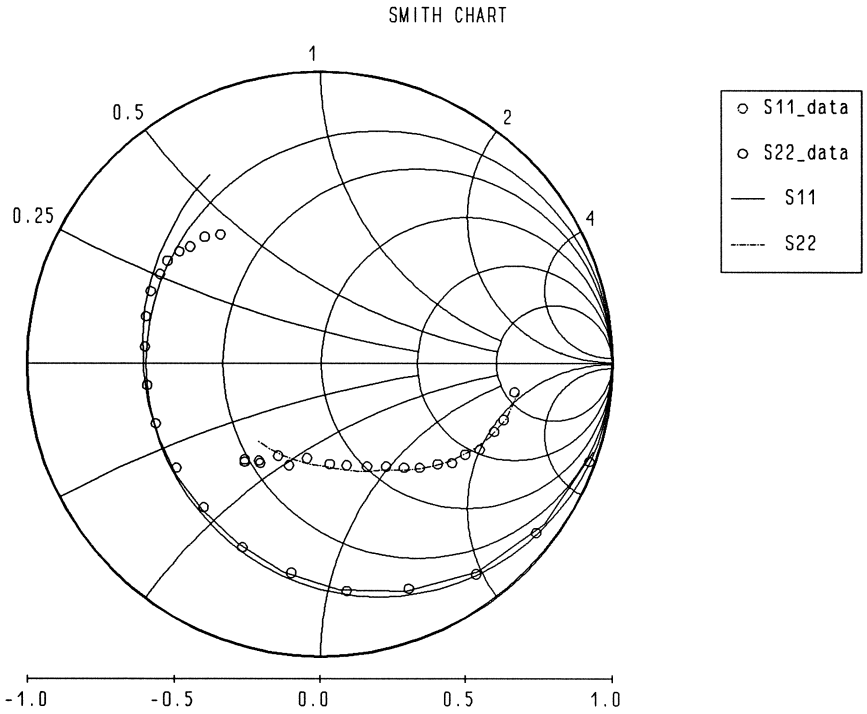

Match Between Simulated and Measured S21

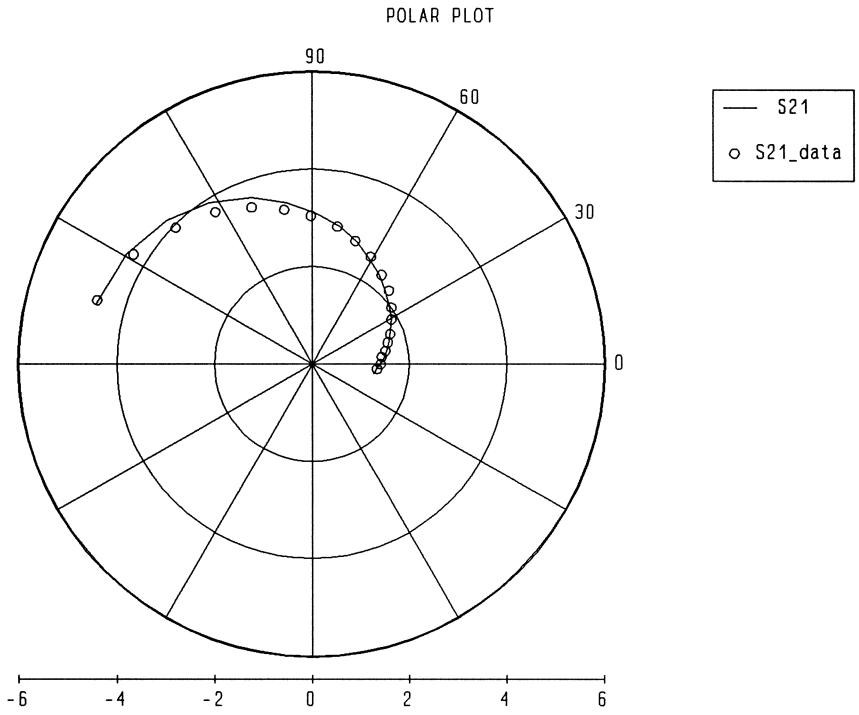

demo48

Illustration of the preprogrammed KTL physics-based small-signal FET model.

KTL has been developed by OSA for physics-based FET modeling. KTL combines the Khatibzadeh and Trew nonlinear model (for solving for the DC operating point) and the Ladbrooke small-signal model.

The preprogrammed equations are supplied in the include file "ktl.inc".

The model parameters are extracted by HarPE from *S*-parameter measurements.

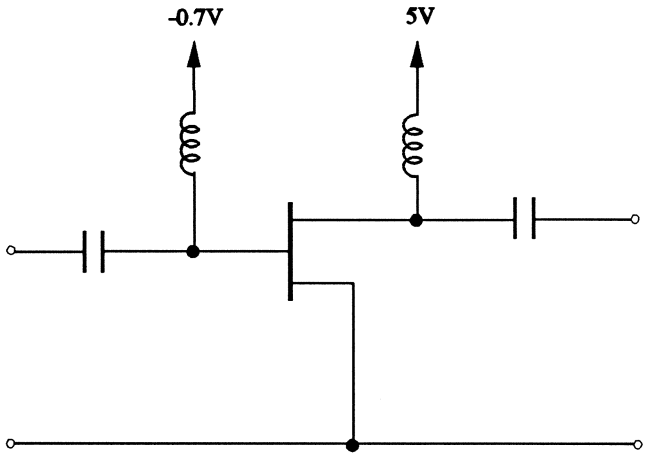

Input File

```
!  Example  demo48.ckt
!  Illustrate preprogrammed physics-based KTL FET model.
!  Show match to measured S parameters and also DC IV curves.

Model
   #include "ktl.inc"

   ! KTL model parameters

   L      = 0.49UM;
   W      = 300UM;
   A      = 0.13UM;
   EPSR   = 12.5;
   VS     = 9.5e-5;
   VBI    = 0.6612;
   U0     = 0.5e-9;
   D      = 1.0E-12;
   ND     = 2.47826E23;
   LAMBDA = 1.0E-8;
   ALPHA  = 0.5;
   AA     = 1.0E6;
   BB     = 1.0;
   CC     = 1.0;
   DD     = 0;
   A0     = 1.0;
   R01    = 0.013286;
```

```
   R02    = 1.82965;
   R03    = 572.253;
   M      = 4;
   LGG0   = 0.0162194;
   CDS    = 0.06pF;
   GDS    = 0.0023;
   RG     = 7.8;
   RD     = 0.5;
   RS0    = 3.8;
   CGE    = 0.055pF;
   CDE    = 0.0002pF;
   CX     = 2pF;
   LD     = 0.06NH;
   LS     = 0.022NH;

   KTL(4, 5, 0,
       L, W, A, EPSR, VS, VBI, U0, D, ND, LAMBDA, ALPHA,
       AA, BB, CC, DD, A0, R01, R02, R03, LGG0, M,
       LD, LS, RG, RD, RS0, GDS, CX,  CDS, CGE, CDE, 1);

   VG: -0.7;
   VD: 5;

   CAP 4 40 C=10nF;
   CAP 5 50 C=10nF;
   IND 4 41 L=1mH;
   IND 5 51 L=1mH;

   VSOURCE 41 0  VDC=VG;
   VSOURCE 51 0  NAME=DRAIN  VDC=VD;

   PORT 40 0;
   PORT 50 0;

   CIRCUIT;

   ID_mA: Idrain_DC * 1000;
end

Sweep
   DC: VG: from -1 to 0 step=0.2  VD: from 0 to 6 step=0.3  ID_mA;

   AC: FREQ: from 1GHz to 21GHz step=2GHz  K=((FREQ+1)/2GHz)
       MS PS MS11_data PS11_data MS21_data PS21_data
             MS12_data PS12_data MS22_data PS22_data
       {Smith MP=(MS11_data,PS11_data)."S11_data".green.circle &
                 (MS22_data,PS22_data)."S22_data".yellow.circle &
                 (MS11,PS11)."S11".green & (MS22,PS22)."S22".yellow}
       {Polar MP=(MS21,PS21)."S21" & (MS21_data,PS21_data)."S21_data".circle}
       {Polar MP=(MS12,PS12)."S12" & (MS12_data,PS12_data)."S12_data".circle};
end

Expression
   ! measured data: MS11 PS11 MS21 PS21 MS12 PS12 MS22 PS22
   ! 1GHz, 3GHz, ..., 21GHz

   Data[11,8] = [
      0.9955 -11.44 2.572 170.1 0.0148 82.57 0.6734 -6.068
      0.9644 -33.42 2.439 152.6 0.04203 69.88 0.6565 -14.22
      0.916 -53.12 2.23 136.5 0.06374 58.7 0.6337 -22.05
      0.8652 -70.02 2.001 122.6 0.07947 49.57 0.6109 -28.95
      0.8203 -84.23 1.785 110.5 0.09031 42.34 0.5922 -35.08
      0.7838 -96.12 1.597 100 0.09762 36.66 0.5786 -40.72
      0.7551 -106.1 1.438 90.78 0.1025 32.18 0.5696 -46.08
      0.733 -114.6 1.304 82.49 0.1057 28.63 0.5645 -51.28
      0.7159 -121.8 1.192 74.96 0.1077 25.8 0.5626 -56.4
      0.7028 -128.1 1.097 68.02 0.1089 23.55 0.5632 -61.46
      0.6926 -133.5 1.016 61.57 0.1096 21.76 0.5658 -66.49];

   K: 1;
```

```
    MS11_data = data[K,1];
    MS21_data = data[K,3];
    MS12_data = data[K,5];
    MS22_data = data[K,7];
    PS11_data = data[K,2];
    PS21_data = data[K,4];
    PS12_data = data[K,6];
    PS22_data = data[K,8];
end
```

Match Between Simulated and Measured S11 and S22

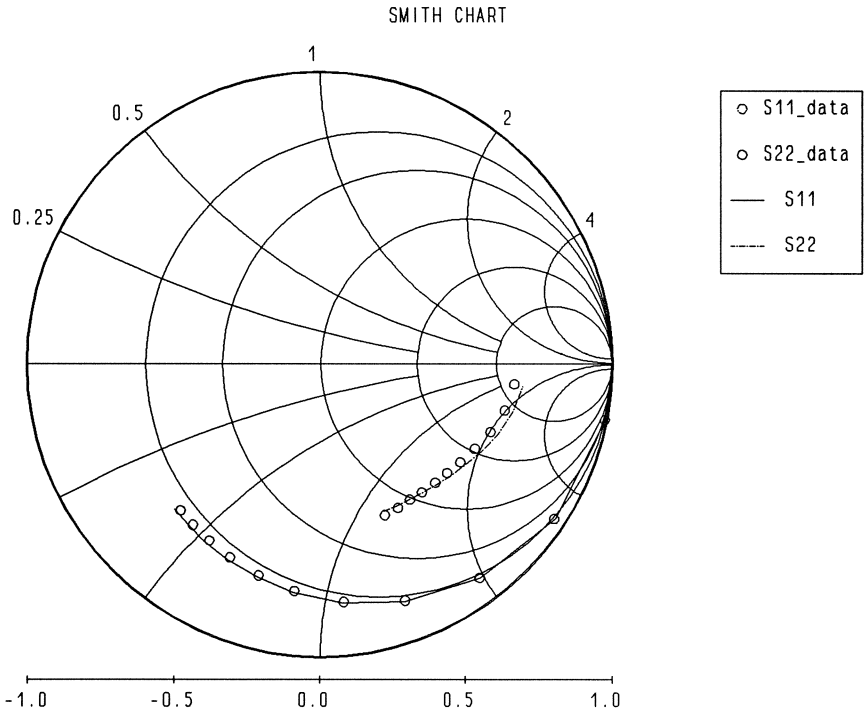

Match Between Simulated and Measured S21

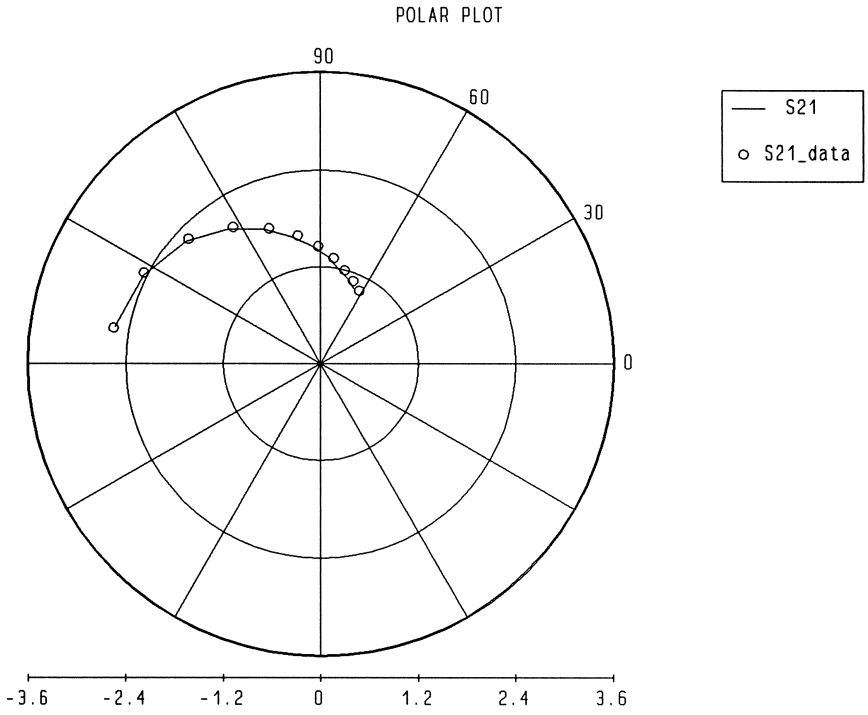

Match Between Simulated and Measured S12

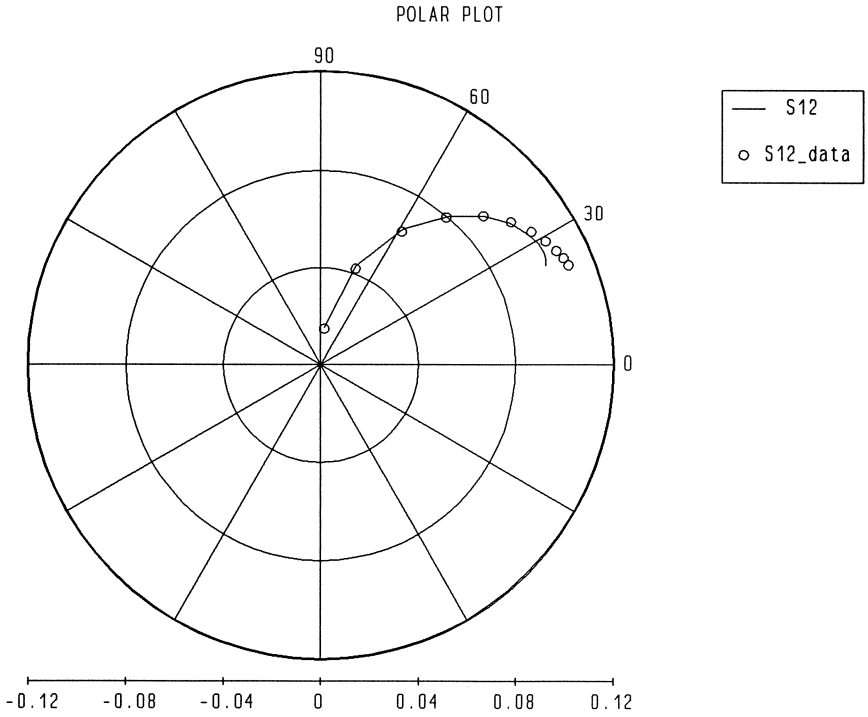

demo49

Illustration of using a linear subcircuit as a port termination. A subcircuit consisting of a resistor and a capacitor in parallel is used as a complex load terminating the output port.

The FET model is extracted by HarPE from *MGF1902* data.

We can plot the phase plane of the time-domain output current (calculated by hamonic balance simulation) versus the output voltage (Parametric display with time as the sweep parameter).

The parametric display of output current versus output voltage can be superimposed on the DC IV characteristics to show the drain load lines at different input power levels and/or frequencies.

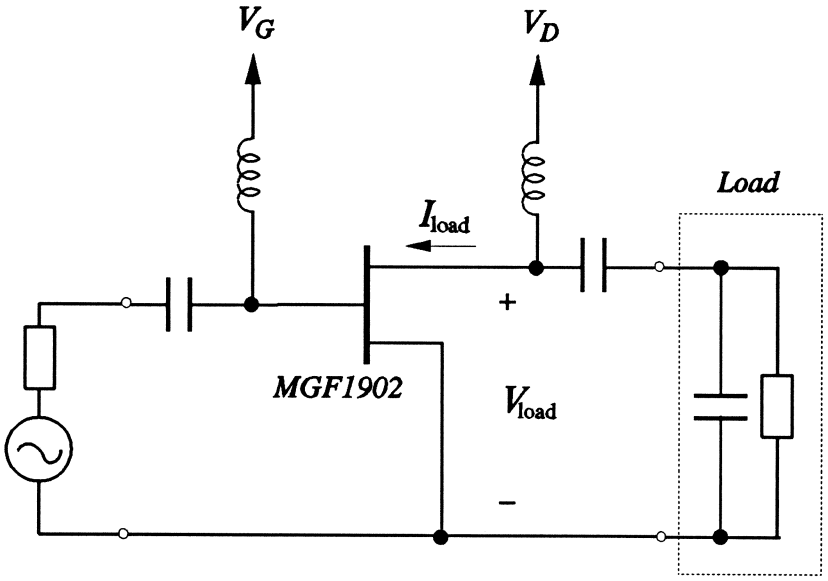

Input File

```
!  Example  demo49.ckt
!  Illustrate the use of a linear subcircuit as a port termination.
!  A subcircuit of parallel RES-CAP is used as the (complex) load.
!  We can show the phase plane plot (load lines) by combining two displays:
!  Parametric display of time-domain output current versus output voltage
!  and Xsweep display of the DC IV characteristics.
!  The FET model for Mitsubishi MGF1902 is extracted by HarPE.

Model
   SUBCIRCUIT  Load  1 0 {
      RES 1 0  R=50;
      CAP 1 0  C=1pF;
   };

   CAP 1 2 C=1000pF;

   Extrinsic4  20 30 40 2 3
```

```
      RG=5          RD=0.2      RS=1.5     LS=0.0948NH
      LG=0.53633NH  LD=0.936NH  GDS=0.002  CDS=0.0278PF
      CDE=0.0682pF  CX=10pF;

   FETM  20 30 40
      E=1.4  SL=0.126  IB0=8e-12    ALPHAB=1     VBC=6
      GAMMA=-0.06356   K1=2         CF0=0.02PF   KF=-0.157
      IDSS=0.04716     VP0=-0.7338  R10=0.00343  C10=0.6294PF;

   CAP 2 0 C=0.184pF;  ! FET parasitic
   CAP 3 0 C=0.216pF;

   CAP 3 4 C=1000pF;

   Pin: -2;
   VG: -0.3;
   VD: 3;

   IND 2 200 L=1000nH;
   VSOURCE 200 0 NAME=gate VDC=VG;

   IND 3 300 L=1000nH;
   VSOURCE 300 0 NAME=drain VDC=VD;

   PORT 1 0  P=Pin;

   PORT 4 0 NAME=out  Z=Load;

   CIRCUIT;

   Id_mA = Idrain_DC * 1000;

   MP2RI(MVout, PVout, RVout[0:N_SPECTRA], IVout[0:N_SPECTRA]);
   MP2RI(MIout, PIout, RIout[0:N_SPECTRA], IIout[0:N_SPECTRA]);

   K: 0;
   T: K / FREQ;

   Vout = DFT_FT(RVout, IVout, Spectral_Freq, T);
   Iout = DFT_FT(RIout, IIout, Spectral_Freq, T);

   Vload = Vout + VD;  ! include the DC component
   Iload = (Iout + MIdrain[0]) * 1000;
end

Sweep
   DC: VG: from -0.8 to 0.2 step=0.1  VD: from 0 to 1 step=0.25 2 3 4 5  ID_mA
       {Xsweep  Y=ID_mA  VG=all Ymin=0 Ymax=60 NYticks=6  NXticks=5};

   HB: FREQ=2GHZ  Pin: -9 -6 -3 0  K: from 0 to 1 N=25  Vload Iload
       {PARAMETRIC  Title="Drain Load Lines"  Comments="Load: PRC R=50 C=1pF"
        Pin=all  X=Vload Xmin=0 Xmax=5 NXticks=5
        Y=Iload Ymin=0 Ymax=60 NYticks=6};

   HB: FREQ: 1 2 4 8  K: from 0 to 1 N=25  Vload Iload
       {PARAMETRIC  Title="Drain Load Lines"  Comments="Load: PRC R=50 C=1pF"
        FREQ=all  X=Vload Xmin=0 Xmax=5 NXticks=5
        Y=Iload Ymin=0 Ymax=60 NYticks=6};
end
```

Drain Load Lines for Different Input Power Levels (Frequency = 2GHz)

The drain load lines shown in the following figures are obtained by superimposing the parametric display of output current versus output voltage on the DC IV characteristics. At the present, this has to be done manually by combining two HPGL plotter files.

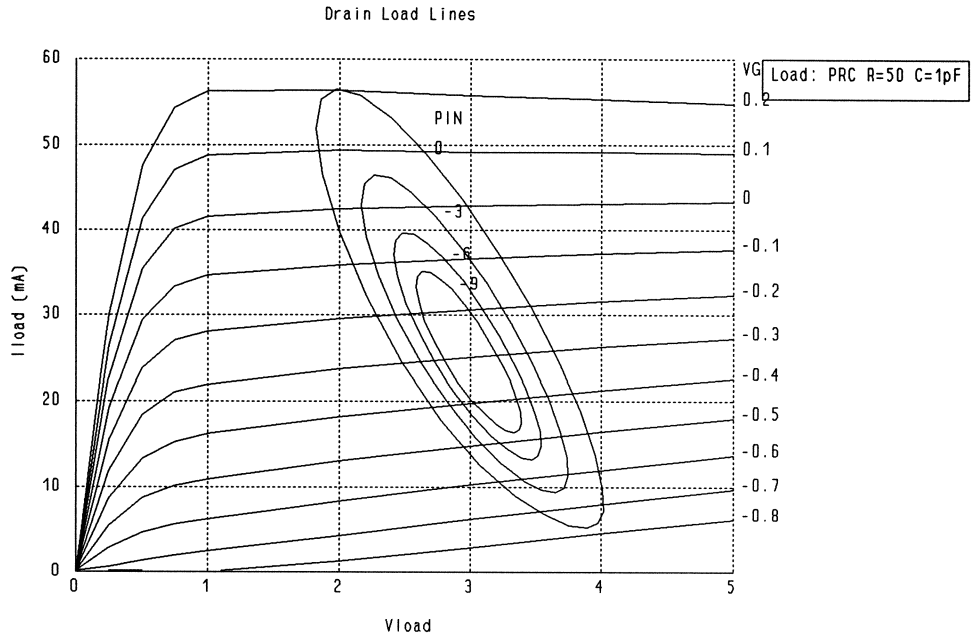

Drain Load Lines at Different Frequencies (Available Input Power = -2dBm)

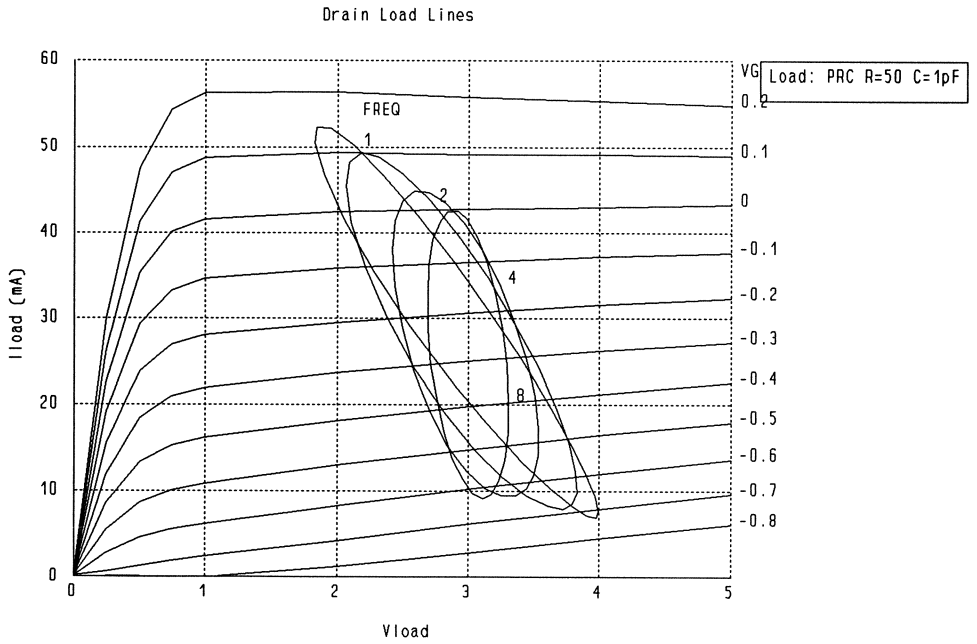

demo50

Illustration of nested linear subcircuits.

This example uses two levels of nested subcircuits.

To demonstrate the benefit of linear subcircuits, we compare this example with another one which defines the same circuit using symbolic subcircuits. The ratio of simulation time between these two is approximately 1:43. Clearly, the use of linear subcircuits, where appropriate, may lead to substantial computational savings.

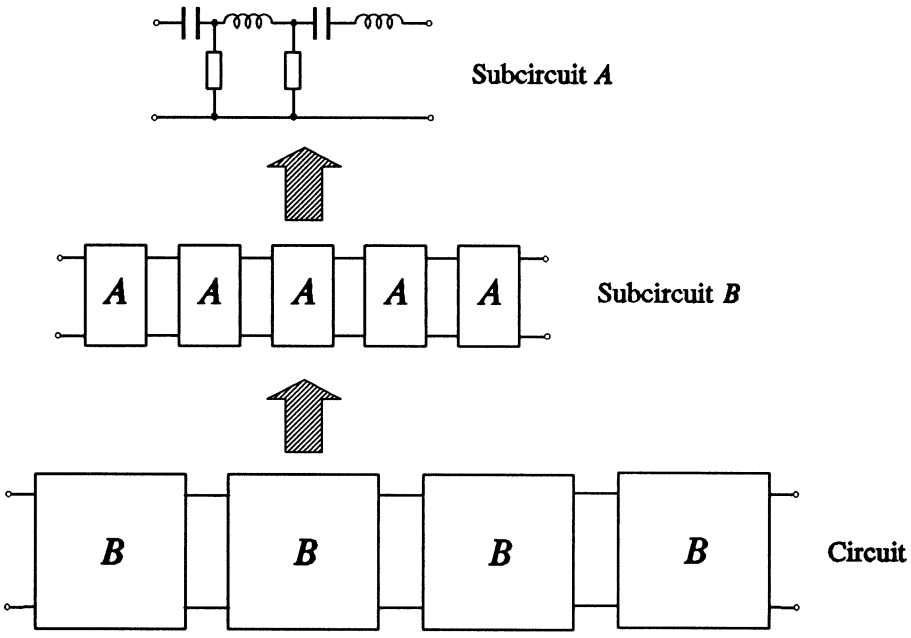

Input File

```
!  Example  demo50.ckt
!  Illustrate the use of nested linear subcircuits.
!  Comparison of simulation time between this example which uses
!  nested subcircuits and one which uses symbolic subcircuits
!  is approximately  1 : 43

Model
   SUBCIRCUIT  SubCkt_A 1 5 0 {
      CAP 1 2 C=1;
      RES 2 0 R=10;
      IND 2 3 L=1;
      RES 3 0 R=10;
      CAP 3 4 C=1;
      IND 4 5 L=1;
   };


   SUBCIRCUIT  SubCkt_B 1 6 0 {
      SubCkt_A 1 2 0;
      SubCkt_A 2 3 0;
```

```
      SubCkt_A 3 4 0;
      SubCkt_A 4 5 0;
      SubCkt_A 5 6 0;
   };


   SubCkt_B 1 2 0;
   SubCkt_B 2 3 0;
   SubCkt_B 3 4 0;
   SubCkt_B 4 5 0;

   PORT 1 0;
   PORT 5 0;

   Circuit;
end

Sweep
   AC: FREQ: from 1 to 10 step=1  MS PS;
end
```

demo51

Illustration of using the built-in matrix functions to solve linear circuit equations.

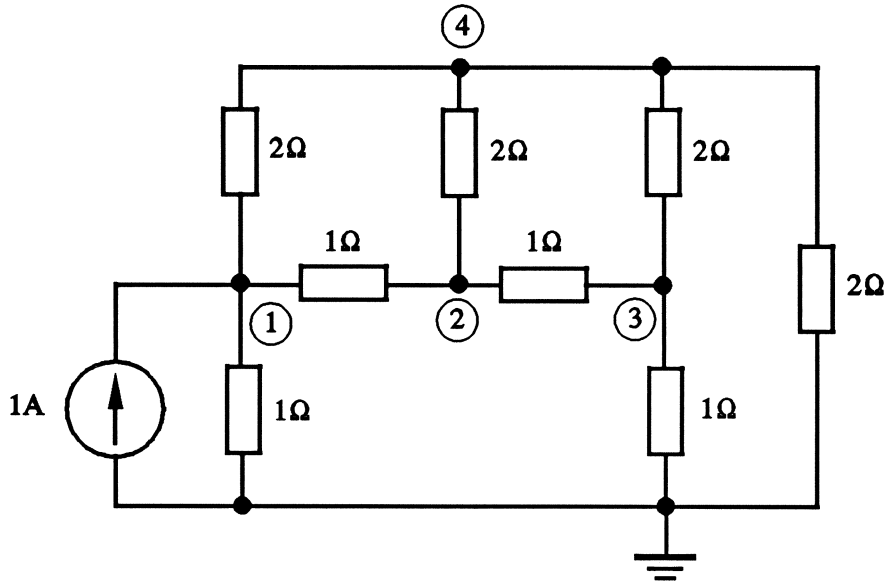

The circuit equations for solving for the nodal voltages are defined as

$$\mathbf{Y}\,\mathbf{V} = \mathbf{I}$$

where **Y** is the nodal admittance matrix, **V** is the vector of nodal voltages and **I** is the right-hand-side vector representing the current excitaion.

The input file of demo51 implements this set of equations using OSA90's array expressions and solves the equations using the built-in matrix function Solve().

The solution obtained from matrix operations is compared with the results from circuit simulation.

Input File

```
! Example  demo51.ckt
! Illustrate the use of matrix operations to solve linear circuit equations.
! This example solves real (resistive) circuit equations.
! demo52 solves complex equations.
! The results are compared with circuit simulation results.

Model
   ISOURCE 1 0 IDC=1;

   RES 1 0 R=1;
   RES 1 2 R=1;
   RES 2 3 R=1;
   RES 3 0 R=1;
```

```
   RES 1 4 R=2;
   RES 2 4 R=2;
   RES 3 4 R=2;
   RES 4 0 R=2;

   VLABEL 1 0  NAME=V1;
   VLABEL 2 0  NAME=V2;
   VLABEL 3 0  NAME=V3;
   VLABEL 4 0  NAME=V4;

   CIRCUIT;

   Y[4,4] = [ 2.5  -1.0   0.0  -0.5
             -1.0   2.5  -1.0  -0.5
              0.0  -1.0   2.5  -0.5
             -0.5  -0.5  -0.5   2.0];

   RHS[4] = [1 0 0 0];

   V[4] = solve(Y, RHS);
end

Sweep
   DC: V1, V2, V3, V4,  V;
end
```

Results

The results obtained by numerical display are as follows.

```
! OSA90 V2.5
! Input File: /home/osa90/demo51.ckt    Wed May 12 10:30:00 1993
! Parameter Sweep
 FORMAT V[1]       V[2]       V[3]       V[4];
      0.6222        0.4     0.2222     0.3111
```

demo52

Illustration of using the built-in matrix functions to solve linear circuit equations. While demo51 deals with real equations (resistive circuit), this example illustrates solution of complex equations.

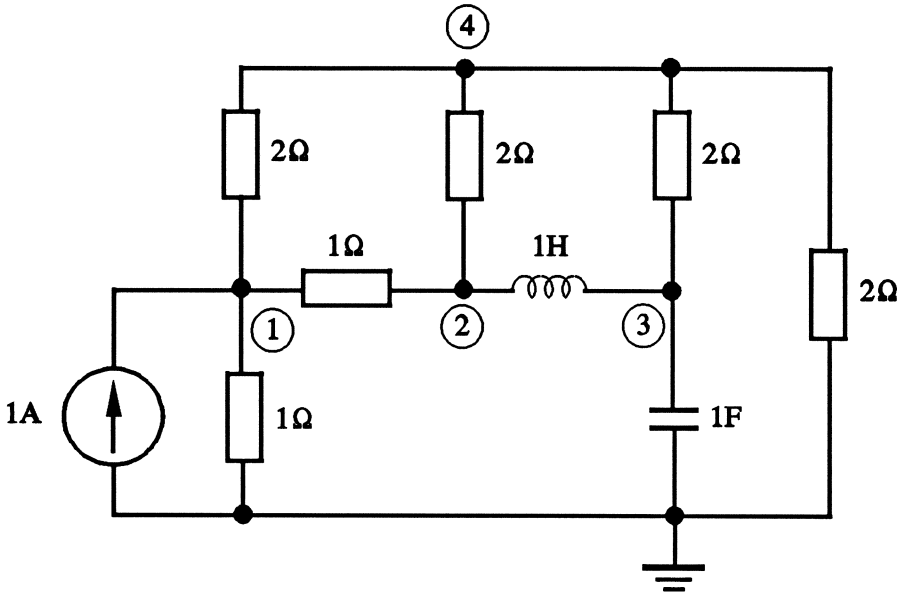

The circuit equations for solving for the nodal voltages are defined as

$$\mathbf{Y}\,\mathbf{V} = \mathbf{I}$$

where Y is the complex nodal admittance matrix, V is the vector of nodal voltages and I is the right-hand-side vector representing the current excitaion.

We split the set of complex equations into real and imaginary parts. For instance, the 4×4 complex Y matrix is represented by an 8×8 real matrix.

The solution obtained from matrix operations is compared with the results from circuit simulation.

Input File

```
!  Example  demo52.ckt
!  Illustrate the use of matrix operations to solve linear circuit equations.
!  demo51 solves real (resistive) circuit equations.
!  This example solves complex equations.
!  The results are compared with circuit simulation results.

Control
   Non_Microwave_Units;
   Display_N_Digits = 6;
end
```

```
Model
   R1: 1;   G1 = 1 / R1;
   R2: 2;   G2 = 1 / R2;
   R3: 1;   G3 = 1 / R3;
   L: 1;    YL = -1 / (2 * PI * FREQ * L);
   C: 2;    YC = 2 * PI * FREQ * C;

   ISOURCE 1 0  I=1;

   RES 1 2 R=R1;
   IND 2 3 L=L;
   CAP 3 0 C=C;

   RES 1 4 R=R2;
   RES 2 4 R=R2;
   RES 3 4 R=R2;
   RES 4 0 R=R2;
   RES 1 0 R=R3;

   VLABEL 1 0  NAME=V1;
   VLABEL 2 0  NAME=V2;
   VLABEL 3 0  NAME=V3;
   VLABEL 4 0  NAME=V4;

   CIRCUIT;

   MV[4] = [MV1[1] MV2[1] MV3[1] MV4[1]];
   PV[4] = [PV1[1] PV2[1] PV3[1] PV4[1]];
   MP2RI(MV, PV, RV_a[4], IV_a[4]);

   RY[4,4] = [ (G1 + G2 + G3)   -G1          0    -G2
               -G1              (G1 + G2)    0    -G2
                0                0           G2   -G2
               -G2              -G2         -G2   (4 * G2)];

   IY[4,4] = [ 0   0    0   0
               0   YL  -YL  0
               0  -YL   YC  0
               0   0    0   0 ];

   Y[8,8] = [ RY  -IY
              IY   RY ];

   RHS[8] = [1 0 0 0 0 0 0 0];

   V[8] = solve(Y, RHS);
   RV_b[4] = subset(V,1);
   IV_b[4] = subset(V,5);

   RY_INV[4,4] = inverse(RY);
   RYIY[4,4] = product(RY_INV,IY);
   IYRYIY[4,4] = product(IY,RYIY);
   RIRI[4,4] = RY + IYRYIY;
   RHS4[4] = [1 0 0 0];

   RV_c[4] = solve(RIRI,RHS4);
   IV_[4] = product(RYIY, RV_c);
   IV_c[4] = -IV_;
end

Sweep
   HB: FREQ: 1 5 10  RV_a, IV_a;
   FREQ: 1 5 10  RV_b, IV_b;
   FREQ: 1 5 10  RV_c, IV_c;
end
```

demo53

Illustration of displaying FET drain load lines. The circuit is the optimized small-signal amplifier from demo12. The FETR model is extracted by HarPE from *NEC700* data.

The FET drain load lines are obtained by superimposing the Parametric display of time-domain drain current versus drain voltage on the Xsweep display of DC IV curves. At the present, this has to be done manually by combining two HPGL plotter files.

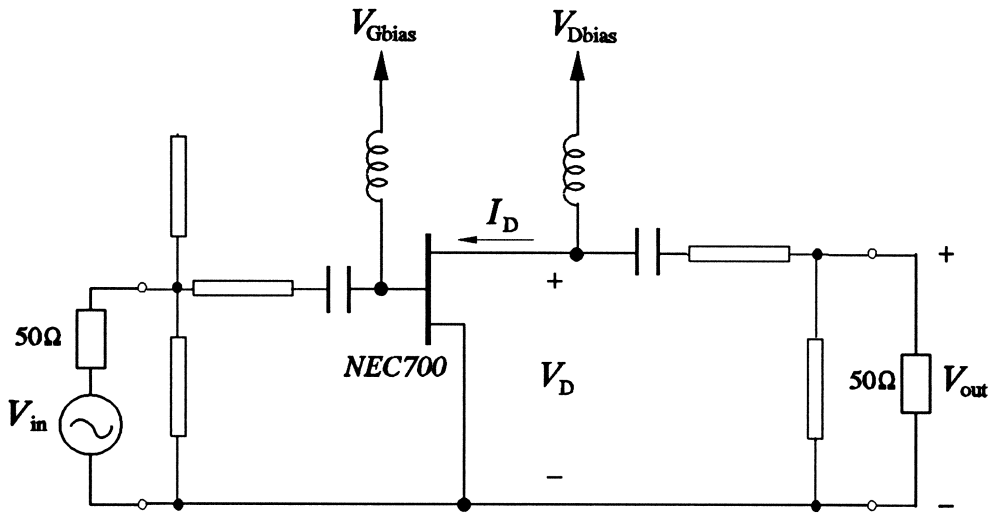

Input File

```
!  Example  demo53.ckt
!  Illustrate the display of FET drain load lines.
!  The circuit is the optimized small-signal amplifier from demo12.
!  FETR model extracted by HarPE from NEC700 data.
!  The FET drain load lines are obtained by combining two displays:
!  Parametric display of time-domain drain current versus drain voltage
!  and Xsweep display of the DC IV characteristics

Model
   TEM  @input  0  Z=70  E=128  F=18GHZ;
   TEM  @output 0  Z=50  E=61.7 F=18GHZ;

   TEM   @input @open1 0 @open2  Z=100 E=65 F=18GHZ;
   OPEN  @open1 @open2;

   TEM  @input @DC_block1  Z=100 E=25 F=18GHZ;

   ! FET model

   CAP @DC_block1 @FET_input  C=10NF;
   IND @Gate_bias @FET_input  L=100NH;

   Extrinsic2  @intrin1 @intrin2 @intrin3 @FET_input @FET_output
      RG=3.5   LG=0.0306NH  RD=0.5       LD=0.00792NH
      RS=4.73  LS=0.0451NH  GDS=0.00345  CDS=0.08738PF  CX=10PF;

   FETR  @intrin1 @intrin2 @intrin3
```

```
      IS=5E-15    N=1         FC=0.5          GMIN=1.0E-07
      VBI=0.8     VBR=20.0    ALPHA=2         THETA=0.003
      BETA=0.029  VT0=-1.637  LAMBDA=0.04978  TAU=2.8PS
      CGS0=0.4428PF  CGD0=0.1066PF;

   CAP @probe @DC_block2   C=10NF;
   SRL @probe @Drain_bias  L=100NH;

   TEM  @DC_block2 @output  Z=100 E=15 F=18GHZ;

   VG: -0.56V;
   VD: 4V;

   VSOURCE  @Gate_bias  0  VDC=VG;
   VSOURCE  @Drain_bias 0  NAME=drain VDC=VD;

   Pin: 0;

   PORT  @input  0  P=Pin;
   PORT  @output 0  NAME=OUT;

   ILABEL @probe @FET_output  NAME=Idac;

   VLABEL @FET_output 0  NAME=Vdac;

   CIRCUIT;

   ID_mA = IDrain_DC * 1000;

   MP2RI(MVdac, PVdac, RVdac[0:N_SPECTRA], IVdac[0:N_SPECTRA]);
   MP2RI(MIdac, PIdac, RIdac[0:N_SPECTRA], IIdac[0:N_SPECTRA]);

   K: 0;
   T: K / FREQ;

   Vd_T = DFT_FT(RVdac, IVdac, Spectral_Freq, T);
   Id_T = DFT_FT(RIdac, IIdac, Spectral_Freq, T);
   Id_T_mA = Id_T * 1000;
end

Sweep
   DC: VG: from -1.4 to 0 step=0.2  VD: from 0 to 1 step=0.25 2 3 4 5 6 ID_mA
       {Xsweep VG=all Y=ID_mA  NXTicks=6  Ymin=0 Ymax=70 NYTicks=7};

   HB: FREQ=15  PIN: from -9 to 3 step=3
       K: from 0 to 1 N=25  Vd_T Id_T_mA
       {Parametric  Pin=all  X=Vd_T Xmin=0 Xmax=6 NXTicks=6
        Y=Id_T_mA Ymin=0 Ymax=70 NYTicks=7};

   HB: FREQ: 6 10 14 18  PIN=-3
       K: from 0 to 1 N=25  Vd_T Id_T_mA
       {Parametric  FREQ=all  X=Vd_T Xmin=0 Xmax=6 NXTicks=6
        Y=Id_T_mA Ymin=0 Ymax=70 NYTicks=7};
end
```

Drain Load Lines at Different Input Power Levels (Frequency = 15GHz)

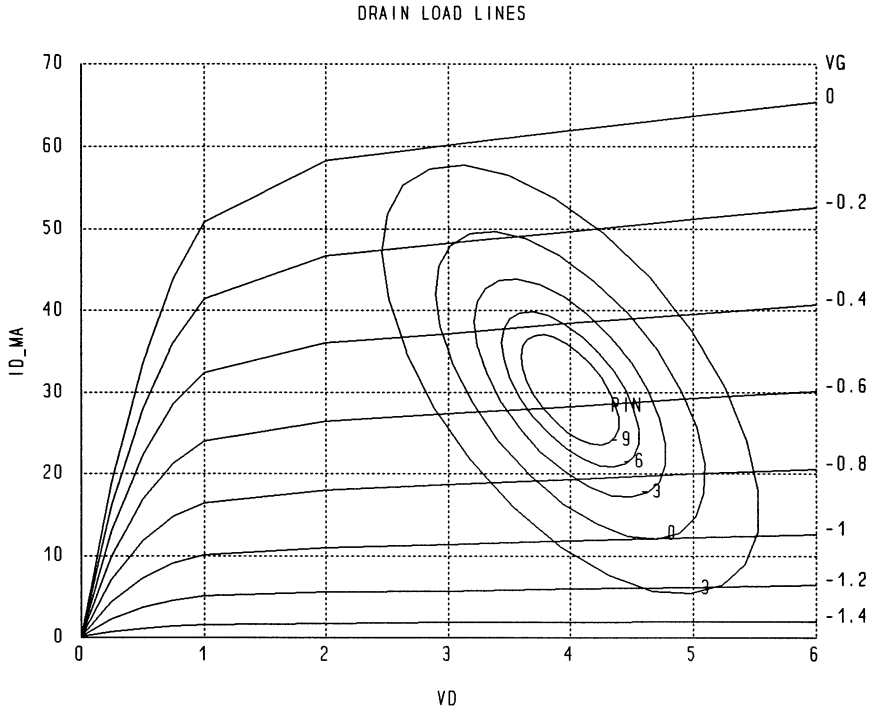

Drain Load Lines at Different Frequencies (Available Input Power = -3dBm)

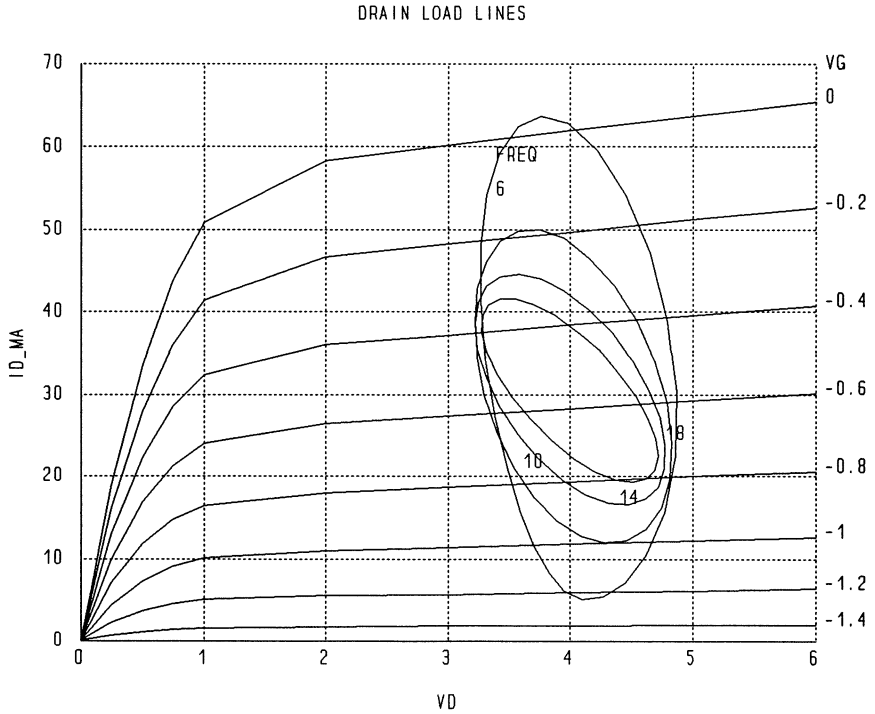

demo54

Demonstration of Huber optimization. A sequence of Huber optimization with decreasing threshold values is shown to converge to the ℓ_1 solution.

The optimization problem is identical to the one considered in demo02. We wish to approximate

$$Goal = \text{sqrt}(t)$$

by

$$Function = (x_1 t + x_2 t^2) / (1 + x_3 t + x_4 t^2)$$

for t = 0, 0.02, 0.04, ..., 1, by optimizing the coefficients x_1, x_2, x_3 and x_4.

The ℓ_1 solution is illustrated in demo02. In this example, we perform a sequence of Huber optimizations with decreasing threshold values of 0.025, 0.01 and 0.005. The Huber solutions are shown to be converging to the ℓ_1 solution.

Input File

```
!  Example  demo54.ckt
!  Demonstration of sequential Huber optimization converging to L1 solution
!  Matching sqrt(t) by a rational function in the interval [0  1] of t
!  The coefficients of the rational function are optimized by the Huber
!  optimizer with decreasing threshold values.
!  The results are shown to be converging to the L1 solution.

control
   optimizer=Huber;    ! IMPORTANT: choose threshold=0.25 (the default)
   no_default_bounds;
   two_sided_perturbation;
end

Expression
   t: 0;
   Goal: sqrt(t);

   x11: ?-0.4?;
   x12: ?-4?;
   x13: ?0.5?;
   x14: ?0.5?;

   Function1: x11 * exp(x12 * t) + x13 * exp(x14 * t);
   error1 = function1 - goal;
   "delta=0.025" = abs(error1);

   x21: ?-0.4?;
   x22: ?-4?;
   x23: ?0.5?;
   x24: ?0.5?;

   Function2: x21 * exp(x22 * t) + x23 * exp(x24 * t);
   error2 = function2 - goal;
   "delta=0.01" = abs(error2);

   x31: ?-0.4?;
   x32: ?-4?;
   x33: ?0.5?;
```

```
   x34: ?0.5?;

   Function3: x31 * exp(x32 * t) + x33 * exp(x34 * t);
   error3 = function3 - goal;
   "delta=0.005" = abs(error3);

   xL11: -0.475112;
   xL12: -3.57642;
   xL13: 0.609186;
   xL14: 0.51505;

   FunctionL1: xL11 * exp(xL12 * t) + xL13 * exp(xL14 * t);
   errorL1 = functionL1 - goal;
   "L1" = abs(errorL1);
end

Sweep
   t: from 0 to 1 step=0.01  "delta=0.025" "delta=0.01" "delta=0.005" "L1"
      {Xsweep Title="Comparison of Optimization Using L1 and Hyber Norms"
       Y=all  Y_title="Absolute Errors"  Ymax=0.02  Ymin=0  NYticks=4};
end

Specification
   t: from 0 to 1 step=0.02
      function1 = goal W=10   ! W=10, equivalent to threshold = 0.025
      function2 = goal W=25   ! W=25, equivalent to threshold = 0.01
      function3 = goal W=50;  ! W=50, equivalent to threshold = 0.005
end
```

Sequence of Huber Optimizations Converging to the L1 Solution

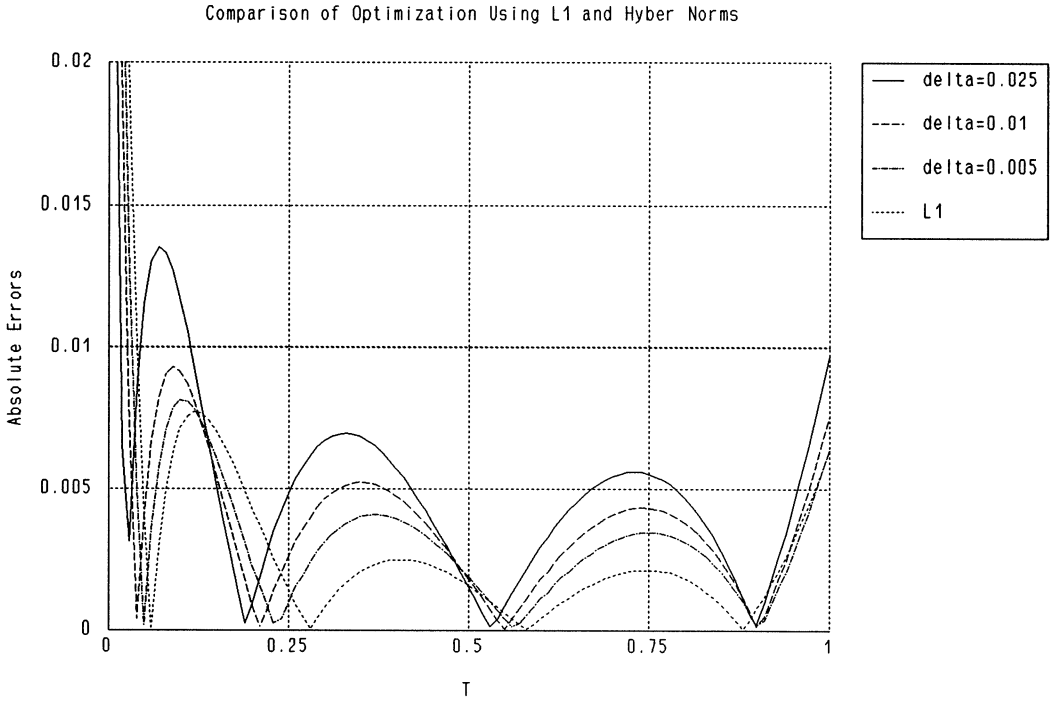

demo55

Monte Carlo analysis of a small-signal X-band amplifier. The three FETs and passive components are represented by physics-based models.

The FET gate length, gate width, channel thickness and doping density as well as MIM capacitor metal plate areas and spiral inductor turns have been optimized for enhanced yield.

This example is consistent with the results published by Bandler *et al.* in "Integrated physics-oriented statistical modeling, simulation and optimization", *IEEE Trans. Microwave Theory Tech.*, vol. 40, pp. 1374-1400, 1992.

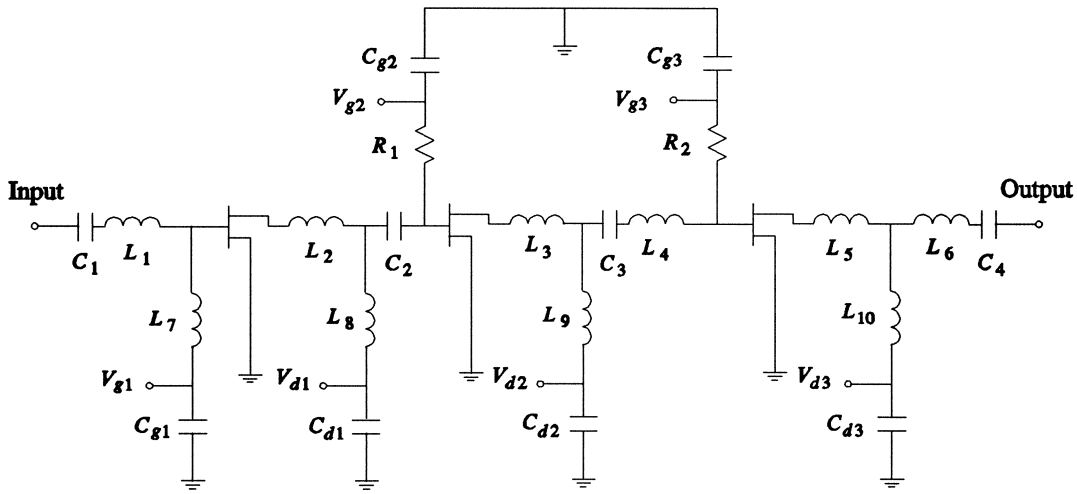

Input File

```
!  Example  demo55.ckt
!  Monte Carlo analysis of a small-signal X-band amplifier.
!  The FETs and passive components are represented by physics-based models.
!  The FET gate length, gate width, channel thickness and doping density
!  as well as MIM capacitor metal plate areas and spiral inductor turns
!  have been optimized for yield.

Model
   ! parameters for calculating capacitors
   Epsr: 7;
   C_d: 0.1 {NORMAL SIGMA=4.0%};
   C_k: Epsr / (36.0 * 3.14159 * C_d) * 1.0e-6;
   C_S1: 322.728 {NORMAL SIGMA=3.5%};  ! metal plate area in square UMs
   C_S2: 2006.25 {NORMAL SIGMA=3.5%};
   C_S3: 222.868 {NORMAL SIGMA=3.5%};
   C_S4: 356.737 {NORMAL SIGMA=3.5%};
   C_S5: 8078;
   C_S6: 24235;

   CalculateCapacitance(1);
   CalculateCapacitance(2);
   CalculateCapacitance(3);
```

```
CalculateCapacitance(4);
CalculateCapacitance(5);
CalculateCapacitance(6);

! parameters for calculating inductors
sh: 200;        ! height of the substract
L_n1:  2.7396;  ! number of turns
L_n2:  3.65507;
L_n3:  3.03115;
L_n4:  3.65057;
L_n5:  2.22971;
L_n6:  2.51133;
L_n7:  2.6174;
L_n8:  2.44414;
L_n9:  2.78489;
L_n10: 3.09459;

CalculateInductance(1);
CalculateInductance(2);
CalculateInductance(3);
CalculateInductance(4);
CalculateInductance(5);
CalculateInductance(6);
CalculateInductance(7);
CalculateInductance(8);
CalculateInductance(9);
CalculateInductance(10);

! resistor
Rsv: 400;
R1_W: 20;
R2_W: 20;
R1_L: 75;
R2_L: 75;
R1 = Rsv * R1_L / R1_W;
R2 = Rsv * R2_L / R2_W;

! FETs in 3 Section
TrewModel(@ge1, @de1, 1, 2, 3, 4, 1);
TrewModel(@ge2, @de2, 5, 6, 7, 8, 2);
TrewModel(@ge3, @de3, 9,10,11,12, 3);

! matching circuits
CAP   @do1     @ge2  C=C2;
SRLC  @do2     @ge3  C=C3  L=L4;
IND   @de1     @do1  L=L2;
IND   @de2     @do2  L=L3;
IND   @de3     @do3  L=L5;
IND   @gbi1    @ge1  L=L7;
RES   @gbi2    @ge2  R=R1;
RES   @gbi3    @ge3  R=R2;
IND   @dbi1    @do1  L=L8;
IND   @dbi2    @do2  L=L9;
IND   @dbi3    @do3  L=L10;
SRLC  @input   @ge1  C=C1  L=L1;
SRLC  @output  @do3  C=C4  L=L6;

! capacitors to the ground
CAP  @gbi1  0  C=C5;
CAP  @gbi2  0  C=C5;
CAP  @gbi3  0  C=C5;
CAP  @dbi1  0  C=C6;
CAP  @dbi2  0  C=C6;
CAP  @dbi3  0  C=C6;

! ac block
IND  @gbi1  @gbv  L=100NH;
IND  @dbi1  @dbv  L=100NH;
IND  @gbi2  @gbv  L=100NH;
IND  @dbi2  @dbv  L=100NH;
IND  @gbi3  @gbv  L=100NH;
```

```
   IND  @dbi3  @dbv  L=100NH;

   VSOURCE  @gbv 0  Vdc=-2.5;
   VSOURCE  @dbv 0  Vdc=5;

   PORT  @input  0;
   PORT  @output 0;

   CIRCUIT;

   Gain = 20 * log10(MS21);
   VSWR1 = if (MS11 < 0.9) ((1 + MS11)/(1 - MS11)) else (20);
   VSWR2 = if (MS22 < 0.9) ((1 + MS22)/(1 - MS22)) else (20);
end

Sweep
   AC: FREQ: from 6GHZ to 15GHZ step=0.2GHZ  Gain VSWR1 VSWR2
       {Xsweep Y=all NXticks=9  Ymin=0 Ymax=16 NYticks=8};
end

MonteCarlo
   AC: N_OUTCOMES=100
       FREQ: from 6GHZ to 15GHZ step=0.2GHZ  Gain VSWR1 VSWR2;
   AC: FREQ: from 8GHZ to 12GHZ step=1GHZ
       Gain > 12.5  Gain < 15.5  VSWR1 < 2.5  VSWR2 < 2.5;
   AC: FREQ: 6GHZ   Gain < 2;
   AC: FREQ: 15GHZ  Gain < 2;
end

Specification
   AC: FREQ: from 8GHZ to 12GHZ step=1GHZ
       Gain > 12.5  Gain < 15.5  VSWR1 < 2.5  VSWR2 < 2.5;
   AC: FREQ: 6GHZ 15GHZ  Gain < 2;
end

#define TrewModel(ge, de, cr1, cr2,cr3, cr4, $) {
   Extrinsic2  @gi$ @di$ @si$ ge de
      RG=2.5  Lg=0.05nH  RD=3.5  Ld=0.08nH  RS=3.5  LS=0.08nH
      Cds=0.001pF  Cge=0.1pF  Cde=0.1pF  Cx=10pF  Gds=0.003;

   FETT1  @gi$ @di$ @si$
      L=0.9909UM  {NORMAL SIGMA=3.5% CORRELATION=FET[cr2]}
      A=0.3081UM  {NORMAL SIGMA=3.5% CORRELATION=FET[cr1]}
      ND=1.028E23 {NORMAL SIGMA=7.0% CORRELATION=FET[cr4]}
      W=308.5UM   {NORMAL SIGMA=2.0% CORRELATION=FET[cr3]}
      EPSR=12.9   EC=3.75E5  VS=1.5E-4  LAMBDA=0.01UM
      U0=4.0E-10  VBI=0.7    D=1.0E-12  ALPHA=0.5
      TAU=3pS;
}

#define CalculateCapacitance($)   C$ = C_k * C_S$;

#define CalculateInductance($) {
   L_wl$: 20 {NORMAL SIGMA=3.0%};
   L_sp$: 10 {NORMAL SIGMA=3.0%};

   L_Kg$ = 0.57 - 0.145*LOG(L_wl$/sh);
   L_K1$ = 0.03937*L_Kg$;
   L_K2$ = 2.0*(L_wl$ + L_sp$);
   L_K3$ = L_wl$ - L_sp$;
   L_K4$ = L_K1$ * 0.375 * 0.375 / 8.5;
   L$: L_K4$ * L_n$ * L_n$ * (L_K2$*L_n$ + L_K3$);
}

Statistics
   Correlation: FET  dimension=12  format=full;
   !A1   L1   W1   Nd1   A2   L2   W2   Nd2   A3   L3   W3   Nd3
  1.00  0.00  0.00 -0.25  0.80  0.00  0.00 -0.20  0.78  0.00  0.00 -0.10
  0.00  1.00  0.00 -0.10  0.00  0.80  0.00 -0.05  0.00  0.78  0.00 -0.05
  0.00  0.00  1.00  0.00  0.00  0.00  0.80  0.00  0.00  0.00  0.78  0.00
 -0.25 -0.10  0.00  1.00 -0.20 -0.05  0.00  0.80 -0.15 -0.05  0.00  0.78
```

```
  0.80  0.00  0.00 -0.20  1.00  0.00  0.00 -0.25  0.80  0.00  0.00 -0.20
  0.00  0.80  0.00 -0.05  0.00  1.00  0.00 -0.10  0.00  0.80  0.00 -0.10
  0.00  0.00  0.80  0.00  0.00  0.00  1.00  0.00  0.00  0.00  0.80  0.00
 -0.20 -0.05  0.00  0.80 -0.25 -0.10  0.00  1.00 -0.20 -0.05  0.00  0.80
  0.78  0.00  0.00 -0.15  0.80  0.00  0.00 -0.20  1.00  0.00  0.00 -0.25
  0.00  0.78  0.00 -0.05  0.00  0.80  0.00 -0.05  0.00  1.00  0.00 -0.10
  0.00  0.00  0.78  0.00  0.00  0.00  0.80  0.00  0.00  0.00  1.00  0.00
 -0.10 -0.05  0.00  0.78 -0.20 -0.10  0.00  0.80 -0.25 -0.10  0.00  1.00
End
```

Monte Carlo Sweep of Amplifier Gain

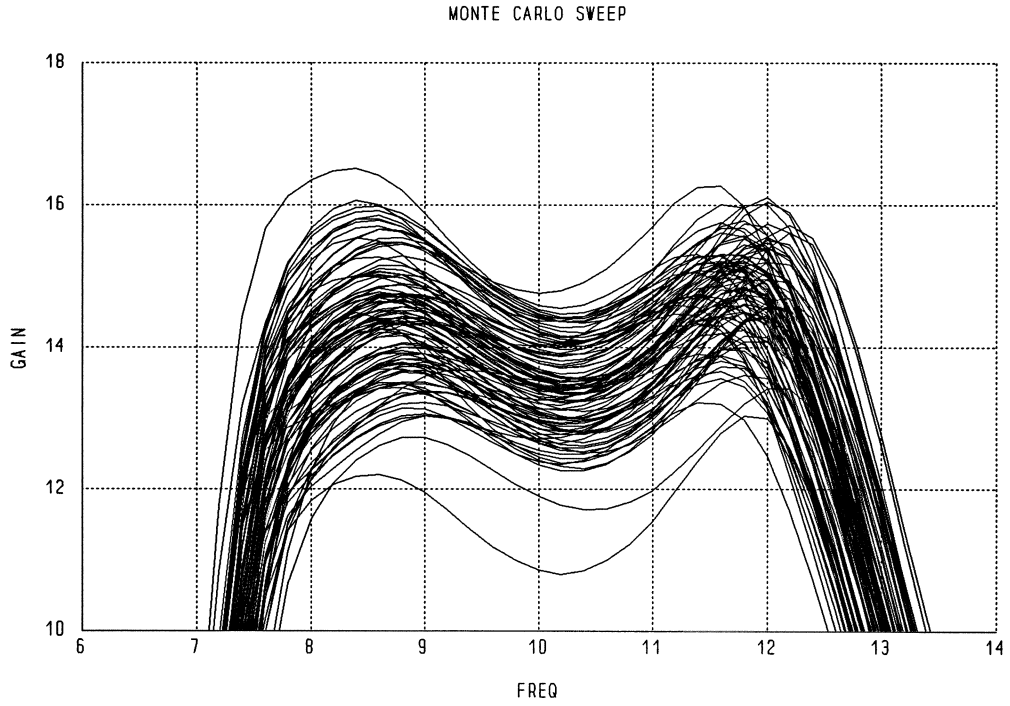

Histogram of the Maximum Errors of Monte Carlo Outcomes

The Monte Carlo analysis in this example involves design specifications on different responses, including the input and output VSWRs, as well as in-band and out-of-band gain of the amplifier. Therefore, the display of any one response shows only a subset of the specifications related to that response, but it does not show the overall yield.

The histogram of the maximum errors is devised to depict a composite picture of the percentage of acceptable outcomes (i.e., yield) and the distribution of outcomes in terms of how much they satisfy or violate the specifications.

A set of error functions e_i is defined according to the specifications, where the index i identifies different responses and discretized frequencies.

For each Monte Carlo outcome, we can calculate the maximum error

$$e_{max} = max \{ e_i \}.$$

The sign of e_{max} indicates the acceptability of the outcome: $e_{max} > 0$ for an unacceptable outcome (one or more specifications violated) or $e_{max} \leq 0$ for an acceptable outcome.

A histogram of e_{max} is shown in the following figure.

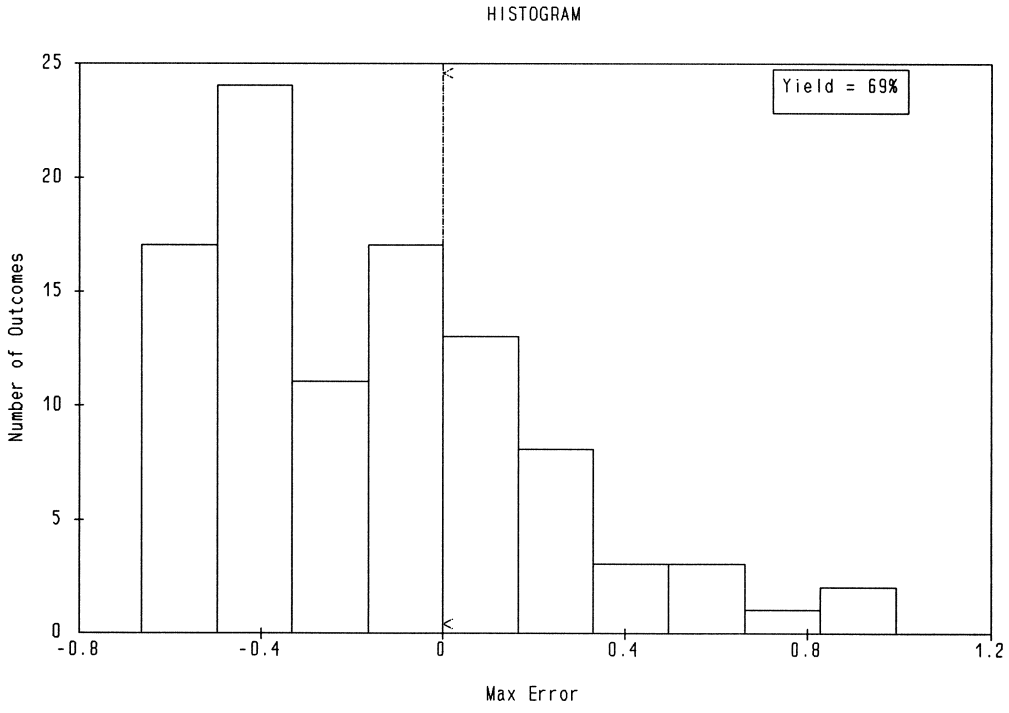

demo56

A test of numerical truncation errors in matrix inversion.

Consider the following matrix

$$\boldsymbol{A} = \begin{bmatrix} 1 & 2 & 3 \\ 2 & 4 & 6+\delta \\ 7 & 8 & 9 \end{bmatrix}$$

When $\delta = 0$, $\boldsymbol{A}$ is singular. When δ is small but nonzero, $\boldsymbol{A}$ is nearly singular and the inversion of $\boldsymbol{A}$ is susceptible to numerical truncation errors with finite precision.

This can be studied statistically using the Monte Carlo method by generating δ from a Gaussian distribution. We assign δ a relative scale of magnitude ranging from 10^{-5} to 1 and calculate the ℓ_1 error defined as

$$e = \sum |\boldsymbol{E}_{i,j}|$$

$$\boldsymbol{E} = \boldsymbol{A}\,\boldsymbol{B} - \mathbf{1}$$

where $\boldsymbol{B}$ is the numerical inversion of $\boldsymbol{A}$ and $\mathbf{1}$ is the identity matrix.

Input File

```
!  Example  demo56.ckt
!  Test the errors in matrix inversion using the Monte Carlo method.
!  One of the elements of the matrix A is perturbed statistically.
!  When the perturbation level is low, A is nearly singular and
!  therefore results in a higher level of errors.

Expression
   Power = -1;

   Pert: 1 {Normal sigma=1%};

   A[3,3] = [ 1 2 3
              2 4 ((1 + Pert * 10^Power) * 6)
              7 8 9 ];

   B[3,3] = INVERSE(A);

   C[3,3] = PRODUCT(A,B);

   Identity[3,3] = [ 1 0 0 0 1 0 0 0 1];

   ErrMat[3,3] = abs(C - Identity);

   ErrTotal = SUM(ErrMat);
end

Sweep
   B;
end

MonteCarlo
```

```
   N_OUTCOMES=100  Power: -5 -4 -3 -2 -1 0 ErrTotal;
end
```

Numerical Errors in Inverting a Nearly Singular Matrix

The following figure shows the errors in inverting a nearly singular matrix using single precision. The horizontal axis represents the relative scale of magnitude of the perturbation δ as powers of 10, i.e., 10^x. The truncation error is negligible for $x \geq -2$.

It is interesting to note that when $x = -5$ (i.e., at the scale of 10^{-5}), the perturbations are so severely truncated that apparently they are reduced to a single significant decimal digit, hence the errors shown in the figure seem to "converge" to a few isolated values.

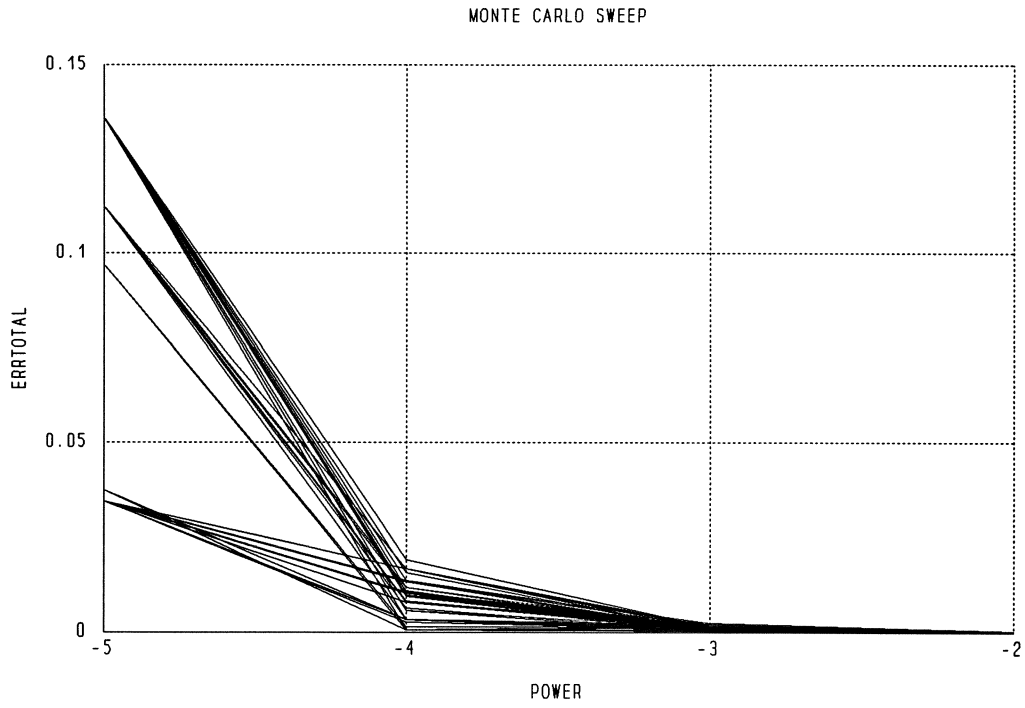

demo57

Illustration of using OSA90 as a child through Datapipe.

A separate copy of OSA90 is called as a Datapipe child to compute the drain voltage and current of a nonlinear FET amplifier for displaying load lines.

The FET amplifier is identical to the one used in demo53. But, in demo53, to obtain the load lines we have to manually combine two HPGL plotter files so that the time-domain IV curves are superimposed on the DC IV curves.

In this example, the time-domain and DC IV curves are computed by the child OSA90 and sent back to the parent OSA90 as data arrays. By displaying the data arrays simultaneously we can plot the load lines without any manual manipulation of HPGL plotter files.

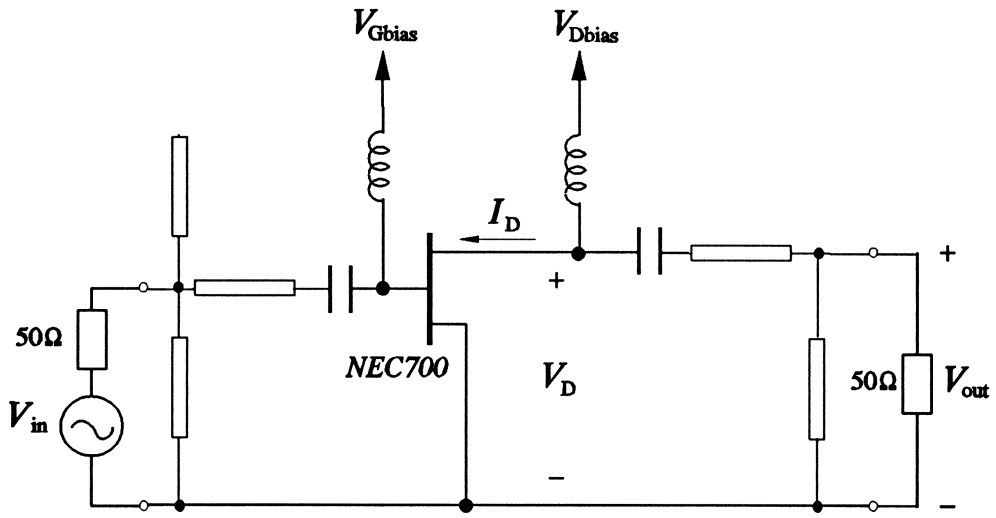

Input File

```
!  Example  demo57.ckt
!  Illustrate using OSA90 as a child through Datapipe.
!  OSA90 (a separate copy) is called to compute the DC IV curves and
!  large-signal time-domain drain voltage and current of a nonlinear
!  FET amplifier.  The results are sent back to the parent OSA90 and
!  utilized to display load lines.
!  This FET amplifier is identical to the one in demo53.  But here
!  we are able to display the load lines without having to manually
!  combining two separate HPGL plotter files.

Expression
   char ckt_file[] = "
Model
   TEM  @input  0  Z=70  E=128  F=18GHZ;
   TEM  @output 0  Z=50  E=61.7 F=18GHZ;

   TEM   @input @open1 0 @open2  Z=100 E=65 F=18GHZ;
   OPEN  @open1 @open2;
```

```
   TEM  @input @DC_block1  Z=100 E=25 F=18GHZ;

   ! FET model

   CAP @DC_block1 @FET_input  C=10NF;
   IND @Gate_bias @FET_input  L=100NH;

   Extrinsic2  @intrin1 @intrin2 @intrin3 @FET_input @FET_output
      RG=3.5   LG=0.0306NH  RD=0.5       LD=0.00792NH
      RS=4.73  LS=0.0451NH  GDS=0.00345  CDS=0.08738PF  CX=10PF;

   FETR  @intrin1 @intrin2 @intrin3
      IS=5E-15    N=1         FC=0.5          GMIN=1.0E-07
      VBI=0.8     VBR=20.0    ALPHA=2         THETA=0.003
      BETA=0.029  VTO=-1.637  LAMBDA=0.04978  TAU=2.8PS
      CGS0=0.4428PF  CGD0=0.1066PF;

   CAP @probe @DC_block2   C=10NF;
   SRL @probe @Drain_bias  L=100NH;

   TEM  @DC_block2 @output  Z=100 E=15 F=18GHZ;

   VG: -0.56V;
   VD: 4V;

   VSOURCE  @Gate_bias  0  VDC=VG;
   VSOURCE  @Drain_bias 0  NAME=drain VDC=VD;

   Pin: 0;

   PORT  @input  0  P=Pin;
   PORT  @output 0  NAME=OUT;

   ILABEL @probe @FET_output  NAME=Idac;

   VLABEL @FET_output 0  NAME=Vdac;

   CIRCUIT;

   ID_mA = IDrain_DC * 1000;

   MP2RI(MVdac, PVdac, RVdac[0:N_SPECTRA], IVdac[0:N_SPECTRA]);
   MP2RI(MIdac, PIdac, RIdac[0:N_SPECTRA], IIdac[0:N_SPECTRA]);

   K: 0;
   T: K / FREQ;

   Vd_T = DFT_FT(RVdac, IVdac, Spectral_Freq, T);
   Id_T = DFT_FT(RIdac, IIdac, Spectral_Freq, T);
   Id_T_mA = Id_T * 1000;
end

Sweep
   DC: VG: from -1.4 to 0 step=0.2  VD: from 0 to 6 N=25  VD ID_mA;

   HB: FREQ=15  PIN: from -9 to 3 step=3
       K: from 0 to 1 N=25  Vd_T Id_T_mA;
end
";

   Datapipe: COM  FILE="osa90 -p"
             N_INPUT=2    INPUT=(1, ckt_file)
             N_OUTPUT=(2*13*26)
             OUTPUT=(VD_DC[8,26], ID_DC[8,26], VD_T[9:13,26], ID_T[9:13,26]);

   I: 1;
   J: 1;

   VD: if (I < 9) (VD_DC[I,J]) else (VD_T[I,J]);
   ID: if (I < 9) (ID_DC[I,J]) else (ID_T[I,J]);
end
```

```
sweep
   I: from 1 to 13 step=1  J: from 1 to 26 step=1  VD ID
      {Parametric  title="Amplifier FET Drain Load Lines"  I=all
       X=VD Xmin=0 Xmax=6 NXTicks=6  Y=ID Ymin=0 Ymax=70 NYTicks=7};
end
```

FET Drain Load Lines

The FET drain lines shown in the following figure are obtained by plotting the drain current versus drain voltage while sweeping the array indices (Parametric display). The DC and time-domain drain currents are displayed as separate curves. The DC IV curves are indicated by the indices 1 - 8, which correspond to gate bias voltage from -1.4V to 0V with a 0.2V step. The time-domain curves are indicated by indices 9 - 13, which correspond to available input power from -9dBm to 3dBm with a 3dBm step.

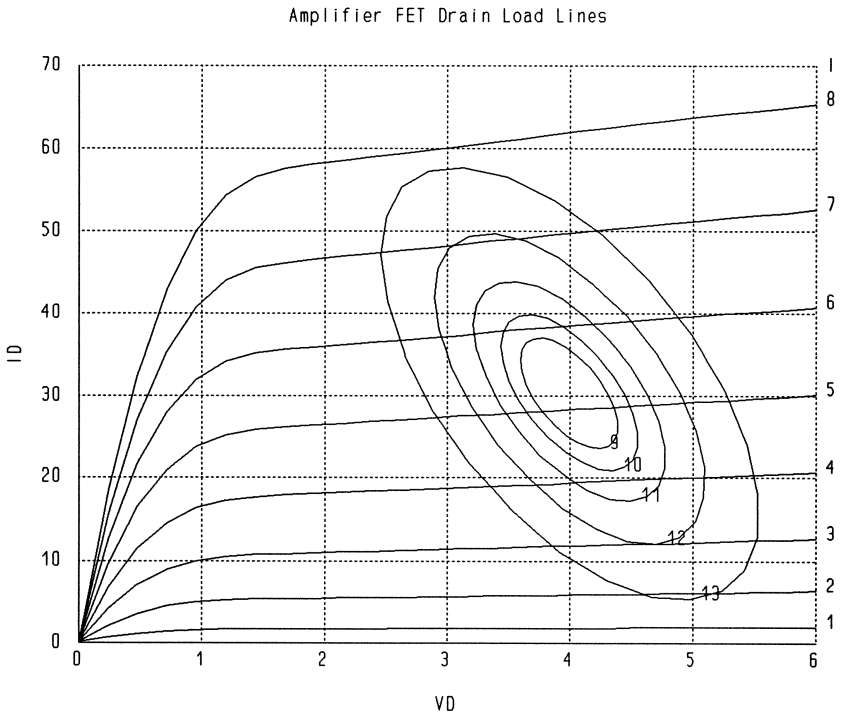

demo58

Illustration of using OSA90 as a child through Datapipe. A separate copy of OSA90 is called as a Datapipe child to compute the power gain of a nonlinear FET circuit at different input power levels. The results are used by the parent OSA90 to calculate the 1-dB compression point.

To be more specific, we consider input power levels from -9dBm to 12dBm with a 3dBm step for a total of 8 different values, denoted by

$$P_{in,k} = \text{-9dBm} + (k - 1) \times \text{3dBm}, \quad k = 1, 2, ..., 8.$$

At these input power levels, the child OSA90 calculates the fundamental output power in dBm, denoted by $P_{out,k}$, and the large-signal power gain in dB, defined as

$$G_{p,k} = P_{out,k} - P_{in,k}.$$

From these data, the parent OSA90 computes the corresponding gain compression as

$$C_k = 20 * \log10(|S_{21}|) - G_{p,k}$$

where the small-signal gain $|S_{21}|$ is also calculated by the child OSA90.

Then, utilizing the built-in cubic spline functions, we construct interpolation models for the output power, power gain and input power as functions of the gain compression, denoted by $P_{out}(C)$, $G_p(C)$ and $P_{in}(C)$, respectively.

From the spline model, we can easily obtain the output power, input power and power gain at 1-dB gain compression as $P_{out}(1)$, $P_{in}(1)$ and $G_p(1)$, respectively.

This example includes frequency as an input parameter to the child OSA90. By sweeping the frequency variable in the parent OSA90, we can display the 1-dB compression point versus frequency.

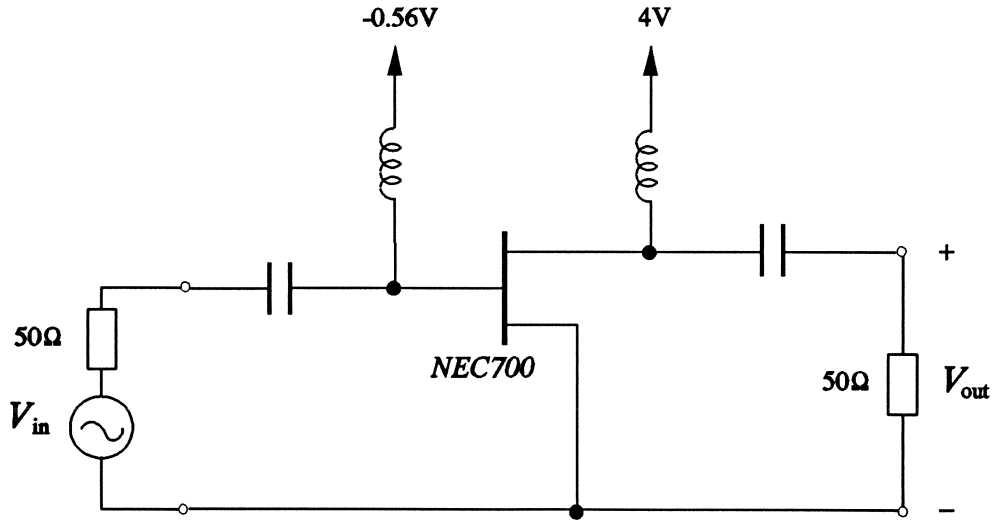

Input File

```
!  Example  demo58.ckt
!  Illustrate using OSA90 as a child through Datapipe.
!  OSA90 (a separate copy) is called to compute the power gain of a
!  nonlinear FET circuit at different input power levels.  The results
!  are sent back to the parent OSA90.  Based on this data, we can
!  calculate compression (small-signal gain - power gain).
!  Cubic spline models are constructed to represent the input power,
!  output power and power gain as functions of compression.
!  Then, we can pin-point the 1-dB compression point by interpolation.
!  This example includes frequency as a variable input parameter to
!  the child.  The parent sweeps frequency in order to calculate and
!  display 1-dB compression point versus frequency.

Expression
   char ckt_file[] = "
Model
   Fx: 2;  ! place holder for frequency

   CAP 1 2 C=1000pF;

   Extrinsic2  20 30 40 2 3
      RG=3.5   LG=0.0306NH  RD=0.5       LD=0.00792NH
      RS=4.73  LS=0.0451NH  GDS=0.00345  CDS=0.08738PF  CX=10PF;

   FETR  20 30 40
      IS=5E-15    N=1         FC=0.5          GMIN=1.0E-07
      VBI=0.8     VBR=20.0    ALPHA=2         THETA=0.003
      BETA=0.029  VT0=-1.637  LAMBDA=0.04978  TAU=2.8PS
      CGS0=0.4428PF  CGD0=0.1066PF;

   CAP 3 4 C=1000pF;

   Pin: 0;

   PORT 1 0  P=Pin;
   PORT 4 0 NAME=out;

   IND 2 200 L=1000nH;
   VSOURCE 200 0 NAME=gate VDC=-0.56;

   IND 3 300 L=1000nH;
   VSOURCE 300 0 NAME=drain VDC=4;

   CIRCUIT;

   Pout = 10 * log10(PWout[1]) + 30;
   Power_Gain = Pout - Pin;

   MS21_dB = 20 * log10(MS21);
end

Sweep
   AC: FREQ=Fx  MS21_dB;
   HB: FREQ=Fx  Pin: from -9dBM to 12DBM step=3dBM  Pin Pout Power_Gain;
end
";

   Datapipe: COM  FILE="osa90 -p"
             N_INPUT=3    INPUT=(2, ckt_file, FREQ)
             N_OUTPUT=25  OUTPUT=(MS21_dB, Pin[8], Pout[8], Power_Gain[8]);

   Compression[8] = MS21_dB - Power_Gain;

   coef1[8] = SPLINE(Compression, Pin);
   coef2[8] = SPLINE(Compression, Pout);
   coef3[8] = SPLINE(Compression, Power_Gain);

   Pin_1dB_Comp = SPLINT(1.0, coef1, Compression, Pin);
```

```
   Pout_1dB_Comp = SPLINT(1.0, coef2, Compression, Pout);
   Gain_1dB_Comp = SPLINT(1.0, coef3, Compression, Power_Gain);
end

Sweep
   FREQ: from 1 to 10 step=1
      MS21_dB Pin_1dB_Comp Pout_1dB_Comp Gain_1dB_Comp
      {Xsweep  Y=Pout_1dB_Comp  NXTicks=9  Ymin=16 Ymax=17 NYticks=5}
      {Xsweep  Y=Gain_1dB_Comp & Pin_1dB_Comp
       NXTicks=9  Ymin=5 Ymax=12 NYticks=7};
end
```

Output Power at 1-dB Compression versus Frequency

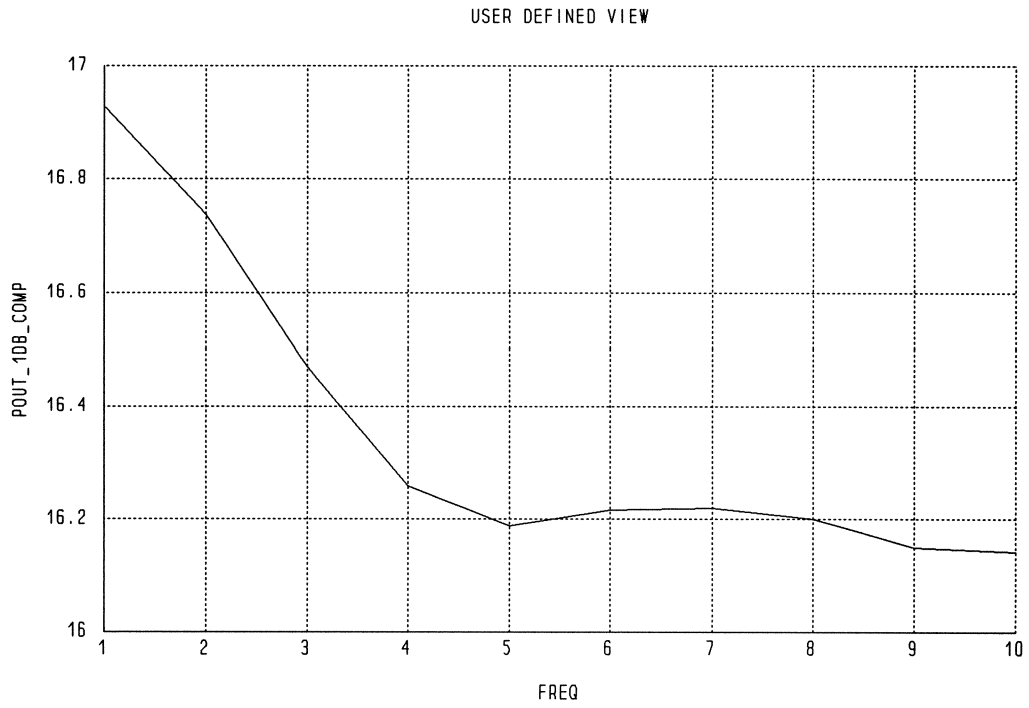

Power Gain and Input Power at 1-dB Compression versus Frequency

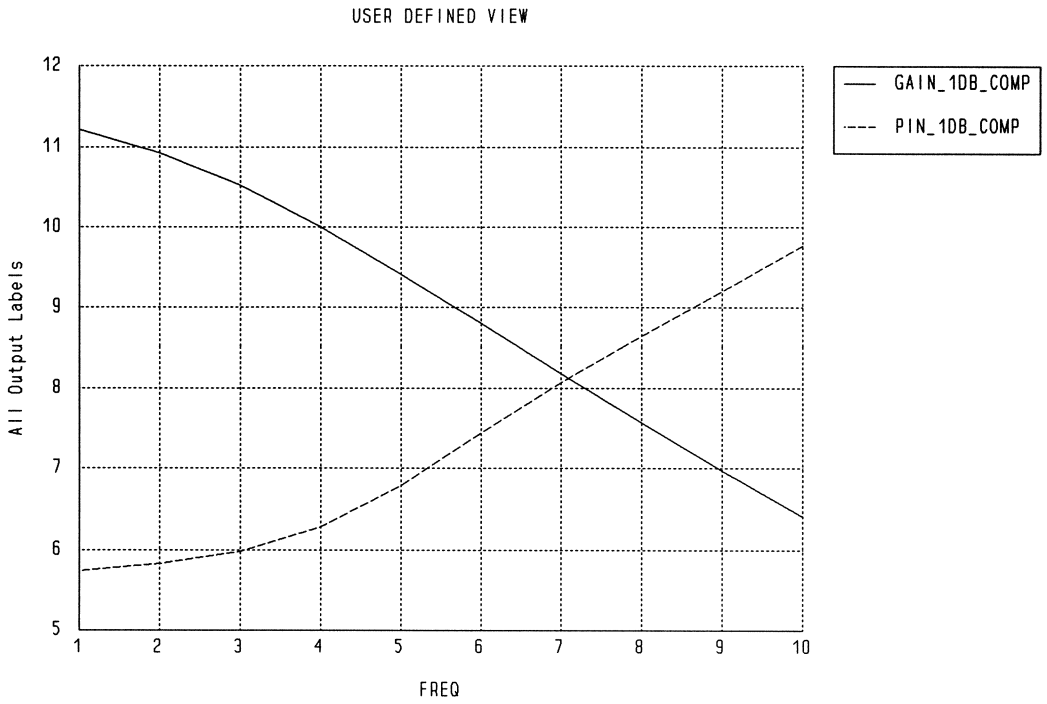

demo59

Illustration of using OSA90 for adjoint sensitivity calculations.

This example considers a simple RC circuit. We wish to calculate the sensitivities of the voltage V_3 w.r.t. the parameters R_1 and C_2 by adjoint analysis.

Both the original and adjoint circuits are defined in the same input file. OSA90 allows definition of multiple, unconnected circuits (except, perhaps, sharing a common ground node). A separate circuit with R_1 and C_2 set to the actual perturbed values is also included for verifying the accuracy of adjoint sensitivities.

The original circuit:

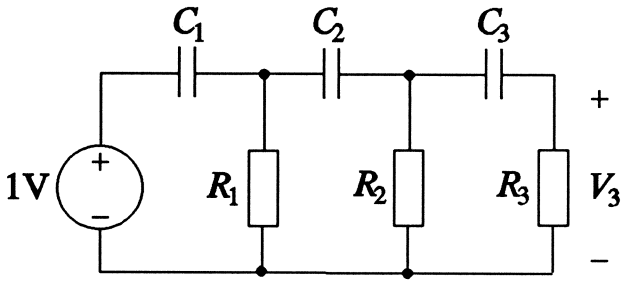

The adjoint circuit:

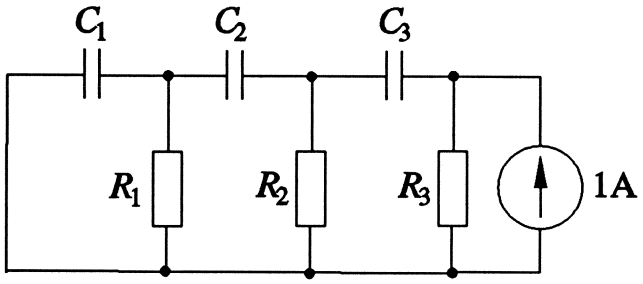

Input File

```
!  Example  demo59.ckt
!  demonstrate adjoint sensitivity calculations using OSA90

Control
   Non_Microwave_Units;
   Display_N_digits = 5;
end

Model
   Omega = 2;

   Perturbation = 5;
   R10 = 2;
   C20 = 1;
   deltaR1 = 0.01 * Perturbation * R10;
   deltaC2 = 0.01 * Perturbation * C20;

   SUBCIRCUIT  RC_CKT  1 2 3 4 0  R1=R10 R2=2 R3=2 C1=1 C2=C20 C3=1 {
      CAP 1 2 C=C1;
      RES 2 0 R=R1;
      CAP 2 3 C=C2;
      RES 3 0 R=R2;
      CAP 3 4 C=C3;
      RES 4 0 R=R3;
   };

 ! the original circuit

   RC_CKT   1 2 3 4 0;

   VSOURCE  1 0  V=1;
   VLABEL   2 3  NAME=VC2;
   VLABEL   2 0  NAME=VR1;
   VLABEL   4 0  NAME=V3;

 ! the adjoint circuit for calculating the sensitivities of
 ! V3 w.r.t. the parameters C2 and R1

   RC_CKT   0 5 6 7 0;

   ISOURCE  7 0  I=1;
   VLABEL   5 6  NAME=VC2_hat;
   VLABEL   5 0  NAME=VR1_hat;

 ! the circuit with C2 and R1 perturbed for verifying
 ! the estimation by sensitivities

   RC_CKT   11 12 13 14 0  R1=(R10 + deltaR1) C2=(C20 + deltaC2);

   VSOURCE  11 0  V=1;
   VLABEL   14 0  NAME=V3_perturbed;
   OPEN     12;
   OPEN     13;

   Circuit;

 ! dV3 / dC2 = -j omega VC2 * VC2_hat

   MdV3dC2 = Omega * MVC2[1] * MVC2_hat[1];
   PdV3dC2 = PVC2[1] + PVC2_hat[1] - 90;

 ! dV3 / dR1 =  VR1 * VR1_hat / (R1 * R1)

   MdV3dR1 = MVR1[1] * MVR1_hat[1] / (R10 * R10);
   PdV3dR1 = PVR1[1] + PVR1_hat[1];

   MP2RI(MdV3dC2, PdV3dC2, RdV3dC2, IdV3dC2);
   MP2RI(MdV3dR1, PdV3dR1, RdV3dR1, IdV3dR1);
```

```
   MP2RI(MV3[1], PV3[1], RV3, IV3);
   MP2RI(MV3_perturbed[1], PV3_perturbed[1], RV3_perturbed, IV3_perturbed);

   delta_RV3_estimate = (RdV3dC2 * deltaC2 + RdV3dR1 * deltaR1) * 100 / RV3;
   delta_IV3_estimate = (IdV3dC2 * deltaC2 + IdV3dR1 * deltaR1) * 100 / IV3;

   delta_RV3 = (RV3_perturbed - RV3) * 100 / RV3;
   delta_IV3 = (IV3_perturbed - IV3) * 100 / IV3;
end

Sweep
   HB: Perturbation: from -5 to 5 step=1  FREQ=(Omega / (2 * PI))
       delta_RV3_estimate  delta_RV3  delta_IV3_estimate  delta_IV3
       RdV3dC2 IdV3dC2 RdV3dR1 IdV3dR1
       {Xsweep  Title="Estimates by Adjoint Sensitivities"
        Y_title="Changes in Real(V3) (%)"  Ymin=-6 Ymax=6 NYTicks=4
        Y=delta_RV3_estimate & delta_RV3
        X_title="Perturbation (%)"  NXticks=10}
       {Xsweep  Title="Estimates by Adjoint Sensitivities"
        Y_title="Changes in Imag(V3) (%)"  Ymin=-1 Ymax=1 NYTicks=4
        Y=delta_IV3_estimate & delta_IV3
        X_title="Perturbation (%)"  NXticks=10};
end
```

Verification of the Adjoint Sensitivities

The changes in V_3 due to perturbations to R_1 and C_2 are predicted based on a first-order approximation using adjoint sensitivities. The result is compared with the exact calculation with the actual perturbed parameter values.

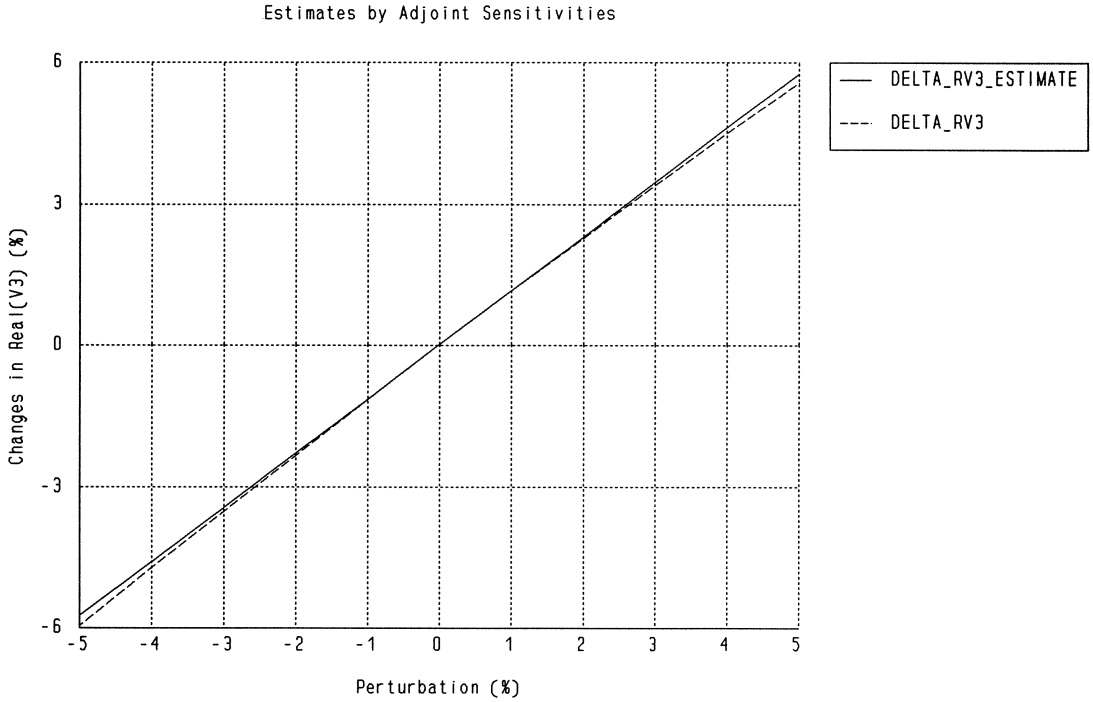

demo60

Implementation of a YIG resonator model published by J.A. Mezak and G.D. Vendelin in *Microwave Journal*, vol. 35, Dec. 1992, pp. 92 - 98.

The equivalent circuit for YIG resonator:

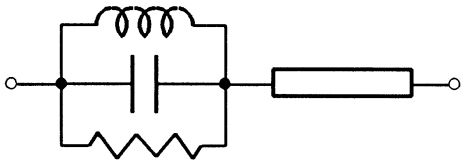

Input File

```
!  Example  demo60.ckt
!  YIG resonator model according to G. Vendelin
!  Microwave Journal, vol. 35, Dec 1992, pp. 92 - 98

Model
   SUBCIRCUIT  YIG  2 0
      F0=1GHz  ! resonant frequency of the YIG sphere
      Mss=1    ! saturation magnetization in Gauss
      Ds=1     ! YIG sphere diameter
      DH=1     ! material line width in Oersted
      DL=1     ! coupling loop diameter
      L1=1     ! start of coupling along loop
      L2=2     ! end of coupling along loop
      L3=1     ! overall length of the coupling loop
      ZL=50    ! characteristic impedance of the coupling loop
   {
      Mu0 = PI * 4e-7;      ! Henry/meter
      Gamma = 1.759e11;     ! the gyromagnetic ratio
      MsMKS = MSS * 1e-4;   ! convert MSS from Gauss to ampere-turn/meter

      Vm = 4 * PI * (DS / 2)^3 / 3;    ! volume of the sphere
      W0 = 2 * PI * F0;
      Beta = W0 / 0.2999797GHz;
      Wm = Gamma * MsMKS;
      AAA = Mu0 * Wm * Vm * (sin(Beta * L2) - sin(Beta * L1))^2;
      BBB = 16 * W0 * PI * PI * ((DL / 2)^4) * Beta * Beta;
      Lyig = AAA / BBB;
      Cyig = 1 / (Lyig * W0 * W0);
      Qu = ((W0 / (1e-4HZ * Gamma) - Mss / 3)) / DH;    ! unloaded Q in Gauss
      Ryig = W0 * Lyig * Qu;

      TRL 1 0 Z=ZL L=L3 K=1;
      PRC 1 2 R=Ryig C=Cyig;
      IND 1 2 L=Lyig;
   };

   YIG  1 0  F0=5GHz Mss=800 Ds=24MIL DH=1 DL=40MIL
             L1=10MIL L2=73MIL L3=125MIL ZL=150;

   PORT 1 0;

   Circuit;
end

Sweep
   AC: FREQ: from 4.94 to 5.06 step=0.001 RREF=1 RZ11 IZ11
```

```
        {Xsweep Title="YIG Resonator Impedance"  Y_title="Impedance (Ohm)"
         Y=RZ11 & IZ11 Ymin=-450 Ymax=900 NYticks=3  NXTicks=6};
end
```

Impedance of a YIG Resonator Model

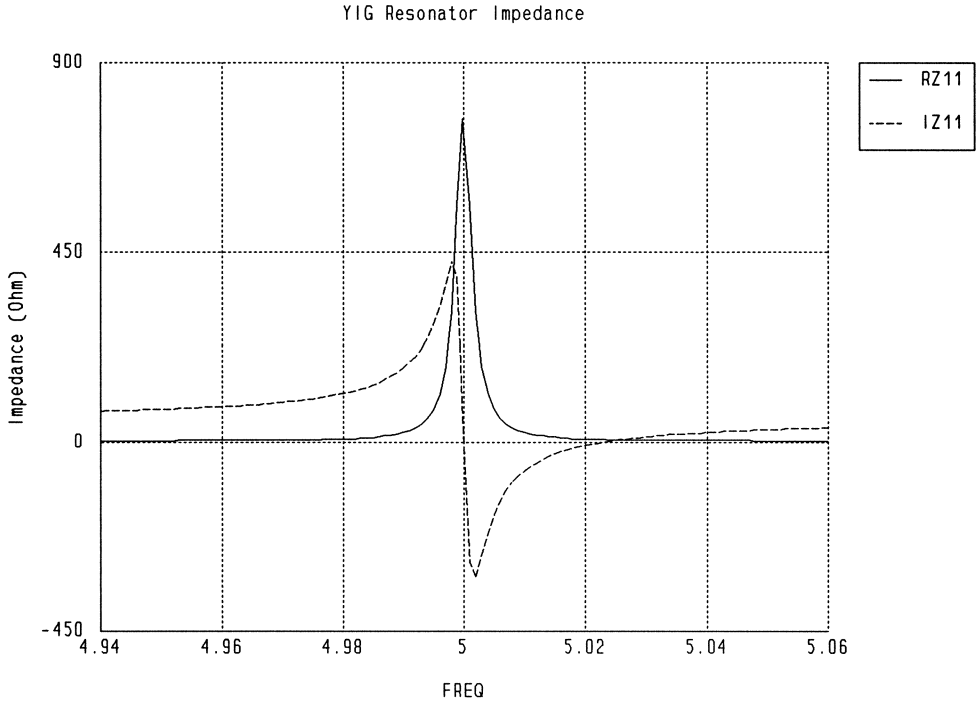

demo61

Oscillator analysis using the OSCPORT element.

The OSCPORT element provides a stimulus voltage to "jump start" the oscillator analysis. The feedback gain and phase are made available through the labels OSC_GAIN (in dB) and OSC_PHASE (in degrees). The free oscillation conditions are

OSC_GAIN = 0 dB

and

OSC_PHASE = 0.

The oscillation frequency and the voltage magnitude at OSCPORT are the unknowns.

This example illustrates oscillator analysis by optimization. The variables are frequency and the stimulus voltage, and the objective is to satisfy the oscillation conditions. A Datapipe child OSA90 is used to calculate OSC_GAIN and OSC_PHASE during optimization.

If the oscillation conditions are satisfied at the solution, then the oscillator output voltage (fundamental spectral component) is equal to the stimulus voltage since the feedback gain is 1.

The oscillator contains an FET represented by the nonlinear FETM model. A transmission line provides the FET gate matching and an RLC resonant circuit is connected to the FET source.

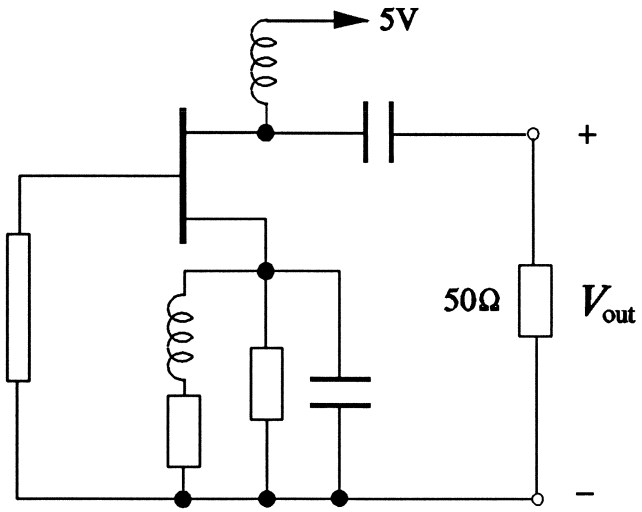

Input File

```
!  Example  demo61.ckt
!  Oscillator analysis using OSCPORT and using a Datapipe child osa90.
!  The oscillation frequency and stimulus voltage magnitude are unknowns
!  to be determined by optimization.
!  The child osa90 performs circuit simulation during optimization and
!  returns OSC_GAIN and OSC_PHASE.
!  The optimization objective is to satisfy the free oscillation
!  conditions: OSC_GAIN = 0dB  and  OSC_PHASE=0.
!  The solution is verified by displaying OSC_GAIN and OSC_PHASE versus
!  frequency sweep and voltage sweep.

Model
   OSC_Freq: ?15?;
   OSC_Volt: ?2?;

   Datapipe: COM  FILE="osa90 -p"
             N_INPUT=4   INPUT=(2, ckt_file, OSC_Freq, OSC_Volt)
             N_OUTPUT=2  OUTPUT=(Gain, Phase);

   TEM  @gate 0  Z=70 E=25 F=16;

   Extrinsic1  1 2 3  @gate @drain @source
      RG=3  RD=2  RS=4  LG=0.03nH  LD=0.07nH  LS=0.05nH  CDS=0.08pF;

   FETM  1 2 3
      GAMMA=-0.1  IG0=5E-10    SL=0.2     KG=-0.25  ALPHAG=20  VBC=20
      KF=-0.1     CF0=0.026pF  IDSS=0.26  VP0=-3    TAU=3pS    R10=0.012
      C10=0.5pF   C1S=0.005pF  K1=1;

   PRC  @source 0  R=50 C=0.5pF;
   SRL  @source 0  R=10 L=6nH;

   IND      @drain 4  L=100nH;
   VSOURCE  4      0  VDC=5V;

   CAP      @drain 5  C=10pF;
   OSCPORT  5      0  NAME=out  V=OSC_Volt;

   CIRCUIT;
end

Sweep
   HB: FREQ: 15.5 15.54 15.58   OSC_PHASE  OSC_GAIN
       {XSweep  Title="Oscillator Feedback Phase and Gain"
        Y=OSC_PHASE & OSC_GAIN  Ymin=-1 Ymax=1 NYTicks=4  NXTicks=8};

   HB: FREQ=OSC_Freq  OSC_Volt: 2.3 2.35 2.4   OSC_PHASE  OSC_GAIN
       {XSweep  Title="Oscillator Feedback Phase and Gain"
        Y=OSC_PHASE & OSC_GAIN  Ymin=-1 Ymax=1 NYTicks=4  NXTicks=10};
end

Spec
   Phase=0  Gain=0;
end

Expression
   char ckt_file[] = "
Model
   OSC_Freq: ?15?;
   OSC_Volt: ?2?;

   TEM  @gate 0  Z=70 E=25 F=16;

   Extrinsic1  1 2 3  @gate @drain @source
      RG=3  RD=2  RS=4  LG=0.03nH  LD=0.07nH  LS=0.05nH  CDS=0.08pF;

   FETM  1 2 3
      GAMMA=-0.1  IG0=5E-10    SL=0.2     KG=-0.25  ALPHAG=20  VBC=20
```

```
      KF=-0.1     CF0=0.026pF  IDSS=0.26  VP0=-3     TAU=3pS     R10=0.012
      C10=0.5pF   C1S=0.005pF  K1=1;

   PRC  @source 0  R=50 C=0.5pF;
   SRL  @source 0  R=10 L=6nH;

   IND      @drain 4  L=100nH;
   VSOURCE  4      0  VDC=5V;

   CAP      @drain 5  C=10pF;
   OSCPORT  5      0  NAME=out  V=OSC_Volt;

   CIRCUIT;
end

Sweep
   HB: FREQ=OSC_Freq  OSC_Gain OSC_Phase;
end
";
end
```

OSC_GAIN and OSC_PHASE versus Frequency

To verify that the free oscillation conditions are satisfied at the solution, OSC_GAIN and OSC_PHASE are displayed versus frequency sweep while the stimulus voltage is held constant at the solution. We can see that OSC_GAIN and OSC_PHASE are simultaneously zero at the frequency of 15.536GHz, which agrees with the optimization result.

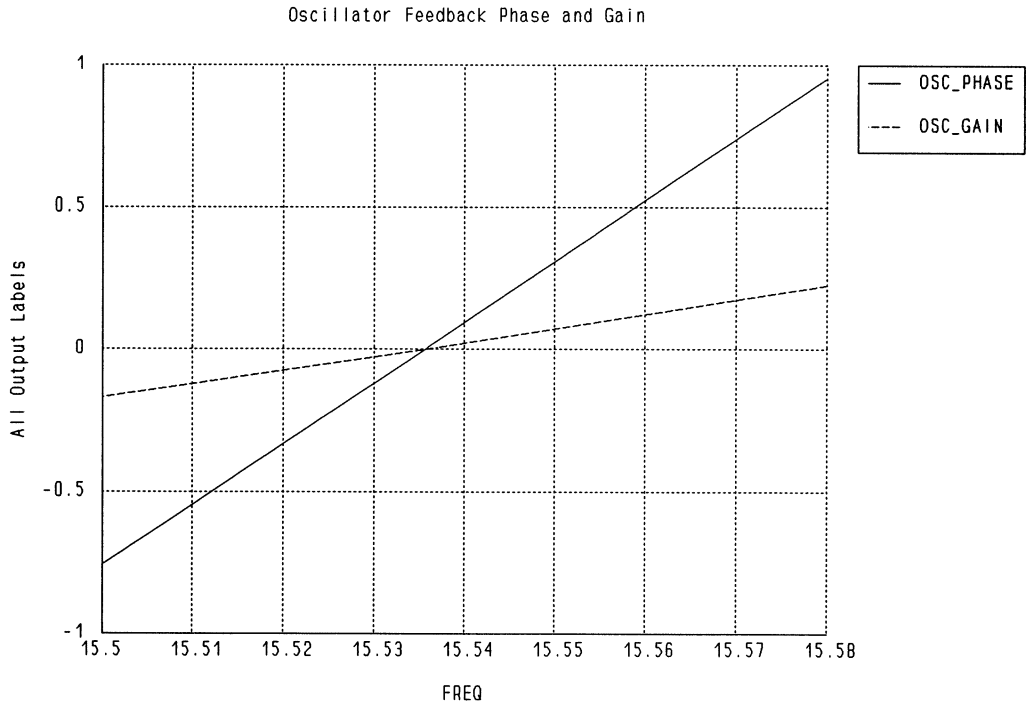

OSC_GAIN and OSC_PHASE versus Stimulus Voltage

We also display OSC_GAIN and OSC_PHASE versus the stimulus voltage while the frequency is held constant at the solution. The oscillation conditions are satisfied at the voltage of 2.348V, which agrees with the optimization result. The oscillator output voltage (the fundamental spectral component) is also 2.348V since the feedback gain is 1.

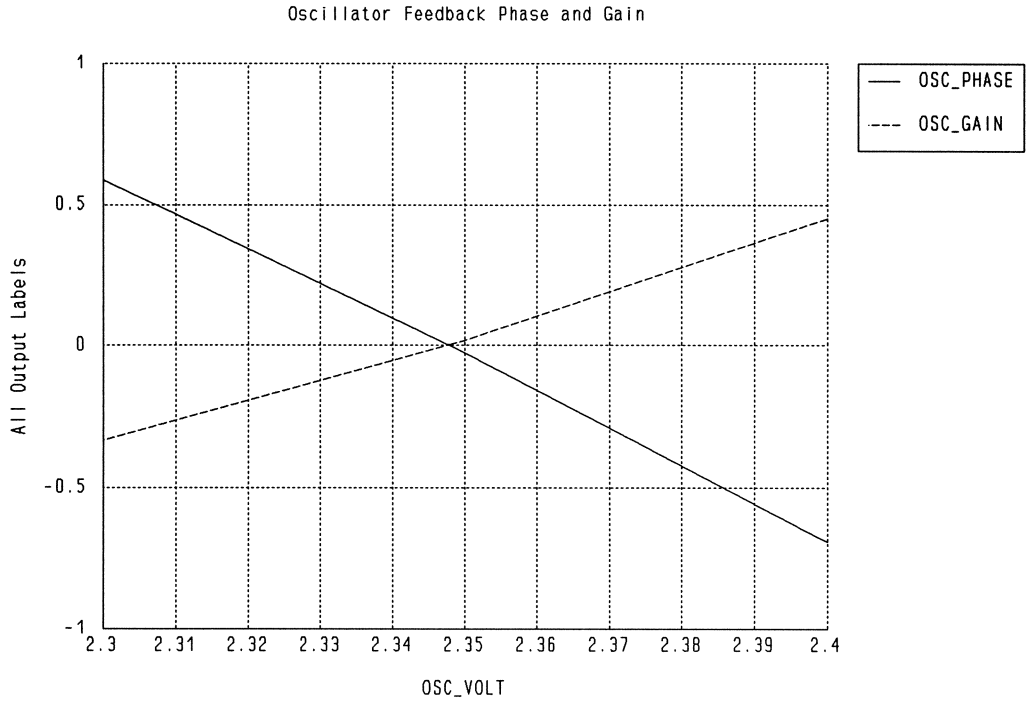

demo62

Oscillator design optimization using the OSCPORT element.

The OSCPORT element provides a stimulus voltage to "jump start" the oscillator analysis. The feedback gain and phase are made available through the labels OSC_GAIN (in dB) and OSC_PHASE (in degrees). The free oscillation conditions are

OSC_GAIN = 0 dB

and

OSC_PHASE = 0.

The oscillator contains an FET represented by the nonlinear FETM model. A transmission line provides the FET gate matching. The resonant circuit connected to the FET source includes a tuning capacitor.

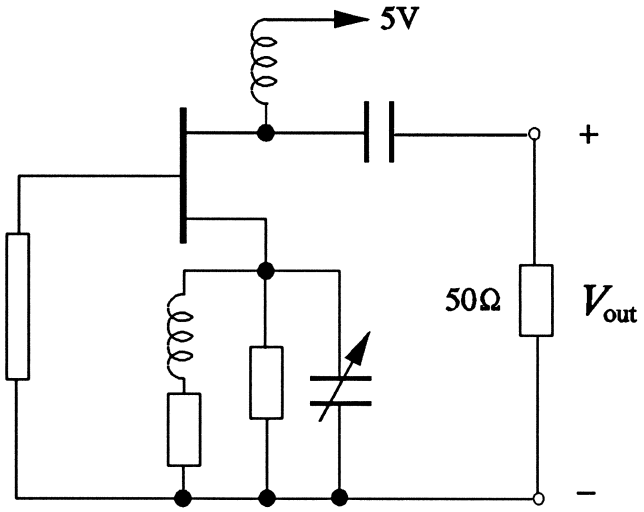

This example optimizes the tuning capacitor to achieve free oscillation at 15GHz. The stimulus voltage is an unknown to be determined by optimization. The objective is to satisfy the oscillation conditions at the desired frequency.

Input File

```
!  Example  demo62.ckt
!  Oscillator design using OSCPORT.
!  A tuning capacitor is optimized.  The simulus voltage is allowed to
!  vary.  The optimization objective is to satisfy the oscillation
!  conditions OSC_Phase=0 and OSC_Gain=0dB at the desired oscillation
!  frequency of 15GHz.

Model
   Tuning_Capacitor: ?0.5pF?;

   TEM  @gate 0  Z=70 E=25 F=16;

   Extrinsic1  1 2 3  @gate @drain @source
      RG=3  RD=2  RS=4  LG=0.03nH  LD=0.07nH  LS=0.05nH  CDS=0.08pF;

   FETM  1 2 3
      GAMMA=-0.1  IG0=5E-10    SL=0.2     KG=-0.25  ALPHAG=20  VBC=20
      KF=-0.1     CF0=0.026pF  IDSS=0.26  VP0=-3    TAU=3pS    R10=0.012
      C10=0.5pF   C1S=0.005pF  K1=1;

   PRC  @source 0  R=50 C=Tuning_Capacitor;
   SRL  @source 0  R=10 L=6nH;

   IND      @drain 4  L=100nH;
   VSOURCE  4      0  VDC=5V;

   CAP      @drain 5  C=10pF;
   OSCPORT  5      0  NAME=out  V=?2?;

   CIRCUIT;
end

Sweep
   HB: FREQ=15GHz   OSC_Phase OSC_Gain MVout PVout
       {Waveform  Title="Oscillator Output Voltage Waveforms"
        Tmin=0 Tmax=0.125 NT=100  NXTicks=5
        Spectrum=(MVout, PVout)."Vout_T"  Ymin=-3 Ymax=3 NYticks=6};
end

Spec
   HB: FREQ=15GHz  OSC_Phase=0  OSC_Gain=0;
end
```

Oscillator Output Voltage Waveform

The optimized solution satisfies the free oscillation conditions at the desired frequency of 15GHz. The optimized capacitance of the tuning capacitor is 0.6387pF. The fundamental spectral component of the output voltage is 2.35V.

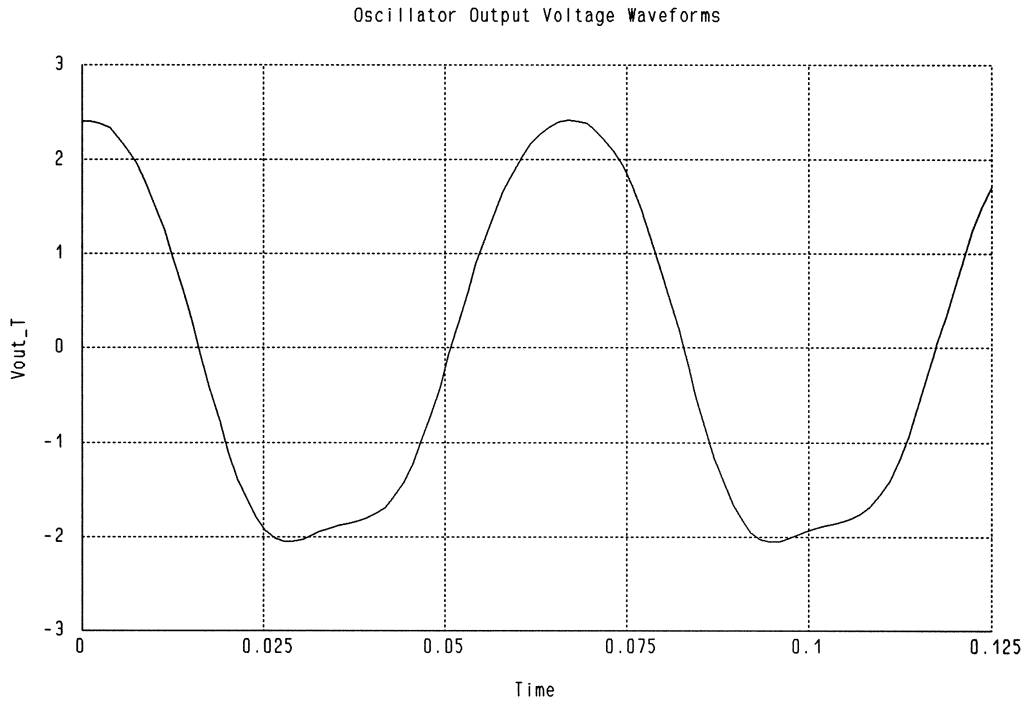

Chapter 4

Non-linear CAD benchmark

(Microwave Engineering Europe, November 1993)

Non-linear CAD benchmark

For the latest in our series of CAD reviews, a challenging bipolar amplifier circuit was supplied to the major rf CAD vendors. An original concern that the results might all prove to be identical proved far from reality. OSA, Hewlett Packard, Eesof and Compact Software took up the challenge and supplied the simulation results here.

The principal aim of this year's CAD review was to challenge companies with simulation products significantly beyond the entry level products featured in the same issue of *Microwave Engineering Europe* last year. The circuit is certainly practical: it is a power amplifier with less than 1W output at 2GHz and is clearly aimed at commercial applications with a standard silicon bipolar transistor and inexpensive FR4 substrate. With a significant body of work aimed at communications applications around 2GHz at present, the circuit outlined is quite a realistic test of a simulation capability.

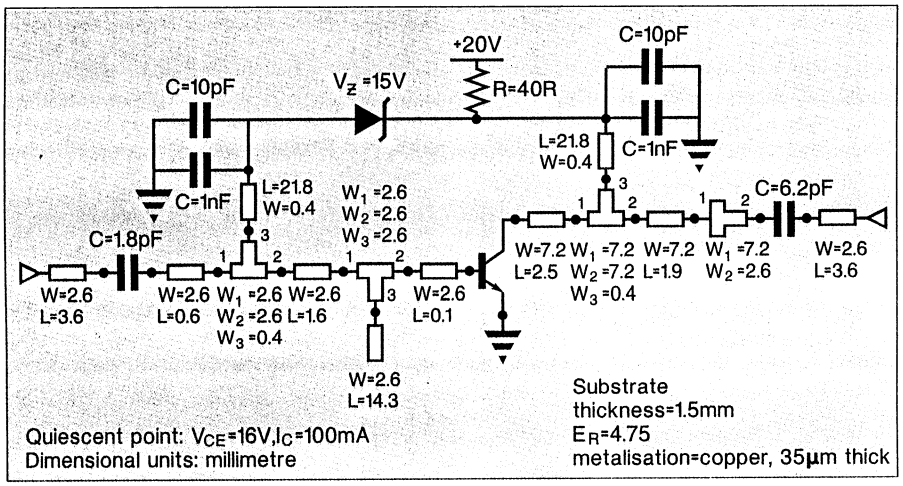

Figure 1: The power amplifier circuit, as supplied to the CAD vendors.

The supply of a circuit example to the software vendors, and the use of their own applications staff to programme the example, answered a criticism levelled at last year's exercise; that an independent review team would not necessarily have all the training needed to get the best out of a particular simulator. Nevertheless, the companies that protested about the training-level of any independent review team also proved the most reluctant to undertake this year's review! We are certainly grateful for the efforts of the four companies reported here, who clearly had the confidence to join this very public debate. You now have an opportunity to form a judgement on whether that confidence has been fully vindicated or shown to be misplaced.

Review process

The circuit details were despatched on the 13th of September to a comprehensive list of rf and microwave CAD vendors and both linear and power sweep results were requested. All companies had prior warning that this and two other circuits would be provided, but with the results from the first circuit not arriving until shortly before going to press, it was concluded that the further two examples should be sent after completion of the first circuit and the results featured in a future issue.

Each company was supplied with the circuit diagram, including physical dimensions of the components, and the part number of the Avantek device, AT 64023. Avantek is now part of Hewlett Packard (HP) but this was not considered to give an unfair advantage to that company since the Spice model from the data book or any vendor's library could be used. To avoid confusion with HP as a software vendor, the Avantek name is used throughout. Similarly, we refer to "Eesof" which is now also owned by HP.

The four companies that followed through the simulation challenge were, in order of response with results: Optimization System Associates, Hewlett Packard, Eesof and Compact Software. Each encountered some problems and stated some limitations on the basis of the circuit information made available to them and these are reported.

Both Jansen Microwave and Ingsoft also proposed to contribute, but Jansen was not prepared to undertake the simulation without a full characterisation of the substrate and measured data for the transistor to derive an alternative model to the manufacturer's and Ingsoft had insufficient resources available to undertake the task in the time allowed, partly due to the imminent release of an enhanced version of the company's RF Designer program.

One further problem could have arisen from the purchase of Eesof by Hewlett Packard after the benchmark process had commenced, but both companies agreed to take part, to some extent driven by the enthusiasm of the Eesof staff in Europe. Eesof was, at least to our knowledge, the only company to undertake the benchmarking with European-based applications staff. HP and OSA used staff at their respective home bases in Santa Rosa, California and Dundas, Ontario while Compact used a specialist in a field office in Dallas, Texas.

The circuit

The amplifier shown in figure 1 was designed at University College Dublin, Ireland by Ruairi Jennings and Philip Perry.

It is used to provide a high power driver to saturate other high power devices which are being tested under non-linear operation.

The design uses mainly distributed elements realised in microstrip on standard 1.5mm thick FR4 board. It consists of a single stub input equaliser, and a quarter wave transformer on the output. The input and output blocking capacitors provide a further degree of freedom in the design of

the matching networks.

This configuration results in a very narrow band response centred on 2GHz, with the power characteristics having been somewhat sacrificed in favour of good impedance and gain characteristics.

The transistor used is the Avantek AT64023, biased for a constant collector current of 100mA and a constant collector emitter voltage of 16V. It is capable of providing +23dBm at 1dB gain compression under these bias conditions. It is a classic power BJT, with a poor S12 (ie the device must be regarded as bilateral), an electrically large package, and an emitter ballast resistor.

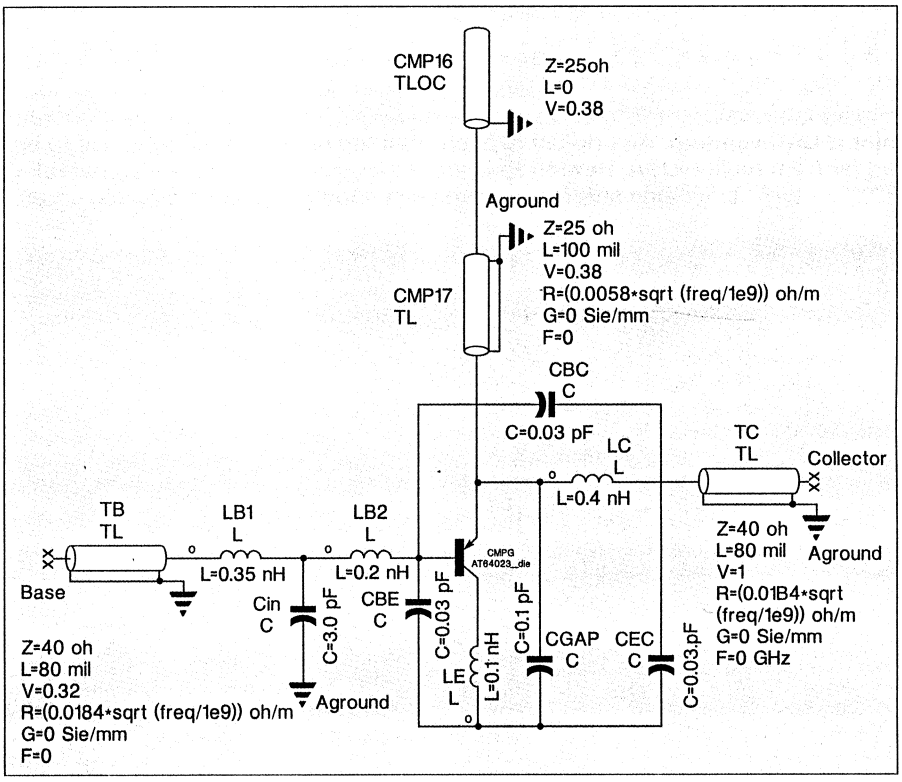

Figure 2: The equivalent circuit model for the transistor, with the package shown too. This format is from Hewlett Packard.

The non-linear model being used in this example is the model provided by Avantek. It consists of a standard SPICE type model, with a distributed RC base, where the capacitances are simulated by nonlinear diodes. The extra elements around the basic device model represent the device package. The entire device model is shown in figure 2.

The amplifier circuit was not chosen for complexity since it is appreciated that application resources are expensive. However, despite the circuit working well in practice it had proved very difficult to simulate using non-linear harmonic-balance simulators and was therefore considered to be an appropriate challenge.

Success and failure

The two most feared scenarios in waiting for the simulation results to be returned were either a complete success where four identical S21 plots proved nothing or a total failure with no convergence. Neither turned out to be the case but at one stage the failure of three simulators to handle the circuit looked likely.

The first company to return results was OSA, but by mid October we had still not received any further simulations and more questions about the circuit were being sent to the journal and to the circuit's designers in Dublin.

There was a common thread in that the linear simulations based on S-parameters in the Avantek data book had been successful but the harmonic balance simulations had failed to produce an amplifier. Hewlett Packard's simulation was an oscillator while both Eesof and Compact were achieving about 40dB of attenuation at 2GHz. Some of the explanations were simple. HP's application engineer had neglected to include the device package in the non-linear simulation. The S-parameters given by Avantek include the package while the Spice parameters do not. This simple oversight was rapidly corrected.

Eesof's "attenuator" was also cured by checking the input parameters and a more realistic simulation produced.

Compact's simulation took significantly longer to return and again the non-linear Microwave Harmonica program initially showed a significant level of insertion loss. This raised the question of the appropriate value to use for a parameter known as the Kirk current or IK. It describes the corner point in the plot of log(Ic) versus Vbe.

The value in the data sheet is quoted for a "unit" transistor and a scaling factor must be applied for a particular transistor. For the device used here, the value of $10^{-4}Am^{-2}$ needs to be scaled by a factor of 1560, yielding a value of 156mA which is compatible with a bias current of 100mA for the circuit. Thus these "process" description parameters can be used for a much wider range of devices. Definition of the Spice model in this way is stated in the data sheets from the transistor manufacturer.

Forward gain

Results for the gain of the amplifier, derived from a linear simulation using S-parameters in the Avantek data book, are broadly similar. They are shown in figure 3.

The frequency range shown is chosen to match the measured data available for the amplifier fabricated at UCD, although this does go beyond the useful operating range of the unit. A good agreement between the different simulators would be expected in this context, although differences in the way that the passive elements in the circuit are modelled in the different simulators will clearly impact the results.

OSA did not supply results above 2.5GHz, and indeed were not asked to, but from the other three simulators a resonance at 2.75GHz is clearly visible. This resonance is notable both as a common feature in the simulations and for its complete absence from the measurements of the actual circuit! Eesof elected to sup-

ply two sets of results, making use of different Tee models. The plots shown here define the Tees in the same way as HP, which was considered to be closer to the reality of the fabricated amplifier. In practice the difference in small signal gain is less than 1dB.

In summary, the small signal gains at 2GHz were 16.35dB (OSA), 11dB (HP), 11.4dB (Eesof) and 11.8dB for (Compact's modified circuit) compared with the measured value of 12.2dB.

Non-linear analysis

It is in the area of non-linear simulation that some of the most interesting features of the simulations have been found. The results are plotted for a 2GHz tone, in figure 4.

The problems with getting to this stage have already been described, although the data made available to each of the companies precisely matched that available to an engineer designing a circuit in the laboratory.

OSA, Eesof and HP simulated the circuit as supplied, although OSA alleged that the measured S-parameters supplied in the databook were not wholly in agreement with the Spice model, and produced an "optimised" model by extraction from the S-parameters. Compact Software predicted the circuit supplied to have an output at the 1dB compression point of only +17dBm, with a linear gain of 7.4dB. The values are significantly below expectations, and the company suggests that this is due to "an improperly matched device". A phase-plane analysis feature in the software was applied to examine the ac load line of the transistor which showed it to have a full range of current swing but a very poor voltage swing of less than ±3.5V. Compact's results are therefore from the simulation of a circuit with a different output match. Subsequent examination of the circuit schematic used by Compact for the simulation led the circuit's designers at UCD to conclude that the company had not included the transistor package with the non-linear simulation, hence causing a mismatch in much the same way experienced by HP.

OSA's reaction to concerns about discrepancies between the S-parameter-derived and Spice models led it to undertake a Monte Carlo sweep of output power versus input power for 100 outcomes. It showed a spread in 1dB compression values between 23.2dBm and 27.2dBm. The former value is actually closer to the measurements at UCD.

A further sensitivity analysis was also carried out which led OSA to suggest that the output power at 1dB gain compression was more sensitive to the length of the open stub in the input matching circuits and the lengths of the microstrip lines in the output matching circuits than to any other parameters in the circuits.

Despite the additional work undertaken by the company, OSA was by far the quickest company to return results. In this context, it is certainly surprising that the total terminal time quoted for the simulation problem, before the additional work, was actually the longest of any of the companies, 10hours.

OSA's results include a small signal gain of 16.35dB and a 1dB compression point of 26.6dBm, rather higher than the 12.2dB and 23.0dBm measured for the actual circuit.

Eesof's results were the next to arrive, and proved to be closer to the measurements. Gain was 11.3dB while the 1dB compression was at 21.8dBm. With the alternative Tee structure, the gain was increased by 0.8dB to provide an even closer value

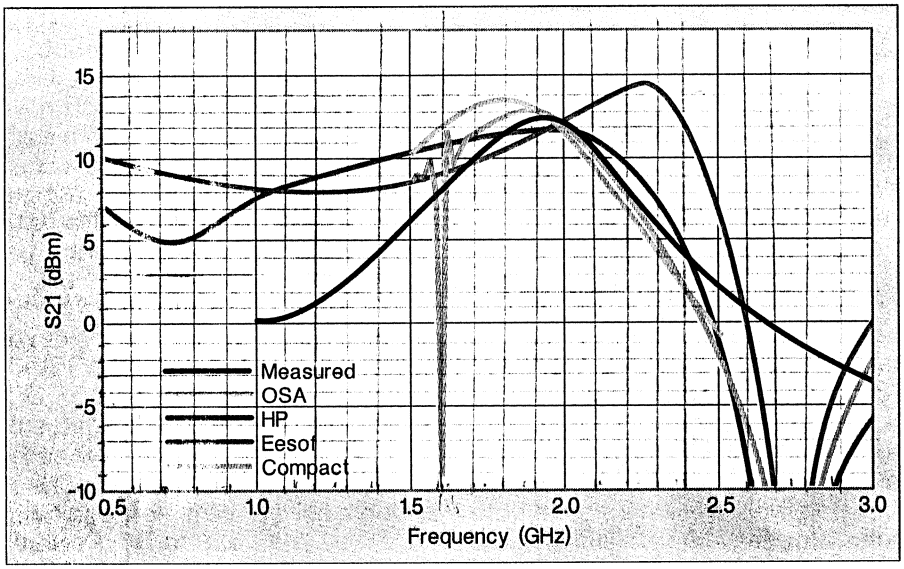

Figure 3 (above left): The linear simulation results for small signal gain, compared with the results measured at University College Dublin.

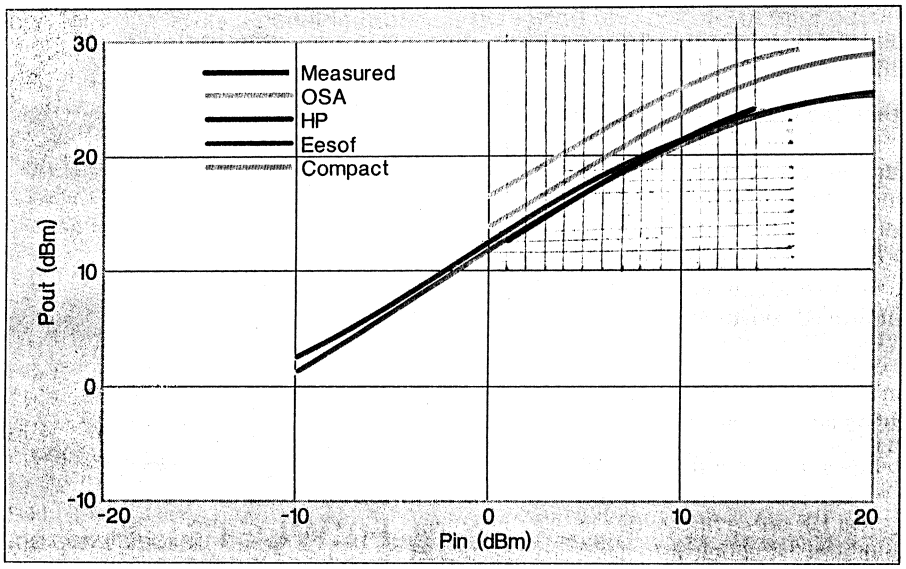

Figure 4 (left): Swept power results at 2GHz for amplifier, showing 1dB saturation point.

Table 1: Simulation times and platforms

	Results received	Terminal time	Simulation time F sweep/Power sweep	Platform
OSA	30/9/93	10 hours	* / 12s (5pts)	Sun Sparcstation 10
HP	19/10/93	40 minutes	0.4 (51pts) / 80 (121pts)	HP735
EEsof	28/10/93	60 minutes	150s (351pts) / 27s (121pts)	HP730
Compact Software	8/11/93	*	15s (101pts) / 180s (41pts)	50MHz 486PC

Benchmark circuit sent 13/9/93 with transistor Spice parameters (i.e. data sheet) 20/9/93.
* Information not supplied.

although the increase in the compression point was rather less, 0.2dB. The results plotted in figures 3 and 4 are not the closest to the measurements but have been selected since the Tee used is believed to be closest to the actual circuit.

Eesof made several comments. All lumped components were modelled as "ideal" and both the connector and the tanδ losses have been ignored.

Turning now to Hewlett Packard, several similar assumptions are quoted which could affect the simulated results. The small capacitors have been modelled as surface mount components while the larger capacitors are assumed ideal. The capacitors in the bias circuit were unfortunately read by the HP application engineer to be 1μF rather than the actual value of 1nF, an error which may well have been caused by the resolution of the FAX transmission. This dramatic change in the value is not, however, thought by the circuit designers to have had a similarly dramatic effect on the performance at 2GHz, and this hypothesis seems to be borne out by the results.

Zener diodes are not common features in microwave simulator libraries so this was created as a "complete fiction" simply to provide the correct dc bias conditions for the transistor. Again substrate loss is ignored.

The predicted performance from S-parameters had understated that obtained from the actual circuit, with 11.0dB gain achieved but the 12.5dB value achieved with the Spice model was very close. The 1dB gain compression point was at 21.5dBm.

The final results to arrive were from Compact Software, a delay that had partly been caused by international travel by leading members of their team, and partly by some confusion over the scaling parameters in the Spice model for the transistor.

The company carried out the work on a 50MHz 486 platform rather than the workstations employed by the other three vendors, so the simulation times quoted should be considered in this context.

In the simulation of the circuit as supplied, Compact suggested that the amplifier would only be capable of 7.4dB linear gain with a 1dB compression point at 17dBm. The explanation for this poor performance has already been reported, but the results plotted in figure 4 are those for an optimised circuit with the netlist changed. Performance achieved is then a 1dB compression point at 2GHz of 25.8dBm with an input of 13dBm. The linear gain prediction had been 11.8dB.

Conclusions

It is certainly rare that four different simulators, should be directed at the same circuit. The efforts of all the companies and their openness in providing the results for scrutiny are appreciated.

Clearly the simulators do not all come up with the same answers. Indeed, taking the results from Compact before modification of the netlist, we have a spread in linear gain predictions and 1dB compression point simulations of 9dB. There is also a significant variation between the small signal gain predictions according to whether they come from the linear simulations or the harmonic balance simulations. The values from Eesof and OSA did not show this discrepancy, although the optimisation by OSA of the non-linear device model using the S-parameters may have made the agreement inevitable.

The closest match to the measured results came from HP and Eesof. Although there were variables in the circuit that could have influenced the results, this would be the case for any real circuit where the simulation is to be undertaken as part of the design process, before building it!

Our original intention was to examine not just single tone responses shown here, but also to look at the first four harmonics, expecting that the results would otherwise be too alike to draw any conclusions. In practice, the time taken by some of the applications engineers to achieve a correct non-linear model for the circuit, basically from a thorough understanding of the Avantek three layer packaged transistor model, precluded that extra level of analysis. This did leave a question mark over the problems an engineer might have with the input of a similar circuit if the world's best CAD-dedicated engineers found it a problem. Beyond that we leave you to judge.

We gratefully acknowledge the contribution of University College Dublin to the CAD review, and here Philip Perry makes some comments on the results.

The CAD review has certainly been an education! The principal problem seems to have come from the use of different models for the bipolar transistor in its packaged form. In the Avantek data book a three layer model is presented with the conventional Spice model embedded in a network of non-linear diodes and capacitors. This, in turn is embedded in a package model of transmission lines, capacitors and inductors.

When Compact presented the full implementation of the model to us, it became apparent that the package model had been omitted. This would account for the discrepancies in the simulated results and the company's inability achieve a good impedance match. HP fully implemented the Avantek model after initially omitting the package.

Upon examining the OSA results, I felt that they too had not included the package. Whilst the optimisation of the model towards the given S-parameters would have offset some of the effects, the use of S-parameters at a single bias point would also have caused some errors. However OSA insists that the package was included in the non-linear model.

It is not clear how Eesof implemented the model, but the simulations do seem close to the measured values.

One common feature of the simulations was the 2.75GHz resonance. This may well be due to the bias circuit, which the companies all chose to simulate, rather than assuming that its effects could be negated by additional circuitry (chokes) as was actually the case, This omission would have allowed a feedback path, but the effect would have been minimal compared to the transistor model problem.

Chapter 5

CAD Review: the 7GHz doubler circuit

(Microwave Engineering Europe, May 1994)

CAD Review: the 7GHz doubler circuit

For our latest CAD benchmark, a doubler circuit was supplied to commercial vendors of non-linear microwave CAD. The results are presented here for simulators from Compact Software, Hewlett Packard and Optimization Systems Associates.

The CAD reviews in Microwave Engineering Europe, run every May and November, have proved to be very popular. In this exercise, the CAD vendors were supplied with circuit details for a class B frequency doubler built on Duroid. Compact Software and Optimization Systems Associates rapidly agreed to take part and had encouraged us to publish additional benchmarks.

Hewlett Packard declined to formally take part, citing the pressure of work after last year's acquisition of Eesof as the principal reason. However, with HP, including Eesof, now representing the largest single vendor of microwave CAD it was thought inappropriate to leave the company out. Hence the circuit designers in Belfast undertook the HP Microwave Design System (MDS) simulation while OSA and Compact devoted their own engineering resources to the problem.

Sonnet Software submitted results for the electromagnetic aspects of the simulation, and Sonnet's "em" planar simulator was also used by OSA.

Engineering resources are valuable and we would like to thank all the companies that gave so freely of their time for taking part. The results have again proved to be interesting.

Doubler circuit

The circuit outline, which was supplied to the vendors with dimensions, is shown in figure 1. Designed by Dr Aaron Tang at Queen's University, Belfast, it uses RT Duroid with a nominal dielectric constant of 2.2 and a height of 0.254mm. The active device is a NEC 7100 FET in die form and the two capacitors are AVX Accuwave 8.2pF.

In common with last November's review, the circuit was intended to be a practical one, using a commercial substrate and active device, but the FET was not packaged on this occasion. Measurements were taken using a Wiltron launcher and a University harmonic balance simulator was also used to provide an alternative set of simulated results.

Models

It will be clear to all users of microwave CAD that the accuracy of the models used for both active and passive devices is the key to good simulation. Both OSA and Compact initially used their own library models for the microstrip elements in the circuit, but their approaches to the active device were different.

Compact's team observed that the NEC FET was well suited to the application but added that modelling the device for harmonic balance simulation is not straightforward. They actually produced two models. NEC's European sales office supplied one, based on a Curtice cubic model (NEC model) while Compact undertook dc IV and bias dependent S-parameter measurements to produce a Materka-

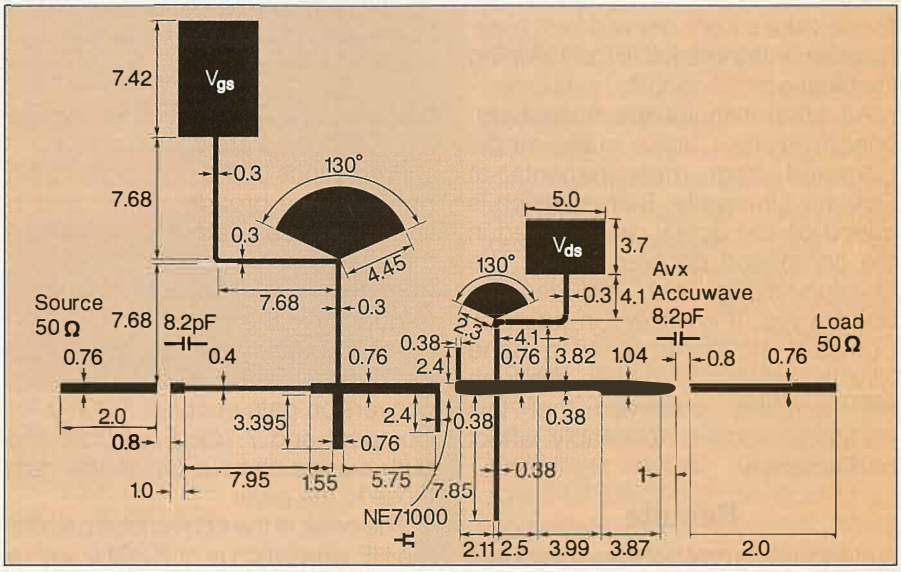

Figure 1: Circuit layout for the 7GHz doubler.

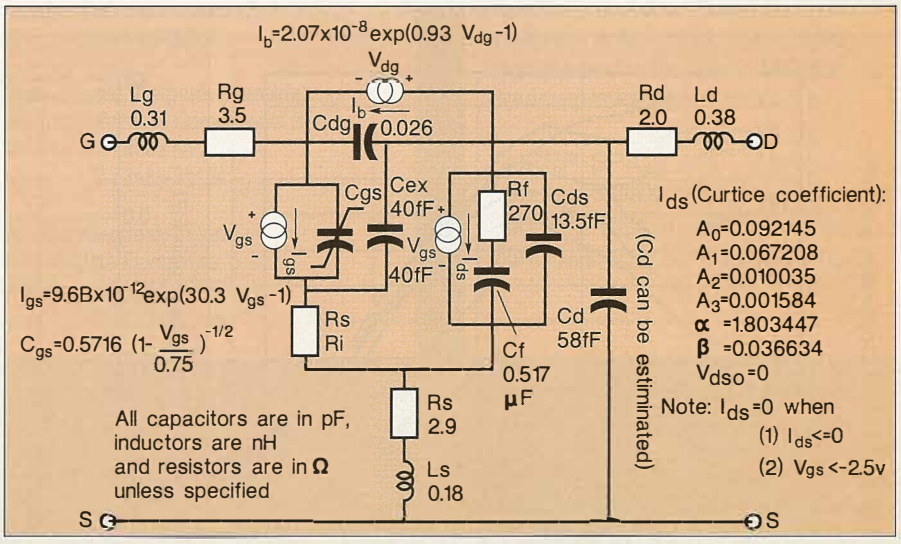

Figure 2: The Queen's model for the NEC 71000 FET.

Kacprzak model, which we will call the CS model. OSA used published data for the device at two bias points and for frequency points at 1GHz increments from 2-26GHz. The company's Harpe parameter extractor derived a Curtice and Ettenberg model from the data.

Hewlett Packard includes a model for the 71000 FET in the MDS "Fetlib" library, so this was used by the team at Queen's in all MDS simulations, with passive elements also drawn from the MDS libraries. Bond wire inductances of 0.3nH were added for the gate and drain, which use two 0.0254mm bond wires in the actual circuit, while the 3 source bond wires were represented by 0.18nH. These values were derived from measurements undertaken in developing the Queen's FET model.

All other simulations have been based on the Curtice cubic model extracted from measurements at Queen's University, Belfast which is based on the actual device used in the completed doubler circuit. The Queen's model also includes the bond wires. It is shown in figure 2. Compact standardized on a bond wire inductance of 0.3nH, although the company observed that this parameter could noticeably affect performance.

Results

A standard format has been adopted to allow easy comparison of the simulations and the measured data. The colours used and notation for the first four harmonics are shown above.

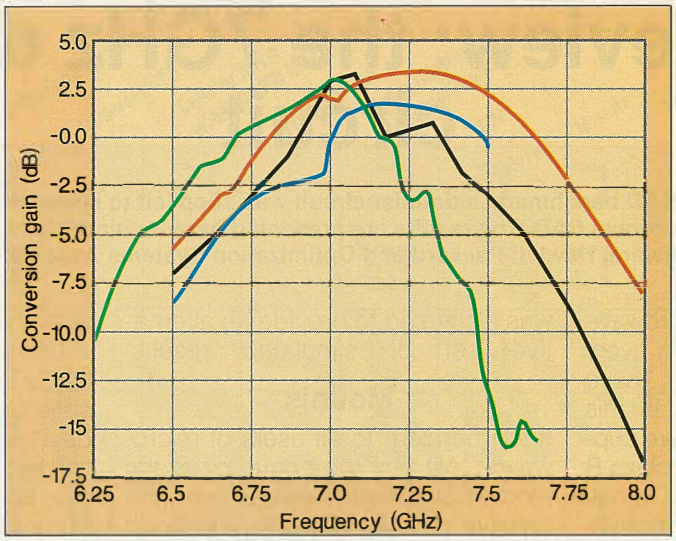

Figure 3: Conversion gain results plotted against frequency.

Key:
Compact
OSA
Measured
HP MDS
+ Fundamental (7GHz)
× 2nd harmonic
○ 3rd harmonic
● 4th harmonic

Predictions of the conversion gain proved to be broadly similar and in line with measurements. However, there were some shifts in frequency from the nominal 7GHz operating frequency at the input.

The frequency sweeps are plotted in figure 3. Peaks in the values of conversion gain occur at 7.3GHz for Compact and 7.1GHz for OSA and both curves show a dip in the gain close to the peak.

The peak in the conversion gain for the HP simulation is at 7.2GHz with a value of 1.4dB at an input power of 9.0dBm. At this frequency, the simulation shows 21dB suppression of the fundamental at the output. The third and fourth harmonics are at -27dBm and -30dBm respectively.

Power sweeps were requested at a nominal 7GHz, so these relatively small frequency shifts should be considered when we compare the power sweeps. One non-constant factor is the drive level applied. OSA used 9dBm as the peak of the conversion gain while Compact used 5dBm. Reference to the power sweeps below will show that this could influence the results but is unlikely to be a dominant factor.

For the HP simulations, a drive level in excess of 9dBm was needed to achieve conversion gain, rather than loss at 7.0GHz.

Measured results for the actual circuit show a conversion gain in excess of 2dB at 7.0GHz for drive levels between -2 and +8dBm, with a 3V Vds, but an increased Vds causes the conversion gain to drop rapidly at the lower drive levels - see figure 4. While Vds determines the different curves in the figure, variations between the active device models might be expected to similarly influence the results.

Conversion gain peaks occur with a +7dBm input or -1dBm input at 2.8dB and 3.8dB respectively.

Compact's second simulation with the 0.6nH bond wires may give us a further explanation. The company

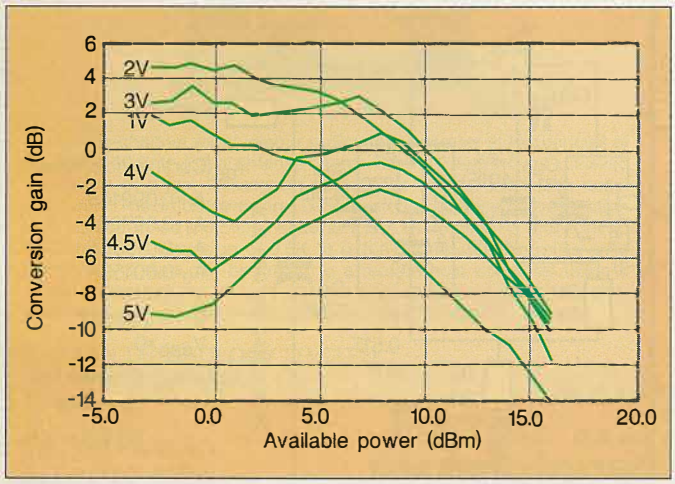

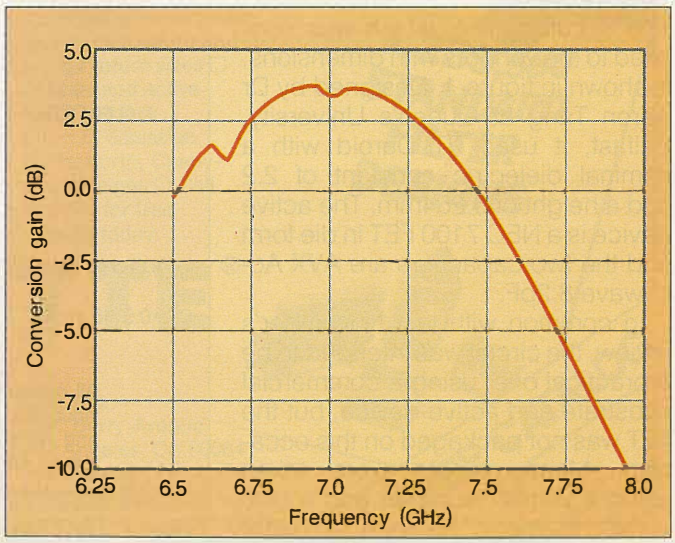

Figure 4: Conversion gain measurements for different Vds. Figure 5 (right): Compact's simulation with 0.6nH bond wires to the chip.

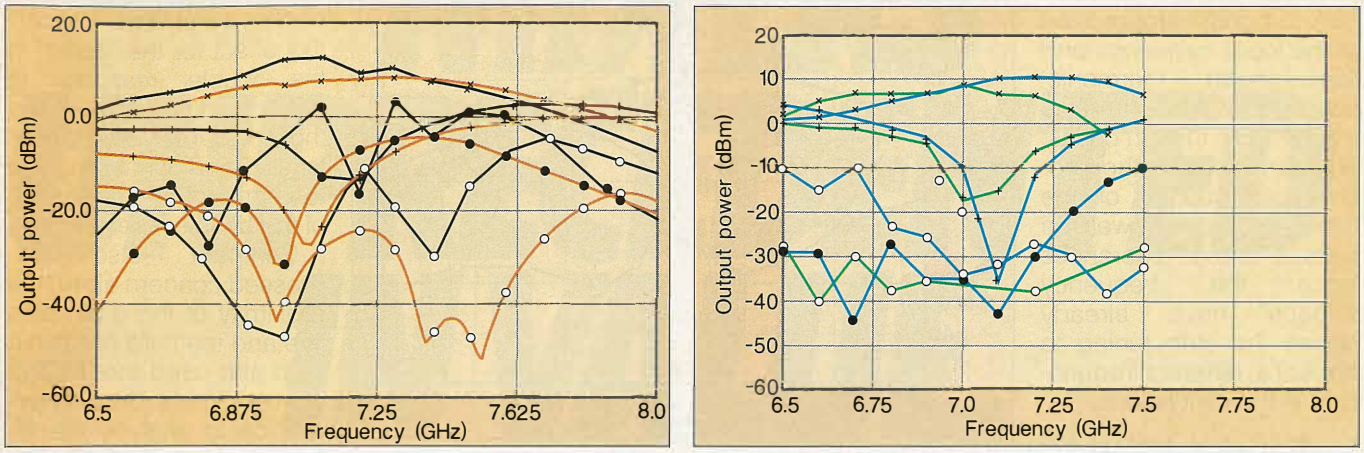

Figure 6 (a) and (b): Swept frequency results for the first four harmonics. Note that drive levels are not constant.

found that the increased inductance caused the centre of the response to be shifted down to 7.0GHz and the conversion gain to slightly increase, to 4.0dB as shown in figure 5. Compact identified the bias decoupling circuit as the cause of the dip at 7.0GHz and an equivalent spike in the predicted return loss.

The results from the frequency sweep for the first four harmonics also prove to be interesting in figure 6. Here the results diverge further than the simple conversion gain plots and the suppression of the input frequency at the output is significantly lower for OSA, at 24dB, than for the Compact simulation, at 36dB or HP at 45dB. The maximum value occurs at 7.1GHz and the 7.85mm drain stub was identified as the reason for this. The 2.4mm third harmonic stubs at the gate and drain are also clearly evident on Compact's and HP's results.

Although the plots show the output power for each simulation to allow a comparison, it should be remembered that the drive levels are not constant. To achieve satisfactory conversion gain levels, HP and OSA used a 9dBm input power, and the respective power sweeps show hor the conversion gain dropped below these input levels. The Compact results are with a 5dBm input, which is closer to the 6dBm value used for the measurements. In practice, conversion gain for the actual circuit was far less sensitive to the input level than the simulations.

In OSA's simulation, the third harmonic stubs have have an almost identical effect at 7.0GHz but the fourth harmonic, is at 7.2GHz compared to Compact's 7.0GHz.

The simulations with HP's MDS are broadly in line with Compact's when the frequency characteristics are considered although the drive levels used to achieve conversion gain is 4dB higher.

The best suppression of the fundamental and the fourth harmonic are at 7.1GHz but the third harmonic stub appears to be most effective at 7.0GHz. Suppression of the fundamental is the highest of all the simulations at 46dB, and well above the best measured result of 26dB, which occurred at 7.0GHz.

These results, so influenced by the modelling of the passive elements, suggest that there is some considerable variation in the passive library elements included with the simulators.

For the only two external passive elements, the AVX Accuwave 8.2pF capacitors, Compact also considered how critical the modelling of these elements would be in the overall simulation. It was concluded that for values above 3pF, the simulation is quite insensitive to the parameters of these devices.

Power sweep

The power sweep simulations again show some significant differences, all using 7GHz as the input frequency. At 5dBm input, the OSA simulation predicts a conversion loss of almost 5dB, while the Compact simulation is predicting a conversion gain in excess of 3dB - see figure 7. Compact's simulation is certainly predicting a rather better doubler,

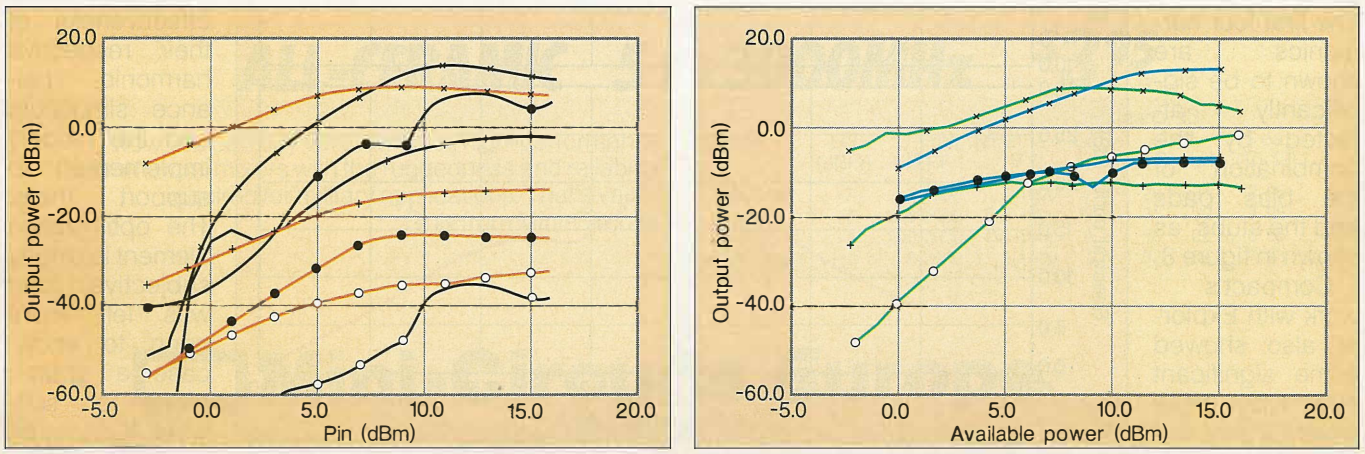

Figure 7 (a) and (b): Swept power simulations and measurements.

with superior suppression of the input frequency and the fourth harmonic' although the third harmonic is well down in both cases. The sensitivity to the precise performance of the tuning stubs may well be behind these differences since the frequency sweeps have already shown the stub tuning to appear at different frequencies in the simulations.

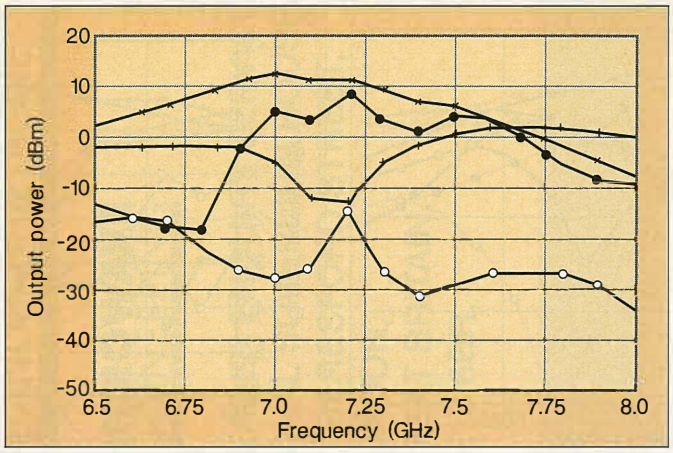

Figure 7: OSA's results with full "em" simulation of the bias pads and third harmonic stubs.

Em simulation

Both Compact and OSA opted to look further into the coupling of the stubs. OSA has links from the OSA90/Hope software into Sonnet's EM planar electromagnetic simulator and used this program, while Compact used its Explorer software. With the third harmonic stub coupling simulated by EM as a four port, OSA's results showed a smoother response for conversion gain against frequency, with 3.5dB gain from 7 to 7.1GHz, again using the 9dBm drive level.

The third harmonic suppression proved not to be as great but the stub resonances were still at 7GHz and 7.4GHz. The predicted increase in the third and fourth harmonic levels produced a more distorted waveform when OSA plotted the input and output voltage waveforms.

OSA went on to consider the effects of the bias pads and the radial stubs adjacent to them, simulating them as a two port in EM. The first four harmonics are shown to be significantly affected by the combination of the bias pads and the stubs, as shown in figure 8.

Compact's work with Explorer also showed some significant effects but these were largely out of band and affected the doubler simulation relatively little.

For the large bias pads, the company found resonances at 19.5GHz and 24.0GHz which were "due to a transverse mode and a patch antenna mode". However, it was observed from a plot of the phase component of S11 that the gate bias stub was operating as a quarter wavelength at 5.0GHz rather than the intended 7.0GHz, due to "the large width of the transmission line and the large impedance step discontinuity from the connecting line". The effect on the circuit is small as the radial stub is "providing a wideband short circuit near 7.0GHz" and this impedance is transformed through the half wavelength connecting line. Compact's engineers blamed this effect for the "bump" in the doubler response at 7.0GHz and recommended the removal of the rectangular stub and connecting line to improve the smoothness of the doubler's response.

Compact also expressed concern about the proximity of the drain bias line and the third harmonic stub and used the "MCPL" element in Microwave Harmonica to analyse the effect. Any resulting change to the conversion gain was found to be very small, varying by less than 0.1dB.

Sonnet's electromagnetic analysis encompassed the second fan stub and the Vds pad. It shows the pad radiating at frequencies between 20 and 25GHz, including the third harmonic, and a magnitude of 0.9 for S_{11} at these frequencies was predicted.

Plots of the current density across the pad show a broadly similar distribution to a patch antenna.

With the Vds probe in the centre of the pad, the distribution is much the same, but short circuiting the end of the pad changes the situation significantly. Hence, the company warns against placing the bias probe in the centre of the pad. Otherwise the current density was insensitive to the impedance of the supply.

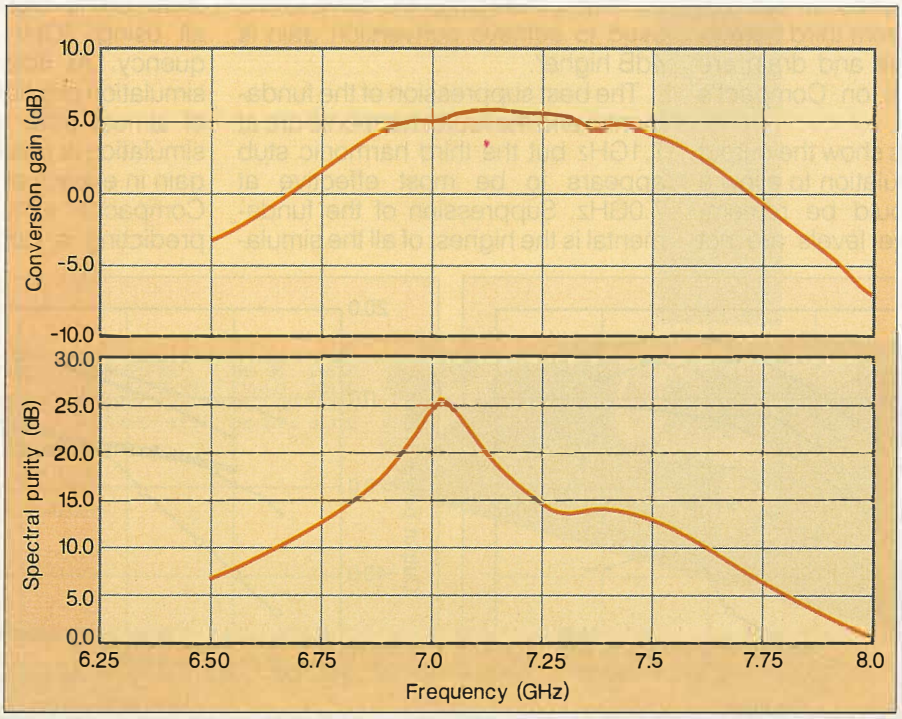

Figure 8: Spectral purity and conversion gain for Compact's optimized circuit.

Optimization

The objective part of the benchmark gave an opportunity for the companies to show the effectiveness of their respective harmonic balance simulators and the models implemented to support them. The optimization element is clearly subjective and was left more open to showcase a greater range of software. It draws on the skill of the

companies' support engineers as well as the scope of the CAD tools.

Compact stayed within the circuit topology given, varying only the lengths and widths of the transmission lines. They aimed to improve the conversion gain to 6dB and the spectral purity of the 2nd harmonic to better than 15dB. They defined a band of interest as 6.8 to 7.6GHz.

The spectral purity is defined by the ratio of the power at the second harmonic divided by the sum of the power in all other harmonics. The results are shown in figure 9.

OSA set the more conservative figure of 3dB conversion gain as a target but aimed for a higher spectral purity of 20dB. Data was based on simulations of the circuit with the EM analysis included for the bias pads and stubs. The fifteen variables picked for the optimization defined lengths of the transmission lines. The conversion gain is shown for the optimized circuit in figure 10.

In the two companies' optimizations, the changes in the lengths are quite different for each. In a majority of cases, one company's increase, corresponds to the other's decrease, as shown in table 2.

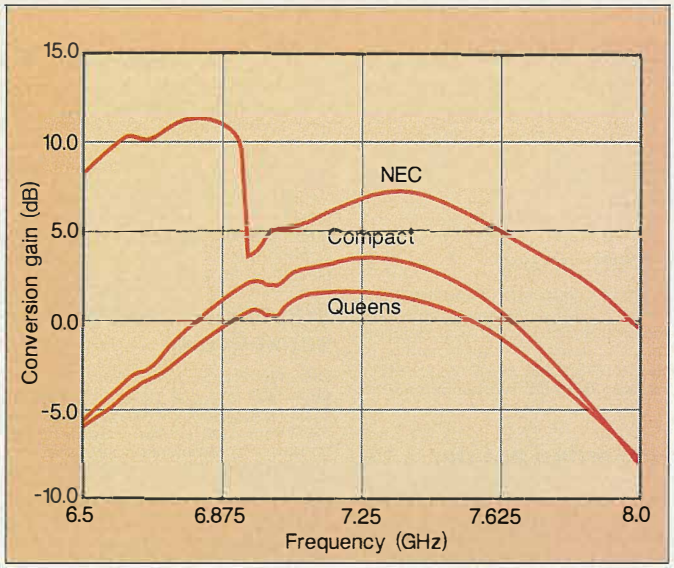

Figure 10: A comparison of results with the three models for the NEC 71000 FET. Shown are the Queen's University model, Compact's model and NEC's model.

Device models

The choice of the correct device model to use when there is not an obvious one in the FET manufacturers data book is clearly critical to a good simulation. OSA and Compact both looked at this problem.

OSA ran a Monte Carlo simulation to assess the effect of model uncertainty on simulation result and assigned a 20% tolerance to all model parameters to do this. The conclusion was that the frequency doubling would not be very sensitive but the spectral purity would be. The conversion gain spread in 50 outcomes was between -2.4dB and 4.7dB.

Compact compared three transistor models. They found that the NEC-Europe-supplied FET model did not exhibit pinch-off and although a hard pinch-off could be forced, this would be at the expense of a discontinuous model with accompanying convergence problems in the simulation. The CS model and the Queen's model were broadly similar except for the variation in Idss and Vpo. Conversion gain results for all three models are compared in figure 10.

Compact also ran multiple conversion gain analyses for the circuit based on different Idss and Vpo values, since the device data sheet predicts that these parameters can vary from 20 to 120mA and from -0.5 to -3.5V respectively. A 20dB range of conversion gain values was actually predicted, suggesting large error bars could be placed on the simulations. Nevertheless, the results had consistently been much closer to measurements for the particular device used at Queen's in the circuit.

HP was the only company with a model for the FET already in the MDS library and, with shared library resources, this should also be available to Libra users. The design team at Queen's were not as confident about the HP model as their won and with HP choosing not to take part in the benchmark, the details were not available as tot he origin of the model. Nevertheless, the ground-rules for the benchmarks were based on each software vendor using their own model.

Table 2

Original (mm)	Optimized Compact (mm)	Optimized OSA (mm)
5.7	5.73	5.182
3.395	3.93	4.5
2.11	2.44	1.601
7.85	7.79	7.903
7.68	7.86	7.51
3.82	3.82	3.804
1.55	1.58	1.759
7.95	8.36	6.792
2.5	2.57	2.842
3.99	4.35	3.903
3.87	4.10	3.698

Conclusions

All three simulators used in the benchmark showed a doubler operating around 7.0GHz. The differences came from the models of both the active device and the passive elements. Subjectively, the HP and Compact simulations are most similar in the prediction of the passive tuning of the circuit, although their simulations diverge in the parameters related to the active device.

The Compact and Queen's models for the FET appear to produce the best results, and both have been extracted from measurements of an actual NE71000 device. Despite the broad specification range on the NEC data sheet, the different transistors measured have produced similar results. Good simulations need good models.

Simulation times were not conclusive. OSA claimed a slightly shorter CPU time of 0.3s per point with a Sun Sparc station 10 workstation. Compact quoted 1.6s and 0.7s/point for frequency and power sweeps respectively.

Acknowledgements

Significant time and resources have gone into the benchmark. We would like to thank Aaron Tang and David Linton at Queen's University, Belfast. Bill McGinn in the USA and Hendrik Nagel at Technical Software Services in Germany undertook the Compact simulations while Radek Biernacki supplied the OSA results. Thanks also to Jim Merrill and Jim Rautio at Sonnet.

Reprint 1

Microwave Device Modeling Using Efficient ℓ_1 Optimization: A Novel Approach

Microwave Device Modeling Using Efficient l_1 Optimization: A Novel Approach

JOHN W. BANDLER, FELLOW, IEEE, SHAO HUA CHEN, STUDENT MEMBER, IEEE, AND SHAHROKH DAIJAVAD, STUDENT MEMBER, IEEE

Abstract—**A powerful modeling technique which exploits the theoretical properties of the l_1 norm is presented. The concept of multicircuit measurements and its advantages for unique identification of parameters are discussed. Self-consistent models for passive and active devices are achieved by an approach that automatically checks the validity of model parameters obtained from optimization. A set of formulas is presented to evaluate the first-order sensitivities of two-port S-parameters with respect to circuit elements appearing in an admittance or impedance matrix description of linear network equivalents. These formulas are used for devices with linear network models in conjunction with an efficient gradient-based l_1 algorithm. Practical use of the efficient l_1 algorithm in complicated problems for which gradient evaluation may not be feasible is also discussed. Two different optimization problems are formulated which connect the concept of modeling to physical adjustments on the device. Detailed examples in modeling of multicoupled cavity filters and GaAs FET's are presented.**

I. Introduction

THE PROBLEM of approximating a measured response by a network or system response has been formulated as an optimization problem with respect to the equivalent circuit parameters of a proposed model. The traditional approach in modeling is almost entirely directed at achieving the best possible match between measured and calculated responses. This approach has serious shortcomings in two frequently encountered cases. The first case is when the equivalent circuit parameters are not unique with respect to the responses selected and the second is when nonideal effects are not modeled adequately, the latter causing an imperfect match even if small measurement errors are allowed for. In both cases, a family of solutions for circuit model parameters may exist which produce reasonable and similar matches between measured and calculated responses.

In this paper, we present a new formulation for modeling that automatically checks the validity of the circuit parameters, with a simultaneous attempt in matching measured and calculated responses. If successful, the method provides confidence in the validity of the model parameters; otherwise, it proves their incorrectness. The use of the l_1 norm, based on its theoretical properties, is an integral part of the approach. We discuss the use of an efficient l_1 algorithm [1]–[3] both in problems for which response gradients can be evaluated and in complicated problems for which gradient evaluation is not feasible. The use of a gradient-based l_1 algorithm and of a variation of Broyden's formula to update gradients internally [3] makes it possible to employ a state-of-the-art optimization algorithm with any simulation package capable simply of providing responses. Therefore, widely used microwave design programs, e.g., SUPER-COMPACT [4] and TOUCHSTONE [5], which do not calculate exact gradients, could employ such an algorithm with an appropriate interface. As a result, it is conceivable that the modeling technique described could find its way into microwave engineering practice in the near future.

Two examples of practical interest, namely, modeling of a narrow-band multicoupled cavity filter and of a wide-band GaAs FET, follow the theoretical description of both the traditional and the new approaches. In both examples, a large number of variables are considered.

II. Review of Concepts in Approximation

A. The Approximation Problem

The traditional approximation problem is stated as follows

$$\underset{x}{\text{minimize}} \| \boldsymbol{f} \| \tag{1}$$

where a typical component of vector $\boldsymbol{f}$, namely f_i evaluated at the frequency point ω_i, is given by

$$f_i \triangleq w_i \left(F_i^c(\boldsymbol{x}) - F_i^m \right), \qquad i = 1, 2, \cdots, k. \tag{2}$$

F_i^m is a measured response at ω_i and F_i^c is the response of an appropriate network which depends nonlinearly on a vector of model parameters $\boldsymbol{x} \triangleq [x_1 \quad x_2 \quad \cdots \quad x_n]^T$ and w_i denotes a nonnegative weighting factor. Here $\| \boldsymbol{f} \|$ denotes the general l_p norm, given by

$$\| \boldsymbol{f} \| = \left(\sum_{i=1}^{k} |f_i|^p \right)^{1/p}. \tag{3}$$

The widely used least-squares norm, or l_2, is obtained with $p = 2$, and as $p \to \infty$ (1) becomes the well-known minimax problem. In this paper, we are primarily concerned with the l_1 norm, i.e., formulating the approximation problem

Manuscript received March 15, 1986; revised June 2, 1986. This work was supported in part by the Natural Sciences and Engineering Research Council of Canada under Grant G1135.

The authors are with the Simulation Optimization Systems Research Laboratory and the Department of Electrical and Computer Engineering, McMaster University, Hamilton, Ont., Canada L8S 4L7. J. W. Bandler is also with Optimization Systems Associates Inc., Dundas, Ont., Canada L9H 6L1.

IEEE Log Number 8610563.

0018-9480/86/1200-1282$01.00 ©1986 IEEE

TABLE I
APPROXIMATION PROBLEM USING l_1 AND l_2 OPTIMIZATION

	Case A		Case B		Case C	
Parameter	ℓ_1	ℓ_2	ℓ_1	ℓ_2	ℓ_1	ℓ_2
x_1	0 0	0 0071	0 0	0 0391	0 0	−0 0261
x_2	8 5629	8 5660	8 6664	5 8050	8 5506	12 8828
x_3	29 3124	29 7515	30 5684	30 0523	29 1070	26 0012
x_4	24 7375	25 0108	25 4261	19 6892	24 6452	32 1023
x_5	12 2285	12 3699	12 9234	21 8794	12 0887	7 4300

as

$$\underset{x}{\text{minimize}} \|f\| \triangleq \sum_{i=1}^{k} |f_i|. \tag{4}$$

B. Properties of l_1 Approximation

The use of the l_1 norm as compared to the other norms l_p with $p>1$ has the distinctive property that some large components of f are ignored; i.e., at the solution there may well be a few f_i's which are much larger than the others. This means that, with the components of f as defined by (2), a few large measurement errors can be tolerated by the l_1 norm better than any other norm. In this paper, we do not need to assume that such large errors exist. We use a formulation in which some components of f are designed to have large values at the solution, thereby justifying the use of l_1. In Section III, we introduce such a formulation using multicircuit measurements where the change in parameters between different circuits forms part of the objective; i.e., they are some of the f_i's. Indeed, these f_i's are expected to have a few large values and many zeros at the solution.

The robustness of the l_1 optimization in dealing with large components of f, as discussed in the literature [2], [6], is the result of a mathematical property related to the necessary conditions for optimality. The solution to (4) is usually situated at a point where one or more of the f_i's equal zero while some large f_i's are in effect ignored completely.

C. Illustration of l_1 Approximation

To illustrate the above property, we consider a rational approximation problem. We obtain a solution to the problem using l_1 and l_2 optimizations. Then, we deliberately create a few large deviations in the actual functions to observe the effect on parameters when large components of f are supposed to be present at the solution. Again, we emphasize that, because of our formulation in Section III, a few large deviations in f_i's are desired and expected. The parameters obtained using the l_1 and l_2 optimizations with and without deviations present are compared.

We want to find the rational approximant of the form [7]

$$K(x) = \frac{x_1 + x_2\omega + x_3\omega^2}{1 + x_4\omega + x_5\omega^2} \tag{5}$$

to the function $\sqrt{\omega}$ in the interval $\omega \in [0,1]$. Using 51 uniformly spaced sample points on the given interval,

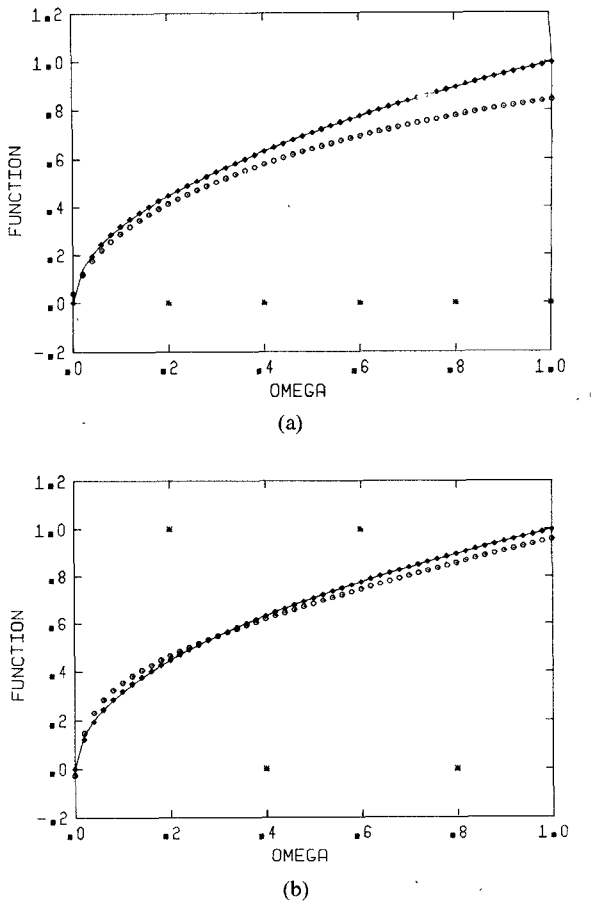

Fig. 1. Approximations using l_1 and l_2 optimizations. Solid line is the actual function. Diamonds identify the approximation using l_1 and circles represent approximations with l_2. Stars represent data points after large deliberate deviations. (a) and (b) correspond, respectively, to cases B and C in Section II.

parameter vector x was obtained by l_1 and l_2 optimizations and the results are summarized in Table I under case A. Using both sets of parameters, the approximating function virtually duplicates the actual function over the whole interval. We now introduce a few large deviations in the actual function in two separate cases. In case B, the actual function value is replaced by zero at five points in the interval, namely, at 0.2, 0.4, $\cdots$, 1.0. In case C we use zero at 0.4 and 0.8, and one at 0.2 and 0.6. In both cases, l_1 and l_2 optimizations are performed and the parameters obtained are summarized in Table I.

The parameters obtained by l_1 optimization in cases B and C are consistent with their values in case A. On the other hand, the presence of large deviations has affected the l_2 optimization results severely, and inconsistent parameters are obtained. Fig. 1(a) and (b) illustrates the approximating and actual functions for cases B and C. Whereas the approximation using l_1 has ignored the large deviations completely and has achieved an excellent match for both cases, the l_2 approximation, which was as good as l_1 in case A, has deteriorated. For instance, the particular arrangement of deviations in case B has caused the approximating function to underestimate the actual function over the whole interval.

The property that a few large individual function f_i's are ignored by l_1 optimization and many f_i's are zero at the solution has also found applications in fault-isolation techniques for linear analog circuits [8] and the functional approach to postproduction tuning [9].

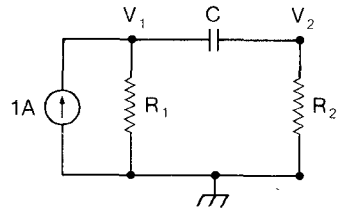

Fig. 2. Simple RC network.

III. New Approach Using Multiple Sets of Measurements

The use of multiple sets of measurements for a circuit was originally thought of by the authors as a way of increasing the "identifiability" of the network. The idea is to overcome the problem of nonuniqueness of parameters that exists when only one set of multifrequency measurements at a certain number of ports (or nodes) is used for identification. By a new set of measurements we mean multifrequency measurements on one or more responses after making a physical adjustment on the device. Such an adjustment results in the deliberate perturbation of one or a few circuit parameters; therefore, to have multiple sets of measurements, multiple circuits differing from each other in one or a few parameters are created. In the above context, the term multicircuit identification may also be used.

In this section, we first use a simple example to illustrate the usefulness of multicircuit measurements in identifying the parameters uniquely. We formulate an appropriate optimization problem and also discuss its limitations. Finally, we develop a model verification method and formulate a second optimization problem which exploits multicircuit measurements and the properties of the l_1 optimization in device modeling.

A. Unique Identification of Parameters Using Multicircuit Measurements

Consider the simple RC passive circuit of Fig. 2. The parameters $\boldsymbol{x} = [R_1 \quad R_2 \quad C]^T$, where T denotes the transpose, are to be identified. If we have measurements only on V_2, given by

$$V_2 = \frac{sCR_1R_2}{1+sC(R_1+R_2)} \tag{6}$$

it is clear by inspection that $\boldsymbol{x}$ cannot be uniquely determined regardless of the number of frequency points and the choice of frequencies used. This is because R_1 and R_2 are observed in exactly the same way by V_2. Formally, the nonuniqueness is proved using the concepts discussed in the subject of fault diagnosis of analog circuits [8] in the following way. Given a complex-valued vector of responses $\boldsymbol{h}(\boldsymbol{x}, s_i)$, $i = 1,2,\cdots,n_\omega$ (from which real-valued vector $\boldsymbol{F}^c(\boldsymbol{x},\omega)$ is obtained), the measure of identifiability of $\boldsymbol{x}$ is determined by testing the rank of the $n_\omega \times n$ Jacobian matrix

$$\boldsymbol{J} \triangleq [\nabla_x \boldsymbol{h}^T(\boldsymbol{x})]^T. \tag{7}$$

If the rank of matrix $\boldsymbol{J}$ denoted by ρ is less than n, $\boldsymbol{x}$ is not uniquely identifiable from $\boldsymbol{h}$. For the RC circuit example, we have

$$\boldsymbol{J} = \begin{bmatrix} \dfrac{s_1CR_2(1+s_1CR_2)}{[1+s_1C(R_1+R_2)]^2} & \dfrac{s_1CR_1(1+s_1CR_1)}{[1+s_1C(R_1+R_2)]^2} & \dfrac{s_1R_1R_2}{[1+s_1C(R_1+R_2)]^2} \\ \vdots & \vdots & \vdots \\ \dfrac{s_{n_\omega}CR_2(1+s_{n_\omega}CR_2)}{[1+s_{n_\omega}C(R_1+R_2)]^2} & \dfrac{s_{n_\omega}CR_1(1+s_{n_\omega}CR_1)}{[1+s_{n_\omega}C(R_1+R_2)]^2} & \dfrac{s_{n_\omega}R_1R_2}{[1+s_{n_\omega}C(R_1+R_2)]^2} \end{bmatrix}. \tag{8}$$

Denoting the three columns of $\boldsymbol{J}$ by $\boldsymbol{J}_1$, $\boldsymbol{J}_2$, and $\boldsymbol{J}_3$, we have

$$\boldsymbol{J}_1 - \left(\frac{R_2}{R_1}\right)^2 \boldsymbol{J}_2 + \frac{C(R_2-R_1)}{R_1^2}\boldsymbol{J}_3 = \boldsymbol{0} \tag{9}$$

i.e., $\boldsymbol{J}$ cannot have a rank greater than 2. Therefore, $\boldsymbol{x}$ is not unique with respect to V_2.

Now, suppose that a second circuit is created when R_2 is adjusted by an unknown amount. Using a superscript to identify the circuit (1 or 2), we have

$$V_2^1 = \frac{sC^1R_1^1R_2^1}{1+sC^1(R_1^1+R_2^1)} \tag{10a}$$

and

$$V_2^2 = \frac{sC^1R_1^1R_2^2}{1+sC^1(R_1^1+R_2^2)} \tag{10b}$$

noting that R_1^2 and C^2 are not present, since only R_2 has changed.

Taking only two frequencies s_1 and s_2, the expanded parameter vector $\boldsymbol{x} = [R_1^1 \quad R_2^1 \quad C^1 \quad R_2^2]^T$ is uniquely

identifiable because the Jacobian J given by

$$J=\begin{bmatrix} \frac{s_1C^1R_2^1(1+s_1C^1R_2^1)}{[1+s_1C^1(R_1^1+R_2^1)]^2} & \frac{s_1C^1R_1^1(1+s_1C^1R_1^1)}{[1+s_1C^1(R_1^1+R_2^1)]^2} & \frac{s_1R_1^1R_2^1}{[1+s_1C^1(R_1^1+R_2^1)]^2} & 0 \\ \frac{s_2C^1R_2^1(1+s_2C^1R_2^1)}{[1+s_2C^1(R_1^1+R_2^1)]^2} & \frac{s_2C^1R_1^1(1+s_2C^1R_1^1)}{[1+s_2C^1(R_1^1+R_2^1)]^2} & \frac{s_1R_1^1R_2^1}{[1+s_2C^1(R_1^1+R_2^1)]^2} & 0 \\ \frac{s_1C^1R_2^2(1+s_2C^1R_2^2)}{[1+s_1C^1(R_1^1+R_2^2)]^2} & 0 & \frac{s_1R_1^1R_2^2}{[1+s_1C^1(R_1^1+R_2^2)]^2} & \frac{s_1C^1R_1^1(1+s_1C^1R_1^1)}{[1+s_1C^1(R_1^1+R_2^2)]^2} \\ \frac{s_2C^1R_2^2(1+s_2C^1R_2^2)}{[1+s_2C^1(R_1^1+R_2^2)]^2} & 0 & \frac{s_2R_1^1R_2^2}{[1+s_2C^1(R_1^1+R_2^2)]^2} & \frac{s_2C^1R_1^1(1+s_2C^1R_1^1)}{[1+s_2C^1(R_1^1+R_2^2)]^2} \end{bmatrix} \tag{11}$$

is of rank 4 if $s_1 \neq s_2$.

To summarize the approach, it can be stated that although the use of unknown perturbations adds to the number of unknown parameters, the addition of new measurements could increase the rank of J by an amount greater than the increase in n, thereby increasing the chance of uniquely identifying the parameters. The originality of the technique lies in the fact that neither additional ports (nodes) nor additional frequencies are required. The additional measurements on the perturbed system can be performed at subsets of the ports (nodes) or frequencies employed for the unperturbed system.

Based on the above ideas and for n_c circuits, we formulate an l_1 optimization problem as follows:

$$\underset{x}{\text{minimize}} \sum_{t=1}^{n_c} \sum_{\iota=1}^{k_t} |f_\iota^t| \tag{12}$$

where

$$f_\iota^t \triangleq w_\iota^t \left[F_\iota^c(x^t) - (F_\iota^m)^t \right] \tag{13}$$

and

$$x = \begin{bmatrix} x^1 \\ x_a^2 \\ \vdots \\ x_a^{n_c} \end{bmatrix} \tag{14}$$

with superscript and index t identifying the tth circuit. Here, x_a^t represents the vector of additional parameters introduced after the $(t-1)$th adjustment. It has only one or a few elements compared to n elements in x^t which contains all circuit parameters after the change, i.e., including the ones which have not changed. The variable k_t is an index whose value depends on t; therefore, a different number of frequencies may be used for different circuits.

B. Model Verification Using Multicircuit Measurements

Although the optimization problem formulated in (12) with the variables given in (14) enhances the unique identification of parameters, its limitations should be considered carefully. The limitations are related to the way in which model parameters x are controlled by physical adjustments on the device.

Parameters x are generally controlled by some physical parameters $\phi \triangleq [\phi_1 \quad \phi_2 \quad \cdots \quad \phi_l]^T$. For instance, in active device modeling, intrinsic network parameters are controlled by bias voltages or currents, and in waveguide filters, the penetration of a screw may control a particular element of the network model. The actual functional relationship between ϕ and x may not be known; however, we often know which element or elements of x are affected by an adjustment on an element of ϕ. The success of the optimization problem (12) is dependent on this knowledge; i.e., after each physical adjustment, the correct candidates should be present in x_a. To ensure this, we should overestimate the number of model parameters which are likely to change after adjusting an element of ϕ. On the other hand, we would like to have as few elements as possible in each x_a vector, so that the increase in the number of variables can be overcompensated for by the increase in rank of matrix J resulting from the addition of new measurements.

In practice, by overestimating the number of elements in x_a or by making physical adjustments which indeed affect many model parameters (a change in bias voltage may affect all intrinsic parameters of a transistor model), the optimization problem of (12) may not be better conditioned than the traditional single-circuit optimization. This means that the chance for unique identification of parameters may not increase. However, multicircuit measurements could still be used as an alternative to selecting different frequency points or a greater number of points, as may be done in the single-circuit approach.

We now formulate another optimization problem, which either verifies the model parameters obtained or proves their inconsistency with respect to physical adjustments. The information about which elements of x are affected by adjusting an element of ϕ, although used to judge the consistency of results, is not required *a priori*. Therefore, the formulation is applicable to all practical cases.

Suppose that we make an easy-to-achieve adjustment on an element of ϕ such that one or a few components of x are changed in a dominant fashion and the rest remain

constant or change slightly. Consider the following l_1 optimization problem

$$\underset{x}{\text{minimize}} \sum_{t=1}^{2} \sum_{i=1}^{k_t} |f_i^t| + \sum_{j=1}^{n} \beta_j |x_j^1 - x_j^2| \qquad (15)$$

where β_j represents an appropriate weighting factor and x is a vector which contains circuit parameters of both the original and perturbed networks, i.e.,

$$x = \begin{bmatrix} x^1 \\ x^2 \end{bmatrix}. \qquad (16)$$

Notice that, despite its appearance, (15) can be rewritten easily in the standard l_1 optimization form, which is minimizing $\Sigma|\cdot|$, by taking the individual functions from either the nonlinear part f_i^t or the linear part $x_j^1 - x_j^2$.

The above formulation has the following properties.

1) Considering only the first part of the objective function, the formulation is equivalent to performing two optimizations, i.e., matching the calculated response of the original circuit model with its corresponding measurements and repeating the procedure for the perturbed circuit.

2) By adding the second part to the objective function, we take advantage of the knowledge that only one or a few model parameters should change dominantly by perturbing a component of ϕ. Therefore, we penalize the objective function for any difference between x^1 and x^2. However, since the l_1 norm is used, one or a few large changes from x^1 to x^2 are still allowed. Discussions on the use of the l_1 norm in Section II should be referred to.

The confidence in the validity of the equivalent circuit parameters increases if a) an optimization using the objective function of (15) results in a reasonable match between calculated and measured responses for both circuits 1 and 2 (original and perturbed) and b) the examination of the solution vector x reveals changes from x^1 to x^2 which are consistent with the adjustment to ϕ; i.e., only the expected components have changed significantly. We can build upon our confidence even more by generalizing the technique to more adjustments to ϕ, i.e., formulating the optimization problem as

$$\underset{x}{\text{minimize}} \sum_{t=1}^{n_c} \sum_{i=1}^{k_t} |f_i^t| + \sum_{t=2}^{n_c} \sum_{j=1}^{n} \beta_j^t |x_j^1 - x_j^t| \qquad (17)$$

when n_c circuits and their corresponding sets of responses, measurements, and parameters are considered and the first circuit is the reference model before any adjustment to ϕ. In this case, x is given by

$$x = \begin{bmatrix} x^1 \\ x^2 \\ \vdots \\ x^{n_c} \end{bmatrix}. \qquad (18)$$

By observing inconsistencies in changes of x with the actual change in ϕ, the new technique exposes the existence of nonideal effects not taken into account in the model. Having confidence in the parameters as well as observing a good match between measured and modeled responses means that the parameters and the model are valid, even if different responses or different frequency ranges are used.

IV. Practical Application of the l_1 Algorithm

Consider the l_1 optimization problem formulated in (17). The success of the new technique described relies upon the use of an efficient and robust l_1 algorithm. Recently, a superlinearly convergent algorithm for nonlinear l_1 optimization has been described [1]. The algorithm, based on the original work of Hald and Madsen [2], is a combination of a first-order method that approximates the solution by successive linear programming and a quasi-Newton method using approximate second-order information to solve the system of nonlinear equations resulting from the first-order necessary conditions for an optimum.

The most efficient use of the l_1 algorithm requires the user to supply function and gradient values of the individual functions in (17); i.e., network responses as well as their gradients are needed. Starting with the impedance or nodal admittance description of a network for which only input and output port responses are of interest, we have derived analytical formulas for evaluation of first-order sensitivities of two-port S parameters with respect to any circuit parameter appearing in the impedance or admittance matrix. The formulas and more explanation are given in the Appendix.

In many practical problems, e.g., in the presence of nonlinear devices or complicated field problems, the evaluation of gradients is not feasible. In such cases, it is possible to estimate the gradients using the numerical difference method. However, this is computationally slow and consequently expensive. To take advantage of a fast gradient-based approach, without requiring user-supplied gradients or using the numerical difference method, the original l_1 algorithm has been modified [3]. Different and flexible versions of the modified algorithm exist. A typical version estimates the gradients using the numerical difference method only once and updates the gradients with minimum extra effort by applying a variation of Broyden's formula as the optimization proceeds. All approximations are performed internally; therefore, the optimization could be linked to any analysis program which provides only the responses.

V. Examples

A. Modeling of Multicoupled Cavity Filters

Test 1: A sixth-order multicoupled cavity filter centered at 11785.5 MHz with a 56.2-MHz bandwidth is considered. Measurements on input and output return loss, insertion loss, and group delay of an optimally tuned filter and the same filter after a deliberate adjustment on the screw which dominantly controls coupling M_{12} were provided by ComDev Ltd., Cambridge, Canada [10]. Although the passband return loss changes significantly, we anticipate

TABLE II
RESULTS FOR THE SIXTH-ORDER FILTER EXAMPLE

Coupling	Original Filter	Perturbed Filter	Change in Parameter
M_{11}	-0 0473	-0 1472	-0 0999*
M_{22}	-0 0204	-0 0696	-0 0492*
M_{33}	-0 0305	-0 0230	0 0075
M_{44}	0 0005	0 0066	0 0061
M_{55}	-0 0026	0 0014	0 0040
M_{66}	0 0177	-0 0047	-0 0224
M_{12}	0.8489	0 7119	-0 1370*
M_{23}	0 6064	0 5969	-0 0095
M_{34}	0 5106	0 5101	-0 0005
M_{45}	0 7709	0 7709	0 0000
M_{56}	0 7898	0 7806	-0 0092
M_{36}	-0 2783	-0 2850	-0 0067

*Significant change in parameter value.

that such a physical adjustment affects only model parameters M_{12}, M_{11}, and M_{22} (the last two correspond to cavity resonant frequencies) in a dominant fashion, possibly with slight changes in other parameters.

Using the new technique described in this paper, we simultaneously processed measurements on passband return loss (input reflection coefficient with a weighting of 1) and stopband insertion loss (with a weighting of 0.05) of both filters, i.e., the original and perturbed models. The l_1 algorithm with exact gradients was used. The evaluation of sensitivities is discussed in detail by Bandler *et al.* [11]. The model parameters identified for the two filters are summarized in Table II. Figs. 3 and 4 illustrate the measured and modeled responses of the original filter and the filter after adjustment, respectively. An examination of the results in Table II and Figs. 3 and 4 shows that not only an excellent match between measured and modeled responses has been achieved, but also the changes in parameters are completely consistent with the actual physical adjustment. Therefore, by means of only one optimization, we have built confidence in the validity of the equivalent circuit parameters. The problem involved 84 nonlinear functions (42×2 responses for original and perturbed filters), 12 linear functions (change in parameters of two circuit equivalents), and 24 variables. The solution was achieved in 72 s of CPU time on the VAX 11/780 system.

Test 2: In this test, we used the new modeling technique to reject a certain set of parameters obtained for an eighth-order multicavity filter by proving their inconsistent behavior with respect to physical adjustments. We then improved the model by including an ideally zero stray coupling in the model and obtained parameters which not only produce a good match between measured and modeled responses, but also behave consistently when perturbed by a physical adjustment.

The eight-order filter is centered at 11 902.5 MHz with a 60-MHz bandwidth. Return loss and insertion loss

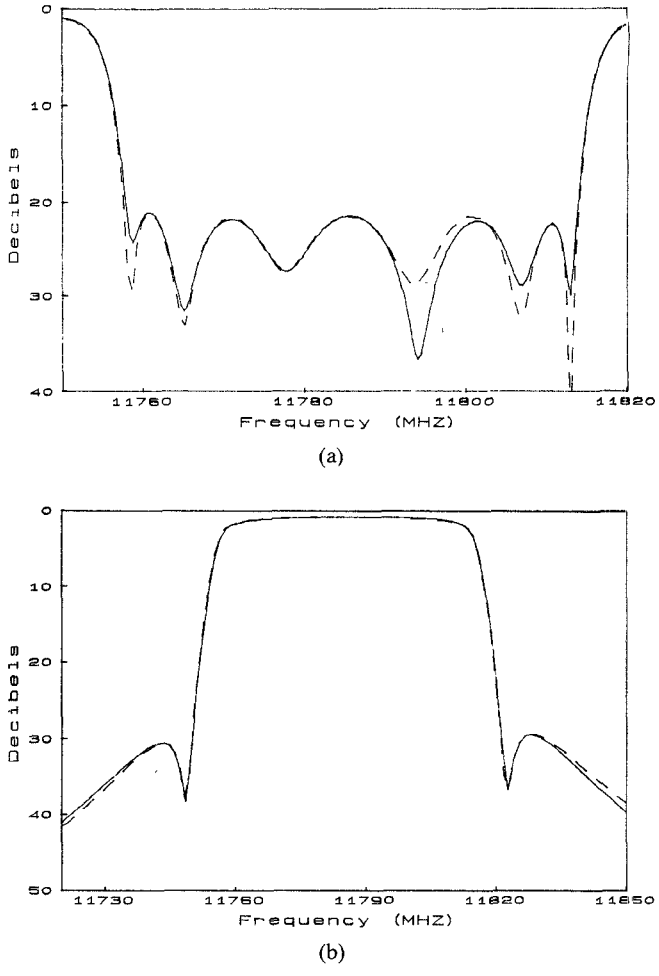

Fig. 3. (a) Input return loss and (b) insertion loss responses of the sixth-order filter before adjusting the screw. Solid line represents the modeled response and dashed line shows measurement data.

measurements of an optimally tuned filter and the same filter after an adjustment on the iris which dominantly controls coupling M_{23} were provided by ComDev Ltd [10]. Based on the physical structure of the filter, screw couplings M_{12}, M_{34}, M_{56}, and M_{78} and the iris couplings M_{23}, M_{14}, M_{45}, M_{67}, and M_{58}, as well as all cavity resonant frequencies and input–output couplings (transformer ratios), are anticipated as possible nonzero parameters to be identified.

In the first attempt, the stray coupling M_{36} was ignored and passband measurements on input and output return loss and stopband isolation for both filters were used to identify the parameters of the filters. The parameters are summarized in Table III. An examination of the results shows no apparent trend for the change in parameters; i.e., it would have been impossible to guess the source of perturbation (adjustment on the iris controlling M_{23}) from these results. This is the kind of inconsistency that would not have been discovered if only the original circuit had been considered.

In a second attempt, we included the stray coupling M_{36} in the circuit model and processed exactly the same measurements as before. Table III also contains the identified parameters of the two filters for this case. A compari-

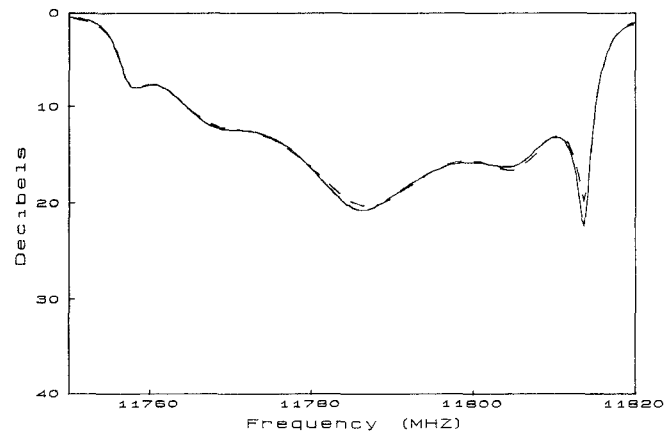

(a)

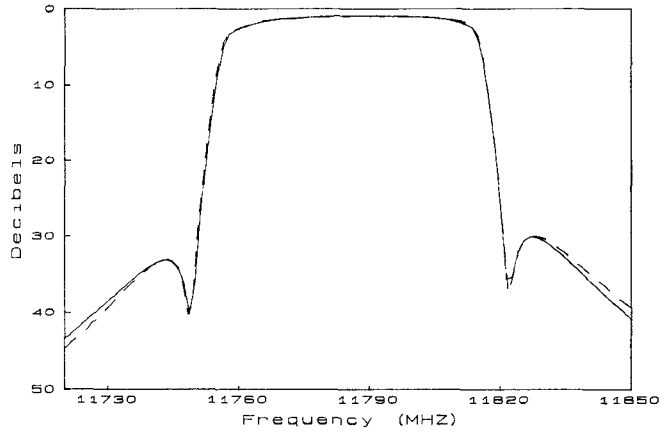

(b)

Fig. 4. (a) Input return loss and (b) insertion loss responses of the sixth-order filter after adjusting the screw. Solid line represents the modeled response and dashed line shows measurement data.

son of the original and perturbed filter parameters reveals that the significant change in couplings M_{12}, M_{23}, and M_{34} and cavity resonant frequencies M_{22} and M_{33} is absolutely consistent with the actual adjustment on the iris; i.e., by inspecting the change in parameters, it is possible to deduce which iris has been adjusted. The measured and modeled input return loss and insertion loss responses of the two filters are illustrated in Figs. 5 and 6. It is interesting to mention that the match between measured and modeled responses in the first attempt, where M_{36} was ignored and inconsistent parameters were found, is almost as good as the match in Figs. 5 and 6. This justifies the essence of this paper, which attempts to identify the most consistent set of parameters among many that produce a reasonable match between measured and calculated responses.

B. FET Modeling

Test 1: Device NEC700, for which measurement data are supplied with TOUCHSTONE, was considered. Using S-parameter data, single-circuit modeling with the l_1 objective was performed. The goal of this experiment was to prepare for the more complicated Test 2 by testing some common formulas and assumptions. The equivalent circuit

TABLE III
RESULTS FOR THE EIGHTH-ORDER FILTER EXAMPLE

	M_{36} ignored		M_{36} present	
Coupling	Original	Perturbed	Original	Perturbed
M_{11}	-0 0306	-0 1122	-0 0260	-0 0529
M_{22}	0 0026	-0 0243	0 0354	0 6503*
M_{33}	-0 0176	-0 0339	-0 0674	-0 6113*
M_{44}	-0 0105	-0 0579	-0 0078	-0 0151
M_{55}	-0 0273	-0 0009	-0 0214	0 0506
M_{66}	-0 0256	0 0457	-0 0179	-0 0027
M_{77}	-0 0502	0 0679	-0 0424	-0 0278
M_{88}	-0 0423	0 0594	-0 0426	-0 0272
M_{12}	0 7789	0 7462	0 3879	0 2876*
M_{23}	0 8061	0 8376	0 9990	0 8160*
M_{34}	0 4460	0 4205	0 0270	-0 1250*
M_{45}	0 5335	0 5343	0 4791	0 5105
M_{56}	0 5131	0 5373	0 5006	0 5026
M_{67}	0 7260	0 7469	0 6495	0 6451
M_{78}	0 8330	0 8476	0 8447	0 8463
M_{14}	0 3470	-0 3582	-0 7648	-0 7959
M_{58}	-0 1995	-0 1892	-0 1000	-0 0953
M_{36}	-	-	0 1314	0 1459

Input and output couplings: $n_1^2 = n_2^2 = 1.067$.
*Significant change in parameter value.

at normal operating bias (including the carrier) with 16 possible variables, as illustrated in Fig. 7, was used. An l_1 optimization with exact gradients, which are evaluated using the formulas derived in the Appendix, was performed. Measurement data were taken from 4 to 20 GHz. Table IV summarizes the identified parameters and Fig. 8 illustrates the measured and modeled responses.

Test 2: Using S-parameter data for the device B1824-20C from 4 to 18 GHz, Curtice and Camisa have achieved a very good model for the FET chip [12]. They have used the traditional least squares optimization of responses utilizing SUPER-COMPACT. Their success is due to the fact that they have reduced the number of possible variables in Fig. 7 from 16 to 8 by using dc and zero-bias measurements. We created two sets of artificial S-parameter measurements with TOUCHSTONE: one set using the parameters reported by Curtice and Camisa (operating bias $V_{ds} =$ 8.0 V, $V_{gs} = -2.0$ V, and $I_{ds} = 128.0$ mA) and the other by changing the values of C_1, C_2, L_g, and L_d to simulate the effect of taking different reference planes for the carriers. Both sets of data are shown in Fig. 9, where the S parameters of the two circuits are plotted on a Smith Chart.

Using the technique described in this paper, we processed the measurements on the two circuits simultaneously by minimizing the function defined in (15). The objective of this experiment is to show that even if the equivalent circuit parameters were not known, as is the case using real measurements, the consistency of the results would be

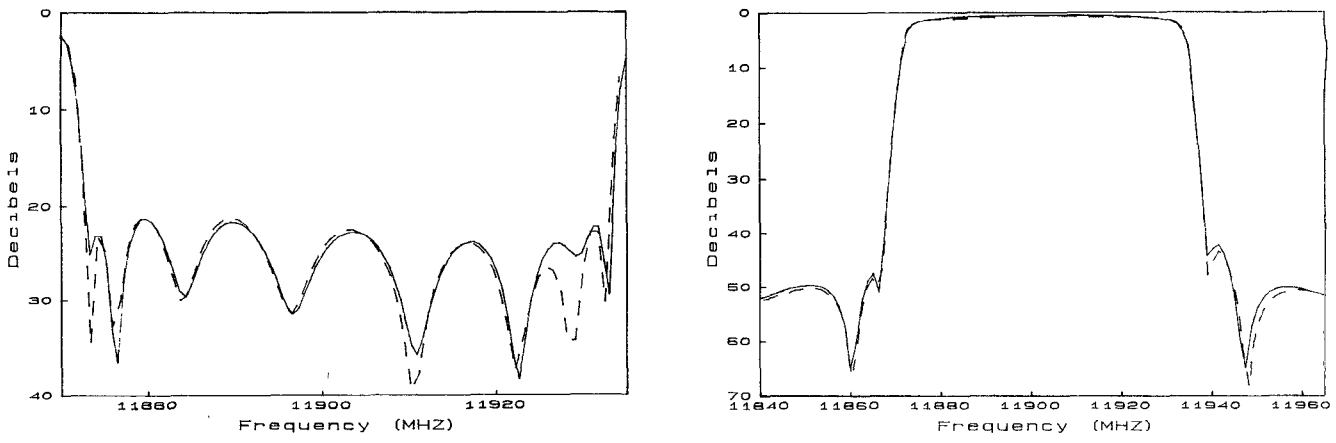

(a) (b)

Fig. 5. (a) Input return loss and (b) insertion loss of the eighth-order filter before adjusting the iris. Solid line represents the modeled response and dashed line shows the measurement data.

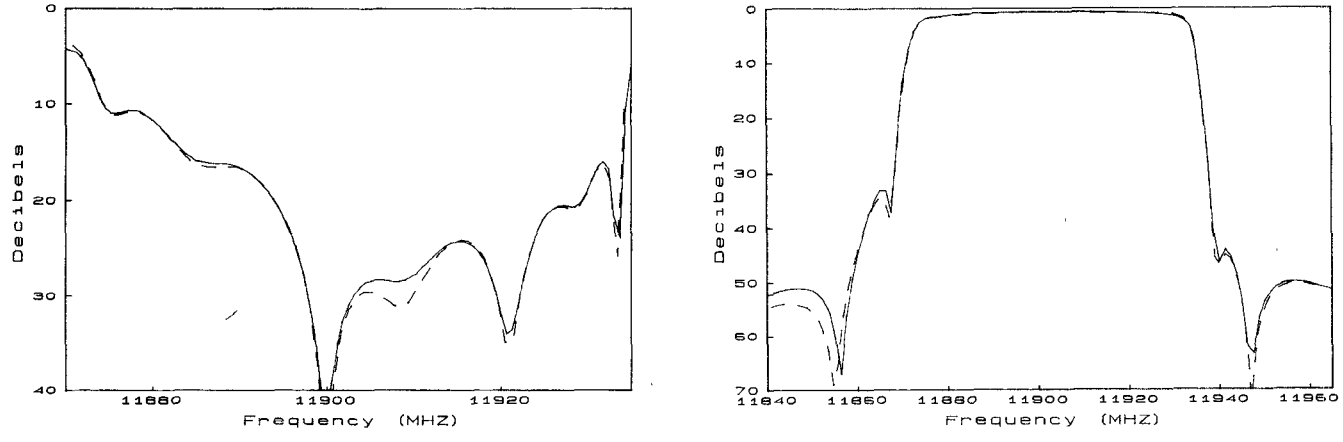

(a) (b)

Fig. 6. (a) Input return loss and (b) insertion loss of the eighth-order filter after adjusting the iris. Solid line represents the modeled response and dashed line shows the measurement data.

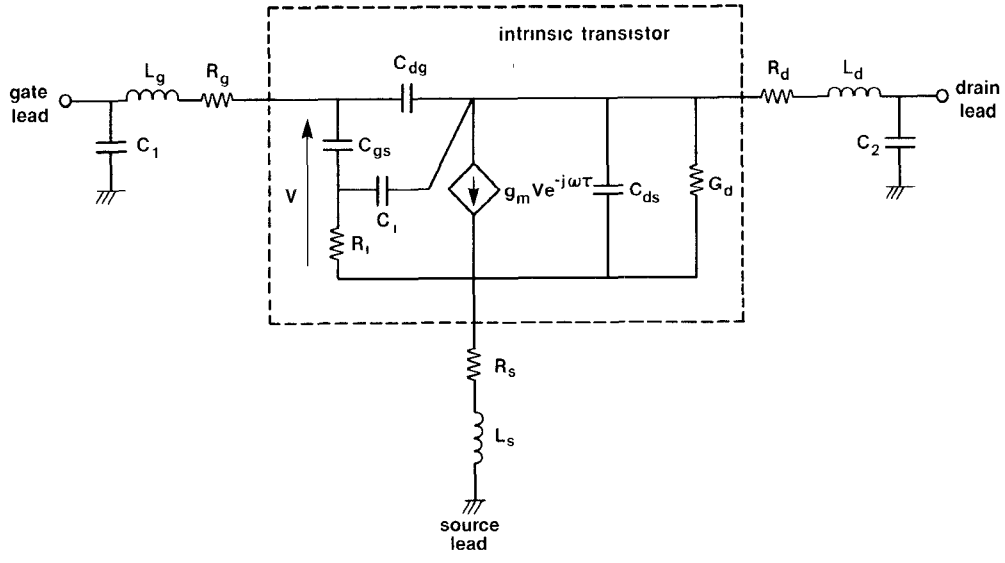

Fig. 7. Equivalent circuit of carrier-mounted FET.

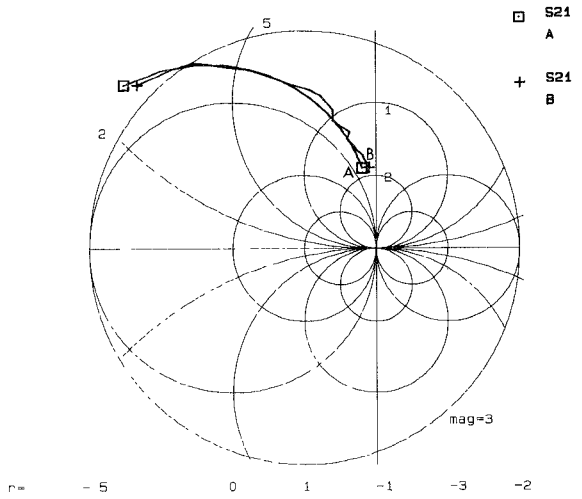

(a)

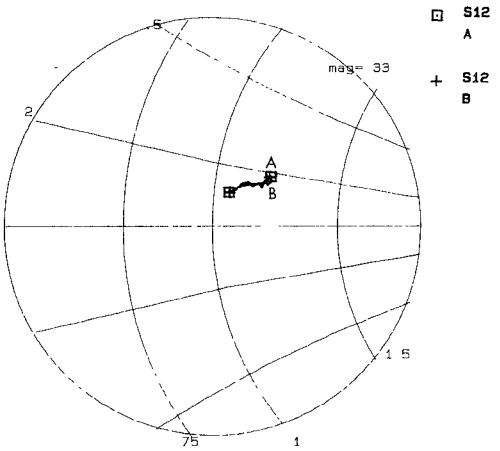

(b)

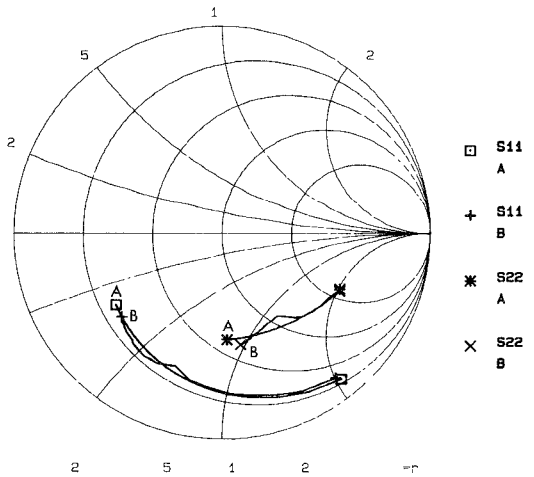

(c)

Fig. 8. Smith Chart display of S_{11}, S_{22}, S_{12}, and S_{21} in modeling of NEC700. The frequency range is 4–20 GHz. Points A and B mark the high-frequency end of modeled and measured responses, respectively.

TABLE IV
RESULTS FOR THE NEC700 FET EXAMPLE

Parameter		Value
C_1	(pF)	0 0448
C_2	(pF)	0 0058
C_{dg}	(pF)	0 0289
C_{gs}	(pF)	0 2867
C_{ds}	(pF)	0 0822
C_i	(pF)	0 0100
R_g	(Ω)	3 5000
R_d	(Ω)	2 0000
R_s	(Ω)	3 6270
R_i	(Ω)	7 3178
G_d^{-1}	(kΩ)	0 2064
L_g	(nH)	0 0585
L_d	(nH)	0 0496
L_s	(nH)	0 0379
g_m	(S)	0 0572
τ	(ps)	3 1711

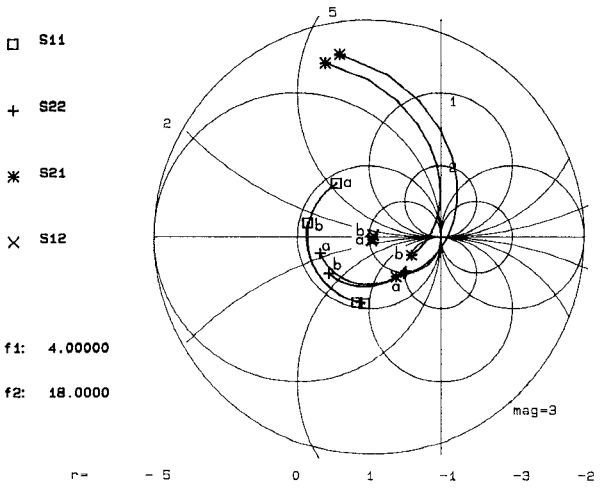

Fig. 9. Smith Chart display of S_{11}, S_{22}, S_{12}, and S_{21} for the carrier-mounted FET device B1824-20C before and after adjustment of parameters. Points a and b mark the high-frequency end of original and perturbed network responses, respectively.

proved only if the intrinsic parameters of the FET remain unchanged between the two circuits. This was indeed the case for the experiment performed. Although the maximum number of possible variables, namely 32 (16 for each circuit), was allowed for in the optimization, the intrinsic parameters were found to be the same between the two circuits and, as expected, C_1, C_2, L_g, and L_d changed from circuit 1 to 2. Table V summarizes the parameter values obtained. The problem involved 128 nonlinear functions (real and imaginary parts of four S parameters, at eight frequencies, for two circuits), 16 linear functions, and 32 variables. The CPU time on the VAX 11/780 system was 79 s.

TABLE V
RESULTS FOR THE GaAs FET B1824-20C EXAMPLE

Parameter		Original Circuit	Perturbed Circuit
C_1	(pF)	0 0440	0 0200*
C_2	(pF)	0 0389	0 0200*
C_{dg}	(pF)	0 0416	0 0416
C_{gs}	(pF)	0 6869	0 6869
C_{ds}	(pF)	0 1900	0 1900
C_i	(pF)	0 0100	0 0100
R_g	(Ω)	0 5490	0 5490
R_d	(Ω)	1 3670	1 3670
R_s	(Ω)	1 0480	1 0480
R_i	(Ω)	1 0842	1 0842
G_d^{-1}	(kΩ)	0 3761	0 3763
L_g	(nH)	0 3158	0 1500*
L_d	(nH)	0 2515	0 1499*
L_s	(nH)	0 0105	0 0105
g_m	(S)	0 0423	0 0423
τ	(ps)	7.4035	7 4035

*Significant change in parameter value.

VI. CONCLUSIONS

We have described a new technique for the modeling of microwave devices which exploits multicircuit measurements. The way in which the multicircuit measurements may contribute to the unique identification of parameters has been described mathematically with the help of a simple example. An optimization problem which is directly aimed at overcoming the nonuniqueness of parameters was formulated. A second formulation, which is aimed at the automatic verification of model parameters by checking the consistency of their behavior with respect to physical adjustments on the device, was proposed.

The use of the l_1 norm is an integral part of the approach. We discussed the use of an efficient l_1 algorithm both in problems for which gradient evaluation is possible (a set of useful formulas was presented) and in complicated problems for which gradient evaluation is not feasible. In the latter case, the technique described in this paper can be used in conjunction with widely used microwave design programs or in-house analysis programs employed in industry.

An important aspect of any optimization problem is the question of starting values. To address this problem, we recommend the use of l_1 optimization with simplified network equivalent models such as low-frequency models. In cases where little information about the range of parameter values is available, a common set of measurements can be used with different network equivalents (different topology) for the optimization. The solutions obtained using simplified models provide good starting values for multicircuit modeling with complicated network equivalents.

The results for the modeling of narrow-band multicoupled cavity filter and wide-band GaAs FET examples are very promising and completely justify the use of our multicircuit approach and formulation. The authors strongly believe that the use of multiple sets of measurements and a formulation which ties modeling (performed by computer) to the actual physical adjustments on the device will enhance further developments in modeling and tuning of microwave circuits.

ACKNOWLEDGMENT

The authors are pleased to acknowledge the assistance of R. Tong and H. AuYeung of ComDev Ltd., Cambridge, Canada, in preparing measurement data for multicoupled cavity filters.

APPENDIX
FIRST-ORDER SENSITIVITY EVALUATION FOR TWO-PORT S PARAMETERS

Here, the details for evaluating the first-order sensitivities of two-port S parameters with respect to the circuit elements are given. It is assumed that the nodal admittance matrix $\boldsymbol{Y}$ for the circuit model is available. For the case in which the impedance matrix is given, the approach is similar.

The open-circuit impedance matrix of the two-port is given by

$$z_{OC} = \begin{bmatrix} (\boldsymbol{Y}^{-1})_{11} & (\boldsymbol{Y}^{-1})_{1n} \\ (\boldsymbol{Y}^{-1})_{n1} & (\boldsymbol{Y}^{-1})_{nn} \end{bmatrix} \tag{A1}$$

where $\boldsymbol{Y}_{n\times n}$ is the admittance matrix arranged such that nodes 1 and n identify the ports at which S parameters are of interest.

Assuming that ϕ is a generic notation for a variable which appears in $\boldsymbol{Y}$ in the locations as shown below

$$\boldsymbol{Y} = \begin{array}{c} \\ i \\ \\ j \\ \\ \end{array} \begin{array}{c} \begin{array}{ccccc} & k & & l & \end{array} \\ \begin{bmatrix} \vdots & \vdots & & \vdots & \\ \cdots & \phi & \cdots & -\phi & \cdots \\ \vdots & \vdots & & \vdots & \\ \cdots & -\phi & \cdots & \phi & \cdots \\ \vdots & \vdots & & \vdots & \end{bmatrix} \end{array} \tag{A2}$$

it can be proved, after a few simple algebraic manipulations, that

$$z_{OC} = \begin{bmatrix} p_1 & q_1 \\ p_n & q_n \end{bmatrix} \tag{A3}$$

and

$$\frac{\partial z_{OC}}{\partial \phi} = -\begin{bmatrix} (\hat{p}_i - \hat{p}_j)(p_k - p_l) & (\hat{p}_i - \hat{p}_j)(q_k - q_l) \\ (\hat{q}_i - \hat{q}_j)(p_k - p_l) & (\hat{q}_i - \hat{q}_j)(q_k - q_l) \end{bmatrix} \tag{A4}$$

where vectors $\boldsymbol{p}$, $\hat{\boldsymbol{p}}$, $\boldsymbol{q}$, and $\hat{\boldsymbol{q}}$ are obtained by solving the

systems of equations

$$\boldsymbol{Y}\boldsymbol{p} = \boldsymbol{e}_1 \tag{A5a}$$

$$\boldsymbol{Y}^T\hat{\boldsymbol{p}} = \boldsymbol{e}_1 \tag{A5b}$$

$$\boldsymbol{Y}\boldsymbol{q} = \boldsymbol{e}_n \tag{A5c}$$

and

$$\boldsymbol{Y}^T\hat{\boldsymbol{q}} = \boldsymbol{e}_n \tag{A5d}$$

where $\boldsymbol{e}_1 = [\,1\ 0 \cdots 0]^T$ and $\boldsymbol{e}_n = [0 \cdots 0\ 1]^T$.

From a computational point of view, the solution to (A.5) requires only one LU factorization of $\boldsymbol{Y}$ (the LU factors of $\boldsymbol{Y}^T$ are obtained from LU factors of $\boldsymbol{Y}$ without calculations) and four forward and backward substitutions. Matrix $\boldsymbol{Y}$ is never inverted in the process.

The two-port S-parameter matrix and its sensitivities with respect to ϕ are then evaluated using the following relationships:

$$(\bar{\boldsymbol{z}} - \mathbf{1}) = \boldsymbol{S}(\bar{\boldsymbol{z}} + \mathbf{1}) \tag{A6}$$

and

$$\frac{\partial \boldsymbol{S}}{\partial \phi} = \frac{1}{2Z_0}(\mathbf{1} - \boldsymbol{S})\frac{\partial z_{OC}}{\partial \phi}(\mathbf{1} - \boldsymbol{S}) \tag{A7}$$

where

$$\bar{\boldsymbol{z}} = \frac{1}{Z_0}\boldsymbol{z}_{OC} \tag{A8}$$

and

$$\boldsymbol{S} = \begin{bmatrix} S_{11} & S_{12} \\ S_{21} & S_{22} \end{bmatrix} \tag{A9}$$

with Z_0 denoting the normalizing impedance and $\mathbf{1}$ representing the 2×2 unit matrix.

The sensitivities of $\boldsymbol{S}$ with respect to circuit elements can be evaluated using $\partial \boldsymbol{S}/\partial \phi$. For instance, for transconductance parameter g_m and delay τ associated with a VCCS in the circuit, we have $\partial \boldsymbol{S}/\partial g_m = e^{-j\omega\tau}\,\partial \boldsymbol{S}/\partial \phi$ and $\partial \boldsymbol{S}/\partial \tau = -\,j\omega g_m e^{-j\omega\tau}\,\partial \boldsymbol{S}/\partial \phi$, where $\phi = g_m e^{-j\omega\tau}$.

References

[1] J. W. Bandler, W. Kellermann, and K. Madsen, "A superlinearly convergent algorithm for nonlinear l_1 optimization with circuit applications," in *Proc. IEEE Int. Symp. Circuits and Systems* (Kyoto, Japan), 1985, pp. 977–980.

[2] J. Hald and K. Madsen, "Combined LP and quasi-Newton methods for nonlinear l_1 optimization," *SIAM J. Numer. Anal.*, vol. 22, pp. 68–80, 1985.

[3] J. W. Bandler, S. H. Chen, S. Daijavad, and K. Madsen, "Efficient gradient approximations for nonlinear optimization of circuits and systems," in *Proc. IEEE Int. Symp. Circuits and Systems* (San Jose, CA), 1986, pp. 964–967.

[4] *SUPER-COMPACT User's Manual*, COMSAT General Integrated Systems Inc., Palo Alto, CA, 1984.

[5] TOUCHSTONE User's Manual, EEsof Inc., Westlake Village, CA, 1986.

[6] R. H. Bartels and A. R. Conn, "An approach to nonlinear l_1 data fitting," Computer Science Department, University of Waterloo, Rep. CS-81-17, 1981.

[7] R. A. El-Attar, M. Vidyasagar, and S. R. K. Dutta, "An algorithm for l_1-norm minimization with application to nonlinear l_1-approximation," *SIAM J. Numer. Anal.*, vol. 16, pp. 70–86, 1979.

[8] J. W. Bandler and A. E. Salama, "Fault diagnosis of analog circuits," *Proc. IEEE*, vol. 73, pp. 1279–1325, 1985.

[9] J. W. Bandler and A. E. Salama, "Functional approach to microwave postproduction tuning," *IEEE Trans. Microwave Theory Tech.*, vol. MTT-33, pp. 302–310, 1985.

[10] ComDev Ltd., 155 Sheldon Drive, Cambridge, Ontario, Canada N1R 7H6, private communication, 1985.

[11] J. W. Bandler, S. H. Chen, and S. Daijavad, "Exact sensitivity analysis for optimization of multi-coupled cavity filters," *Int. J. Circuit Theory and Applic.*, vol. 14, pp. 63–77, 1986.

[12] W. R. Curtice and R. L. Camisa, "Self-consistent GaAs FET models for amplifier design and device diagnostics," *IEEE Trans. Microwave Theory Tech.*, vol. MTT-32, pp. 1573–1578, 1984.

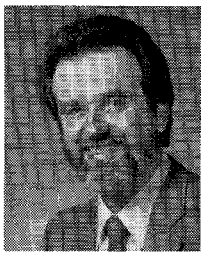

John W. Bandler (S'66–M'66–SM'74–F'78) was born in Jerusalem, Palestine, on November 9, 1941. He studied at Imperial College of Science and Technology, London, England, from 1960–1966. He received the B.Sc. (Eng.), Ph.D., and D.Sc. (Eng.) degrees from the University of London, London, England, in 1963, 1967, and 1976, respectively.

He joined Mullard Research Laboratories, Redhill, Surrey, England, in 1966. From 1967 to 1969, he was a postdoctorate fellow and sessional lecturer at the University of Manitoba, Winnipeg, Canada. He joined McMaster University, Hamilton, Canada, in 1969, where he is currently a Professor of electrical and computer engineering. He has served as Chairman of the Department of Electrical Engineering and Dean of the Faculty of Engineering. He currently directs research, which has received substantial support by the Natural Sciences and Engineering Research Council of Canada under its Operating and Strategic Grants Awards, in the Simulation Optimization Systems Research Laboratory. Dr. Bandler is also currently president of Optimization Systems Associates, Inc. He has provided consulting services and software to numerous organizations in the electronic, microwave, and electrical power industry, specializing in advanced applications of simulation, sensitivity analysis, and mathematical optimization techniques.

Dr. Bandler is a contributor to *Modern Filter Theory and Design* (Wiley-Interscience, 1973). He has more than 210 publications, four of which appear in *Computer-Aided Filter Design* (IEEE Press, 1973), one in *Microwave Integrated Circuits* (Artech House, 1985), and one in *Low-Noise Microwave Transistors and Amplifiers* (IEEE Press, 1981). Dr. Bandler was an Associate Editor of the IEEE TRANSACTIONS ON MICROWAVE THEORY AND TECHNIQUES (1969–1974). He was Guest Editor of the special issue of the IEEE TRANSACTIONS ON MICROWAVE THEORY AND TECHNIQUES on Computer-Oriented Microwave Practices (March 1974). Dr. Bandler is a Fellow of the Royal Society of Canada and of the Institution of Electrical Engineers (Great Britain). He is a member of the Association of Professional Engineers of the Province of Ontario (Canada).

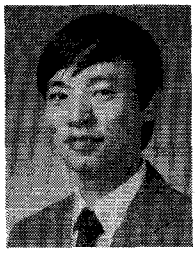

Shao Hua Chen (S'84) was born in Swatow, Guangdong, China, on September 27, 1957. He received the B.S. degree from South China Institute of Technology, Guangzhou, China, in 1982.

From July 1982 to August 1983, he was with the Department of Automation, South China Institute of Technology, Guangzhou, China, as a teaching assistant. He was awarded a Chinese Government Scholarship and joined the Department of Electrical and Computer Engineering, McMaster University, Hamilton, Canada, in September 1983, where he is currently a teaching assistant and graduate student working towards the Ph.D. degree. He has been awarded an Ontario Graduate Scholarship for the academic years 1985/86 and 1986/87. His research interests are in optimization methods, sensitivity analysis, modeling, tuning, and CAD software on personal computers.

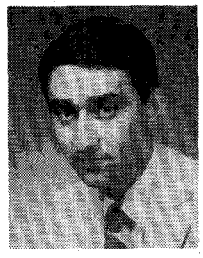

Shahrokh Daijavad (S'82) was born in Isfahan, Iran, on July 7, 1960. He received the B.Eng. (summa cum laude) and Ph.D. degrees in electrical engineering from McMaster University, Hamilton, Ontario, Canada, in 1983 and 1986, respectively.

From 1983 to 1986, he worked as a teaching assistant in the Department of Electrical and Computer Engineering, McMaster University, while holding an Ontario Graduate Scholarship from 1983 to 1985 and a Natural Sciences and Engineering Research Council of Canada Scholarship from 1985 to 1986. His research interests are in computer-aided design with emphasis on applications of optimization theory in modeling, fault location, and tuning.

Reprint 2

A Nonlinear ℓ_1 Optimization Algorithm for Design, Modeling and Diagnosis of Networks

Transaction Briefs

A Nonlinear l_1 Optimization Algorithm for Design, Modeling, and Diagnosis of Networks

JOHN W. BANDLER, FELLOW, IEEE, WITOLD KELLERMANN, MEMBER, IEEE, AND KAJ MADSEN

Abstract—**This paper presents a fast and highly efficient algorithm for nonlinear l_1 optimization and its applications to circuits employing the properties of the l_1 norm. The algorithm, based on the work of Hald and Madsen, is similar to a minimax algorithm originated by the same authors. It is a combination of a first-order method that approximates the solution by successive linear programming and a quasi-Newton method using approximate second-order information to solve a system of nonlinear equations resulting from the first-order necessary conditions for an optimum. The new l_1 algorithm is particularly useful in fault location methods using the l_1 norm. A new technique for isolating the most likely faulty elements, based on an exact penalty function, is presented. Another important application of the algorithm is the design of contiguous-band multiplexers consisting of multicavity filters distributed along a waveguide manifold which is illustrated by a 12-channel multiplexer design. We also present a formulation using the l_1 norm for model parameter identification problems in the presence of large isolated errors in measurements and illustrate it with a sixth-order filter.**

I. Introduction

The optimization problem to be considered has the following mathematical formulation:

Let $f_j(\boldsymbol{x}) = f_j(x_1, \cdots, x_n)$, $j = 1, \cdots, m$, be a set of m nonlinear, continuously differentiable functions. The vector $\boldsymbol{x} \triangleq [x_1\ x_2 \cdots x_n]^T$ is the set of n parameters to be optimized. We consider the following problem:

$$\underset{\boldsymbol{x}}{\text{minimize}}\ \boldsymbol{F}(\boldsymbol{x}) \triangleq \sum_{j=1}^{m} |f_j(\boldsymbol{x})|$$

subject to

$$\begin{aligned} \boldsymbol{a}_i^T\boldsymbol{x} + b_i &= 0, \qquad i = 1, \cdots, l_{\text{eq}} \\ \boldsymbol{a}_i^T\boldsymbol{x} + b_i &\geq 0, \qquad i = (l_{\text{eq}}+1), \cdots, l \end{aligned} \tag{1}$$

where $\boldsymbol{a}_i$ and b_i, $i = 1, \cdots, l$, are constants. This is called the linearly constrained l_1 problem.

The problem arises in a variety of areas. The most popular application of the l_1 norm is the problem of approximating a function to data that might be contaminated with some wild points or gross errors. In this case, the minimization of the l_1 norm residual is superior to using other norms l_p with $p > 1$ [1]. The larger the value of p, the more focus is put on the data points with largest deviation from the approximating function.

The number of applications of the l_1 norm to circuit problems is increasing. The l_1 norm has been successfully used to isolate the most likely faulty elements in fault isolation techniques for linear analog circuits [2]. We present a new technique for isolating the most likely faulty elements which is based on an exact penalty function.

Another important application of the l_1 norm is the functional approach to post-production tuning [3], where the l_1 type of objective function is used to select the number of tunable parameters needed to tune all possible outcomes of a manufactured design.

In this paper, the l_1 norm is employed in a general multiplexer design procedure and in model parameter identification from measurements with large isolated errors. Therefore, a highly efficient and fast algorithm for l_1 optimization is of great importance to many circuit designers and engineers. It is the purpose of this paper to present such an algorithm.

We present an iterative algorithm for solving (1), which requires the user to supply function and gradient values of the nonlinear functions f_j. The algorithm also uses some second-order information, i.e., information about the second-order derivatives of the functions. This is approximated from the user-supplied gradients.

The algorithm is similar to that of Hald and Madsen in [4]. It has been reported by Hald in [5], which describes and lists a Fortran subroutine implementing a version of the algorithm. Hald and Madsen [6] have demonstrated that the algorithm has sure convergence properties. Their results indicate that this algorithm may be the best of its class currently available. A survey of l_1 algorithms has also been given in [6].

The plan of the paper is as follows. The algorithm of this paper is described in more detail in Section II, where the two methods (namely, the first-order method and the approximate second-order method) are presented and the switching conditions between the two methods are given. A new technique for isolating the most likely faulty elements, based on an exact penalty function, is presented in Section III and illustrated by a simple mesh network example. In Section IV, we describe an optimization procedure using the l_1 norm for contiguous-band multiplexer design. Section V illustrates the application of the l_1 norm to model parameter identification from measurements. We conclude in Section VI with an assessment of the potential impact of the l_1 algorithm in the area of circuit design, fault location, and model parameter identification.

II. Description of the Algorithm

The algorithm of this paper is based on the work of Hald and Madsen [6]. It is a hybrid method combining a first-order method with an approximate second-order method. The first-order method is a robust trust region method which provides convergence to the neighborhood of a solution. It is based on linear model problems. These are solved subject to the constraints of the original problem (1) and a bound on the step length $\|\boldsymbol{h}\|$. The

Manuscript received August 7, 1985; revised May 12, 1986. This work was supported in part by the Natural Sciences and Engineering Research Council of Canada under Grants A7239 and G1135.

J. W. Bandler is with the Simulation Optimization Systems Research Laboratory and the Department of Electrical and Computer Engineering, McMaster University, Hamilton, Canada L8S 4L7. He is also with Optimization Systems Associates Inc., Dundas, Ontario, Canada, L9H 6L1.

W. Kellermann is with Ontario Hydro, Toronto, Canada, M5G 1X6.

K. Madsen is with the Institute for Numerical Analysis, Technical University of Denmark, Building 303, DK-2800 Lyngby, Denmark.

IEEE Log Number 8611460.

0098-4094/87/0200-0174$01.00 ©1987 IEEE

latter bound reflects the neighborhood of the iterate x_k in which the kth model function (see (2)) is a good approximation to the nonlinear l_1 function. When a good approximation to the solution seems to have been obtained, then a higher order method must be used in order to obtain a fast ultimate rate of convergence. Therefore, a switch is made to a quasi-Newton method that solves a set of nonlinear equations that necessarily hold at a solution of (1). This method has superlinear final convergence. Several switches between the first-order and the quasi-Newton method may take place. The reason for allowing this is that the latter method works only close to a solution so that, if it is started too early, a switch back to the (more robust) trust region method is necessary. Notice that the user of this algorithm is required to supply function values and first-order derivatives, whereas the necessary second derivative information is generated by the algorithm.

We now give a detailed description of the method which is a combination of Method 1 and Method 2. We first describe the two basic methods and next the combined method, including switching rules.

A. Method 1

This is a method providing global convergence. At the kth step a feasible approximation x_k to a solution of (1) and a local bound Λ_k are given. In order to find a better estimate, the following linearized problem is solved:

$$\underset{h}{\text{minimize}}\, \bar{F}(x_k, h) \triangleq \sum_{j=1}^{m} |f_j(x_k) + f_j'(x_k)^T h|$$

subject to

$$\begin{aligned} &\|h\|_\infty \leq \Lambda_k \\ &a_i^T(x_k + h) + b_i = 0, \qquad i = 1, \cdots, l_{\text{eq}}, \\ &a_i^T(x_k + h) + b_i \geq 0, \qquad i = (l_{\text{eq}} + 1), \cdots, l. \end{aligned} \tag{2}$$

The solution of (2), h_k, may be found by a standard linear programming routine. However, we use an implementation of the algorithm of Bartels, Conn, and Sinclair [7], which is more efficient. Notice that $(x_k + h_k)$ is feasible.

The next iterate is $(x_k + h_k)$ provided that this point is better than x_k in the sense of F, i.e., if $F(x_k + h_k) < F(x_k)$. Otherwise, $x_{k+1} = x_k$.

The local bound Λ_k is adjusted in every iteration based on comparison between the decrease in the nonlinear objective function and the decrease predicted by the model $\bar{F}$. If the ratio between the two is small

$$F(x_k) - F(x_k + h_k) \leq 0.25[\bar{F}(x_k, 0) - \bar{F}(x_k, h_k)] \tag{3}$$

then the bound is decreased: $\Lambda_{k+1} = \Lambda_k/4$. Otherwise, if

$$F(x_k) - F(x_k + h_k) \geq 0.75[\bar{F}(x_k, 0) - \bar{F}(x_k, h_k)] \tag{4}$$

then $\Lambda_{k+1} = 2\Lambda_k$. If neither (3) nor (4) hold, then we leave the bound unchanged, $\Lambda_{k+1} = \Lambda_k$.

Experiments have shown that the method is insensitive to small changes in the constants used in this updating procedure of the local bound. Notice that if the new point $(x_k + h_k)$ is not accepted, then the bound is decreased.

B. Method 2

This is a local method. It is assumed that a point near a solution x^* is known and that the set of zero functions

$$Z(x^*) \triangleq \{ j | f_j(x^*) = 0 \} \tag{5}$$

and the set of active constraints

$$A(x^*) \triangleq \{ i | a_i^T x^* + b_i = 0 \} \tag{6}$$

are known.

At a solution x^* of the linearly constrained l_1 problem (1), the functions whose values are zero play a special role since they contribute to the kinks of F. The functions which are nonzero at x^* give smooth contributions to F since $|f_j(x)|$ is smooth near x^* when $f_j(x^*) \neq 0$. Therefore, we partition F into a smooth and a nonsmooth part

$$\begin{aligned} F(x) &= \sum_{j \notin Z} |f_j(x)| + \sum_{j \in Z} |f_j(x)| \\ &= g(x) + \sum_{j \in Z} |f_j(x)| \end{aligned}$$

where $Z = Z(x^*)$ is defined by (5) and $g = g(x^*)$ is smooth in a neighborhood of x^*.

It is easily shown (see for instance Charalambous, [8]) that the following set of equations hold at the local minimum $x = x^*$:

$$\begin{aligned} g'(x) + \sum_{j \in Z} \delta_j f_j'(x) - \sum_{i \in A} \mu_i a_i &= 0 \\ f_j(x) &= 0, \qquad j \in Z \\ a_i^T x + b_i &= 0, \qquad i \in A \end{aligned} \tag{7}$$

where $|\delta_j| \leq 1$, $\mu_i \geq 0$, $Z = Z(x^*)$ and $A = A(x^*)$ are defined by (5) and (6), and

$$g(x) = \sum_{j \notin Z} |f_j(x)|.$$

This set of equations corresponds to the Kuhn-Tucker conditions for the nonlinear programming problem which is equivalent to (1). The unknowns are x, δ_j, and μ_i, and it is seen that the number of unknowns equals the number of equations. If we use vector notation, (7) can be expressed as follows:

$$R(x, \delta, \mu) = 0. \tag{8}$$

Method 2 is an approximate Newton method for solving the nonlinear system (7) (in the variables (x, δ, μ)). Exact first derivatives are used but the matrix

$$g''(x^*) + \sum_{j \in Z} \delta_j f_j''(x^*)$$

is approximated using a modified Broyden-Fletcher-Goldfarb-Shanno update. In this way, an approximate Jacobian J_k is obtained at the estimate $(x_k, \delta^{(k)}, \mu^{(k)})$ of the solution of (7). The next estimate is obtained by

$$\begin{aligned} J_k \begin{bmatrix} \Delta x_k \\ \Delta\delta^{(k)} \\ \Delta\mu^{(k)} \end{bmatrix} &= -R(x_k, \delta^{(k)}, \mu^{(k)}) \\ (x_{k+1}, \delta^{(k+1)}, \mu^{(k+1)}) &= (x_k, \delta^{(k)}, \mu^{(k)}) \\ &\quad + (\Delta x_k, \Delta\delta^{(k)}, \Delta\mu^{(k)}) \end{aligned} \tag{9}$$

where R is defined by (8). Notice that no line search is involved.

C. The Combined Method

The combined method is the algorithm which we recommend to use in this paper. Method 1 is intended to provide the global convergence and Method 2 is used to obtain fast local convergence.

Initially, Method 1 is used and the sets (5) and (6) are estimated. When a local minimum seems to be approached, a

switch to Method 2 is made. If the Method 2 iteration is unsuccessful, then Method 1 is used again. Several switches between the two methods may take place. When Method 1 is used, we say that the iteration is in Stage 1; otherwise, it is in Stage 2. A detailed description of the two stages follows.

D. The Stage 1 Iteration

We have a point x_k, a local bound Λ_k, and a matrix J_k which should approximate the Jacobian of (7).

1) x_{k+1} and Λ_{k+1} are found using Method 1, and approximations Z_{k+1} and A_{k+1} of the sets (5) and (6) are found via the zero and active sets at the solution h_k of the linear model problem (2).

2) An estimate $(\delta^{(k+1)}, \mu^{(k+1)})$ of the multipliers is found through a least-squares solution of (A1) with $(x_{k+1}, Z_{k+1}, A_{k+1})$ inserted for $(x, Z(x), A(x))$. This estimate is used for finding a new Jacobian estimate J_{k+1} by the BFGS method.

3) A switch to Stage 2 is made if the following two conditions hold:

(a) the estimates Z_{k+1} and A_{k+1} have been constant over v consecutive different Stage 1 iterates ($v \geq 3$);

(b) the multiplier estimates are in the correct ranges

$$|\delta_j^{(k+1)}| \leq 1$$

$$\mu_j^{(k+1)} \geq 0.$$

E. The Stage 2 Iteration

We have an estimate $(x_k, \delta^{(k)}, \mu^{(k)})$, estimates Z_k and A_k of (5) and (6), and a matrix J_k which should approximate the Jacobian of (7).

1) Find $(x_{k+1}, \delta^{(k+1)}, \mu^{(k+1)})$ and J_{k+1} using Method 2 with (Z_k, A_k) inserted for $(Z(x^*), A(x^*))$.

2) Let $A_{k+1} = A_k$, $Z_{k+1} = Z_k$ and $\Lambda_{k+1} = \Lambda_k$.

3) Switch to Stage 1 if one of the following conditions holds:

(a) a function f_j with $j \notin Z_k$ has changed sign, or a constraint corresponding to an index i with $i \notin A_k$ has become violated;

(b) a component of $\delta^{(k+1)}$ or of $\mu^{(k+1)}$ is outside its range

$$|\delta_j^{(k+1)}| > 1$$

or

$$\mu_j^{(k+1)} < 0$$

(c) $\|R(x_{k+1}, \delta^{(k+1)}, \mu^{(k+1)}\| > 0.999\|R(x_k, \delta^{(k)}, \mu^{(k)})\|$ (see (8) for the definition of R).

This completes the description of the combined method.

It has been shown by Hald and Madsen [6] that the method has safe global convergence properties: it can only converge to stationary points. Furthermore, the final rate of convergence is at least superlinear, i.e.,

$$\|x_{k+1} - x^*\| \leq \epsilon_k \|x_k - x^*\| \tag{10}$$

where $\epsilon_k \to 0$ for $k \to \infty$.

III. Fault Isolation Using the l_1 Norm

A. Formulation of the Problem

In this section, we deal with fault isolation in linear analog circuits under an insufficient number of independent voltage measurements. The l_1 norm is used to isolate the most likely faulty elements. Practically, the faulty components are very few and the relative change in their values is significantly larger than in the nonfaulty ones [9].

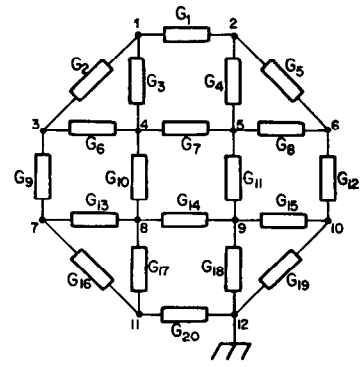

Fig. 1. The resistive mesh network.

The method presented here is a modification of the method utilizing multiple test vectors to obtain the measurements [2].

For k different excitations applied to the faulty network, we consider the following optimization problem:

$$\underset{x}{\text{minimize}} \sum_{i=1}^{n} |\Delta x_i / x_i^0| \tag{11a}$$

subject to

$$V_1^c - V_1^m = 0$$

$$\vdots$$

$$V_k^c - V_k^m = 0 \tag{11b}$$

where $x \triangleq [x_1 \quad x_2 \quad \cdots \quad x_n]^T$ is a vector of network parameters, x^0 represents the nominal parameter values, $\Delta x_i \triangleq x_i - x_i^0$, $i = 1,2,\cdots,n$, represent the deviations in network parameters from nominal values, V_k^m is a p-dimensional vector of voltage measurements performed at the accessible nodes for the kth excitation, and V_k^c is a p-dimensional vector of voltages at accessible nodes calculated using the vector x as parameter values.

The corresponding nonlinear l_1 problem can be formulated based on an exact penalty function [8] as follows:

$$\underset{x}{\text{minimize}} \sum_{j=1}^{n+k\times p} |f_j(x)| \tag{12}$$

where

$$f_i(x) \triangleq \Delta x_i / x_i^0, \qquad i = 1,2,\cdots,n \tag{13}$$

$$f_{n+i}(x) \triangleq \beta_i (V_i^c - V_i^m), \qquad i = 1,2,\cdots,k\times p \tag{14}$$

and β_i, $i = 1,2,\cdots,k\times p$, are appropriate multipliers (satisfying certain conditions stated in [8]).

B. Mesh Network Example [2]

Consider the resistive network shown in Fig. 1 with the nominal values of elements $G_i = 1.0$ and tolerances $\epsilon_i = \pm 0.05$, $i = 1,2,\cdots,20$. All outside nodes are assumed to be accessible with node 12 taken as the reference node. Nodes 4, 5, 8, and 9 are assumed internal, where no measurements can be performed.

Two faults are assumed in the network in elements G_2 and G_{18}. For Case 1, we applied the new l_1 algorithm to optimization problem (12) with a single excitation at node 1. For Case 2, we considered two excitations applied at nodes 3 and 6 sequentially. The results of both optimization problems are summarized in Table I. The nominal component values have been used as a

TABLE I
RESULTS FOR THE MESH NETWORK EXAMPLE

Element	Nominal Value	Actual Value	Percentage Deviation		
			Actual	Case 1	Case 2
G_1	1.0	0.98	-2.0	0.00	0.13
G_2	1.0	0.50	-50.0*	-48.78	-49.44
G_3	1.0	1.04	4.0	0.00	3.60
G_4	1.0	0.97	-3.0	0.00	0.00
G_5	1.0	0.95	-5.0	-2.26	-1.71
G_6	1.0	0.99	-1.0	0.00	0.00
G_7	1.0	1.02	2.0	0.00	0.00
G_8	1.0	1.05	5.0	0.00	0.00
G_9	1.0	1.02	2.0	2.80	0.97
G_{10}	1.0	0.98	-2.0	0.00	0.00
G_{11}	1.0	1.04	4.0	0.00	0.00
G_{12}	1.0	1.01	1.0	3.45	2.08
G_{13}	1.0	0.99	-1.0	0.00	-0.44
G_{14}	1.0	0.98	-2.0	0.00	0.00
G_{15}	1.0	1.02	2.0	0.00	1.55
G_{16}	1.0	0.96	-4.0	-2.42	-5.71
G_{17}	1.0	1.02	2.0	0.00	2.67
G_{18}	1.0	0.50	-50.0*	-52.16	-48.94
G_{19}	1.0	0.98	-2.0	0.00	-1.95
G_{20}	1.0	0.96	-4.0	-3.67	-4.88
Number of Function Evaluations				8	8
Execution Time (secs) on Cyber 170/815				3.0	3.9

* Faults

starting point since just a few elements change significantly from nominal.

In both cases, the actual faulty elements have been identified, but in Case 2, the estimated changes in the faulty elements are closer to their true values. Also, some of the changes in the nonfaulty components approach better their true values in Case 2.

The estimated changes in the faulty elements are much closer to the actual changes as compared to the results reported in [2].

IV. CONTIGUOUS-BAND MULTIPLEXER DESIGN USING THE l_1 NORM

A. Introductory Remarks

Practical design and manufacture of contiguous- and noncontiguous-band microwave multiplexers consisting of multicavity filters distributed along a waveguide manifold has been a problem of significant interest [10]–[13]. Recently, a general multiplexer optimal design procedure using a powerful gradient-based minimax algorithm has been described [14]. The simulation and sensitivity analysis aspect of the problem together with a number of examples of multiplexer optimization have been presented in [15]. A typical structure under consideration is shown in Fig. 2. All design parameters of interest, e.g., waveguide spacings, input–output, and filter coupling parameters, can be directly optimized. A wide range of possible multiplexer optimization problems can be formulated and solved by appropriately defining specifications on common port return loss and individual channel insertion loss functions.

A major task in designing a multiplexer is to determine the location of the channel filters along the waveguide manifold [12]. This is very important for designs using the common port return loss as the only optimization criterion. A typical value of lower specification on return loss over the passbands of all multiplexer channels is 20 dB.

The error functions $f_j(\boldsymbol{x})$, $j \in J$, are of the form

$$-w_L(\omega_i)\left(F(\boldsymbol{x},\omega_i)-S_L(\omega_i)\right) \tag{15}$$

where $F(\boldsymbol{x},\omega_i)$ is the return loss at the common port at the ith frequency, $S_L(\omega_i)$ is the lower specification on return loss at the ith frequency, $\boldsymbol{x} \triangleq [x_1 \quad x_2 \quad \cdots \quad x_n]^T$ is the vector of design parameters, and w_L is an arbitrary user chosen nonnegative weighting factor.

If we perform a minimax optimization based on these error functions and, at the solution, the minimax objective function value is negative, then the goal has been achieved. In many cases, however, using the filter spacings as the only optimization variables may not be sufficient to satisfy all specifications, and minimax optimization gives results corresponding to the situation where the specification violations are distributed over all multiplexer channels. In that case, the use of the one-sided l_1 optimization of the same error functions may lead to more desirable results where the violations occur only over a few multiplexer channels. This process of identifying "bad channels" has two very important consequences. First, the results indicate in which channels the additional variables have to be released to improve locally (in the frequency domain) the performance of the multiplexer, and second, it gives very good starting values of the waveguide spacings to be used in the subsequent minimax optimization. The idea presented is illustrated by designing a 12-GHz, 12-channel multiplexer without dummy channels. The 12-channel contiguous-band multiplexer has a channel frequency separation of 40 MHz and a usable bandwidth of 39 MHz with the center frequency of channel no. 1 being 12 180.0 MHz.

B. 12-Channel 12-GHz Multiplexer Design

Suppose we want to design this multiplexer such that a lower specification of 20 dB on the common port return loss over the passbands of all 12 channels should be satisfied.

We start the design process with 12 identical sixth-order filters with the coupling coefficients given in the following matrix [16]:

$$M = \begin{bmatrix} 0 & 0.594 & 0 & 0 & 0 & 0 \\ 0.594 & 0 & 0.535 & 0 & 0 & 0 \\ 0 & 0.535 & 0 & 0.425 & 0 & -0.400 \\ 0 & 0 & 0.425 & 0 & 0.834 & 0 \\ 0 & 0 & 0 & 0.834 & 0 & 0.763 \\ 0 & 0 & -0.400 & 0 & 0.763 & 0 \end{bmatrix}.$$

Initially, we select the spacing lengths along the waveguide manifold as the only optimization variables with starting values set equal to $\lambda_{gk}/2$ (half the wavelength corresponding to the kth center frequency). For the kth channel, the waveguide spacing is measured along the manifold from the adjacent $(k-1)$th channel. For the first channel, the spacing is the distance from the short circuit. The filters are assumed lossy and dispersive. Waveguide junctions are assumed nonideal.

Fig. 3 shows the return-loss response of the multiplexer at the start of the optimization process. The specification on the common port return loss is seriously violated, especially in the lower frequency range (corresponding to channels 9–12).

The filter spacings are the dominant variables of the problem. This is based on the initial sensitivity analysis of the common port return loss function w.r.t. all variables at selected frequency points.

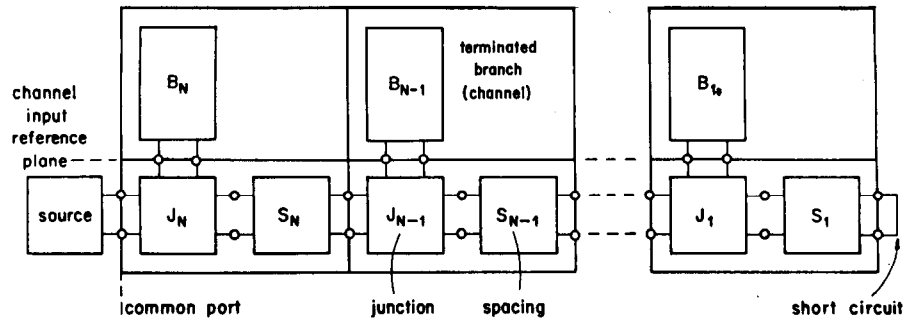

Fig. 2. The multiplexer configuration under consideration. $J_1, J_2, \cdots, J_N$ are arbitrarily defined 3-port junctions. $B_1, B_2, \cdots, B_N$ are terminated branches or channels which may each be represented in reduced cascade form and $S_1, S_2, \cdots, S_N$ are usually waveguide spacing elements.

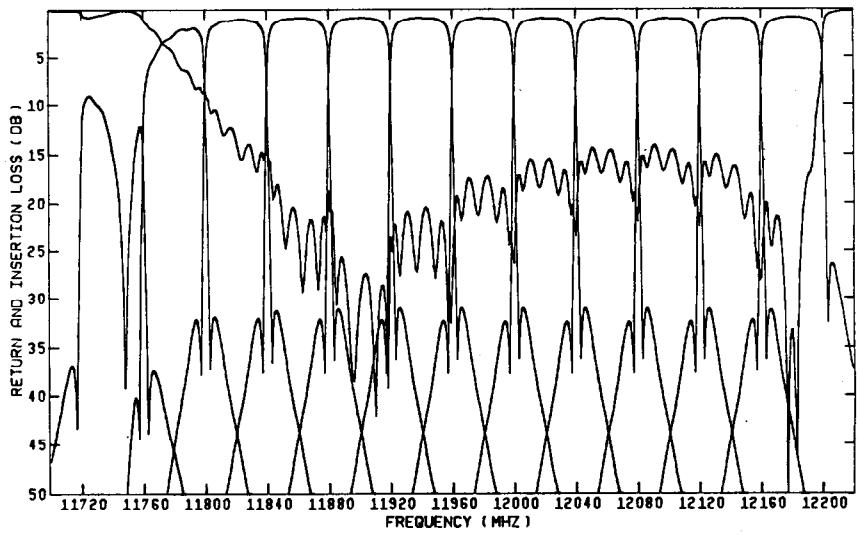

Fig. 3. Responses of the 12-channel multiplexer at the start of the optimization process.

We perform the one-sided l_1 optimization which is defined in the following way:

$$\underset{x}{\text{minimize}} \sum_{i=1}^{m} |f_i^*(x)| \tag{16}$$

where

$$f_i^* \triangleq \begin{cases} f_i(x) & \text{if } f_i(x) \geq 0 \\ 0 & \text{if } f_i(x) < 0. \end{cases} \tag{17}$$

The functions $f_i(x)$ are the original error functions defined in (15).

We define also the gradients of the functions $f_i^*(x)$ in the following way:

$$\frac{\partial f_i^*(x)}{\partial x} \triangleq \begin{cases} \dfrac{\partial f_i(x)}{\partial x} & \text{if } f_i(x) \geq 0 \\ 0 & \text{if } f_i(x) < 0 \end{cases} \tag{18}$$

The results of the l_1 optimization defined above are shown in Fig. 4. The violations of the 20-dB specification are most serious in the frequency range corresponding to channels 1–2 and 9–12. This motivates us to release additional optimization variables in the filters corresponding to these channels. As additional optimization variables we release the input–output transformer ratios, cavity resonant frequencies, as well as intercavity couplings. From that point, minimax optimization is employed using the l_1 optimized spacings as the starting values for the spacings. The final optimized return loss of the 12-channel multiplexer is shown in Fig. 5. The problem involves 60 nonlinear design variables.

V. Model Parameter Identification Using the l_1 Norm

A. Formulation of the Problem

This application of the l_1 norm to circuit problems deals with model parameter identification from measurements. The problem of approximating a measured response by a network or system response can be formulated as an optimization problem

$$\underset{\phi}{\text{minimize}} \|f\| \tag{19}$$

where

$$f \triangleq [f_1 \quad f_2 \quad \cdots \quad f_k]^T \tag{20}$$

$$f_i(\phi) \triangleq F^c(\phi, \omega_i) - F^m(\omega_i), \qquad i = 1,2,\cdots,k. \tag{21}$$

$F^c(\phi, \omega_i)$ is the response of an appropriate model which depends nonlinearly on a vector of parameters $\phi \triangleq [\phi_1 \quad \phi_2 \cdots \phi_n]^T$ and $F^m(\omega_i)$ is a measured response corresponding to measurements at data (frequency) points $\omega_i, i = 1,2,\cdots,k$.

It is usually assumed that the expected values of components of f are zero, but due to the presence of measurement errors in

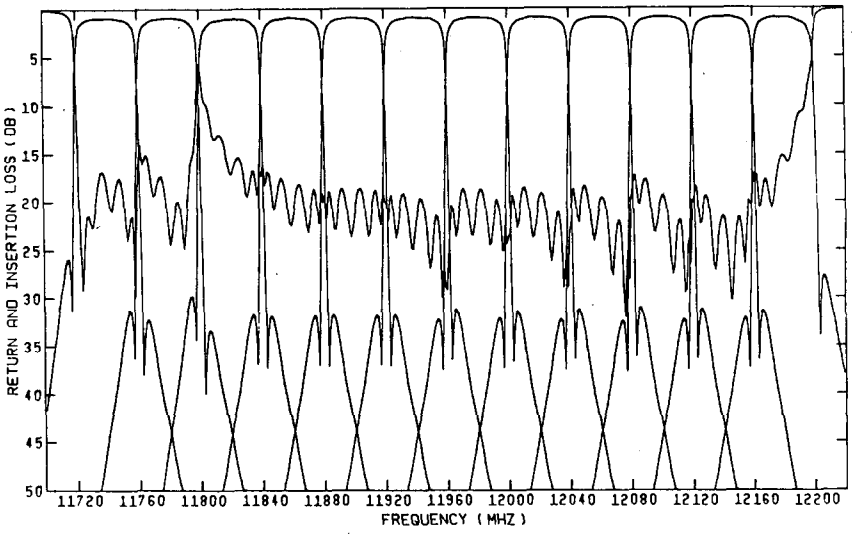

Fig. 4. Responses of the 12-channel multiplexer with optimized spacings only using l_1 optimization.

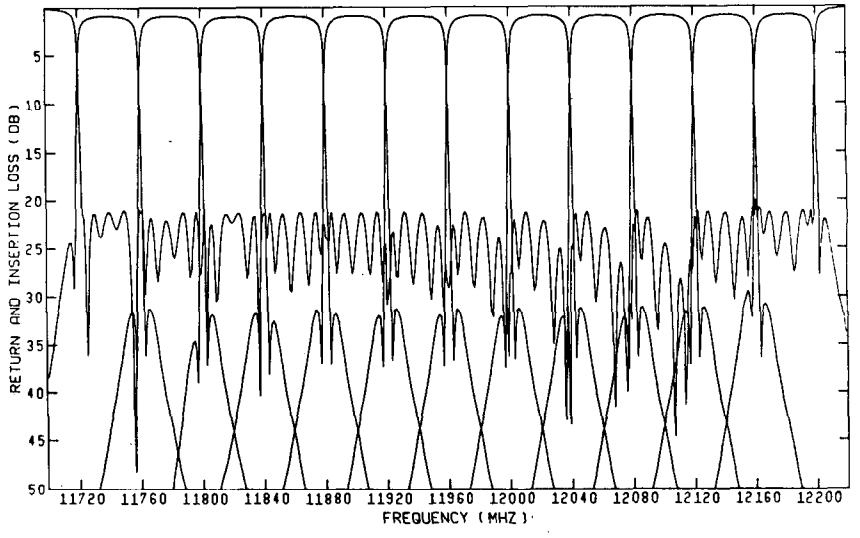

Fig. 5. Responses of the 12-channel multiplexer with optimized spacings, input–output transformer ratios, cavity resonances, and coupling parameters using minimax optimization.

observing $F^m(\omega_i)$, this cannot be realized in practice. The particular norm to be used depends on the distribution of these errors, represented by the components of $\boldsymbol{f}$.

It is commonly supposed that the values of the f_i's are independent and normally distributed, when the maximum likelihood estimate of the data is given by choosing the norm to be the least-squares norm [17]. The measurements, however, might contain some isolated large errors, and in this case, minimization of the l_1 norm residual is recommended due to its "filtering" properties w.r.t. large errors.

Using the l_1 norm, the identification problem becomes

$$\underset{\phi}{\text{minimize}} \sum_{i=1}^{k} |f_i(\phi)| \tag{22}$$

where $f_i(\phi)$, $i=1,2,\cdots,k$, are defined in (21).

D. Sixth-Order Multicoupled Cavity Filter Example

In this example, we deal with multicoupled cavity narrow bandpass filters used in microwave communication systems (see Fig. 6).

A narrow-band lumped model of an unterminated multicavity filter has been given by Atia and Williams [18] as

$$\boldsymbol{ZI} = \boldsymbol{V} \tag{23}$$

where

$$\boldsymbol{Z} = j(s\mathbf{1} + \boldsymbol{M}), \tag{24}$$

$$s = \frac{\omega_0}{\Delta\omega}\left(\frac{\omega}{\omega_0} - \frac{\omega_0}{\omega}\right). \tag{25}$$

$\mathbf{1}$ denotes an $n \times n$ identity matrix, $\boldsymbol{M}$ is an $n \times n$ coupling matrix whose (i, j) element represents the normalized coupling between the ith and jth cavities, ω_0 is the center frequency, and $\Delta\omega$ is the bandwidth parameter. The diagonal entries M_{ii} represent the deviations from the synchronous tuning.

In practice, it is often desired to determine the actual filter couplings based on response (return loss or insertion loss) measurements. The problem can be formulated as an optimization problem (22) with the l_1 objective function.

In this example, reflection coefficient has been used as the filter response. A sixth-order filter centered at 4000 MHz with 40-MHz bandwidth is considered.

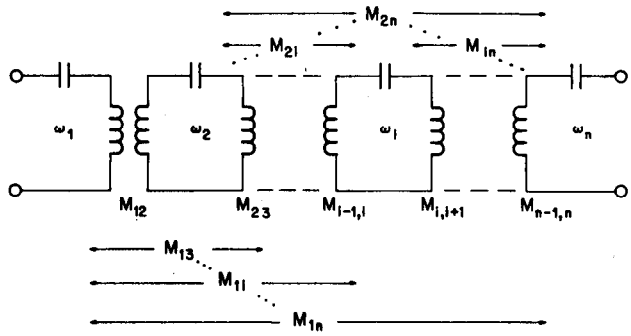

Fig. 6. Unterminated coupled-cavity filter illustrating the coupling coefficients.

TABLE II
DATA USED AS MEASUREMENTS IN THE SIXTH-ORDER FILTER EXAMPLE

Frequency (MHz)	Reflection Coefficient
3975.0	0.99
3977.0	1.00
3979.0	0.89
3980.0	0.58
3982.0	0.26
3984.0	0.23
3986.0	0.23
3986.0	0.23 → 0.75
3988.0	0.20
3990.0	0.14 → 0.40
3992.0	0.08
3994.0	0.01
3996.0	0.05
3998.0	0.08
4000.0	0.09
4002.0	0.08
4004.0	0.05
4006.0	0.01
4008.0	0.08
4010.0	0.14
4012.0	0.20
4014.0	0.23
4016.0	0.23
4018.0	0.25
4020.0	0.55
4022.0	0.99
4024.0	0.99

To demonstrate the properties of the l_1 norm in the identification problem, we deliberately introduce large errors to data representing the measurements. Table II contains data (frequency point, reflection coefficient) used in the example. Measurement 0.23 at 3986.0 MHz has been replaced by 0.75 and measurement 0.14 at 3990.0 by 0.40. The optimization problem (22) has been solved with the data containing two large errors. The results of identification are summarized in Table III. All the couplings have been identified successfully in the presence of large errors. The l_1 objective function of the solution is equal to the sum of the absolute values of the errors introduced in the measurements.

VI. CONCLUSIONS

We have described a highly efficient algorithm for nonlinear l_1 optimization problems. The algorithm combines linear programming methods with quasi-Newton methods and the convergence is at least superlinear.

TABLE III
RESULTS OF IDENTIFICATION FOR THE SIXTH-ORDER FILTER PROBLEM WITH DATA CONTAINING LARGE ERRORS

Coupling	Actual Value	Identified Value
M_{12}	0.859956	0.860312
M_{23}	0.526602	0.527016
M_{34}	0.791894	0.791897
M_{45}	0.526602	0.526184
M_{56}	0.859956	0.859608
M_{16}	0.087293	0.087273
M_{25}	-0.393685	-0.393680
Number of Function Evaluations		19
ℓ_1 Objective Function at the Solution		0.77628
Execution Time (secs) on VAX 11/780		12.5

The importance of the algorithm stems from the fact that the number of applications of the l_1 norm to circuit and system problems has been increasing in recent years. The necessary conditions for optimality of the nonlinear l_1 problem (see, e.g., [8]) indicate that zeros of the nonlinear functions $f_j(x)$ play an important role in the characteristics of the l_1 problem. This fact has been used in fault isolation techniques for linear analog circuits and we have demonstrated that the new l_1 algorithm is very successful in methods for fault isolation in linear analog circuits under an insufficient number of independent voltage measurements.

A formulation using the l_1 norm for the initial stage of multiplexer design has been presented and illustrated by a 12-channel 12-GHz multiplexer. The one-sided l_1 optimization sets to zero as many error functions as possible and this results in identifying channels of the multiplexer where the specification violations are most serious.

We also presented a formulation using the l_1 norm for model parameter identification problems in the presence of large isolated errors in the measurements.

We feel that the properties of the l_1 norm will be used more and more frequently in solving circuit and system problems, including diagnosis of networks, selection of tunable parameters in post-production tuning, and model parameter identification from measurements.

ACKNOWLEDGMENT

The authors acknowledge the contribution of Dr. S. Daijavad, now at the University of California, Berkeley, CA, to this research project. The assistance of M. L. Renault of McMaster University in preparing the numerical examples is also gratefully acknowledged.

REFERENCES

[1] R. H. Bartels and A. R. Conn, "An approach to nonlinear l_1 data fitting," Univ. of Waterloo, Computer Science Dep., Rep. CS-81-17, 1981.

[2] J. W. Bandler, R. M. Biernacki, A. E. Salama, and J. A. Starzyk, "Fault isolation in linear analog circuits using the l_1 norm," in *Proc. IEEE Int. Symp. Circuits Syst.* (Rome, Italy), 1982, pp. 1140-1143.

[3] J. W. Bandler and A. E. Salama, "Functional approach to microwave postproduction tuning," *IEEE Trans. Microwave Theory Tech.*, vol. MTT-33, pp. 302–310, 1985.
[4] J. Hald and K. Madsen, "Combined LP and quasi-Newton methods for minimax optimization," *Math. Programming*, vol. 20, pp. 49–62, 1981.
[5] J. Hald, "A 2-stage algorithm for nonlinear l_1 optimization," Rep. No. NI-81-03, Inst. for Num. Analysis, Tech. Univ. of Denmark, 1981.
[6] J. Hald and K. Madsen, "Combined LP and quasi-Newton methods for nonlinear l_1 optimization," *SIAM J. Numerical Analy.*, vol. 22, pp. 68–80, 1985.
[7] R. H. Bartels, A. R. Conn, and J. W. Sinclair, "Minimization techniques for piecewise differentiable functions: The l_1 solution to an overdetermined linear system," *SIAM J. Numerical Analy.*, vol. 15, pp. 224–241, 1978.
[8] C. Charalambous, "On conditions for optimality of the nonlinear l_1 problem," *Math. Programming*, vol. 17, pp. 123–135, 1979.
[9] H. M. Merrill, "Failure diagnosis using quadratic programming," *IEEE Trans. Reliability*, vol. R-22, pp. 207–213, 1973.
[10] A. E. Atia, "Computer-aided design of waveguide multiplexers," *IEEE Trans. Microwave Theory Tech.*, vol. MTT-22, pp. 332–336, 1974.
[11] M. H. Chen, F. Assal, and C. Mahle, "A contiguous-band multiplexer," *COMSAT Tech. Rev.*, vol. 6, pp. 285–306, 1976.
[12] M. H. Chen, "A 12-channel contiguous-band multiplexer at *Ku*-band," in *1983 IEEE Int. Microwave Symp. Dig.* (Boston), 1983, pp. 77–79.
[13] E. R. Egri, A. E. Williams, and A. E. Atia, "A contiguous-band multiplexer design," in *1983 IEEE Int. Microwave Symp. Dig.*, (Boston), 1983, pp. 86–88.
[14] J. W. Bandler, W. Kellermann, and K. Madsen, "A superlinearly convergent minimax algorithm for microwave circuit design," *IEEE Trans. Microwave Theory Tech.*, vol. MTT-33, pp. 1519–1530, 1985.
[15] J. W. Bandler, S. H. Chen, S. Daijavad, and W. Kellermann, "Optimal design of multicavity filters and contiguous-band multiplexers," in *Proc. 14th Euro. Microwave Conf.* (Liege, Belgium), 1984, pp. 863–868.
[16] R. Tong and D. Smith, "A 12-channel contiguous-band multiplexer for satellite application," in *1984 IEEE Int. Microwave Symp. Dig.*, (San Francisco), 1984, pp. 297–298.
[17] G. A. Watson, "Discrete l_1 approximation by rational functions," *IMA J. Numerical Analysis*, vol. 4, pp. 275–288, 1984.
[18] A. E. Atia and A. E. Williams, "Narrow-bandpass waveguide filters," *IEEE Trans. Microwave Theory Tech.*, vol. MTT-20, pp. 258–265, 1972.

Fast Algorithms for 2-D FIR Wiener Filtering and Linear Prediction

DIMITRIS G. MANOLAKIS
AND VINAY K. INGLE, MEMBER, IEEE

Abstract—**This paper deals with the development of computationally efficient algorithms for 2-D finite-impulse response (FIR) Wiener filters and linear predictors which are optimum in the mean-square-error (MSE) sense. It turns out that the computational effort to determine the coefficients of the 2-D FIR restoration filter depends heavily on the statistical features of the input signal. It is shown that in the case of homogeneous signals, one can develop two very efficient algorithms which are, at least, 30-percent faster than other existing schemes. These algorithms are subsequently used for the efficient implementation of the introduced restoration techniques. Experimental results as well as performance evaluations of this technique are included.**

I. Introduction

The state of the art in digital computers, special-purpose signal processors, and VLSI has recently opened the way for high-resolution 2-D digital signal processing.

Manuscript received October 24, 1985; revised June 2, 1986. This work was supported in part by the Center for Electromagnetics Research, Northeastern University.
The authors are with the Department of Electrical and Computer Engineering, Northeastern University, Boston, MA 02115.
IEEE Log Number 8611461.

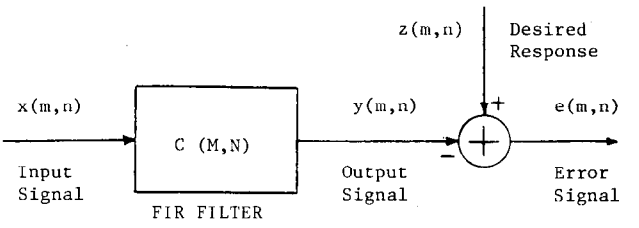

Fig. 1. Illustration of 2-D linear FIR least-squares filtering problem.

The subject of this paper is the development of fast algorithms for 2-D finite-impulse response (FIR) Wiener filters which minimize the mean-square-error (MSE) criterion of performance. Assuming a 2-D FIR filter with quarter-plane support, the minimization in the spatial-domain results in a linear system of normal equations whose solution provides the coefficients of the Wiener filter. The solution of these normal equations requires a tremendous amount of computational effort. However, if the input signal is either horizontally or vertically stationary, then a proper arrangement of the normal equations results in a block Toeplitz system of linear equations, which can be efficiently solved using the multichannel Levinson algorithm [4], [5]. If the input signal is featured by both vertical and horizontal stationarity (homogeneous signal), then the normal equation matrix attains a Toeplitz–Toeplitz (TT) structure (block Toeplitz with Toeplitz entries). Although the multichannel Levinson algorithm [6] can also be used in this case, we introduce two new algorithms which offer a computational saving of 30 percent compared to the Levinson scheme. Moreover, both algorithms possess a structure which reveals many interesting physical aspects of the problem.

The remainder of the paper is organized as follows. In Section II, we introduce the basic 2-D FIR MSE filtering problem. This material serves both to establish notation and to provide the background for the rest of the paper. Section III provides a brief discussion of the multichannel Levinson algorithm and prepares the ground for Section IV, which deals with the introduction of the new algorithms. The application of these algorithms to the restoration of degraded images is the subject of Section V.

II. 2-D FIR Mean-Square-Error Filtering

We shall deal with the optimum filtering problem, shown in Fig. 1. The 2-D FIR filter used in this arrangement has a finite quarter-plane support and is described by the following convolution summation:

$$y(m,n) = -\sum_{k=1}^{M}\sum_{l=1}^{N} c_{kl}\,x(m+1-k, n+1-l) \qquad (1)$$

where $\{c_{kl}\colon 1 \leqslant k \leqslant M,\ 1 \leqslant l \leqslant N\}$ is the array of the filter coefficients, m is the horizontal index, and n is the vertical index. We will use the symbol $C(M,N)$ to denote this kind of filter.

A simple look at Fig. 2 indicates that the computation of the output sample $y(m,n)$ requires the present and $M-1$ "previous" columns, with each column having N samples, if the filter input data are arranged column-wise. If the input data are arranged row-wise, the present and $N-1$ "previous" rows, with M elements each, are needed for the computation of the output $y(m,n)$.

0098-4094/87/0200-0181$01.00 ©1987 IEEE

Reprint 3

Circuit Optimization: The State of the Art

Circuit Optimization: The State of the Art

JOHN W. BANDLER, FELLOW, IEEE, AND SHAO HUA CHEN, STUDENT MEMBER, IEEE

Invited Paper

Abstract—**This paper reviews the current state of the art in circuit optimization, emphasizing techniques suitable for modern microwave CAD. It is directed at the solution of realistic design and modeling problems, addressing such concepts as physical tolerances and model uncertainties. A unified hierarchical treatment of circuit models forms the basis of the presentation. It exposes tolerance phenomena at different parameter/response levels. The concepts of design centering, tolerance assignment, and postproduction tuning in relation to yield enhancement and cost reduction suitable for integrated circuits are discussed. Suitable techniques for optimization oriented worst-case and statistical design are reviewed. A generalized l_p centering algorithm is proposed and discussed. Multicircuit optimization directed at both CAD and robust device modeling is formalized. Tuning is addressed in some detail, both at the design stage and for production alignment. State-of-the-art gradient-based nonlinear optimization methods are reviewed, with emphasis given to recent, but well-tested, advances in minimax, l_1, and l_2 optimization. Illustrative examples as well as a comprehensive bibliography are provided.**

I. INTRODUCTION

COMPUTER-AIDED circuit optimization is certainly one of the most active areas of interest. Its advances continue; hence the subject deserves regular review from time to time. The classic paper by Temes and Calahan in 1967 [102] was one of the earliest to formally advocate the use of iterative optimization in circuit design. Techniques that were popular at the time, such as one-dimensional (single-parameter) search, the Fletcher–Powell procedure and the Remez method for Chebyshev approximation, were described in detail and well illustrated by circuit examples. Pioneering papers by Lasdon, Suchman, and Waren [73], [74], [108] demonstrated optimal design of linear arrays and filters using the penalty function approach. Two papers in 1969 by Director and Rohrer [48], [49] originated the adjoint network approach to sensitivity calculations, greatly facilitating the use of powerful gradient-based optimization methods. In the same period, the work by Bandler [4], [5] systematically treated the formulation of error functions, the least pth objective, nonlinear constraints, optimization methods, and circuit sensitivity analysis.

Manuscript received May 4, 1987; revised August 20, 1987. This work was supported in part by the Natural Sciences and Engineering Research Council of Canada under Grant A7239 and in part by Optimization Systems Associates Inc.

J. W. Bandler is with the Simulation Optimization Systems Research Laboratory and the Department of Electrical and Computer Engineering, McMaster University, Hamilton, Canada L8S 4L7. He is also with Optimization Systems Associates Inc., Dundas, Ontario, Canada L9H 6L1.

S. H. Chen was with the Department of Electrical and Computer Engineering, McMaster University, Hamilton, Canada. He is now with Optimization Systems Associates Inc., Dundas, Ontario, Canada L9H 6L1.

IEEE Log Number 8717974.

Since then, advances have been made in several major directions. The development of large-scale network simulation and optimization techniques have been motivated by the requirements of the VLSI era. Approaches to realistic circuit design where design parameter tolerances and yield are taken into account have been pioneered by Elias [52] and Karafin [68] and furthered by many authors over the ensuing years. Optimization methods have evolved from simple, low-dimension-oriented algorithms into sophisticated and powerful ones. Highly effective and efficient solutions have been found for a large number of specialized applications. The surveys by Calahan [37], Charalambous [39], Bandler and Rizk [26], Hachtel and Sangiovanni-Vincentelli [63], and Brayton *et al.* [32] are especially relevant to circuit designers.

In the present paper, we concentrate on aspects that are relevant to and necessary for the continuing move to optimization of increasingly more complex microwave circuits, in particular to MMIC circuit modeling and design. Consequently, we emphasize optimization-oriented approaches to deal more explicitly with process imprecision, manufacturing tolerances, model uncertainties, measurement errors, and so on. Such realistic considerations arise from design problems in which a large volume of production is envisaged, e.g., integrated circuits. They also arise from modeling problems in which consistent and reliable results are expected despite measurement errors, structural limitations such as physically inaccessible nodes, and model approximations and simplifications. The effort to formulate and solve these problems represents one of the driving forces of theoretical study in the mathematics of circuit CAD. Another important impetus is provided by progress in computer hardware, resulting in drastic reduction in the cost of mass computation. Finally, the continuing development of gradient-based optimization techniques has provided us with powerful tools.

In this context, we review the following concepts: realistic representations of a circuit design and modeling problem, nominal (single) circuit optimization, statistical circuit design, and multicircuit modeling, as well as recent gradient-based optimization methods.

Nominal design and modeling are the conventional approaches used by microwave engineers. Here, we seek a single point in the space of variables selected for optimization which best meets a given set of performance specifications (in design) or best matches a given set of response measurements (in modeling). A suitable scalar measure

0018-9480/88/0200-0424$01.00 ©1988 IEEE

of the deviation between responses and specifications which forms the objective function to be minimized is the ubiquitous least squares measure (see, for example, Morrison [83]), the more esoteric generalized l_p objective (Charalambous [41]) or the minimax objective (Madsen *et al.* [80]). We observe here that the performance-driven (single-circuit) least squares approach that circuit design engineers have traditionally chosen has proved unsuccessful both in addressing design yield and in serious device modeling.

Recognition that an actual realization of a nominal design is subject to fluctuation or deviation led, in the past, to the so-called sensitivity minimization approach (see, for example, Schoeffler [94] and Laker *et al.* [71]). Employed by filter designers, the approach involves measures of performance sensitivity, typically first-order, that are included in the objective function.

In reality, uncertainties which deteriorate performance may be due to physical (manufacturing, operating) tolerances as well as to parasitic effects such as electromagnetic coupling between elements, dissipation, and dispersion (Bandler [6], Tromp [107]). In the design of substantially untunable circuits these phenomena lead to two important classes of problems: worst-case design and statistical design. The main objective is the reduction of cost or the maximization of production yield.

Worst-case design (Bandler *et al.* [23], [24]), in general, requires that all units meet the design specifications under all circumstances (i.e., a 100 percent yield), with or without tuning, depending on what is practical. In statistical design [1], [26], [30], [47], [97], [98], [100], [101] it is recognized that a yield of less than 100 percent is likely; therefore, with respect to an assumed probability distribution function, yield is estimated and enhanced by optimization. Typically, we either attempt to center the design with fixed assumed tolerances or we attempt to optimally assign tolerances and/or design tunable elements to reduce production cost.

What distinguishes all these problems from nominal designs or sensitivity minimization is the fact that a single design point is no longer of interest: a (tolerance) region of multiple possible outcomes is to be optimally located with respect to the acceptable (feasible, constraint) region.

Modeling, often unjustifiably treated as if it were a special case of design, is particularly affected by uncertainties and errors at many levels. Unavoidable measurement errors, limited accessibility to measurement points, approximate equivalent circuits, etc., result in nonunique and frequently inconsistent solutions. To overcome these frustrations, we advocate a properly constituted multicircuit approach (Bandler *et al.* [12]).

Our presentation is outlined as follows.

In Section II, in relation to a physical engineering system of interest, a typical hierarchy of simulation models and corresponding response and performance functions are introduced. Error functions arising from given specifications and a vector of optimization variables are defined. Performance measures such as l_p objective functions (l_p norms and generalized l_p functions) are introduced and their properties discussed.

We devote to Section III a brief review of the relatively well-known and successful approach of nominal circuit design optimization.

In Section IV, uncertainties that exist in the physical system and at different levels of the model hierarchy are discussed and illustrated by a practical example. Different cases of multicircuit design, namely centering, tolerancing (optimal tolerance assignment), and tuning at the design stage, are identified. A multicircuit modeling approach and several possible applications are described.

Some important and representative techniques in worst-case and statistical design are reviewed in Section V. These include the nonlinear programming approach to worst-case design (Bandler *et al.* [24], Polak [89]), simplicial (Director and Hachtel [47]) and multidimensional (Bandler and Abdel-Malek [7]) approximations of the acceptable region, the gravity method (Soin and Spence [98]), and the parametric sampling method (Singhal and Pinel [97]). A generalized l_p centering algorithm is proposed as a natural extension to l_p nominal design. It provides a unified formulation of yield enhancement for both the worst case and the case where yield is less than 100 percent.

Illustrations of statistical design are given in Section VI.

The studies in the last two decades on the theoretical and algorithmic aspects of optimization techniques have produced a great number of results. In particular, gradient-based optimization methods have gained increasing popularity in recent years for their effectiveness and efficiency. The essence of gradient-based l_p optimization methods is reviewed in Section VII. Emphasis is given to the trust region Gauss–Newton and the quasi-Newton algorithms (Madsen [78], Moré [82], Dennis and Moré [46]).

The subject of gradient calculation and approximation is briefly discussed in Section VIII.

II. Variables and Functions

In this section, we review some basic concepts of practical circuit optimization. In particular, we identify a physical system and its simulation models. We discuss a typical hierarchy of models and the associated designable parameters and response functions. We also define specifications, error functions, optimization variables and objective functions.

A. The Physical System

The physical engineering system under consideration can be a network, a device, a process, and so on, which has both a fixed structure and given element types. We manipulate the system through some adjustable parameters contained in the column vector ϕ^M. The superscript M identifies concepts related to the physical system. Geometrical dimensions such as the width of a strip and the length of a waveguide section are examples of adjustable parameters.

In the production of integrated circuits, ϕ^M may include some fundamental variables which control, say, a doping or photomasking process and, consequently, determine the geometrical and electrical parameters of a chip. External controls, such as the biasing voltages applied to an active device, are also possible candidates for ϕ^M.

The performance and characteristics of the system are described in terms of some measurable quantities. The usual frequency and transient responses are typical examples. These measured responses, or simply measurements, are denoted by $F^M(\phi^M)$.

B. The Simulation Models

In circuit optimization, some suitable models are used to simulate the physical system. Actually, models can be usefully defined at many levels. Tromp [106], [107] has considered an arbitrary number of levels (also see Bandler *et al.* [19]). Here, for simplicity, we consider a hierarchy of models consisting of four typical levels as

$$F^H = F^H(F^L)$$
$$F^L = F^L(\phi^H)$$
$$\phi^H = \phi^H(\phi^L). \tag{1}$$

ϕ^L is a set of low-level model parameters. It is supposed to represent, as closely as possible, the adjustable parameters in the actual system, i.e., ϕ^M. ϕ^H defines a higher-level model, typically an equivalent circuit, with respect to a fixed topology. Usually, we use an equivalent circuit for the convenience of its analysis. The relationship between ϕ^L and ϕ^H is either derived from theory or given by a set of empirical formulas.

Next on the hierarchy we define the model responses at two possible levels. The low-level external representation, denoted by F^L, can be the frequency-dependent complex scattering parameters, unterminated y-parameters, transfer function coefficients, etc. Although these quantities may or may not be directly measurable, they are very often used to represent a subsystem. The high-level responses F^H directly correspond to the actual measured responses, namely F^M, which may be, for example, frequency responses such as return loss, insertion loss, and group delay of a suitably terminated circuit.

A realistic example of a one-section transformer on stripline was originally considered by Bandler *et al.* [25]. The circuits and parameters, physical as well as model, are shown in Fig. 1. The physical parameters ϕ^M (and the low-level model ϕ^L) include strip widths, section lengths, dielectric constants, and strip and substrate thicknesses. The equivalent circuit has six parameters, considered as ϕ^H, including the effective line widths, junction parasitic inductances, and effective section length. The scattering matrix of the circuit with respect to idealized (matched) terminations is a candidate for a low-level external representation (F^L). The reflection coefficient by taking into account the actual complex terminations could be a high-level response of interest (F^H).

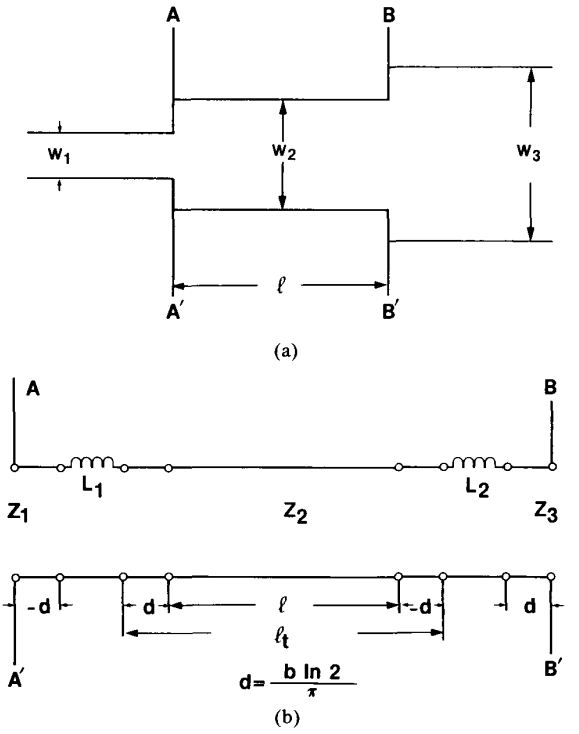

Fig. 1. A microwave stripline transformer showing (a) the physical structure and (b) the equivalent circuit model [25]. The physical parameters are

$$\phi^M = [\, w_1\, w_2\, w_3 : l \sqrt{\varepsilon_{r1}}\, \sqrt{\varepsilon_{r2}}\, \sqrt{\varepsilon_{r3}}\, b_1\, b_2\, b_3\, t_{s1}\, t_{s2}\, t_{s3} \,]^T$$

where w is the strip width, l the length of the middle section, ε_r the dielectric constant, b the substrate thickness, and t_s the strip thickness. ϕ^M is represented in the simulation model by ϕ^L. The high-level parameters of the equivalent circuit are

$$\phi^H = [\, D_1\, D_2\, D_3\, L_1\, L_2\, l_t \,]^T$$

where D is the effective linewidth, L the junction parasitic inductance, and l_t the effective section length. Suitable empirical formulas that relate ϕ^L to ϕ^H can be found in [25].

For a particular case, we may choose a certain section of this hierarchy to form a design problem. We can choose either ϕ^L or ϕ^H as the designable parameters. Either F^L or F^H or a suitable combination of both may be selected as the response functions. Bearing this in mind, we simplify the notation by using ϕ for the designable parameters and F for the response functions.

C. Specifications and Error Functions

The following discussion on specifications and error functions is based on presentations by Bandler [5], and Bandler and Rizk [26], where more exhaustive illustrations can be found.

We express the desirable performance of the system by a set of specifications which are usually functions of certain independent variable(s) such as frequency, time, and temperature. In practice, we have to consider a discrete set of samples of the independent variable(s) such that satisfying the specifications at these points implies satisfying them

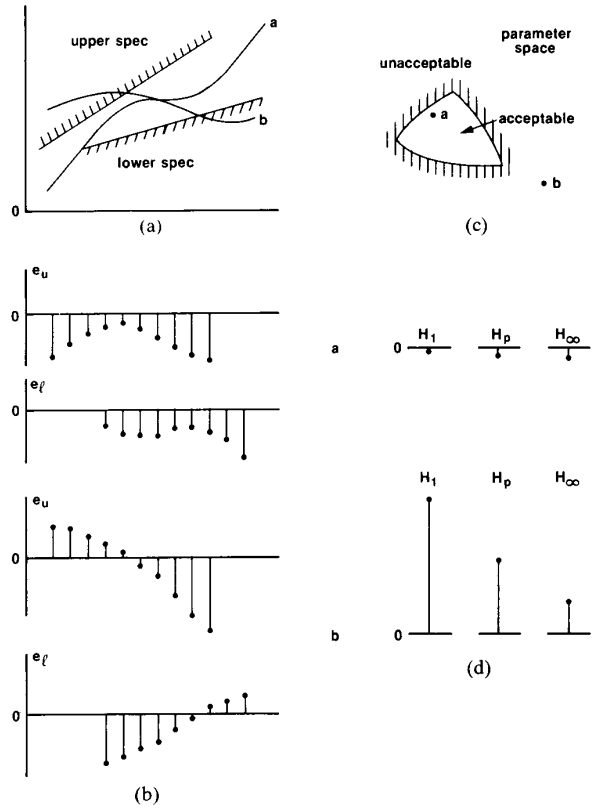

Fig. 2. Illustrations of (a) upper specifications, lower specifications, and the responses of circuits a and b, (b) error functions corresponding to circuits a and b, (c) the acceptable region, and (d) generalized l_p objective functions defined in (13).

almost everywhere. Also, we may consider simultaneously more than one kind of response. Thus, without loss of generality, we denote a set of sampled specifications and the corresponding set of calculated response functions by, respectively,

$$S_j, \qquad j=1,2,\cdots,m$$
$$F_j(\phi), \qquad j=1,2,\cdots,m. \tag{2}$$

Error functions arise from the difference between the given specifications and the calculated responses. In order to formulate the error functions properly, we may wish to distinguish between having upper and lower specifications (windows) and having single specifications, as illustrated in Figs. 2(a) and 3(a). Sometimes the one-sidedness of upper and lower specifications is quite obvious, as in the case of designing a bandpass filter. On other occasions the distinction is more subtle, since a single specification may as well be interpreted as a window having zero width.

In the case of having single specifications, we define the error functions by

$$e_j(\phi) = w_j|F_j(\phi) - S_j|, \qquad j=1,2,\cdots,m \tag{3}$$

where w_j is a nonnegative weighting factor.

We may also have an upper specification S_{uj} and a lower specification S_{lj}. In this case we define the error

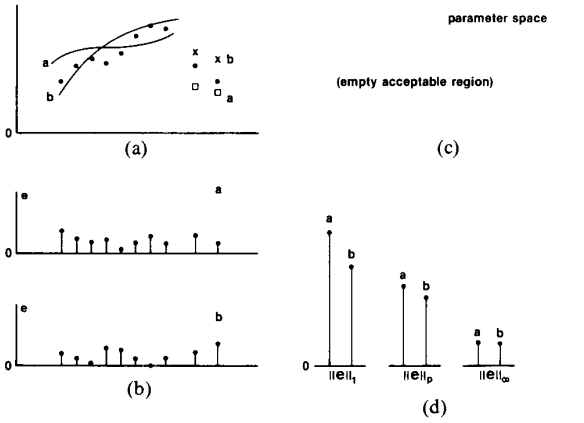

Fig. 3. Illustrations of (a) a discretized single specification and two discrete single specifications (e.g., expected parameter values to be matched), as well as the responses of circuits a and b, (b) error functions related to circuits a and b, (c) the (empty) acceptable region (i.e., a perfect match is not possible) and (d) the corresponding l_p norms.

functions as

$$e_{uj}(\phi) = w_{uj}\big(F_j(\phi) - S_{uj}\big), \qquad j \in J_u$$
$$e_{lj}(\phi) = w_{lj}\big(F_j(\phi) - S_{lj}\big), \qquad j \in J_l \tag{4}$$

where w_{uj} and w_{lj} are nonnegative weighting factors. The index sets as defined by

$$J_u = \{j_1, j_2, \cdots, j_k\}$$
$$J_l = \{j_{k+1}, j_{k+2}, \cdots, j_m\} \tag{5}$$

are not necessarily disjoint (i.e., we may have simultaneous specifications). In order to have a set of uniformly indexed error functions, we let

$$e_i = e_{uj}(\phi), \qquad j=j_i, \quad i=1,2,\cdots,k$$
$$e_i = -e_{lj}(\phi), \qquad j=j_i, \quad i=k+1,k+2,\cdots,m. \tag{6}$$

The responses corresponding to the single specifications can be real or complex, whereas upper and lower specifications are applicable to real responses only. Notice that, in either case, the error functions are real. Clearly, a positive (nonpositive) error function indicates a violation (satisfaction) of the corresponding specification. Figs. 2(b) and 3(b) depict the concept of error functions.

D. Optimization Variables and Objective Functions

Mathematically, we abstract a circuit optimization problem by the following statement:

$$\underset{x}{\text{minimize}}\ U(x) \tag{7}$$

where x is a set of optimization variables and $U(x)$ a scalar objective function.

Optimization variables and model parameters are two separate concepts. As will be elaborated on later in this paper, x may contain a subset of ϕ which may have been normalized or transformed, it may include some statistical variables of interest, several parameters in ϕ may be tied to one variable in x, and so on.

Typically, the objective function $U(\boldsymbol{x})$ is closely related to an l_p norm or a generalized l_p function of $\boldsymbol{e}(\boldsymbol{\phi})$. We shall review the definitions of such l_p functions and discuss their appropriate use in different contexts.

E. The l_p Norms

The l_p norm (Temes and Zai [103]) of $\boldsymbol{e}$ is defined as

$$\|\boldsymbol{e}\|_p = \left[\sum_{j=1}^{m} |e_j|^p\right]^{1/p}. \tag{8}$$

It provides a scalar measure of the deviations of the model responses from the specifications. Least-squares (l_2) is perhaps the most well-known and widely used norm (Morrison [83]), which is

$$\|\boldsymbol{e}\|_2 = \left[\sum_{j=1}^{m} |e_j|^2\right]^{1/2}. \tag{9}$$

The l_2 objective function is differentiable and its gradient can be easily obtained from the partial derivatives of $\boldsymbol{e}$. Partly due to this property, a large variety of l_2 optimization techniques have been developed and popularly implemented. For example, the earlier versions of the commercial CAD packages TOUCHSTONE [104] and SUPER-COMPACT [99] have provided designers solely the least-squares objective.

The parameter p has an important implication. By choosing a large (small) value for p, we in effect place more emphasis on those error functions (e_j's) that have larger (smaller) values. By letting $p = \infty$ we have the minimax norm

$$\|\boldsymbol{e}\|_\infty = \max_j |e_j| \tag{10}$$

which directs all the attention to the worst case and the other errors are in effect ignored. Minimax optimization is extensively employed in circuit design where we wish to satisfy the specifications in an optimal equal-ripple manner [3], [13], [14], [21], [40], [42], [65], [67], [80], [85].

On the other hand, the use of the l_1 norm, as defined by

$$\|\boldsymbol{e}\|_1 = \sum_{j=1}^{m} |e_j| \tag{11}$$

implies attaching more importance to the error functions that are closer to zero. This property has led to the application of l_1 to data-fitting in the presence of gross errors [22], [29], [66], [86] and, more recently, to fault location [8], [9], [27] and robust device modeling [12].

Notice that neither $\|\boldsymbol{e}\|_\infty$ nor $\|\boldsymbol{e}\|_1$ is differentiable in the ordinary sense. Therefore, their minimization requires algorithms that are much more sophisticated than those for the l_2 optimization.

F. The One-Sided and Generalized l_p Functions

By using an l_p norm, we try to minimize the errors towards a zero value. In cases where we have upper and lower specifications, a negative value of e_j simply indicates that the specification is exceeded at that point which, in a sense, is better than having $e_j = 0$. This fact leads to the one-sided l_p function defined by

$$H_p^+(\boldsymbol{e}) = \left[\sum_{j \in J} |e_j|^p\right]^{1/p} \tag{12}$$

where $J = \{j | e_j \geqslant 0\}$. Actually, if we define $e_j^+ = \max\{e_j, 0\}$, then $H_p^+(\boldsymbol{e}) = \|\boldsymbol{e}^+\|_p$.

Bandler and Charalambous [10], [41] have proposed the use of a generalized l_p function defined by

$$H_p(\boldsymbol{e}) = \begin{cases} H_p^+(\boldsymbol{e}) & \text{if the set } J \text{ is not empty} \\ H_p^-(\boldsymbol{e}) & \text{otherwise} \end{cases} \tag{13}$$

where

$$H_p^-(\boldsymbol{e}) = -\left[\sum_{j=1}^{m} (-e_j)^{-p}\right]^{-1/p}. \tag{14}$$

In other words, when at least one of the e_j is nonnegative we use H_p^+, and H_p^- is defined if all the error functions have become negative.

Compared to (12), the generalized l_p function has an advantage in the fact that it is meaningfully defined for the case where all the e_j are negative. This permits its minimization to proceed even after all the specifications have been met, so that the specifications may be further exceeded.

A classical example is the design of Chebyshev-type bandpass filters, where we have to minimize the generalized minimax function

$$H_\infty(\boldsymbol{e}) = \max_j \{e_j\}. \tag{15}$$

The current Version 1.5 of TOUCHSTONE [105] offers the generalized l_p optimization techniques, including minimax.

G. The Acceptable Region

We use $H(\boldsymbol{e})$ as a generic notation for $\|\boldsymbol{e}\|_p$, $H_p^+(\boldsymbol{e})$, and $H_p(\boldsymbol{e})$. The sign of $H(\boldsymbol{e}(\boldsymbol{\phi}))$ indicates whether or not all the specifications are satisfied by $\boldsymbol{\phi}$. An acceptable region is defined as

$$R_a = \{\boldsymbol{\phi} | H(\boldsymbol{e}(\boldsymbol{\phi})) \leqslant 0\} \tag{16}$$

Figs. 2(c), 2(d), 3(c), and 3(d) depict the l_p functions and the acceptable regions.

III. Nominal Circuit Optimization

In a nominal design, without considering tolerances (i.e., assuming that modeling and manufacturing can be done with absolute accuracy), we seek a single set of parameters, called a nominal point and denoted by $\boldsymbol{\phi}^0$, which satisfies the specifications. Furthermore, if we consider the functional relationship of $\boldsymbol{\phi}^H = \boldsymbol{\phi}^H(\boldsymbol{\phi}^L)$ to be precise, then it does not really matter at which level the design is conceived. In fact, traditionally it is often oriented to an equivalent circuit. A classical case is network synthesis

where $\phi^{H,0}$ is obtained through the use of an equivalent circuit and/or a transfer function. A low-level model $\phi^{L,0}$ is then calculated from $\phi^{H,0}$, typically with the help of an empirical formula (e.g., the number of turns of a coil is calculated for a given inductance). Finally, we try to realize $\phi^{L,0}$ by its physical counterpart $\phi^{M,0}$.

With the tool of mathematical optimization, the nominal point ϕ^0 (at a chosen level) is obtained through the minimization of $U(\boldsymbol{x})$, where the objective function is typically defined as an l_p function $H(\boldsymbol{e})$. The vector $\boldsymbol{x}$ contains all the elements of or a subset of the elements of ϕ^0. It is a common practice to have some of the variables normalized. It is also common to have several model parameters tied to a single variable. This is true, e.g., for symmetrical circuit structures but, most importantly, it is a fact of life in integrated circuits. Indeed, such dependencies should be taken into account both in design and in modeling to reduce the dimensionality. The minimax optimization of manifold multiplexers as described by Bandler *et al.* [18], [22], [28] provides an excellent illustration of large-scale nominal design of microwave circuits.

Traditionally, the approach of nominal design has been extended to solving modeling problems. A set of measurements made on the physical system serves as single specifications. Error functions are created from the differences between the calculated responses $\boldsymbol{F}(\phi^0)$ and the measured responses $\boldsymbol{F}^M$. By minimizing an l_p norm of the error functions, we attempt to identify a set of model parameters ϕ^0 such that $\boldsymbol{F}(\phi^0)$ best matches $\boldsymbol{F}^M$. This is known as data fitting or parameter identification.

Such a casual treatment of modeling as if it were a special case of design is often unjustifiable, due to the lack of consideration to the uniqueness of the solution. In design, one satisfactory nominal point, possibly out of many feasible solutions, may suffice. In modeling, however, the uniqueness of the solution is almost always essential to the problem. Affected by uncertainties at many levels, unavoidable measurement errors and limited accessibility to measurement points, the model obtained by a nominal optimization is often nonunique and unreliable. To overcome these frustrations, a recent multicircuit approach will be described in Section IV.

IV. A Multicircuit Approach

The approach of nominal circuit optimization, which we have described in Section III, focuses attention on a certain kind of idealized situation. In reality, unfortunately, there are many uncertainties to be accounted for. For the physical system, without going into too many details, consider

$$\begin{aligned} \boldsymbol{F}^M &= \boldsymbol{F}^{M,0}(\phi^M) + \Delta\boldsymbol{F}^M \\ \phi^M &= \phi^{M,0} + \Delta\phi^M \end{aligned} \tag{17}$$

where $\Delta\boldsymbol{F}^M$ represents measurement errors, $\phi^{M,0}$ a nominal value for ϕ^M, and $\Delta\phi^M$ some physical (manufacturing, operating) tolerances.

For simulation purposes, we may consider a realistic representation of the hierarchy of possible models as

$$\begin{aligned} \boldsymbol{F}^H &= \boldsymbol{F}^{H,0}(\boldsymbol{F}^L) + \Delta\boldsymbol{F}^H \\ \boldsymbol{F}^L &= \boldsymbol{F}^{L,0}(\phi^H) + \Delta\boldsymbol{F}^L \\ \phi^H &= \phi^{H,0}(\phi^L) + \Delta\phi^H \\ \phi^L &= \phi^{L,0} + \Delta\phi^L \end{aligned} \tag{18}$$

where $\phi^{L,0}$, $\phi^{H,0}$, $\boldsymbol{F}^{L,0}$, and $\boldsymbol{F}^{H,0}$ are nominal models applicable at different levels. $\Delta\phi^L$, $\Delta\phi^H$, $\Delta\boldsymbol{F}^L$, and $\Delta\boldsymbol{F}^H$ represent uncertainties or inaccuracies associated with the respective models. $\Delta\phi^L$ corresponds to the tolerances $\Delta\phi^M$. $\Delta\phi^H$ may be due to the approximate nature of an empirical formula. Parasitic effects which are not adequately modeled in ϕ^H will contribute to $\Delta\boldsymbol{F}^L$, and finally we attribute anything else that causes a mismatch between $\boldsymbol{F}^{H,0}$ and $\boldsymbol{F}^{M,0}$ to $\Delta\boldsymbol{F}^H$.

These concepts can be illustrated by the one-section stripline transformer example [25] which we have considered in Section II. Tolerances may be imposed on the physical parameters including the strip widths and thicknesses, the dielectric constants, the section length and substrate thicknesses (see Fig. 1). Such tolerances correspond to $\Delta\phi^M$ and are represented in the model by $\Delta\phi^L$. We may also use $\Delta\phi^H$ to represent uncertainties associated with the empirical formulas which relate the physical parameters to the equivalent circuit parameters (the effective line widths, the junction inductances, and the effective section length). Mismatches in the terminations at different frequencies may be estimated by $\Delta\boldsymbol{F}^H$ ($\boldsymbol{F}^H$ being the actual reflection coefficient; see [25] for more details).

The distinction between different levels of model uncertainties can be quite subtle. As an example, consider the parasitic resistance r associated with an inductor whose inductance is L. Both L and r are functions of the number of turns of a coil (which is a physical parameter). Depending on whether or not r is modeled by the equivalent circuit (i.e., whether or not r is included in ϕ^H), the uncertainty associated with r may appear in $\Delta\phi^H$ or in $\Delta\boldsymbol{F}^L$.

When such uncertainties are present, a single nominal model often fails to represent satisfactorily the physical reality. One effective solution to the problem is to simultaneously consider multiple circuits. We discuss the consequences for design and modeling separately.

A. Multicircuit Design

Our primary concern is to improve production yield and reduce cost in the presence of tolerances $\Delta\phi^L$ and model uncertainties $\Delta\phi^H$. First of all, we represent a realistic situation by multiple circuits as

$$\phi^k = \phi^0 + s^k, \qquad k = 1,2,\cdots,K \tag{19}$$

where ϕ^0, ϕ^k, and s^k are generic notation for the nominal parameters, the kth set of parameters, and a deviate due to the uncertainties, respectively. A more elaborate definition is developed as we proceed.

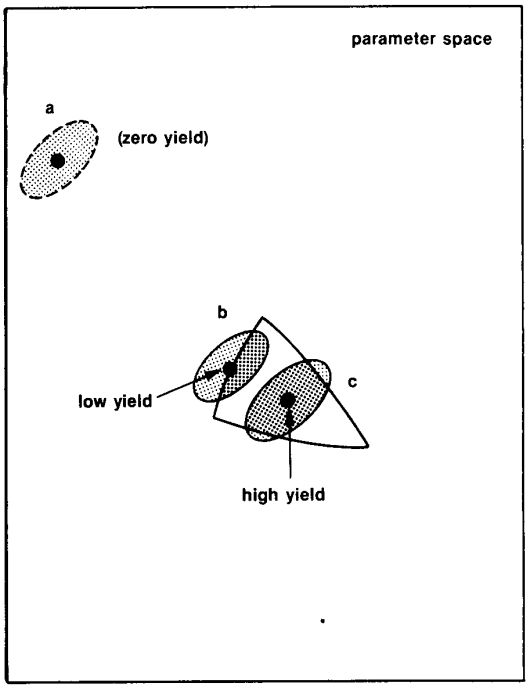

Fig. 4. Three nominal points and the related yield.

For each circuit, we define an acceptance index by

$$I_a(\phi) = \begin{cases} 1, & \text{if } H(e(\phi)) \leqslant 0 \\ 0, & \text{otherwise} \end{cases} \tag{20}$$

where $H(e) \leqslant 0$, defined in (13), indicates satisfaction of the specifications by ϕ. An estimate of the yield is given by the percentage of acceptable samples out of the total, as

$$Y \simeq \left[\sum_{k=1}^{K} I_a(\phi^k) \right] \Big/ K. \tag{21}$$

The merit of a design can then be judged more realistically according to the yield it promises, as illustrated in Fig. 4. Now we shall have a closer look at the definition of multiple circuits.

In the Monte Carlo method the deviates s^k are constructed by generating random numbers using a physical process or arithmetical algorithms. Typically, we assume a statistical distribution for $\Delta\phi^L$, denoted by $D^L(\varepsilon^L)$ where ε^L is a vector of tolerance variables. For example, we may consider a multidimensional uniform distribution on $[-\varepsilon^L, \varepsilon^L]$. Similarly, we assume a $D^H(\varepsilon^H)$ for $\Delta\phi^H$. The uniform and Gaussian (normal) distributions are illustrated in Fig. 5.

At the low level, consider

$$\phi^{L,k} = \phi^{L,0} + s^{L,k}, \qquad k = 1,2,\cdots,K^L \tag{22}$$

where $s^{L,k}$ are samples from D^L. At the higher level, we have, for each k,

$$\phi^{H,k,i} = \phi^{H,0} + s^{H,k,i}, \qquad i = 1,2,\cdots,K^H \tag{23}$$

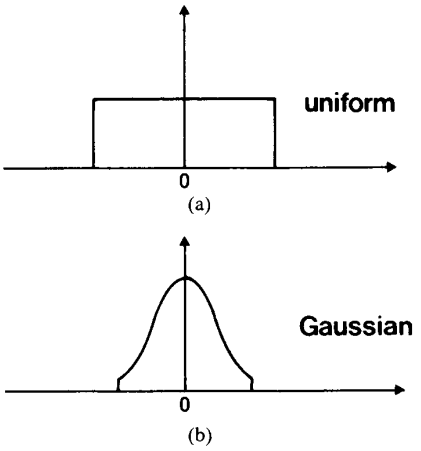

Fig. 5. Typical tolerance distributions: uniform and Gaussian (normal).

where

$$\phi^{H,0} = \phi^{H,0}\left(\phi^{L,0}\right)$$
$$s^{H,k,i} = \phi^{H,0}\left(\phi^{L,k}\right) - \phi^{H,0}\left(\phi^{L,0}\right) + \delta^{k,i} \tag{24}$$

with $\delta^{k,i}$ being samples from D^H.

One might propose a distribution for $s^{H,k,i}$ which presumably encompasses the effect of distribution D^L and distribution D^H. But, while we may reasonably assume simple and independent distributions for $\Delta\phi^L$ and $\Delta\phi^H$, the compound distribution is likely to be complicated and correlated.

B. Centering, Tolerancing, and Tuning

Again, in order to simplify the notation, we use ϕ^0 for the nominal circuit and ε for the tolerance variables.

An important problem involves design centering with fixed tolerances, usually relative to corresponding nominal values. We call this the fixed tolerance problem (FTP). The optimization variables are elements of ϕ^0, the elements of ε are constant or dependent on the variables, and the objective is to improve the yield. Incidentally, the nominal optimization problem, i.e., the traditional design problem, is sometimes referred to as the zero tolerance problem (ZTP).

Since imposing tight tolerances on the parameters will increase the cost of component fabrication or process operation, we may attempt to maximize the allowable tolerances subject to an acceptable yield. In this case both ϕ^0 and ε may be considered as variables. Such a problem is referred to as optimal tolerancing, optimal tolerance assignment, or the variable tolerance problem (VTP).

Tuning some components of ϕ^M after production, whether by the manufacturer or by a customer, is quite commonly used as a means of improving the yield. This process can also be simulated using the model by introducing a vector of designable tuning adjustments τ^k for each circuit, as

$$\phi^k = \phi^0 + s^k + \tau^k, \qquad k = 1,2,\cdots,K. \tag{25}$$

We have to determine, through optimization, the value of

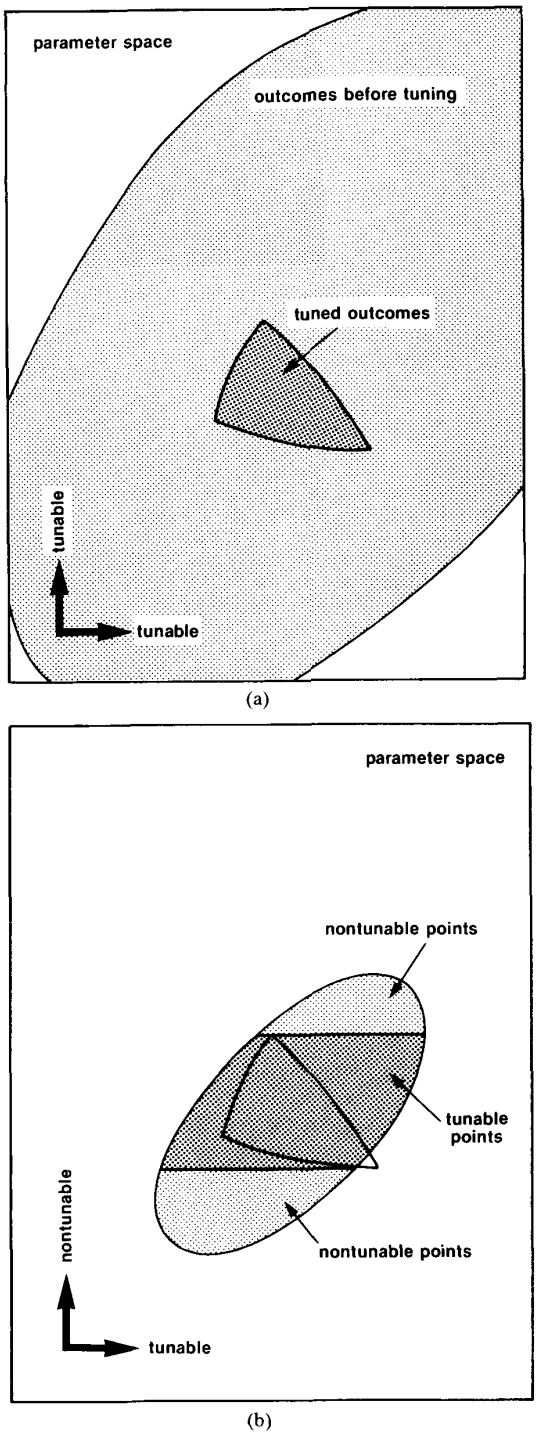

Fig. 6. Illustrations of tuning: (a) both parameters are tunable for a case in which the probability that an untuned design meets the specifications is very low and (b) only one parameter is tunable.

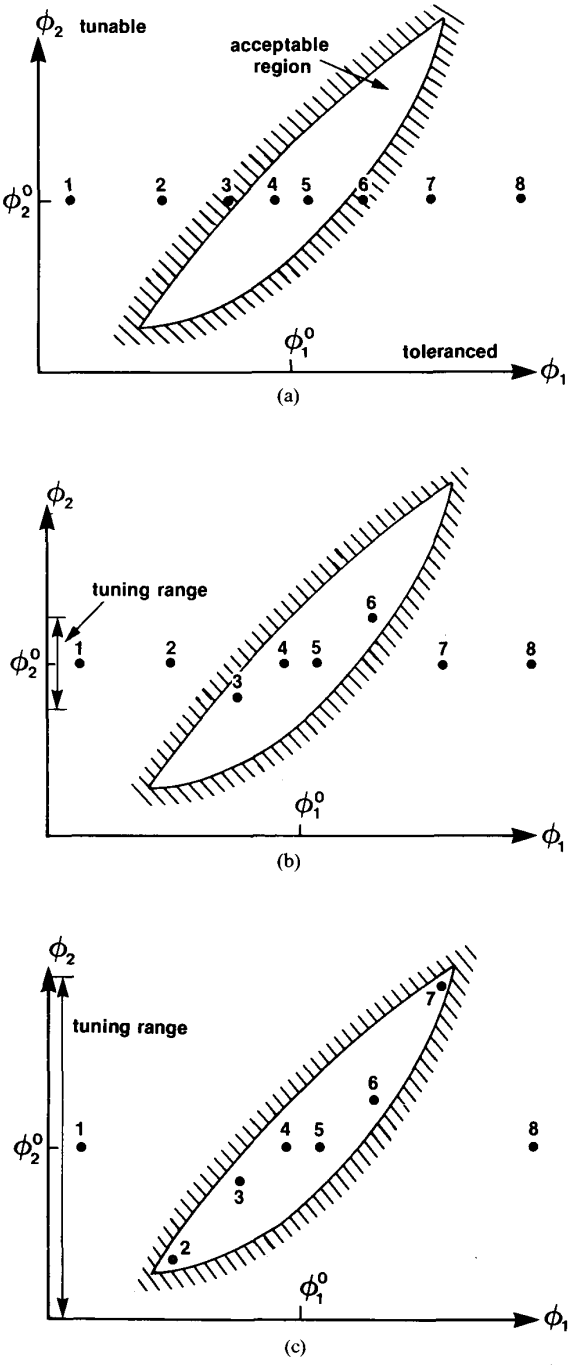

Fig. 7. An illustration of multicircuit design considering eight circuit outcomes. ϕ_1 is toleranced and ϕ_2 is tunable. (a) Without tuning the yield is 2/8 (25 percent). (b) Tuning on ϕ_2 is restricted to a small range. The improved yield is 4/8 (50 percent). (c) A 75 percent yield is achieved by allowing a large tuning range.

τ^k such that the specifications will be satisfied at ϕ^k which may otherwise be unacceptable, as depicted in Figs. 6 and 7. The introduction of tuning, on the other hand, also increases design complexity and manufacturing cost. We seek a suitable compromise by solving an optimization problem in which τ^k are treated as part of the variables.

From nominal design, centering, optimal tolerancing, to optimal tuning, we have defined a range of problems which lead to increasingly improved yield but, on the other hand, correspond to increasing complexity. Some specific formulations are discussed in Section V. Analogously to ZTP, FTP, and VTP, we can define zero tuning, fixed tuning, and variable tuning problems [20].

C. Multicircuit Modeling

The uncertainties that affect circuit modeling can be discussed under the following categories.

1) Measurement errors will inevitably exist in practice, as represented by $\Delta \boldsymbol{F}^M$ in (17): $\boldsymbol{F}^M = \boldsymbol{F}^{M,0}(\boldsymbol{\phi}^M) + \Delta \boldsymbol{F}^M$.
2) Even without measurement errors, the calculated response $\boldsymbol{F}^{H,0}$ may never be able to match $\boldsymbol{F}^{M,0}$ perfectly, due to, for example, the use of a model of insufficient order or inadequate complexity. Such an inherent mismatch is accounted for in (18) by $\boldsymbol{F}^H = \boldsymbol{F}^{H,0} + \Delta \boldsymbol{F}^H$.
3) Even if neither $\Delta \boldsymbol{F}^M$ nor $\Delta \boldsymbol{F}^H$ exists so that $\boldsymbol{F}^{H,0} = \boldsymbol{F}^M$, we may still not be able to uniquely identify $\boldsymbol{\phi}$ from the set of measurements that has been selected. This happens when the system of (generally nonlinear) equations $\boldsymbol{F}^{H,0}(\boldsymbol{\phi}) - \boldsymbol{F}^M = \boldsymbol{0}$, where $\boldsymbol{F}^M$ is the data, is underdetermined. Typically, this problem occurs when, for any reason, many internal nodes are inaccessible to direct measurement. An overcomplicated equivalent circuit, including unknown parasitic elements, is frequently at the heart of this phenomenon.
4) The parasitic effects that are not adequately modeled by $\boldsymbol{\phi}^H$ contribute to the uncertainty $\Delta \boldsymbol{F}^L$. This is another source of interference with the modeling process.

First we consider the case in which modeling is applied to obtain a suitable $\boldsymbol{\phi}$ such that $\boldsymbol{F}^H(\boldsymbol{\phi})$ approximates $\boldsymbol{F}^M$. The nominal circuit approach may be able to cope with the uncertainties in 1) and 2), and comes up with a $\boldsymbol{\phi}$ which minimizes the errors $\Delta \boldsymbol{F}^M$ and $\Delta \boldsymbol{F}^H$ in a certain sense. But it will not be able to overcome the problem of uniqueness. In practice, we are often unable to determine unambiguously the identifiability of a system, because all these uncertainties can be present at the same time. There will be, typically, a family of solutions which produce reasonable and similar matches between the measured and the calculated responses. We cannot, therefore, rely on any particular set of parameters.

The approach of multicircuit modeling by Bandler *et al.* [12] can be used to overcome these difficulties. Multiple circuits are created by making deliberate adjustments on the physical parameters $\boldsymbol{\phi}^M$. For example, we can change the biasing conditions for an active device and obtain multiple sets of measurements. By doing so, we introduce perturbations to the model which cause some parameters in $\boldsymbol{\phi}$ to change by an unknown amount. For this approach to be successful, each physical adjustment should produce changes in only a few parameters in $\boldsymbol{\phi}$.

Although we do not know the changes in $\boldsymbol{\phi}$ quantitatively, it is often possible to identify which model parameters may have been affected by the physical adjustments. Such a qualitative knowledge may be apparent from the definition of the model or it may come from practical experience. In the attempt to process multiple circuits simultaneously, we define those model parameters that are not supposed to change as common variables and, at the same time, allow the others to vary between different circuits. By doing so, we force the solution to exhibit the desired consistency and, therefore, improve the reliability of the result. In other words, from a family of possible solutions we select the one that conforms to the topological constraints. Bandler *et al.* have shown an example [12, Section III-A] in which $\boldsymbol{\phi}$ can not be uniquely identified due to inaccessible nodes. The problem was effectively addressed using the multicircuit approach.

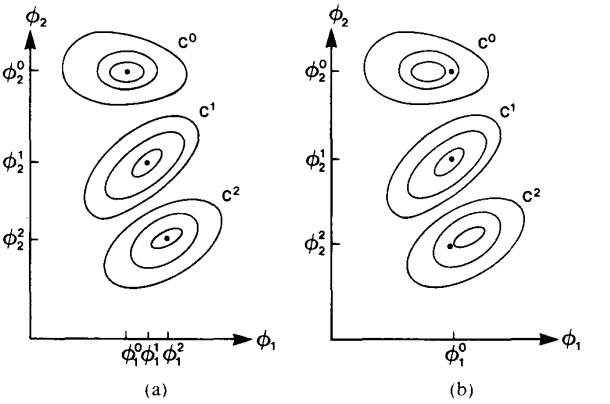

Fig. 8. An illustration of multicircuit modeling. Three circuits are created by making two physical adjustments. Assume that we know that ϕ_1 should not be affected by the physical adjustments. C^0, C^1, and C^2 are contours of the error functions corresponding to the three circuits. (a) By treating the three circuits separately, we obtain $\boldsymbol{\phi}^0$, $\boldsymbol{\phi}^1$, and $\boldsymbol{\phi}^2$. ϕ_1^0, ϕ_1^1, and ϕ_1^2 turn out to have different values (which is inconsistent with our knowledge) because of uncertainties. (b) Consistent results can be obtained by defining ϕ_1 as a common variable and processing three circuits simultaneously.

To formulate this mathematically, let

$$\boldsymbol{\phi}^k = \begin{bmatrix} \boldsymbol{\phi}_c^k \\ \boldsymbol{\phi}_a^k \end{bmatrix} \tag{26}$$

where $\boldsymbol{\phi}_c^k$ contains the common variables and $\boldsymbol{\phi}_a^k$ contains the variables which are allowed to vary between the kth circuit and the reference circuit $\boldsymbol{\phi}^0$. We then define the optimization variables by

$$\boldsymbol{x} = \left[\left(\boldsymbol{\phi}^0\right)^T \left(\boldsymbol{\phi}_a^1\right)^T \cdots \left(\boldsymbol{\phi}_a^K\right)^T \right]^T \tag{27}$$

and state the optimization problem as to

$$\underset{\boldsymbol{x}}{\text{minimize}}\, U(\boldsymbol{x}) = \| \boldsymbol{f} \|_p \tag{28}$$

where

$$\boldsymbol{f} = \left[\boldsymbol{e}^T(\boldsymbol{\phi}^0)\ \boldsymbol{e}^T(\boldsymbol{\phi}^1) \cdots \boldsymbol{e}^T(\boldsymbol{\phi}^K) \right]^T. \tag{29}$$

Although any l_p norm may be used, the unique property of l_1 discussed in detail by Bandler *et al.* [12] can be exploited to great advantage. The concept of common and independent variables is depicted in Fig. 8.

Now, suppose that we do not have a clear idea about which model parameters may have been affected by the

adjustment on ϕ^M. In this case, we let

$$x = \left[(\phi^0)^T\ (\phi^1)^T \cdots (\phi^K)^T\right]^T \tag{30}$$

and change the objective function to an l_p norm of

$$f = \left[e^T(\phi^0) \cdots e^T(\phi^K)\ \alpha_1(\phi^1 - \phi^0)^T \cdots \alpha_K(\phi^K - \phi^0)^T\right]^T \tag{31}$$

where $\alpha_1, \alpha_2, \cdots, \alpha_K$ are nonnegative multipliers (weights).

Using this formulation, while minimizing the errors e, we penalize the objective function for any deviates between ϕ^k and ϕ^0, since our only available knowledge is that only a few parameters in ϕ^k should have any significant changes. To be effective, an l_1 norm should be used. A similar principle has been successfully applied to the analog circuit fault location problem [9], [27].

A practical application to FET modeling has been described by Bandler *et al.* in [16], where multiple circuits were created by taking three sets of actual measurements under different biasing conditions.

Another important application of multicircuit modeling is to create analytical formulas which link the model ϕ to the actual physical parameters ϕ^M. Such formulas will become extremely useful in guiding an actual production alignment or tuning procedure. A sequence of adjustments on ϕ^M can be systematically made and multiple sets of measurements are taken. By nominal circuit optimization, these measurements would be processed separately to obtain a set of static models. In the presence of uncertainties, a single change in ϕ^M may seem to cause fluctuations in all the model parameters. Obviously, such results are of very little use. In contrast, multicircuit modeling is more likely to produce models that are consistent and reliable. Since the measurements are made systematically, it certainly makes sense to process them simultaneously. Actually, the variables need not be equivalent circuit model parameters. They can include coefficients of a proposed formula as well.

An example of establishing an experimental relationship between the physical and model parameters for a multicavity filter using multiple sets of actual measurements has been described by Daijavad [44].

The multicircuit approach can also be applied to model verification. This is typically related to cases where the parasitic uncertainty ΔF^L has put the validity of a model in doubt. Instead of defining common and independent variables explicitly, we use the formulation of (30) and (31). If consistent results are obtained, then our confidence in the model is strengthened. Otherwise we should probably reject the current model and consider representing the parasitics more adequately. A convincing example has been demonstrated by Bandler *et al.* [12, section V, test 2].

The commercial packages TOUCHSTONE [104], [105] and SUPER-COMPACT [99] allow a hierarchy of circuit blocks and permit the use of variable labels. Multiple circuits and common variables can be easily defined utilizing these features.

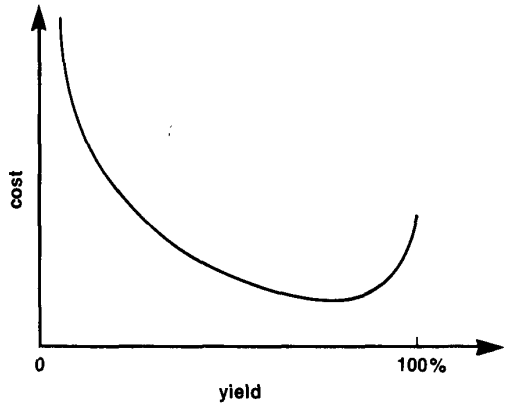

Fig. 9. A typical cost-versus-yield curve [97].

V. Techniques for Statistical Design

In Section IV we have generally discussed uncertainties at different levels, and, in particular, we have expressed our desire to maximize yield in the presence of uncertainties. Optimal tolerancing and tuning have also been identified as means to further reduce cost in the actual production.

We begin this section with a review of some existing techniques for statistical design. Some of the earliest work in this area came from Karafin [68], Pinel and Roberts [87], Butler [36], Elias [52], Bandler, Liu, and Tromp [24]. During the years, significant contributions have been made by, among others, Director and Hachtel [47] (the simplicial method), Soin and Spence [98] (the gravity method), Bandler and Abdel-Malek [1], [2], [7] (multidimensional approximation), Biernacki and Styblinski [30] (dynamic constraint approximation), Polak and Sangiovanni-Vincentelli [90] (a method using outer approximation), as well as Singhal and Pinel [97] (the parametric sampling method). Following the review, we propose a generalized l_p centering algorithm.

A commonly assumed cost versus yield curve [97] is shown in Fig. 9. Actually, hard data are difficult to obtain, and, as we shall see, rather abstract objective functions are often selected for the tolerance-yield design problem. Fig. 10 shows a design with a 100 percent yield and a second design corresponding to the minimum cost.

A. Worst-Case Design

By this approach, we attempt to achieve a 100 percent yield. Since it means that the specifications have to be satisfied for all the possible outcomes, we need to consider only the worst cases.

Bandler et al. [23], [24] have formulated it as a nonlinear programming problem

$$\begin{aligned} &\underset{x}{\text{minimize}}\ C(x) \\ &\text{subject to } e(\phi^k) \leqslant 0, \qquad \text{for all } k \end{aligned} \tag{32}$$

where $C(x)$ is a suitable cost function and the points ϕ^k

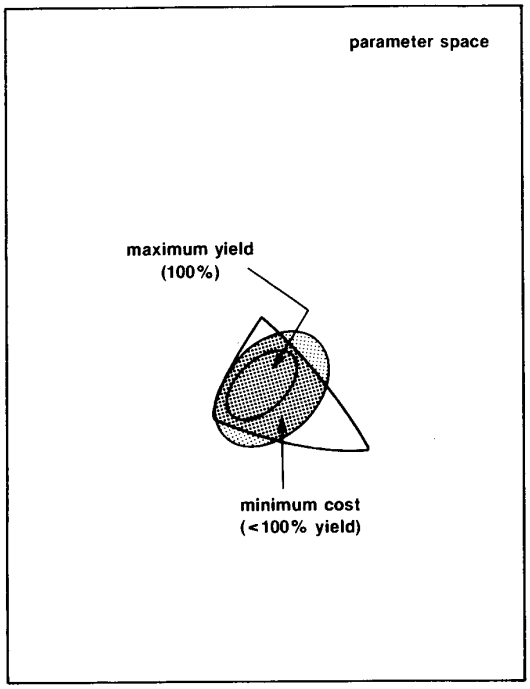

Fig. 10. A maximum yield design and a minimum cost design.

are the worst cases. For instance, we may have

$$C(\boldsymbol{x}) = \sum_{i \in I_e} \frac{a_i}{\varepsilon_i} + \sum_{i \in I_t} b_i t_i \tag{33}$$

where I_e and I_t are index sets identifying the toleranced and tunable parameters, respectively. ε_i and t_i are the tolerance and the tuning range, respectively, associated with the ith parameter. a_i and b_i are nonnegative weights. A cost function can also be defined for relative tolerances and tuning by including ϕ_i^0 into (33). A critical part of this approach is the determination of the worst cases. Vertices of the tolerance region, for example, are possible candidates for the worst cases by assuming one-dimensional convexity. The yield function does not enter (32) explicitly; instead, a 100 percent yield is implied by a feasible solution.

Bandler and Charalambous [11] have demonstrated a solution to (32) by minimax optimization. Polak and Sangiovanni-Vincentelli [90] have proposed a different but equivalent formulation which involves a nondifferentiable optimization.

A worst-case design is not always appropriate. While attempting to obtain a 100 percent yield, the worst-case approach may necessitate unrealistically tight tolerances, or demand excessive tuning. In either case, the cost may be too high. A perfect 100 percent yield may not even be realizable.

B. Methods of Approximating the Acceptable Region

Since yield is given by the percentage of model outcomes that fall into the acceptable region, we may wish to find an approximation to that region. The acceptable region has been defined in (16) as $R_a = \{\boldsymbol{\phi} | H(\boldsymbol{e}(\boldsymbol{\phi})) \leqslant 0\}$.

Director and Hachtel [47] have devised a simplicial approximation approach. It begins by determining points $\boldsymbol{\phi}^k$ on the boundary of R_a which is given by $\Omega_a = \{\boldsymbol{\phi} | H(\boldsymbol{e}(\boldsymbol{\phi})) = 0\}$. The convex hull of these points forms a polyhedron. The largest hypersphere inscribed within the polyhedron gives an approximation to R_a and is found by solving a linear programming problem. Using line searches, more points on the boundary are located and the polyhedron is expanded. The process thus provides a monotonically increasing lower bound on the yield. The center and radius of the hypersphere can be used to determine the centered nominal point and the tolerances, respectively. The application of this method is, however, severely limited by the assumption of a convex acceptable region.

Bandler and Abdel-Malek [1], [2], [7] have presented a method which approximates each $e_j(\boldsymbol{\phi})$ by a low-order multidimensional polynomial. Model simulations are performed at some $\boldsymbol{\phi}^k$ selected around a reference point. From the values of $e_j(\boldsymbol{\phi}^k)$ the coefficients of the approximating polynomial are determined by solving a linear system of equations. Appropriate linear cuts are constructed to approximate the boundary Ω_a. The yield is estimated through evaluation of the hypervolumes that lie outside R_a but inside the tolerance region. In critical regions these polynomial approximations are updated during optimization. The one-dimensional convexity assumption for this method is much less restrictive than the multidimensional convexity required by the simplicial approach. Sensitivities for the estimated yield are also available.

Recently, Biernacki and Styblinski [30] have extended the work on multidimensional polynomial approximation by considering a dynamic constraint approximation scheme. It avoids the large number of base points required for a full quadratic interpolation by selecting a maximally flat interpolation. During optimization, whenever a new base point is added, the approximation is updated. It shows improved accuracy compared with a linear model as well as reduced computational effort compared with a full quadratic model.

C. The Gravity Method

Soin and Spence [98] proposed a statistical exploration approach. Based on a Monte Carlo analysis, the centers of gravity of the failed and passed samples are determined as, respectively,

$$\boldsymbol{\phi}^f = \left[\sum_{k \in J} \boldsymbol{\phi}^k\right] \Big/ K_{\text{fail}}$$

$$\boldsymbol{\phi}^p = \left[\sum_{k \notin J} \boldsymbol{\phi}^k\right] \Big/ K_{\text{pass}} \tag{34}$$

where J is the index set identifying the failed samples. K_{fail} and K_{pass} are the numbers of failed and passed samples, respectively. The nominal point $\boldsymbol{\phi}^0$ is then adjusted along the direction $\boldsymbol{s} = \boldsymbol{\phi}^p - \boldsymbol{\phi}^f$ using a line search.

This algorithm is simple but also heuristic. It is not clear as to how the gravity centers are related to the yield in a general multidimensional problem.

D. The Parametric Sampling Method

The parametric sampling approach by Singhal and Pinel [97] has provided another promising direction. A continuous estimate of yield (as opposed to the Monte Carlo estimate, using discrete samples) is given by the following integral:

$$Y(\boldsymbol{x}) = \int_{-\infty}^{+\infty} I_a(\boldsymbol{\phi}) \Gamma(\boldsymbol{\phi}, \boldsymbol{x})\, d\boldsymbol{\phi} \tag{35}$$

where $I_a(\boldsymbol{\phi})$ is the acceptance index defined in (20) and $\Gamma(\boldsymbol{\phi}, \boldsymbol{x})$ the parameter distribution density function which depends on the design variables $\boldsymbol{x}$ (e.g., the nominal point specifies the mean value and the tolerances control the standard deviations). Normally, in order to estimate the yield, we generate samples $\boldsymbol{\phi}^k$, $k = 1,2,\cdots,K$, from the component density Γ, perform K circuit analyses, and then take the average of $I_a(\boldsymbol{\phi}^k)$. For each new set of variables $\boldsymbol{x}$ we would have a new density function, and therefore, the sampling and circuit analyses have to be repeated.

The parametric sampling method is based on the concept of importance sampling as

$$Y(\boldsymbol{x}) = \int_{-\infty}^{+\infty} I_a(\boldsymbol{\phi}) \frac{\Gamma(\boldsymbol{\phi}, \boldsymbol{x})}{h(\boldsymbol{\phi})} h(\boldsymbol{\phi})\, d\boldsymbol{\phi} \tag{36}$$

where $h(\boldsymbol{\phi})$ is called the sampling density function. The samples $\boldsymbol{\phi}^k$ are generated from $h(\boldsymbol{\phi})$ instead of $\Gamma(\boldsymbol{\phi}, \boldsymbol{x})$. An estimate of the yield is made as

$$\begin{aligned} Y(\boldsymbol{x}) &\simeq \frac{1}{K} \sum_{k=1}^{K} I_a(\boldsymbol{\phi}^k) \frac{\Gamma(\boldsymbol{\phi}^k, \boldsymbol{x})}{h(\boldsymbol{\phi}^k)} \\ &= \frac{1}{K} \sum_{k=1}^{K} I_a(\boldsymbol{\phi}^k) W(\boldsymbol{\phi}^k, \boldsymbol{x}). \end{aligned} \tag{37}$$

The weights $W(\boldsymbol{\phi}^k, \boldsymbol{x})$ compensate for the use of a sampling density different from the component density.

This approach has two clear advantages. First, once the indices $I_a(\boldsymbol{\phi}^k)$ are calculated, no more model simulations are required when $\boldsymbol{x}$ is changed. Furthermore, if Γ is a differentiable density function, then gradients of the estimated yield are readily available. Hence, powerful optimization techniques may be employed. In practice, the algorithm starts with a large number of base points sampled from $h(\boldsymbol{\phi})$ to construct the initial databank. To maintain a sufficient accuracy, the databank needs to be updated by adding new samples during optimization.

This approach, however, cannot be applied to nondifferentiable density functions such as uniform, discrete, and truncated distributions. It can be extended to include some tunable parameters if the tuning ranges are fixed or practically unlimited. In this case the acceptance index $I_a(\boldsymbol{\phi}^k)$ is defined as 1 if $\boldsymbol{\phi}^k$ is acceptable after tuning. If $\boldsymbol{\phi}^k$ is unacceptable before tuning, then whether it can be tuned and, if so, by how much, may have to be determined through optimization. Variable tuning ranges (in order to minimize cost) cannot be accommodated by the parametric sampling method.

E. Generalized l_p Centering

Here, we propose a generalized l_p centering algorithm which encompasses, in a unified formulation, problems of 100 percent yield (worst-case design) and less than 100 percent yield.

First, we consider the centering problem where we have fixed tolerances and no tuning. Only the nominal point $\boldsymbol{\phi}^0$ is to be optimized. Define

$$\boldsymbol{f} = \left[\boldsymbol{e}^T(\boldsymbol{\phi}^1) \cdots \boldsymbol{e}^T(\boldsymbol{\phi}^K)\right]^T \tag{38}$$

as the set of multicircuit error functions. We can achieve a worst-case minimax design by

$$\underset{\boldsymbol{x}}{\text{minimize}}\, U(\boldsymbol{x}) = H_\infty(\boldsymbol{f}) = \max_k \max_j \left\{ e_j(\boldsymbol{\phi}^k) \right\} \tag{39}$$

where the multiple circuits $\boldsymbol{\phi}^k$ are related to $\boldsymbol{\phi}^0$ according to (19).

If a 100 percent yield is not attainable, we would naturally look for a solution where the specifications are met by as many points (out of K circuits) as possible. For this purpose minimax is not a proper choice, since unless and until the worst case is dealt with nothing else seems to matter. We may attempt to use a generalized l_2 or l_1 function (i.e., $H_2(\boldsymbol{f})$ or $H_1(\boldsymbol{f})$) instead of $H_\infty(\boldsymbol{f})$ in (39), hoping to reduce the emphasis given to the worst case.

In order to gain more insight into the problem, we define, for each $\boldsymbol{\phi}^k$, a scalar function which will indicate directly whether $\boldsymbol{\phi}^k$ satisfies or violates the specifications and by how much. For this purpose, we choose a set of generalized l_p functions as

$$v_k(\boldsymbol{x}) = H_p(\boldsymbol{e}(\boldsymbol{\phi}^k)), \qquad k = 1,2,\cdots,K. \tag{40}$$

The sign of v_k indicates the acceptability of $\boldsymbol{\phi}^k$ while the magnitude of v_k measures, so to speak, the distance between $\boldsymbol{\phi}^k$ and the boundary of the acceptable region. For example, with $p = \infty$ the distance is measured in the worst-case sense whereas for $p = 2$ it will be closer to a Euclidean norm.

We can define a generalized l_p centering as

$$\underset{\boldsymbol{x}}{\text{minimize}}\, U(\boldsymbol{x}) = H_p(\boldsymbol{u}(\boldsymbol{x})) \tag{41}$$

where

$$\boldsymbol{u}(\boldsymbol{x}) = \begin{bmatrix} \alpha_1 v_1 \\ \vdots \\ \alpha_K v_K \end{bmatrix} \begin{bmatrix} \alpha_1 H_q(\boldsymbol{e}(\boldsymbol{\phi}^1)) \\ \vdots \\ \alpha_K H_q(\boldsymbol{e}(\boldsymbol{\phi}^K)) \end{bmatrix} \tag{42}$$

and $\alpha_1, \alpha_2, \cdots, \alpha_K$ are a set of positive multipliers. With different p and q it leads to a variety of algorithms for yield enhancement. We discuss separately the case where a nonpositive $U(\boldsymbol{x})$ exists and the case where we always have $U(\boldsymbol{x}) > 0$.

In the first case, the existence of a $U(\boldsymbol{x}) \leqslant 0$ indicates that a 100 percent yield is attainable. We should point out

that for a given x the sign of $U(x)$ does not depend on p, q, or α_k. However, the optimal solution x at which $U(x)$ attains its minimum is dependent on p, q, and α. This means that using any values of p, q, and α we will be able to achieve a $U(x) \leq 0$ (i.e., to achieve a 100 percent yield). Furthermore, by using different p, q, and α, we influence the centering of ϕ^0. Interestingly, the worst-case centering (39) becomes a special case by letting both $p, q = \infty$ and using unit multipliers.

Now consider the case where the optimal yield is less than 100 percent. In this case we propose the use of $p = 1$ and $q = 1$ in (41). Also, given a starting point x_0, we define the set of multipliers by

$$\alpha_k = 1/|v_k(x_0)|, \qquad k = 1,2,\cdots,K. \tag{43}$$

Our proposition is based on the following reasoning (a more complete theoretical justification is reserved for a future paper).

Consider the l_p sum given by

$$\sum_{k \in J} [u_k(x)]^p \tag{44}$$

where $J = \{k | u_k > 0\}$. As $p \to 0$ (44) approaches the total number of unacceptable circuits which we wish to minimize. The smallest p that gives a convex approximation is 1. This leads to the generalized l_1 objective function given by

$$U(x) = \sum_{k \in J} u_k(x) = \sum_{k \in J} \alpha_k v_k(x). \tag{45}$$

With the multipliers defined by (43), the value of the objective function at the starting point, namely $U(x_0)$, is precisely the count of unacceptable circuits. Also, notice that the magnitude of v_k measures the closeness of ϕ^k to the acceptable region. A small $|v_k|$ indicates that ϕ^k is close to satisfying or violating the specifications. Therefore, we assign a large multiplier to it so that more emphasis will be given to ϕ^k during optimization. On the other hand, we de-emphasize those points that are far away from the boundary of the acceptable region because their contributions to the yield are less likely to change.

One important feature of this approach is its capability of accommodating arbitrary tolerance distributions, since they only influence the generation of ϕ^k. The numerical results we have obtained are very promising. The generalized l_p centering algorithm can also be extended to include variable tolerances and tuning.

VI. Examples of Statistical Design

Example 1

The classical two-section 10:1 transmission line transformer, originally proposed by Bandler *et al.* [23] to test minimax optimizers, is a good example for illustrating graphically the basic ideas of centering and tolerancing. An upper specification on the reflection coefficient as $|\rho| \leq 0.55$ and 11 frequencies $\{0.5, 0.6, \cdots, 1.5$ GHz$\}$ are considered. The lengths of the transmission lines are fixed at the quarter-wavelength while the characteristic impedances Z_1 and Z_2 are to be toleranced and optimized. Fig. 11 shows the minimax contours, the minimax nominal solution, and the worst-case solutions [23] for

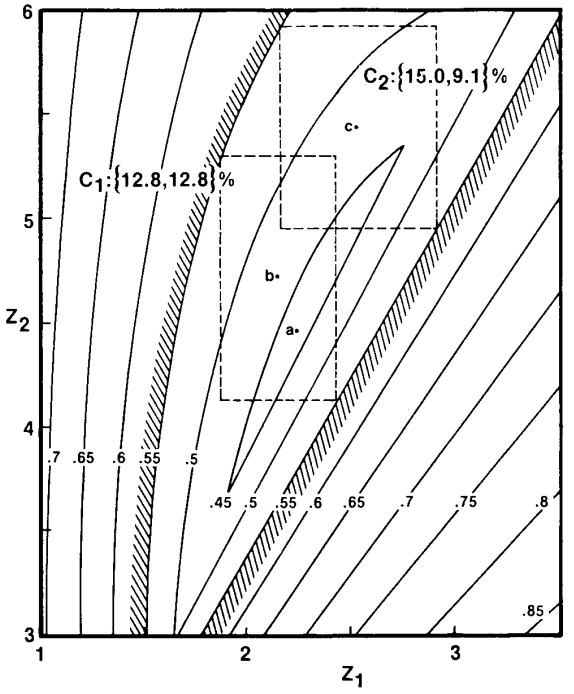

Fig. 11. Contours of max $|\rho_j|$ with respect to Z_1 and Z_2 for the two-section transformer indicating the minimax nominal solution a, the centered design with relative tolerances b, and the centered design with absolute tolerances c. The values in brackets are the optimized tolerances (as percentages of the nominal values). The specification is $|\rho| \leq 0.55$.

$P0$: minimize $C_1 = Z_1^0/\varepsilon_1 + Z_2^0/\varepsilon_2$
subject to $Y = 100$ percent

$P1$: minimize $C_2 = 1/\varepsilon_1 + 1/\varepsilon_2$ subject to $Y = 100$ percent

where $\varepsilon_1, \varepsilon_2$ denote tolerances on Z_1 and Z_2 (assuming independent uniform distributions), and Y is the yield. The cost functions C_1 and C_2 correspond to, respectively, relative and absolute tolerancing problems. Two problems of less than 100 percent yield have also been considered by Bandler and Abdel-Malek [7] as

$P2$: minimize C_2 subject to $Y \geq 90$ percent

$P3$: minimize C_2/Y.

The optimal tolerance regions and nominal values for $P2$ and $P3$ are shown in Fig. 12. For more details see the original paper [7].

Example 2

The statistical design of a Chebyshev low-pass filter (Singhal and Pinel [97]) is used as the second example. Fifty-one frequencies $\{0.02, 0.04, \cdots, 1.0, 1.3$ Hz$\}$ are considered. An upper specification of 0.32 dB on the insertion loss is defined for frequencies from 0.02 to 1.0 Hz. A lower specification of 52 dB on the insertion loss is defined at 1.3 Hz.

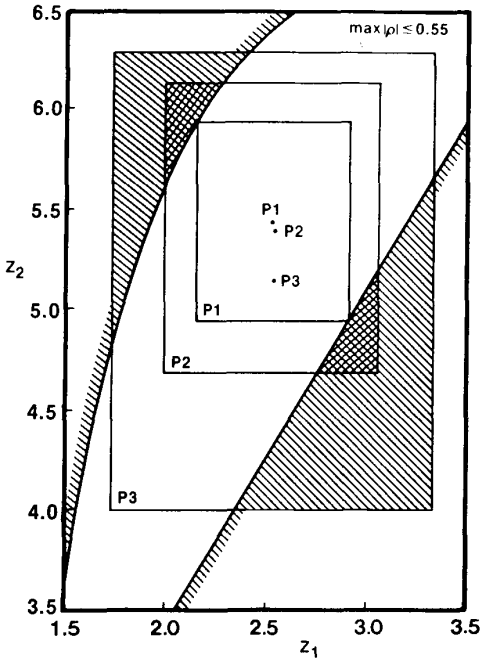

Fig. 12. The optimized tolerance regions and nominal values for the worst case design $P1$, 90 percent yield design $P2$, and minimum cost design $P3$ of the two-section transformer.

TABLE I
STATISTICAL DESIGN OF A LOW-PASS FILTER USING GENERALIZED l_1 CENTERING TECHNIQUE

Component ϕ_i	Nominal Design $\phi_i^{0,0}$	Case 1 $\phi_i^{0,1}$	Case 2 $\phi_i^{0,2}$	Case 3 $\phi_i^{0,3}$
x_1	0.2251	0.21954	0.21705	0.21530
x_2	0.2494	0.25157	0.24677	0.23838
x_3	0.2523	0.25529	0.24784	0.24120
x_4	0.2494	0.24807	0.24019	0.23687
x_5	0.2251	0.22042	0.21753	0.21335
x_6	0.2149	0.22627	0.23565	0.23093
x_7	0.3636	0.36739	0.37212	0.38225
x_8	0.3761	0.36929	0.38012	0.39023
x_9	0.3761	0.37341	0.38371	0.39378
x_{10}	0.3636	0.36732	0.37716	0.38248
x_{11}	0.2149	0.22575	0.22127	0.23129
Yield	49%	77.67%	79.67%	83.67%
Number of samples used for design		50	100	100
Starting point		$\phi^{0,0}$	$\phi^{0,1}$	$\phi^{0,2}$
Number of iterations		16	18	13
CPU time (VAX 8600)		10 sec.	30 sec.	26 sec.

Independent uniform distributions are assumed for each component with fixed tolerances $\epsilon_i = 1.5\%\ \phi_i^0$. The yield is estimated based on 300 samples.

Singhal and Pinel [97] have applied the parametric sampling method to the same circuit, assuming normal distributions for the toleranced elements. But, as we have pointed out earlier in this paper, the parametric sampling method cannot be applied to nondifferentiable (such as uniform) distributions. Here, we consider a uniformly distributed 1.5 percent relative tolerance for each component. The generalized l_p centering algorithm described in Section V is used with $p=1$. The nominal solution by standard synthesis as given in [97] was used as starting point, which has a 49 percent yield (w.r.t. the tolerances specified). An 84 percent yield is achieved at the solution which involves a sequence of three design cycles with a total CPU time of 66 seconds on the VAX 8600. Some details are provided in Table I.

VII. GRADIENT-BASED OPTIMIZATION METHODS

So far we have concentrated on translating our practical concerns into mathematical expressions. Now we turn our attention to the solution methods for optimization problems.

The studies in the last two decades on the theoretical and algorithmic aspects of optimization techniques have produced a great number of results. Modern state-of-the-art methods have largely replaced the primitive trial-and-error-approach. In particular, gradient-based optimization methods have gained increasing popularity in recent years for their effectiveness and efficiency.

The majority of gradient-based methods belong to the Gauss–Newton, quasi-Newton, and conjugate gradient families. All these are iteraiive algorithms which, from a given starting point $\boldsymbol{x}_0$, generate a sequence of points $\{\boldsymbol{x}_k\}$. The success of an algorithm depends on whether $\{\boldsymbol{x}_k\}$ will converge to a point $\boldsymbol{x}^*$ and, if so, whether $\boldsymbol{x}^*$ will be a stationary point. An iterative algorithm is described largely by one of its iterations as how to obtain $\boldsymbol{x}_{k+1}$ from $\boldsymbol{x}_k$.

We use the notation $U(\boldsymbol{x})$ for the objective function and ∇U for the gradient vector of U. When $U(\boldsymbol{x})$ is defined by an l_p function, we use $\boldsymbol{f}$ to denote the set of individual error functions so that $U = H(\boldsymbol{f})$. We also use $\boldsymbol{f}_j'$ for the first-order derivatives of f_j and $\boldsymbol{G}$ for the Jacobian matrix of $\boldsymbol{f}$.

A. l_p Optimization and Mathematical Programming

Of the l_p family, l_1, l_2, and l_∞ are the most distinctive and by far the most useful members. Apart from their unique theoretical properties, it is very important from the algorithmic point of view that linear l_1, l_2, and l_∞ problems can be solved exactly using linear or quadratic programming techniques. Besides, all the other members of the l_p family have a continuously differentiable function and, therefore, can be treated similarly to the l_2 case.

An l_1, l_2, or l_∞ optimization problem can be converted into a mathematical program. The concepts of local linearization and optimality conditions are often clarified by the equivalent formulation.

For instance, the minimization of $\|\boldsymbol{f}\|_1$ is equivalent to

$$\underset{x,y}{\text{minimize}} \sum_{j=1}^{m} y_j \tag{46}$$

TABLE II
MATHEMATICAL PROGRAMMING EQUIVALENT FORMULATIONS FOR l_1, l_2, AND l_∞ OPTIMIZATION

The original problem: $\min_{\mathbf{x}} H(\mathbf{f})$

The equivalent problem: $\min_{\mathbf{x},\mathbf{y}} V(\mathbf{x},\mathbf{y})$ subject to the constraints as defined below

$H(\mathbf{f})$	$V(\mathbf{x},\mathbf{y})$	constraints (for $j = 1, 2, \ldots, m$)
$\|\mathbf{f}\|_1$	$\sum_{j=1}^{m} y_j$	$y_j \geq f_j,\ y_j \geq -f_j$
$\|\mathbf{f}\|_2$	$\mathbf{y}^T\mathbf{y}$	$y_j = f_j$
$\|\mathbf{f}\|_\infty$	y	$y \geq f_j,\ y \geq -f_j$
$H_1^+(\mathbf{f})$	$\sum_{j=1}^{m} y_j$	$y_j \geq f_j,\ y_j \geq 0$
$H_2^+(\mathbf{f})$	$\mathbf{y}^T\mathbf{y}$	$y_j \geq f_j,\ y_j \geq 0$
$H_\infty^+(\mathbf{f})$	y	$y \geq f_j, y \geq 0$
$H_\infty(\mathbf{f})$	y	$y \geq f_j$

Note: A generalized ℓ_p function $H_p(\mathbf{f})$ is defined through $H_p^+(\mathbf{f})$ and $H_p^-(\mathbf{f})$. H_p^- is a continuously differentiable function for all $p < \infty$.

subject to

$$y_j \geq f_j(\boldsymbol{x}), \qquad y_j \geq -f_j(\boldsymbol{x}), \qquad j = 1,2,\cdots,m.$$

Other equivalent formulations are summarized in Table II. For the convenience of presentation, we denote these mathematical programming problems by $P(\boldsymbol{x}, \boldsymbol{f})$. One important feature of $P(\boldsymbol{x}, \boldsymbol{f})$ is that it has a linear or quadratic objective function. If $\boldsymbol{f}$ is a set of linear functions, then $P(\boldsymbol{x}, \boldsymbol{f})$ becomes a linear or quadratic program which can be solved using standard techniques. Equally importantly, linear constraints can be easily incorporated into the problem. Let $P(\boldsymbol{x}, \boldsymbol{f}, D)$ be the problem of $P(\boldsymbol{x}, \boldsymbol{f})$ subject to a set of linear constraints of the form

$$D: \begin{array}{ll} \boldsymbol{a}_l^T\boldsymbol{x} + b_l = 0, & l = 1,2,\cdots,L_{eq} \\ \boldsymbol{a}_l^T\boldsymbol{x} + b_l \geq 0, & l = L_{eq}+1,\cdots,L \end{array} \tag{47}$$

where $\boldsymbol{a}_l$ and b_l are constants. If $P(\boldsymbol{x}, \boldsymbol{f})$ is a linear or quadratic program, so is $P(\boldsymbol{x}, \boldsymbol{f}, D)$. In other words, unconstrained and linearly constrained linear l_1, l_2, and l_∞ problems can be solved using standard linear or quadratic programming techniques.

B. Gauss–Newton Methods Using Trust Regions

For a general problem, we may, at each iteration, substitute $\boldsymbol{f}$ with a linearized model $\bar{\boldsymbol{f}}$ so that $P(\boldsymbol{x}, \bar{\boldsymbol{f}})$ can be solved.

For a Gauss–Newton type method, at a given point $\boldsymbol{x}_k$, a linearization of $\boldsymbol{f}$ is made as

$$\bar{\boldsymbol{f}}(\boldsymbol{h}) = \boldsymbol{f}(\boldsymbol{x}_k) + \boldsymbol{G}(\boldsymbol{x}_k)\boldsymbol{h} \tag{48}$$

where $\boldsymbol{G}$ is the Jacobian matrix. We then solve the linear or quadratic program $P(\boldsymbol{h}, \bar{\boldsymbol{f}}, D)$, where

$$D: \begin{array}{ll} \Lambda_k \geq h_j, & j = 1,2,\cdots,n \\ \Lambda_k \geq -h_j, & j = 1,2,\cdots,n. \end{array} \tag{49}$$

These additional constraints define a trust region in which the linearized model $\bar{\boldsymbol{f}}$ is believed to be a good approximation to $\boldsymbol{f}$.

Another way to look at it is that we have applied a semilinearization (Madsen [78]) to $U(\boldsymbol{x}) = H(\boldsymbol{f})$ resulting in

$$\bar{U}(\boldsymbol{h}) = H(\bar{\boldsymbol{f}}(\boldsymbol{h})). \tag{50}$$

It is important to point out that (50) is quite different from a normal linearization as $U(\boldsymbol{h}) \simeq U(\boldsymbol{x}_k) + [\nabla U(\boldsymbol{x}_k)]^T\boldsymbol{h}$ which corresponds to a steepest descent method. In fact ∇U may not even exist.

Denote the solution of $P(\boldsymbol{h}, \bar{\boldsymbol{f}}, D)$ by $\boldsymbol{h}_k$. If $\boldsymbol{x}_k + \boldsymbol{h}_k$ reduces the original objective function, we take it as the next iterate; i.e., if $U(\boldsymbol{x}_k + \boldsymbol{h}_k) < U(\boldsymbol{x}_k)$ then $\boldsymbol{x}_{k+1} = \boldsymbol{x}_k + \boldsymbol{h}_k$. Otherwise we let $\boldsymbol{x}_{k+1} = \boldsymbol{x}_k$. In the latter case, the trust region is apparently too large and, consequently, should be reduced. At each iteration, the local bound Λ_k in (49) is adjusted according to the goodness of the linearized model.

The above describes the essence of a class of algorithms due to Madsen, who has called it method 1. Madsen [78] has shown that the algorithm provides global convergence in which the proper use of trust regions constitutes a critical part. Such a method has been implemented as an important element in the minimax and l_1 algorithms of Hald and Madsen [65], [66]. In some other earlier work by Osborne and Watson [85], [86] the problem $P(\boldsymbol{h}, \bar{\boldsymbol{f}})$ was solved without incorporating a trust region and the solution $\boldsymbol{h}_k$ was used as the direction for a line search. For their methods no convergence can be guaranteed and $\{\boldsymbol{x}_k\}$ may even converge to a nonstationary point.

Normally for the least-squares objective we have to solve a quadratic program at each iteration, which can be a time-consuming process. A remarkable alternative is the Levenberg–Marquardt [76], [81] method. Given $\boldsymbol{x}_k$, it solves

$$\min_{\boldsymbol{h}} \boldsymbol{h}^T(\boldsymbol{G}^T\boldsymbol{G} + \theta_k\mathbf{1})\boldsymbol{h} + 2\boldsymbol{f}^T\boldsymbol{G}\boldsymbol{h} + \boldsymbol{f}^T\boldsymbol{f} \tag{51}$$

where $\boldsymbol{G} = \boldsymbol{G}(\boldsymbol{x}_k)$, $\boldsymbol{f} = \boldsymbol{f}(\boldsymbol{x}_k)$, and $\mathbf{1}$ is an identity matrix. The minimizer $\boldsymbol{h}_k$ is obtained simply by solving the linear system

$$(\boldsymbol{G}^T\boldsymbol{G} + \theta_k\mathbf{1})\boldsymbol{h}_k = -\boldsymbol{G}^T\boldsymbol{f} \tag{52}$$

using, for example, LU factorization. The Levenberg–Marquardt parameter θ_k is very critical for this method. First of all, it is made to guarantee the positive definiteness of (52). Furthermore, it plays, roughly speaking, an inversed role of Λ_k to control the size of a trust region. When $\theta_k \to \infty$, $\boldsymbol{h}_k$ gives an infinitesimal steepest descent step. When $\theta_k = 0$, $\boldsymbol{h}_k$ becomes the solution to $P(\boldsymbol{h}, \bar{\boldsymbol{f}})$ without bounds, which is equivalent to having $\Lambda_k \to \infty$.

The concept of trust region has been discussed in a broader context by Moré in a recent survey [82].

C. Quasi-Newton Methods

Quasi-Newton methods (also known as variable metric methods) are originated in and steadily upgraded from the work of Davidon [45] and Broyden [33], [34], as well as Fletcher and Powell [55].

For a differentiable $U(\boldsymbol{x})$, a quasi-Newton step is given by

$$\boldsymbol{h}_k = -\alpha_k \boldsymbol{B}_k^{-1} \nabla U(\boldsymbol{x}_k) \tag{53}$$

where $\boldsymbol{B}_k$ is an approximation to the Hessian of $U(\boldsymbol{x})$ and the step size controlling parameter α_k is to be determined through a line search. However, on some occasions such as in the l_1 or minimax case, the gradient ∇U may not exist, much less the Hessian.

We can gain more insight to the general case by examining the optimality conditions. Applying the Kuhn–Tucker conditions for nonlinear programming [70] to the equivalent problem $P(\boldsymbol{x}, \boldsymbol{f})$, we shall find a set of optimality equations

$$\boldsymbol{R}(\boldsymbol{x}) = \boldsymbol{0}. \tag{54}$$

Since a local optimum $\boldsymbol{x}^*$ must satisfy these equations, we are naturally motivated to solve (54), as a means of finding the minimizer of $U(\boldsymbol{x})$. A quasi-Newton step for solving nonlinear equations (54) is given by

$$\boldsymbol{h}_k = -\alpha_k \boldsymbol{J}_k^{-1} \boldsymbol{R}(\boldsymbol{x}_k) \tag{55}$$

where $\boldsymbol{J}_k$ is an approximate Jacobian of $\boldsymbol{R}(\boldsymbol{x})$. Only when $U(\boldsymbol{x})$ is differentiable will we have the optimality equations as $\boldsymbol{R}(\boldsymbol{x}) = \nabla U(\boldsymbol{x}) = \boldsymbol{0}$ and (55) reverts to (53).

Hald and Madsen [65], [66] and Bandler *et al.* [21], [22] have described the implementation of a quasi-Newton method for the minimax and l_1 optimization in which the objective functions are not differentiable. Clarke [43] has introduced the concept of generalized gradient, with which optimality conditions can be derived for a broad range of problems.

Quasi-Newton methods, whether in (53) or (55), all require updates of certain approximate Hessians. Many formulas have been proposed over the years. The best known are the Powell symmetric Broyden (PSB) update [91], the Davidon–Fletcher–Powell (DFP) update [45], [55], and the Broyden–Fletcher–Goldfarb–Shanno (BFGS) update [35], [53], [60], [95]. The merits of these formulas and a great many other variations are often compared in terms of their preservation of positive definiteness, convergence to the true Hessian, and numerical performance (see, for instance, Fletcher [54] and Gill and Murray [59]).

Another important point to be considered is the line search. Ideally, α_k is chosen as the minimizer of U in the direction of line search so that $\boldsymbol{h}_k^T \nabla U(\boldsymbol{x}_k + \boldsymbol{h}_k) = 0$. If exact line searches are executed, Dixon [50] has shown that theoretically all members of the Broyden family [34], [53] would have the same performance. In practice, however, exact line search is deemed too expensive and is therefore replaced by other methods. An inexact line search usually limits the evaluation of U and ∇U to only a few points. Interpolation and extrapolation techniques (such as a quadratic or cubic fit) are then incorporated.

D. Combined Methods

The distinguishing advantage of a quasi-Newton method is that it enjoys a fast rate of convergence near a solution. However, like the Newton method for nonlinear equations, the quasi-Newton method is not always reliable from a bad starting point.

Hald and Madsen [65], [66], [78] have suggested a class of two-stage algorithms. A first-order method of the Gauss–Newton type is employed in stage 1 to provide global convergence to a neighborhood of a solution. When the solution is singular, method 1 suffers from a very slow rate of convergence and a switch is made to a quasi-Newton method (stage 2). Several switches between the two methods may take place and the switching criteria ensure the global convergence of the combined algorithm. Numerical examples of circuit applications have demonstrated a very strong performance of the approach [21], [22], [79], [80].

Powell [92] has extended the Levenberg–Marquardt method and suggested a trust-region strategy which interpolates between a steepest descent step and a Newton step. When far away from the solution, the step is biased toward the steepest descent direction to make sure that it is downhill. Once close to the solution, taking a full Newton step will provide rapid final convergence.

E. Conjugate Gradient Methods

Some extremely large-scale engineering applications involve hundreds of variables and functions. Although the rapid advances in computer technology have enabled us to solve increasingly larger problems, there may be cases in which even the storage of a Hessian matrix and the solution of an n by n linear system become unmanageable.

Conjugate gradient methods [56], [75], [88] provide an alternative for such problems. A distinct advantage of conjugate gradient methods is the minimal requirement of storage. Typically three to six vectors of length n are needed, which is substantially less than the requirement by the Gauss–Newton or quasi-Newton methods. However, proper scaling or preconditioning, near-perfect line searches and appropriate restart criteria are usually necessary to ensure convergence. In general, we have to pay the price for the reduced storage by enduring a longer computation time.

VIII. Gradient Calculation and Approximation

The application of gradient-based l_p optimization methods requires the first-order derivatives of the error functions with respect to the variables.

In circuit optimization, these derivatives are usually obtained from a sensitivity analysis of the network under consideration. For linearized circuits in the frequency domain, it is often possible to calculate the exact sensitivities by the adjoint network approach [5], [31], [48].

However, we ought to recognize that an explicit and elegant sensitivity expression is not always available. For time-domain responses and nonlinear circuits, an exact formula may not exist. Even for linear circuits in the frequency domain, large-scale networks present new problems which need to be addressed.

Often, a large-scale network can be described through compounded and interconnected subnetworks. Many commercial CAD packages such as SUPER-COMPACT [99] and TOUCHSTONE [104], [105] have facilitated such a block structure. In this case, one possible approach would be to assemble the overall nodal matrix and solve the system of equations using sparse techniques (see, e.g., Duff [51], Gustavson [61], Hachtel *et al.* [62]). Another possibility is to rearrange the overall nodal matrix into a bordered block structure which is then solved using the Sherman–Morrison–Woodbury formula [63], [96]. Sometimes it is also possible to develop efficient formulas for a special structure, such as the approach of Bandler *et al.* [17] for branched cascaded networks.

In practice, perhaps the most perplexing and time-consuming part of the task is to devise an index scheme through which pieces of lower level information can be brought into the overall sensitivity expression. It may also require a large amount of memory storage for the various intermediate results. Partly due to these difficulties, methods of exact sensitivity calculations have yet to find their way into general-purpose CAD software packages, although the concept of adjoint network has been in existence for nearly two decades and has had success in many specialized applications.

In cases where either exact sensitivities do not exist or are too difficult to calculate, we can utilize gradient approximations [15], [16], [77], [109]. A recent approach to circuit optimization with integrated gradient approximations has been described by Bandler *et al.* [16]. It has been shown to be very effective and efficient in practical applications including FET modeling and multiplexer optimization.

IX. Conclusions

In this review, we have formulated realistic circuit design and modeling problems and described their solution methods. Models, variables, and functions at different levels, as well as the associated tolerances and uncertainties, have been identified. The concepts of design centering, tolerancing, and tuning have been discussed. Recent advances in statistical design, yield enhancement, and robust modeling techniques suitable for microwave CAD have been discussed in detail. State-of-the-art optimization techniques have been addressed from both the theoretical and algorithmic points of view.

We have concentrated on aspects that are felt to be immediately relevant to and necessary for modern microwave CAD. There are, of course, other related subjects that have not been treated or not adequately treated in this paper. Notable among these are special techniques for very large systems (Geoffrion [57], [58], Haimes [64], Lasdon [72]), third-generation simulation techniques (Hachtel and Sangiovanni-Vincentelli [63]), fault diagnosis (Bandler and Salama [27]), supercomputer-aided CAD (Rizzoli *et al.* [93]), the simulated annealing and combinatorial optimization methods and their application to integrated circuit layout problems [38], [69], [84], and the new automated decomposition approach to large scale optimization (Bandler and Zhang [28]).

The paper is particularly timely in that software based on techniques which we have described is being integrated by Optimization Systems Associates Inc. into SUPER-COMPACT by arrangement with Compact Software Inc.

Acknowledgment

The authors would like to thank Dr. K. C. Gupta, Guest Editor of this Special Issue on Computer-Aided Design, for his invitation to write this review paper. The useful comments offered by the reviewers are also appreciated. The authors must acknowledge original work done by several researchers which has been integrated into our presentation, including that of Dr. H. L. Abdel-Malek, Dr. R. M. Biernacki, Dr. C. Charalambous, Dr. S. Daijavad, Dr. W. Kellermann, Dr. P. C. Liu, Dr. K. Madsen, Dr. M. R. M. Rizk, Dr. H. Tromp, and Dr. Q. J. Zhang. M. L. Renault is thanked for her contributions, including assistance in preparing data, programs, and results. The opportunity EEsof Inc. provided to develop state-of-the-art optimizers into practical design tools, through interaction with Dr. W. H. Childs, Dr. C. H. Holmes, and Dr. D. Morton, is appreciated. Thanks are extended to Dr. R. A. Pucel of Raytheon Company, Research Division, Lexington, MA, for reviving the first author's interest and work in design centering and yield optimization. Dr. U. L. Rohde of Compact Software Inc., Paterson, NJ, is facilitating the practical implementation of advanced mathematical techniques of CAD. The stimulating environment provided by Dr. Pucel and Dr. Rohde to the first author is greatly appreciated.

References

[1] H. L. Abdel-Malek and J. W. Bandler, "Yield optimization for arbitrary statistical distributions, Part I: Theory", *IEEE Trans. Circuits Syst.*, vol. CAS-27, pp. 245–253, 1980.

[2] H. L. Abdel-Malek and J. W. Bandler, "Yield optimization for arbitrary statistical distributions, Part II: Implementation," *IEEE Trans. Circuits Syst.*, vol. CAS-27, pp. 253–262, 1980.

[3] D. Agnew, "Improved minimax optimization for circuit design," *IEEE Trans. Circuits Syst.*, vol. CAS-28, pp. 791–803, 1981.

[4] J. W. Bandler, "Optimization methods for computer-aided design," *IEEE Trans. Microwave Theory Tech.*, vol. MTT-17, pp. 533–552, 1969.

[5] J. W. Bandler, "Computer-aided circuit optimization," in *Modern Filter Theory and Design*, G. C. Temes and S. K. Mitra, Eds. New York: Wiley, 1973, pp. 211–271.

[6] J. W. Bandler, "Engineering modelling and design subject to model uncertainties and manufacturing tolerances," in *Methodology in Systems Modelling and Simulation*, B. P. Zeigler, *et al.*, Eds. Amsterdam: North-Holland, 1979, pp. 399–421.

[7] J. W. Bandler and H. L. Abdel-Malek, "Optimal centering, tolerancing, and yield determination via updated approximations and cuts," *IEEE Trans. Circuits Syst.*, vol. CAS-25, pp. 853–871, 1978.

[8] J. W. Bandler, R. M. Biernacki, and A. E. Salama, "A linear programming approach to fault location in analog circuits," in

Proc. IEEE Int. Symp. Circuits Syst., (Chicago, IL), 1981, pp. 256–260.

[9] J. W. Bandler, R. M. Biernacki, A. E. Salama, and J. A. Starzyk, "Fault isolation in linear analog circuits using the L_1 norm," in *Proc. IEEE Int. Symp. Circuits Syst.*, (Rome, Italy), 1982, pp. 1140–1143.

[10] J. W. Bandler and C. Charalambous, "Theory of generalized least pth approximation," *IEEE Trans. Circuit Theory*, vol. CT-19, pp. 287–289, 1972.

[11] J. W. Bandler and C. Charalambous, "Nonlinear programming using minimax techniques," *J. Opt. Theory Appl.*, vol. 13, pp. 607–619, 1974.

[12] J. W. Bandler, S. H. Chen, and S. Daijavad, "Microwave device modeling using efficient l_1 optimization: A novel approach," *IEEE Trans. Microwave Theory Tech.*, vol. MTT-34, pp. 1282–1293, 1986.

[13] J. W. Bandler, S. H. Chen, S. Daijavad, and W. Kellermann, "Optimal design of multicavity filters and contiguous-band multiplexers," in *Proc. 14th European Microwave Conf.* (Liege, Belgium), 1984, pp. 863–868.

[14] J. W. Bandler, S. H. Chen, S. Daijavad, W. Kellermann, M. Renault, and Q. J. Zhang, "Large scale minimax optimization of microwave multiplexers," in *Proc. 16th European Microwave Conf.* (Dublin, Ireland), 1986, pp. 435–440.

[15] J. W. Bandler, S. H. Chen, S. Daijavad, and K. Madsen, "Efficient gradient approximations for nonlinear optimization of circuits and systems," in *Proc. IEEE Int. Symp. Circuits Syst.*, (San Jose, CA), 1986, pp. 964–967.

[16] J. W. Bandler, S. H. Chen, S. Daijavad, and K. Madsen, "Efficient optimization with integrated gradient approximations," pp. 444–455, this issue.

[17] J. W. Bandler, S. Daijavad and Q. J. Zhang, "Computer aided design of branched cascaded networks," in *Proc. IEEE Int. Symp. Circuits Syst.*, (Kyoto, Japan), 1985, pp. 1579–1582.

[18] J. W. Bandler, S. Daijavad, and Q. J. Zhang, "Exact simulation and sensitivity analysis of multiplexing networks," *IEEE Trans. Microwave Theory Tech.*, vol. MTT-34, pp. 93–102, 1986.

[19] J. W. Bandler, M. A. El-Kady, W. Kellermann, and W. M. Zuberek, "An optimization approach to the best alignment of manufactured and operating systems," in *Proc. IEEE Int. Symp. Circuits Syst.*, (Newport Beach, CA), 1983, pp. 542–545.

[20] J. W. Bandler and W. Kellermann, "Selected topics in optimal design centering, tolerancing and tuning," Department of Electrical and Computer Engineering, McMaster University, Hamilton, Canada, Rep. SOS-83-28, 1983.

[21] J. W. Bandler, W. Kellermann, and K. Madsen, "A superlinearly convergent minimax algorithm for microwave circuit design," *IEEE Trans. Microwave Theory Tech.*, vol. MTT-33, pp. 1519–1530, 1985.

[22] J. W. Bandler, W. Kellermann, and K. Madsen, "A nonlinear l_1 optimization algorithm for design, modelling and diagnosis of networks," *IEEE Trans. Circuits Syst.*, vol. CAS-34, pp. 174–181, 1987.

[23] J. W. Bandler, P. C. Liu, and J. H. K. Chen, "Worst case network tolerance optimization," *IEEE Trans. Microwave Theory Tech.*, vol. MTT-23, pp. 630–641, 1975.

[24] J. W. Bandler, P. C. Liu, and H. Tromp, "A nonlinear programming approach to optimal design centering, tolerancing and tuning," *IEEE Trans. Circuits Syst.*, vol. CAS-23, pp. 155–165, 1976.

[25] J. W. Bandler, P. C. Liu, and H. Tromp, "Integrated approach to microwave design," *IEEE Trans. Microwave Theory Tech.*, vol. MTT-24, pp. 584–591, 1976.

[26] J. W. Bandler and M. R. M. Rizk, "Optimization of electrical circuits," *Math. Program. Study*, vol. 11, pp. 1–64, 1979.

[27] J. W. Bandler and A. E. Salama, "Fault diagnosis of analog circuits," *Proc. IEEE*, vol. 73, pp. 1279–1325, 1985.

[28] J. W. Bandler and Q. J. Zhang, "An automatic decomposition technique for device modelling and large circuit design," in *IEEE Int. Microwave Symp. Dig.*, (Las Vegas, NV), 1987, pp. 709–712.

[29] R. H. Bartels and A. R. Conn, "An approach to nonlinear l_1 data fitting," Computer Science Department, University of Waterloo, Waterloo, Canada, Rep. CS-81-17, 1981.

[30] R. M. Biernacki and M. A. Styblinski, "Statistical circuit design with a dynamic constraint approximation scheme," in *Proc. IEEE Int. Symp. Circuits Syst.*, (San Jose, CA), 1986, pp. 976–979.

[31] F. H. Branin, Jr., "Network sensitivity and noise analysis simplified," *IEEE Trans. Circuit Theory*, vol. CT-20, pp. 285–288, 1973.

[32] R. K. Brayton, G. D. Hachtel, and A. L. Sangiovanni-Vincentelli, "A survey of optimization techniques for integrated-circuit design," *Proc. IEEE*, vol. 69, pp. 1334–1362, 1981.

[33] C. G. Broyden, "A class of methods for solving nonlinear simultaneous equations," *Math. Comp.*, vol. 19, pp. 577–593, 1965.

[34] C. G. Broyden, "Quasi-Newton methods and their application to function minimization," *Math. Comp.*, vol. 21, pp. 368–381, 1967.

[35] C. G. Broyden, "A new double-rank minimization algorithm," *Notices Amer. Math. Soc.*, vol. 16, p. 670, 1969.

[36] E. M. Butler, "Realistic design using large-change sensitivities and performance contours," *IEEE Trans. Circuit Theory*, vol. CT-18, pp. 58–66, 1971.

[37] D. A. Calahan, *Computer-Aided Network Design*, rev. ed. New York: McGraw Hill, 1972.

[38] A. Casotto, F. Romeo, and A. L. Sangiovanni-Vincentelli, "A parallel simulated annealing algorithm for the placement of macro-cells," in *Proc. IEEE Int. Conf. Computer-Aided Design* (Santa Clara, CA), 1986, pp. 30–33.

[39] C. Charalambous, "A unified review of optimization," *IEEE Trans. Microwave Theory Tech.*, vol. MTT-22, pp. 289–300, 1974.

[40] C. Charalambous, "Minimax design of recursive digital filters," *Computer Aided Design*, vol. 6, pp. 73–81, 1974.

[41] C. Charalambous, "Nonlinear least pth optimization and nonlinear programming," *Math. Program.*, vol. 12, pp. 195–225, 1977.

[42] C. Charalambous and A. R. Conn, "Optimization of microwave networks," *IEEE Trans. Microwave Theory Tech.*, vol. MTT-23, pp. 834–838, 1975.

[43] F. H. Clarke, "Generalized gradients and applications," *Trans. Amer. Math. Soc.*, vol. 205, pp. 247–262, 1975.

[44] S. Daijavad, "Design and modelling of microwave circuits using optimization methods," Ph.D. thesis, McMaster University, Hamilton, Canada, 1986.

[45] W. C. Davidon, "Variable metric method for minimization," Rep. ANL-5990 Rev., Argonne National Laboratories, Argonne, IL, 1959.

[46] J. E. Dennis, Jr., and J. J. Moré, "Quasi-Newton methods, motivation and theory," *SIAM Rev.*, vol. 19, pp. 46–89, 1977.

[47] S. W. Director and G. D. Hachtel, "The simplicial approximation approach to design centering," *IEEE Trans. Circuits Syst.*, vol. CAS-24, pp. 363–372, 1977.

[48] S. W. Director and R. A. Rohrer, "Generalized adjoint network and network sensitivities," *IEEE Trans. Circuit Theory*, vol. CT-16, pp. 318–323, 1969.

[49] S. W. Director and R. A. Rohrer, "Automated network design: The frequency domain case," *IEEE Trans. Circuit Theory*, vol. CT-16, pp. 330–337, 1969.

[50] L. C. W. Dixon, "Quasi-Newton algorithms generate identical points," *Math. Program.*, vol. 2, pp. 383–387, 1972.

[51] I. S. Duff, "A survey of sparse matrix research," *Proc. IEEE*, vol. 65, pp. 500–535, 1977.

[52] N. J. Elias, "New statistical methods for assigning device tolerances," in *Proc. IEEE Int. Symp. Circuits Syst.*, (Newton, MA), 1975, pp. 329–332.

[53] R. Fletcher, "A new approach to variable metric algorithms," *Comput. J.*, vol. 13, pp. 317–322, 1970.

[54] R. Fletcher, "A survey of algorithms for unconstrained optimization," in *Numerical Methods for Unconstrained Optimization*, W. Murray, Ed. London: Academic Press, 1972.

[55] R. Fletcher and M. J. D. Powell, "A rapidly convergent descent method for minimization," *Comput. J.*, vol. 6, pp. 163–168, 1963.

[56] R. Fletcher and C. M. Reeves, "Function minimisation by conjugate gradients," *Comput. J.*, vol. 7, pp. 149–154, 1964.

[57] A. M. Geoffrion, "Elements of large-scale mathematical programming—Part I: Concepts," *Management Sci.*, vol. 16, pp. 652–675, 1970.

[58] A. M. Geoffrion, "Elements of large-scale mathematical programming—Part II: Synthesis of algorithms and bibliography," *Management Sci.*, vol. 16, pp. 676–691, 1970.

[59] P. E. Gill and W. Murray, "Quasi-Newton methods for unconstrained minimization," *J. Inst. Math. Appl.*, vol. 9, pp. 91–108, 1972.

[60] D. Goldfarb, "A family of variable-metric methods derived by variational means," *Math. Comp.*, vol. 24, pp. 23–26, 1970.

[61] F. G. Gustavson, "Some basic techniques for solving sparse systems of linear equations," in *Sparse Matrices and Their Applications*, D. J. Rose and R. A. Willoughby, Eds. New York: Plenum Press, 1971.

[62] G. D. Hachtel, R. K. Brayton, and F. G. Gustavson, "The sparse

tableau approach to network analysis and design," *IEEE Trans. Circuit Theory*, vol. CT-18, pp. 101–113, 1971.
[63] G. D. Hachtel and A. L. Sangiovanni-Vincentelli, "A survey of third-generation simulation techniques," *Proc. IEEE*, vol. 69, pp. 1264–1280, 1981.
[64] Y. Y. Haimes, Ed., *Large Scale Systems*. Amsterdam: North Holland, 1982.
[65] J. Hald and K. Madsen, "Combined LP and quasi-Newton methods for minimax optimization," *Math. Program.*, vol. 20, pp. 49–62, 1981.
[66] J. Hald and K. Madsen, "Combined LP and quasi-Newton methods for nonlinear l_1 optimization," *SIAM J. Numer. Anal.*, vol. 22, pp. 68–80, 1985.
[67] R. Hettich, "A Newton-method for nonlinear Chebyshev approximation," in *Approximation Theory*, R. Schaback and K. Scherer, Eds. (Lecture Notes in Mathematics, 556). Berlin: Springer, 1976, pp. 222–236.
[68] B. J. Karafin, "The optimum assignment of component tolerances for electrical networks," *Bell Syst. Tech. J.*, vol. 50, pp. 1225–1242, 1971.
[69] S. Kirkpatrick, C. D. Gelatt, and M. P. Vecchi, "Optimization by simulated annealing," *Science*, vol. 220, pp. 671–680, 1983.
[70] H.W. Kuhn and A. W. Tucker, "Non-linear programming," in *Proc. 2nd Symp. Math. Statistics Probability* (Berkeley, CA), 1951, pp. 481–493.
[71] K. R. Laker, M. S. Ghausi, and J. J. Kelly, "Minimum sensitivity active (leapfrog) and passive ladder bandpass filters," *IEEE Trans. Circuits Syst.*, vol. CAS-22, pp. 670–677, 1975.
[72] L. S. Lasdon, *Optimization Theory for Large Systems*. New York: Macmillan, 1970.
[73] L. S. Lasdon, D. F. Suchman, and A. D. Waren, "Nonlinear programming applied to linear array design," *J. Acoust. Soc. Amer.*, vol. 40, pp. 1197–1200, 1966.
[74] L. S. Lasdon and A. D. Waren, "Optimal design of filters with bounded, lossy elements," *IEEE Trans. Circuit Theory*, vol. CT-13, pp. 175–187, 1966.
[75] D. Le, "A fast and robust unconstrained optimization method requiring minimum storage," *Math. Program.*, vol. 32, pp. 41–68, 1985.
[76] K. Levenberg, "A method for the solution of certain problems in least squares," *Quart. Appl. Math.*, vol. 2, pp. 164–168, 1944.
[77] K. Madsen, "Minimax solution of nonlinear equations without calculating derivatives," *Math. Program. Study*, vol. 3, pp. 110–126, 1975.
[78] K. Madsen, "Minimization of non-linear approximation functions," Dr. techn. thesis, Institute of Numerical Analysis, Tech. Univ. of Denmark, DK2800 Lyngby, Denmark, 1985.
[79] K. Madsen and H. Schjaer-Jacobsen, "New algorithms for worst case tolerance optimization," in *Proc. IEEE Int. Symp. Circuits Syst.*, (New York), 1978, pp. 681–685.
[80] K. Madsen, H. Schjaer-Jacobsen, and J. Voldby, "Automated minimax design of networks," *IEEE Trans. Circuits Syst.*, vol. CAS-22, pp. 791–796, 1975.
[81] D. Marquardt, "An algorithm for least-squares estimation of nonlinear parameters," *SIAM J. Appl. Math.*, vol. 11, pp. 431–441, 1963.
[82] J. J. Moré, "Recent developments in algorithms and software for trust region methods," in *Mathematical Programming, The State of the Art*. Bonn: Springer Verlag, 1982, pp. 258–287.
[83] D. D. Morrison, "Optimization by least squares," *SIAM J. Numer. Anal.*, vol. 5, pp. 83–88, 1968.
[84] S. Nahar, S. Sahni, and E. Shragowitz, "Simulated annealing and combinatorial optimization," in *Proc. 23rd Design Automat. Conf.*, (Las Vegas, NV), 1986, pp. 293–299.
[85] M. R. Osborne and G. A. Watson, "An algorithm for minimax optimization in the nonlinear case," *Comput. J.*, vol. 12, pp. 63–68, 1969.
[86] M. R. Osborne and G. A. Watson, "On an algorithm for discrete nonlinear l_1 approximation," *Comput. J.*, vol. 14, pp. 184–188, 1971.
[87] J. F. Pinel and K. A. Roberts, "Tolerance assignment in linear networks using nonlinear programming," *IEEE Trans. Circuit Theory*, vol. CT-19, pp. 475–479, 1972.
[88] E. Polak, *Computational Methods in Optimization: A Unified Approach*. New York: Academic Press, 1971, pp. 53–54.
[89] E. Polak, "An implementable algorithm for the optimal design centering, tolerancing, and tuning problem," *J. Opt. Theory Appl.*, vol. 37, pp. 45–67, 1982.
[90] E. Polak and A. L. Sangiovanni-Vincentelli, "Theoretical and computational aspects of the optimal design centering, tolerancing, and tuning problem," *IEEE Trans. Circuits Syst.*, vol. CAS-26, pp. 795–813, 1979.
[91] M. J. D. Powell, "A new algorithm for unconstrained optimization," in *Nonlinear Programming*, J. B. Rosen, O. L. Mangasarian and K. Ritter, Eds. New York: Academic Press, 1970.
[92] M. J. D. Powell, "A hybrid method for nonlinear equations," in *Numerical Methods for Nonlinear Algebraic Equations*, P. Rabinowitz, Ed. London: Gordon and Breach, 1970.
[93] V. Rizzoli, M. Ferlito, and A. Neri, "Vectorized program architectures for supercomputer-aided circuit design," *IEEE Trans. Microwave Theory Tech.*, vol. MTT-34, pp. 135–141, 1986.
[94] J. Schoeffler, "The synthesis of minimum sensitivity networks," *IEEE Trans. Circuit Theory*, vol. CT-11, pp. 271–276, 1964.
[95] D. F. Shanno, "Conditioning of quasi-Newton methods for function minimization," *Math. Comp.*, vol. 24, pp. 647–656, 1970.
[96] J. Sherman and W. J. Morrison, "Adjustment of an inverse matrix corresponding to changes in the elements of a given column or row of the original matrix," *Annu. Math. Statist.*, vol. 20, p. 621, 1949.
[97] K. Singhal and J. F. Pinel, "Statistical design centering and tolerancing using parametric sampling," *IEEE Trans. Circuits Syst.*, vol. CAS-28, pp. 692–701, 1981.
[98] R. S. Soin and R. Spence, "Statistical exploration approach to design centering," *Proc. Inst. Elec. Eng.*, vol. 127, pt. G., pp. 260–269, 1980.
[99] *SUPER-COMPACT User's Manual*, Compact Software Inc., Paterson, NJ 07504, May 1986.
[100] K. S. Tahim and R. Spence, "A radial exploration approach to manufacturing yield estimation and design centering," *IEEE Trans. Circuits Syst.*, vol. CAS-26, pp. 768–774, 1979.
[101] T. S. Tang and M. A. Styblinski, "Yield gradient estimation for non-differentiable density functions using convolution techniques and their application to yield optimization," in *Proc. IEEE Int. Symp. Circuits Syst.*, (San Jose, CA), 1986, pp. 1306–1309.
[102] G. C. Temes and D. A. Calahan, "Computer-aided network optimization the state-of-the-art," *Proc. IEEE*, vol. 55, pp. 1832–1863, 1967.
[103] G. C. Temes and D. Y. F. Zai, "Least pth approximation," *IEEE Trans. Circuit Theory*, vol. CT-16, pp. 235–237, 1969.
[104] *TOUCHSTONE User's Manual*, EEsof Inc., Westlake Village, CA 91362, Aug. 1985.
[105] *TOUCHSTONE Reference Manual*, (Version 1.5), EEsof Inc., Westlake Village, CA 91362, Mar. 1987.
[106] H. Tromp, "The generalized tolerance problem and worst case search," in *Proc. Conf. Computer-Aided Design of Electronic and Microwave Circuits Syst.*, (Hull, England), 1977, pp. 72–77.
[107] H. Tromp, "Generalized worst case design, with applications to microwave networks," Doctoral thesis (in Dutch), Faculty of Engineering, University of Ghent, Ghent, Belgium, 1978.
[108] A. D. Waren, L. S. Lasdon, and D. F. Suchman, "Optimization in engineering design," *Proc. IEEE*, vol. 55, pp. 1885–1897, 1967.
[109] W. M. Zuberek, "Numerical approximation of gradients for circuit optimization," in *Proc. 27th Midwest Symp. Circuits Syst.*, (Morgantown, WV), 1984, pp. 200–203.

✠

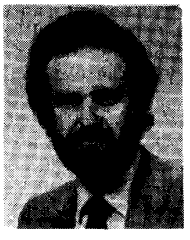

John W. Bandler (S'66–M'66–SM'74–F'78) was born in Jerusalem, Palestine, on November 9, 1941. He studied at Imperial College of Science and Technology, London, England, from 1960 to 1966. He received the B.Sc. (Eng.), Ph.D. and D.Sc. (Eng.) degrees from the University of London, England, in 1963, 1967, and 1976, respectively.

He joined Mullard Research Laboratories, Redhill, Surrey, England, in 1966. From 1967 to 1969 he was a Postdoctorate Fellow and Ses-

sional Lecturer at the University of Manitoba, Winnipeg, Canada. He joined McMaster University, Hamilton, Canada, in 1969, where he is currently a Professor of Electrical and Computer Engineering. He has served as Chairman of the Department of Electrical Engineering and Dean of the Faculty of Engineering. He currently directs research in the Simulation Optimization Systems Research Laboratory. Dr. Bandler is President of Optimization Systems Associates Inc., which he established in 1983. OSA currently provides consulting services and software, specializing in advanced applications of simulation, sensitivity analysis, and mathematical optimization techniques for CAE of microwave integrated circuits.

Dr. Bandler is a contributor to *Modern Filter Theory and Design* (Wiley-Interscience, 1973) and to the forthcoming *Analog Circuits: Computer-aided Analysis and Diagnosis* (Marcel Dekker). He has more than 220 publications, four of which appear in *Computer-Aided Filter Design* (IEEE Press, 1973), one in *Microwave Integrated Circuits* (Artech House, 1975), one in *Low-Noise Microwave Transistors and Amplifiers* (IEEE Press, 1981), one in *Microwave Integrated Circuits* (2nd ed., Artech House, 1985), one in *Statistical Design of Integrated Circuits* (IEEE Press, 1987), and one to be published in *Analog Fault Diagnosis* (IEEE Press). Dr. Bandler was an Associate Editor of the IEEE TRANSACTIONS ON MICROWAVE THEORY AND TECHNIQUES (1969–1974). He was Guest Editor of the Special Issue of the IEEE TRANSACTIONS ON MICROWAVE THEORY AND TECHNIQUES on Computer-Oriented Microwave Practices (March 1974). Dr. Bandler is a Fellow of the Royal Society of Canada and of the Institution of Electrical Engineers (Great Britain). He is a member of the Association of Professional Engineers of the Province of Ontario (Canada).

✠

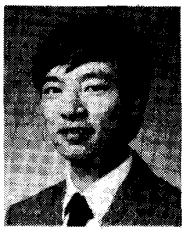

Shao Hua Chen (S'84) was born in Swatow, Guangdong, China, on September 27, 1957. He received the B.S. degree from the South China Institute of Technology, Guangzhou, China, in 1982 and the Ph.D. degree in electrical engineering from McMaster University, Hamilton, Canada, in 1987.

From July 1982 to August 1983, he was a teaching assistant in the Department of Automation at the South China Institute of Technology. He received a graduate scholarship from the Chinese Ministry of Education and worked in the Department of Electrical and Computer Engineering at McMaster University from 1983 to 1987. He held an Ontario Graduate Scholarship for the academic years 1985/86 and 1986/87. Currently he is working as a research engineer for Optimization Systems Associates Inc., Dundas, Ontario, Canada. His research interests include optimization methods, sensitivity analysis, device modeling, design centering, tolerancing and tuning, as well as interactive CAD software.

Reprint 4

A Unified Theory for Frequency-Domain Simulation and Sensitivity Analysis of Linear and Nonlinear Circuits

A Unified Theory for Frequency-Domain Simulation and Sensitivity Analysis of Linear and Nonlinear Circuits

JOHN W. BANDLER, FELLOW, IEEE, QI-JUN ZHANG, MEMBER, IEEE, AND RADOSLAW M. BIERNACKI, SENIOR MEMBER, IEEE

Abstract—**In this paper, a unified theory for frequency-domain simulation and sensitivity analysis of linear and nonlinear circuits is presented. An elegant derivation expands the harmonic balance technique from nonlinear simulation to nonlinear adjoint sensitivity analysis. This provides an efficient tool for the otherwise expensive but essential gradient calculations in design optimization. The hierarchical approach, widely used for circuit simulation, is generalized to sensitivity analysis and to computing responses in any subnetwork at any level of the hierarchy. Therefore, important aspects of frequency-domain circuit CAD such as simulation and sensitivity analysis, linear and nonlinear circuits, hierarchical and nonhierarchical approaches, voltage and current excitations, or open- and short-circuit terminations are unified in this general framework. Our theory provides a key for the coming generation of microwave CAD software. It will take advantage of the many existing and mature techniques such as the syntax-oriented hierarchical analysis, optimization, and yield driven design to handle nonlinear as well as linear circuits. Our novel sensitivity analysis approach has been verified by a MESFET mixer example exhibiting a 90 percent saving of CPU time over the prevailing perturbation method.**

I. INTRODUCTION

IN THIS PAPER, we present a unified approach to the simulation and sensitivity analysis of linear/nonlinear circuits in the frequency domain. The linear part of the circuit can be large and can be hierarchically decomposed, highly suited to modern microwave CAD. Analysis of the nonlinear part is performed in the time domain and the large-signal steady-state periodic analysis of the overall circuit is carried out by means of the harmonic balance (HB) method. In the sensitivity analysis we exploit the concept of the adjoint network technique.

The HB method has become an important tool for the analysis of nonlinear circuits. The work of Rizzoli *et al.* [1], Curtice and Ettenberg [2], Curtice [3], [4], Gilmore and Rosenbaum [5], Gilmore [6], Camacho-Penalosa and Aitchison [7] stimulated work on HB in the microwave CAD community. The excellent paper by Kundert and Sangiovanni-Vincentelli [8] provided systematic insight into the HB method. Many others, e.g., [9]–[15], have also contributed substantially to the state of the art of the HB technique. The first step toward design optimization was made by Rizzoli *et al.* [1], who used the perturbation method to approximate the gradients. A recent review of this area was given by Rizzoli and Neri [16].

The adjoint network approach has been a classical vehicle for sensitivity analysis of linear circuits [17], [18] and of nonlinear time-domain or dc circuits [18], [19]. The existing methods, however, are not suitable for the sensitivity analysis of nonlinear circuits operating under large-signal steady-state periodic or almost periodic conditions, especially in the context of the HB method. The HB analysis is performed in the frequency domain and generates the circuit responses through their spectra. The time-domain approach, such as that of SPICE, is very inefficient in the steady-state case since the analysis must be carried out until the transient responses vanish. Therefore, the adjoint network nonlinear time-domain sensitivity analysis, even if applicable, would be inefficient as well. On the other hand, the nonlinear dc analysis is only a part of the harmonic balance analysis; moreover, it is integrated with the calculation of all harmonics simultaneously. If there are large-signal ac sources in the circuit, the dc analysis cannot be separated from the ac analysis. Therefore, the existing nonlinear dc adjoint network technique is not directly applicable to the HB method.

In our paper, we extend to the HB technique the powerful adjoint network concept. The concept involves solving a set of linear equations whose coefficient matrix is available in many existing HB programs. The solution of a single adjoint system is sufficient for the computation of sensitivities with respect to all parameters in both the linear and nonlinear subnetworks, in the bias circuit, driving sources, and terminations. No parameter perturbation or iterative simulations are required.

To make our theory highly suitable for microwave oriented CAD programs, we have also developed a hierarchical treatment of the adjoint system analysis. Preferred by leading experts, e.g. Jansen [20], and used in circuit simulators such as Super-Compact and Touchstone, the syntax-oriented hierarchical approach has proved very convenient and efficient in analyzing linear circuits. Our theory further extends such an approach to adjoint sensitivity analysis.

Manuscript received April 11, 1988; revised August 23, 1988.

The authors are with Optimization Systems Associates Inc., Dundas, Ont., Canada L9H 5E7. J. W. Bandler and R. M. Biernacki are also with the Simulation Optimization Systems Research Laboratory and the Department of Electrical and Computer Engineering, McMaster University, Hamilton, Canada L8S 4L7.

IEEE Log Number 8824205.

0018-9480/88/1200-1661$01.00 ©1988 IEEE

TABLE I
NOTATION AND DEFINITION

Notation	Definition
N_t	total number of nodes (internal and external) of a linear subnetwork.
N	number of circuit nodes (or ports) used in harmonic analysis. Also, it is the number of external nodes for a typical subnetwork of Fig. 2.
H	number of harmonics, including DC.
k	harmonic index. k = 0 for DC, k = 1 for the fundamental harmonic, k = 2, 3, ..., H-1 for other harmonics.
$V_t(k)$, $I_t(k)$	complex N_t-vectors indicating kth harmonic voltages or currents at all nodes (both internal and external) of a linear subnetwork.
V(k), I(k)	complex N-vectors indicating kth harmonic voltages or currents at all external nodes of any linear subnetwork (at the highest level of hierarchy the nodes or ports at which the harmonic balance equations are formulated).
$\bar{V}_t$, $\bar{I}_t$	real $2HN_t$-vectors containing real and imaginary parts of $V_t(k)$ or $I_t(k)$ at all harmonics k, k = 0, 1, ..., H-1.
$\bar{V}$, $\bar{I}$	real 2HN-vectors containing real and imaginary parts of V(k) or I(k) at all harmonics k, k = 0, 1, ..., H-1.
$Y_t(k)$	N_t by N_t matrix representing the unreduced nodal admittance matrix of a linear subnetwork at harmonic k.
Y(k)	N by N matrix representing the reduced nodal admittance matrix of a linear subnetwork at harmonic k.

Notation	Definition
$\bar{Y}_t$	$2HN_t$ by $2HN_t$ real matrix obtained by splitting the real and imaginary parts of $Y_t(k)$ for all harmonics k, k = 0, 1, ..., H-1.
$\bar{Y}$	2HN by 2HN real matrix obtained by splitting the real and imaginary parts of Y(k) for all harmonics k, k = 0, 1, ..., H-1.
$\bar{J}_t$	$2HN_t$ by $2HN_t$ real matrix representing the Jacobian defined in (A2).
$\bar{J}$	2HN by 2HN real matrix representing the Jacobian defined by (5). The internal nodes of the linear subcircuit are suppressed.
$\bar{e}_t$	$2HN_t$ real vector selecting the output voltage from the vector $\bar{V}_t$.
$\bar{e}$	2HN real vector selecting the output voltage from the vector $\bar{V}$.
A(k)	$\begin{bmatrix} Y_t(k) & -U \\ U^T & 0 \end{bmatrix}$ where U is $\begin{bmatrix} 0 \\ 1 \end{bmatrix}$ and 1 is an N by N identity matrix.
$Z_s(k)$	n_E by n_E diagonal matrix whose diagonal entries are the terminating impedances Z_i, i = 1, 2, ..., n_E.
$Y_s(k)$	n_I by n_I diagonal matrix whose diagonal entries are the terminating admittances Y_i, i = 1, 2, ..., n_I.
$V_s(k)$	n_E-vector containing voltage excitations E_i, i = 1, 2, ..., n_E.
$I_s(k)$	n_I-vector containing current excitations I_{si}, i = 1, 2, ..., n_I.

The sensitivities we propose are exact in terms of the harmonic balance method itself. Our exact adjoint sensitivity analysis can be used with various existing HB simulation techniques, e.g., the basic HB [8], the modified HB [6], and the APFT HB [15]. *The only computational effort includes solving the adjoint linear equations and calculating the Fourier transforms of all time-domain derivatives at the nonlinear element level.* Significant CPU time savings are achieved over the perturbation method.

In Section II, we define the notation used throughout this paper. In Section III, the simulation of linear and nonlinear circuits is reviewed under a general circuit hierarchy. In Section IV, a new and unified treatment to adjoint systems for linear and nonlinear circuits is introduced. Novel sensitivity formulas for nonlinear circuits are derived in Section V. Finally, in Section VI, a MESFET mixer example is used to verify our theory.

II. NOTATION AND DEFINITION

We follow the notation of [8]. Real vectors containing voltages and currents at time t are denoted by $\boldsymbol{v}(t)$ and $\boldsymbol{i}(t)$. Capitals $\boldsymbol{V}(k)$ and $\boldsymbol{I}(k)$ are used to indicate complex vectors of voltages and currents at harmonic k. A subscript t at $\boldsymbol{V}_t(k)$ indicates that the vector contains the nodal voltages at all N_t nodes (both internal and external) of a linear subnetwork. If there is no subscript, then the vector corresponds to the port voltages (currents) at all N ports of the reduced subnetwork. A bar denotes the split real and imaginary parts of a complex vector. In particular, $\bar{\boldsymbol{V}}$ or $\bar{\boldsymbol{I}}$ are real vectors containing the real and the imaginary parts of $\boldsymbol{V}(k)$ or $\boldsymbol{I}(k)$, respectively, for all harmonics k, $k = 0, 1, \cdots, H-1$. The total number of harmonics taken into consideration, including dc, is H. The hat distinguishes quantities of the adjoint system. For example, $\hat{\boldsymbol{V}}_t(k)$ represents adjoint voltages at internal and external nodes of a subnetwork at harmonic k. A detailed definition of the notation is given in Table I.

III. LINEAR AND NONLINEAR SIMULATION

A. Circuit Structure

Our exact adjoint sensitivity analysis can be used for hierarchically structured linear subcircuits. Consider the arbitrary circuit hierarchy of Fig. 1. A typical subnetwork containing internal and external nodes is shown in Fig. 2. A general representation of a terminated circuit is depicted in Fig. 3. An unpartitioned or nonhierarchical approach is a special case of Fig. 1 when only one level exists.

For a completely linear circuit, the sources and loads are applied at the highest level of the hierarchy, as depicted in Fig. 3. For a nonlinear circuit, the linear part of the overall circuit can have an arbitrary hierarchy as illustrated by Fig. 1 while the nonlinear part is connected directly at the highest level to the linear part. Therefore, in any case we consider an unterminated N-port circuit at the highest level of hierarchy. Such an approach simultaneously facilitates both the effect of the reference plane in microwave circuits and the need for the harmonic balance equations.

B. Hierarchical Simulation of the Linear Network

Hierarchical simulation of linear circuits has been successfully used in many microwave CAD packages. It is summarized and expanded here into a set of formulas, enabling voltage responses at any nodes (internal or external) for any subnetwork at any level to be systematically computed. Firstly, we solve the terminated circuit at the

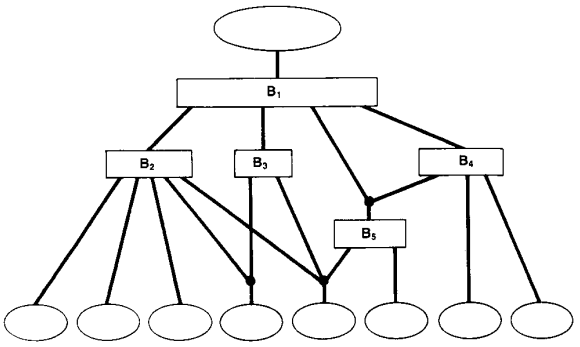

Fig. 1. An arbitrary circuit hierarchy. Each thick line represents a group of nodes. Each rectangular box represents a connection block for a subcircuit. Each bottom circular box represents a circuit element and the top circular box represents the sources and loads.

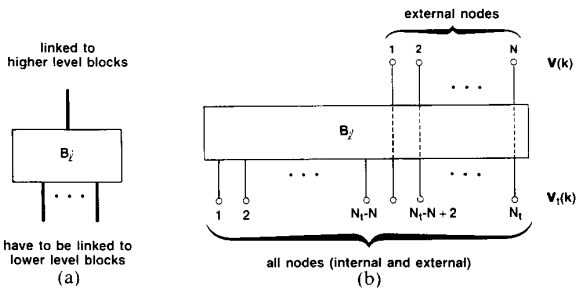

Fig. 2. A typical subcircuit connection block: (a) as seen from Fig. 1; (b) detailed representation of all the nodes of the subnetwork. Nodes at the top (bottom) of the rectangular box are the external (external and internal) nodes of the subnetwork.

highest level of the hierarchy using

$$\left\{\begin{bmatrix}\mathbf{1} & \mathbf{0}\\ \mathbf{0} & \boldsymbol{Y}_s(k)\end{bmatrix}+\begin{bmatrix}\boldsymbol{Z}_s(k) & \mathbf{0}\\ \mathbf{0} & \mathbf{1}\end{bmatrix}\boldsymbol{Y}(k)\right\}\boldsymbol{V}(k)=\begin{bmatrix}\boldsymbol{V}_s(k)\\ \boldsymbol{I}_s(k)\end{bmatrix} \tag{1}$$

where the overall quantity in the curly bracket is an N by N matrix linking the port voltages $\boldsymbol{V}(k)$ with the external sources for the terminated circuit. As defined in Table I, $\boldsymbol{Y}_s(k)$ and $\boldsymbol{Z}_s(k)$ are diagonal matrices containing terminating admittances and impedances, respectively, of the circuit shown in Fig. 3. $\boldsymbol{Y}(k)$ is the admittance matrix of the unterminated circuit. $\boldsymbol{V}_s(k)$ and $\boldsymbol{I}_s(k)$ denote the voltage and current excitations of the circuit, respectively. The solution vector $\boldsymbol{V}(k)$ contains external voltages of the circuit block under consideration. Then, all (both internal and external) nodal voltages $\boldsymbol{V}_t(k)$ of this subnetwork can be obtained from the equation

$$\boldsymbol{A}(k)\begin{bmatrix}\boldsymbol{V}_t(k)\\ \boldsymbol{I}(k)\end{bmatrix}=\begin{bmatrix}\mathbf{0}\\ \boldsymbol{V}(k)\end{bmatrix} \tag{2}$$

where $\boldsymbol{A}(k)$ is the modified nodal admittance matrix of the subnetwork, as defined in Table I. $\boldsymbol{I}(k)$ represents currents into the subcircuit through its external ports.

The solution of (2), i.e., $\boldsymbol{V}_t(k)$, provides external voltages of all the subnetworks at the next level down the hierarchy. Therefore, (2) is used iteratively for the first, second, $\cdots$ levels of the hierarchy until all desired nodal voltages are found.

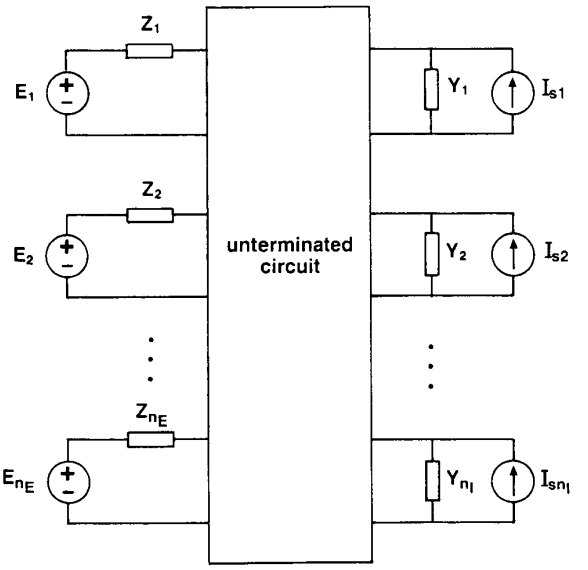

Fig. 3. A representation of a terminated subnetwork. Both current and voltage sources can be accommodated. The overall port sequence is such that ports $1,2,\cdots,n_E$ correspond to voltage sources and ports $n_E+1,\ n_E+2,\cdots,n_E+n_I$ correspond to current sources. The total number of ports is N, i.e., $N=n_E+n_I$.

Our formulas can directly accommodate both open- and short-circuit terminations. For example, a short-circuit termination at port 1 simply means $Z_1=0$ in the matrix $\boldsymbol{Z}_s$ in (1). An open-circuit termination at port n_E+2 simply means $Y_2=0$ in the matrix $\boldsymbol{Y}_s$ in (1).

C. Simulation of Nonlinear Circuits

The frequency-domain simulation of a nonlinear circuit is done effectively by the harmonic balance technique [1]–[16]. The problem is to find a $\bar{\boldsymbol{V}}$ such that

$$\bar{\boldsymbol{F}}(\bar{\boldsymbol{V}})\triangleq\bar{\boldsymbol{I}}_{NL}(\bar{\boldsymbol{V}})+\bar{\boldsymbol{I}}_L(\bar{\boldsymbol{V}})=\mathbf{0} \tag{3}$$

where the vectors $\bar{\boldsymbol{I}}_L$ and $\bar{\boldsymbol{I}}_{NL}$ are defined as the currents into the linear and nonlinear parts at the ports of their connection. $\bar{\boldsymbol{V}}$ contains the split real and imaginary parts of voltages, as defined in Table I. The Newton update for solving (3) is

$$\bar{\boldsymbol{V}}_{\text{new}}=\bar{\boldsymbol{V}}_{\text{old}}-\bar{\boldsymbol{J}}^{-1}\bar{\boldsymbol{F}}(\bar{\boldsymbol{V}}_{\text{old}}) \tag{4}$$

where $\bar{\boldsymbol{J}}$ is the Jacobian matrix defined by

$$\bar{\boldsymbol{J}}\triangleq\left(\partial\bar{\boldsymbol{F}}^T/\partial\bar{\boldsymbol{V}}\right)^T. \tag{5}$$

The (i,j)th entry of the Jacobian matrix $\bar{\boldsymbol{J}}$ is the derivative of the ith entry of $\bar{\boldsymbol{F}}$ with respect to the jth entry of $\bar{\boldsymbol{V}}$.

In the context of the overall hierarchical structure, the solution of (3) provides the external voltages $\boldsymbol{V}(k)$, $k=$

IV. Adjoint System Simulation

Efficient and exact sensitivity analysis can be achieved by solving an adjoint system. In this section, a new and unified formulation of adjoint systems for hierarchically structured linear/nonlinear circuits is presented.

A. Adjoint System for Linear Networks

At the highest level of the hierarchy, the adjoint system is excited by a unit source at the output port. Suppose the output voltage V_{out} can be selected from $V(k)$ by an N-vector $\boldsymbol{e}$ as

$$V_{\text{out}} = \boldsymbol{e}^T \boldsymbol{V}(k). \tag{6}$$

For example, if V_{out} is chosen as the voltage at the first port, then the vector $\boldsymbol{e}$ contains 1 as the first entry and zeros everywhere else. By solving

$$\left\{ \begin{bmatrix} \mathbf{1} & \mathbf{0} \\ \mathbf{0} & \boldsymbol{Y}_s(k) \end{bmatrix} + \begin{bmatrix} \boldsymbol{Z}_s(k) & \mathbf{0} \\ \mathbf{0} & \mathbf{1} \end{bmatrix} \boldsymbol{Y}^T(k) \right\} \hat{\boldsymbol{V}}(k) = \boldsymbol{e} \tag{7}$$

we obtain adjoint voltages $\hat{\boldsymbol{V}}(k)$ at external ports at the highest level of the hierarchy. $\boldsymbol{Y}_s(k)$, $\boldsymbol{Z}_s(k)$, and $\boldsymbol{Y}(k)$ are the same matrices as used in (1). In order to obtain adjoint voltages $\hat{\boldsymbol{V}}_t(k)$ at all (both internal and external) nodes of the circuit block, we solve the equation

$$\boldsymbol{A}^T(k) \begin{bmatrix} \hat{\boldsymbol{V}}_t(k) \\ -\hat{\boldsymbol{I}}(k) \end{bmatrix} = \begin{bmatrix} \mathbf{0} \\ -\hat{\boldsymbol{V}}(k) \end{bmatrix} \tag{8}$$

where $\boldsymbol{A}^T(k)$ is the transpose of the modified nodal admittance matrix of the subnetwork used in (2). The solution vector $\hat{\boldsymbol{V}}_t(k)$ provides external adjoint voltages for all subnetworks at the next level down the hierarchy. Therefore, (8) can be used iteratively for the first, second, $\cdots$ levels of the hierarchy until all desired adjoint voltages are found.

Notice that (8) is a convenient formulation of the adjoint system since the LU factors of $\boldsymbol{A}(k)$ can already be available from solving (2).

B. Adjoint System for Nonlinear Networks

Suppose $\bar{V}_{\text{out}}$ is the real or imaginary part of output voltage V_{out} and can be selected from the voltage vector $\bar{\boldsymbol{V}}$ by a vector $\bar{\boldsymbol{e}}$ as

$$\bar{V}_{\text{out}} = \bar{\boldsymbol{e}}^T \bar{\boldsymbol{V}}. \tag{9}$$

The adjoint system is the linear equation

$$\bar{\boldsymbol{J}}^T \hat{\bar{\boldsymbol{V}}} = \bar{\boldsymbol{e}} \tag{10}$$

where $\bar{\boldsymbol{J}}$ is the Jacobian at the solution of (3). Notice that $\bar{\boldsymbol{V}}$ and $\hat{\bar{\boldsymbol{V}}}$ are both 2HN-vectors containing the split real and imaginary parts of voltages at the connection ports of the linear and nonlinear subcircuits. According to our notation $\bar{\boldsymbol{V}}$ is defined for the original network and $\hat{\bar{\boldsymbol{V}}}$ is defined for the adjoint network. Also notice that the LU factors of $\bar{\boldsymbol{J}}$ can be available from the last iteration of (4). Therefore, to obtain $\hat{\bar{\boldsymbol{V}}}$ from (10), we need only the forward and backward substitutions.

The adjoint voltages can be computed even if the output port is suppressed from the harmonic equation (3). Although the theoretical derivation for this case is rather involved, as given in the Appendix, we found a very logical and easy-to-implement method to handle this situation. First, we compute the adjoint voltages at the external ports of the linear subnetwork. This can be done by disconnecting the nonlinear part and then solving the linear part for individual harmonics separately. The resulting vector, denoted by $\hat{\bar{\boldsymbol{V}}}_L$, is then transformed to the actual adjoint excitations of the overall circuit (including both linear and nonlinear parts) to be incorporated to (10) in place of $\bar{\boldsymbol{e}}$. The final equation takes the form

$$\bar{\boldsymbol{J}}^T \hat{\bar{\boldsymbol{V}}} = \bar{\boldsymbol{Y}}^T \hat{\bar{\boldsymbol{V}}}_L. \tag{11}$$

In (11), $\hat{\bar{\boldsymbol{V}}}$ and $\hat{\bar{\boldsymbol{V}}}_L$ have exactly the same dimensions and both represent the split real and imaginary parts of adjoint voltages at the connection ports of the linear and nonlinear subcircuits. The former is computed from the overall circuit and the latter is computed from the linear subcircuit only.

Equations (10) or (11) provide adjoint voltages at external ports at the highest level of the hierarchy. We then use (8) iteratively for the first, second, $\cdots$ levels of the hierarchy to obtain adjoint voltages at both internal and external nodes of all subnetworks.

V. Sensitivity Analysis

A. Adjoint System Approach to Sensitivity Evaluation

Let x be a design variable of the nonlinear circuit. Differentiating (3) with respect to x gives

$$\left(\partial \bar{\boldsymbol{F}}^T / \partial \bar{\boldsymbol{V}}\right)^T \left(\partial \bar{\boldsymbol{V}} / \partial x\right) + \left(\partial \bar{\boldsymbol{F}} / \partial x\right) = \mathbf{0} \tag{12}$$

or

$$\partial \bar{\boldsymbol{V}} / \partial x = -\bar{\boldsymbol{J}}^{-1} \left(\partial \bar{\boldsymbol{F}} / \partial x\right) \tag{13}$$

where $\bar{\boldsymbol{J}}$ has been defined in (5). Premultiplying (13) by $\bar{\boldsymbol{e}}^T$ results in

$$\begin{aligned} \partial \bar{V}_{\text{out}} / \partial x &= -\bar{\boldsymbol{e}}^T \bar{\boldsymbol{J}}^{-1} \left(\partial \bar{\boldsymbol{F}} / \partial x\right) \\ &= -\hat{\bar{\boldsymbol{V}}}^T \left(\partial \bar{\boldsymbol{F}} / \partial x\right). \end{aligned} \tag{14}$$

This expression is further simplified by considering the locations of x in $\bar{\boldsymbol{F}}$. Notice that each entry of vector $\bar{\boldsymbol{F}}$ corresponds to a port and to a harmonic of the circuit. Take, for instance, a nonlinear resistor described by $i(t) = i(v(t), x)$ and connected across the jth port. The variable x enters $\bar{\boldsymbol{F}}$ at the positions relating to port j and harmonic k, $k = 0, 1, \cdots, H-1$, by the Fourier transform of $i(v(t), x)$. In this case, (14) is simplified to

$$\partial \bar{V}_{\text{out}} / \partial x = -\sum_k \text{Real}\left[\hat{V}_j(k) G^*(k)\right] \tag{15}$$

where $\hat{V}_j(k)$ is the adjoint voltage at the jth port, $G(k)$ is the kth Fourier coefficient of $\partial i / \partial x$ and superscript * denotes the complex conjugate.

TABLE II
SENSITIVITY EXPRESSIONS AT THE ELEMENT LEVEL

Type of Element*	Expression for $G_b(k)$	Applicable Equation
linear G	1	(16a)
linear R	$-1/R^2$	(16a)
linear C	$j\omega_k$	(16a)
linear L	$-1/(j\omega_k L^2)$	(16a)
nonlinear VCCS or resistor $i = i(v(t),x)$	[kth Fourier coefficient of $\partial i/\partial x$]	(16b)
nonlinear capacitor $q = q(v(t),x)$	ω_k [kth Fourier coefficient of $\partial q/\partial x$]	(16c)
current driving source	1	(16b) or (16c)+
voltage driving source	$\frac{1}{\text{source impedance}}$	(16b) or (16c)+

* element is in branch b and contains x

\+ (16b) for the real part and (16c) for the imaginary part of the driving source

ω_k is the kth harmonic angular frequency

TABLE III
GRADIENTS OF MIXER CONVERSION GAIN

Variable x	Gradient Expression
RF power	$c\ \text{Real}\{(\partial V_{out}/\partial x)/V_{out}\} - 1$
$R_g(f_{RF})$	$c\ \text{Real}\{(\partial V_{out}/\partial x)/V_{out}\} + c/(2R_g(f_{RF}))$
$R_d(f_{IF})$	$c\ \text{Real}\{(\partial V_{out}/\partial x)/V_{out} - 1/(R_d(f_{IF}) + jX_d(f_{IF}))\} + c/(2R_d(f_{IF}))$
$X_d(f_{IF})$	$c\ \text{Real}\{(\partial V_{out}/\partial x)/V_{out} - j/(R_d(f_{IF}) + jX_d(f_{IF}))\}$
any other parameter	$c\ \text{Real}\{(\partial V_{out}/\partial x)/V_{out}\}$

$c = 20/\ell n 10$

R and X represent the real and the imaginary parts of the impedance terminations, respectively. Subscripts g and d represent the gate and the drain terminations, respectively.

complex quantity $\partial V_{out}/\partial x$ is obtained by solving (9), (10) and (16) twice, once for the real part and the other for the imaginary part. The LU factors of $\bar{J}$ and the Fourier transforms of element sensitivities are common between the two operations.

$0, 1, \cdots, H-1$, at the highest level of the linear part. The desired internal and external voltages at all levels of the hierarchy can be solved by using (2) iteratively.

B. Sensitivity Expressions

Suppose a variable x belongs to branch b. We have derived the following general formula for computing the exact sensitivity of V_{out} with respect to x:

$$\frac{\partial \bar{V}_{out}}{\partial x} = \begin{cases} -\sum_k \text{Real}\left[\hat{V}_b(k) V_b^*(k) G_b^*(k)\right] & \text{if } x \in \text{linear subnetwork} \quad (16a) \\ -\sum_k \text{Real}\left[\hat{V}_b(k) G_b^*(k)\right] & \text{if } x \in \text{nonlinear VCCS or nonlinear resistor or real part of a complex driving source} \quad (16b) \\ -\sum_k \text{Imag}\left[\hat{V}_b(k) G_b^*(k)\right] & \text{if } x \in \text{nonlinear capacitor or imaginary part of a complex driving source.} \quad (16c) \end{cases}$$

Complex quantities $V_b(k)$ and $\hat{V}_b(k)$ are the voltages of branch b at harmonic k and are obtained from vectors $\bar{V}_t(k)$ and $\hat{\bar{V}}_t(k)$, respectively. $G_b(k)$ denotes the sensitivity expression of the element containing variable x. For example, if x is the conductance of a linear resistor, $G_b(k) = 1$. If x belongs to a nonlinear resistor represented by $i = i(v(t), x)$, $G_b(k)$ is the *kth Fourier coefficient* of $\partial i/\partial x$. A list of various cases of $G_b(k)$ is given in Table II.

Our sensitivity formula (16) has no restrictions on the selection of harmonic frequencies or the time samples. In a multitone case, the index k in (16) corresponds to all the harmonics used in the harmonic equation (3). When the multidimensional Fourier transform is used, we simply place a multidimensional summation in (16).

Notice that our sensitivity formulas permit variable x to appear in any subcircuit at any level of the hierarchy since all required voltages can be calculated as needed.

C. Comparison with the Perturbation Method

To approximate the sensitivities using the traditional perturbation method, one needs a circuit simulation for each variable. The best possible situation for this method is that all simulations finish in one iteration. For our exact adjoint sensitivity analysis, the major computation, i.e., solving the adjoint equations, is done only once for *all* variables. A detailed comparison reveals that the worst case for our approach takes less computation than the best situation of the perturbation method. In our experiment, we used only 1.6 percent of the CPU time required by the perturbation method to obtain all sensitivities.

D. Gradient Vector for Optimization

The novel formula (16) can be used as a key to formulate the gradient vectors for design optimization and yield maximization of nonlinear circuits. Table III lists the gradients of a FET mixer conversion gain with respect to various variables, expressed as simple functions of $\partial V_{out}/\partial x$.

VI. Examples

Example 1: Hierarchical Circuit Description

Many researchers, e.g., [3], and [7], have used FET mixer examples to test harmonic balance simulators. Here, we describe a mixer under the framework of hierarchical analysis. Such a description fits in with existing commercial software such as Super-Compact. The overall nonlinear circuit with its biasing and driving sources is described by a Super-Compact–like circuit file as follows.

```
* HIERARCHICAL ANALYSIS OF A MESFET MIXER
BLOCK
* INPUT MATCHING AND GATE BIAS SUBNETWORK
  IND  3 4 L=15NH
  IND  2 3 L=.5NH
  CAP  3 0 C=2.2PF
  CAP  1 2 C=2.2PF
  IND  2 5 L=.55NH
* DEFINE THE SUBCIRCUIT AS A 3-PORT
  CKT1: 3PORT 1 4 5
END
BLOCK
* OUTPUT MATCHING AND DRAIN BIAS SUBNETWORK
  IND  2 3 L=15NH
  IND  1 2 L=1.1NH
  CAP  2 0 C=20PF
  CAP  1 4 C=20PF
* DEFINE THE SUBCIRCUIT AS A 3-PORT
  CKT2: 3PORT 1 4 3
END
BLOCK
* THE HIGHEST HIERARCHY
  CKT1 1 3 5
  CKT2 7 2 4
  CAP  6 C=2PF
* A TRANSMISSION LINE BETWEEN PORT 6 0 AND PORT 7
  MIC  6 7
* BIAS SOURCES
  BIAS  3 V=-.9
  BIAS  4 V=3.
* NONLINEAR FET
* NODE NUMBERS REFER TO GATE, DRAIN AND SOURCE
  NFET 5 6 0
END
FREQUENCIES
* DEFINE LO FREQUENCY
  TONE 1
  11GHZ
* DEFINE RF FREQUENCY
  TONE 2
  12GHZ
END
SOURCES
* DEFINE LO DRIVING SOURCE
  TONE 1
  POWER 1 0 P=7DBM
* DEFINE RF DRIVING SOURCE
  TONE 2
  POWER 1 0 P=-15DBM
END
```

The LO and RF input matching and the gate bias circuits are analyzed separately in subnetwork CKT1. The IF output matching and drain bias circuits are analyzed in subnetwork CKT2. These subnetworks are then connected to a higher level of the hierarchy formulating an unterminated circuit block. This circuit block is then connected to nonlinear device ports. Using formulas developed in Sections III and IV, we are able to hierarchically simulate the original circuit as well as the adjoint circuit. This is a direct realization of the syntax-oriented step-by-step topological description [20], permitting the sensitivity analysis of a large circuit to be performed by solving a set of small original and adjoint systems.

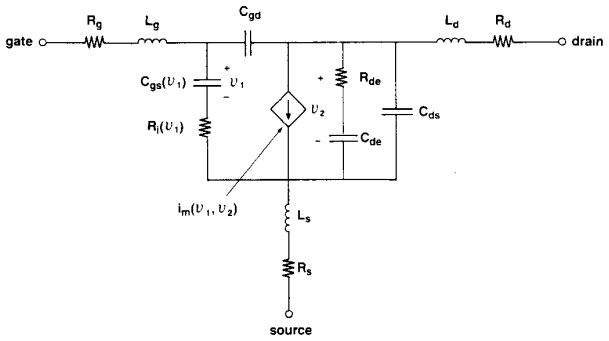

Fig. 4. A large-signal MESFET model. All parameter values are consistent with [7].

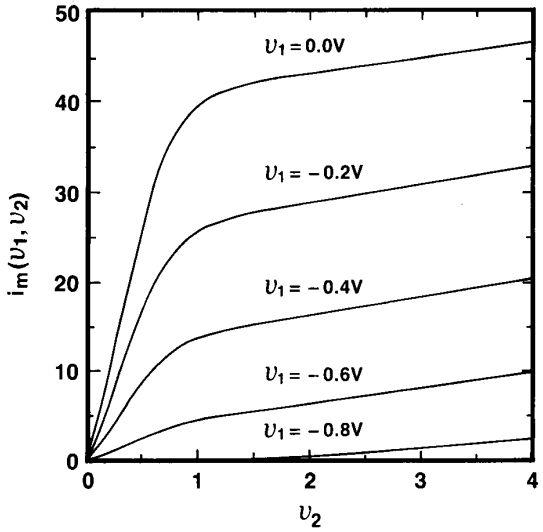

Fig. 5. The dc characteristics of the MESFET model.

Example 2: Simulation and Sensitivity Analysis of a MESFET Mixer

The MESFET mixer example reported in [7] was used to verify our theory. Figs. 4 and 5 show the large-signal MESFET model and the dc characteristics of the device. The frequencies are $f_{LO} = 11$ GHz, $f_{RF} = 12$ GHz, and $f_{IF} = 1$ GHz. The dc bias voltages are $V_{GS} = -0.9$ V and $V_{DS} = 3.0$ V. With LO power $P_{LO} = 7$ dBm and RF power $P_{RF} = -15$ dBm, the conversion gain was 6.4 dB. Twenty-six variables were considered, including all parameters in the linear as well as the nonlinear parts, dc bias, LO power, RF power, and IF, LO, and RF terminations. Exact sensitivities of the conversion gain with respect to all the variables are computed using our novel theory. The results were in excellent agreement with those from the perturbation method, as shown in Table IV. The circuit was solved in 22 seconds on a VAX 8600. The CPU time

TABLE IV
NUMERICAL VERIFICATION OF SENSITIVITIES OF THE MIXER

Location of Variable	Variable	Exact Sensitivity	Numerical Sensitivity	Difference (%)
linear subnetwork	C_{ds}	2.23080	2.23042	0.02
	C_{gd}	-29.44595	-29.44659	0.00
	C_{de}	0.00000	0.00000	0.03
	R_g	3.17234	3.17214	0.01
	R_d	6.42682	6.42751	0.01
	R_s	11.50766	11.50805	0.00
	R_{de}	-0.02396	-0.02412	0.66
	L_g	-0.50245	-0.50346	0.20
	L_d	-0.20664	-0.20679	0.07
	L_s	1.15334	1.15333	0.00
nonlinear subnetwork*	C_{gs0}	-6.17770	-6.17786	0.00
	τ	0.49428	0.49414	0.03
	V_ϕ	-20.85730	-20.85758	0.00
	V_{p0}	-26.48210	-26.48041	0.01
	V_{dss}	0.01064	0.01028	3.33
	I_{dsp}	9.93696	9.93680	0.00
bias and driving sources	V_{GS}	-31.62080	-31.62423	0.01
	V_{DS}	-2.17821	-2.17823	0.00
	P_{LO}	2.76412	2.76412	0.00
	P_{RF}	-0.05401	-0.05392	0.16
terminations	$R_g(f_{LO})$	0.06671	0.06657	0.22
	$X_g(f_{LO})$	0.37855	0.37854	0.00
	$R_g(f_{RF})$	0.78812	0.78798	0.02
	$X_g(f_{RF})$	0.45120	0.45119	0.00
	$R_d(f_{IF})$	0.71451	0.71436	0.02
	$X_d(f_{IF})$	0.10886	0.10871	0.14

* Nonlinear elements are characterized by

$$C_{gs}(v_1) = C_{gs0} / \sqrt{1 - v_1 / V_\phi},$$

$$R_i(v_1)C_{gs}(v_1) = \tau$$

and the function for $i_m(v_1, v_2)$ is shown in Fig. 5, whose mathematical expression is consistent with [7]. V_ϕ, V_{p0}, V_{dss} and I_{dsp} are parameters in the function $i_m(v_1, v_2)$.

for sensitivity analysis using our method and the perturbation method are 3.7 seconds and 240 seconds, respectively. The CPU time saving of our method is 90 percent for both simulation and sensitivity calculations, and 98 percent if only sensitivity analysis is compared.

The dangling node between the nonlinear elements C_{gs} and R_i, a case which could cause trouble in HB programs, is directly accommodated in our approach.

We have plotted selected sensitivities versus LO power in Fig. 6. For example, as LO power is increased, conversion gain becomes less sensitive to changes in gate bias V_{GS}.

VII. CONCLUSIONS

This paper presents a unified theory for frequency-domain simulation and sensitivity analysis of linear and nonlinear circuits. Our formula (16) encompasses the adjoint network approach previously used in linear [17], [18] and nonlinear dc circuits [18], [19] as special cases. Since the simulation of nonlinear circuits is expensive, gradient approximations for nonlinear circuits using repeated simulation are very costly. Consequently, the adjoint sensitivity analysis becomes far more significant for nonlinear circuits than for linear ones.

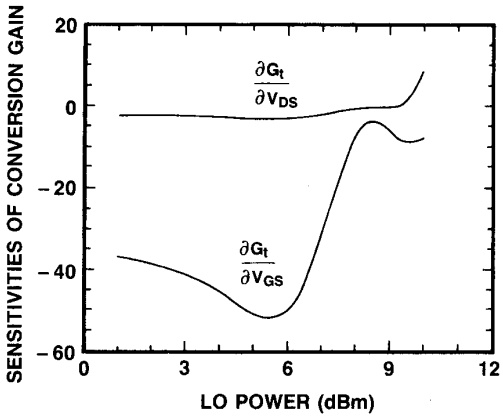

Fig. 6. Sensitivities of conversion gain with respect to bias voltages as functions of LO power.

The hierarchical approach widely used for circuit simulation is generalized for sensitivity analysis and for computing responses in any subnetwork at any level of the hierarchy. Therefore, important aspects of frequency-domain circuit CAD such as simulation and sensitivity analysis, linear and nonlinear circuits, hierarchical and nonhierarchical approaches, voltage and current excitations, and open- and short-circuit terminations are unified in this general framework.

An immediate application of our theory would be the parameter extraction of nonlinear devices under RF large-signal excitations. The optimization criterion is to match computed responses with the measured ones at dc and at fundamental and higher harmonics. A powerful gradient optimizer should be used. Gradient information would be obtained using the adjoint network approach.

Our theory provides a key for the coming generation of microwave CAD software. It can take advantage of many existing and mature techniques such as the syntax-oriented hierarchical analysis and optimization and yield driven design to handle nonlinear as well as linear circuits.

Our novel sensitivity analysis approach has been verified by a MESFET mixer example. Compared with the perturbation method, the CPU time saving of our method is 90 percent for both simulation and sensitivity calculations, and 98 percent for sensitivity analysis only.

APPENDIX A
DERIVATION OF EQUATION 11

Suppose

$$\bar{V}_{\text{out}} = \bar{e}_t^T \bar{V}_t. \tag{A1}$$

The harmonic balance equations can be formulated with respect to all nodes of the circuit, i.e., without suppressing the internal nodes in a single level description of the circuit. In such a case the Jacobian matrix $\bar{J}_t$ can be

defined similarly to (5), and

$$\bar{J}_t = \bar{Y}_t + QD^T P^T \tag{A2}$$

where D is a $2HN \times 2HN$ matrix representing the contribution to $\bar{J}$ from nonlinear components, i.e.,

$$\bar{J} = \bar{Y} + D^T. \tag{A3}$$

Matrices P and Q are $2HN_t \times 2HN$ incidence matrices containing 0's and ± 1's.

Let

$$T = \bar{Y}_t^T. \tag{A4}$$

As with (9) and (10), based on (A1) the adjoint voltages at both internal and external nodes can be computed as

$$\hat{\bar{V}}_t \triangleq \left(\bar{J}_t^T\right)^{-1} \bar{e}_t = \left(T + PDQ^T\right)^{-1} \bar{e}_t. \tag{A5}$$

Applying the Householder formula [21] to (A5) we have

$$\hat{\bar{V}}_t = T^{-1}\bar{e}_t - T^{-1}P\left(D^{-1} + Q^T T^{-1} P\right)^{-1} Q^T T^{-1} \bar{e}_t. \tag{A6}$$

Notice that

$$\left(\bar{Y}^T\right)^{-1} = Q^T T^{-1} P. \tag{A7}$$

Let

$$X = \bar{Y}^T \tag{A8}$$

$$\hat{\bar{V}}_L = Q^T T^{-1} \bar{e}_t. \tag{A9}$$

Premultiplying (A6) by Q^T gives

$$\hat{\bar{V}} \triangleq Q^T \hat{\bar{V}}_t = \hat{\bar{V}}_L - X^{-1}\left(D^{-1} + X^{-1}\right)^{-1} \hat{\bar{V}}_L. \tag{A10}$$

Again, using the Householder formula [21],

$$\left(D^{-1} + X^{-1}\right)^{-1} = X - X(D + X)^{-1} X \tag{A11}$$

and substituting (A3) and (A8) into (A10) we get

$$\hat{\bar{V}} = \left(\bar{J}^T\right)^{-1} \bar{Y}^T \hat{\bar{V}}_L \tag{A12}$$

or

$$\bar{J}^T \hat{\bar{V}} = \bar{Y}^T \hat{\bar{V}}_L. \tag{A13}$$

ACKNOWLEDGMENT

Technical discussions with Dr. R. A. Pucel of Raytheon Company, Research Division, Lexington, MA, Dr. F. J. Rosenbaum of Washington University, St. Louis, MO, and Dr. R. Gilmore of Compact Software Inc., Paterson, NJ, on nonlinear circuits and devices and on harmonic balance simulation techniques are gratefully appreciated.

REFERENCES

[1] V. Rizzoli, A. Lipparini and E. Marazzi, "A general-purpose program for nonlinear microwave circuit design," *IEEE Trans. Microwave Theory Tech.*, vol. MTT-31, pp. 762–769, 1983.

[2] W. R. Curtice and M. Ettenberg, "A nonlinear GaAs FET model for use in the design of output circuits for power amplifiers," *IEEE Trans. Microwave Theory Tech.*, vol. MTT-33, pp. 1383–1394, 1985.

[3] W. R. Curtice, "Nonlinear analysis of GaAs MESFET amplifiers, mixers, and distributed amplifiers using the harmonic balance technique," *IEEE Trans. Microwave Theory Tech.*, vol. MTT-35, pp. 441–447, 1987.

[4] W. R. Curtice, "GaAs MESFET modeling and nonlinear CAD," *IEEE Trans. Microwave Theory Tech.*, vol. MTT-36, pp. 220–230, 1988.

[5] R. J. Gilmore and F. J. Rosenbaum, "Modelling of nonlinear distortion in GaAs MESFET's," in *IEEE Int. Microwave Symp. Dig.* (San Francisco, CA), 1984, pp. 430–431.

[6] R. Gilmore, "Nonlinear circuit design using the modified harmonic balance algorithm," *IEEE Trans. Microwave Theory Tech.*, vol. MTT-34, pp. 1294–1307, 1986.

[7] C. Camacho-Penalosa and C. S. Aitchison, "Analysis and design of MESFET gate mixers," *IEEE Trans. Microwave Theory Tech.*, vol. MTT-35, pp. 643–652, 1987.

[8] K. S. Kundert and A. Sangiovanni-Vincentelli, "Simulation of nonlinear circuits in the frequency domain," *IEEE Trans. Computer-Aided Design*, vol. CAD-5, pp. 521–535, 1986.

[9] S. Egami, "Nonlinear, linear analysis and computer-aided design of resistive mixers," *IEEE Trans. Microwave Theory Tech.*, vol. MTT-22, pp. 270–275, 1974.

[10] F. Filicori, V. A. Monaco, and C. Naldi, "Simulation and design of microwave class-C amplifiers through harmonic analysis," *IEEE Trans. Microwave Theory Tech.*, vol. MTT-27, pp. 1043–1051, 1979.

[11] R. G. Hicks and P. J. Khan, "Numerical analysis of subharmonic mixers using accurate and approximate models," *IEEE Trans. Microwave Theory Tech.*, vol. MTT-30, pp. 2113–2120, 1982.

[12] C. Camacho-Penalosa, "Numerical steady-state analysis of nonlinear microwave circuits with periodic excitation," *IEEE Trans. Microwave Theory Tech.*, vol. MTT-31, pp. 724–730, 1983.

[13] M. S. Nakhla and J. Vlach, "A piecewise harmonic balance technique for determination of periodic response of nonlinear systems," *IEEE Trans. Circuits Syst.*, vol. CAS-23, pp. 85–91, 1976.

[14] A. Ushida and L. O. Chua, "Frequency-domain analysis of nonlinear circuits driven by multi-tone signals," *IEEE Trans. Circuits Syst.*, vol. CAS-31, pp. 766–779, 1984.

[15] K. S. Kundert, G. B. Sorkin, and A. Sangiovanni-Vincentelli, "Applying harmonic balance to almost-periodic circuits," *IEEE Trans. Microwave Theory Tech.*, vol. MTT-36, pp. 366–378, 1988.

[16] V. Rizzoli and A. Neri, "State of the art and present trends in nonlinear microwave CAD techniques," *IEEE Trans. Microwave Theory Tech.*, vol. MTT-36, pp. 343–365, 1988.

[17] S. W. Director and R. A. Rohrer, "The generalized adjoint network and network sensitivities," *IEEE Trans. Circuit Theory*, vol. CT-16, pp. 318–323, 1969.

[18] L. O. Chua and P. M. Lin, *Computer-Aided Analysis of Electronic Circuits*. Englewood Cliffs, NJ: Prentice-Hall, 1975.

[19] D. A. Calahan, *Computer-Aided Network Design*, 2nd ed. New York, NY: McGraw-Hill, 1972.

[20] R. H. Jansen, "Computer-aided design of hybrid and monolithic microwave integrated circuits—State of the art, problems and trends," in *Proc. European Microwave Conf.* (Nurnberg, West Germany), 1983, pp. 67–78.

[21] A. S. Householder, "A survey of some closed methods for inverting matrices," *SIAM J.*, vol. 5, pp. 155–169, 1957.

✠

John W. Bandler (S'66–M'66–SM'74–F'78) was born in Jerusalem, Palestine, on November 9, 1941. He studied at the Imperial College of Science and Technology, London, England, from 1960 to 1966. He received the B.Sc. (Eng.), Ph.D and D.Sc. (Eng.) degrees from the University of London, London, England, in 1963, 1967, and 1976, respectively.

He joined Mullard Research Laboratories, Redhill, Surrey, England, in 1966. From 1967 to 1969 he was a Postdoctorate Fellow and Sessional Lecturer at the University of Manitoba, Winnipeg, Canada. He joined McMaster University, Hamilton, Canada, in 1969, where he is currently a Professor of Electrical and Computer Engineering. Dr. Bandler has served as Chairman of the Department of Electrical Engineering and Dean of the Faculty of Engineering. He currently directs research in the Simulation Optimization Systems Research Laboratory. He is President of Optimization Systems Associates Inc., Dundas, Ont.,

Canada, which he established in 1983. OSA currently provides consulting services and software to numerous microwave clients in CAE of microwave integrated circuits.

Dr. Bandler contributed to *Modern Filter Theory and Design* (Wiley-Interscience, 1973) and to *Analog Methods for Computer-Aided Circuit Analysis and Diagnosis* (Marcel Dekker, 1988). He has more than 220 publications, four of which appear in *Computer-Aided Filter Design* (IEEE Press, 1973), one in *Microwave Integrated Circuits* (Artech House, 1975), one in *Low-Noise Microwave Transistors and Amplifiers* (IEEE Press, 1981), one in *Microwave Integrated Circuits* (2nd ed., Artech House, 1985), one in *Statistical Design of Integrated Circuits* (IEEE Press, 1987), and one in *Analog Fault Diagnosis* (IEEE Press, to be published). Dr. Bandler was an Associate Editor of the IEEE TRANSACTIONS ON MICROWAVE THEORY AND TECHNIQUES (1969–1974). He was Guest Editor of the Special Issue of the IEEE TRANSACTIONS ON MICROWAVE THEORY AND TECHNIQUES on Computer-Oriented Microwave Practices (March 1974).

Dr. Bandler is a Fellow of the Royal Society of Canada and of the Institution of Electrical Engineers (Great Britain). He is a member of the Association of Professional Engineers of the Province of Ontario (Canada).

✠

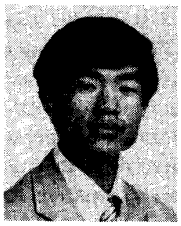

Qi-jun Zhang (S'84–M'87) was born in Xianyan, Shanxi, China, on October 8, 1959. He received the B.Eng. degree from the East China Engineering Institute, Nanjing, China in 1982, and the Ph.D. Degree from McMaster University, Hamilton, Canada in 1987, all in electrical engineering.

He was a research assistant in the Institute of Systems Engineering, Tianjin University, Tianjin, China, from 1982 to 1983. He was a teaching assistant in the Department of Electrical and Computer Engineering, McMaster University, from 1984 to 1987. He was a postdoctoral fellow in the Department of Electrical and Computer Engineering, McMaster University from September 1987 to March 1988. Presently he is a research engineer with Optimization Systems Associates Inc., Dundas, Ontario, Canada. His professional interests include all aspects of circuit CAD with emphasis on large-scale simulation and optimization, design and modelling of nonlinear microwave circuits, statistical modeling, sensitivity analysis, and the diagnosis and tuning of analog circuits.

Dr. Zhang is a contributor to *Analog Methods for Computer-Aided Circuit Analysis and Diagnosis* (Marcel Dekker, 1988).

✠

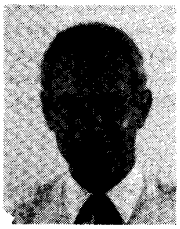

Radoslaw M. Biernacki (M'85–SM'86) was born in Warsaw, Poland. He received the Ph.D. degree from the Technical University of Warsaw, Warsaw, Poland, in 1976.

He became a Research and Teaching Assistant in 1969 and an Assistant Professor in 1976 at the Institute of Electronics Fundamentals, Technical University of Warsaw. From 1978 to 1980 he was on leave with the Research Group on Simulation, Optimization and Control and the Department of Electrical and Computer Engineering, McMaster University, Hamilton, Canada, as a Post-Doctorate Fellow. From 1984 to 1986 he was a Visiting Associate Professor at Texas A&M University, College Station, TX. He joined Optimization Systems Associates, Inc., Dundas, Ontario, Canada, in 1986, as Senior Research Engineer. In 1988 he also became a Professor (part-time) in the Department of Electrical and Computer Engineering, McMaster University. His research interests include system theory, optimization and numerical methods, and computer-aided design of integrated circuits and control systems.

Dr. Biernacki has more than 50 publications and has been awarded prizes several times for his research and teaching activities.

Reprint 5

Integrated Model Parameter Extraction Using Large-Scale Optimization Concepts

Integrated Model Parameter Extraction Using Large-Scale Optimization Concepts

JOHN W. BANDLER, FELLOW, IEEE, SHAO HUA CHEN, MEMBER, IEEE, SHEN YE, STUDENT MEMBER, IEEE, AND QI-JUN ZHANG, MEMBER, IEEE

Abstract—**This paper presents a robust approach to model parameter extraction. The approach not only attempts to match dc and ac measurements under different bias conditions simultaneously, but also employs the dc characteristics of the device as constraints on bias-dependent parameters, hence improving the uniqueness and reliability of the solution. The approach is an expansion of the hierarchical modeling techniques recently proposed by Bandler and Chen. Based on Bandler and Zhang's automatic decompositon concepts for large-scale optimization, a sequential model building method is proposed which, combined with powerful l_1 optimization techniques, can be used to establish a model with simple topology and sufficient accuracy.**

Practical FET models proposed by Materka and Kacprzak and by Curtice and Ettenberg are used to illustrate our formulation. A detailed numerical example based on the Materka and Kacprzak model is presented which has up to 28 optimization variables and 414 nonlinear error functions. The results show that a unique solution can be reached even after perturbing the original starting point (initial model parameter values) by 20 to 200 percent. The results also demonstrate the effectiveness of applying the sequential model building method to the FET modeling problem.

I. INTRODUCTION

MODEL parameter extraction, i.e., the determination of equivalent circuit parameters from dc, RF, and microwave measurements on devices (such as FET's), is of fundamental importance to microwave circuit designers. Conventionally, we seek a set of model parameters which minimizes the difference between the model responses and the measurements. To alleviate indeterminacy as well as for simplicity, techniques have been implemented (e.g., [1]–[3]) which separate the dc, low-frequency, and high-frequency measurements and divide the model parameters into corresponding subsets. This defines a set of subproblems to be solved sequentially. Such a sequentially decoupled solution, however, may not be reliable: a parameter determined solely from dc measurements may not be suitable for the purpose of microwave simulation, and the information contained in ac measurements is not fully utilized.

The multicircuit algorithm [4], [5] can improve the uniqueness of the solution by simultaneously processing multiple sets of S-parameter measurements made under different bias conditions. However, the authors [4], [5] assumed for computational purposes that the model parameters were either completely bias-independent or arbitrarily bias-dependent.

The approach presented in this paper not only attempts to match dc and ac measurements simultaneously, but also employs the dc characteristics of the device as constraints on the bias-dependent parameters. This enables us to use more efficiently the information contained in dc and nonzero frequency measurements and to reduce the degrees of freedom by imposing constraints on bias-dependent parameters. In this way we aim at improving the uniqueness and reliability of the solution.

Bandler and Zhang [6] have proposed a decomposition dictionary to reveal the interdependency between functions and their variables. In this paper, such a dictionary and the powerful l_1 optimization algorithm [7] are integrated to explore the relations between the model responses and model parameters during the modeling process, so that possible model defects can be overcome sequentially. In other words, we start the modeling process with the simplest model structure, subsequently adding elements according to the l_1 optimization result and the dictionary for a better match between the model responses and the measurements.

In Section II, through a simple circuit example, we demonstrate the feasibility and usefulness of integrating dc and ac modeling in one optimization problem. In Section III, general and abstract definitions for the model parameters are given. The definitions are illustrated by examples of significant interest, namely the Materka and Kacprzak FET model [2] and the Curtice and Ettenberg FET model [8]. The modeling optimization problem with both dc and ac responses is formulated in Section IV. In Section V, we present the sequential model building approach. In Section VI, a FET modeling example using the Materka and Kacprzak model is described in detail to demonstrate our new approach.

Manuscript received April 11, 1988; revised August 23, 1988. This work was supported in part by Optimization Systems Associates Inc. and in part by the Natural Sciences and Engineering Research Council of Canada under Grant A7239.

J. W. Bandler, S. H. Chen, and Q. J. Zhang are with Optimization Systems Associates Inc., Dundas, Ont., Canada L9H 5E7. J. W. Bandler is also with the Simulation Optimization Systems Research Laboratory and the Department of Electrical and Computer Engineering, McMaster University, Hamilton, Canada L8S 4L7.

S. Ye is with the Department of Electrical and Computer Engineering, McMaster University, Hamilton, Canada L8S 4L7.

IEEE Long Number 8824202.

0018-9480/88/1200-1629$01.00 ©1988 IEEE

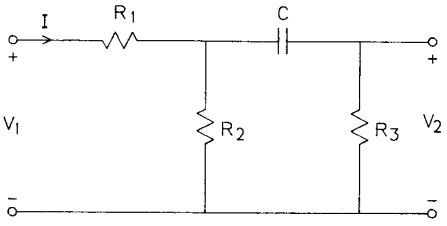

Fig. 1. Simple *RC* linear circuit example.

TABLE I
DEFINITIONS OF THE MODEL PARAMETERS

Category	Notation	Brief definition
Bias-independent	ϕ_a	affect dc and ac circuits
	ϕ_b	affect ac circuit
Unconstrained bias-dependent	ϕ_c^k	affect dc and ac circuits on the kth bias condition
	ϕ_d^k	affect ac circuit on the kth bias condition
Constrained bias-dependent	$\phi_e(\alpha, v^k)$	α affects dc and ac circuits
	$\phi_f(\alpha, \beta, v^k)$	β affects ac circuit only

$v^k = v(\phi_a, \phi_c^k, \alpha)$ denotes the dc state variables (such as the voltages and currents) under the kth bias condition.

II. A Simple Circuit Example

As a simple example to illustrate that combining dc and ac modeling is both feasible and useful, let us examine the linear *RC* circuit shown in Fig. 1. The unknown parameters are $\phi = [R_1 \quad R_2 \quad C]^T$. R_3 is assumed to be a known resistor. We also assume the responses to be the dc current I, under dc excitation $V_1 = V_{dc}$, as

$$I = \frac{V_{dc}}{R_1 + R_2} \tag{1}$$

and ac (complex) voltage V_2, under ac excitation $V_1 = V_{ac}$, as

$$V_2 = \frac{V_{ac} R_2 R_3 sC}{sC(R_1R_2 + R_1R_3 + R_2R_3) + R_1 + R_2} \tag{2}$$

where s denotes the complex frequency variable.

It is obvious that we cannot distinguish R_1 and R_2 if only the dc response I is used. It can also be verified that if only the ac response V_2 is taken we cannot uniquely determine ϕ either, no matter how many frequency points are applied.

It can be proved, however, that ϕ will be uniquely determined when we utilize both dc and ac measurements simultaneously, i.e., to match the dc response and ac response to the corresponding measurements at the same time. (The detailed proof of this observation is provided in Appendix I.)

III. Classification of Model Parameters

A. The General Case

In general, consider a device model with its equivalent circuit. The model parameters can be individually classified as bias-independent, unconstrained bias-dependent, or constrained bias-dependent. We also separate the parameters that appear in both dc and ac (small-signal) models from those appearing only in the ac model. Therefore, we define six subsets of model parameters, denoted by ϕ_a, ϕ_b, ϕ_c, ϕ_d, ϕ_e and ϕ_f, respectively, where ϕ_a and ϕ_b are bias-independent, ϕ_c and ϕ_d are unconstrained bias-dependent, and ϕ_e and ϕ_f are constrained bias-dependent. The parameters ϕ_a and ϕ_c appear in both the dc and ac models, whereas ϕ_b and ϕ_d affect only the ac small-signal equivalent circuit.

We use a superscript k to indicate a different bias point and the corresponding device model. Therefore, ϕ_c^k, ϕ_d^k, ϕ_e^k, and ϕ_f^k belong to the model under the kth bias, whereas ϕ_a and ϕ_b remain unchanged for different bias points.

We express the functional dependency of ϕ_e and ϕ_f on the bias condition by $\phi_e^k = \phi_e(\alpha, v^k)$ and $\phi_f^k = \phi_f(\alpha, \beta, v^k)$, where α and β are the coefficients of the constraints, and $v^k = v(\phi_a, \phi_c^k, \alpha)$ denotes the dc state variables (such as the voltages and currents). The coefficient α affects the dc equivalent circuit but β does not.

Table I summarizes the foregoing definitions.

This categorization stems from the consideration of the physical device and a feasible model. It is clear that we neeed ϕ_a and ϕ_b to represent the parameters which do not vary or vary only slightly with the bias conditions, such as the package capacitance and lead inductance of an FET. We need ϕ_c^k and ϕ_d^k to represent those bias-dependent parameters whose functional bias dependency expressions may not be known or available; on the other hand ϕ_c^k and ϕ_d^k may be used to test or investigate the functional bias-dependent properties of the model parameters.

Introducing $\phi_e(\alpha, v^k)$ and $\phi_f(\alpha, \beta, v^k)$ allows us to describe other bias-dependent parameters whose bias-dependent properties can be expressed by functions or, as we refer to them, constraints. Such constraints may be derived from physical characteristics of the device. They may be introduced empirically to simulate the pattern of the dc characteristic curves. They may also include mathematical expressions, such as polynomials. These constraints reduce the degrees of freedom in modeling, since the number of variables in this group, namely α and β, does not increase when more bias points are used, so that the uniqueness of the solution can be improved.

Our classification of the model parameters is consistent with the hierarchical parameter descriptions of Bandler and Chen [5]. From the definitions presented above, for example, we can see that for the ac responses, α and β are low-level parameters compared with ϕ_a, ϕ_b, ϕ_c, ϕ_d, ϕ_e, and ϕ_f. However, we should notice that a parameter can appear as a low-level and a high-level parameter simultaneously. For example, ϕ_e is at the same level as ϕ_a but it depends on ϕ_a as well.

B. Two Practical FET Device Examples

To illustrate the definitions presented in the previous subsection, we consider a typical nonlinear FET model of the type proposed by Materka and Kacprzak [2]. The model and its corresponding small-signal equivalent circuit are shown in Fig. 2 (a) and (b), respectively.

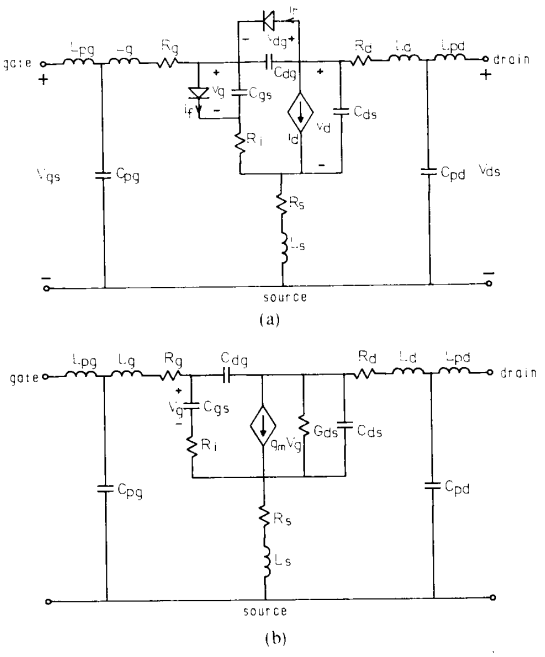

Fig. 2. (a) The Materka and Kacprzak nonlinear FET model [2] and (b) the corresponding small-signal equivalent circuit.

In the Materka and Kacprzak model, there are three bias-dependent current sources i_f, i_r, and i_d (see Fig. 2 (a)), which are defined as [2]

$$i_f = I_s\left[\exp(\alpha_s v_g) - 1\right]$$

$$i_r = I_{sr}\left[\exp(\alpha_{sr} v_{dg}) - 1\right]$$

$$i_d = I_{dss}\left(1 - \frac{v_g}{V_p}\right)^2 \tanh\left(\frac{\alpha_d v_d}{v_g - V_p}\right) \tag{3}$$

where

$$V_p = V_{po} + \gamma v_d$$

and where I_s, α_s, I_{sr}, α_{sr}, I_{dss}, α_d, V_{po}, and γ are parameters to be determined. Three other bias-dependent parameters, G_{ds}, g_m, and C_{gs} (see also Fig. 2 (b)), are constrained by [2]

$$G_{ds} = \frac{\partial i_d}{\partial v_d}$$

$$g_m = \frac{\partial i_d}{\partial v_g}$$

$$C_{gs} = C_{go}\left(1 - \frac{v_g}{V_{bi}}\right)^{-0.5} \qquad \text{for } v_g < 0.8V_{bi} \tag{4}$$

where C_{go} and V_{bi} are also parameters to be determined.

Table II gives clear classifications for all the parameters of the Materka and Kacprzak model.

We have also considered another typical nonlinear FET model, namely that proposed by Curtice and Ettenberg [8], as shown in Fig. 3 (a). Its small-signal equivalent circuit is shown in Fig. 3 (b). Following the considerations and the notations of [8], I_{gs} is a function of $\{R_F, V_{bi}\}$; I_{dg} is a function of $\{R_1, R_2, V_{B0}\}$; I_{ds}, g_{ds} and g_m are functions of $\{A_0, A_1, A_2, A_3, \gamma, \beta, V_{\text{out}}^0\}$; C_{gs} is a function of $\{V_{BI}\}$; and τ is a function of $\{A_5\}$. The classifications of the parameters are listed in the last column of Table II. (For details of the Curtice and Ettenberg model, see [8].)

TABLE II
PARAMETER DEFINITIONS FOR FET MODELS

Category	Subset	Parameters		
		Model 1	Model 1*	Model 2
bias-independent	ϕ_a	R_g, R_d, R_s, R_i	R_g, R_d	R_g, R_d, R_s
	ϕ_b	L_g, L_d, L_s, L_{pg} L_{pd}, C_{pg}, C_{pd} C_{dg}, C_{ds}, τ	L_g, L_d, L_s, L_{pg} L_{pd}, C_{pg}, C_{pd} τ	R_{in}, C_{ds}
unconstrained bias-dependent	ϕ_c^k		R_i^k, R_s^k	R_{ds}^k
	ϕ_d^k		C_{dg}^k, C_{ds}^k	C_{dg}^k
constrained bias-dependent	ϕ_e	G_{ds}, g_m	G_{ds}, g_m	g_{ds}, g_m
	ϕ_f	C_{gs}	C_{gs}	C_{gs}, τ
	α	I_s, α_s, I_{sr}, α_{sr} I_{dss}, α_d, V_{po}, γ	I_s, α_s, I_{sr}, α_{sr} I_{dss}, α_d, V_{po}, γ	A_0, A_1, A_2, A_3 γ, β, V_{out}^0 R_1, R_2, V_{B0} V_{bi}, R_F
	β	C_{go}, V_{bi}	C_{go}, V_{bi}	V_{BI}, A_5

Notes:

(1) The parameters under **Model 1** are defined according to Materka and Kacprzak [2].

(2) The parameters under **Model 1*** are the same as those in **Model 1** except that we assume R_i, R_s, C_{dg} and C_{ds} to be bias-dependent but we do not enforce their bias-dependent characteristics.

(3) The parameters under **Model 2** are defined following the considerations and the notation of Curtice and Ettenberg [8].

(4) The dc state variables are $v = [v_g\ v_d\ v_{dg}]^T$ for the Materka and Kacprzak model and $v = [V_{in}\ V_{out}\ V_{dg}]^T$ for the Curtice and Ettenberg model.

IV. MULTIBIAS DC AND AC MODELING OPTIMIZATION

Assume that the dc and ac measurements are S_{dc}^k and $S_{\text{ac}}^k(\omega_n)$, respectively, where ω_n, $n = 1, 2, \cdots, N$, is a set of frequency points. Correspondingly, we assume

$$\boldsymbol{F}_{\text{dc}}^k = \boldsymbol{F}_{\text{dc}}\left(\phi_a, \phi_c^k, \alpha\right) \tag{5}$$

as the dc model response, and

$$\boldsymbol{F}_{\text{ac}}^k(\omega_n) = \boldsymbol{F}_{\text{ac}}\left(\phi_a, \phi_b, \phi_c^k, \phi_d^k, \phi_e(\alpha, v^k), \phi_f(\alpha, \beta, v^k); \omega_n\right) \tag{6}$$

as the ac model response. Thus, the error functions corresponding to the dc model responses can be expressed as

$$e_{\text{dc}j}^k = w_{\text{dc}j}^k\left(F_{\text{dc}j}^k - S_{\text{dc}j}^k\right), \qquad j = 1, 2, \cdots, M_{\text{dc}}^k; \quad k \in K_{\text{dc}} \tag{7}$$

where $w_{\text{dc}j}^k$ is the weighting factor, M_{dc}^k is the number of dc measurements taken at the kth bias point, and K_{dc} is the set of bias points at which dc measurements are taken. The error functions corresponding to the ac model responses can be expressed as

$$e_{\text{ac}j}^k(\omega_n) = w_{\text{ac}j}^k\left[F_{\text{ac}j}^k(\omega_n) - S_{\text{ac}j}^k(\omega_n)\right],$$
$$j = 1, 2, \cdots, M_{\text{ac}}^k; \quad n = 1, 2, \cdots, N; \quad k \in K_{\text{ac}} \tag{8}$$

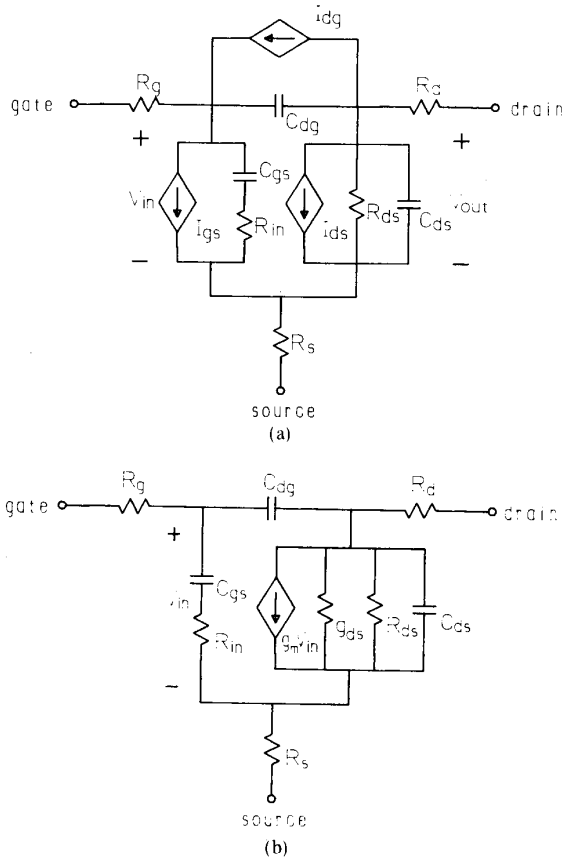

Fig. 3. (a) The Curtice and Ettenberg nonlinear FET model [8] and (b) the corresponding small-signal equivalent circuit.

where w_{acj}^k is the weighting factor, M_{ac}^k is the number of ac measurements taken at the kth bias point, and K_{ac} is the set of bias points at which ac measurements are taken.

If we use K to indicate the set of all bias points, then

$$K = K_{dc} \cup K_{ac} = \{1, 2, \cdots, K_{bias}\}. \tag{9}$$

Usually M_{dc}^k could be the same for different k, $k \in K_{dc}$, such as the number of dc current responses at different bias conditions. Similarly M_{ac}^k could be the same for different k, $k \in K_{ac}$, such as the number of S-parameter responses.

To obtain a uniform set of error functions, we define

$$f_i = e_{dcj}^k, \qquad j = 1, 2, \cdots, M_{dc}^k; \quad k \in K_{dc}; \quad i \in J_{dc} \tag{10}$$

and

$$f_i = e_{acj}^k(\omega_n), \qquad j = 1, 2, \cdots, M_{ac}^k; \quad n = 1, 2, \cdots, N; \quad k \in K_{ac}; \quad i \in J_{ac} \tag{11}$$

where $J_{dc} = \{1, 2, \cdots, M_1\}$, M_1 is the total number of dc measurements, $J_{ac} = \{M_1 + 1, M_1 + 2, \cdots, M_2\}$, and M_2 is the total number of measurements. Then we can formulate the l_1 modeling optimization problem

$$\text{minimize} \left\{ \sum_{i \in J_{dc}} |f_i| + \sum_{i \in J_{ac}} |f_i| \right\} \tag{12}$$

where the optimization variables are α, β, ϕ_a, ϕ_b, ϕ_c^k for $k \in K$, and ϕ_d^k for $k \in K_{ac}$, since ϕ_c^k is required for calculating both dc and ac responses, whereas ϕ_d^k is required only for calculating ac responses.

In order to calculate the model responses, we first solve the nonlinear dc circuit of the model for ϕ_a, ϕ_c^k and α, $k \in K$, so that F_{dc}^k, if $k \in K_{dc}$, can be determined. If $k \in K_{ac}$, $\phi_e(\alpha, v^k)$ and $\phi_f(\alpha, \beta, v^k)$ are calculated with v^k obtained from the dc solution. And then $F_{ac}^k(\omega_n)$, $n = 1, 2, \cdots, N$, can be determined.

The derivatives of the error functions required by the optimization can be obtained by the perturbation method. However, since the equivalent circuit of the device model is usually not very complicated, it is both feasible and efficient to get them analytically by adjoint analyses. The details of the analytic derivative calculations are discussed in Appendix II.

V. Sequential Model Building

A device model, such as the FET model in Super-Compact [9], may have a complicated topology and a comprehensive set of possible model parameters. In practice, we prefer a simplified model, provided that the match between the model responses and the measurements is satisfactory. It not only simplifies the computation, but also increases the identifiability.

Approaches have been proposed (e.g., [10], [11]) which optimize both the element values and the model topology. However, the topology optimization part of these approaches is entirely by trial and error and quite often has no physical justification.

For sequential model building, we start with a simple basic model structure, and sequentially add parameter(s) that would most effectively improve the match between the model responses and the measurements, where we assume that a comprehensive model which is physically meaningful is available. The iterative process continues until the match is satisfactory or no more parameter could be added. In order to find out the relationship between the model responses and parameters, we have applied the decomposition approach of Bandler and Zhang [6] to construct a decomposition dictionary to identify the interdependency between the model responses and parameters.

Consider a function $f_j(x)$ and a parameter x_i. A measure of the degree of interdependency between x_i and f_j can be defined, following [6], as

$$C_{ij} = \sum_{r=1}^{L} \left| \frac{\partial f_j(x^r)}{\partial x_i} x_i^0 \right|^p \tag{13}$$

where L is the number of points randomly chosen around x, x_i^0 is a scaling factor, and p can be 1 or 2. (In the example discussed in the next section we will choose $p = 1$.) The decompositon dictionary is constructed by fur-

ther grouping closely related functions

$$D_{it} = \sum_{j \in J_t} C_{ij} \tag{14}$$

where $J_1 \cup J_2 \cup \cdots \cup J_q = J_{dc} \cup J_{ac}$, and q is the number of function groups. For instance, we may designate all the error functions related to the complex S parameter S_{11} to one function group. The relative magnitude of D_{it} indicates the relative degree of interdependency between parameter x_i and the tth function group.

By virtue of the l_1 optimization algorithm [7], which has the very desirable feature of isolating large errors among all the error functions, the sequential model building procedure can practically be implemented: during the modeling process the l_1 solution and the corresponding decomposition dictionary at a specific model structure can indicate the most appropriate element(s) to be included in the model if the match has not been satisfactory. (See case 2 of the example in the next section.)

The decomposition dictionary may reveal parameters that are impossible or very difficult to identify from the available measurements; i.e, if the dictionary entries corresponding to a parameter are very small, this parameter may be very insensitive to any functions. Such parameters could be kept fixed at standard values. They may even be eliminated from the model if they have little effect on the match between the model responses and the measurements.

VI. A FET Example

Consider again the Materka and Kacprzak model discussed in Section III-B. The FET equivalent circuit model is shown in Fig. 2(a) and the corresponding small-signal equivalent circuit is shown in Fig. 2(b). We use measurements made under three different bias conditions (the same data have been considered by Bandler *et al.* [12]).

Following the assumptions in [12], we will use the classification of the parameters under **Model 1*** in Table II; however, we ignore the package parasitics L_{pg}, L_{pd}, C_{pg}, and C_{pd}. Since there are three bias points, altogether we have 28 optimization variables in ϕ_a, ϕ_b, ϕ_c^k, and ϕ_d^k for $k = 1, 2, 3$, α, and β. The units of the related parameters are listed in Table III.

The error functions are defined according to (7) and (8). Here $K_{dc} = K_{ac} = \{1, 2, 3\}$ for three different bias points; $M_{dc}^k = 2$ corresponding to the dc measurements on the gate and source currents; $M_{ac}^k = 8$ representing the real and imaginary parts of the S parameters; and $N = 17$ representing 17 frequency points from 2 to 18 GHz, 1 GHz apart. The weighting factors w_{dcj}^k and w_{acj}^k are properly chosen to balance the dc and ac error functions. The total number of nonlinear error functions for this example is 414.

At each bias point, we use Powell's algorithm [13] to solve the nonlinear dc equivalent circuit. The adjoint network analysis technique is applied to efficiently calculate the sensitivities of both dc and ac equivalent circuits.

Three cases are discussed as follows. In case 1, we will show the robustness of the modeling approach proposed in Section IV. In case 2, an experiment will be shown to demonstrate the feasibility of the sequential model building procedure in Section V. A similar experiment will be discussed briefly in case 3 with a different scaling factor in (13).

Case 1: At the starting point, we construct the decomposition dictionary. The scaling factor x_i^0 in (13) for this

TABLE III
UNITS OF THE FET MODEL PARAMETERS

Parameter	Unit	Parameter	Unit
R_g	Ω	I_s	A
R_i	Ω	α_s	1/V
R_d	Ω	I_{sr}	A
R_s	Ω	α_{sr}	1/V
G_{ds}	1/Ω	I_{dss}	A
g_m	1/Ω	α_d	-
L_g	nH	V_{po}	V
L_d	nH	γ	-
L_s	nH	C_{go}	pF
C_{dg}	pF	V_{bi}	V
C_{ds}	pF		
C_{gs}	pF		
τ	ps		

TABLE IV
PARAMETER VALUES OF THE FET MODEL

Parameter	Bias 1		Bias 2		Bias 3	
	start	solution	start	solution	start	solution
R_g+	1.0	0.0119	1.0	0.0119	1.0	0.0119
R_d+	1.0	0.0006	1.0	0.0006	1.0	0.0006
G_{ds}	*	0.0049	*	0.0058	*	0.0063
R_i	1.0	3.4731	1.0	4.2221	1.0	5.5954
R_s	1.0	0.5234	1.0	0.3675	1.0	0.2312
L_s	0.02	0.0107	0.02	0.0107	0.02	0.0107
C_{gs}	*	0.5929	*	0.3992	*	0.3333
C_{dg}	0.07	0.0287	0.07	0.0428	0.07	0.0533
C_{ds}	0.04	0.1958	0.04	0.1917	0.04	0.1905
g_m	*	0.0569	*	0.0437	*	0.0302
τ	7.0	3.6540	7.0	3.6540	7.0	3.6540
L_g	0.01	0.1257	0.01	0.1257	0.01	0.1257
L_d	0.01	0.0719	0.01	0.0719	0.01	0.0719

Parameter	start	solution
I_{dss}	0.2	0.1888
α_d	4.0	3.0523
V_{po}	-4.0	-4.3453
γ	-0.2	-0.3958
C_{go}	1.0	0.6137
V_{bi}	1.0	1.3011

See bias conditions in Table V.
+ values may not be reliable as the decomposition dictionary shows weak identifiability.
• values determined by α, β and dc solution.

TABLE V
DC RESPONSES AND MEASUREMENTS

DC current	Bias 1	Bias 2	Bias 3
	V_{gs} = 0V V_{ds} = 4V	V_{gs} = -1.74V V_{ds} = 4V	V_{gs} = -3.10V V_{ds} = 4V
I_{gs} assumed	0.0A	0.0A	0.0A
i_{gs} calculated	-2.7×10^{-8}A	-1.5×10^{-7}A	-6.1×10^{-7}A
I_{ds} measured	0.177A	0.092A	0.037A
i_{ds} calculated	0.177A	0.092A	0.043A

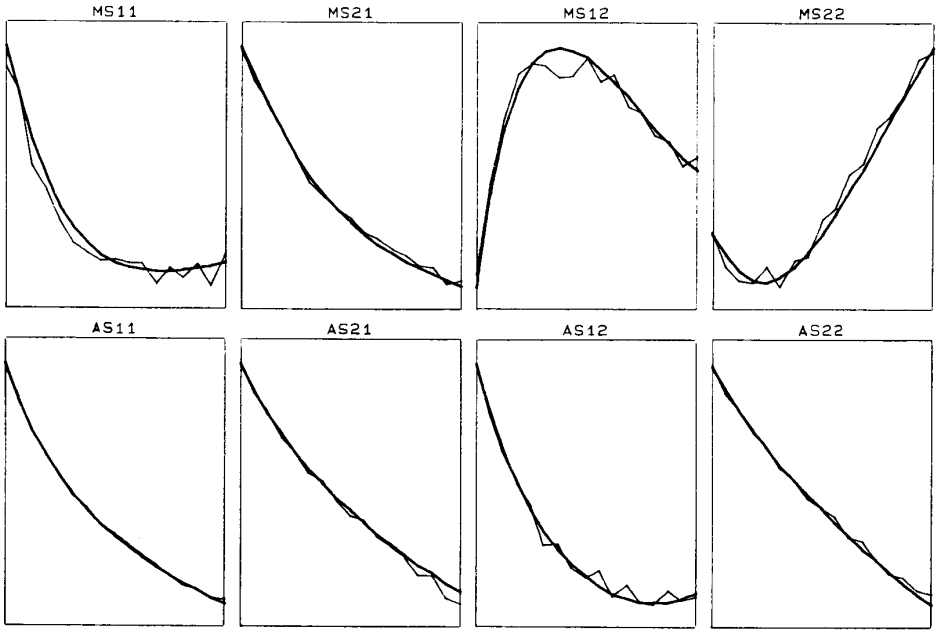

Fig. 4. The S-parameter match at the solution of case 1 for $V_{ds} = 4$ V and $V_{gs} = 0$ V.

dictionary is chosen to be x_i^r, which corresponds to the exponential transformation on the variables used by the optimization. This dictionary shows very small entries for I_s, α_s, I_{sr}, and α_{sr}. An l_1 optimization is performed, fixing $I_s = I_{sr} = 0.5$ nA, $\alpha_s = 20\ \mathrm{V}^{-1}$, and $\alpha_{sr} = 1\ \mathrm{V}^{-1}$. The resulting parameter values are listed in Table IV. Table V shows the dc responses, and Fig. 4 depicts the ac responses at the solution for one bias point.

To check whether we should consider I_s, α_s, I_{sr}, and α_{sr} as variables, we set up the dictionary at the solution, as shown in Table VI. The fact that the entries for I_s, α_s, I_{sr}, and α_{sr} remain very small confirms the validity of eliminating them as optimization variables. As a further verification, we attempted another optimization which included all possible variables. As expected, it did not improve the match between the model responses and the measurements.

The insensitivity of I_s, α_s, I_{sr}, and α_{sr} is, in fact, expected, since it is known that special bias conditions are needed in order to effectively determine the forward-biasing and breakdown properties of the FET [2].

To test the robustness of our approach, we randomly perturbed the starting point by 20 to 200 percent and restated the optimization. All the variables converged to virtually the same solution.

Case 2: As in case 1, the decomposition dictionaries in this case are constructed by choosing the scaling factor x_i^0 in (13) to be x_i^r, which corresponds to the exponential transformation on the variables used by the optimization. To demonstrate the feasibility of the sequential model building procedure, we restart the modeling process with a simplified model which does not include L_g and L_d. Also, R_g, R_d, R_i, I_s, α_s, I_{sr}, and α_{sr} are kept constant according to their relatively small entries in the decomposition

TABLE VI
DECOMPOSITION DICTIONARY AT THE SOLUTION

Parameter	I_{gs}	I_{ds}	S_{11}	S_{21}	S_{12}	S_{22}
R_g	0.00	0.00	0.02	0.01	0.01	0.02
L_g	-	-	15.	3.8	10.	1.1
L_d	-	-	0.32	1.6	4.6	9.2
L_s	-	-	0.91	0.24	16.	0.89
R_d	0.00	0.00	0.00	0.00	0.00	0.00
r	-	-	1.0	6.3	1.5	2.6
C_{dg}^1	-	-	1.7	1.7	28.	4.4
C_{ds}^1	-	-	0.36	4.1	9.8	16.
R_i^1	0.00	0.00	1.4	0.54	3.5	0.16
R_s^1	0.00	0.55	0.64	0.39	6.6	0.53
C_{dg}^2	-	-	3.4	3.0	21.	6.6
C_{ds}^2	-	-	0.80	4.4	9.3	16.
R_i^2	0.00	0.00	1.6	0.60	2.1	0.24
R_s^2	0.00	0.15	0.20	0.18	1.8	0.13
C_{dg}^3	-	-	4.2	3.3	19.	6.9
C_{ds}^3	-	-	0.94	4.0	9.2	16.
R_i^3	0.00	0.00	2.1	0.61	2.1	0.26
R_s^3	0.00	0.03	0.07	0.08	0.74	0.09
I_s	0.00	0.00	0.00	0.00	0.00	0.00
α_s	0.00	0.00	0.00	0.00	0.00	0.00
I_{sr}	0.00	0.00	0.00	0.00	0.00	0.00
α_{sr}	0.00	0.00	0.00	0.00	0.00	0.00
I_{dss}	0.00	29.	4.2	33.	18.	42.
α_d	0.00	2.8	1.2	12.	11.	25.
V_{po}	0.00	13.	2.8	26.	12.	28.
γ	0.00	4.6	1.4	12.	7.1	19.
C_{go}	-	-	40.	26.	49.	9.9
V_{bi}	-	-	9.3	5.5	9.7	2.4

The dictionary was set up using 50 random points over a 25 percent range around the solution point.

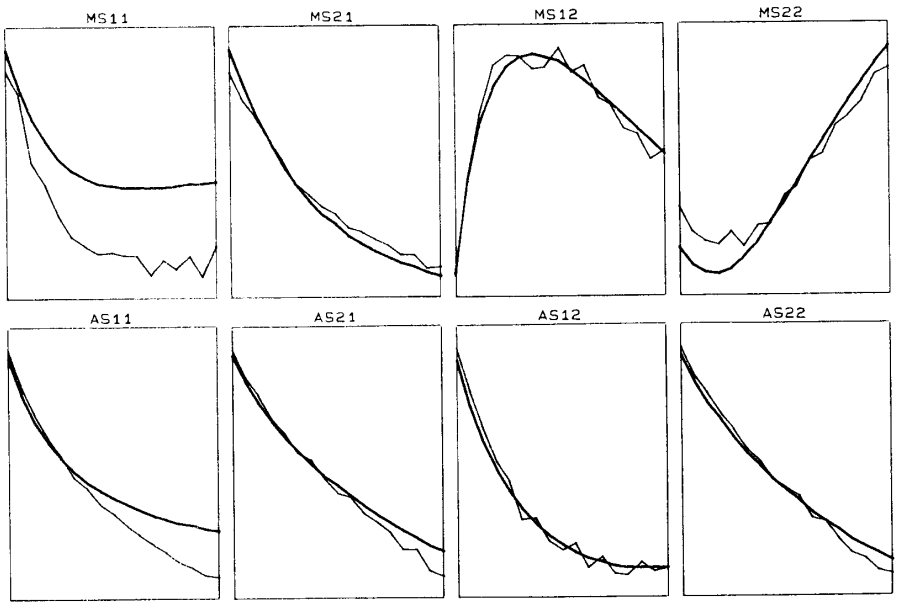

Fig. 5. The S-parameter match at the solution of case 2 using a simplified model for $V_{ds} = 4$ V and $V_{gs} = 0$ V.

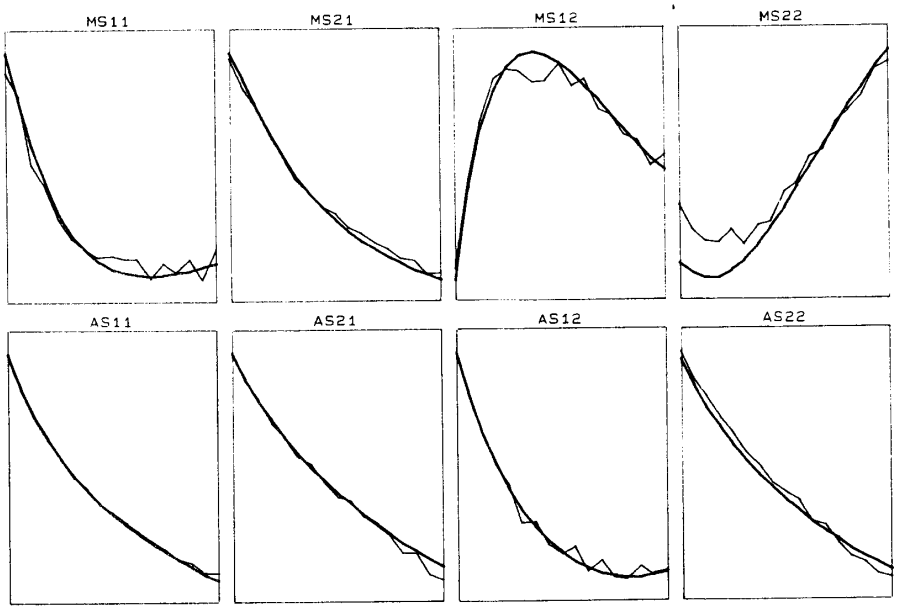

Fig. 6. The S-parameter match at the solution of case 2 for $V_{ds} = 4$ V and $V_{gs} = 0$ V. R_g and L_g were included as optimization variables.

dictionary. Fig. 5 depicts the model responses and the measurements at one bias point after the l_1 optimization using this simplified model.

It is obvious from Fig. 5 that the worst match is for S_{11}. According to the decomposition dictionary at this stage, as shown in Table VII, the most effective candidates for improving the match in S_{11} are R_g and L_g because of their larger entries under S_{11}. The result of a subsequent optimization which includes R_g and L_g as variables is shown in Fig. 6, from which a significant improvement on the match of S_{11} can be observed.

Further steps of sequential model building based on the decomposition dictionary include adding R_d and L_d to improve S_{22} and eventually converge to the same solution as in case 1.

By such a sequential model building, we have obtained a clear view of the relationship between a model parameter and the model responses, and we have the ability to avoid possible redundant model parameters. If the match between the model responses and measurements is sufficiently good, we do not have to include more optimizable parameters even if there are still some left.

TABLE VII
DECOMPOSITION DICTIONARY AT AN INTERMEDIATE STAGE

Parameter	S_{11}	S_{21}	S_{12}	S_{22}
R_g	1.7	0.56	1.2	0.16
L_g	1.1	0.27	0.84	0.08
L_d	0.05	0.19	0.65	1.2
R_d	0.07	0.70	1.1	2.9
R_i^1	0.48	0.16	0.98	0.05
R_i^2	0.41	0.14	0.51	0.06
R_i^3	0.41	0.10	0.39	0.05
I_s	0.00	0.00	0.00	0.00
α_s	0.00	0.00	0.00	0.00
I_{sr}	0.00	0.00	0.00	0.00
α_{sr}	0.00	0.00	0.00	0.00

Notes:

(1) Only relevant function groups and possible parameter candidates are listed.

(2) The dictionary is constructed by assuming an initial value of 0.01nH for L_g and L_d.

(3) 50 points and a 25 percent range were used to set up the dictionary.

Case 3: We also conducted an experiment where the decomposition dictionary was constructed by setting the scaling factor x_i^0 in (13) to 1, which corresponds to the sensitivities of the error functions with respect to the actual parameters.

At the starting point, we construct the dictionary with respect to all the possible variables. The actual variables used first in the optimization are those whose entries in the dictionary are relatively large, and other variables are kept constant. Then each time an optimization is completed but the result is not satisfactory, we check the match between the model responses and measurements, and select new variable(s) according to the updated dictionary which would most effectively improve the match.

Following such a procedure, results similar to those in case 2 were clearly observed. However, also observed from this experiment is that the parameters first chosen as optimization variables, i.e., the parameters whose entries are dominant in the decomposition dictionary, appeared to stay quite close to the first solution in the subsequent optimizations. Therefore, alternative decompositions for the optimization problem could be investigated.

VII. CONCLUSIONS

By introducing dc constraints and formulating the modeling process as a complete and integrated optimization problem, i.e., including simultaneously the dc and ac responses, we have improved the uniqueness and reliability of the extracted model parameters. A sequential model building approach has been proposed based on a decomposition dictionary. It can be used to arrive at a suitable compromise between the simplicity and adequacy of the model.

A powerful l_1 optimization technique, which is essential to the implementation of the sequential model building, has been employed in our algorithm. All the required gradients have been provided through efficient adjoint analyses.

Practical FET models have been considered. A FET modeling example using the Materka and Kacprzak model has been described in detail which clearly demonstrates the advantages of the new approach.

It should be noted, however, that when dc characteristics are used as constraints, they should be compatible with the actual device to be modeled; otherwise inappropriate dc constraints could cause large intrinsic discrepancies between the model responses and measurements.

As to the prospects of the approach proposed in this paper, we can see that

1) The model parameters extracted can be used directly by the harmonic balance method.
2) We can establish a more reliable small-signal model when dc constraints are considered.
3) The approach is applicable to other device modeling problems since it is quite general.
4) The sequential model building procedure is particulary promising.

A computer program RoMPE (Robust Model Parameter Extractor) [16] has recently been developed by Optimization Systems Associates Inc. It offers the techniques presented in this paper to microwave community through a user-friendly interface which includes state-of-the-art graphics and a simple yet flexible input file format.

APPENDIX I
VERIFICATION OF THE IDENTIFIABILITY OF THE *RC* CIRCUIT

The *RC* circuit under consideration is shown in Fig. 1. As in the derivations in [14], we use the concept of analog circuit fault diagnosis [4] to verify the identifiability of R_1, R_2, and C in the circuit. Briefly, given a complex-valued vector of responses $\boldsymbol{h}(\phi) = [h_1(\phi) \cdots h_m(\phi)]^T$, where $\phi = [\phi_1 \cdots \phi_n]^T$, the measure of identifiability of ϕ is determined by testing the rank of the $m \times n$ Jacobian matrix

$$\boldsymbol{J} = \left[\nabla \boldsymbol{h}^T(\phi)\right]^T \tag{A1}$$

where ∇ is the partial derivative operator $\partial/\partial\phi$. If the rank of matrix $\boldsymbol{J}$ is less than n, then ϕ will not be uniquely identifiable from $\boldsymbol{h}$.

1) Only a dc Response: The dc response I is

$$I = \frac{V_{\mathrm{dc}}}{R_1 + R_2}. \tag{A2}$$

The corresponding Jacobian matrix is

$$\boldsymbol{J}_{\mathrm{dc}} = \left[-V_{\mathrm{dc}}/(R_1+R_2)^2 \;\; -V_{\mathrm{dc}}/(R_1+R_2)^2\right]. \tag{A3}$$

It is clear that rank $\boldsymbol{J}_{\mathrm{dc}} = 1$. Therefore, R_1 and R_2 are not identifiable from the dc response I. This result is also straightforward intuitively.

2) Only an ac Response: The ac response V_2 is calculated as

$$V_2 = \frac{V_{ac} R_2 R_3 \, sC}{sC(R_1R_2 + R_1R_3 + R_2R_3) + R_1 + R_2}. \quad \text{(A4)}$$

The corresponding Jacobian matrix

$$\boldsymbol{J}_{ac} = \begin{bmatrix} -H[s_1C(R_2+R_3)+1] & H[R_1(s_1CR_3+1)/R_2] & H[(R_1+R_2)/C] \\ \vdots & \vdots & \vdots \\ -H[s_mC(R_2+R_3)+1] & H[R_1(s_mCR_3+1)/R_2] & H[(R_1+R_2)/C] \end{bmatrix} \quad \text{(A5)}$$

where s_i, $i = 1, \cdots, m$, indicate different frequencies, and

$$H = \frac{V_{ac} R_2 R_3 sC}{[sC(R_1R_2 + R_1R_3 + R_2R_3) + R_1 + R_2]^2}.$$

Denoting the three columns of $\boldsymbol{J}_{ac}$ by $\boldsymbol{J}_1$, $\boldsymbol{J}_2$, and $\boldsymbol{J}_3$, we can obtain

$$\frac{(R_2+R_3)}{R_1}\boldsymbol{J}_2 + \frac{R_3}{R_2}\boldsymbol{J}_1 - \frac{C}{(R_1+R_2)}\boldsymbol{J}_3 = \boldsymbol{0} \quad \text{(A6)}$$

which means that the rank of $\boldsymbol{J}_{ac}$ is less than 3, no matter how many frequency points are used. Hence we cannot uniquely determine ϕ from the response V_2.

3) Combined dc and ac Responses: When we consider both dc and ac responses simultaneously then, combining (A3) and (A5), the Jacobian matrix becomes

$$\boldsymbol{J} = \begin{bmatrix} -V_{dc}/(R_1+R_2)^2 & -V_{dc}/(R_1+R_2)^2 & 0 \\ -H[s_1C(R_2+R_3)+1] & H[R_1(s_1CR_3+1)/R_2] & H[(R_1+R_2)/C] \\ \vdots & \vdots & \vdots \\ -H[s_mC(R_2+R_3)+1] & H[R_1(s_mCR_3+1)/R_2] & H[(R_1+R_2)/C] \end{bmatrix} \quad \text{(A7)}$$

which is of full column rank. This indicates that ϕ is identifiable from the response $\boldsymbol{h} = [I(\phi)\, V_2(\phi, s_1) \cdots V_2(\phi, s_m)]^T$.

All three situations discussed above have been numerically verified.

Appendix II
Derivative Computations of the Model Responses

For $j \in J_{dc}$, f_j is a function of ϕ_a, ϕ_c^k, and α, $k \in K_{dc}$. The corresponding $\partial f_j/\partial \phi_a$, $\partial f_j/\partial \phi_c^k$, and $\partial f_j/\partial \alpha$ can be derived by nonlinear dc adjoint analysis [15].

For $j \in J_{ac}$, we know that

$$f_j = f_j\big(\phi_a, \phi_b, \phi_c^k, \phi_d^k, \phi_e(\alpha, v^k), \phi_f(\alpha, \beta, v^k)\big), \qquad k \in {}^k_{ac} \quad \text{(A8)}$$

where the true variables are $\phi_a, \phi_b, \phi_c^k, \phi_d^k, \alpha$ and β, and v^k was defined in Section III-A. Therefore, we can use the chain rule to obtain the required derivatives:

$$\frac{\partial f_j}{\partial \phi_{ai}} = \frac{\partial f_j}{\partial \phi_{ai}} + \frac{\partial v^{kT}}{\partial \phi_{ai}} \frac{\partial \phi_e^{kT}}{\partial v^k} \frac{\partial f_j}{\partial \phi_e^k} + \frac{\partial v^{kT}}{\partial \phi_{ai}} \frac{\partial \phi_f^{kT}}{\partial v^k} \frac{\partial f_j}{\partial \phi_f^k}$$

$$\frac{\partial f_j}{\partial \phi_{bi}} = \frac{\partial f_j}{\partial \phi_{bi}} \quad \text{(A9)}$$

$$\frac{\partial f_j}{\partial \phi_{ci}^k} = \frac{\partial f_j}{\partial \phi_{ci}^k} + \frac{\partial v^{kT}}{\partial \phi_{ci}^k} \frac{\partial \phi_e^{kT}}{\partial v^k} \frac{\partial f_j}{\partial \phi_e^k} + \frac{\partial v^{kT}}{\partial \phi_{ci}^k} \frac{\partial \phi_f^{kT}}{\partial v^k} \frac{\partial f_j}{\partial \phi_f^k}$$

$$\frac{\partial f_j}{\partial \phi_{di}^k} = \frac{\partial f_j}{\partial \phi_{di}^k} \quad \text{(A10)}$$

$$\frac{\partial f_j}{\partial \alpha_i} = \frac{\partial \phi_e^{kT}}{\partial \alpha_i} \frac{\partial f_j}{\partial \phi_e^k} + \frac{\partial v^{kT}}{\partial \alpha_i} \frac{\partial \phi_e^{kT}}{\partial v^k} \frac{\partial f_j}{\partial \phi_e^k} + \frac{\partial \phi_f^{kT}}{\partial \alpha_i} \frac{\partial f_j}{\partial \phi_f^k} + \frac{v^{kT}}{\partial \alpha_i} \frac{\partial \phi_f^{kT}}{\partial v^k} \frac{\partial f_j}{\partial \phi_f^k}$$

$$\frac{\partial f_j}{\partial \beta_i} = \frac{\partial \phi_f^{kT}}{\partial \beta_i} \frac{\partial f_j}{\partial \phi_f^k} \quad \text{(A11)}$$

where the superscript T stands for transposition. The derivative of f_j with respect to ϕ_a, ϕ_b, ϕ_e, ϕ_f, ϕ_c^k, and ϕ_d^k for $k \in K_{ac}$ on the right-hand side of (A9)–(A11) can be obtained by standard ac adjoint analysis, while the derivative of v^k with respect to α, β, ϕ_a, and ϕ_c^k for $k \in K_{ac}$ can be obtained by nonlinear dc adjoint analysis [15].

Acknowledgment

The first author would like to acknowledge Dr. R. A. Pucel of Raytheon Company, Research Division, Lexington, MA, for many helpful discussions on device modeling for CAD.

References

[1] H. Kondoh, "An accurate FET modelling from measured *S*-parameters," in *IEEE Int. Microwave Symp. Dig.* (Baltimore, MD), 1986, pp. 377–380.

[2] A. Materka and T. Kacprzak, "Computer calculation of large-signal GaAs FET amplifier characteristics," *IEEE Trans. Microwave Theory Tech.*, vol. MTT-33, pp. 129–135, 1985.

[3] W. R. Curtice, "GaAs MESFET modeling and nonlinear CAD," *IEEE Trans. Microwave Theory Tech.*, vol. 36, pp. 220–229, 1988.

[4] J. W. Bandler, S. H. Chen, and S. Daijavad, "Microwave device modeling using efficient l_1 optimization: A novel approach," *IEEE Trans. Microwave Theory Tech.*, vol. MTT-34, pp. 1282–1293, 1986.

[5] J. W. Bandler and S. H. Chen, "Circuit optimization: The state of the art," *IEEE Trans. Microwave Theory Tech.*, vol. 36, pp. 424–443, 1988.

[6] J. W. Bandler and Q. J. Zhang, "An automatic decompositon approach to optimization of large microwave systems," *IEEE Trans. Microwave Theory Tech.*, vol. MTT-35, pp. 1231–1239, 1987.

[7] J. W. Bandler, W. Kellermann, and K. Madsen, "A nonlinear l_1 optimization algorithm for design, modeling and diagnosis of networks," *IEEE Trans. Circuits Syst.*, vol. CAS-34, pp. 174–181, 1987.

[8] W. R. Curtice and M. Ettenberg, "A nonlinear GaAs FET model for use in the design of output circuits for power amplifiers," *IEEE Trans. Microwave Theory Tech.*, vol. MTT-33, pp. 1383–1394, 1985.
[9] *SUPER-COMPACT User's Manual*, Compact Software Inc., Patterson, NJ 07504, Apr. 1987.
[10] O. P. D. Cutteridge and Y. S. Zhang, "Computer-aided linear modelling of high-frequency bipolar transistors", *Proc. Inst. Elec. Eng.*, vol. 131, part G, pp. 252–260, 1984.
[11] M. Dowson, "Computer-aided design of equivalent circuit models for microwave frequencies," *Computer-aided Design*, vol. 17, no. 8, pp. 353–362, 1985.
[12] J. W. Bandler, S. H. Chen, S. Daijavad, and K. Madsen, "Efficient optimization with integrated gradient approximations," *IEEE Trans. Microwave Theory Tech.*, vol. 36, pp. 444–455, 1988.
[13] P. Rabinowitz, *Numerical Methods for Nonlinear Algebraic Equations*. New York: Gordon and Breach, 1970, pp. 87–161.
[14] J. W. Bandler and A. E. Salama, "Fault diagnosis of analog circuits," *Proc. IEEE*, vol. 73, pp. 1279–1325, 1985.
[15] L. O. Chua and P. Lin, *Computer-aided Analysis of Electronic Circuits: Algorithms and Computational Techniques*. Englewood Cliffs, N.J.: Prentice-Hall. 1975.
[16] *RoMPE User's Manual*, Optimization systems Associates Inc., Dundas, Ontario, Canada, Report OSA-88-RO-19-M, Oct. 1988.

John W. Bandler (S'66–M'66–SM'74–F'78) was born in Jerusalem, Palestine, on November 9, 1941. He studied at the Imperial College of Science and Technology, London, England, from 1960 to 1966. He received the B.Sc. (Eng.), Ph.D and D.Sc. (Eng.) degrees from the University of London, London, England. in 1963, 1967, and 1976, respectively.

He joined Mullard Research Laboratories, Redhill, Surrey, England, in 1966. From 1967 to 1969 he was a Postdoctorate Fellow and Sessional Lecturer at the University of Manitoba, Winnipeg, Canada. He joined McMaster University, Hamilton, Canada, in 1969, where he is currently a Professor of Electrical and Computer Engineering. Dr. Bandler has served as Chairman of the Department of Electrical Engineering and Dean of the Faculty of Engineering. He currently directs research in the Simulation Optimization Systems Research Laboratory.

Dr. Bandler is President of Optimization Systems Associates Inc., Dundas, Ont., Canada, which he established in 1983.

Dr. Bandler contributed to *Modern Filter Theory and Design* (Wiley-Interscience, 1973) and to *Analog Methods for Computer-Aided Circuit Analysis and Diagnosis* (Marcel Dekker, 1988). He has more than 220 publications, four of which appear in *Computer-Aided Filter Design* (IEEE Press, 1973), one in *Microwave Integrated Circuits* (Artech House, 1975), one in *Low-Noise Microwave Transistors and Amplifiers* (IEEE Press, 1981), one in *Microwave Integrated Circuits* (2nd ed., Artech House, 1985), one in *Statistical Design of Integrated Circuits* (IEEE Press, 1987), and one in *Analog Fault Diagnosis* (IEEE Press, to be published). Dr. Bandler was an Associate Editor of the IEEE TRANSACTIONS ON MICROWAVE THEORY AND TECHNIQUES (1969–1974). He was Guest Editor of the Special Issue of the IEEE TRANSACTIONS ON MICROWAVE THEORY AND TECHNIQUES on Computer-Oriented Microwave Practices (March 1974). Dr. Bandler is a Fellow of the Royal Society of Canada and of the Institution of Electrical Engineers (Great Britain). He is a member of the Association of Professional Engineers of the Province of Ontario (Canada).

Shao Hua Chen (S'84–M'88) was born in Swatow, Guangdong, China, on September 27, 1957. He received the B.S. (Eng.) degree from the South China Institute of Technology, Guangzhou, China, in 1982

and the Ph.D. degree in electrical engineering from McMaster University, Hamilton, Canada, in 1987.

From July 1982 to August 1983, he was a teaching assistant in the Department of Automation at the South China Institute of Technology. He received a graduate scholarship from the Chinese Ministry of Education and joined the Department of Electrical and Computer Engineering at McMaster University in 1983. He held an Ontario Graduate Scholarship for the academic years 1985/86 and 1986/87. Currently he is working as a research engineer for Optimization Systems Associates Inc., Dundas, Ontario, Canada. His research interests include optimization methods, sensitivity analysis, device modeling, design centering, tolerancing and tuning, as well as user-friendly computer graphics.

Shen Ye (S'88) was born in Shanghai, China, on January 31, 1957. He received the B. E. and M. E. degrees in electrical engineering from Shanghai University of Technology, Shanghai, China, in 1982 and 1984, respectively.

From August 1984 to August 1986 he was with the Department of Electrical Engineering, Shanghai University of Technology. Since September 1986, he has been working towards the Ph.D. degree in the Department of Electrical and Computer Engineering, McMaster University, Hamiltion, Canada. His main research interests include analog fault diagnosis, device modeling, and computer-aided design using optimization methods.

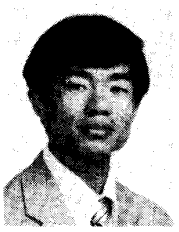

Qi-jun Zhang (S'84–M'87) was born in Xianyan, Shanxi, China, on October 8, 1959. He received the B. Eng. degree from the East China Engineering Institute, Nanjing. China in 1982, and the Ph. D. Degree from McMaster University, Hamilton, Canada in 1987, all in electrical engineering.

He was a research assistant in the Institute of Systems Engineering, Tianjin University, Tianjin, China, from 1982 to 1983. He was a teaching assistant in the Department of Electrical and Computer Engineering, McMaster University, from 1984 to 1987. He was a postdoctoral fellow in the Department of Electrical and Computer Engineering, McMaster University, from September 1987 to March 1988. Presently he is a research engineer with Optimization Systems Associates Inc., Dundas, Ontario, Canada. His professional interests include all aspects of circuit CAD with emphasis on large-scale simulation and optimization, design and modeling of nonlinear microwave circuits, statistical modeling, sensitivity analysis, and the diagnosis and tuning of analog circuits.

Dr. Zhang is a contributor to *Analog Methods for Computer-Aided Circuit Analysis and Diagnosis* (Marcel Dekker, 1988).

Reprint 6

Efficient Large-Signal FET Parameter Extraction Using Harmonics

Efficient Large-Signal FET Parameter Extraction Using Harmonics

JOHN W. BANDLER, FELLOW, IEEE, QI-JUN ZHANG, MEMBER, IEEE, SHEN YE, STUDENT MEMBER, IEEE, AND SHAO HUA CHEN, MEMBER, IEEE

Abstract—**We present a novel approach to nonlinear large-signal FET model parameter extraction for GaAs MESFET devices measured under large-signal conditions. Powerful nonlinear adjoint-based optimization, which employs the harmonic balance method as the nonlinear circuit simulation technique, simultaneously processes multibias, multipower inputs, multi-fundamental-frequency excitations, and multiharmonic measurements to uniquely reveal the parameters of the intrinsic FET. In contrast to other methods by which the model parameters are extracted using dc and small-signal measurements, our new approach can provide more accurate and reliable large-signal model parameters extracted under actual operating conditions. The modified Materka and Kacprzak FET model serves as an example. Numerical results verify that our approach can effectively determine the parameters of this model. Including harmonics in parameter extraction results in a reliable large-signal model. Real data provided by Texas Instruments have also been employed. The technique has been implemented in a new program called HarPE.**

I. Introduction

AN ACCURATE nonlinear large-signal FET model is critical to nonlinear microwave CAD. Various approaches to FET modeling have been proposed, e.g., [1]–[5]. The dominant nonlinear bias-dependent current source in these models, namely, the drain-to-source current source, is commonly determined by fitting static or dynamic dc $I-V$ characteristics only [1], [2], [4]–[7] or by matching dc characteristics and small-signal S parameters simultaneously [3]. Other nonlinear elements in the model are determined either by applying special dc biases so as to determine the parameters of the gate-to-source nonlinear current source in the Materka and Kacprzak model [2] or by using small-signal S parameters so as to determine the gate-to-source nonlinear capacitor [3].

The FET models obtained by those methods may provide accurate results under dc and/or small-signal operating conditions. They may not, however, be accurate enough for high-frequency large-signal applications [8], since they are determined under small-signal conditions and then used to *predict* the behavior for large-signal operations. Parameter extraction using large-signal measurements, e.g., power measurements [9], has recently been proposed. However the approach in [9] does not distinguish individual harmonics.

In this paper, we present a truly nonlinear large-signal FET parameter extraction procedure which utilizes spectrum measurements, including dc bias information and power output at different harmonics under practical working conditions [10]. Besides multibias and multifrequency excitations, multipower inputs are introduced for large-signal parameter extraction. The harmonic balance method [11] is employed for fast nonlinear frequency domain simulation in conjunction with ℓ_1 [12] and ℓ_2 optimization for extracting the parameters of the nonlinear elements in the large-signal FET model. Powerful nonlinear adjoint analysis for sensitivity computation [13] is implemented with attendant advantages in computation time.

Numerical experiments show that all the parameters can be identified under practical large-signal conditions and that including higher harmonics in large-signal parameter extraction is crucial to the reliability of the model. Numerical results are also obtained in processing actual measurement data provided by Texas Instruments. Good agreement between the measurements and the model responses is reached, demonstrating the feasibility of our new parameter extraction approach.

In Section II, the formulation of the large-signal parameter extraction optimization problem is presented. Section III describes the applications of the harmonic balance technique to model response simulations and nonlinear adjoint sensitivity analysis to gradient calculations. An automatic weight assignment algorithm enhancing parameter extraction optimization is given in Section IV. Numerical examples are discussed in Section V, where we use the modified Materka and Kacprzak FET model [14], which has 21 parameters characterizing the nonlinear intrinsic part of this large-signal FET model.

II. Optimization for Large-Signal Parameter Extraction

Consider the FET model and its measurement environment shown in Fig. 1, where Y_{in} and Y_{out} are input and output 2-ports, and Y_g and Y_d are gate and drain bias

Manuscript received April 3, 1989; revised July 19, 1989. This work was supported in part by Optimization Systems Associates Inc. and in part by the Natural Sciences and Engineering Research Council of Canada under Grant A7239.

J. W. Bandler and Q.-J. Zhang are with Optimization Systems Associates Inc., P.O. Box 8083, Dundas, Ont., Canada L9H 5E7, and with the Simulation Optimization Systems Research Laboratory and the Department of Electrical and Computer Engineering, McMaster University, Hamilton, Ont., Canada L8S 4L7.

S. H. Chen is with Optimization Systems Associates Inc., P.O. Box 8083, Dundas, Ont., Canada L9H 5E7.

S. Ye is with the Simulation Optimization Systems Research Laboratory and the Department of Electrical and Computer Engineering, McMaster University, Hamilton, Ont., Canada L8S 4L7.

IEEE Log Number 8931360.

0018-9480/90/1200-2099$01.00 ©1990 IEEE

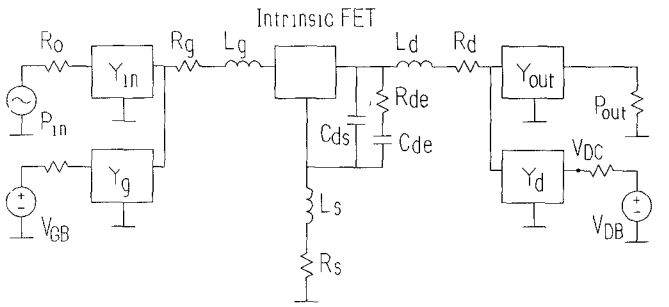

Fig. 1. Circuit setup for large-signal multiharmonic FET measurement.

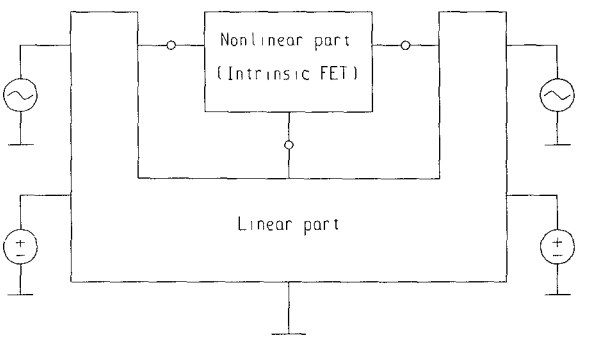

Fig. 2. Block diagram for illustrating circuit simulation using the harmonic balance method.

2-ports, respectively. A large-signal power input P_{in} is applied to the circuit. The responses including dc and several harmonic components are measured.

In addition to the multibias, multifrequency concept we pioneered for small-signal parameter extraction [3], [15], we allow the circuit to be excited at several input power levels. Various combinations of bias points, fundamental frequencies, and input power levels together with multiharmonic measurements contribute to the information needed for real large-signal parameter extraction. In the following discussion we use the term *bias–input-frequency combination* to indicate the modeling circuit working at a bias point with a particular input power level and at a particular fundamental frequency.

Assume for the jth bias–input-frequency combination, $j=1,2,\cdots,M$, the measurement is

$$\boldsymbol{S}_j = \left[S_j(0)\ \ S_j(\omega_{j1})\cdots S_j(\omega_{jH})\right]^T \tag{1}$$

where M is the number of bias–input-frequency combinations, $S_j(0)$ is the dc component of the measurement, $S_j(\omega_{jk})$, $k=1,2,\cdots,H$, are the kth harmonic components at the jth bias–input-frequency combination, and H is the number of harmonics contained in the measurement. $S_j(0)$ can be taken as the bias-related dc voltage or current, which varies at different fundamental frequencies and input levels even at a fixed bias point. When using power spectrum measurement, $S_j(\omega_{jk})$ denotes the kth harmonic of the output power spectrum measured at the jth bias–input-frequency combination. (The equivalent output voltage with phase information might also be employed [10].)

Corresponding to (1), the model response $\boldsymbol{F}_j(\phi)$ can be expressed as

$$\boldsymbol{F}_j(\phi) = \left[F_j(\phi,0)\ \ F_j(\phi,\omega_{j1})\cdots F_j(\phi,\omega_{jH})\right]^T, \quad j=1,2,\cdots,M \tag{2}$$

where ϕ stands for the parameters of the model to be determined. The parameter extraction problem can be formulated as the following optimization problem:

$$\min_{\phi}\sum_{j=1}^{M}\left(w_{j\mathrm{dc}}|F_j(\phi,0)-S_j(0)|^p + \sum_{k=1}^{H} w_{jk}|F_j(\phi,\omega_{jk})-S_j(\omega_{jk})|^p\right) \tag{3}$$

where $w_{j\mathrm{dc}}$ and w_{jk} are weighting factors, and $p=1$ or 2 corresponds to ℓ_1 or ℓ_2 optimization, respectively. The criterion of the above optimization is to match the model responses to the measurements at dc and several harmonics. It is clear that the practical usefulness of this parameter extraction approach depends on the effectiveness of calculating the model responses $\boldsymbol{F}_j(\phi)$, $j=1,2,\cdots,M$, and their derivatives. (In the next section we will show that the numerical computation of $\boldsymbol{F}_j(\phi)$ and its derivatives is not a trivial task.)

The magnitude of the circuit responses varies widely at different bias–input-frequency combinations and different harmonics. An automatic weight assignment algorithm has been developed to improve robustness and enhance convergence speed. If the harmonic measurement is made in the form of output power, the conditioning of the optimization problem can be further improved by converting the output power to its equivalent output voltage.

III. Nonlinear Circuit Simulation and Gradient Calculation

For a nonlinear large-signal FET model, the circuit model in Fig. 1 is nonlinear. This means that the model response $\boldsymbol{F}_j(\phi)$ in (2) must be obtained by solving a dynamic nonlinear circuit, and the gradient of the objective function in (3) involves calculation of the derivatives of the dynamic nonlinear circuit response.

To solve these two difficult problems, we have employed the efficient harmonic balance method [11] for fast nonlinear circuit simulation in the frequency domain. A powerful nonlinear adjoint sensitivity analysis technique [13] has been implemented to calculate the derivatives of the model response and therefore the gradient of the objective function in (3) with respect to ϕ. In this section we discuss the applications of the harmonic balance technique to model response simulation, and of nonlinear adjoint sensitivity analysis to gradient calculations.

Let the nonlinear circuit model be partitioned into linear and nonlinear subcircuits, as illustrated in Fig. 2. Assume that the multiport Y matrix of the linear subcircuit can be established, all the nonlinear elements are voltage-controlled, and there is no nonlinear inductor inside the intrinsic FET model. Also, for simplicity, we assume that the parameters in the linear subcircuits are known. In the rest of this section, we will focus our discussions on the jth

bias–input-frequency combination; therefore the corresponding subscript j will be omitted to simplify the notation. Other bias–input-frequency combinations can be treated similarly.

A. Nonlinear Circuit Simulation Using Harmonic Balance Method

Following [11], the harmonic balance equation for our model can be expressed as

$$\boldsymbol{I}_d(\phi, \boldsymbol{V}(\phi), \omega_k) + j\Omega(\omega_k)\boldsymbol{Q}(\phi, \boldsymbol{V}(\phi), \omega_k) + \boldsymbol{Y}(\omega_k)\boldsymbol{V}(\phi, \omega_k) + \boldsymbol{I}_s(\omega_k) = \boldsymbol{0}, \qquad k = 0, 1, \cdots, H' \tag{4}$$

where k represents the kth harmonic, $\omega_0 = 0$ corresponds to the dc component, $\boldsymbol{V}(\phi) = [\boldsymbol{V}^T(\phi, 0)\ \boldsymbol{V}^T(\phi, \omega_1) \cdots \boldsymbol{V}^T(\phi, \omega_{H'})]^T$ is the voltage vector to be solved for, $\boldsymbol{Y}$ stands for the multiport admittance matrix of the linear subcircuit, $\boldsymbol{I}_s$ is the equivalent current excitation from the external excitations, $\boldsymbol{I}_d$ corresponds to the current from the nonlinear current sources, $\Omega(\omega_k)$ is a diagonal matrix with ω_k as diagonal elements, and $\boldsymbol{Q}$ corresponds to the charge from the nonlinear capacitors. For example, $\boldsymbol{I}_d$ may contain the drain-to-source and drain-to-gate nonlinear current sources, and $\boldsymbol{Q}$ may include the gate-to-source nonlinear capacitor.

In (4) ϕ represents the optimization variables, i.e., the parameters to be determined, and H' the number of harmonics considered in the harmonic balance simulation. It should be noticed that $H' \geqslant H$ (the number of measured harmonics used), and H' can be different for different bias–input frequency combinations. For higher accuracy H' could be greater than H.

We solve (4) by organizing it into a scalar form:

$$\begin{bmatrix} \boldsymbol{I}_d^R(\phi, \boldsymbol{V}(\phi), 0) \\ \boldsymbol{I}_d^R(\phi, \boldsymbol{V}(\phi), \omega_1) \\ \vdots \\ \boldsymbol{I}_d^R(\phi, \boldsymbol{V}(\phi), \omega_{H'}) \\ \boldsymbol{I}_d^I(\phi, \boldsymbol{V}(\phi), 0) \\ \boldsymbol{I}_d^I(\phi, \boldsymbol{V}(\phi), \omega_1) \\ \vdots \\ \boldsymbol{I}_d^I(\phi, \boldsymbol{V}(\phi), \omega_{H'}) \end{bmatrix} + \begin{bmatrix} & & & & -\Omega(0) & & & \\ & & & & & -\Omega(\omega_1) & & \\ & & & & & & \ddots & \\ & & & & & & & -\Omega(\omega_{H'}) \\ \Omega(0) & & & & & & & \\ & \Omega(\omega_1) & & & & & & \\ & & \ddots & & & & & \\ & & & \Omega(\omega_{H'}) & & & & \end{bmatrix} \begin{bmatrix} \boldsymbol{Q}^R(\phi, \boldsymbol{V}(\phi), 0) \\ \boldsymbol{Q}^R(\phi, \boldsymbol{V}(\phi), \omega_1) \\ \vdots \\ \boldsymbol{Q}^R(\phi, \boldsymbol{V}(\phi), \omega_{H'}) \\ \boldsymbol{Q}^I(\phi, \boldsymbol{V}(\phi), 0) \\ \boldsymbol{Q}^I(\phi, \boldsymbol{V}(\phi), \omega_1) \\ \vdots \\ \boldsymbol{Q}^I(\phi, \boldsymbol{V}(\phi), \omega_{H'}) \end{bmatrix}$$

$$+ \begin{bmatrix} \boldsymbol{Y}^R(0) & & & & -\boldsymbol{Y}^I(0) & & & \\ & \boldsymbol{Y}^R(\omega_1) & & & & -\boldsymbol{Y}^I(\omega_1) & & \\ & & \ddots & & & & \ddots & \\ & & & \boldsymbol{Y}^R(\omega_{H'}) & & & & -\boldsymbol{Y}^I(\omega_{H'}) \\ \boldsymbol{Y}^I(0) & & & & \boldsymbol{Y}^R(0) & & & \\ & \boldsymbol{Y}^I(\omega_1) & & & & \boldsymbol{Y}^R(\omega_1) & & \\ & & \ddots & & & & \ddots & \\ & & & \boldsymbol{Y}^I(\omega_{H'}) & & & & \boldsymbol{Y}^R(\omega_{H'}) \end{bmatrix} \begin{bmatrix} \boldsymbol{V}^R(\phi, 0) \\ \boldsymbol{V}^R(\phi, \omega_1) \\ \vdots \\ \boldsymbol{V}^R(\phi, \omega_{H'}) \\ \boldsymbol{V}^I(\phi, 0) \\ \boldsymbol{V}^I(\phi, \omega_1) \\ \vdots \\ \boldsymbol{V}^I(\phi, \omega_{H'}) \end{bmatrix} + \begin{bmatrix} \boldsymbol{I}_s^R(0) \\ \boldsymbol{I}_s^R(\omega_1) \\ \vdots \\ \boldsymbol{I}_s^R(\omega_{H'}) \\ \boldsymbol{I}_s^I(0) \\ \boldsymbol{I}_s^I(\omega_1) \\ \vdots \\ \boldsymbol{I}_s^I(\omega_{H'}) \end{bmatrix} = \boldsymbol{0}$$

or, simply

$$\bar{\boldsymbol{I}}_d(\phi, \bar{\boldsymbol{V}}(\phi)) + \bar{\Omega}\bar{\boldsymbol{Q}}(\phi, \bar{\boldsymbol{V}}(\phi)) + \bar{\boldsymbol{Y}}\bar{\boldsymbol{V}}(\phi) + \bar{\boldsymbol{I}}_s = \boldsymbol{0} \tag{5}$$

where the superscripts R and I represent real and imaginary parts of the corresponding component, respectively. Note that in solving the harmonic balance equation (5), ϕ is constant and $\bar{\boldsymbol{V}}(\phi)$ is the variable. Powell's algorithm for solving nonlinear equations [16] is used, where in order to save computation time and provide higher accuracy the exact Jacobian matrix is calculated in our program, i.e.,

$$\bar{\boldsymbol{J}}(\phi, \bar{\boldsymbol{V}}(\phi)) = \left(\frac{\partial \bar{\boldsymbol{I}}_d^T(\phi, \bar{\boldsymbol{V}}(\phi))}{\partial \bar{\boldsymbol{V}}(\phi)}\right)^T + \bar{\Omega}\left(\frac{\partial \bar{\boldsymbol{Q}}^T(\phi, \bar{\boldsymbol{V}}(\phi))}{\partial \bar{\boldsymbol{V}}(\phi)}\right)^T + \bar{\boldsymbol{Y}}. \tag{6}$$

The detailed calculations of the entries of $\bar{\boldsymbol{J}}(\phi, \bar{\boldsymbol{V}}(\phi))$ are discussed in [11].

When the solution $\bar{\boldsymbol{V}}(\phi)$ is reached, the model response $\boldsymbol{F}(\phi)$ can be easily obtained:

$$\boldsymbol{F}(\phi, \omega_k) = \boldsymbol{a}^T(\omega_k)\boldsymbol{V}(\phi, \omega_k) + \boldsymbol{b}^T(\omega_k)\boldsymbol{E}(\omega_k), \qquad k = 0, 1, \cdots, H \tag{7}$$

where $\boldsymbol{a}(\omega_k)$ and $\boldsymbol{b}(\omega_k)$ are constant vectors determined by the linear subcircuit, and $\boldsymbol{E}(\omega_k)$ corresponds to the external excitations including power input source and bias sources.

B. Gradient Calculation by Nonlinear Adjoint Sensitivity Analysis

Let N be an index set indicating interfacing ports between linear and nonlinear parts, and $\boldsymbol{e}_{n1}(k)$ and $\boldsymbol{e}_{n2}(k)$ be such unit vectors that $V_n(\phi, \omega_k) = (\boldsymbol{e}_{n1}(k) + j\boldsymbol{e}_{n2}(k))^T\bar{\boldsymbol{V}}(\phi)$, $n \in N$. The circuit response $\boldsymbol{F}(\phi, \omega_k)$ in (7)

can be rewritten as

$$\boldsymbol{F}(\phi,\omega_k) = \sum_{n\in N} a_n(\omega_k)\left(\boldsymbol{e}_{n1}(k)+j\boldsymbol{e}_{n2}(k)\right)^T\bar{\boldsymbol{V}}(\phi)+\boldsymbol{b}^T(\omega_k)\boldsymbol{E}(\omega_k). \tag{8}$$

The derivative of $\boldsymbol{F}(\phi,\omega_k)$ w.r.t. ϕ_t is then

$$\frac{\partial \boldsymbol{F}(\phi,\omega_k)}{\partial\phi_t} = \sum_{n\in N} a_n(\omega_k)\left(\boldsymbol{e}_{n1}^T(k)\frac{\partial\bar{\boldsymbol{V}}(\phi)}{\partial\phi_t}+j\boldsymbol{e}_{n2}^T(k)\frac{\partial\bar{\boldsymbol{V}}(\phi)}{\partial\phi_t}\right). \tag{9}$$

To realize the above derivative, we first derive from (5) that

$$\frac{\partial\bar{\boldsymbol{V}}(\phi)}{\partial\phi_t} = -\bar{\boldsymbol{J}}^{-1}(\phi,\bar{\boldsymbol{V}}(\phi))\left(\frac{\partial\bar{\boldsymbol{I}}_d(\phi,\bar{\boldsymbol{V}}(\phi))}{\partial\phi_t}+\bar{\Omega}\frac{\partial\bar{\boldsymbol{Q}}(\phi,\bar{\boldsymbol{V}}(\phi))}{\partial\phi_t}\right) \tag{10}$$

where $\bar{\boldsymbol{J}}(\phi,\bar{\boldsymbol{V}}(\phi))$ is defined in (6) and is available at the solution of the harmonic balance equation. Then by multiplying both sides of (10) by $\boldsymbol{e}_{n1}^T(k)$, we get

$$\boldsymbol{e}_{n1}^T(k)\frac{\partial\bar{\boldsymbol{V}}(\phi)}{\partial\phi_t} = -\hat{\bar{\boldsymbol{V}}}^T(\phi)\left(\frac{\partial\bar{\boldsymbol{I}}_d(\phi,\bar{\boldsymbol{V}}(\phi))}{\partial\phi_t}+\bar{\Omega}\frac{\partial\bar{\boldsymbol{Q}}(\phi,\bar{\boldsymbol{V}}(\phi))}{\partial\phi_t}\right) \tag{11}$$

where

$$\hat{\bar{\boldsymbol{V}}}^T(\phi) = \left[\left(\hat{\boldsymbol{V}}^R(\phi,0)\right)^T\left(\hat{\boldsymbol{V}}^R(\phi,\omega_1)\right)^T\cdots\left(\hat{\boldsymbol{V}}^R(\phi,\omega_{H'})\right)^T \cdot\left(\hat{\boldsymbol{V}}^I(\phi,0)\right)^T\left(\hat{\boldsymbol{V}}^I(\phi,\omega_1)\right)^T\cdots\left(\hat{\boldsymbol{V}}^I(\phi,\omega_{H'})\right)^T\right]$$

and is determined by solving the adjoint system

$$\bar{\boldsymbol{J}}^T(\phi,\bar{\boldsymbol{V}}(\phi))\hat{\bar{\boldsymbol{V}}}(\phi) = \boldsymbol{e}_{n1}(k). \tag{12}$$

It can be proved that if ϕ_t is a parameter of a nonlinear element at branch b, then

$$\boldsymbol{e}_{n1}^T(k)\frac{\partial\bar{\boldsymbol{V}}(\phi)}{\partial\phi_t} = \begin{cases} -\sum_{\ell=0}^{H'}\text{Real}\left[\hat{\bar{\boldsymbol{V}}}_b(\phi,\omega_\ell)G_{bIt}^*(\phi,\omega_\ell)\right] & \text{if } b\in\{\text{nonlinear current sources}\} \\ -\sum_{\ell=0}^{H'}\text{Imag}\left[\hat{\bar{\boldsymbol{V}}}_b(\phi,\omega_\ell)G_{bQt}^*(\phi,\omega_\ell)\right] & \text{if } b\in\{\text{nonlinear capacitors}\} \end{cases} \tag{13}$$

where the superscript $*$ stands for complex conjugate, and $G_{bIt}(\phi,\omega_\ell)$ and $G_{bQt}(\phi,\omega_\ell)$ are the ℓth Fourier coefficients of the partial derivatives of the current $i_b(\phi,v(t))$ and charge $q_b(\phi,v(t))$ w.r.t. ϕ_t, respectively (see [13]). For example, if branch b is the gate-to-source diode with characteristics

$$i_b(\phi,v(t)) = I_{G0}\left[\exp\left(\alpha_G v_b(t)\right)-1\right]$$

and $\phi_t=\alpha_G$, we will have

$$\frac{\partial i_b(\phi,v(t))}{\partial\phi_t} = I_{G0}v_b(t)\exp\left(\alpha_G v_b(t)\right)$$

and

$$G_{bIt}(\phi,\omega_\ell) = \frac{1}{N_T}\sum_{m=0}^{N_T-1}\frac{\partial i_b(\phi,v(mT_1))}{\partial\phi_i}\exp\left(-j\ell m\cdot 2\pi/N_T\right)$$

where discrete Fourier transformation is used, $N_T\geq(2H'+1)$ is the number of samples in the time domain within one period T, $T_1=T/N_T$, and $T=1/$(fundamental frequency).

The same derivations can be applied to

$$\boldsymbol{e}_{n2}^T(k)\frac{\partial\bar{\boldsymbol{V}}(\phi)}{\partial\phi_t}.$$

Hence, $\partial\boldsymbol{F}(\phi,\omega_k)/\partial\phi_t$ in (9) can be obtained. Consequently, the gradient of the objective function in (3) can be obtained.

Summing up, we can see that the gradient of the nonlinear circuit response $\boldsymbol{F}(\phi)$ w.r.t. ϕ can be calculated by nonlinear adjoint analysis which utilizes the existing Jacobian matrix from the solution of the harmonic balance equation to complete all the adjoint analysis. The equivalent conductances at the nonlinear element level, i.e., $G_{bIi}(\phi,\omega_\ell)$ or $G_{bQi}(\phi,\omega_\ell)$, are the same for different adjoint systems, and therefore only need to be calculated once. Compared with the perturbation method for gradient computations, which requires solving one nonlinear circuit for each optimization variable, the nonlinear adjoint analysis not only provides the exact gradient of the objective function, but, what is more important, significantly reduces the computation time and makes our parameter extraction approach computationally practical [13], [17].

IV. Weight Assignment Procedure

In the large-signal parameter extraction approach, presented in Section II, the model response is optimized to match several harmonics at various bias–input-frequency combinations. Two difficulties must be overcome to optimize the objective function in (3): the magnitude differences between different harmonic measurements, and the differences between different bias–input-frequency combinations. Suitably chosen weighting factors can balance these differences and improve the convergence of the opti-

mization. This weight assignment procedure assumes that (a) the possibility of having large measurement errors is small, (b) the power measurement has been converted to the magnitude of the output voltage, and (c) we want one harmonic in a bias–input-frequency combination to have the same opportunity in the objective function as the same harmonic in another bias–input-frequency combination.

A. Balance of a Harmonic Between Different Bias–Input-Frequency Combinations

In (1) of Section II, we have defined the kth harmonic measurement $S_j(\omega_{jk})$, where $j=1,2,\cdots,M$ corresponds to the jth bias–input-frequency combination. Let $\bar{S}_k$ be the mean value of the kth harmonic measurement over M combinations:

$$\bar{S}_k = \frac{1}{M}\sum_{j=1}^{M} S_j(\omega_{jk}), \qquad k=0,1,\cdots,H. \tag{14}$$

Since the measurement will not be zero, we can balance the kth harmonic by

$$w'_{jk} = \frac{\bar{S}_k}{S_j(\omega_{jk})}. \tag{15}$$

Minimum and maximum bounds can be imposed on w'_{jk}; i.e., simple interpolation adjustment can be used within the kth harmonic if some w'_{jk}, $j=1,\cdots,M$, lies outside the bound(s).

B. Balance Between Different Harmonics

In practice we may want to emphasize some harmonics over the others; e.g., the lower harmonic measurements may be emphasized due to their larger magnitudes and therefore higher measurement accuracy. This requires adjustment between different harmonics. Let K_k be the weight adjustment factor for the kth harmonic. Then the weighting factors for the optimization problem (3) can be expressed as

$$w_{jk} = K_k w'_{jk}\frac{\bar{S}_1}{\bar{S}_k}, \qquad k=1,2,\cdots,H \tag{16}$$

and

$$w_{j\mathrm{dc}} = K_0 w'_{j0}\frac{\bar{S}_1}{\bar{S}_0} \tag{17}$$

where we take the mean value of the first harmonic measurement as a reference. As an example, if we want to place equal emphasis on the dc and fundamental harmonic measurements and lower emphasis on higher harmonic measurement, we can choose $K_k=1$ for $k=0$ and 1, and $K_k = B^{-k}$ for $k=2,\cdots,H$ where $B>1$.

V. Numerical Examples

In the numerical examples, we use the Microwave Harmonica [14] modified Materka and Kacprzak FET model as the intrinsic FET, as shown in Fig. 3. All the linear FET model parameters such as the parasitics in Fig. 1 are extracted using small-signal measurement data. The nonlinear elements of the model are described by [14]

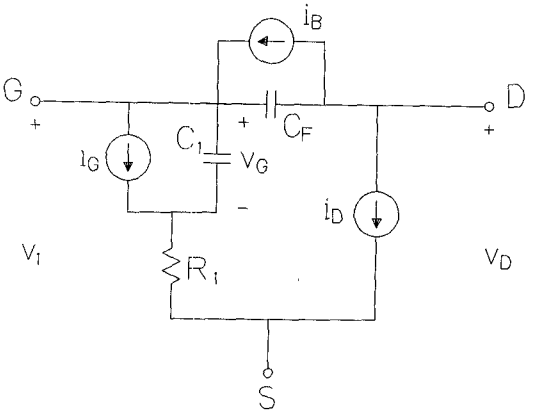

Fig. 3. Intrinsic part of the modified Materka and Kacprzak FET model.

$$i_D = F[v_G(t-\tau), v_D(t)]\left(1+S_S\frac{v_D}{I_{DSS}}\right)$$

$$F(v_G,v_D) = I_{DSS}\left(1-\frac{v_G}{V_{P0}+\gamma v_D}\right)^{(E+K_E v_G)} \cdot\tanh\left(\frac{S_1 v_D}{I_{DSS}(1-K_G v_G)}\right)$$

$$i_G = I_{G0}[\exp(\alpha_G v_G)-1]$$

$$i_B = I_{B0}\exp[\alpha_B(v_D - v_1 - V_{BC})]$$

$$\begin{cases} R_1 = R_{10}(1-K_R v_G) \\ R_1 = 0 \quad \text{if } K_R v_G \geq 1 \end{cases}$$

$$\begin{cases} C_1 = C_{10}(1-K_1 v_G)^{-1/2} + C_{1S} \\ C_1 = C_{10}\sqrt{5} + C_{1S} \quad \text{if } K_1 v_G \geq 0.8 \end{cases} \tag{18}$$

and

$$\begin{cases} C_F = C_{F0}[1-K_F(v_1 - v_D)]^{-1/2} \\ C_F = C_{F0}\sqrt{5} \quad \text{if } K_F(v_1 - v_D) \geq 0.8 \end{cases}$$

where I_{DSS}, V_{P0}, γ, E, K_E, S_1, K_G, τ, S_S, I_{G0}, α_G, I_{B0}, α_B, V_{BC}, R_{10}, K_R, C_{10}, K_1, C_{1S}, C_{F0}, and K_F are the parameters to be determined. Since only one of I_{B0} and V_{BC} is independent (see the Appendix), we fix V_{BC} and optimize the other 20 parameters:

$$\phi = [I_{DSS}\ V_{P0}\ \gamma\ E\ K_E\ S_1\ K_G\ \tau\ S_s\ I_{G0}\ \alpha_G\ I_{B0}\ \alpha_B\ R_{10}\ K_R\ C_{10}\ K_1\ C_{1S}\ C_{F0}\ K_F]^T. \tag{19}$$

During the optimization the nonlinear circuit is solved using the harmonic balance method, where the excitation of the circuit is the available input power P_{in}, which can be converted to an equivalent input voltage source V_{in} by

$$P_{\mathrm{in}} = \frac{|V_{\mathrm{in}}|^2}{8R_0}. \tag{20}$$

TABLE I
PARAMETER VALUES OF THE INTRINSIC PART OF THE MODIFIED MATERKA AND KACPRZAK FET MODEL

Name	Unit	Value Case 1	Case 2	Case 3
I_{DSS}	A	0.1888	0.0521	0.0740
V_{P0}	V	-4.3453	-1.267	-3.185
γ	-	-0.3958	-0.0877	0.0177
E	-	2.0	1.269	2.937
K_E	1/V	0.0	-0.3224	-0.9077
S_1	1/Ω	0.0972	0.0731	0.1527
K_G	1/V	-0.1678	-0.6482	-0.4912
τ	pS	3.654	5.322	0.1011
S_s	1/Ω	0.0	4.462×10^{-5}	0.0022
I_{G0}	A	0.5×10^{-9}	8.782×10^{-9}	4.965×10^{-11}
α_G	1/V	20.0	34.04	20.32
I_{B0}	A	0.5×10^{-9}	5.960×10^{-12}	1.000×10^{-12}
α_B	1/V	1.0	4.245	2.000
V_{BC}	V	0.0*	20.0*	20.0*
R_{10}	Ω	4.4302	0.0361	0.1243
K_R	1/V	0.0	9.892×10^{-3}	0.0
C_{10}	pF	0.6137	1.066	1.170
K_1	1/V	0.7686	1.531	1.201
C_{1S}	pF	0.0	0.0314	-0.5243
C_{F0}	pF	0.0416	1.321	0.0623
K_F	1/V	0.0	1.638	-0.0959

* Since only one of I_{B0} and V_{BC} is independent (see the Appendix), we fix V_{BC} and optimize I_{B0}.

Three cases are discussed. In case 1, we will show the theoretical aspects of the proposed approach, i.e., the robustness, reliability and efficiency of our parameter extraction approach if there is no model deficiency. Case 2 gives a numerical experiment of matching the modified Materka and Kacprzak model to the Curtice model. In case 3, we will discuss practical large-signal FET model parameter extraction for the measurement data provided by Texas Instruments.

Case 1: Robustness and Efficiency of the Parameter Extraction Approach

We use the MESFET parasitics from [3]:

$$[R_g\ L_g\ R_s\ L_s\ R_d\ L_d\ C_{ds}\ R_{de}\ C_{de}]$$
$$= [0.0119\ \Omega\ 0.1257\ \text{nH}$$
$$0.3740\ \Omega\ 0.0107\ \text{nH}\ 0.0006\ \Omega\ 0.0719\ \text{nH}$$
$$0.1927\ \text{pF}\ 440\ \Omega\ 1.5\ \text{pF}]$$

and assume that the solution of the model is also from [3], which is listed in Table I. The circuit is simulated at four bias points: ($V_{GB}=-0.5$ V, $V_{DB}=2$ V), ($V_{GB}=-2$ V, $V_{DB}=2$ V), ($V_{GB}=-0.5$ V, $V_{DB}=5$ V), and ($V_{GB}=-2$ V, $V_{DB}=5$ V). At each bias point three input power levels ($P_{in}=5$, 10, and 15 dBm) and two fundamental frequencies ($f_1=1$ and 2 GHz) are applied, respectively. There are a total of 24 bias–input-frequency combinations. Six harmonics are considered in the harmonic balance simulation. The output power P_{out} and the dc voltage V_{DC} (see Fig. 1) of the simulation results are then used as the simulated measurements. This corresponds to the situation of no model deficiencies.

To examine the robustness of the approach, we generated several starting points by uniformly perturbing the assumed solution by 20 to 40 percent and optimized them with the ℓ_1 norm, i.e., $p=1$ in (3). The circuit response $\boldsymbol{F}_j(\phi)$ in (2) was computed using six harmonics ($H'=6$). In the case where there is no measurement error, i.e., the exact simulation results obtained at the assumed solution are used as the measurement data, all the starting points converged to the known solution exactly when we included the first three harmonics, the first two harmonics, or one harmonic (plus dc) in the objective function; i.e., $H=3$, 2, or 1 in (3), respectively. However, it has been observed that the speed of convergence is usually faster when more harmonics are considered in the optimization.

TABLE II
MATCH ERRORS BETWEEN THE MEASUREMENTS AND MODEL RESPONSES IN CASE 1

Harm. Match	P_{out} matching errors in (%) (H=1)	(H=2)	(H=3)
First harm.	-0.53	-0.84	-1.08
Second harm.	21.32	7.58	6.77
Third harm.	-37.48	-14.36	-9.31

where H=1, 2, or 3 corresponds to the number of harmonics included in the objective function (3), and the comparisons here are made at bias point (V_{GB}=-2V, V_{DB}=2V), available input power P_{in}=10dBm and fundamental frequency f_1=1GHz.

To simulate a real measurement environment we added 10 percent normally distributed random noise to the simulated measurements. The same starting points were optimized with the ℓ_2 norm, i.e., $p=2$ in (3), and the same conditions were tested. When $H=3$ or 2 in (3), all the starting points converged to virtually one solution which is close to the assumed solution and gave very good match to the measurement with noise. When $H=1$, however, those different starting points did not converge to a single solution close to the assumed solution. Although at these solutions the matches to the measurements with noise at dc and fundamental harmonic are better than those achieved when $H=3$ or 2, poor matches at second, third, and/or higher harmonics exist. Table II shows the match errors at one of the bias–input-frequency combinations at the solutions obtained when $H=1$, 2, and 3 in the objective function.

From these experiments, we can see that with our approach the nonlinear parameters can theoretically be determined even when $H=1$ in (3). In practice when the model is not perfect and the measurement contains error, it is necessary to include higher harmonic measurements in the nonlinear large-signal model parameter extraction, for it not only improves convergence, but, what is more important, results in a more reliable model.

Two different starting points were used to compare the CPU execution time with and without nonlinear adjoint

TABLE III
PARAMETERS OF THE CURTICE MODEL USED IN CASE 2

Parameter	β_2 (1/V)	A_0 (A)	A_1 (A/V)	A_2 (A/V^2)
Value	0.04062	0.05185	0.04036	-0.009478
Parameter	A_3 (A/V^3)	γ (1/V)	V_{DS0} (V)	I_S (A)
Value	-0.009058	1.608	4.0	1.05×10^{-9}
Parameter	N (-)	C_{GS0} (pF)	C_{GD0} (pF)	F_C (-)
Value	1.0	1.1	1.25	0.5
Parameter	G_{MIN}(1/Ω)	V_{BI} (V)	V_{BR} (V)	τ (ps)
Value	0.0	0.7	20	5.0

see [4]

TABLE IV
INPUT LEVELS USED WITH DIFFERENT FUNDAMENTAL FREQUENCIES AND DIFFERENT BIASES IN CASE 2

(V_{GB}, V_{DB})	P_{in} (dBm)			
	f_1=0.5GHz	f_1=1.0GHz	f_1=1.5GHz	f_1=2.0GHz
(-0.3, 3)	0, 4	0, 4	0, 4	0, 4
(-0.3, 7)	0, 4	0, 4	0, 4	0, 4
(-1.0, 3)	0	0	0	0
(-1.0, 7)	0	0, 4	0, 4	0
(-0.5, 3)	--	8	8	--
(-0.5, 7)	8	8	8	8

f_1 denotes the fundamental frequency

analysis for gradient computation. To reach an ℓ_1 objective function value of about 1.0×10^{-3} for another example having 16 bias–input-frequency combinations, 20 variables, and 64 error functions, the Fortran program with the adjoint analysis runs approximately 10 times faster than that without adjoint analysis (about 200 s versus 2000 s on a VAX 8650 computer).

Case 2: Fitting to the Curtice Model

Here we use a set of data generated by the Curtice model [4]. The circuit is similar to that of Fig. 1 except that the intrinsic FET is replaced by the intrinsic part of the Curtice model. Some of the parameters of the Curtice model are taken from [4, fig. 13]. See Table III. The parameters in the linear part of the circuit are the same as in case 1.

We selected 32 bias–input-frequency combinations, as shown in Table IV. The first three harmonics were assumed as measurement data. Any signal below −30 dBm was discarded. There were 111 error functions in total.

To extract the model parameters, ℓ_2 optimization was applied and the result is listed under the case 2 column in Table I. Fig. 4 illustrates the modeling results at a bias point other than those considered in the optimization. Excellent agreement is observed.

As for case 1, parameters at the solution were perturbed uniformly by 20 to 40 percent and reoptimized. Of six starting points, four converged to the same solution with little variances in R_{10} and K_R. The other two converged to different local solutions with higher final objective function values.

Fig. 5 shows the characteristics of drain-to-source nonlinear current sources of the Curtice model and the modified Materka and Kacprzak model, and again we have reached an excellent match. Notice that only six bias points are used in the optimization, which is even less than the total number of parameters for this current source. However, since we modeled under actual large-signal conditions, employing higher harmonic measurements, a much larger range of information has been covered than individual points on the dc $I-V$ curve can provide.

Case 3: Processing Measurement Data from Texas Instruments

Actual GaAs FET measurement data were obtained from Texas Instruments [18] including small-signal and large-signal measurements. We used the small-signal S parameter measurement data to extract the linear parameters of the model. Large-signal measurements taken at 36 bias–input-frequency combinations were used for nonlinear parameter extraction. Table V illustrates the bias–input frequency combinations in detail. At each combination, the dc bias current and up to three RF harmonic output power measurements are available.

Optimization with the ℓ_1 norm was performed where, depending on the scales of the input and the corresponding output powers, the circuit was simulated using three to seven harmonics. There are 20 optimization variables and 113 error functions. Among ten different starting points, six converged to virtually one single solution with variations of I_{G0}, I_{B0}, α_B, and R_{10} because of their relatively low sensitivities to the response functions. One typical solution is listed under the case 3 column in Table I. Fig. 6 shows the match at the solution between the model responses and measurements at one of the bias points taken into account in the optimization, while Fig. 7 shows the match at a bias point not included in the optimization. Good agreement at both bias points is observed.

Fig. 8 depicts the $I-V$ characteristics of the drain-to-source nonlinear current source at the solution. Notice that this set of curves is obtained from large-signal parameter extraction, not from typical dc $I-V$ curve fitting.

VI. CONCLUSIONS

An accurate and truly nonlinear large-signal parameter extraction approach has been presented where not only dc bias and fundamental frequency but also higher harmonic responses have been used. The harmonic balance method for nonlinear circuit simulation, adjoint analysis for nonlinear circuit sensitivity calculation, and state-of-the-art optimization methods have been applied. Improvements to the convergence of the optimization process have been discussed. Numerical results have demonstrated that the method is both theoretically and computationally feasible, i.e., the method can uniquely and efficiently determine the parameters of the nonlinear elements of the GaAs MESFET model under actual large-signal operating conditions. Numerical results have also shown that under multibias, multipower inputs and multifrequency excitations, spectrum measurements can effectively reflect the nonlin-

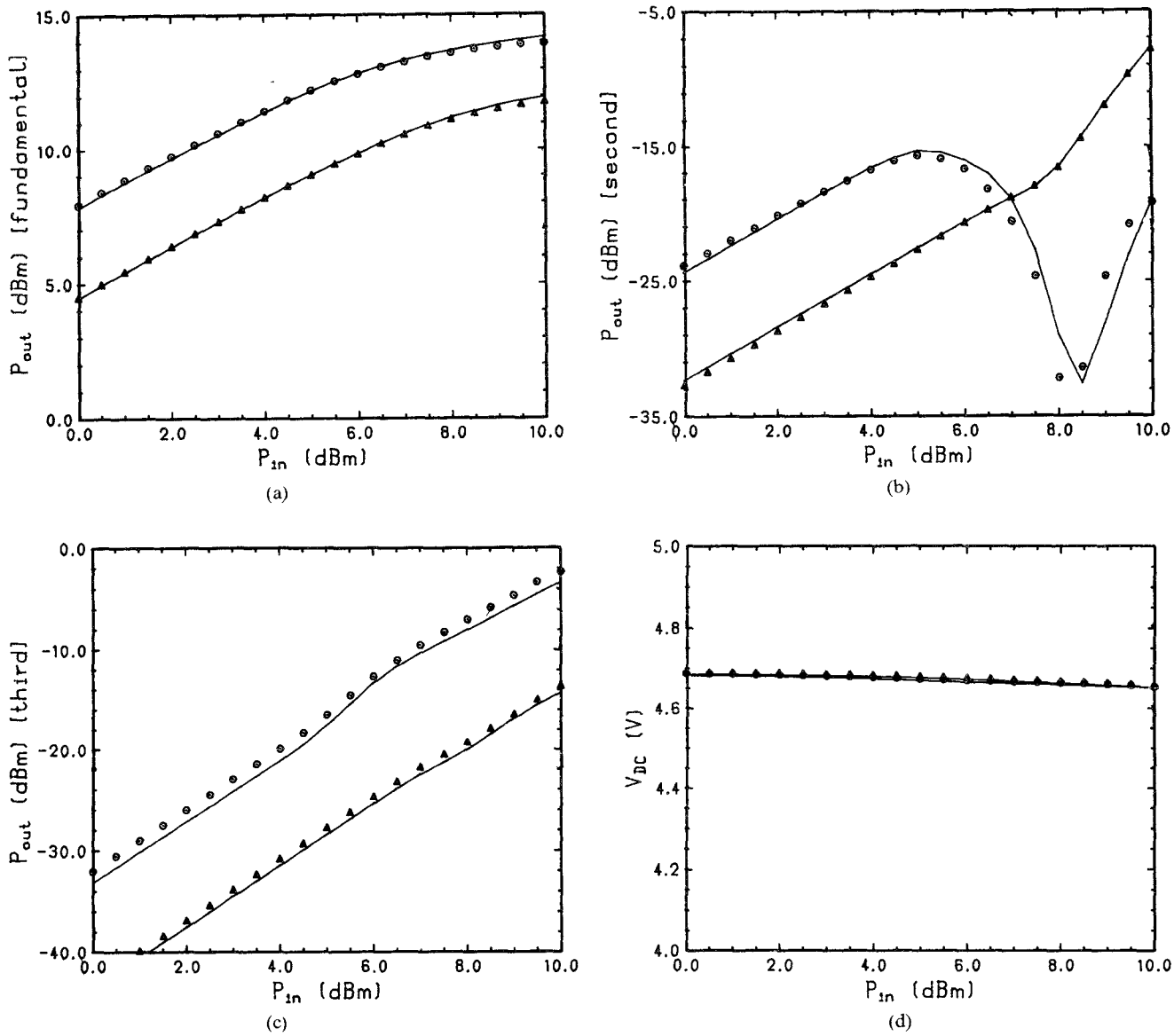

Fig. 4. Agreement between the (Materka) model response and the simulated measurements (using the Curtice model) at $V_{GB} = -0.5$ and $V_{DB} = 5$ in case 2 Solid lines represent the (Materka) computed model response. Circles denote the simulated measurements at fundamental frequency 0.5 GHz and triangles the simulated measurements at fundamental frequency 1 5 GHz (a) Fundamental component. (b) Second harmonic component. (c) Third harmonic component. (d) dc

TABLE V
BIAS–INPUT-FREQUENCY MEASUREMENT COMBINATIONS FOR THE NUMERICAL EXAMPLE OF CASE 3

	P_{in} = -15, -10, -5, 0, 5, 10 dBm		
	f_1=0.2GHz	f_1=6.0GHz	f_1=10GHz
Bias 1	(-0.373,2)	(-0.372,2)	(-0.372,2)
Bias 2	(-1.072,6)	(-1.073,6)	(-1.069,6)

where f_1 means fundamental frequency and the number pairs in the brackets are the bias voltages (V_{GB},V_{DB})

earities of the model and improve model reliability when used in nonlinear large-signal model parameter extraction.

A computer program, called HarPE, has been developed by Optimization Systems Associates Inc. It offers a user-friendly implementation of the technique presented in this paper to the microwave community.

APPENDIX
RELATIONSHIP BETWEEN I_{B0} AND V_{BC}

For the drain-to-gate diode of the Materka and Kacprzak FET model (see Fig. 3), we have

$$i_B = I_{B0}\exp\left[\alpha_B(v_D - v_1 - V_{BC})\right]. \quad \text{(A1)}$$

This can be rewritten as

$$i_B = I_{B0}\exp\left[\alpha_B(v_D - v_1)\right]\cdot\exp\left[-\alpha_B V_{BC}\right] \quad \text{(A2)}$$

or

$$i_B = I'_{B0}\exp\left[\alpha_B(v_D - v_1)\right] \quad \text{(A3)}$$

where

$$I'_{B0} = I_{B0}\exp\left[-\alpha_B V_{BC}\right]. \quad \text{(A4)}$$

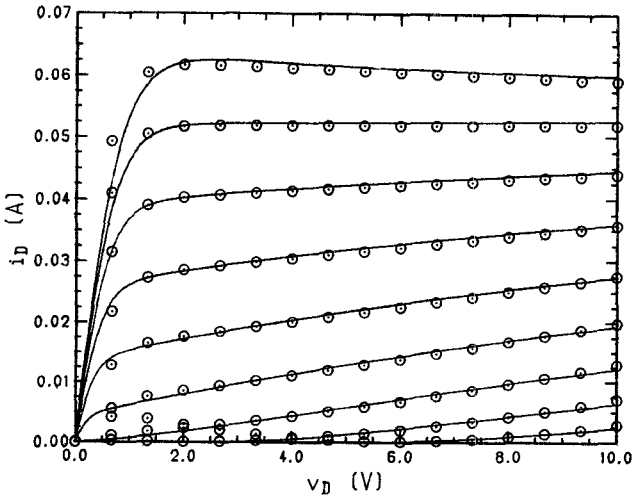

Fig. 5. Agreement between the dc characteristics of the modified Materka and Kacprzak model and the simulated measurements (from the Curtice model) in case 2. V_G is from -1.75 V to 0.25 V in steps of 0.25 V, and V_D is from 0 to 10 V. (Curtice uses V_{in} and V_{out}, respectively.) Solid lines represent the (Materka) model, and the circles represent the measurements.

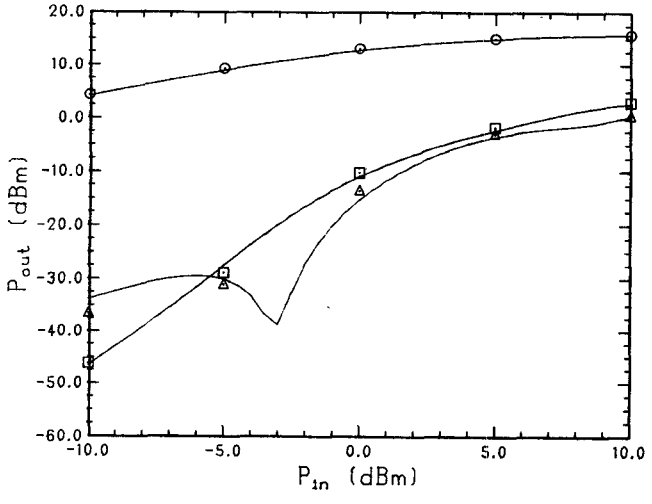

Fig. 6. Agreement between the (Materka) model responses and the measurements from Texas Instruments at fundamental frequency 0.2 GHz, and bias point $V_{GB} = -0.373$ V and $V_{DB} = 2$ V. (This bias point has been included in the optimization.) Solid lines represent computed model responses. Circles, triangles, and squares denote fundamental, second harmonic, and third harmonic measurements, respectively.

It is clear that for a given value of I'_{B0} there is no unique solution for I_{B0} and V_{BC}. In other words, only one of the two parameters I_{B0} and V_{BC} is independent. Therefore, we can fix V_{BC} and optimize I_{B0} during parameter extraction.

ACKNOWLEDGMENT

The authors thank Dr. R. A. Pucel of Raytheon Company, Lexington, MA, for suggesting the numerical example of case 2. They thank Dr. A. M. Pavio of Texas Instruments, Dallas, TX, for several detailed discussions and for providing experimental data to test the algorithm. Thanks are also due to Dr. R. M. Biernacki of Optimization Systems Associates Inc., Dundas, Ontario, Canada, for helpful technical discussions and suggestions.

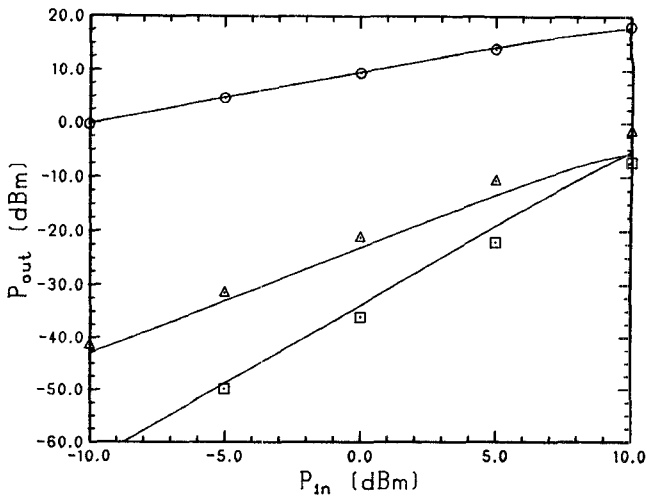

Fig. 7. Agreement between the (Materka) model responses and the measurements from Texas Instruments at fundamental frequency 6 GHz, and bias point $V_{GB} = -0.673$ V and $V_{DB} = 4$ V. (This bias point has not been included in the optimization.) Solid lines represent computed model responses. Circles, triangles, and squares denote fundamental, second harmonic, and third harmonic measurements, respectively.

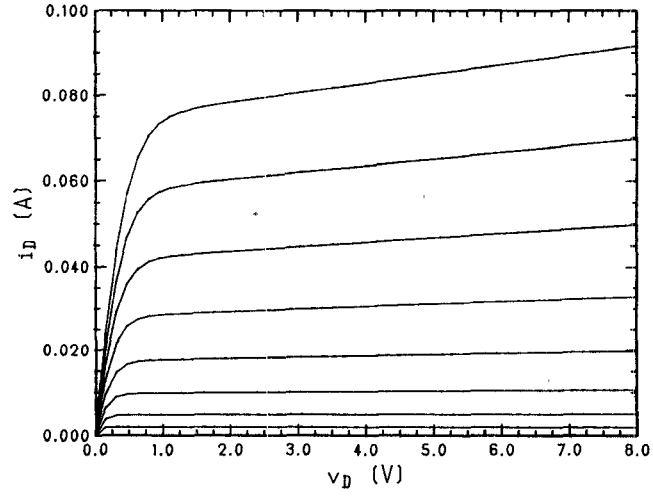

Fig. 8. dc characteristics of the drain-to-source nonlinear current source of the modified Materka and Kacprzak model after the optimization to match the large-signal measurement data provided by Texas Instruments. V_G is from -1.75 V to 0.25 V in steps of 0.25 V, and V_D is from 0 to 10 V.

REFERENCES

[1] Y. Tajima, B. Wrona, and K. Mishima, "GaAs FET large-signal model and its application to circuit designs," *IEEE Trans. Electron Devices*, vol. ED-28, pp. 171–175, 1981.

[2] A. Materka and T. Kacprzak, "Computer calculation of large-signal GaAs FET amplifier characteristics," *IEEE Trans. Microwave Theory Tech.*, vol. MTT-33, pp. 129–135, 1985.

[3] J. W. Bandler, S. H. Chen, S. Ye, and Q. J. Zhang, "Integrated model parameter extraction using large-scale optimization concepts," *IEEE Trans. Microwave Theory Tech.*, vol. 36, pp. 1629–1638, 1988.

[4] W. R. Curtice, "GaAs MESFET modeling and nonlinear CAD," *IEEE Trans. Microwave Theory Tech.*, vol. 36, pp. 220–230, 1988.

[5] H. Statz, P. Newman, I. R. Smith, R. A. Pucel, and H. A. Haus, "GaAs FET device and circuit simulation in SPICE," *IEEE Trans. Electron Devices*, vol. ED-34, pp. 160–169, 1987.

[6] M. A. Smith, T. S. Howard, K. J. Anderson, and A. M. Pavio, "RF nonlinear device characterization yields improved modeling accuracy," in *IEEE MTT-S Int. Microwave Symp. Dig.* (Baltimore, MD), 1986, pp. 381–384.

[7] M. Paggi, P. H. Williams, and J. M. Borrego, "Nonlinear GaAs MESFET modeling using pulsed gate measurements," in *IEEE MTT-S Int. Microwave Symp. Dig.* (New York, NY), 1988, pp. 229–231.
[8] B. Kopp and D. D. Heston, "High-efficiency 5-watt power amplifier with harmonic tuning," in *IEEE MTT-S Int. Microwave Symp. Dig.* (New York, NY), 1988, pp. 839–842.
[9] B. R. Epstein *et al.*, "Large-signal MESFET characterization using harmonic balance," in *IEEE MTT-S Int. Microwave Symp. Dig.* (New York, NY), 1988, pp. 1045–1048.
[10] U. Lott, "A method for measuring magnitude and phase of harmonics generated in nonlinear microwave two-ports," in *IEEE MTT-S Int. Microwave Symp. Dig.* (New York, NY), 1988, pp. 225–228.
[11] K. S. Kundert and A. Sangiovanni-Vincentelli, "Simulation of nonlinear circuits in the frequency domain," *IEEE Trans. Computer-Aided Design*, vol. CAD-5, pp. 521–535, 1986.
[12] J. W. Bandler, W. Kellermann, and K. Madsen, "A nonlinear ℓ_1 optimization algorithm for design, modeling and diagnosis of networks," *IEEE Trans. Circuits Syst.*, vol. 34, pp. 174–181, 1987.
[13] J. W. Bandler, Q. J. Zhang, and R. M. Biernacki, "A unified theory for frequency-domain simulation and sensitivity analysis of linear and nonlinear circuits," *IEEE Trans. Microwave Theory Tech.*, vol. 36, pp. 1661–1669, 1988.
[14] *Microwave Harmonica User's Manual*, Compact Software Inc., Paterson, NJ 07504, 1987.
[15] J. W. Bandler, S. H. Chen, and S. Daijavad, "Microwave device modeling using efficient ℓ_1 optimization: A novel approach," *IEEE Trans. Microwave Theory Tech.*, vol. MTT-34, pp. 1282–1293, 1986.
[16] P. Rabinowitz, *Numerical Methods for Nonlinear Algebraic Equations*. New York: Gordon and Breach, 1970, pp. 87–161.
[17] J. W. Bandler, Q. J. Zhang, and R. M. Biernacki, "Practical, high speed gradient computation for harmonic balance simulators," in *IEEE MTT-S Int. Microwave Symp. Dig.* (Long Beach, CA), 1989, pp. 363–366.
[18] Measurement data provided by Texas Instruments, Dallas, TX, Jan. 1989.

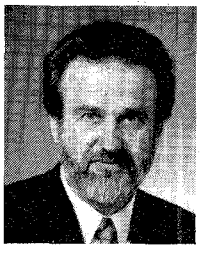

John W. Bandler (S'66–M'66–SM'74–F'78) was born in Jerusalem, Palestine, on November 9, 1941. He studied at the Imperial College of Science and Technology, London, England, from 1960 to 1966. He received the B.Sc. (Eng.), Ph.D. and D.Sc. (Eng.) degrees from the University of London, London, England, in 1963, 1967, and 1976, respectively.

He joined Mullard Research Laboratories, Redhill, Surrey, England, in 1966. From 1967 to 1969 he was a Postdoctorate Fellow and Sessional Lecturer at the University of Manitoba, Winnipeg, Canada. He joined McMaster University, Hamilton, Canada, in 1969, where he is currently a Professor of Electrical and Computer Engineering. Dr. Bandler has served as Chairman of the Department of Electrical Engineering and Dean of the Faculty of Engineering. He currently directs research in the Simulation Optimization Systems Research Laboratory. He is President of Optimization Systems Associates Inc., Dundas, Ont., Canada, which he established in 1983. OSA currently provides consulting services and software to numerous microwave clients in CAE of microwave integrated circuits.

Dr. Bandler contributed to *Modern Filter Theory and Design* (Wiley-Interscience, 1973) and to *Analog Methods for Computer-Aided Circuit Analysis and Diagnosis* (Marcel Dekker, 1988). He has more than 220 publications, four of which appear in *Computer-Aided Filter Design* (IEEE Press, 1973), one in *Microwave Integrated Circuits* (Artech House, 1975), one in *Low-Noise Microwave Transistors and Amplifiers* (IEEE Press, 1981), one in *Microwave Integrated Circuits* (2nd ed., Artech House, 1985), and one in *Statistical Design of Integrated Circuits* (IEEE Press, 1987). Dr. Bandler was an Associate Editor of the IEEE TRANSACTIONS ON MICROWAVE THEORY AND TECHNIQUES (1969–1974). He was Guest Editor of the Special Issue of the IEEE TRANSACTIONS ON MICROWAVE THEORY AND TECHNIQUES on Computer-Oriented Microwave Practices (March 1974).

Dr. Bandler is a Fellow of the Royal Society of Canada and of the Institution of Electrical Engineers (Great Britain). He is a member of the Association of Professional Engineers of the Province of Ontario (Canada).

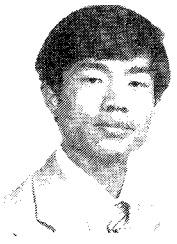

Qi-jun Zhang (S'84–M'87) was born in Xianyan, Shanxi, China on October 8, 1959. He received the B.Eng. degree from the East China Engineering Institute, Nanjing, China in 1982, and the Ph.D. degree from McMaster University, Hamilton, Ontario, Canada, in 1987, both in electrical engineering.

He was a research assistant in the Institute of Systems Engineering, Tianjin University, Tianjin, China, from 1982 to 1983. He joined the Simulation Optimization Systems Research Laboratory and the Department of Electrical and Computer Engineering at McMaster University in 1983 as a graduate student. He was awarded an Ontario Graduate Scholarship for the academic years 1985/86 and 1986/87. He was a teaching assistant in the Department of Electrical and Computer Engineering, McMaster University, from 1984 to 1987 and a post-doctorate fellow there from 1987 to 1988. Presently he is a Research Engineer with Optimization Systems Associates Inc., Dundas, Ontario, Canada. In 1989, he also became an Assistant Professor (part-time) of Electrical and Computer Engineering at McMaster University. His professional interests include all aspects of circuit CAD, with emphasis on large-scale simulation and optimization, design and modeling of nonlinear microwave circuits, statistical modeling, sensitivity analysis, and the diagnosis and tuning of analog circuits.

Dr. Zhang was a contributor to *Analog Methods for Computer-Aided Circuit Analysis and Diagnosis* (Marcel Dekker, 1988).

Shen Ye (S'88) was born in Shanghai, China, on January 31, 1957. He received the B.E. and M.E. degrees in electrical engineering from Shanghai University of Technology, Shanghai, China, in 1982 and 1984, respectively.

From 1984 to 1986 he was with the Department of Electrical Engineering, Shanghai University of Technology. Since 1986, he has been with the Simulation Optimization Systems Research Laboratory and the Department of Electrical and Computer Engineering, McMaster University, Hamilton, Ontario, Canada, working towards the Ph.D. degree. He is also a teaching assistant there. His main research interests include analog fault diagnosis, device modeling and parameter extraction, and computer-aided design using optimization methods.

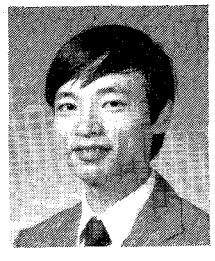

Shao Hua Chen (S'84–M'88) was born in Swatow, Guangdong, China, on September 27, 1957. He received the B.S. (Eng.) degree from the South China Institute of Technology, Guangzhou, China, in 1982 and the Ph.D. degree in electrical engineering from McMaster University, Hamilton, Ontario, Canada, in 1987.

From 1982 to 1983, he was a teaching assistant in the Department of Automation at the South China Institute of Technology. He joined the Simulation Optimization Systems Research Laboratory and the Department of Electrical and Computer Engineering at McMaster University, Hamilton, Ontario, Canada, in 1983 as a graduate student. He was awarded an Ontario Graduate Scholarship for the academic years 1985/86 and 1986/87. He was a teaching assistant in the Department of Electrical and Computer Engineering, McMaster University, from 1984 to 1987. Currently he is working as Research Engineer for Optimization Systems Associates Inc., Dundas, Ontario, Canada. His professional interests include CAD software architecture, optimization methods, sensitivity analysis, device modeling, circuit statistics, design centering, computer graphics, and user interfaces.

Reprint 7

FAST Gradient Based Yield Optimization of Nonlinear Circuits

FAST Gradient Based Yield Optimization of Nonlinear Circuits

JOHN W. BANDLER, FELLOW, IEEE, QI-JUN ZHANG, MEMBER, IEEE, JIAN SONG, AND RADOSLAW M. BIERNACKI, SENIOR MEMBER, IEEE

Abstract—**This paper meets the challenge of yield optimization of nonlinear microwave circuits operating in the steady state under large-signal periodic excitations. Yield-driven design is formulated as a one-sided ℓ_1 optimization problem. We introduce two novel, high-speed methods of gradient calculation, the integrated gradient approximation technique (IGAT) and the feasible adjoint sensitivity technique (FAST). IGAT utilizes the Broyden formula with special iterations of Powell to update the approximate gradients. FAST combines the efficiency and accuracy of the adjoint sensitivity technique with the simplicity of the perturbation technique. IGAT and FAST are compared with the simple perturbation approximate sensitivity technique (PAST) on the one extreme and the theoretical exact adjoint sensitivity technique (EAST) on the other. FAST, linking state-of-the-art optimization and efficient harmonic balance simulation, is the key to making our approach to nonlinear microwave circuit design the most powerful available. A FET frequency doubler example treats statistics of both linear elements and nonlinear device parameters. This design has six optimizable variables including input power and bias conditions, and 34 statistical parameters. Using either IGAT or FAST, yield is driven from 40% to 70%. FAST exhibits superior efficiency.**

I. INTRODUCTION

STATISTICAL circuit design has been recognized as an indispensable tool for modern CAD of integrated circuits [1]–[3]. A number of algorithms for yield optimization have been developed within the past 15 years, e.g., Director and Hachtel [4] (simplicial approximation), Soin and Spence [5] (the center of gravity method), Bandler and Abdel-Malek [6], [7] (updated approximations and cuts), Styblinski and Ruszczynski [8] (stochastic approximation), Polak and Sangiovanni-Vincentelli [9] (outer approximation), Singhal and Pinel [10] (parametric sampling), Bandler and Chen [3] (generalized ℓ_p centering), and Biernacki *et al.* [11] (efficient quadratic approximation). This paper deals with yield optimization of nonlinear microwave circuits within the harmonic balance (HB) simulation environment.

Manuscript received March 6, 1990; revised July 12, 1990. This work was supported in part by Optimization Systems Associates Inc. and in part by the Natural Sciences and Engineering Research Council of Canada under Grants OGP0007239, OGP0042444, and STR0040923.

J. W. Bandler, Q. Zhang, and R. M. Biernacki are with Optimization Systems Associates Inc., P.O. Box 8083, Dundas, Ontario, Canada L9H 5E7, and with the Simulation Optimization Systems Research Laboratory and the Department of Electrical and Computer Engineering, McMaster University, Hamilton, Canada L8S 4L7.

J. Song is with the Simulation Optimization Systems Research Laboratory and the Department of Electrical and Computer Engineering, McMaster University, Hamilton, Canada L8S 4L7.

IEEE Log Number 9038712.

Statistical design of practical nonlinear microwave circuits is a challenge. One serious inherent difficulty is the potentially prohibitively high computational cost: many circuits have to be simulated repeatedly and each circuit simulation involves CPU-intensive iterations to solve the HB equations. Furthermore, gradient-based optimization requires effort to estimate the gradients of the error functions. Therefore, an effective and efficient approach to gradient calculation is of utmost importance.

The conventional perturbation approximate sensitivity technique (PAST) is conceptually simple. Since PAST needs to perturb all variables one at a time, the computational effort involved grows in proportion to the number of variables. Rizzoli *et al.* [12] used this method in their single-loop approach for nominal circuit design. In yield optimization, however, PAST becomes extremely inefficient because of the large number of circuit outcomes to be dealt with.

The exact adjoint sensitivity technique (EAST) has been recently developed by Bandler, Zhang, and Biernacki [13], [14] for the HB technique. In contrast to PAST, EAST involves solving a set of linear equations whose coefficient matrix is available after circuit simulation. The solution of a single adjoint system is sufficient for the calculation of sensitivities with respect to all variables. No perturbation or iterative simulations are required. EAST enjoys high computational efficiency, but is very difficult to implement.

In this paper, we formulate the yield-driven design of nonlinear circuits as a one-sided ℓ_1 optimization problem [15] allowing the powerful, robust one-sided ℓ_1 algorithm proposed by Bandler *et al.* [16] to be employed. We introduce two powerful approaches to gradient calculation. One is the integrated gradient approximation technique (IGAT), presented by Bandler *et al.* [17], which is adapted here to the needs of yield optimization. The other is the feasible adjoint sensitivity technique (FAST), first reported by Bandler *et al.* [18]. Motivated by the potential impact of the adjoint sensitivity approach on general-purpose CAD programs, we have studied its implementational aspects. FAST is demonstrated to be an implementable, high-speed gradient calculation technique. FAST retains most of the efficiency and accuracy of EAST while accommodating the simplicity of PAST.

0018-9480/90/1100-1701$01.00 ©1990 IEEE

IGAT and FAST are applied to yield optimization of a microwave frequency doubler. In this example, normal and uniform distributions describing large-signal FET model parameters and passive elements are fully accommodated. The performance yield is increased from 40% to 70%.

In Section II we formulate the yield optimization problem for nonlinear circuits as a one-sided ℓ_1 optimization problem. Sections III and IV are devoted to IGAT and FAST, respectively. Comparisons between the various approaches are made in Section V. Section VI presents the details of the FET frequency doubler example.

II. The Yield Problem for Nonlinear Circuits

A. Specifications and Errors for Nonlinear Circuit Yield Optimization

Consider a nonlinear microwave circuit operating under large-signal, steady-state periodic conditions. Response functions for such a circuit may involve dc and harmonic components of the output signal. Therefore, design specifications can be imposed at dc and several harmonics. The jth specification can be denoted by

$$S_{uj}(\boldsymbol{h}) \tag{1a}$$

if it is an upper specification, or

$$S_{lj}(\boldsymbol{h}) \tag{1b}$$

in the case of lower specifications, where

$$\boldsymbol{h} = [0 \quad 1 \quad 2 \quad \cdots \quad H]^T \tag{2}$$

is the harmonic index vector, and 0 and H represent dc and the highest harmonic, respectively. A specific circuit response may involve all or some of the $(H+1)$ spectral components.

Manufactured outcomes are spread over a region which can be described by the nominal design, $\boldsymbol{\phi}^0$, along with a statistical distribution of parameters. Parameters in $\boldsymbol{\phi}^0$ can be lumped element values, device model parameters, dimensions of a physical realization, etc. For statistical design, many circuits are needed to represent the distribution of manufactured outcomes. Such circuit outcomes, denoted by $\boldsymbol{\phi}^i$, can be written as

$$\boldsymbol{\phi}^i = \boldsymbol{\phi}^0 + \Delta\boldsymbol{\phi}^i, \qquad i = 1,2,\cdots,N \tag{3}$$

where $\Delta\boldsymbol{\phi}^i$ is the deviation of the ith outcome from the nominal circuit and N is the number of outcomes considered. In yield optimization, each $\boldsymbol{\phi}^i$ is determined by statistically perturbing $\boldsymbol{\phi}^0$ according to a known or assumed statistical distribution of the manufactured outcomes.

The response of each outcome, denoted by

$$R_j(\boldsymbol{\phi}^i, \boldsymbol{h}) \tag{4}$$

is calculated after solving the HB equations [19]

$$\bar{\boldsymbol{F}}(\boldsymbol{\phi}^i, \bar{\boldsymbol{V}}) = \boldsymbol{0} \tag{5}$$

where $\bar{\boldsymbol{V}}$ comprises the split real and imaginary parts of the state variables in the HB equation. The corresponding error function is defined as

$$R_j(\boldsymbol{\phi}^i, \boldsymbol{h}) - S_{uj}(\boldsymbol{h}) \tag{6a}$$

or as

$$S_{lj}(\boldsymbol{h}) - R_j(\boldsymbol{\phi}^i, \boldsymbol{h}). \tag{6b}$$

We assemble all errors for the outcome $\boldsymbol{\phi}^i$ into one vector $\boldsymbol{e}^i$. If all entries of this vector are nonpositive, the outcome $\boldsymbol{\phi}^i$ represents an acceptable circuit.

For N statistical outcomes generated, the production yield can be estimated by

$$Y \approx \frac{\text{number of acceptable circuits}}{N}. \tag{7}$$

B. Formulation of One-Sided ℓ_1 Objective Function

The problem of yield optimization can be properly converted to a mathematical programming problem so that modern mathematical optimization techniques can be applied. In the following the design variables are nominal values $\boldsymbol{\phi}^0$. Although only the outcomes $\boldsymbol{\phi}^i$ appear in the error functions, they depend on $\boldsymbol{\phi}^0$ because the $\boldsymbol{\phi}^i$ are related to $\boldsymbol{\phi}^0$.

After the error vector $\boldsymbol{e}^i$ for the outcome $\boldsymbol{\phi}^i$ has been assembled as

$$\boldsymbol{e}^i = [e_1(\boldsymbol{\phi}^i) \quad e_2(\boldsymbol{\phi}^i) \cdots e_M(\boldsymbol{\phi}^i)]^T \tag{8}$$

where M is the total number of errors considered, the formulation of the objective function for optimization can follow the procedure described in [3]. First, we create the generalized ℓ_p function v^i from $\boldsymbol{e}^i$ [3]:

$$v^i = \begin{cases} \left[\sum_{j \in J(\boldsymbol{\phi}^i)} \left(e_j(\boldsymbol{\phi}^i)\right)^p\right]^{1/p} & \text{if } J(\boldsymbol{\phi}^i) \neq \varnothing \quad (9a) \\ -\left[\sum_{j=1}^{M} \left(-e_j(\boldsymbol{\phi}^i)\right)^{-p}\right]^{-1/p} & \text{if } J(\boldsymbol{\phi}^i) = \varnothing \quad (9b) \end{cases}$$

where

$$J(\boldsymbol{\phi}^i) = \left\{ j \middle| e_j(\boldsymbol{\phi}^i) \geq 0 \right\}. \tag{10}$$

Then we define the one-sided ℓ_1 objective function for yield optimization [3] as

$$U(\boldsymbol{\phi}^0) = \sum_{i \in I} \alpha_i v^i \tag{11}$$

where

$$I = \{i | v^i > 0\} \tag{12}$$

and α_i are positive multipliers. If the α_i were chosen as [3]

$$\alpha_i = \frac{1}{|v^i|} \tag{13}$$

then the function $U(\boldsymbol{\phi}^0)$ would become the exact number

of unacceptable circuits and the yield would be

$$Y(\phi^0) = 1 - \frac{U(\phi^0)}{N}. \tag{14}$$

The mechanism of the one-sided ℓ_1 function naturally imitates the relation between the yield and unacceptable or acceptable outcomes. Now, the task of maximizing yield Y is converted to one of minimizing $U(\phi^0)$; that is,

$$\underset{\phi^0}{\text{minimize}}\, U(\phi^0). \tag{15}$$

We use (13) to assign multipliers α_i at the starting point and fix them during the optimization process. Then $U(\phi^0)$ is no longer the count of unacceptable outcomes during optimization, but a continuous approximate function to it.

Suppose the value of p is chosen as 1. The objective function for the one-sided ℓ_1 optimization becomes

$$U(\phi^0) = \sum_{i \in I} \sum_{j \in J(\phi^i)} \alpha_i e_j(\phi^i) \tag{16}$$

where α_i, I, and $J(\phi^i)$ are defined as before. In (16), error functions for optimization are $e_j(\phi^i)$. In (11), error functions for optimization are v^i. The functions $e_j(\phi^i)$ are differentiable, but the functions v^i of (9) may not be. Therefore, we use (16) in our yield optimization.

Several reoptimizations with updated α_i may be applied to further increase yield. Each can use a different number of statistical outcomes or a different set of outcomes.

C. The One-Sided ℓ_1 Optimization Algorithm

We use a highly efficient one-sided ℓ_1 optimization algorithm [16] to solve (15). The algorithm is based on a two-stage method combining a first-order method, the trust region Gauss–Newton method, with a second-order method, the quasi-Newton method. Switching between the two methods is automatically done to ensure global convergence of the combined algorithm.

To summarize the discussion in this section, all steps involved in our yield optimization are shown in Fig. 1.

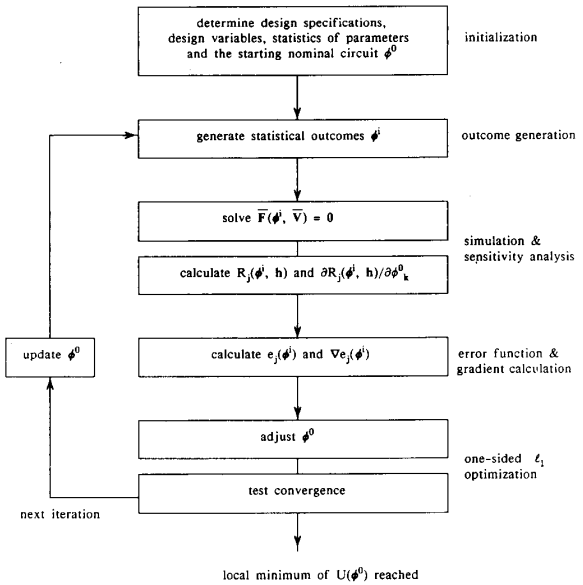

Fig. 1. Flowchart for yield optimization.

III. Integrated Gradient Approximation Technique

After a review of PAST, IGAT is discussed for the case of a single function. The application of IGAT in yield optimization follows.

Because the application of IGAT is not restricted to circuit response functions, let us use $f(\phi)$ to denote a generic function.

A. Approximating Derivatives by PAST

The first-order derivative of $f(\phi)$ with respect to the kth variable can be estimated by

$$\frac{\partial f(\phi)}{\partial \phi_k} \approx \frac{f(\phi + \Delta\phi_k \boldsymbol{u}_k) - f(\phi)}{\Delta\phi_k} \tag{17}$$

where $\phi + \Delta\phi_k \boldsymbol{u}_k$ denotes the perturbation of the kth variable, $\Delta\phi_k$ is the perturbation length and $\boldsymbol{u}_k$ is a column vector which has 1 in the kth position and zeros elsewhere. An approximation to the gradient, $\nabla f(\phi)$, can be obtained by perturbing all variables one at a time.

B. IGAT for General Functions [17]

To start the process, PAST is used as in (17) to calculate the approximate gradient.

The Broyden update generates the new approximate gradient from the previous gradient,

$$\nabla f(\phi_{\text{new}}) = \nabla f(\phi_{\text{old}}) + \frac{f(\phi_{\text{new}}) - f(\phi_{\text{old}}) - (\nabla f(\phi_{\text{old}}))^T \Delta\phi}{\Delta\phi^T \Delta\phi} \Delta\phi \tag{18}$$

where ϕ_{old} and ϕ_{new} are two different points and $\Delta\phi = \phi_{\text{new}} - \phi_{\text{old}}$. If ϕ_{old} and ϕ_{new} are iterates of optimization, $f(\phi_{\text{old}})$ and $f(\phi_{\text{new}})$ need to be evaluated anyway. Thus the updated gradient can be obtained without additional function evaluations (circuit simulations).

To overcome a particular deficiency of the Broyden update, after a few updates, a special iteration of Powell generates a special step $\Delta\phi$ to guarantee strictly linearly independent directions. After a number of optimization iterations, we may also apply PAST (17) to maintain the accuracy of the approximate gradients at a desirable level.

C. Application of IGAT in Yield Optimization

In circuit simulation, there are usually several response levels involved. Suppose the response of interest, on which the design specification is imposed, is the power gain. In the circuit simulation, the power gain is calculated from the output power, which, in turn, is calculated from the

output voltage. This implies three different response levels. IGAT can be applied at any response level. We still use f to denote a particular response function whose gradient is to be approximated.

Because the nominal values, ϕ^0, are design variables, all perturbations are made to ϕ^0 in the initialization and reinitialization steps using PAST (17). When ϕ^0 is perturbed to $\phi^0 + \Delta\phi_k^0 u_k$, denoted by $\phi_{k,\text{pert}}^0$ for short, outcomes should be regenerated from $\phi_{k,\text{pert}}^0$ in order to get perturbed circuit responses. These outcomes are denoted by $\phi_{k,\text{pert}}^i$. Then from (17), the approximate derivative of the response $f(\phi^i)$ is defined as

$$\frac{\partial f(\phi^i)}{\partial \phi_k^0} \approx \frac{f(\phi_{k,\text{pert}}^i) - f(\phi^i)}{\Delta\phi_k^0}. \tag{19}$$

When the Broyden update or the special iteration of Powell is used, $\Delta\phi^0$ is computed from ϕ_{old}^0 and ϕ_{new}^0 as generated either by the optimizer or by the special iteration. Outcomes ϕ_{old}^i and ϕ_{new}^i are outcomes generated from ϕ_{old}^0 and ϕ_{new}^0, respectively. The gradient of the response $f(\phi^i)$ w.r.t. ϕ^0 can be updated as

$$\nabla f(\phi_{\text{new}}^i) = \nabla f(\phi_{\text{old}}^i) + \frac{f(\phi_{\text{new}}^i) - f(\phi_{\text{old}}^i) - (\nabla f(\phi_{\text{old}}^i))^T \Delta\phi^0}{(\Delta\phi^0)^T \Delta\phi^0} \Delta\phi^0. \tag{20}$$

IV. Feasible Adjoint Sensitivity Technique

In the HB simulation environment, the sensitivity of a response with respect to one variable, ϕ_k,

$$\frac{\partial R_j(\phi, h)}{\partial \phi_k} \tag{21}$$

should be computed subject to the constraints of the HB equation, e.g., [19]

$$\bar{F}(\phi, \bar{V}) = 0. \tag{22}$$

Bandler *et al.* [13], [14] proposed EAST, and the sensitivity expressions for various elements were derived and listed [14].

Here, we propose FAST, which is also based on adjoint sensitivity principles. Suppose that the circuit is divided into linear and nonlinear subnetworks and that the response of interest is the voltage at the output port. Normally, the response is taken from the linear subnetwork.

The response can be calculated by

$$\bar{V}_{\text{out}} = [a^T \quad b^T] \begin{bmatrix} \bar{V} \\ \bar{V}_s \end{bmatrix} = c^T \begin{bmatrix} \bar{V} \\ \bar{V}_s \end{bmatrix} \tag{23}$$

where $\bar{V}_s$ denotes the split real and imaginary parts in the spectra of excitation voltages, $\bar{V}$ denotes the solution to the HB equations (22), and

$$c = [a^T \quad b^T]^T \tag{24}$$

is a linear transfer vector linking the output voltage with $\bar{V}_s$ and $\bar{V}$. $\bar{V}$ and c are functions of ϕ. $\bar{V}_s$ can also be a function of ϕ if we want to change $\bar{V}_s$ to improve the circuit performance.

A. FAST for the Nominal Circuit Case

To make the derivation procedure concise, we concentrate on a single circuit design with variables ϕ. From (23) the approximate derivative of $\bar{V}_{\text{out}}$ w.r.t. ϕ_k can be calculated as

$$\frac{\Delta\bar{V}_{\text{out}}}{\Delta\phi_k} \approx \frac{\Delta c^T}{\Delta\phi_k} \begin{bmatrix} \bar{V} \\ \bar{V}_s \end{bmatrix} + a^T \frac{\Delta\bar{V}}{\Delta\phi_k} + b^T \frac{\Delta\bar{V}_s}{\Delta\phi_k} \tag{25}$$

by perturbing ϕ to $\phi + \Delta\phi_k u_k$. Let $\hat{\bar{V}}$ be the adjoint voltages obtained by solving the set of linear equations

$$J^T \hat{\bar{V}} = a \tag{26}$$

where J is the Jacobian of $\bar{F}$ w.r.t. $\bar{V}$ at the HB solution. We can express

$$\Delta\bar{V}_{\text{out}} \approx \left[c^T(\phi + \Delta\phi_k u_k) - c^T\right] \begin{bmatrix} \bar{V} \\ \bar{V}_s \end{bmatrix} + b^T\left[\bar{V}_s(\phi + \Delta\phi_k u_k) - \bar{V}_s\right] - \hat{\bar{V}}^T \Delta\bar{F}. \tag{27}$$

The incremental term $\Delta\bar{F}$ can be approximated by

$$\Delta\bar{F} \approx \bar{F}(\phi + \Delta\phi_k u_k, \bar{V}) \tag{28}$$

for a small $\Delta\phi_k$.

Considering the different elements, (27) can be further expressed as

$$\Delta\bar{V}_{\text{out}} \approx \begin{cases} \left[c^T(\phi + \Delta\phi_k u_k) - c^T\right] \begin{bmatrix} \bar{V} \\ \bar{V}_s \end{bmatrix} - \hat{\bar{V}}^T \bar{F}(\phi + \Delta\phi_k u_k, \bar{V}), & \phi_k \in \text{linear subnetwork} \\ b^T\left[\bar{V}_s(\phi + \Delta\phi_k u_k) - \bar{V}_s\right] - \hat{\bar{V}}^T \bar{F}(\phi + \Delta\phi_k u_k, \bar{V}), & \phi_k \in \text{sources} \\ -\hat{\bar{V}}^T \bar{F}(\phi + \Delta\phi_k u_k, \bar{V}), & \phi_k \in \text{nonlinear subnetwork}. \end{cases} \tag{29}$$

This formula is much easier to implement than the corresponding formula for EAST [13], [14]. The function $\bar{F}(\phi + \Delta\phi_k u_k, \bar{V})$ is evaluated by perturbation. The effort for solving the linear equations (26) is small since the LU factors of the Jacobian matrix are already available from the final HB iteration. The terms $\bar{V}$ and $\bar{V}_s$ are also available from the HB simulation. The perturbed vectors $a(\phi + \Delta\phi_k u_k)$ and $b(\phi + \Delta\phi_k u_k)$ can be easily calculated since they involve the linear subnetwork only. Finally, the perturbed excitations $\bar{V}_s(\phi + \Delta\phi_k u_k)$ can be effortlessly obtained. It is clear that the calculation of all the terms in (27) or (29) can be readily implemented.

Finally, the approximate sensitivity of output voltage $\bar{V}_{\text{out}}$ w.r.t. ϕ_k can be computed as

$$\frac{\partial \bar{V}_{\text{out}}}{\partial \phi_k} \approx \frac{\Delta \bar{V}_{\text{out}}}{\Delta \phi_k}. \tag{30}$$

B. FAST for Yield Optimization

Similar to IGAT perturbations in yield optimization, perturbations used in FAST are also made to the nominal values ϕ^0. The outcomes ϕ^i and $\phi^i_{k,\text{pert}}$ are generated from the unperturbed and perturbed nominal values ϕ^0 and $\phi^0_{k,\text{pert}}$, respectively. The increment of the output voltage of the ith outcome due to the perturbation is calculated by

$$\begin{aligned}\Delta \bar{V}_{\text{out}}(\phi^i) \approx & \left[c^T\left(\phi^i_{k,\text{pert}}\right) - c^T(\phi^i)\right]\begin{bmatrix}\bar{V} \\ \bar{V}_s(\phi^i)\end{bmatrix} \\ & + b^T(\phi^i)\left[\bar{V}_s\left(\phi^i_{k,\text{pert}}\right) - \bar{V}_s(\phi^i)\right] \\ & - \hat{\bar{V}}^T \Delta \bar{F}\end{aligned} \tag{31}$$

where

$$\Delta \bar{F} \approx \bar{F}\left(\phi^i_{k,\text{pert}}, \bar{V}\right). \tag{32}$$

$\bar{V}$ is the solution to the HB equation (5), and $\hat{\bar{V}}$ is the solution to (26).

V. Comparisons of Various Approaches

A. Comparisons of PAST, IGAT, EAST, and FAST

PAST and IGAT do not need any modification of the circuit simulator.

PAST is a widely used approach, because it is very easy to implement. However, the cost may be prohibitive. Suppose there are ten design variables in the nonlinear circuit. Using PAST to calculate the gradient, one needs to perturb all design variables and to solve the entire nonlinear circuit for each perturbation, i.e., ten times. The best possible situation for this approach is that all ten simulations use the same Jacobian and all converge in one iteration. This applies to nominal circuit design. For yield optimization, a large number of statistically generated circuit outcomes may make PAST prohibitive.

The distinct advantage of IGAT over PAST is that IGAT only requires the circuit response function once to update the previously calculated gradient for most optimization iterations. IGAT enjoys the simplicity of the perturbation method so that yield optimization can be carried out without modifying the circuit simulator to calculate exact derivatives. IGAT is very desirable when the circuit simulator cannot be modified.

Both EAST and FAST require modification to the circuit simulator.

The generic exact adjoint sensitivity technique [13], [14] is accepted by all circuit theoreticians as the most powerful tool. However, to implement it, we have to keep track of all arbitrary locations of variables and to compute branch voltages at all these locations. Microwave software engineers have, to date, found these obstacles insurmountable.

Using FAST, we also need to perturb all variables. For a circuit with ten design variables, instead of completely solving ten nonlinear circuits, we only evaluate ten residuals in the form of (28) and calculate the perturbed linear subnetwork. The solution of adjoint equation (26) can be accomplished by using forward and backward substitutions. In FAST, we completely eliminate the need to track variable locations. We only need to identify the output port, which is the simplest step in adjoint sensitivity theory.

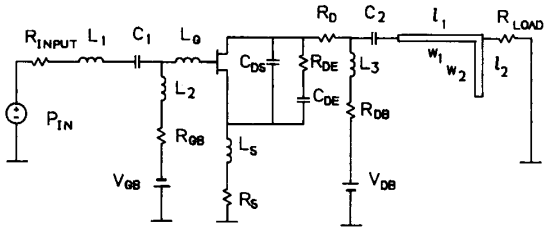

Fig. 2. Circuit diagram of the FET microwave frequency doubler. The nominal values for nonoptimizable variables are: $L_2 = 15$ nH, $L_3 = 15$ nH, $C_1 = 20$ pF, $C_2 = 20$ pF, $w_1 = 0.1 \times 10^{-3}$ m, $w_2 = 0.635 \times 10^{-3}$ m, $R_{\text{LOAD}} = R_{\text{INPUT}} = 50\ \Omega$, and $R_{GB} = R_{DB} = 10\ \Omega$.

B. Numerical Comparison of FAST, EAST, and PAST

We use a MESFET mixer [13], [14] to investigate the accuracy and actual time efficiency of FAST [18]. Sensitivities of the mixer conversion gain w.r.t. 26 variables were calculated by the FAST, EAST, and PAST approaches, respectively. The variables included all parameters in the linear as well as the nonlinear part, dc bias, LO power, and IF, LO, and RF terminations. The results show that the FAST sensitivities are almost identical to the exact sensitivities, whereas the sensitivities computed by PAST are typically 1 to 2% different from their exact values. This fact reveals that FAST promises to be much more reliable than PAST. The CPU time comparison shows that FAST is three times slower than EAST but 23 times faster than PAST for one complete sensitivity analysis of the mixer circuit.

VI. Yield Optimization of a Frequency Doubler

The FET frequency doubler shown in Fig. 2 is considered. It consists of a common-source FET with a lumped input matching network and a microstrip output matching

TABLE I
ASSUMED STATISTICAL DISTRIBUTIONS FOR THE FET PARAMETERS

FET Parameter	Nominal Value	Standard Deviation (%)	FET Parameter	Nominal Value	Standard Deviation (%)
L_G(nH)	0.16	5	S_I	0.676×10^{-1}	0.65
$R_D(\Omega)$	2.153	3	K_G	1.1	0.65
L_S(nH)	0.07	5	τ(pS)	7.0	6
$R_S(\Omega)$	1.144	5	S_S	1.666×10^{-3}	0.65
$R_{DE}(\Omega)$	440	14	I_{G0}(A)	0.713×10^{-5}	3
C_{DE}(pF)	1.15	3	α_G	38.46	3
C_{DS}(pF)	0.12	4.5	I_{B0}(A)	-0.713×10^{-5}	3
I_{DSS}(A)	6.0×10^{-2}	5	α_B	-38.46	3
V_{p0}(V)	-1.906	0.65	$R_{I0}(\Omega)$	3.5	8
γ	-15×10^{-2}	0.65	C_{I0}(pF)	0.42	4.16
E	1.8	0.65	C_{F0}(pF)	0.02	6.64

The following parameters are considered as deterministic: K_E = 0.0, K_R = 1.111, K_I = 1.282, C_{IS} = 0.0, and K_F = 1.282. For definitions of the FET parameters, see [20].

TABLE II
FET MODEL PARAMETER CORRELATIONS [22]

	L_G	R_S	L_S	R_{DE}	C_{DS}	g_m	τ	R_{IN}	C_{GS}	C_{GD}
L_G	1.00	-0.16	0.11	-0.22	-0.20	0.15	0.06	0.15	0.25	0.04
R_S	-0.16	1.00	-0.28	0.02	0.06	-0.09	-0.16	0.12	-0.24	0.26
L_S	0.11	-0.28	1.00	0.11	-0.26	0.53	0.41	-0.52	0.78	-0.12
R_{DE}	-0.22	0.02	0.11	1.00	-0.44	0.03	0.04	-0.54	0.02	-0.14
C_{DS}	-0.20	0.06	-0.26	-0.44	1.00	-0.13	-0.14	0.23	-0.24	-0.04
g_m	0.15	-0.09	0.53	0.03	-0.13	1.00	-0.08	-0.26	0.78	0.38
τ	0.06	-0.16	0.41	0.04	-0.14	-0.08	1.00	-0.19	0.27	-0.46
R_{IN}	0.15	0.12	-0.52	-0.54	0.23	-0.26	-0.19	1.00	-0.35	0.05
C_{GS}	0.25	-0.24	0.78	0.02	-0.24	0.78	0.27	-0.35	1.00	0.15
C_{GD}	0.04	0.26	-0.12	-0.14	-0.04	0.38	-0.46	0.05	0.15	1.00

Certain modifications have been made to adjust these small-signal parameter correlations to be consistent with the large-signal FET model.

and filter section. The optimization variables include the input inductance L_1 and the microstrip lengths l_1 and l_2. Two bias voltages V_{GB} and V_{DB} and the driving power level P_{IN} are also considered as optimization variables. The fundamental frequency is 5 GHz. Responses of interest are the conversion gain and spectral purity, which are defined by

$$\text{conversion gain} = 10\log\frac{\text{power of the second harmonic at the output port}}{\text{power of the fundamental frequency at the input port}}$$

and

$$\text{spectral purity} = 10\log\frac{\text{power of the second harmonic at the output port}}{\text{total power of all other harmonics at the output port}}$$

respectively. The specifications for the conversion gain and spectral purity are 2.5 dB and 20 dB, respectively. They are both lower specifications.

Our large-signal FET statistical model includes an intrinsic large-signal FET model modified from the Materka and Kacprzak model [21], statistical distributions, and correlations of parameters. The multidimensional normal distribution is assumed for all FET intrinsic and extrinsic parameters. The means and standard deviations are listed in Table I. The correlations between parameters are assumed according to the results published by Purviance *et al.* [22]. Certain modifications have been made to make the correlations for the large-signal FET model consistent with those for the small-signal FET model dealt with in [22]. The correlation coefficients are given in Table II. Uniform distributions with fixed tolerances of 3% are assumed for P_{IN}, V_{GB}, V_{DB}, L_1, l_1, and l_2. Finally, uniform distributions with fixed tolerances of 5% are assumed for L_2, L_3, C_1, C_2, w_1 and w_2. The random number generator used is capable of generating outcomes from the independent and multidimensional correlated normal distributions and from uniform distributions.

In our program, the formulation (16) is used. In more detail, the error functions resulting from the simulated conversion gain and spectral purity are calculated, and then these error functions with their multipliers defined in (13) are fed into the one-side ℓ_1 optimizer. IGAT and FAST are implemented to provide gradients. IGAT calculates approximate sensitivities of the conversion gain and spectral purity. The computer used is a Multiflow Trace 14/300.[1]

The starting point for yield optimization is the solution of the minimax nominal design w.r.t. the same specifications, using the same six design variables. At this point, the estimated yield based on 500 outcomes is 39.6%.

We conduct two designs using IGAT and FAST gradient calculation in the same environment. Computational details are given in Tables III and IV. Each design has two consecutive phases; that is, the starting point for the second phase is the solution of the first phase. The second phase is to reoptimize the first solution with updated α_i.

Using IGAT, the first phase reaches 71% yield, and the second phase confirms that the solution of the first phase has been optimized in terms of the estimated yield. The two phases use 61 optimization iterations and 184 function evaluations. For FAST, the first phase uses 19 function evaluations and gradient calculations to give 70.6% yield. The second phase slightly increases the estimated yield to 71%, verifying the solution of the first phase. The efficiency of FAST is well demonstrated. To reach the same yield level, the CPU time used by the FAST approach is much less than that used by the IGAT ap-

[1]A test at McMaster University using LINPACK to solve 100 linear equations indicated a performance for this machine of 10 MFLOPS. A VAX 11/780 exhibited 0.14 MFLOPS in a similar test.

TABLE III
YIELD OPTIMIZATION OF THE FREQUENCY DOUBLER USING IGAT

Variable	Starting Point	Nominal Design	Solution I	Solution II
P_{IN}(W)	2.0×10^{-3}	2.49048×10^{-3}	1.98488×10^{-3}	1.92366×10^{-3}
V_{GB}(V)	-1.9	-1.70329	-1.93468	-1.92542
V_{DB}(V)	5.0	6.50000	6.50000	6.50000
L_1(nH)	5.0	5.29066	5.68905	5.63822
l_1(m)	1.0×10^{-3}	1.77190×10^{-3}	1.73378×10^{-3}	1.73740×10^{-3}
l_2(m)	5.0×10^{-3}	5.73087×10^{-3}	5.75011×10^{-3}	5.74907×10^{-3}
Yield		39.6%	71.0%	71.0%
No. of Optimization Iterations			23	38
No. of Function Evaluations			89	95
CPU Time (Multiflow Trace 14/300)			18.6min	19.1min

The yield is estimated from 500 outcomes.

TABLE IV
YIELD OPTIMIZATION OF THE FREQUENCY DOUBLER USING FAST

Variable	Starting Point	Nominal Design	Solution I	Solution II
P_{IN}(W)	2.0×10^{-3}	2.49048×10^{-3}	2.02313×10^{-3}	1.94444×10^{-3}
V_{GB}(V)	-1.9	-1.70329	-1.93930	-1.92927
V_{DB}(V)	5.0	6.50000	6.50000	6.5000
L_1(nH)	5.0	5.29066	5.71547	5.63312
l_1(m)	1.0×10^{-3}	1.77190×10^{-3}	1.73531×10^{-3}	1.74046×10^{-3}
l_2(m)	5.0×10^{-3}	5.73087×10^{-3}	5.74965×10^{-3}	5.74956×10^{-3}
Yield		39.6%	70.6%	71.0%
No. of Optimization Iterations			19	29
No. of Function Evaluations and Sensitivity Analyses			19	29
CPU Time (Multiflow Trace 14/300)			7.9min	12.1min

The yield is estimated from 500 outcomes.

proach. Although IGAT is slower than FAST, it is very robust in terms of the final yield reached.

Figs. 3 and 4 show histograms of the conversion gain and the spectral purity, respectively. Five hundred outcomes are used to calculate both distributions. Fig. 3(a) is the conversion gain distribution before yield optimization. The histograms in parts (b) and (c) of Fig. 3 are based on the solutions using IGAT and FAST, respectively. Fig. 4(a) is the spectral purity distribution before yield optimization. The histograms in parts (b) and (c) of Fig. 4 are based on solutions using IGAT and FAST, respectively. The improvement in spectral purity is very clearly illustrated by the histograms in Fig. 4. Before yield optimization, the center of the distribution is close to the design specification of 20 dB, indicating that many outcomes are unacceptable. After yield optimization, the center of the distribution is shifted to the right-hand side of the specification. Most outcomes then satisfy the specification.

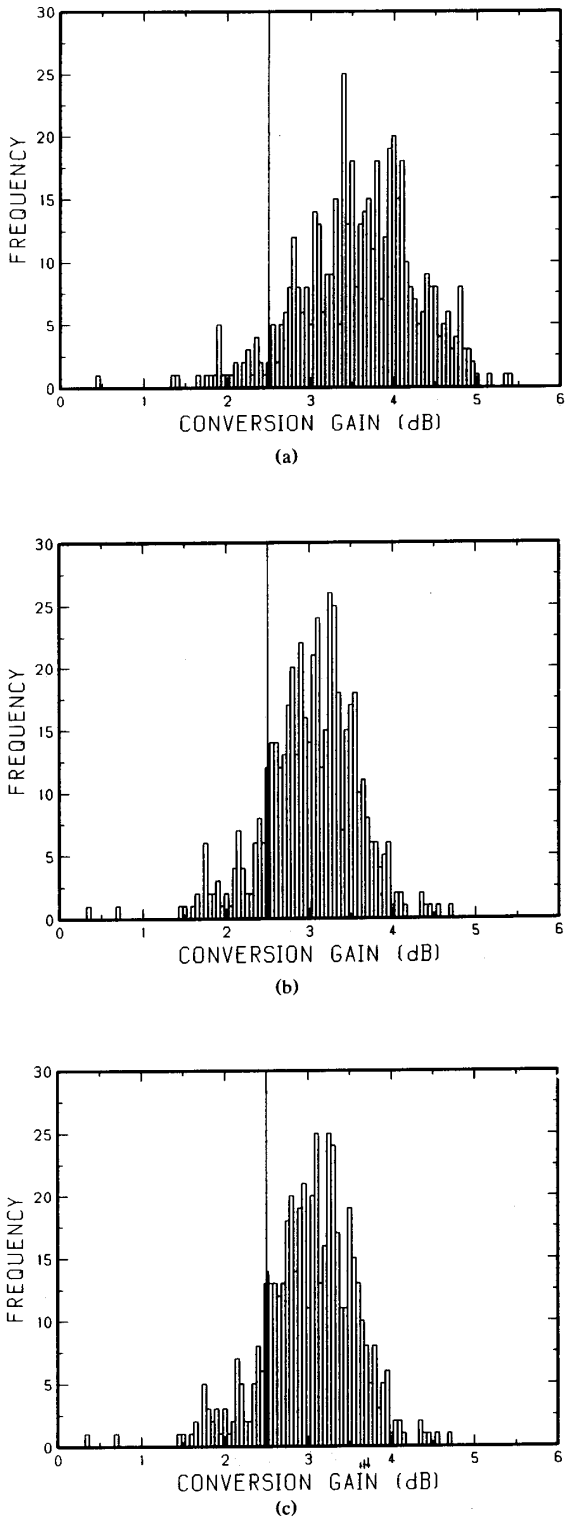

Fig. 3. Histogram of conversion gains of the frequency doubler based on 500 statistical outcomes. The specification is shown by a vertical line. (a) At the starting point. (b) At the solution of yield optimization using IGAT. (c) At the solution of yield optimization using FAST.

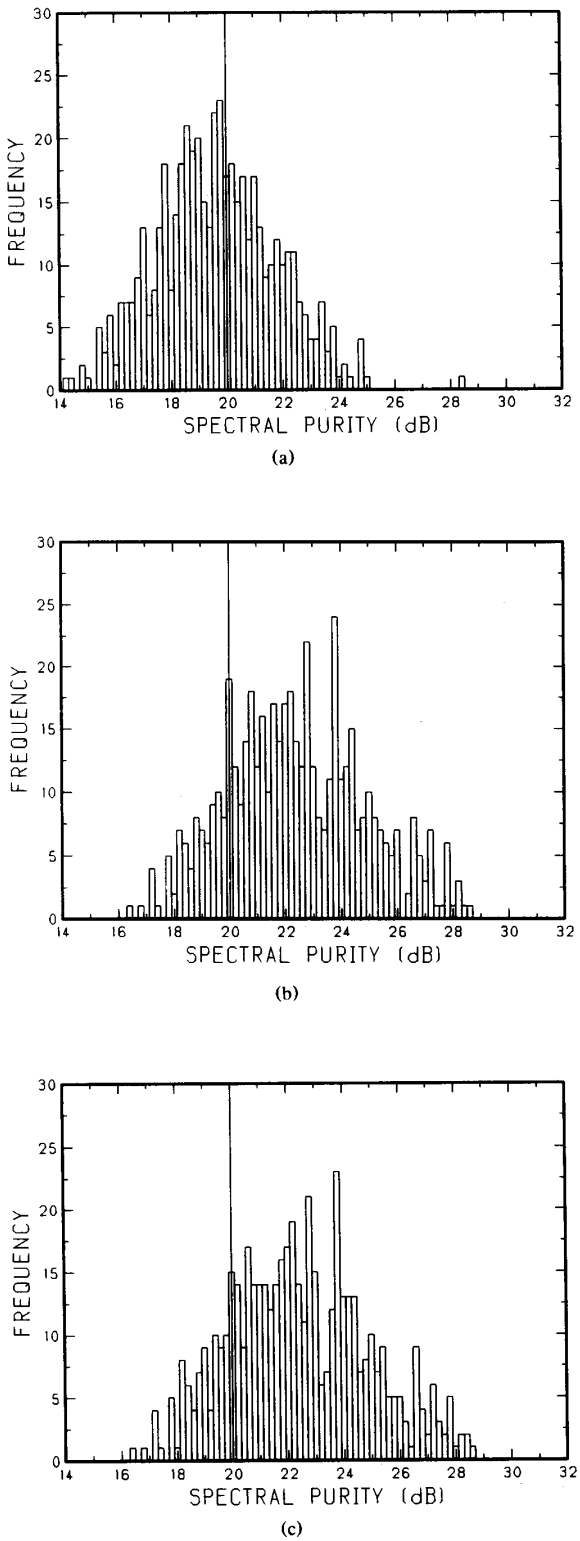

Fig. 4. Histogram of spectral purities of the frequency doubler based on 500 statistical outcomes. The specification is shown by a vertical line. (a) At the starting point. (b) At the solution of yield optimization using IGAT. (c) At the solution of yield optimization using FAST.

VII. Conclusions

This paper presents a comprehensive formulation for yield optimization of nonlinear circuits operating within the harmonic balance simulation environment. We have conducted a convincing demonstration of yield optimization of statistically characterized nonlinear microwave circuits using our two best approaches to gradient calculation, namely, IGAT and FAST. These two approaches are expedient tools for gradient calculation in the HB environment. The significant advantages of IGAT and FAST over PAST are their unmatched speeds, and over EAST are their implementational simplicity. IGAT is a desirable choice when the circuit simulator cannot be modified. FAST is particularly suitable for implementation in general-purpose microwave CAD software.

Numerical experiments directed at yield-driven optimization of a FET frequency doubler verify our two gradient calculation approaches. Large-signal FET parameter statistics are fully facilitated. The substantial computational advantages of IGAT and FAST have been observed. Our approaches provide powerful tools to meet the very pressing need for efficient microwave nonlinear circuit design. Our success should strongly motivate the development of statistical modeling of microwave devices for large-signal applications.

Acknowledgment

The authors wish to thank Dr. S. H. Chen of Optimization Systems Associates Inc., Dundas, Ontario, Canada, for providing some necessary software and suggestions.

References

[1] A. J. Strojwas, *Statistical Design of Integrated Circuits*. New York, NY: IEEE Press, 1987.

[2] E. Wehrhahn and R. Spence, "The performance of some design centering methods," in *Proc. IEEE Int. Symp. Circuits Syst.* (Montreal, Canada), 1984, pp. 1424–1438.

[3] J. W. Bandler and S. H. Chen, "Circuit optimization: The state of the art," *IEEE Trans. Microwave Theory Tech.*, vol. 36, pp. 424–443, 1988.

[4] S. W. Director and G. D. Hachtel, "The simplicial approximation approach to design centering," *IEEE Trans. Circuits Syst.*, vol. CAS-24, pp. 363–372, 1977.

[5] R. S. Soin and R. Spence, "Statistical exploration approach to design centering," *Proc. Inst. Elec. Eng.*, vol. 127, pt. G., pp. 260–269, 1980.

[6] J. W. Bandler and H. L. Abdel-Malek, "Optimal centering, tolerancing, and yield determination via updated approximations and cuts," *IEEE Trans. Circuits Syst.*, vol. CAS-25, pp. 853–871, 1978.

[7] H. L. Abdel-Malek and J. W. Bandler, "Yield optimization for arbitrary statistical distributions: Part I—Theory," *IEEE Trans. Circuits Syst.*, vol. CAS-27, pp. 245–253, 1980.

[8] M. A. Styblinski and A. Ruszczynski, "Stochastic approximation approach to statistical circuit design," *Electron. Lett.*, vol. 19, no. 8, pp. 300–302, 1980.

[9] E. Polak and A. L. Sangiovanni-Vincentelli, "Theoretical and computational aspects of the optimal design centering, tolerancing, and tuning problem," *IEEE Trans. Circuits Syst.*, vol. CAS-26, pp. 795–813, 1979.

[10] K. Singhal and J. F. Pinel, "Statistical design centering and tolerancing using parametric sampling," *IEEE Trans. Circuits Syst.*, vol. CAS-28, pp. 692–701, 1981.

[11] R. M. Biernacki, J. W. Bandler, J. Song, and Q. J. Zhang, "Efficient quadratic approximation for statistical design," *IEEE Trans. Circuits Syst.*, vol. 36, pp. 1449–1454, 1989.

[12] V. Rizzoli, A. Lipparini, and E. Marazzi, "A general-purpose program for nonlinear microwave circuit design," *IEEE Trans. Microwave Theory Tech.*, vol. MTT-31, pp. 762–770, 1983.
[13] J. W. Bandler, Q. J. Zhang, and R. M. Biernacki, "A unified framework for harmonic balance simulation and sensitivity analysis," in *IEEE MTT-S Int. Microwave Symp. Dig.* (New York, NY), 1988, pp. 1041–1044.
[14] J. W. Bandler, Q. J. Zhang, and R. M. Biernacki, "A unified theory for frequency domain simulation and sensitivity analysis of linear and nonlinear circuits," *IEEE Trans. Microwave Theory Tech.*, vol. 36, pp. 1661–1669, 1988.
[15] J. W. Bandler, Q. J. Zhang, J. Song, and R. M. Biernacki, "Yield optimization of nonlinear circuits with statistically characterized devices," in *IEEE MTT-S Int. Microwave Symp. Dig.* (Long Beach, CA), 1989, pp. 649–652.
[16] J. W. Bandler, S. H. Chen, and K. Madsen, "An algorithm for one-sided ℓ_1 optimization with application to circuit design centering," in *Proc. IEEE Int. Symp. Circuits Syst.* (Espoo, Finland), 1988, pp. 1795–1798.
[17] J. W. Bandler, S. H. Chen, S. Daijavad, and K. Madsen, "Efficient optimization with integrated gradient approximations," *IEEE Trans. Microwave Theory Tech.*, vol. 36, pp. 444–454, 1988.
[18] J. W. Bandler, Q. J. Zhang, and R. M. Biernacki, "Practical, high-speed gradient computation for harmonic balance simulators," in *IEEE MTT-S Int. Microwave Symp. Dig.* (Long Beach, CA), 1989, pp. 363–367.
[19] K. S. Kundert and A. L. Sangiovanni-Vincentelli, "Simulation of nonlinear circuits in the frequency domain," *IEEE Trans. Computer-Aided Design*, vol. CAD-5, pp. 521–535, 1986.
[20] J. W. Bandler, Q. J. Zhang, S. Ye, and S. H. Chen, "Efficient large-signal FET parameter extraction using harmonics," *IEEE Trans. Microwave Theory Tech.*, vol. 37, pp. 2099–2108, 1989.
[21] A. Materka and T. Kacprzak, "Computer calculation of large-signal GaAs FET amplifier characteristics," *IEEE Trans. Microwave Theory Tech.*, vol. MTT-33, pp. 129–135, 1985.
[22] J. Purviance, D. Criss, and D. Monteith, "FET model statistics and their effects on design centering and yield prediction for microwave amplifiers," in *IEEE MTT-S Int. Microwave Symp. Dig.* (New York, NY), 1988, pp. 315–318.

✠

John W. Bandler (S'66–M'66–SM'74–F'78) was born in Jerusalem on November 9, 1941. He studied at the Imperial College of Science and Technology, London, England, from 1960 to 1966. He received the B.Sc. (Eng.), Ph.D., and D.Sc. (Eng.) degrees from the University of London, London, England, in 1963, 1967, and 1976, respectively.

He joined Mullard Research Laboratories, Redhill, Surrey, England, in 1966. From 1967 to 1969 he was a Postdoctorate Fellow and Sessional Lecturer at the University of Manitoba, Winnipeg, Canada. He joined McMaster University, Hamilton, Canada, in 1969, where he is currently a Professor of Electrical and Computer Engineering. Dr. Bandler has served as Chairman of the Department of Electrical Engineering and Dean of the Faculty of Engineering. He currently directs research in the Simulation Optimization Systems Research Laboratory. He is President of Optimization Systems Associates Inc., Dundas, Ontario, Canada, which he established in 1983. OSA currently provides consulting services and software to numerous microwave clients in CAE of microwave integrated circuits. He is also President of Bandler Research Inc., Dundas, Ontario, Canada, which he founded in 1989.

Dr. Bandler contributed to *Modern Filter Theory and Design* (Wiley-Interscience, 1973) and to *Analog Methods for Computer-Aided Analysis and Diagnosis* (Marcel Dekker, 1988). He has more than 230 publications, four of which appear in *Computer-Aided Filter Design* (IEEE Press, 1973), one in *Microwave Integrated Circuits* (Artech House, 1975), one in *Low-Noise Microwave Transistors and Amplifiers* (IEEE Press, 1981), one in *Microwave Integrated Circuits* (2nd ed., Artech House, 1985), and one in *Statistical Design of Integrated Circuits* (IEEE Press, 1987). Dr. Bandler was an Associate Editor of the IEEE TRANSACTIONS ON MICROWAVE THEORY AND TECHNIQUES (1969–1974). He was Guest Editor of a special issue of the IEEE TRANSACTIONS ON MICROWAVE THEORY AND TECHNIQUES on computer-oriented microwave practices (March 1974). Dr. Bandler is on the editorial boards of the *International Journal of Numerical Modelling* and the *International Journal of Microwave and Millimeterwave Computer-Aided Engineering*. Dr. Bandler is a Fellow of the Royal Society of Canada and of the Institution of Electrical Engineers (Great Britain). He is a member of the Association of Professional Engineers of the province of Ontario (Canada) and a member of the Electromagnetics Academy.

✠

Qi-jun Zhang (S'84–M'87) was born in Xianyan, Shanxi, China, on October 8, 1959. He received the B.Eng. degree from the East China Engineering Institute, Nanjing, China, in 1982, and the Ph.D. degree from McMaster University, Hamilton, Canada, in 1987, both in electrical engineering.

He was a research assistant at the Institute of Systems Engineering, Tianjin University, Tianjin, China, from 1982 to 1983. He joined the Simulation Optimization Systems Research Laboratory and the Department of Electrical and Computer Engineering at McMaster University in 1983 as a graduate student. He was awarded an Ontario Graduate Scholarship for the academic years 1985/86 and 1986/87. He was a teaching assistant in the Department of Electrical and Computer Engineering, McMaster University, from 1984 to 1987 and a postdoctorate fellow there from 1987 to 1988. Presently he is a research engineer with Optimization Systems Associates Inc., Dundas, Ontario, Canada. In 1989, he also became an Assistant Professor (part-time) in the Department of Electrical and Computer Engineering at McMaster University. His professional interests include all aspects of circuit CAD with emphasis on large-scale simulation and optimization, design and modeling of nonlinear microwave circuits, statistical modeling, sensitivity analysis, and the diagnosis and tuning of analog circuits.

Dr. Zhang was a contributor to *Analog Methods for Computer-Aided Analysis and Diagnosis* (Marcel Dekker, 1988).

✠

Jian Song was born in Anshan, Liaoning, China, on May 5, 1956. He received the B.Eng. degree and the M.Eng. degree from Chongqing University, Chongqing, China, in 1982 and 1984, respectively, both in electrical engineering.

In 1984 he joined the Electrical Engineering Department, Chongqing University, Chongqing, China, where he was involved in research in the area of circuit theory and applications. Since 1986, he has been with the Simulation Optimization Systems Research Laboratory and the Department of Electrical and Computer Engineering, McMaster University, Hamilton, Ontario, Canada, as a graduate student working toward the Ph.D. degree. His research interests include general circuit theory, statistical circuit design, yield optimization techniques, device statistical modeling, optimization methods, and large-scale numerical techniques.

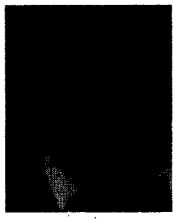

Radoslaw M. Biernacki (M'86–SM'86) was born in Warsaw, Poland. He received the Ph.D. degree from the Technical University of Warsaw, Warsaw, Poland, in 1976.

He became a Research and Teaching Assistant in 1969 and an Assistant Professor in 1976 at the Institute of Electronics Fundamentals, Technical University of Warsaw, Warsaw, Poland. From 1978 to 1980 he was on leave with the Research Group on Simulation, Optimization and Control and with the Department of Electrical and Computer Engineering, McMaster University, Hamilton, Canada, as a Post-Doctorate Fellow. From 1984 to 1986 he was a Visiting Associate Professor at Texas A&M University, College Station, TX. He joined Optimization Systems Associates, Inc., Dundas, Ontario, Canada, in 1986 as Senior Research Engineer. In 1988 he also became a Professor (part-time) in the Department of Electrical and Computer Engineering, McMaster University, Hamilton, Canada. His research interests include system theory, optimization and numerical methods, computer-aided design of integrated circuits, and control systems.

Dr. Biernacki has more than 50 publications and has received a number of prizes for his research and teaching activities.

Reprint 8

Analytically Unified DC/Small-Signal/Large-Signal Circuit Design

Analytically Unified DC/Small-Signal/Large-Signal Circuit Design

John W. Bandler, *Fellow, IEEE*, Radoslaw M. Biernacki, *Senior Member, IEEE*, Shao Hua Chen, *Member, IEEE*, Jian Song, *Student Member, IEEE*, Shen Ye, *Student Member, IEEE*, and Qi-Jun Zhang, *Member, IEEE*

Abstract—**This paper exploits the inherent analytical relationship between the dc, small-signal, and harmonic balance circuit equations. This provides the basis for unified dc, small-signal, and large-signal analyses using a single nonlinear circuit description. Our approach ensures consistent circuit simulation results and permits simultaneous optimization of dc, small-signal, and large-signal responses with multidimensional specifications. Applying this concept to FET parameter extraction leads to nonlinear device models suitable for both small-signal and large-signal analyses. We also demonstrate simultaneous small-signal and large-signal minimax optimization of an FET broad-band amplifier to extend the dynamic operating range.**

I. Introduction

In microwave circuit design, we use a variety of CAD techniques to simulate actual circuit performance. The small-signal simulation focuses on a linear equivalent circuit: the nonlinear devices are represented by measured S parameters, by a linear model extracted from appropriate measurements, or by a linearized model with respect to a specific operating point. In dc simulation, the nonlinear circuit equations at dc are solved to determine the circuit operating point and to study the device characteristics. The harmonic balance (HB) method offers efficient large-signal steady-state simulation of nonlinear circuits in the frequency domain [1], [2].

It is desirable to perform dc, small-signal, and large-signal analyses using a single circuit description and to optimize different types of responses simultaneously. CAD software systems generally implement separate small-signal linear models and large-signal nonlinear models. This can lead to inconsistent simulation results.

This paper verifies and exploits the analytical relationship between the linear small-signal circuit equations and the nonlinear harmonic balance equations. It shows that the results from small-signal simulation and from harmonic balance simulation under sufficiently small signals (HBSS) are inherently consistent. This allows us to use a single nonlinear circuit description which simultaneously takes into account factors such as bias, temperature, and input signal level in the various types of simulations. Consequently, we are able to combine dc, small-signal, and large-signal specifications in a unified optimization problem.

Applying this concept, we extract the parameters of a nonlinear FET model from dc, small-signal, and large-signal measurements. The model we obtained is more consistent than it would be if the small- and large-signal measurements were treated separately. A small-signal broad-band amplifier demonstrates optimization with simultaneous small- and large-signal design specifications. The dynamic operating range of the optimized amplifier is superior to that obtained by conventional small-signal design.

II. Consistency of DC/Small-Signal/Large-Signal Analysis

In our presentation, boldface letters denote vectors and matrices, uppercase letters denote frequency-domain phasors, lower-case letters denote time-domain waveforms, and the superscript T denotes vector or matrix transposition.

Following the notation of Kundert and Sangiovanni-Vincentelli [1], the harmonic balance (HB) equation for a nonlinear circuit is

$$\boldsymbol{F}(\boldsymbol{V}) = \boldsymbol{I}(\boldsymbol{V}) + j\boldsymbol{\Omega}\boldsymbol{Q}(\boldsymbol{V}) + \boldsymbol{Y}\boldsymbol{V} + \boldsymbol{I}_s = \boldsymbol{0} \qquad (1)$$

where $\boldsymbol{V}$ is the vector of unknowns, usually the voltage spectra (phasors) at the nodes connecting the linear and nonlinear subcircuits. $\boldsymbol{I}(\boldsymbol{V})$ represents the current spectra

Manuscript received August 2, 1990; revised January 22, 1991. This work was supported in part by Optimization Systems Associates Inc. and in part by the Natural Sciences and Engineering Research Council of Canada under Grants OGP0042444, OGP0007239, and STR0040923.

J. W. Bandler, R. M. Biernacki, and S. H. Chen are with Optimization Systems Associates Inc., P.O. Box 8083, Dundas, Ontario, Canada L9H 5E7, and with the Simulation Optimization Systems Research Laboratory and the Department of Electrical and Computer Engineering, McMaster University, Hamilton, Ontario, Canada L8S 4L7.

J. Song and S. Ye are with the Simulation Optimization Systems Research Laboratory and the Department of Electrical and Computer Engineering, McMaster University, Hamilton, Ontario, Canada L8S 4L7.

Q.-J. Zhang is with the Department of Electronics, Carleton University, Ottawa, Canada K1S 5B6.

IEEE Log Number 9100148.

0018-9480/91/0700-1076$01.00 ©1991 IEEE

of nonlinear resistive elements and voltage-controlled nonlinear current sources. $\boldsymbol{Q}(V)$ represents the charge spectra of nonlinear capacitors. $\boldsymbol{\Omega} = \text{diag}\{\boldsymbol{\Omega}(0), \boldsymbol{\Omega}(1), \cdots, \boldsymbol{\Omega}(H)\}$, where $\boldsymbol{\Omega}(k) = k\omega_0 \mathbf{1}$, ω_0 is the fundamental angular frequency, and $\mathbf{1}$ is the identity matrix. $Y = \text{diag}\{Y(0), Y(1), \cdots, Y(H)\}$, where $Y(k)$ is the admittance matrix of the linear subcircuit at the kth harmonic frequency. I_s contains the Norton equivalent excitations. We use the notation $V(k)$, $I(V,k)$, $Q(V,k)$ and $I_s(k)$ to represent the kth harmonic components of the respective vectors.

Assuming $v(t)$ is a periodic function, we separate the time invariant and variant terms in its Fourier series as

$$v(t) = V(0) + \Delta v(t) \tag{2}$$

where $V(0)$ is the dc component and

$$\Delta v(t) = \text{Re}\left[\sum_{k=1}^{H} V(k) e^{jk\omega_0 t}\right] \tag{3}$$

where H is the highest harmonic index considered.

Consider the time-domain currents $i(v(t))$ corresponding to $I(V)$ in (1). Under the small-signal assumption (i.e., $\|\Delta v(t)\| \approx 0$), we approximate $i(v(t))$ by the first-order Taylor expansion in terms of $v(t)$ about the dc operating point $V(0)$ as

$$\begin{aligned} i(v(t)) &\approx i(V(0)) + \left(\frac{\partial i^T(v(t))}{\partial v(t)}\right)^T_{v(t)=V(0)} \Delta v(t) \\ &= i(V(0)) + J_I(V(0))\Delta v(t). \end{aligned} \tag{4}$$

Notice that the Jacobian $J_I(V(0))$ is time invariant and depends only on $V(0)$.

Using (4), the dc current is

$$I(V,0) \approx \frac{1}{T_0}\int_0^{T_0} [i(V(0)) + J_I(V(0))\Delta v(t)]\, dt \tag{5}$$

where $T_0 = 2\pi/\omega_0$ is the period. Since the average of $\Delta v(t)$ over one period is zero, i.e.,

$$\frac{1}{T_0}\int_0^{T_0} \Delta v(t)\, dt = 0 \tag{6}$$

we have

$$I(V,0) \approx i(V(0)). \tag{7}$$

Also using (4), we express the ac current phasors as

$$\begin{aligned} I(V,k) &\approx \frac{2}{T_0}\int_0^{T_0} [i(V(0)) + J_I(V(0))\Delta v(t)] e^{-jk\omega_0 t}\, dt \\ &= J_I(V(0))V(k), \qquad k = 1, \cdots, H. \end{aligned} \tag{8}$$

Equation (8) shows that $I(V,k)$ depends only on $V(0)$ and $V(k)$, i.e.,

$$\frac{\partial I^T(V,k)}{\partial V(l)} \approx \begin{cases} J_I^T(V(0)), & k = l \\ \mathbf{0}, & k \neq l. \end{cases} \tag{9}$$

Similar results can be derived for $Q(V)$. Equation (9) and a similar expression for $Q(V)$ indicate that, under the small-signal assumption, the harmonic balance equation

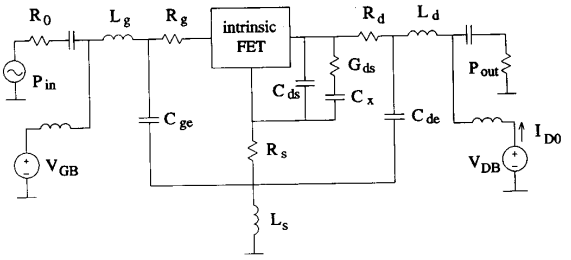

Fig. 1. Single FET circuit with the Curtice nonlinear model.

(1) becomes a block diagonal system of equations. Therefore, we can first solve the dc nonlinear equations

$$F(V(0)) = I(V(0)) + Y(0)V(0) + I_s(0) = \mathbf{0}. \tag{10}$$

Then, for each harmonic of interest, we consider a set of linear equations

$$[J_I(V(0)) + jk\omega_0 J_Q(V(0)) + Y(k)]V(k) + I_s(k) = \mathbf{0}, \quad k \in \{1, \cdots, H\} \tag{11}$$

where $J_I(V(0))$ and $J_Q(V(0))$ are the Jacobians evaluated at the solution of (10).

Not all H sets of linear equations given by (11) need to be solved. We need to consider only the harmonic frequencies for which the excitation $I_s(k)$ is nonzero. In particular, if the excitation is a single-tone sinusoidal signal, then we only need to solve (11) at the fundamental frequency (i.e., $k = 1$).

We can easily reconcile (10) and (11) with the equations for the conventional dc and small-signal analyses. We recognize $J_I(V(0))$ as the conductances and transconductances, and $J_Q(V(0))$ as the capacitances of the small-signal equivalent model of the nonlinear subcircuit. This in itself is not new, but its analytical relationship to the harmonic balance equations as shown here affirms the inherent consistency between dc, small-signal, and large-signal analyses. In this sense, dc and small-signal simulation can be considered a special case of the general HB simulation.

While we have verified that dc/small-signal simulation and harmonic balance simulation under sufficiently small signals (HBSS) lead to consistent results, their solution methods are quite different. In particular, dc/small-signal simulation does not require explicit ac excitations, whereas HBSS simulation does. To illustrate our derivation numerically, we compare the results from HBSS simulation at different input signal levels with the results from dc/small-signal simulation. The circuit with the Curtice FET model [3] is shown in Fig. 1. The comparison in Fig. 2 shows that the results from HBSS and dc/small-signal simulation are almost identical when the input signal is sufficiently small, except when numerical errors become dominant at extremely low signal levels.

It is interesting to note the wide range of the ac excitation power levels for valid HBSS simulations. The upper bound depends on the nonlinearity of the circuit at the actual operating point and may vary substantially with

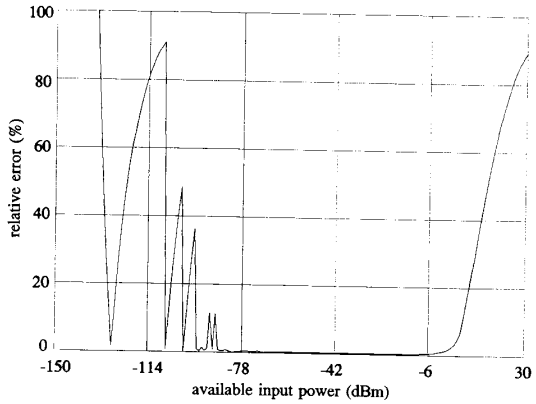

Fig. 2. Relative errors between the voltage gain calculated by HB and $|S_{21}|$ by small-signal analysis with respect to different available input power levels.

the operating point. From our experience, the level of -20 dBm seems to be quite reasonable for many practical situations, e.g., for linear amplifiers. The lower bound depends on the numerical techniques used for solving the nonlinear equations. Surprisingly, our implementation allows as low a power level as -90 dBm to still get reliable, numerically stable solutions. The choice of the starting point for the nonlinear solver is of some importance. We scale the starting point with respect to the excitation level. Another limitation for the lower bound is inherent in the HB method. The HB equations tend to be block diagonal, but in reality they are not. The off-diagonal blocks may contain some residual nonzero values. To some of them the values of dc voltages are applied. Such values may be several orders of magnitude larger than the values of the ac voltages. This may result in adding some errors to the diagonal ac equations and, if the errors become large, may effectively destroy the theoretical block-diagonal property indicated by (10) and (11).

III. Seamlessly Unified Simulation and Optimization

The theoretical consistency between dc, small-signal, and large-signal analyses is the basis for seamlessly unified simulation and optimization in the new generation of CAD systems.

Following our analytical derivation, a block diagram suitable for software implementation can be constructed, as shown in Fig. 3. Regardless of the type of simulation, we always start with the same nonlinear circuit description and operating conditions, such as the bias and the temperature. For small-signal simulation, at each bias point we first solve the nonlinear dc equations given by (10), evaluate the Jacobians as described in (4), and then solve the set of linear equations given by (11). This ensures that all the circuit equations are derived from the same model and therefore the results will be consistent.

Another significance of this approach is that dc, small-signal, and large-signal responses and specifications can

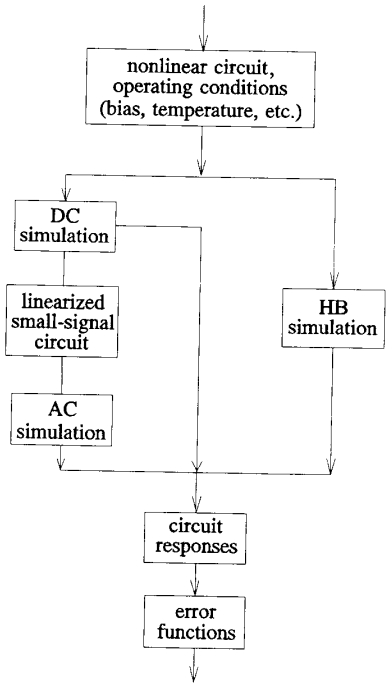

Fig. 3. Block diagram illustrating unified circuit simulation and optimization.

be formulated into one unified optimization problem. We optimize the parameters of a single circuit model from which all the responses are computed. The vector of error functions can be defined as

$$e(\phi) = \begin{bmatrix} e_{dc}(\phi) \\ e_{ss}(\phi) \\ e_{ls}(\phi) \end{bmatrix} \tag{12}$$

where e_{dc}, e_{ss}, and e_{ls} represent error functions that arise from dc, small-signal, and large-signal specifications, respectively. ϕ contains the optimization variables which include model parameters and other designable parameters such as the bias voltages.

The ability to optimize different types of responses simultaneously can bring important benefits to a CAD system. In modeling, it can improve the uniqueness and reliability of the extracted model by simultaneously matching dc, small-signal, and large-signal measurements. In design cases which involve both small- and large-signal performance criteria, the advantage of simultaneous optimization is obvious. Especially when some of the variables affect both the small- and large-signal performance, separate small-signal optimization and large-signal optimization could lead to conflicting parameter values.

IV. Examples

Two numerical examples are used to demonstrate our approach. One involves parameter extraction of a MESFET model, and the other is design optimization of a

TABLE I
MESFET MEASUREMENTS

DC Measurements
Data: drain current
Bias: $V_{GB} = -0.361$ V $V_{DB} = 2$ V
$V_{GB} = -1.062$ V $V_{DB} = 6$ V
Small-Signal Measurements
Data: S parameters (magnitude and phase)
Bias: $V_{GB} = -0.361$ V $V_{DB} = 2$ V
$V_{GB} = -1.062$ V $V_{DB} = 6$ V
Frequencies (GHz): 1, 3, 5, 7, 9, 11, 13, 15
Large-Signal Measurements
Data: dc drain current
output power spectra at the fundamental, second and third harmonics
Bias: $V_{GB} = -0.373$ V $V_{DB} = 2$ V
$V_{GB} = -1.072$ V $V_{DB} = 6$ V
Available input power (dBm): -15, -5, 5
Fundamental frequencies (GHz): 0.2, 6

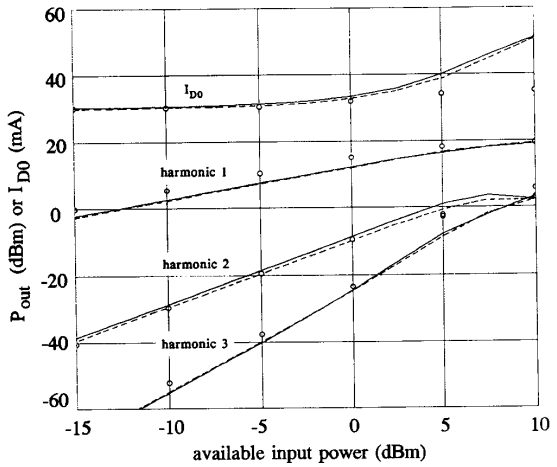

Fig. 4. Agreement between measured and simulated output power spectra at fundamental frequency 2 GHz and bias $V_{GB} = -0.667$ V and $V_{DB} = 4$ V. Solid lines represent the responses of the model extracted from simultaneous dc, small- and large-signal matching. Dashed lines represent the responses of the model extracted from large-signal measurements alone. Circles represent the measured data.

broad-band amplifier. The results are obtained from a research system based on OSA90 [4].

A. MESFET Parameter Extraction

The parameters of the Curtice nonlinear MESFET model [3] are extracted from the measurements summarized in Table I [5]. A total of 27 parameters in both the intrinsic and extrinsic models are extracted [6].

The measurements include dc drain currents, small-signal S parameters, and large-signal power spectra. Following (12), e_{dc} contains the errors between measured and modeled dc drain currents at each bias point, e_{ss} contains the errors in S parameters at each bias point and frequency, and e_{ls} contains the errors in harmonic output powers at each bias point, fundamental frequency, and input power level. There is a total of 178 error functions.

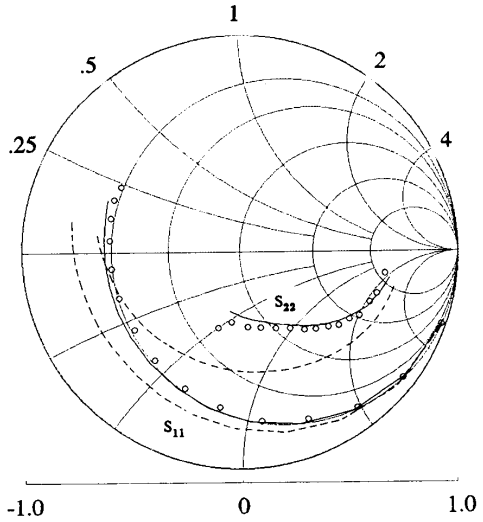

Fig. 5. Agreement between measured and simulated S_{11} and S_{22} at bias $V_{GB} = -0.667$ V and $V_{DB} = 4$ V. Solid lines represent the responses of the model extracted from simultaneous dc, small-signal, and large-signal matching. Dashed lines represent the responses of the model extracted from large-signal measurements alone. Circles represent the measured data.

For comparison, we obtain two solutions, one by simultaneously matching the dc, small-signal, and large-signal measurements, and the other by matching large-signal measurements only. The consistency of the two solutions is tested by matching the measured and modeled responses at an operating point not included in the optimization. From Fig. 4, it seems that both solutions are equally capable of matching the large-signal measurements. However, the S parameter match in Figs. 5 and 6 shows that the solution from simultaneous optimization is significantly more reliable than the one obtained by considering large-signal data alone.

B. Broad-Band Amplifier Design

A small-signal broad-band amplifier [7], as illustrated in Fig. 7, is considered. The FET model described in our first example is used. The specifications for the amplifier are given as

$$\text{gain} = 8 \pm 0.5 \text{ dB}$$
$$|S_{11}| \leq 0.4$$
$$|S_{22}| \leq 0.4$$
$$|S_{12}| \leq 0.15$$

at frequencies of 4, 5, 6, 7, and 8 GHz. The design variables include 11 parameters in the matching network and two resistor values in the bias circuit. Minimax optimization [8] is used.

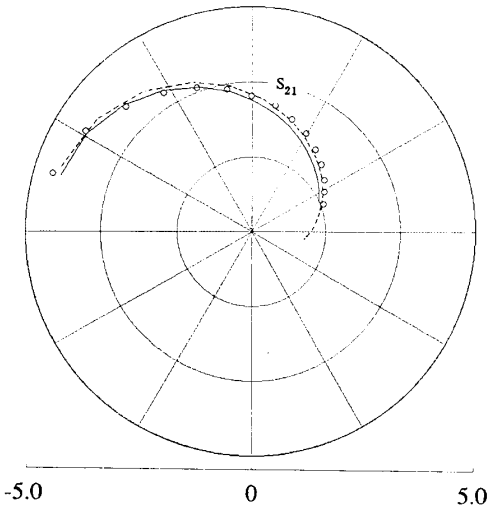

Fig. 6. Agreement between measured and simulated S_{21} at bias $V_{GB} = -0.667$ V and $V_{DB} = 4$ V. The solid line represents S_{21} of the model extracted from simultaneous dc, small-signal, and large-signal matching. The dashed line represents S_{21} of the model extracted from large-signal measurements alone. The circles represent the measured data.

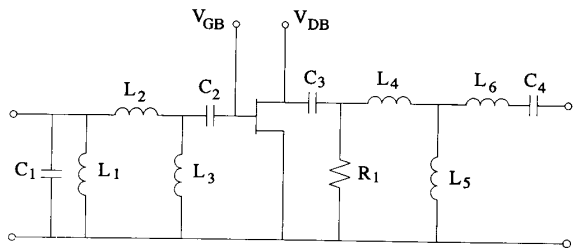

Fig. 7. 4–8 GHz broad-band small-signal amplifier [7].

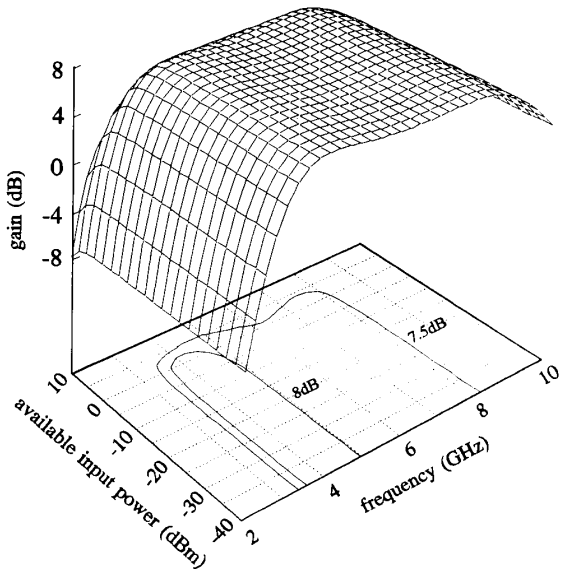

Fig. 8. The gain response surface and selected contour projections for the solution obtained by conventional small-signal design. The specification is 8 ± 0.5 dB.

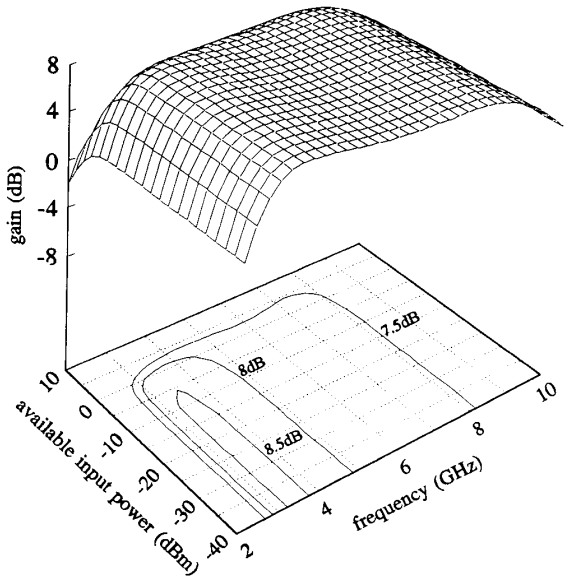

Fig. 9. The gain response surface and selected contour projections for the solution obtained by simultaneous small- and large-signal optimization. The specification is 8 ± 0.5 dB.

First, we design the amplifier by the conventional small-signal approach. The bias point is chosen from the FET dc I–V curves. All the specifications are met by the optimized design.

To exploit our unified optimization approach, we take into consideration the dynamic range of the amplifier, in addition to the small-signal specifications. The specification on the amplifier gain is extended to multiple available input power levels at -10, -5, and 0 dBm. Also, we enforce the second and third harmonic output power levels to be at least 40 dB below the fundamental output power level. The small- and large-signal specifications result in a total of 85 error functions. All the specifications are met at the solution.

The results of the two solutions are compared in Figs. 8 to 11. In Figs. 8 and 9, the gain response surfaces are depicted over fundamental frequency 2 to 10 GHz and available input power -40 to 10 dBm. The solution from simultaneous small- and large-signal optimization exhibits a flatter gain surface than that obtained by small-signal optimization alone. It also provides a wider area in which the gain specification is met.

Figs. 10 and 11 depict the second harmonic error surface over the same range. Any excursion above the flat surface indicates that the specification is violated; i.e., the second harmonic output power exceeds the specified level, which is 40 dB below the fundamental output power. For the design obtained by small-signal optimization alone, a

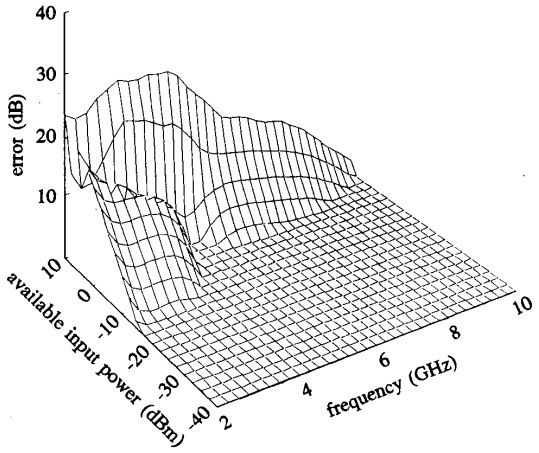

Fig. 10. The error surface of the second harmonic output power with respect to the design specification for the solution obtained by small-signal design. The specifications are given for fundamental frequency from 4 GHz to 8 GHz and for available input power from −10 dBm to 0 dBm. The flat part of the surface indicates zero error.

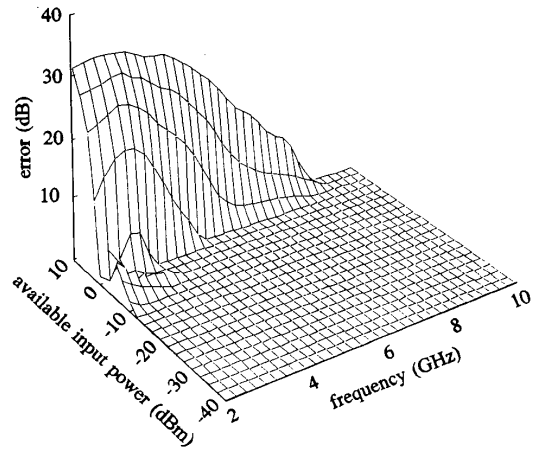

Fig. 11. The error surface of the second harmonic output power with respect to the design specification for the solution obtained by simultaneous small- and large-signal optimization. The specifications are given for fundamental frequency from 4 GHz to 8 GHz and for available input power from −10 dBm to 0 dBm. The flat part of the surface indicates zero error.

nonzero error occurs when the input power is above −10 dBm. For the design which includes large-signal specifications, the zero error area is extended to 0 dBm input power.

V. Conclusions

We have presented a unified approach to dc, small-signal, and large-signal simulation and optimization of microwave circuits. The analytical relationship between the linear equations for small-signal analysis and the harmonic balance equations for large-signal analysis has been derived, which has verified the inherent consistency between the various types of analyses. Following the analytical derivation, a suitable software implementation has been illustrated.

We have demonstrated that, based on a unified nonlinear circuit description, dc, small-signal, and large-signal responses can be simultaneously optimized. When applied to parameter extraction, this approach has led to models that are more consistent and reliable. It can also expand design optimization from the traditional frequency dimension to a multidimensional space [9], by taking into account other factors such as bias and input power levels.

We believe that the new generation of CAD systems must feature unified linear and nonlinear circuit models, as well as simultaneous small-signal and large-signal optimization capabilities.

References

[1] K. S. Kundert and A. Sangiovanni-Vincentelli, "Simulation of nonlinear circuits in the frequency domain," *IEEE Trans. Computer-Aided Design*, vol. CAD-5, pp. 521–535, 1986.

[2] J. W. Bandler, Q. J. Zhang, and R. M. Biernacki, "A unified theory for frequency-domain simulation and sensitivity analysis of linear and nonlinear circuits," *IEEE Trans. Microwave Theory Tech.*, vol. 36, pp. 1661–1669, 1988.

[3] W. R. Curtice, "GaAs MESFET modeling and nonlinear CAD," *IEEE Trans. Microwave Theory Tech.*, vol. 36, pp. 220–230, 1988.

[4] *OSA90*, Optimization Systems Associates Inc., Dundas, Canada, L9H 5E7, 1990.

[5] Measurement data provided by Texas Instruments, Dallas, TX, 1989.

[6] J. W. Bandler, Q. J. Zhang, S. Ye, and S. H. Chen, "Efficient large-signal FET parameter extraction using harmonics," *IEEE Trans. Microwave Theory Tech.*, vol. 37, pp. 2099–2108, 1989.

[7] R. S. Pengelly, *Microwave Field-Effect Transistors—Theory, Design and Applications*. New York: Research Studies Press, 1986.

[8] J. W. Bandler, W. Kellermann, and K. Madsen, "A superlinearly convergent minimax algorithm for microwave circuit design," *IEEE Trans. Microwave Theory Tech.*, vol. MTT-33, pp. 1519–1530, 1985.

[9] J. W. Bandler and M. R. M. Rizk, "Optimization of electrical circuits," *Math. Program. Study on Eng. Optimization*, vol. 11, pp. 1–64, 1979.

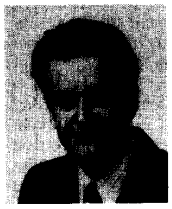

John W. Bandler (S'66–M'66–SM'74–F'78) was born in Jerusalem on November 9, 1941. He studied at Imperial College of Science and Technology, London, England, from 1960 to 1966. He received the B.Sc.(Eng.), Ph.D, and D.Sc.(Eng.) degrees from the University of London, London, England, in 1963, 1967, and 1976, respectively.

He joined Mullard Research Laboratories, Redhill, Surrey, England, in 1966. From 1967 to 1969 he was a Postdoctorate Fellow and Sessional Lecturer at the University of Manitoba, Winnipeg, Canada. He joined McMaster University, Hamilton, Canada, in 1969, where he is currently a Professor of Electrical and Computer Engineering. Dr. Bandler has served as Chairman of the Department of Electrical Engineering and Dean of the Faculty of Engineering. He currently directs research in the Simulation Optimization Systems Research Laboratory. Dr. Bandler is President of Optimization Systems Associates Inc., Dundas, Ontario, Canada, which he established in 1983. OSA currently provides consulting services and software to numerous microwave clients in CAE of microwave integrated circuits. He is also President of Bandler Research Inc., Dundas, Ontario, Canada, which he founded in 1989.

Dr. Bandler contributed to *Modern Filter Theory and Design* (Wiley-Interscience, 1973) and to *Analog Methods for Computer-Aided Analysis and Diagnosis* (Marcel Dekker, 1988). He has published more than 230

papers, of which four appear in *Computer-Aided Filter Design* (IEEE Press, 1973), one in *Microwave Integrated Circuits* (Artech House, 1975), one in *Low-Noise Microwave Transistors and Amplifiers* (IEEE Press, 1981), one in *Microwave Integrated Circuits*, 2nd ed. (Artech House, 1985), and one in *Statistical Design of Integrated Circuits* (IEEE Press, 1987). Dr. Bandler was an Associate Editor of the IEEE TRANSACTIONS ON MICROWAVE THEORY AND TECHNIQUES (1969–1974). He was Guest Editor of the Special Issue of the IEEE TRANSACTIONS ON MICROWAVE THEORY AND TECHNIQUES on Computer-Oriented Microwave Practices (March 1974). He is Guest Coeditor of the forthcoming Special Issue of the IEEE TRANSACTIONS ON MICROWAVE THEORY AND TECHNIQUES on Process-Oriented Microwave CAD and Modeling (July 1992). He joined the Editorial Board of the *International Journal of Numerical Modelling* in 1987 and the Editorial Board of the *International Journal of Microwave and Millimeterwave Computer-Aided Engineering* in 1989. Dr. Bandler is a Fellow of the Royal Society of Canada. He is a Fellow of the Institution of Electrical Engineers (Great Britain). He is a member of the Association of Professional Engineers of the Province of Ontario (Canada) and a member of the Electromagnetics Academy.

Radoslaw M. Biernacki (M'85–SM'86) was born in Warsaw, Poland. He received the Ph.D. degree from the Technical University of Warsaw, Warsaw, Poland, in 1976.

He became a Research and Teaching Assistant in 1969 and an Assistant Professor in 1976 at the Institute of Electronics Fundamentals, Technical University of Warsaw, Warsaw, Poland. From 1978 to 1980 he was on leave with the Research Group on Simulation, Optimization and Control and with the Department of Electrical and Computer Engineering, McMaster University, Hamilton, Canada, as a Post-Doctorate Fellow. From 1984 to 1986 he was a Visiting Associate Professor at Texas A&M University, College Station, TX. He joined Optimization Systems Associates, Inc., Dundas, Ontario, Canada, in 1986 as Senior Research Engineer. In 1988 he also became a Professor (part-time) in the Department of Electrical and Computer Engineering, McMaster University, Hamilton, Canada. His research interests include system theory, optimization and numerical methods, computer-aided design of integrated circuits, and control systems.

Dr. Biernacki has more than 60 publications and has been the recipient of several prizes for his research and teaching activities.

Shao Hua Chen (S'84–M'87) was born in Swatow, Guangdong, China, on September 27, 1957. He received the B.S.(Eng.) degree from the South China Institute of Technology, Guangzhou, China, in 1982 and the Ph.D. degree in electrical engineering from McMaster University, Hamilton, Canada, in 1987.

From July 1982 to August 1983, he was a teaching assistant in the Department of Automation at the South China Institute of Technology. He joined the Department of Electrical and Computer Engineering at McMaster University in 1983 as a graduate student and was awarded an Ontario Graduate Scholarship for the academic years 1985/86 and 1986/87. Since 1987 he has been with Optimization Systems Associates, Inc., Dundas, Canada. Currently he is on leave from Optimization Systems Associates working as a Research Engineer in the Simulation Optimization Systems Research Laboratory, McMaster University. His professional interests include CAD software architecture, optimization theory and algorithms, sensitivity analysis, device modeling, circuit statistics, design centering, computer graphics, and user interfaces.

Jian Song (S'90) was born in Anshan, Liaoning, China, on May 5, 1956. He received the B.Eng. and M.Eng. degrees in electrical engineering from Chongqing University, Chongqing, China, in 1982 and 1984, respectively.

In 1984 he joined the Electrical Engineering Department at Chongqing University, where he was involved in research in circuit theory and applications. Since 1986, he has been with the Simulation Optimization Systems Research Laboratory and the Department of Electrical and Computer Engineering, McMaster University, Hamilton, Canada, as a graduate student working toward the Ph.D. degree. His research interests include general circuit theory, statistical modeling and design, yield optimization, device modeling, optimization methods, and large-scale numerical techniques.

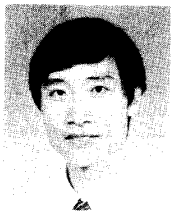

Shen Ye (S'88) was born in Shanghai, China, on January 31, 1957. He received the B.E. and M.E. degrees in electrical engineering from the Shanghai University of Technology, Shanghai, China, in 1982 and 1984, respectively.

From August 1984 to August 1986 he was with the Department of Electrical Engineering, Shanghai University of Technology. Since 1986, he has been with the Simulation Optimization Systems Research Laboratory and the Department of Electrical and Computer Engineering, McMaster University, Hamilton, Canada, working toward the Ph.D. degree. He was a Teaching Assistant from 1986 to 1990. He was awarded an Ontario Graduate Scholarship for the academic year 1989/1990. His research interests are in circuit CAD, including circuit simulation and optimization, device modeling and parameter extraction, statistical modeling, design centering, and software design.

Qi-Jun Zhang (S'84–M'87) was born in Xianyan, Shanxi, China, on October 8, 1959. He received the B.Eng. degree from the East China Engineering Institute, Nanjing, China, in 1982 and the Ph.D. degree from McMaster University, Hamilton, Canada, in 1987, both in electrical engineering.

He was a research assistant in the Institute of Systems Engineering, Tianjin University, Tianjin, China, from 1982 to 1983. He was a teaching assistant in the Department of Electrical and Computer Engineering, McMaster University, from 1984 to 1987 and a postdoctoral fellow there in 1987 and 1988. He was a research engineer with Optimization Systems Associates Inc., Dundas, Ontario, Canada, from 1988 to 1990. During 1989 and 1990 he was also an Assistant Professor (part-time) of Electrical and Computer Engineering at McMaster University. He joined the Department of Electronics, Carleton University, Ottawa, Canada, in 1990, where he is presently an Assistant Professor. His professional interests include all aspects of circuit CAD with emphasis on large-scale simulation and optimization, statistical design and modeling, parameter extraction, sensitivity analysis, and optimization of microwave circuits and high-speed VLSI interconnections.

Dr. Zhang is a contributor to *Analog Methods for Computer-Aided Analysis and Diagnosis* (Marcel Dekker, 1988). Currently he is the holder of the Junior Industrial Chair in CAE established at Carleton University by Bell-Northern Research and the Natural Sciences and Engineering Research Council of Canada.

Reprint 9

Harmonic Balance Simulation and Optimization of Nonlinear Circuits

HARMONIC BALANCE SIMULATION AND OPTIMIZATION OF NONLINEAR CIRCUITS

J.W. Bandler, R.M. Biernacki and S.H. Chen

Optimization Systems Associates Inc.
P.O. Box 8083, Dundas, Canada L9H 5E7

Abstract - This paper addresses the recent advances in harmonic balance simulation and optimization of nonlinear circuits operating in the steady state. The basic concepts and formulations for single tone and multitone simulation are reviewed. A unified theory for nonlinear adjoint sensitivity analysis is summarized. The novel *FAST* technique linking efficient simulation to gradient-based optimization is described. The application of the harmonic balance method is expanded from circuit analysis to modeling, nominal design and yield optimization.

I. INTRODUCTION

Harmonic balance is an attractive method for steady-state simulation of nonlinear circuits because of its efficiency and flexibility [1-3]. By directly calculating the steady-state solution, it avoids the transient analysis performed by traditional time-domain simulators. When the circuit contains widely separated time constants, the transient analysis can be lengthy and expensive. With multitone input signals, it can be difficult to predict the length of the transient state. Harmonic balance is a mixed domain method: the linear elements are evaluated in the frequency domain and the nonlinear devices are modeled in the time domain. Distributed elements and time delays, which are difficult to handle by time-domain simulators, can be easily accommodated by the harmonic balance method.

Harmonic balance simulation has applications to a wide range of nonlinear circuits. For some circuits, the harmonics generated by the nonlinearity are detrimental to performance (e.g., causing distortion in power amplifiers). Using harmonic balance, we can analyze and even minimize such undesirable effects. Yet, harmonic balance simulation is particularly valuable when nonlinearity is exploited as an essential part of the circuit design (e.g., for mixers, oscillators, frequency multipliers and dividers).

This paper reviews recent advances in applying the harmonic balance concept to nonlinear circuit simulation, sensitivity analysis and optimization. A unified theory for nonlinear adjoint sensitivity analysis is summarized. The novel *Feasible Adjoint Sensitivity Technique* (*FAST*) which provides an efficient link between harmonic balance simulation and gradient-based optimization is described. The recent advances have expanded the scope of circuit applications from nonlinear analysis to modeling, nominal design and statistical yield optimization.

This work was supported in part by Optimization Systems Associates Inc. and in part by the Natural Sciences and Engineering Research Council of Canada under Grants OGP0007239, OGP0042444 and STR0040923.

The authors are also with the Simulation Optimization Systems Research Laboratory and the Department of Electrical and Computer Engineering, McMaster University, Hamilton, Canada L8S 4L7.

II. HARMONIC BALANCE EQUATIONS

In harmonic balance simulation, the circuit is partitioned into a linear subcircuit and a nonlinear subcircuit connected through a number of ports. A suitable set of state variables is chosen, such as the port voltages represented by frequency-domain complex phasors at all the harmonic frequencies of interest. The linear subcircuit is evaluated in the frequency domain, given the excitations and state variables. The nonlinear subcircuit is simulated in the time-domain, and the responses are converted into the frequency domain by the Fourier transform.

The set of harmonic balance equations can be defined as

$$\mathbf{F}(\mathbf{V}) = \mathbf{I}_{NL}(\mathbf{V}) + \mathbf{I}_{L}(\mathbf{V}) = \mathbf{0} \qquad (1)$$

where $\mathbf{V}$ represents the state variables, $\mathbf{I}_{NL}$ and $\mathbf{I}_{L}$ are the responses of the nonlinear and linear subcircuits, respectively.

The nonlinear harmonic balance equations can be solved by Newton iterations or by optimization. The choice of starting point is important or even crucial for convergence. The continuation method is often used to overcome convergence difficulties. For instance, to improve convergence at high input power levels, we can first solve the harmonic balance equations at a low input power level and gradually increase the input power to the desired levels. A starting point may also be obtained from small-signal simulation of the linearized circuit around the dc operating point. It has been shown [4] that at sufficiently low input power levels, dc/small-signal simulation and harmonic balance simulation lead to consistent results, as illustrated in Fig. 1.

A different approach suggested by Rizzoli *et al.* [2] employs a quasi-Newton iteration to obtain starting points.

Harmonic balance simulation is certainly not limited to circuits with single-frequency sinusoidal excitations. The input signal may contain nonzero higher harmonic components. For instance, an input of triangular waveforms may be represented by its truncated frequency spectrum. For frequency dividers, the input is treated as the second harmonic of the desired output frequency.

0-7803-0593-0/92 $3.00 1992 IEEE

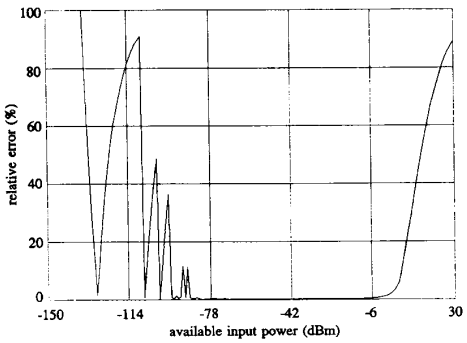

Fig. 1. Relative errors between the voltage gain calculated by harmonic balance and $|S_{21}|$ by small-signal analysis with respect to different input power levels. The errors at high input power levels are due to circuit nonlinearity. Numerical errors become dominant at extremely low input power levels.

Harmonic balance simulation under multitone excitations is useful for intermodulation and mixer analyses. The number of spectral frequencies which need to be considered grows rapidly with the number of tones. The selection of time samples (for the simulation of the nonlinear subcircuit) is another challenging aspect of multitone simulation. A number of competing approaches have been proposed: random sampling, the APFT algorithm by Kundert and Sangiovanni-Vincentelli [5], multidimensional FFT [6], and a recent quasi-orthogonal matrix sampling algorithm by Ngoya *et al.* [7]. Mixers, as a special case of multitone circuits, can also be analyzed by the frequency conversion method [8].

III. HARMONIC BALANCE SENSITIVITIES

In order to incorporate harmonic balance simulation into gradient-based optimization, we need to estimate the sensitivities of circuit responses. The simplest way is by perturbations, but it would require that the nonlinear harmonic balance equations be repeatedly solved after each perturbation.

Exact harmonic balance sensitivity expressions have been derived by Bandler *et al.* [9]. Suppose we are interested in the sensitivity of

$$V_{out} = \mathbf{c}^T \mathbf{V} \tag{2}$$

where $\mathbf{c}$ is a linear transfer vector linking the output voltage with the state variables. An adjoint system is then defined as

$$\mathbf{J}^T \hat{\mathbf{V}} = \mathbf{c} \tag{3}$$

The adjoint system is a set of linear equations whose coefficient matrix $\mathbf{J}$ is the Jacobian matrix at the solution of the harmonic balance equations (1). Once (1) is solved by Newton iterations, little additional effort is required to solve the adjoint system. Detailed adjoint sensitivity expressions are given in [9].

The exact adjoint analysis is theoretically the most precise and efficient method for calculating sensitivities. To implement it in practice, however, can be a very complicated task, especially for general-purpose applications. A novel approach called *Feasible Adjoint Sensitivity Technique* (*FAST*) was proposed by Bandler *et al.* [10,11]. The *FAST* technique exploits the adjoint principles to derive high-level sensitivity expressions in which some of the terms are calculated by perturbations at the elementary level. It retains most of the elegance and accuracy of exact adjoint analysis while avoiding the implementational complexity.

For brevity, we consider ϕ as one of the designable variables. If we perturb ϕ by $\Delta\phi$, the corresponding change in V_{out} can be approximated by

$$\Delta V_{out} \approx \Delta \mathbf{c}^T \mathbf{V} + \mathbf{c}^T \Delta \mathbf{V} \tag{4}$$

To obtain the incremental change in the state variables $\Delta\mathbf{V}$, we utilize the adjoint solution given by (3):

$$\Delta V_{out} \approx \Delta \mathbf{c}^T \mathbf{V} - \hat{\mathbf{V}}^T \Delta \mathbf{F} \tag{5}$$

where $\Delta\mathbf{F}$ is the residual function of the harmonic balance equations (1) at $\phi + \Delta\phi$ ($\mathbf{F}$ is theoretically zero at the harmonic balance solution). The evaluation of $\Delta\mathbf{F}$ at $\phi + \Delta\phi$ requires much less effort than to repeat the harmonic balance solution. The incremental change in the linear transfer vector, namely $\Delta\mathbf{c}$, can be obtained by either an adjoint analysis of the linear subcircuit or perturbation. In fact, if ϕ is a parameter in the nonlinear subcircuit, $\Delta\mathbf{c}$ is not needed:

$$\Delta V_{out} \approx -\hat{\mathbf{V}}^T \Delta \mathbf{F} \tag{6}$$

The *FAST* technique is substantially more efficient than the perturbation method, and it is also much easier to implement than the exact nonlinear adjoint formulas in [9]. Another alternative is the approach of optimization with integrated gradient approximations [12].

IV. NONLINEAR MODELING USING HARMONICS

In conventional frequency-domain linear analysis, nonlinear devices are represented by linearized equivalent circuit models around the dc operating point. Typically, the models are extracted from small-signal and/or dc measurements. Such models can be inadequate or even unsuitable for large-signal simulation. Using harmonic balance, large-signal nonlinear models can be extracted directly from power spectrum and/or waveform measurements [13]. Fig. 2 shows the match between FET power spectrum measurements and the simulated responses of a large-signal nonlinear model obtained using our modeling system HarPE [14].

V. UNIFIED SMALL- AND LARGE-SIGNAL DESIGN

Another significant approach is to combine dc, small-signal and large-signal performance specifications into one unified design optimization problem. This is possible if the same nonlinear circuit model is used in dc, small-signal and large-signal analyses, providing analytically consistent results [4]. The ability to optimize different types of responses simultaneously instead of separately brings important benefits to a CAD system, especially when some of the variables affect both the small- and large-signal performance.

This approach can be illustrated through a broad-band amplifier [4]. The dynamic range of the amplifier is taken into consideration in addition to the small-signal gain. The small-signal gain of the amplifier is optimized simultaneously for a range of input power levels. The higher harmonic responses (undesirable) are also minimized, using our CAD

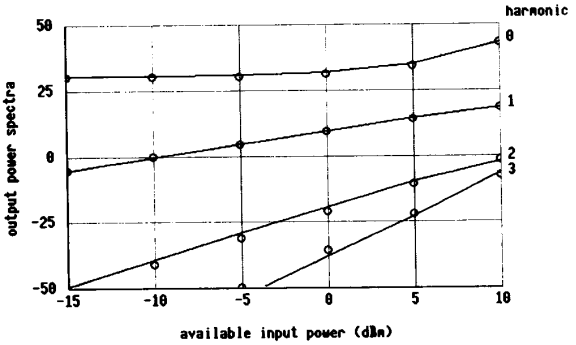

Fig. 2. Measured (circles) and simulated (solid lines) output power spectra of a MESFET.

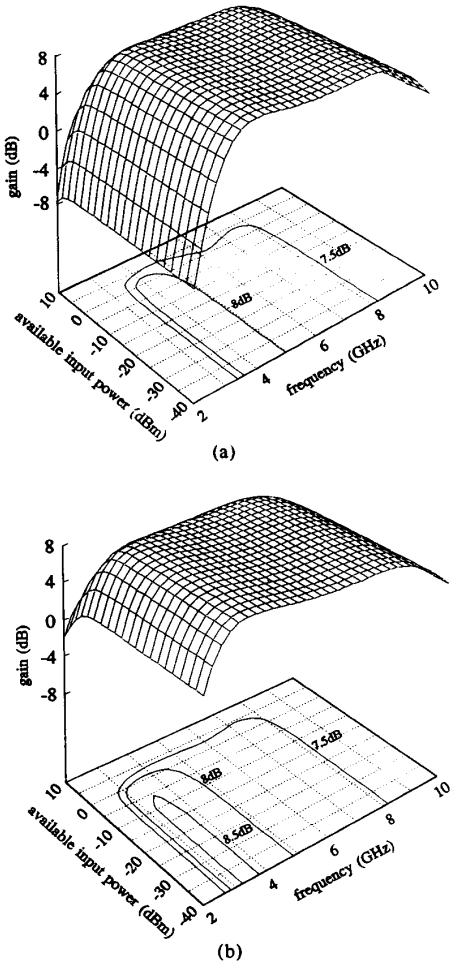

Fig. 3. The gain surface and selected contour projections for the amplifier (a) by conventional small-signal design and (b) by simultaneous small- and large-signal design. The specification is 8 ± 0.5dB.

system OSA90/hope [15]. As shown in Fig. 3, the simultaneous optimization of small- and large-signal responses leads to a flatter gain surface and larger area in which the gain specification is met, as compared with a conventional small-signal design.

VI. NONLINEAR YIELD OPTIMIZATION

Harmonic balance can also be applied to statistical optimization of nonlinear circuits. In order to reduce the computational effort involved in the Monte Carlo simulation of a large number of random outcomes (i.e., circuits with statistically perturbed parameter values), a recent approach applies quadratic approximation not only for the circuit responses but also for their derivatives [16]. Since the determination of the quadratic model coefficients is independent of the number of outcomes, we can improve the sampling accuracy using a large number of outcomes without excessive computational effort.

Nonlinear yield optimization can be demonstrated through a frequency doubler [11]. The doubler consists of a common-source FET with a lumped input matching network and a microstrip output matching and filter section. The statistics of the nonlinear FET model parameters are described by a multidimensional normal distribution, including correlations. The statistics of the linear parameters are represented by uniform distributions. The optimization variables are parameters of the matching circuit. Responses to be optimized include conversion gain and spectral purity. Using the one-sided ℓ_1 centering algorithm [17] implemented in OSA90/hope [15], the yield of the doubler, as estimated from 500 random outcomes, was increased from 31% to 74%. The histograms of the spectrual purity before and after yield optimization are shown in Fig. 4.

VII. DATAPIPE ARCHITECTURE

As optimization is applied to an expanding variety of circuit applications, software modules of diverse origins such as specialized simulators must be accommodated in a general CAD system.

We developed a software architecture called Datapipe which utilizes UNIX interprocess pipes for high speed data communication between independent programs. Utilizing the Datapipe architecture, an optimizer in the parent program will be able accept response functions and gradients from external simulators running as child programs. For example, we are able to interface our optimizers and statistical modules with SPICE-PAC [18].

One of the most active research areas at the present is the development of nonlinear device models for harmonic balance and/or time-domain simulation. The Datapipe concept can facilitate the testing of such models without interfering with an existing CAD system.

VIII. CONCLUSIONS

The basic formulation and advantages of harmonic balance simulation have been described. Recent advances in circuit applications, including device modeling, nominal design and statistical optimization, have been reviewed and illustrated through examples. Nonlinear adjoint sensitivity analysis and especially the *FAST* technique have been discussed. The harmonic balance concept combined with adequate nonlinear circuit models can provide a unifying basis for consistent dc, small-signal and large-signal simulation and optimization.

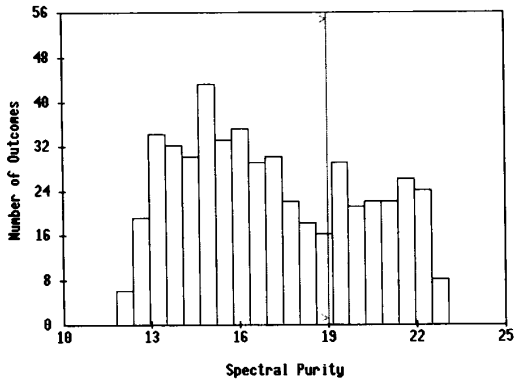

Fig. 3. Histogram of spectral purity of the frequency doubler based on 500 outcomes (a) before yield optimization and (b) after yield optimization. The specification is shown by a vertical line.

REFERENCES

[1] K.S. Kundert and A. Sangiovanni-Vincentelli, "Simulation of nonlinear circuits in the frequency domain", *IEEE Trans. Computer-Aided Design*, vol. CAD-5, pp. 521-535, 1986.

[2] V. Rizzoli and A. Neri, "State of the art and present trends in nonlinear microwave CAD techniques", *IEEE Trans. Microwave Theory Tech.*, vol. 36, pp. 343-365, 1988.

[3] R. Gilmore, "Nonlinear circuit design using the modified harmonic balance algorithm", *IEEE Trans. Microwave Theory Tech.*, vol. MTT-34, pp. 1294-1307, 1986.

[4] J.W. Bandler, R.M. Biernacki, S.H. Chen, J. Song, S. Ye and Q.J. Zhang, "Analytically unified DC/small-signal /large-signal circuit design", *IEEE Trans. Microwave Theory Tech.*, vol. 39, pp. 1076-1082, 1991.

[5] K.S. Kundert and A. Sangiovanni-Vincentelli, "Applying harmonic balance to almost-periodic circuits", *IEEE Trans. Microwave Theory Tech.*, vol. 36, pp. 366-378, 1988.

[6] V. Rizzoli, C. Cecchetti, A. Lipparini and F. Mastri, "General-purpose harmonic balance analysis of nonlinear microwave circuits under multitone excitation", *IEEE Trans. Microwave Theory Tech.*, vol. 36, pp. 1650-1660, 1988.

[7] E. Ngoya, J. Rousset, M. Gayral, R. Quere and J. Obregon, "Efficient algorithms for spectral calculations in nonlinear microwave circuits simulators", *IEEE Trans. Circuits and Systems*, vol. 37, pp. 1339-1355, 1990.

[8] S.A. Maas, *Nonlinear Microwave Circuits*, Norwood, MA: Artech House, 1988.

[9] J.W. Bandler, Q.J. Zhang and R.M. Biernacki, "A unified theory for frequency-domain simulation and sensitivity analysis of linear and nonlinear circuits", *IEEE Trans. Microwave Theory Tech.*, vol. 36, pp. 1661-1669, 1988.

[10] J.W. Bandler, Q.J. Zhang and R.M. Biernacki, "Practical, high-speed gradient computation for harmonic balance simulators", *IEEE MTT-S Int. Microwave Symp. Digest* (Long Beach, CA), pp. 363-367, 1989.

[11] J.W. Bandler, Q.J. Zhang, J. Song and R.M. Biernacki, "FAST gradient based yield optimization of nonlinear circuits", *IEEE Trans. Microwave Theory Tech.*, vol. 38, pp. 1701-1709, 1990.

[12] J.W. Bandler, S.H. Chen, S. Daijavad and K. Madsen, "Efficient optimization with integrated gradient approximations", *IEEE Trans. Microwave Theory Tech.*, vol. 36, pp. 444-454, 1988.

[13] J.W. Bandler, Q.J. Zhang, S. Ye and S.H. Chen, "Efficient large-signal FET parameter extraction using harmonics", *IEEE Trans. Microwave Theory Tech.*, vol. 37, pp. 2099-2108, 1989.

[14] *HarPE™ User's Manual*, Optimization Systems Associates Inc., P.O. Box 8083, Dundas, Canada, L9H 5E7, 1991.

[15] *OSA90/hope™ User's Manual*, Optimization Systems Associates Inc., P.O. Box 8083, Dundas, Canada, L9H 5E7, 1991.

[16] J.W. Bandler, R.M. Biernacki, S.H. Chen, J. Song, S. Ye and Q.J. Zhang, "Gradient quadratic approximation scheme for yield-driven design", *IEEE MTT-S Int. Microwave Symp. Digest* (Boston, MA), pp. 1197-1200, 1991.

[17] J.W. Bandler and S.H. Chen, "Circuit optimization: the state of the art", *IEEE Trans. Microwave Theory Tech.*, vol. 36, pp. 424-443, 1988.

[18] W.M. Zuberek, "SPICE-PAC 2G6c - User's Guide", Technical Report #8902, Department of Computer Science, Memorial University of Newfoundland, St. John's, Canada A1C 5S7, 1989.

Reprint 10

Integrated Physics-Oriented Statistical Modeling, Simulation and Optimization

Integrated Physics-Oriented Statistical Modeling, Simulation and Optimization

John W. Bandler, *Fellow, IEEE,* Radoslaw M. Biernacki, *Senior Member, IEEE,* Qian Cai, *Student Member, IEEE,* Shao Hua Chen, *Member, IEEE,* Shen Ye, *Member, IEEE* and Qi-Jun Zhang, *Member, IEEE*

***Abstract*—We contribute herein to the effective utilization of physics-, geometry- and process-related parameters for yield-driven microwave device modeling and circuit design. We address physics-based modeling of MESFETs from the point of view of efficient simulation, accurate behavior prediction and robust parameter extraction. We present a novel integration of a large-signal physics-based model into the harmonic balance equations for simulation of nonlinear circuits, involving an efficient Newton update. We exploit this integration in gradient-based FAST (*Feasible Adjoint Sensitivity Technique*) circuit optimization. For the purpose of yield-driven circuit design we present a relevant physics-based statistical modeling methodology. Our statistical implementations use models originated by Ladbrooke and Khatibzadeh and Trew. We embed these physics-based device models in the yield optimization process for MMICs using appropriate multidimensional statistical distributions. Quadratic approximation of responses and gradients suitable for yield optimization is discussed. We verify our theoretical contributions and exemplify our computational results using built-in and user-programmable modeling capabilities of the CAE systems OSA90/hope™ and HarPE™. In this context, we report on results of device modeling using a field-theoretic nonlinear device simulator.**

I. Introduction

WE BELIEVE that microwave computer-aided engineering (CAE) technology must address physics-based circuit optimization, directly linking geometrical, material and process-related parameters, or simply, physical parameters, with system performance and production yield. Field theory, circuit theory and system theory need to be integrated into hierarchically structured computer-aided design (CAD) systems for linear, nonlinear and statistical microwave circuit simulation and design.

For active microwave circuit design the effectiveness of modern CAD methods relies heavily on accurate device models. Approaches to device modeling have been developed and a variety of models have been implemented into circuit simulators for such purposes as small- and large-signal circuit design. Generally, the methods for device modeling can be classified into two categories: equivalent circuit-based models (ECMs) and physics-based models (PBMs).

ECM modeling assumes an equivalent circuit to simulate the external behavior of the device under consideration. Such models consist of a number of linear and nonlinear circuit elements connected in a predefined manner. To approximate device characteristics, empirical equations are devised *a priori* for those nonlinear circuit elements. Various FET ECMs, including small-signal and nonlinear large-signal (e.g., Curtice and Ettenberg, Materka and Kacprzak, Statz *et al.*) models [1]–[5], have been widely used in microwave CAD. To properly utilize these models, devices must be characterized through an accurate parameter extraction process where the ECM parameter values are determined from dc, *S*-parameter and/or large-signal measurement data (e.g., Bandler *et al.* [6]–[7]). ECMs enjoy high computational efficiency and are relatively easy to implement into circuit simulators. They have been the foundation of pre-MMIC (monolithic microwave integrated circuits) CAD and continue to dominate today's microwave simulators. However, there is no obvious relationship between ECM parameters and device physical parameters. Also, since the model parameters are usually identified after device fabrication, they have limited extrapolative or statistically meaningful forecasting abilities. This opens the door to PBM modeling.

PBMs address the fundamental device equations and characterize device behavior in terms of physical parameters such as gate length, channel thickness, doping profile, etc. Circuit design can then be considered at the device parameter level. In other words, the design variables can directly include device geometrical, material and process-related parameters [8]. Therefore, PBMs should be very effective in terms of predictability and first-pass success in the design of microwave integrated circuits (MICs) and MMICs.

Efficient microwave nonlinear circuit analysis has been a subject of serious research for a long time. Its importance has resurged with the development of MICs and MMICs, where nonlinear active devices are components critical to performance. Simulation of nonlinear circuits

Manuscript received September 4, 1991; revised March 5, 1992. This work was supported in part by Optimization Systems Associates Inc., by the Natural Sciences and Engineering Research Council of Canada under Grants OGP0007239, OGP0042444, and STR0040923 and by the National Research Council of Canada through its IRAP-M program.

J. W. Bandler, R. M. Biernacki, Q. Cai and S. H. Chen are with the Simulation Optimization Systems Research Laboratory, Department of Electrical and Computer Engineering, McMaster University, Hamilton, ON, Canada L8S 4L7. J. W. Bandler, R. M. Biernacki and S. H. Chen are also with and S. Ye is with Optimization Systems Associates Inc., P.O. Box 8083, Dundas, ON, Canada L9H 5E7. Q.-J. Zhang is with the Department of Electronics, Carleton University, Ottawa, ON, Canada K1S 5B6.

IEEE Log Number 9200458.

0018-9480/92$03.00 © 1992 IEEE

is much more complicated than that of linear circuits. It can be carried out in the time domain, frequency domain, and mixed frequency/time domains, as reviewed by Gilmore and Steer in [9].

Time-domain methods try to solve the circuit equations entirely in the time domain using numerical methods. There are three major time-domain simulation techniques [9]: direct methods [10]–[15], associated discrete circuit model approaches [10], [16] and shooting methods [17]–[22]. Frequency-domain methods, recently reviewed by Steer, Chang and Rhyne [23], attempt to analyze nonlinear circuits entirely in the frequency domain. Functional expansions enable the frequency components of the output spectrum to be calculated directly from the input spectrum. Frequency-domain methods such as power series expansion analysis [24]–[27], Volterra series analysis [28]–[33] and spectral balance analysis [34]–[36], have been used successfully for the analysis of microwave nonlinear circuits [37]–[44].

Mixed frequency/time-domain methods include the harmonic balance (HB) technique [45]–[51] which was significantly advanced by Nakhla and Vlach, Kundert and Sangiovanni-Vincentelli, Rizzoli *et al.*, and several other authors. The HB technique was recently reviewed by Gilmore and Steer [9], [52]. The HB technique is an efficient tool for the simulation of steady-state responses of nonlinear microwave circuits [53]–[58]. The waveform balance (or sample balance) technique is another mixed frequency/time-domain method and can be considered a dual to the HB method. It was, for example, used by Hwang *et al.* for nonlinear modeling and verification of MMIC amplifiers [59].

Nonlinear circuit optimization requires efficient nonlinear circuit simulation. It has become feasible because of the efficiency of the HB method. Optimization employing the HB method has been applied to large-signal FET model parameter extraction [7], nonlinear circuit design [60]–[62] and nonlinear circuit yield optimization [63], although most of the developments have been based on ECMs. Active and passive elements are explicitly represented through their equivalent circuit models. Direct treatment of the effects of device physical parameters on the overall MMIC circuit performance has been studied by a number of researchers [8], [64]–[71]. One of the most significant benefits of PBMs over ECMs is the opportunity of directly optimizing controllable/designable physical parameters of the passive and active devices for low noise, high power, high yield, etc.

Statistical device modeling is a prerequisite for accurate yield-driven or cost-driven circuit analysis and optimization [72], [73]. The model statistics originate from random variations of geometrical, material and process-related parameter values during manufacturing. Those random variations result in complicated distributions and correlations of device responses. The aim of statistical device modeling is to provide tools for generating random device outcomes which can reproduce the actual distribution of the device responses. Statistical modeling has been extensively studied for passive devices, bipolar junction transistors (BJT), metal-oxide semiconductor (MOS) and complementary metal-oxide semiconductor (CMOS) circuits for more than a decade [74]–[82]. Statistical modeling techniques have also been applied to microwave devices [73], [83]–[86].

With the rapid progress of GaAs fabrication technology, MMICs are becoming increasingly practical [87]. During the past two decades, hybrid microwave integrated circuits (HMICs) have been used in the microwave industry, where active and passive discrete components such as transistors, thin- or thick-film capacitors, inductors and resistors are connected on a dielectric substrate. In MMICs, all the active and passive components are fabricated on a common semi-insulating substrate. Post-production tuning of MMICs is restricted, and device replacement is not possible. In the production of MMICs, circuits are manufactured in batches rather than individually. The cost of manufacturing is directly affected by yield. Therefore, yield analysis and optimization, which take into account the manufacturing tolerances, model uncertainties, variations in the process parameters, environmental uncertainties, etc., have become widely accepted as indispensable components of the MMIC design methodology.

Pioneering work on yield optimization was carried out in the early 1970's by a number of researchers (e.g., Karafin, Pinel and Roberts, Bandler [88]–[92]) and was advanced subsequently during the last two decades [93]–[118]. Yield optimization of nonlinear microwave circuits with statistically characterized devices has been reported in the literature, e.g., [63], [119], [120]. Purviance and Meehan [121] recently reviewed statistical analysis and design of microwave circuits. Many approaches developed for yield optimization are restricted to circuits employing ECMs. Statistics are then applied to the equivalent circuit elements such as capacitances, inductances or resistances. There is doubt as to whether such an approach is capable of reflecting the actual statistical behavior of the physical parameters. In MMICs, a change of one device physical parameter may result in correlated changes in all elements of the equivalent circuit model. Furthermore, the resulting correlations may be very complicated and quite difficult to describe. Therefore, conventional design methods at the circuit level are of limited value for yield optimization of MMICs. PBMs, on the other hand, are more likely to reliably simulate statistical behavior because of the physical nature of the model. Consequently, meaningful results of yield optimization should be attainable [122]–[123].

State-of-the-art microwave circuit analysis and design require comprehensive general-purpose CAD softwave to integrate device modeling, steady-state and transient circuit simulation, sensitivity analysis, statistical modeling and analysis, performance- and yield-driven design optimization, as well as physics-based and process-oriented circuit design within the same framework. Different aspects of a CAD system, such as technology optimiza-

tion, cell design, software modularity and adaptability, have been discussed [124]–[126]. The open architecture of the software systems OSA90/hope™ [127] and HarPE™ [128] is designed to address these challenges. These two systems are used to carry out the calculations presented in this paper and implement our new theoretical contributions.

In Section II, we present PBM modeling of MESFETs. Nonlinear circuit analysis using PBMs integrated with the HB method is addressed in Section III. Circuit design exploiting gradient optimizers is discussed in Section IV. Sections V and VI are devoted, respectively, to statistical modeling and yield optimization using PBMs. Section VII describes how an external simulator, such as a two-dimensional (2D) field-based MESFET simulator, can be integrated with OSA90/hope.

II. Physics-Based MESFET Modeling

The fundamental device equations for PBMs may be solved either numerically or analytically. Numerical models typically employ finite-difference or finite-element techniques [129]–[134]. They are potentially the most accurate and play an important role in understanding device physics. However, they are slow and have been hitherto regarded as cumbersome.

Analytical PBM modeling can be traced back to the early pioneering work of Shockley [135] in 1952. He invented the JFET and developed a detailed analysis based on three major assumptions: constant carrier mobility, gradual channel approximation and abrupt transition between the depletion region and the conducting channel [71]. His model was applicable to long gate devices operating in a non-saturated mode, and therefore is not suitable for modern high-frequency transistors. The Shockley model was subsequently improved by including velocity saturation effects and nonuniform doping profiles in the channel [136]–[141]. All these models are based on one-dimensional or quasi one-dimensional analysis and are suitable for dc and small-signal ac operation. They are restricted to devices with large ratios of gate-length to channel thickness. These restrictions were lifted for large-signal analytical models proposed in [142]–[145]. Large-signal analytical models try to solve the device equations with a minimum number of simplifying assumptions. These models offer a reasonable compromise between model accuracy and simulation efficiency. They are quite promising for circuit design and optimization.

A. Basic Device Equations [144]

Following Khatibzadeh and Trew's approach [144], the device model is formulated for the active, or "intrinsic", region, i.e., the channel directly under the gate electrode, as shown in Fig. 1. All other regions of the device are modeled phenomenologically using external or "extrinsic" linear elements. How to derive the values of these extrinsic elements in terms of physical parameters is not yet well established. Usually, their values are assumed according to practical knowledge or obtained through parameter extraction from measurements.

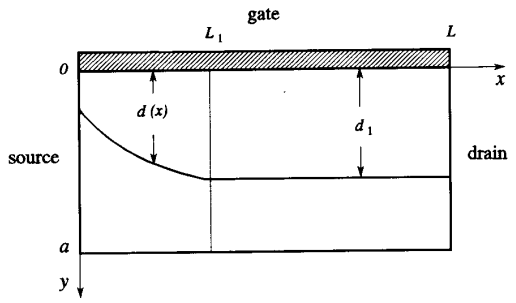

Fig. 1. Active region of a MESFET.

The basic device equations in the active region are

$$\nabla^2\psi = -\frac{q}{\epsilon}[N(y) - n(x, y)] \tag{1}$$

$$\boldsymbol{J} = -qn\boldsymbol{v} + qD\nabla n \tag{2}$$

$$\nabla \cdot \boldsymbol{J} = q\frac{\partial n}{\partial t} \tag{3}$$

and

$$\boldsymbol{J}_t = \boldsymbol{J} + \epsilon\frac{\partial \boldsymbol{E}}{\partial t} \tag{4}$$

where

$$\boldsymbol{E} = -\nabla\psi \tag{5}$$

is the electric field, ψ the electrostatic potential, q the electron charge, ϵ the permittivity of the active layer material, N the donor concentration in the channel, n the free-electron density, v the electron velocity, $\boldsymbol{J}$ the conduction (drift + diffusion) current density, D the diffusion coefficient, and $\boldsymbol{J}_t$ the total (conduction + displacement) current density. It is assumed that $\boldsymbol{v}$ and $\boldsymbol{E}$ are codirectional, i.e.,

$$\boldsymbol{v} = -\mu(E)\boldsymbol{E} \tag{6}$$

where E is the magnitude of $\boldsymbol{E}$ and $\mu(E)$ is the field-dependent mobility. Among the basic device equations, (1) is Poisson's equation, and (3) is the current continuity equation. They contribute to a "drift-diffusion" PBM which characterizes the behavior of the FET devices.

The active region is divided into three parts: a depletion region under the gate Schottky barrier where $n = 0$, a free channel region where $n = N_d$ (N_d is the doping density) and a transition region where n varies smoothly from zero to N_d as indicated by Yamaguchi and Kodera [142] and Madjar and Rosenbaum [143]. The free electron density in the transition region may be expressed as [142]–[144]

$$n(x, y) = N(y)[1 + \gamma(x - L_1)]\ T(d(x), y) \tag{7}$$

where γ and L_1 are the parameters to be determined from the boundary and bias conditions, and the transition func-

tion $T(d(x), y)$ can be defined as [144]

$$T(d(x), y) = 1 - \frac{1}{1 + \exp\left(\dfrac{y - d(x)}{\lambda}\right)}. \tag{8}$$

$d(x)$ is considered in [144] as an "effective depletion-layer width" and λ is a model parameter allowed to vary. Function (8) increases from almost 0 to almost 1 within the range of $y - d(x)$ from -3λ to 3λ, so according to [142], [143] λ should be of the order of the Debye length λ_D. Alternatively, adapting the sinusoidal expression proposed in [142], [143] to the notation of Fig. 1 and allowing λ to vary, the transition function can be defined as

$$T(d(x), y) = \begin{cases} \dfrac{1}{2} + \dfrac{1}{2}\sin\left(\pi \dfrac{y - d(x)}{6\lambda}\right) \\ \qquad \text{if } d(x) - 3\lambda < y < d(x) + 3\lambda \\ 0 \quad \text{if } y \le d(x) - 3\lambda \\ 1 \quad \text{if } y \ge d(x) + 3\lambda. \end{cases} \tag{9}$$

Equation (7) with (8) or (9) eliminates the assumption of abrupt transition between the depletion region and the conducting channel.

B. Dependence of Electron Velocity on Electric Field

In [143], [144], the dependence of the electron drift velocity v on the electric field E is modeled either by a piecewise linear or a quadratic function, both shown in Fig. 2. This neglects the negative differential mobility of GaAs, exemplified by a typical $v - E$ curve, also shown in Fig. 2. An equation with a step function was used by Chang and Day [145] to approximate the negative differential mobility, though the calculated and measured mobilities did not match well.

A good fit to the measured $v - E$ data can be achieved using the Snowden formula [133]

$$\mu(E) = \frac{300\mu_0}{T}\left[\frac{1 + \dfrac{8.5 \times 10^4 E^3}{\mu_0 E_0^4 (1 - 5.3 \times 10^{-4} T)}}{1 + \left(\dfrac{E}{E_0}\right)^4}\right] \tag{10}$$

where

$$\mu_0 = \frac{0.8}{1 + \sqrt{N \times 10^{-23}}}$$

is the doping-dependent low field mobility. Incorporating the functional form of (10) into (6) we express the $v - E$ curve as

$$v = v_s \frac{\dfrac{E}{E_1} + \left(\dfrac{E}{E_0}\right)^\beta}{1 + \left(\dfrac{E}{E_0}\right)^\beta} \tag{11}$$

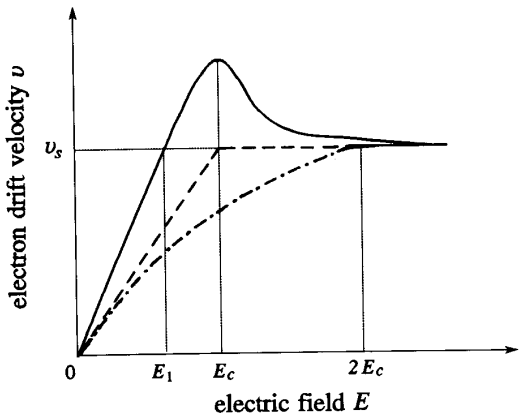

Fig. 2. Electron drift velocity versus electric field: (——) typical $v - E$ curve, (– – –) piecewise linear approximation and (– · –) quadratic approximation.

where v_s (the saturation velocity), E_0 (the characteristic field), E_1 and β are fitting parameters. Equations (10) and (11) can be reconciled if

$$\beta = 4$$

$$E_1 = \frac{v_{s0}}{\mu_0}$$

$$v_{s0} = \frac{T}{300} v_s = \frac{8.5 \times 10^4}{1 - 5.3 \times 10^{-4} T}.$$

When $T = 300°\text{K}$ we have $v_s = v_{s0} = \mu_0 E_1$ (as shown in Fig. 2). Thus E_1 is defined similarly to the critical field E_c (see Fig. 2) introduced in [143], [144]. However, while E_1 denotes the intersection of $v = v_s$ and the line tangent at the origin to the $v - E$ curve, E_c corresponds to the maximum velocity. Therefore, μ_0 is, in general, interpreted differently in the two definitions.

As in [133], in our implementation β is fixed as $\beta = 4$. In Fig. 3 we show the $v - E$ curve calculated by (11) with $v_s = 1.023 \times 10^5$ m/s, $E_1 = 1.173 \times 10^5$ V/m and $E_0 = 3.792 \times 10^5$ V/m. Also shown is the experimental data used by Chang and Day [145] and attributed to Ruch and Kino [146], and Houston and Evans [147]. The match is excellent.

C. Solution for the Potential Distribution

The general solution of Poisson's equation (1) can be expressed as a linear superposition of two components [142]–[144]

$$\psi = \psi_0 + \psi_1, \tag{12}$$

where ψ_0 is the Laplacian potential due to the impressed voltages on the electrodes and satisfies the equation

$$\nabla^2 \psi_0 = 0 \tag{13}$$

with the boundary conditions (see Fig. 1)

$$\psi_0(0, a) = 0 \tag{14a}$$

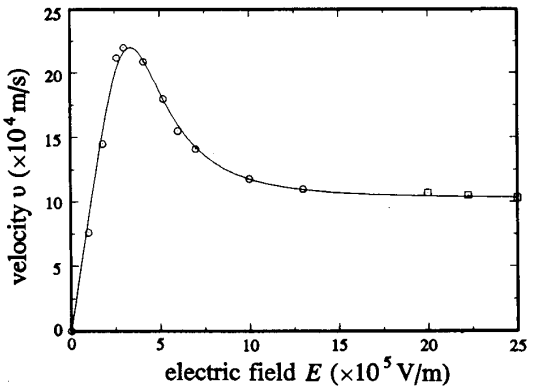

Fig. 3. Comparison of calculated and experimental $v - E$ data for GaAs: (—) calculated from Equation (11), (○) experimental data from Ruch and Kino [146], and (□) experimental data from Houston and Evans [147].

$$\psi_0(L, a) = v_0 \tag{14b}$$

$$\frac{\partial \psi_0(x, a)}{\partial y} = 0 \tag{14c}$$

$$\psi_0(x, 0) = 0. \tag{14d}$$

ψ_1 is due to the space charge in the channel and satisfies the equation

$$\nabla^2 \psi_1 = -\frac{q}{\epsilon}(N - n) \tag{15}$$

with the boundary conditions

$$\psi_1(0, a) = 0 \tag{16a}$$

$$\psi_1(L, a) = v_1 \tag{16b}$$

$$\frac{\partial \psi_1(x, a)}{\partial y} = 0 \tag{16c}$$

$$\psi_1(x, 0) = v_{gs} - V_{bi} \tag{16d}$$

where L and a are the gate length and channel thickness, respectively, V_{bi} is the built-in voltage of the gate Schottky contact, and v_{gs} is the applied intrinsic gate-source voltage, v_0 and v_1 are unknown fractions of v_{ds}, the applied intrinsic drain-source voltage, resulting from the boundary conditions (14b) and (16b) and must be solved for in order to determine the performance of the devices. Since $v_{ds} = v_1 + v_0$, it is sufficient to solve for v_1 only.

Khatibzadeh and Trew [144] showed that a simplified solution to (13) with the boundary conditions (14a)–(14d) is given by

$$\psi_0(x, y) = \frac{v_0}{\sinh\left(\frac{\pi L}{2a}\right)} \sinh\left(\frac{\pi x}{2a}\right) \sin\left(\frac{\pi y}{2a}\right) \tag{17}$$

and the solution to (15) with the boundary conditions (16a)–(16c) can be expressed as

$$\psi_1(x, y) = \begin{cases} -\frac{q}{\epsilon} F_1(d(x), y) + \frac{v_1}{L} x \\ \quad 0 \le x \le L_1 \\ -\frac{q}{\epsilon} F_1(d_1, y) + \frac{v_1}{L} x \\ + \frac{q}{\epsilon} \gamma (x - L_1) F_2(d_1, y) \\ \quad L_1 < x \le L \end{cases} \tag{18}$$

where

$$F_1(d(x), y) = \int_y^a \int_z^a [1 - T(d(x), \tau)] N(\tau)\, d\tau\, dz \tag{19}$$

$$F_2(d_1, y) = \int_y^a \int_z^a T(d_1, \tau) N(\tau)\, d\tau\, dz, \tag{20}$$

where T is the transition function defined by (8) and d_1 is the effective depletion-layer width in the saturation region. The piecewise transition function of (9) could be used here as well. The boundary condition (16d) was applied to (18) to solve for $d(x)$ and γ [144].

Solving for the potential ψ_1 in (18) involves two double integrations F_1 and F_2 which require significant computational effort. These numerical integrations are necessary if the doping profile is arbitrary. However, for uniform doping, i.e., if $N(y) = N_d$ in (7), the efficiency of the model can be greatly improved if (9) is used instead of (8) in (19) and (20) since (9) can be analytically integrated. This has been implemented in both OSA90/hope and HarPE [127], [128] and our experiments show that the simulation time can be reduced by more than two thirds as compared with using (8).

D. Intrinsic Currents

The gate, drain and source currents can be expressed by the equations

$$i_g = i_{gc}(\phi, v_1(\phi, t), v_{gs}(\phi, t), v_{ds}(\phi, t), t) + \frac{\partial q_g(\phi, v_1(\phi, t), v_{gs}(\phi, t), v_{ds}(\phi, t), t)}{\partial t} \tag{21}$$

$$i_d = i_{dc}(\phi, v_1(\phi, t), v_{gs}(\phi, t), v_{ds}(\phi, t), t) + \frac{\partial q_d(\phi, v_1(\phi, t), v_{gs}(\phi, t), v_{ds}(\phi, t), t)}{\partial t} \tag{22}$$

$$i_s = i_{sc}(\phi, v_1(\phi, t), v_{gs}(\phi, t), v_{ds}(\phi, t), t) + \frac{\partial q_s(\phi, v_1(\phi, t), v_{gs}(\phi, t), v_{ds}(\phi, t), t)}{\partial t} \tag{23}$$

where i_{gc}, i_{dc} and i_{sc} are the gate, drain and source conduction currents, respectively, q_g, q_d and q_s stand for the total charges, respectively on the gate, drain and source electrodes, and ϕ is the parameter vector including gate length, gate width, channel thickness, doping density, etc.

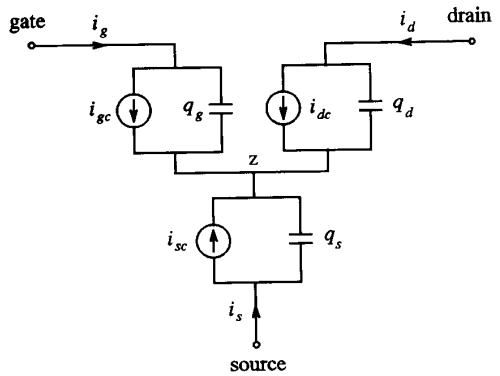

Fig. 4. Equivalent circuit for the intrinsic model.

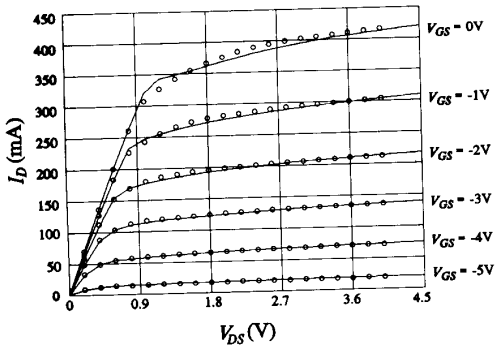

Fig. 5. Comparison of our approach with that of Khatibzadeh's on dc characteristics: (——) our results and (○) Khatibzadeh's results [148].

Equations (21)–(23) can be represented by the equivalent circuit shown in Fig. 4.

i_{gc}, i_{dc} and i_{sc} of (21)–(23) are calculated by integrating the current density $\boldsymbol{J}$ in (2) over the corresponding areas in the planes $y = 0$, $x = L$ and $x = 0$, respectively, (see Fig. 1). For example, the drain conduction current i_{dc} can be written in integral form as [148]

$$i_{dc} = \int \boldsymbol{J} \cdot d\boldsymbol{S} = -qW \int_0^a (\mu(E(L, y))\, n(L, y) \cdot E_x(L, y) + D\, \nabla_x n(L, y))\, dy \tag{24}$$

where E_x and $\nabla_x n$ are the x components of $\boldsymbol{E}$ and ∇n, respectively, and W is the gate width.

The partial derivatives of the total charges q_g, q_d and q_s w.r.t. time t represent the displacement currents through the corresponding electrodes. Again, q_g, q_d, and q_s can be written in integral form [148], for instance,

$$q_g = \epsilon W \int_0^L E_y(x, 0)\, dx \tag{25}$$

where E_y is the y component of $\boldsymbol{E}$.

Since $\boldsymbol{E}(x, y)$ and $n(x, y)$ depend on the voltages v_1, v_{gs} and v_{ds}, the conduction currents and the total charges are nonlinear functions of v_1, v_{gs} and v_{ds}. Under normal working conditions, the gate is reversed biased and the gate conduction current i_{gc} can be neglected. (The gate forward biasing and drain breakdown conditions may be included by introducing diodes into the model [148].) Under this assumption, the drain and source conduction currents are equal at dc. In [142]–[144], the solution of v_1 is obtained iteratively by forcing the difference between the drain and source conduction currents to be sufficiently small. In Section III, we discuss HB simulation where the nonlinear HB equations need to be solved iteratively. In order to avoid a double iteration loop and make the PBM computationally more efficient, we combine solving for v_1 with the HB iterations while satisfying the boundary conditions.

Using the MESFET physical parameters given in [148] we compare dc simulation results of the PBM described in this section to those of Khatibzadeh, as shown in Fig. 5. Slight discrepancies can be attributed to our modifications w.r.t. the original model of [144].

E. Performance Prediction and Parameter Extraction

A significant advantage of the PBMs over the ECMs is that directly from the physical parameter values PBM simulation can predict device performance, or even the performance of the overall circuit embedding the device. This could be done before the device is manufactured and for any range of working conditions. Obviously, validity of this approach strongly depends on model accuracy. We believe that the predictive potential of PBMs should and will provide device and circuit engineers with the opportunity to extend and improve their design capabilities.

Parameter extraction, indispensable for ECMs [5]–[7], [149], [150], may also prove useful for PBMs. Firstly, as was already mentioned in Section II-A, we use parameter extraction to determine the extrinsic device parameters. Secondly, the intrinsic physical parameters, even if they are known or measured, can be fine tuned, for example, to account for measurement errors. It should be noted that, unlike ECMs, it is relatively easy to estimate a good starting point for parameter extraction of PBMs, since the model parameters are physically meaningful and tangible. Another significant application of PBM parameter extraction is for statistical modeling at the device physical and geometrical level, in which a number of devices must be characterized from measurements. This is further discussed in Section IV.

To illustrate PBM parameter extraction of a FET we consider the extrinsic and intrinsic model shown in Fig. 6. The intrinsic parameters are defined in Table I. S-parameter measurements [151] in the frequency range 1 GHz to 21 GHz at 3 bias points (gate bias 0 V, −0.84 V, −1.54 V and drain bias 5 V) are processed simultaneously. The $v - E$ curve obtained by fitting (11) to the

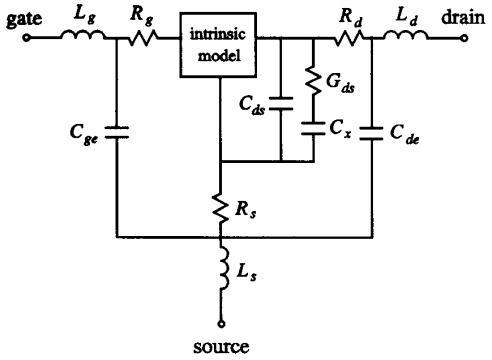

Fig. 6. Circuit topology for parameter extraction showing the intrinsic FET and its associated extrinsic elements.

TABLE I
MESFET INTRINSIC PARAMETERS

Parameter	Notation	Unit
Gate Length	L	μm
Gate Width	W	μm
Channel Thickness	a	μm
Doping Density	N_d	$1/m^3$
Critical Electric Field	E_c	V/m
Saturation Velocity	v_s	m/s
Relative Permittivity	ϵ_r	—
Built-in Potential	V_{bi}	V
Low-Field Mobility	μ_0	m^2/Vs
High-Field Diffusion Coefficient	D_0	m^2/s

experimental data [146], [147] is used here since no $v - E$ measurements for this particular device are available.

Parameter extraction was carried out using the ℓ_2 optimizer [152] of HarPE [128]. Measured values of gate length L, gate width W and doping density N_d were assigned as the starting values. The optimization was performed in two stages. First, the extrinsic parasitic parameters were optimized while the intrinsic physical parameters were kept fixed. In the second stage both the intrinsic and extrinsic parameters were optimized starting from the result of the first stage. The entire parameter extraction process took approximately 5 CPU minutes and 30 iterations on a Sun SPARCstation 1. Optimizable extrinsic and intrinsic parameters before and after optimization are listed in Table II. The measured [151] and simulated S parameters at the three bias points are shown in Fig. 7.

Finally, it should be pointed out that extracting parameter values by simultaneously optimizing a large number of parameters may lead to non-unique results. Some parameter values may become non-physical due to factors such as model simplifications, insufficient measurements or measurement errors. Therefore, model tuning, keeping the parameters within their physical limits, or parameter control, may be necessary. Based on practical knowledge of the device, these concepts can be accommodated in parameter extraction by applying constraints to the parameters being optimized.

TABLE II
EXTRACTED PARAMETERS FOR THE KHATIBZADEH AND TREW MODEL

Parameter	Before Optimization	After Optimization	Plessey Data [151]
L (μm)	0.551	0.571	0.551
W (μm)	300.0	301.6	300.0
N_d ($1/m^3$)	2.235×10^{23}	2.093×10^{23}	2.235×10^{23}
a (μm)	0.200	0.167	—
V_{bi} (V)	0.700	0.672	—
R_g (Ω)	2.200	2.302	—
R_d (Ω)	3.500	3.524	—
R_s (Ω)	2.500	2.704	—
L_g (nH)	0.050	0.028	—
L_d (nH)	0.050	0.010	—
L_s (nH)	0.080	0.036	—
C_{ge} (pF)	0.100	0.123	—
C_{de} (pF)	0.050	0.055	—
G_{ds} ($1/\Omega$)	0.003	0.003	—

Other parameters are fixed as

$E_1 = 1.173 \times 10^5$ V/m $\quad v_s = 1.023 \times 10^5$ m/s
$D_0 = 0.001$ m^2/s $\quad \epsilon_r = 12.9$
$C_x = 10$ pF

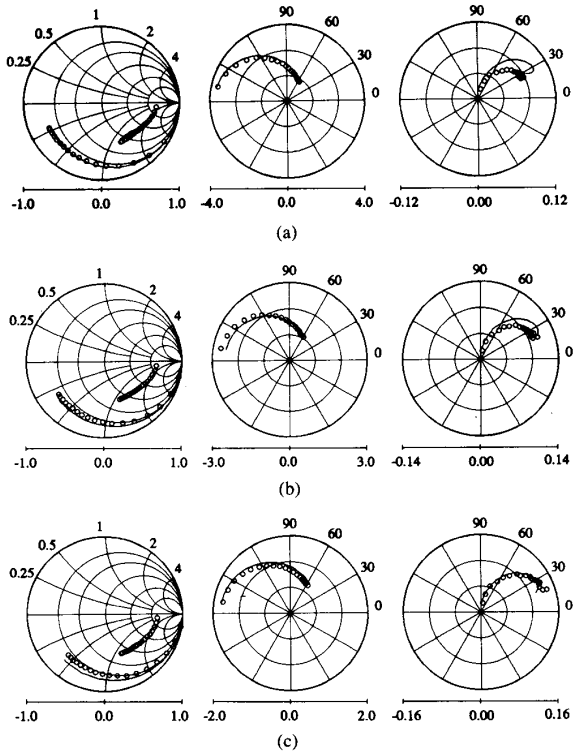

Fig. 7. Comparison of measured (○) and calculated (——) S parameters at 3 bias points for parameter extraction. (a) Gate bias 0 V. (b) Gate bias −0.84 V. (c) Gate bias −1.54 V. Drain bias is 5 V.

III. HARMONIC BALANCE NONLINEAR CIRCUIT ANALYSIS

The responses of a nonlinear circuit can be determined by solving a set of nonlinear state equations

$$f(\dot{x}, x, u, t) = 0 \tag{26}$$

where $\boldsymbol{x} = [x_1 \ x_2 \ \cdots \ x_n]^T$ is the vector of state variables, typically certain voltages and/or currents, and $\boldsymbol{u} = [u_1 \ u_2 \ \cdots \ u_m]^T$ is the excitation vector. (26) can be solved in the time domain, the frequency domain, or a mixed frequency/time domain using respective methods.

In this section, we discuss nonlinear steady-state circuit analysis with PBMs of FETs using the mixed frequency/time-domain HB method.

A. Formulation of the Harmonic Balance Equations

The circuit nodal equations in the time domain can be written as [50]

$$\boldsymbol{f}(\boldsymbol{v}(t), t) = \boldsymbol{i}(\boldsymbol{v}(t)) + \frac{d}{dt}\boldsymbol{q}(\boldsymbol{v}(t)) + \int_{-\infty}^{t} \boldsymbol{y}(t-\tau)\,\boldsymbol{v}(\tau)\,d\tau + \boldsymbol{i}_{ss}(t) = \boldsymbol{0} \tag{27}$$

where t is time, $\boldsymbol{v}$ is the vector of node voltage waveforms, $\boldsymbol{i}$ is the vector of the currents entering the nodes from nonlinear resistors or nonlinear voltage controlled current sources, $\boldsymbol{q}$ is the vector of the charges entering the nodes from nonlinear capacitors, $\boldsymbol{y}$ is the matrix-valued impulse response of linear components, and $\boldsymbol{i}_{ss}$ is the vector of independent current source waveforms.

To use the HB technique, (27) is Fourier transformed into the frequency domain [50] as

$$\boldsymbol{F}(\boldsymbol{V}) = \boldsymbol{I}(\boldsymbol{V}) + j\boldsymbol{\Omega}\boldsymbol{Q}(\boldsymbol{V}) + \boldsymbol{Y}\boldsymbol{V} + \boldsymbol{I}_{ss} = \boldsymbol{0} \tag{28}$$

where $\boldsymbol{V}$, $\boldsymbol{I}_{ss}$, $\boldsymbol{I}$ and $\boldsymbol{Q}$ are the vectors that contain the Fourier coefficients of the respective time-domain waveforms at each node and all harmonics, and $\boldsymbol{Y}$ is the nodal admittance matrix for the linear elements. $\boldsymbol{\Omega}$ is the angular frequency matrix, as defined in [50].

In order to reduce the number of equations the circuit can be divided into a linear subcircuit, a nonlinear subcircuit and an excitation subcircuit, as shown in Fig. 8. Then, the quantities in (28) can be limited to the connection nodes with $\boldsymbol{Y}$ being the equivalent admittance matrix for the linear subcircuit. Further reduction can be achieved by replacing the linear and the excitation subcircuits by their Norton equivalent at the nonlinear ports. The state variables are then limited to the nonlinear port voltages, and $\boldsymbol{I}_{ss}$ and $\boldsymbol{Y}$ represent the Norton equivalent.

To use the Newton method to solve the complex HB equations, (28) is reorganized into the following real equation form by splitting the real and imaginary parts of the complex quantities

$$\overline{\boldsymbol{F}}(\overline{\boldsymbol{V}}) = \overline{\boldsymbol{I}}(\overline{\boldsymbol{V}}) + \overline{\boldsymbol{\Omega}}\,\overline{\boldsymbol{Q}}(\overline{\boldsymbol{V}}) + \overline{\boldsymbol{Y}}\,\overline{\boldsymbol{V}} + \overline{\boldsymbol{I}}_{ss} = \boldsymbol{0} \tag{29}$$

where a bar stands for real quantities resulting from their complex counterparts. For example,

$$\overline{\boldsymbol{V}} = \begin{bmatrix} \text{Real } (\boldsymbol{V}) \\ \text{Imag } (\boldsymbol{V}) \end{bmatrix}, \quad \overline{\boldsymbol{F}} = \begin{bmatrix} \text{Real } (\boldsymbol{F}) \\ \text{Imag } (\boldsymbol{F}) \end{bmatrix}$$

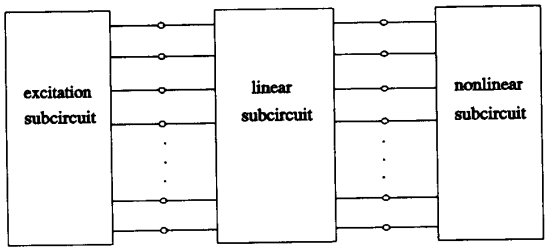

Fig. 8. Partition of a circuit for harmonic balance simulation.

and $\overline{\boldsymbol{\Omega}}$ is a frequency matrix which can be written as

$$\overline{\boldsymbol{\Omega}} = \begin{bmatrix} -\boldsymbol{\Omega}(0) & & & & \\ & -\boldsymbol{\Omega}(\omega_1) & & & \\ & & \cdots & & \\ & & & -\boldsymbol{\Omega}(\omega_H) & \\ \boldsymbol{\Omega}(0) & & & & \\ & \boldsymbol{\Omega}(\omega_1) & & & \\ & & \cdots & & \\ & & & \boldsymbol{\Omega}(\omega_H) & \end{bmatrix} \tag{30}$$

where $\boldsymbol{\Omega}(\omega_i)$ is a diagonal matrix whose diagonal elements are ω_i's. H is the number of harmonics used in the simulation.

It should be noted that the size of the system of equations (28) is directly proportional to the number of harmonics H. It is known that the trigonometric Fourier series exhibits slow convergence. Therefore, truncating the number of harmonic components, needed for efficiency or even feasibility, may strongly affect accuracy and convergence of the HB method, especially for high nonlinearities or excitations with many spectral components.

B. Integration of Physics-Based Model with HB Equations

We now turn to the problem of efficient integration of the MESFET PBM described in Section II into the HB equations (29). The model is solved in the time domain for the gate, drain and source currents at given intrinsic voltages. In order to do that, however, one must first determine the value of the intermediate parameter v_1 in (16). In the original approach [142]–[144], the "pseudo-static" dc condition $i_{dc} = -i_{sc}$ was used to solve for v_1. This condition is valid at dc only when the displacement currents of (21)–(23) assume zero values. For instantaneous currents under ac excitations both terms in (21)–(23) must be considered. Solving first for v_1 would require an additional iteration loop within the HB Newton iteration.

To avoid such a double iteration loop, our implementation treats v_1 of (16b) as an additional state variable, although it has no circuit interpretation. v_1 is directly in-

tegrated into the HB equations and allowed to vary w.r.t. time, RF input levels, and operating frequencies [8], while satisfying the boundary conditions (16). Including v_1 in the state variable vector requires augmenting (28) by the KCL equation for the pseudo-node "Z", as indicated in Fig. 4. This procedure is applied to all FETs in the circuit. For example, for a single FET circuit the state vector can be defined as

$$\boldsymbol{v}(\phi, t) = [v_1(\phi, t)\ v_{gs}(\phi, t)\ v_{ds}(\phi, t)]^T. \quad (31)$$

The nonlinear current and charge vectors of (27) can be expressed as

$$\boldsymbol{i}(\phi, \boldsymbol{v}(\phi, t), t) = \boldsymbol{A}\begin{bmatrix} i_{gc}(\phi, \boldsymbol{v}(\phi, t), t) \\ i_{dc}(\phi, \boldsymbol{v}(\phi, t), t) \\ i_{sc}(\phi, \boldsymbol{v}(\phi, t), t) \end{bmatrix} \quad (32)$$

and

$$\boldsymbol{q}(\phi, \boldsymbol{v}(\phi, t), t) = \boldsymbol{B}\begin{bmatrix} q_g(\phi, \boldsymbol{v}(\phi, t), t) \\ q_d(\phi, \boldsymbol{v}(\phi, t), t) \\ q_s(\phi, \boldsymbol{v}(\phi, t), t) \end{bmatrix} \quad (33)$$

where $\boldsymbol{A}$ and $\boldsymbol{B}$ are simple incidence matrices containing 0's, 1's, and/or -1's needed to express the terminal currents and charges in terms of quantities used in (21)–(23). For an arbitrary value of v_1 (21)–(23) may not satisfy the current continuity condition

$$i_g(t) + i_d(t) + i_s(t) = 0. \quad (34)$$

However, if we augment the HB equations

$$\bar{\boldsymbol{F}}(\phi, \bar{\boldsymbol{V}}(\phi)) = \bar{\boldsymbol{I}}(\phi, \bar{\boldsymbol{V}}(\phi)) + \bar{\boldsymbol{\Omega}}\bar{\boldsymbol{Q}}(\phi, \bar{\boldsymbol{V}}(\phi)) + \bar{\boldsymbol{Y}}\bar{\boldsymbol{V}}(\phi) + \bar{\boldsymbol{I}}_{ss} = \boldsymbol{0} \quad (35)$$

with the admittance matrix $\bar{\boldsymbol{Y}}$ modified to include the pseudo-node "Z", which is isolated from the linear part of the circuit, the solution of (35) ensures current continuity for all harmonics, i.e.,

$$\bar{\boldsymbol{I}}_g + \bar{\boldsymbol{I}}_d + \bar{\boldsymbol{I}}_s = \boldsymbol{0}. \quad (36)$$

This ensures the current continuity condition (34) in the time domain. Therefore, our formulation is valid not only for dc but also for small- and large-signal RF operations, and it does not require a double iteration loop.

C. Notes on Solving the HB Equations

The Newton update for solving the HB equations can be written as

$$\bar{\boldsymbol{V}}_{\text{new}}(\phi) = \bar{\boldsymbol{V}}_{\text{old}}(\phi) - [\bar{\boldsymbol{J}}(\phi, \bar{\boldsymbol{V}}_{\text{old}}(\phi))]^{-1}\bar{\boldsymbol{F}}(\phi, \bar{\boldsymbol{V}}_{\text{old}}(\phi)) \quad (37)$$

where $\bar{\boldsymbol{J}}(\phi, \bar{\boldsymbol{V}}(\phi))$ is the Jacobian matrix used in the algorithm. From (35) (or (29)), we see that the Jacobian has the form

$$\bar{\boldsymbol{J}}(\phi, \bar{\boldsymbol{V}}(\phi)) = \left[\frac{\partial \bar{\boldsymbol{I}}^T(\phi, \bar{\boldsymbol{V}}(\phi))}{\partial \bar{\boldsymbol{V}}(\phi)}\right]^T + \bar{\boldsymbol{\Omega}}\left[\frac{\partial \bar{\boldsymbol{Q}}^T(\phi, \bar{\boldsymbol{V}}(\phi))}{\partial \bar{\boldsymbol{V}}(\phi)}\right]^T + \bar{\boldsymbol{Y}}. \quad (38)$$

Note that in solving the HB equations, ϕ is constant and $\bar{\boldsymbol{V}}(\phi)$ is variable. Following [50], in order to calculate the entries of $\bar{\boldsymbol{J}}(\phi, \bar{\boldsymbol{V}}(\phi))$, we must first obtain the time-domain derivatives of $\boldsymbol{i}$ and $\boldsymbol{q}$ w.r.t. $\boldsymbol{v}$. The time-domain derivatives of $\boldsymbol{i}$ and $\boldsymbol{q}$ w.r.t. $\boldsymbol{v}$ are evaluated by differentiating the corresponding terms of (21)–(23) w.r.t. $\boldsymbol{v}$. After the derivatives of $\boldsymbol{i}$ and $\boldsymbol{q}$ w.r.t. $\boldsymbol{v}$ are obtained, the entries of the Jacobian matrix $\bar{\boldsymbol{J}}$ can be evaluated by the Fourier transform.

Since v_1 is considered as a state variable, the entries of $\bar{\boldsymbol{J}}(\phi, \bar{\boldsymbol{V}}(\phi))$ include the derivatives of $\bar{\boldsymbol{I}}$ and $\bar{\boldsymbol{Q}}$ w.r.t. $\bar{\boldsymbol{V}}_1$. For instance, if $\bar{\boldsymbol{I}}_{dc}(\phi, \bar{\boldsymbol{V}}(\phi), \omega_k)$ denotes the split real and imaginary parts of the kth harmonic component of the drain conduction current and $\bar{\boldsymbol{V}}_1(\phi, \omega_l)$ represents the split real and imaginary parts of the lth harmonic component of variable v_1, then

$$\frac{\partial \bar{\boldsymbol{I}}_{dc}^T(\phi, \bar{\boldsymbol{V}}(\phi), \omega_k)}{\partial \bar{\boldsymbol{V}}_1(\phi, \omega_l)} = \begin{bmatrix} G_{v_1}^R(\omega_{k-l}) + G_{v_1}^R(\omega_{k+l}) & G_{v_1}^I(\omega_{k+l}) - G_{v_1}^I(\omega_{k-l}) \\ G_{v_1}^I(\omega_{k-l}) + G_{v_1}^I(\omega_{k+l}) & G_{v_1}^R(\omega_{k-l}) - G_{v_1}^R(\omega_{k+l}) \end{bmatrix}^T \quad (39)$$

where

$$G_{v_1}^R(\omega_i) \triangleq \frac{1}{T_0}\int_0^{T_0} \frac{\partial i_{dc}(\phi, \boldsymbol{v}(\phi), t)}{\partial v_1(\phi, t)} \cos(\omega_i t)\, dt \quad (40a)$$

and

$$G_{v_1}^I(\omega_i) \triangleq -\frac{1}{T_0}\int_0^{T_0} \frac{\partial i_{dc}(\phi, \boldsymbol{v}(\phi), t)}{\partial v_1(\phi, t)} \sin(\omega_i t)\, dt \quad (40b)$$

and ω_i is the ith harmonic frequency. T_0 is the fundamental period. The time-domain derivative in (40) is evaluated by differentiating (24) w.r.t. v_1

$$\frac{\partial i_{dc}}{\partial v_1} = -qW\int_0^a \left(\frac{\partial \mu}{\partial E}\frac{\partial E}{\partial v_1} nE_x + \mu\frac{\partial n}{\partial v_1}E_x + \mu n\frac{\partial E_x}{\partial v_1} + D\frac{\partial(\nabla_x n)}{\partial v_1}\right)_{x=L} dy. \quad (41)$$

Equation (41) involves additional integrations, so in our actual implementation the perturbation technique is used instead.

In Section IV we discuss further utilization of the Jacobian matrix $\bar{\boldsymbol{J}}$ at the solution of the HB equations: it can be reused in adjoint analysis for optimization.

IV. Gradient-Based Optimization

Circuit design optimization with ECMs has been extensively studied and is available in some commercial software packages. Such optimization adjusts passive components to achieve desired circuit performance or yield with fixed active devices. Little work has been devoted so far to design optimization with PBMs. This section addresses several aspects of physics-based circuit design using gradient optimization and HB simulation.

A. Sensitivity Analysis

To facilitate efficient gradient-based optimization for circuit design we need to provide the optimizer with the gradient, i.e., the partial derivatives of circuit responses w.r.t. design variables. This is commonly referred to as sensitivity analysis. The most popular method of sensitivity analysis is the conventional *P*erturbation *A*pproximate *S*ensitivity *T*echnique (PAST). In this method, the first-order derivative of $f(\phi)$ w.r.t. ϕ_i is estimated by

$$\frac{\partial f(\phi)}{\partial \phi_i} = \frac{f(\phi + \Delta\phi_i \boldsymbol{u}_i) - f(\phi)}{\Delta\phi_i} \tag{42}$$

where $\Delta\phi_i \boldsymbol{u}_i$ denotes the perturbation of the ith variable, $\Delta\phi_i$ is the perturbation size and $\boldsymbol{u}_i$ is a unit vector which has 1 in the ith position and zeros elsewhere. This method is straightforward and easy to implement. However, it may not be accurate enough and the computational effort involved, especially for large-scale problems, may be prohibitive.

Bandler, Chen, Daijavad and Madsen [153] proposed an *I*ntegrated *G*radient *A*pproximation *T*echnique (IGAT) which utilizes the Broyden update [154]

$$\nabla f(\phi_{\text{new}}) = \nabla f(\phi_{\text{old}}) + \frac{f(\phi_{\text{new}}) - f(\phi_{\text{old}}) - (\nabla f(\phi_{\text{old}}))^T \Delta\phi}{\Delta\phi^T \Delta\phi} \Delta\phi \tag{43}$$

and the special iteration of Powell [155]. Perturbations with (42) are used to obtain an initial approximation as well as regular corrections. ϕ_{old} and ϕ_{new} are two different points and $\Delta\phi = \phi_{\text{new}} - \phi_{\text{old}}$. IGAT is robust and has been applied to both microwave performance-driven design [153] and yield optimization [63].

Efficient and accurate sensitivity analysis for HB can be achieved by the *E*xact *A*djoint *S*ensitivity *T*echnique (EAST) developed by Bandler, Zhang and Biernacki [156], which is a generalization of the linear adjoint sensitivity analysis technique. For example, the sensitivity of an output voltage V_{out} w.r.t. a parameter ϕ_i of a nonlinear element at branch b can be expressed by

$$\frac{\partial \overline{V}_{\text{out}}}{\partial \phi_i} = \begin{cases} -\sum_k \text{Real}\,[\hat{V}_b(k)\, G_b^*(k)] \\ \quad \text{if } \phi_i \in \text{nonlinear current sources} \\ -\sum_k \text{Imag}\,[\hat{V}_b(k)\, G_b^*(k)] \\ \quad \text{if } \phi_i \in \text{nonlinear capacitors} \end{cases} \tag{44}$$

where the complex quantity $\hat{V}_b(k)$ is the voltage of branch b at harmonic k and is obtained from the adjoint network. $G_b(k)$ denotes the sensitivity expression of the element containing variable ϕ_i [156]. * stands for the conjugate of a complex number. This technique exhibits high accuracy and computational efficiency but suffers from implementation complexity.

To combine the efficiency of EAST and simplicity of PAST, Bandler *et al.* proposed the *F*easible *A*djoint *S*ensitivity *T*echnique (FAST) [157]. It features high speed gradient computation as well as ease in implementation. It is particularly suitable for general purpose CAD programs. We choose FAST here for incorporating PBMs into efficient gradient-based optimization.

B. Integration of FAST with Physics-Based Models

Consider a vector of circuit responses

$$\boldsymbol{R}(\phi) = \mathfrak{R}(\phi, \overline{V}(\phi)) \tag{45}$$

which may include output voltages, currents, powers, power gains, etc. Let $\boldsymbol{S}$ be a set of design specifications. Then the objective function for a design problem can be expressed as

$$U(\phi) = U(\boldsymbol{R}(\phi), \boldsymbol{S}). \tag{46}$$

The corresponding design optimization problem is to

$$\underset{\phi}{\text{minimize}}\ U(\phi). \tag{47}$$

In order to use a gradient-based optimizer to solve (47), the derivatives of U w.r.t. each variable ϕ_i in ϕ need to be calculated. Let ϕ_i be a generic design variable such as a device dimension or doping density. The sensitivity of U w.r.t. ϕ_i can be obtained by differentiating (46) w.r.t. ϕ_i

$$\frac{\partial U}{\partial \phi_i} = \left[\frac{\partial U}{\partial \boldsymbol{R}}\right]^T \frac{\partial \boldsymbol{R}}{\partial \phi_i}. \tag{48}$$

$\partial U/\partial \boldsymbol{R}$ depends on the form of the objective function. $\partial \boldsymbol{R}/\partial \phi_i$ can be derived from (45) as

$$\frac{\partial \boldsymbol{R}(\phi)}{\partial \phi_i} = \frac{\partial \mathfrak{R}(\phi, \overline{V}(\phi))}{\partial \phi_i} + \left[\frac{\partial \mathfrak{R}^T(\phi, \overline{V}(\phi))}{\partial \overline{V}(\phi)}\right]^T \frac{\partial \overline{V}(\phi)}{\partial \phi_i} \tag{49}$$

where $\partial \mathfrak{R}/\partial \phi_i$ and $\partial \mathfrak{R}^T/\partial \overline{V}$ may be calculated analytically or by perturbation. The FAST technique is applied to calculate $\partial \overline{V}/\partial \phi_i$.

Assume that the solution of the HB equation is $\overline{V} = \overline{V}_{\text{sol}}$, i.e.,

$$\overline{F}(\phi, \overline{V}_{\text{sol}}) = \boldsymbol{0}. \tag{50}$$

The FAST technique approximates the gradient by

$$\bar{e}^T \frac{\partial \overline{V}(\phi)}{\partial \phi_i} \approx -\hat{\overline{V}}^T \frac{\overline{F}(\phi + \Delta\phi_i \boldsymbol{u}_i, \overline{V}_{\text{sol}})}{\Delta\phi_i} \tag{51}$$

where $\bar{e}$ is a vector containing 1's and 0's used to select the real or imaginary part of an output voltage of interest.

$\hat{\bar{V}}$ is obtained by solving the adjoint system

$$[\bar{J}(\phi, \bar{V}(\phi))]^T \hat{\bar{V}} = \bar{e} \tag{52}$$

where $\bar{J}(\phi, \bar{V}(\phi))$ is the Jacobian matrix, as defined by (38), at the solution of the HB equations. In an efficient implementation, it can be available in the form of LU factors.

As an example, consider the sensitivity of an output voltage w.r.t. the gate width W of a FET, i.e., $\bar{e}^T(\partial \bar{V}(\phi)/\partial W)$. We need to obtain the adjoint solution $\hat{\bar{V}}$ and evaluate the HB residual function $\bar{F}(W + \Delta W, \bar{V}_{\text{sol}})$. By reusing the Jacobian matrix available at the HB solution, the adjoint system can be solved with relatively little additional effort. The HB residual function is evaluated from (34) as

$$\begin{aligned}\bar{F}(W + \Delta W, \bar{V}_{\text{sol}}) &= \bar{I}(W + \Delta W, \bar{V}_{\text{sol}}) \\ &\quad + \bar{\Omega}\bar{Q}(W + \Delta W, \bar{V}_{\text{sol}}) \\ &\quad + \bar{Y}\bar{V}_{\text{sol}} + \bar{I}_{ss}. \end{aligned} \tag{53}$$

Note that $\bar{V}_{\text{sol}}$ is constant at this stage, so no iterations are necessary. For instance, i_{dc}, needed to evaluate the first term in the r.h.s. of (53), can be calculated by replacing W by $W + \Delta W$ in (24), where E and n are determined from v_{sol}, the inverse Fourier transform of $\bar{V}_{\text{sol}}$. The resulting i_{dc} is then transformed to the frequency domain and used in (53). This provides a high speed yet simple gradient evaluation procedure for gradient optimizers.

C. Algorithm for Optimization

Step 1: Initialization for Optimization.

Step 1.1: Input the circuit topology, design specifications, matching circuit elements and device physical parameters.

Step 1.2: Initialize the design variable vector ϕ. Assign values to all parameters in the circuit including the physical parameters and parasitic parameters of the FETs.

Step 2: Time Domain Simulation.

Step 2.1: Initialize $\bar{V}(\phi)$.

Step 2.2: Convert $\bar{V}(\phi)$ to $\boldsymbol{v}(\phi, t)$, i.e., v_1, v_{gs} and v_{ds}, using the inverse Fourier transform. Calculate the gate, drain and source conduction currents $\boldsymbol{i}(\phi, \boldsymbol{v}(\phi, t), t)$ and gate, drain and source total charges $\boldsymbol{q}(\phi, \boldsymbol{v}(\phi, t), t)$.

Step 3: Frequency Domain Simulation.

Step 3.1: Use the forward Fourier transform to obtain $\bar{I}(\phi, \bar{V}(\phi))$ and $\bar{Q}(\phi, \bar{V}(\phi))$ from $\boldsymbol{i}(\phi, \boldsymbol{v}(\phi, t), t)$ and $\boldsymbol{q}(\phi, \boldsymbol{v}(\phi, t), t)$.

Step 3.2: Solve the HB equations using the Newton update (37). Note that at this stage ϕ is constant and $\bar{V}(\phi)$ is variable. If $\bar{V}(\phi)$ is the solution of the HB equations $\bar{F}(\phi, \bar{V}(\phi)) = \mathbf{0}$, then go to *Step 4*. Otherwise, update $\bar{V}(\phi)$ and go to *Step 2.2*.

Step 4: Optimization of Parameter ϕ.

Step 4.1: If ϕ is optimal, stop.

Step 4.2: Solve the adjoint system (52) using the Jacobian matrix at the solution of the HB equations. Calculate $\partial \bar{V}(\phi)/\partial \phi_i$ using (51). Evaluate $\partial \boldsymbol{R}(\phi)/\partial \phi_i$ using (49) and then $\partial U(\phi)/\partial \phi_i$ using (48), for $i = 1, 2, \cdots, n$, where n is the number of optimizable parameters.

Step 4.3: Update ϕ according to the optimization algorithm. Go to *Step 2*.

This algorithm is illustrated by the flowchart in Fig. 9.

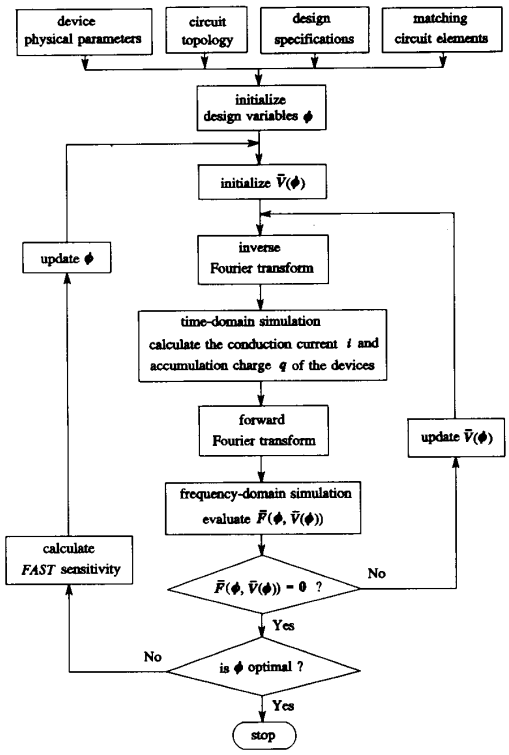

Fig. 9. Flowchart for design optimization of nonlinear FET circuits using HB.

V. Statistical Modeling

Statistical variations of device parameters in the manufacturing process cause performance deviations. The ultimate purpose of statistical modeling is to characterize devices for accurate yield analysis and optimization. In this section we address statistical modeling of FETs with PBMs.

A. Parameter Extraction and Statistical Estimation

Our approach to statistical modeling is based on parameter extraction and statistical estimation through postprocessing. It requires measurements taken on a large sample of devices, which may include dc, small-signal and large-signal data. For each device, the model parameters are extracted from the corresponding measurements, resulting in a sample of models. This sample of models is postprocessed to estimate the statistics of the model parameters, including the mean values, standard deviations,

correlation matrix, etc. Efficient, consistent and reliable parameter extraction is essential for this approach.

Suppose we have K sets of measurement data, each containing m measured responses

$$\boldsymbol{S}^i = [S_1^i \quad S_2^i \quad \cdots \quad S_m^i]^T \tag{54}$$

corresponding to the ith device, $i = 1, 2, \cdots, K$, where K is the total number of devices measured. Let

$$\boldsymbol{\phi}^i = [\phi_1^i \quad \phi_2^i \quad \cdots \quad \phi_n^i]^T \tag{55}$$

denote the model parameters of the ith device and

$$\boldsymbol{R}(\boldsymbol{\phi}^i) = [R_1(\boldsymbol{\phi}^i) \quad R_2(\boldsymbol{\phi}^i) \quad \cdots \quad R_m(\boldsymbol{\phi}^i)]^T \tag{56}$$

be the model responses corresponding to the measurements $\boldsymbol{S}^i$. The parameter extraction problem can be formulated as

$$\min_{\boldsymbol{\phi}^i} \sum_{j=1}^{m} w_j^i |R_j(\boldsymbol{\phi}^i) - S_j^i|^p \qquad 1 \le p \tag{57}$$

where w_j^i is a weighting factor and $p = 1$ or $p = 2$ leads to ℓ_1 or ℓ_2 (least squares) optimization, respectively. Optimization is performed for each device measured, i.e., for $i = 1, 2, \cdots, K$.

Often, a multidimensional normal distribution is assumed for the model parameters. It is fully described by the mean values, standard deviations and pair-wise correlation coefficients estimated from the sample of models. In cases where the sample distribution appears substantially different from normal, we utilize the marginal discrete density function (DDF) approach [84]. A discretized joint probability density function has also been proposed [74], [158].

B. Statistical ECMs

Statistical models can be considered at the device response level, the equivalent circuit model level (statistical ECMs) and the physical parameter level (statistical PBMs), as shown in Fig. 10.

ECM statistical modeling attempts to characterize the distribution of the equivalent circuit parameters such as inductances and capacitances [73], [84]. The main advantage of this approach is that many ECMs are available in microwave CAD software and ECM simulation is usually efficient. However, it is difficult or even impossible to relate the statistical distributions of ECM parameters to those of the device physical parameters. Statistical variations in a single physical parameter may affect many ECM parameters, and at the same time each ECM parameter may be affected by many physical parameters. Consequently, the equivalent circuit model parameters are correlated and such correlations are difficult to estimate. Furthermore, this nonlinear mapping may result in complicated and non-Gaussian distributions.

In a recent paper by Bandler *et al.* [86], statistical modeling of GaAs MESFETs using the Materka ECM [3] was investigated. Even though for individual device models the fit of the ECM responses to the measurements is excellent, the statistical model based on the extracted ECM sample fails to satisfactorily reproduce the original measurement statistics.

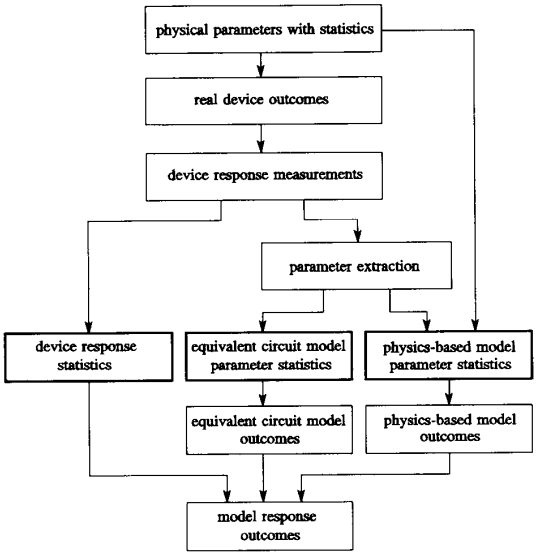

Fig. 10. Different levels of statistical modeling.

C. Statistical PBMs

Statistical PBMs characterize the distributions of device physical parameters [86]. With PBMs it is easier to identify the parameters that are subject to significant statistical variations and the parameters which are correlated (e.g., geometrical dimensions). The statistics of some physical parameters may even be directly available from measurements. At this level, the typical assumption of normal distribution is often justified. Unlike ECMs, by attempting to characterize statistical behavior of the parameters that are actually subject to random variations in the real world, PBM statistical modeling is closer to reality and we believe it is more accurate and reliable. An obvious disadvantage of PBMs is that simulation may be more time consuming.

As an example, we use the Ladbrooke model [159] and the Khatibzadeh and Trew model [144] to illustrate PBM statistical modeling.

The Ladbrooke model uses a small-signal equivalent circuit whose component values are derived from the physical parameters and the bias conditions. The equivalent circuit of the Ladbrooke model is shown in Fig. 11. g_m, τ, r_0, C_{gs}, C_{gd}, R_i, R_d, R_s, and L_g are functions of the physical parameters and bias conditions, for example [159],

$$g_m = \frac{\epsilon v_s W}{d} \tag{58}$$

$$C_{gd} = \frac{2\epsilon W}{1 + \dfrac{2X}{L}} \tag{59}$$

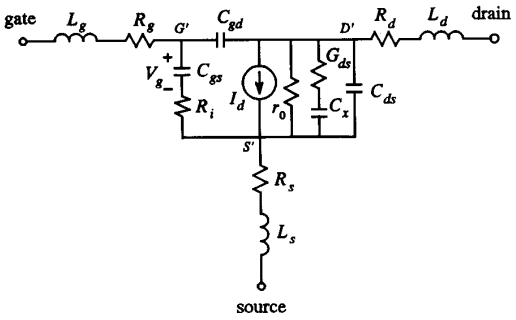

Fig. 11. Topology for the Ladbrooke GaAs MESFET small-signal model where $I_d = g_m V_g \exp(-j\omega\tau)$.

$$L_g = \frac{\mu_0\, dW}{m^2 L} + L_{g0} \tag{60}$$

where ϵ is the permittivity of GaAs, v_s the saturation electron drift velocity, W the gate width, L the gate length, μ_0 the permeability of free space, m the number of gate fingers, and L_{g0} is introduced to include the inductances from gate bond wires and pads. d is the equivalent depletion depth which is determined as

$$d = \sqrt{2\epsilon \frac{V_{B0} - V_{G'S'}}{qN_d}} \tag{61}$$

and X is the voltage dependent space-charge layer extension calculated as

$$X = a_0(V_{D'G'} + V_{B0}) \sqrt{\frac{2\epsilon}{qN_d(V_{B0} - V_{G'S'})}} \tag{62}$$

where V_{B0} is the zero-bias barrier potential, N_d the doping density, and a_0 is a proportionality coefficient. In our implementation the drain output resistor r_0 is approximated by [86]

$$r_0 = r_{01} V_{D'S'}(r_{03} - V_{G'S'}) + r_{02} \tag{63}$$

where r_{01}, r_{02} and r_{03} are fitting parameters, $V_{G'S'}$, $V_{D'G'}$ and $V_{D'S'}$ are the intrinsic gate-to-source, drain-to-gate and drain-to-source dc operating voltages, respectively (see Fig. 11). R_g, L_d, L_s, G_{ds} and C_{ds} are assumed to be linear elements. The value of the gate width W is known and we keep it as a constant. The model parameters to be extracted are

$$\{L,\ a,\ N_d,\ v_s,\ V_{B0},\ a_0,\ r_{01},\ r_{02},\ r_{03},\ L_{g0},$$
$$R_g,\ L_d,\ L_s,\ G_{ds},\ C_{ds}\}$$

where a is the channel thickness.

The parameters of the Khatibzadeh and Trew model are listed in Table I.

Statistical modeling was performed on a sample of GaAs MESFET measurements provided by Plessey Research Caswell [151]. 69 individual devices (data sets) from two wafers were used. Each device represents a four finger 0.5 μm gate length GaAs MESFET with equal finger width of 75 μm. Each data set contains small-signal S parameters measured under three different bias conditions and at frequencies from 1 GHz to 21 GHz with a 0.4 GHz step. The dc drain bias current is also included in the measurements.

HarPE [128] was used to carry out statistical modeling. Parameter extraction was performed first for each individual device by matching simultaneously the dc and small-signal S-parameter responses to the corresponding measurements [6]. Then, the resulting sample of 69 models was postprocessed to obtain the mean values of the parameters. In order to improve consistency of the parameter extraction process, individual device models were extracted again using those mean values as the initial starting point. The new resulting sample of models was then postprocessed to obtain the parameter statistics, including the mean values, standard deviations, discrete distribution functions (DDF) [84], as well as the correlation matrix.

The parameter mean values and standard deviations for the Ladbrooke model and for the Khatibzadeh and Trew model are listed in Table III. The histograms of the FET gate length L and doping density N_d for both models are shown in Figs. 12 and 13. Table III indicates that there exist significant discrepancies in some common parameters in the two models. For example, the standard deviations of the parameters of the Khatibzadeh and Trew model are noticeably smaller than those of the Ladbrooke model. Although slight differences may exist because of different approximations and structures adopted by the two models these results are not satisfactory and further investigation is under way [160].

The two statistical models were examined using Monte Carlo simulations. The statistical S-parameter responses generated by the models were compared with the measurements. The comparison was made at the bias point $V_{GS} = 0$ V and $V_{DS} = 5$ V and at the frequency 11 GHz. Monte Carlo simulation was performed with 400 outcomes from the mean values, standard deviations, correlations and DDFs of the model parameters. The mean values and standard deviations of the measured and the simulated S parameters from the Ladbrooke model and from the Khatibzadeh and Trew model are listed in Table IV. The histograms of one S parameter are plotted in Fig. 14.

The match of the standard deviations of the measured S parameters and of those simulated by the Ladbrooke model is quite good, as shown in Table IV. The mean values from the Ladbrooke model do not fit the measurements well, which may indicate that the model is not flexible enough. The mean value match by the Khatibzadeh and Trew model is better than that by the Ladbrooke model. However, the standard deviations of the S parameters from the Khatibzadeh and Trew model are smaller than those from the measurements except for $|S_{21}|$. This is consistent with the observation that the standard deviations in the Khatibzadeh and Trew model are very small (see Table III).

TABLE III
STATISTICAL PARAMETERS FOR THE LADBROOKE AND THE KHATIBZADEH AND TREW MODELS

Ladbrooke Model			Khatibzadeh and Trew Model		
Parameter	Mean	Deviation (%)	Parameter	Mean	Deviation (%)
L (μm)	0.559	2.93	L (μm)	0.5496	1.29
a (μm)	0.1059	3.64	a (μm)	0.1310	1.38
N_d ($1/m^3$)	3.140×10^{23}	1.71	N_d ($1/m^3$)	2.219×10^{23}	0.98
v_s (m/s)	7.608×10^4	3.48	W (μm)	295.24	1.48
V_{B0} (V)	0.6785	4.94	V_{bi} (V)	0.699	1.62
a_0	1.031	7.03	μ_0 (m^2/Vs)	0.3932	1.16
r_{01} (Ω/V^2)	1.090×10^{-2}	0.44	E_c (V/m)	3.255×10^5	1.38
r_{02} (Ω)	628.2	6.86	R_d (Ω)	4.001	0.06
r_{03} (V)	13.99	0.44	R_s (Ω)	1.697	0.17
R_g (Ω)	3.392	4.99	R_g (Ω)	3.500	0.12
L_{g0} (nH)	2.414×10^{-2}	20.7	L_g (nH)	2.94×10^{-2}	0.13
L_d (nH)	6.117×10^{-2}	18.6	L_d (nH)	8.0×10^{-3}	0.06
L_s (nH)	2.209×10^{-2}	10.6	L_s (nH)	3.9×10^{-2}	0.85
G_{ds} ($1/\Omega$)	2.163×10^{-3}	2.72	G_{ds} ($1/\Omega$)	3.6×10^{-3}	0.61
C_{ds} (pF)	5.429×10^{-2}	2.71	C_{dc} (pF)	5.27×10^{-2}	0.78
			C_{ge} (pF)	0.1504	1.89

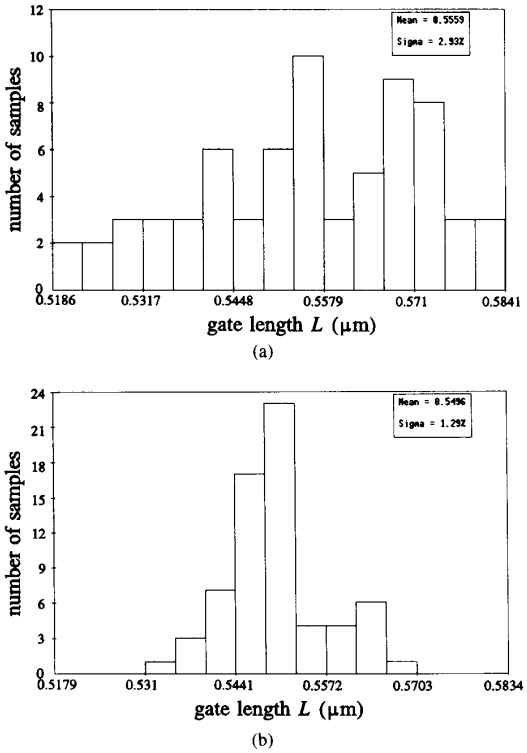

Fig. 12. Histograms of gate length L. (a) The Ladbrooke model. (b) The Khatibzadeh and Trew model.

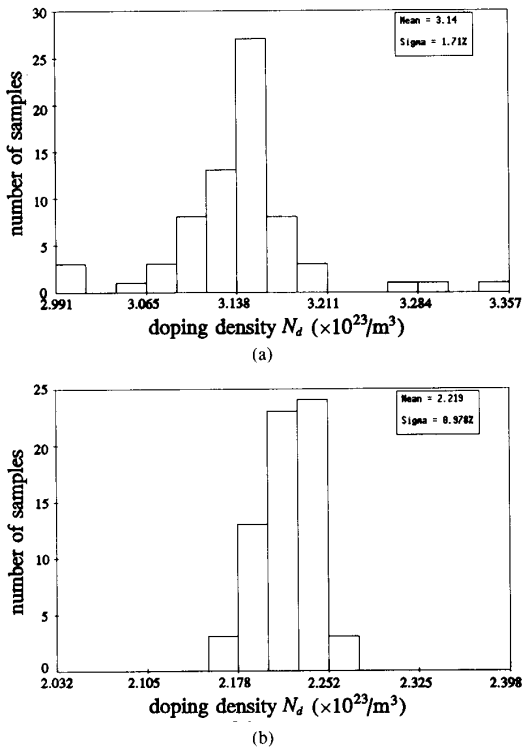

Fig. 13. Histograms of doping density N_d. (a) The Ladbrooke model. (b) The Khatibzadeh and Trew model.

VI. YIELD OPTIMIZATION OF MMICS

Random variations in the manufacturing process may lead to some circuits failing to meet design specifications. Yield optimization, which takes into account the manufacturing tolerances, model uncertainties, variations of process parameters, environmental uncertainties, etc., has become an important design tool to reduce the cost of manufacturing.

In this section, we present yield optimization of MMICs with PBMs. As design variables we directly consider physical parameters for both active devices and passive components. The parameters may include, for example, FET gate length, gate width, doping density, the number of turns of spiral inductors, geometrical dimensions of metal-insulator-metal (MIM) capacitors, etc. Statistical PBMs are employed to generate random circuit outcomes for simulation. The efficient FAST sensitivity

TABLE IV
MEAN VALUES AND STANDARD DEVIATIONS OF MEASURED AND SIMULATED S PARAMETERS AT 11 GHz

	Measured S Parameters [151]		Simulated S Parameters			
			Ladbrooke Model		Khatibzadeh and Trew Model	
	Mean	Deviation (%)	Mean	Deviation (%)	Mean	Deviation (%)
$\|S_{11}\|$	0.773	.988	.7856	.764	.8085	0.32
$\angle S_{11}$	−114.3	1.36	−119.3	1.10	−116.2	0.69
$\|S_{21}\|$	1.919	.802	1.679	1.34	1.834	1.22
$\angle S_{21}$	93.35	.856	94.06	.835	91.69	0.33
$\|S_{12}\|$	.0765	3.77	.07542	3.68	.0785	2.07
$\angle S_{12}$	34.00	2.51	31.98	2.33	31.61	0.94
$\|S_{22}\|$	0.5957	1.48	.5838	1.54	.5446	1.11
$\angle S_{22}$	−38.69	2.10	−36.86	1.42	−40.64	0.98

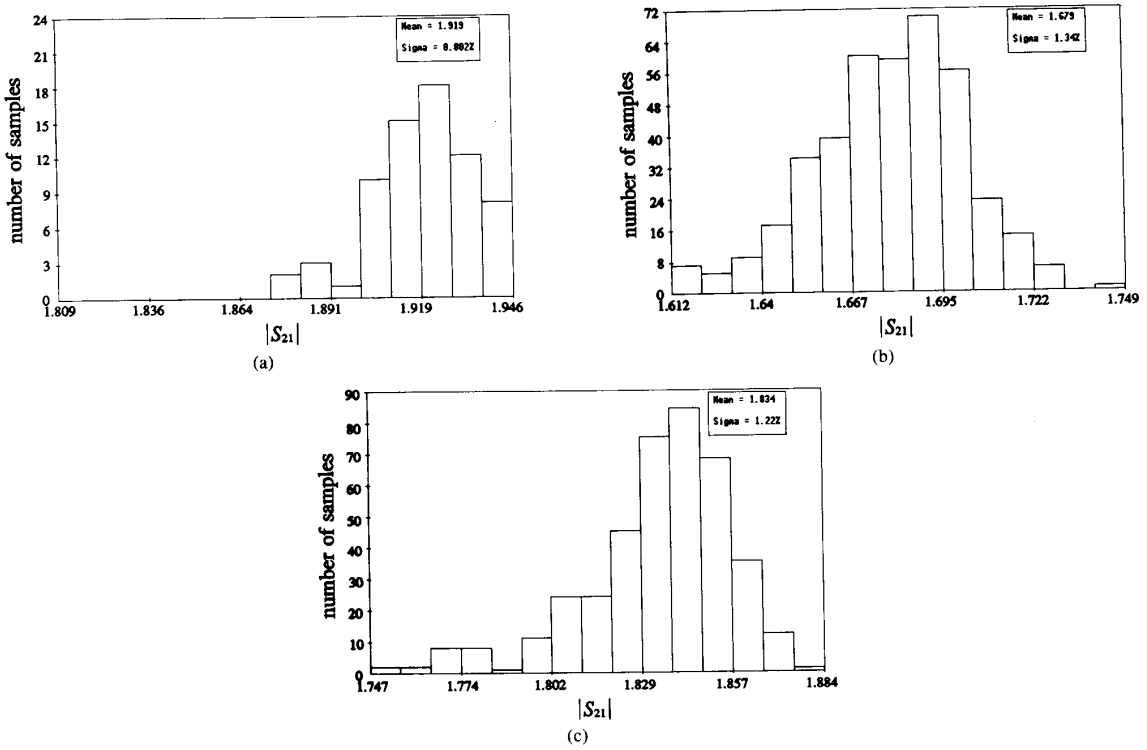

Fig. 14. Histograms of $|S_{21}|$ at $V_{GS} = 0$ V and $V_{DS} = 5$ V and at 11 GHz from: (a) measurements, (b) the Ladbrooke model, (c) the Khatibzadeh and Trew model.

technique is utilized to permit high speed gradient-based yield optimization.

A. Formulation of Yield Optimization Problem

Assume that there are N_{fail} failed circuits out of a total of N outcomes. The production yield is simply defined as

$$Y = 1 - \frac{N_{\text{fail}}}{N}. \tag{64}$$

Let the parameters of a nominal circuit be ϕ^0. The manufactured outcomes ϕ^i, $i = 1, 2, \cdots, N$, are spread around ϕ^0 according to the statistical distributions of the parameters and can be represented by

$$\phi^i = \phi^0 + \Delta\phi^i. \tag{65}$$

For the ith outcome and the jth design specification S_j, $j = 1, 2, \cdots, m$, the error is defined as

$$e_j(\phi^i) = R_j(\phi^i) - S_j \tag{66a}$$

if S_j is an upper specification, or as

$$e_j(\phi^i) = S_j - R_j(\phi^i) \tag{66b}$$

if S_j is a lower specification.

During yield optimization, which takes place at the design stage, the outcomes ϕ^i cannot be the manufactured ones. Instead, they are generated from the statistical models, and the yield optimization problem is defined for those simulated random outcomes. Let all the errors for the ith outcome be assembled into the vector

$$e(\phi^i) = [e_1(\phi^i) \quad e_2(\phi^i) \quad \cdots \quad e_m(\phi^i)]^T. \tag{67}$$

If all the entries of $e(\phi^i)$ are nonpositive, the outcome ϕ^i is acceptable, i.e., it meets all the specifications. From (67) we create the generalized ℓ_p function $v(\phi^i)$ as

$$v(\phi^i) = \begin{cases} \left(\sum\limits_{j \in J(\phi^i)} [e_j(\phi^i)]^p \right)^{1/p} & \text{if } J(\phi^i) \neq \varnothing \\ -\left(\sum\limits_{j=1}^{m} [-e_j(\phi^i)]^{-p} \right)^{-1/p} & \text{if } J(\phi^i) = \varnothing \end{cases} \tag{68}$$

where

$$J(\phi^i) = \{ j | e_j(\phi^i) \geq 0 \}. \tag{69}$$

The one-sided ℓ_1 objective function for yield optimization [72] can be formulated as

$$U(\phi^0) = \sum_{i \in I} \alpha_i v(\phi^i) \tag{70}$$

where

$$I = \{ i | v(\phi^i) > 0 \} \tag{71}$$

and α_i are positive multipliers. If we chose α_i as [72]

$$\alpha_i = \frac{1}{|v(\phi^i)|} \tag{72}$$

the value of the function $U(\phi^0)$ would be equal to N_{fail} and the yield would be

$$Y(\phi^0) = 1 - \frac{U(\phi^0)}{N}. \tag{73}$$

Hence, the relation between yield and the error functions is established, so maximization of yield can be converted to minimization of $U(\phi^0)$, i.e.,

$$\underset{\phi^0}{\text{minimize}}\ U(\phi^0). \tag{74}$$

In our implementation the α_i are assigned according to (72) only at the starting point and then they are kept fixed during optimization. As a consequence, $U(\phi^0)$ is no longer equal to N_{fail} when optimization proceeds, but it provides a continuous approximation to N_{fail} [72]. A continuous "yield probability function" has been recently proposed in [161] to be used in place of (70).

B. Physics-Based Models for MMIC Passive Components

We use the PBM described in Section II to model GaAs MESFETs. Passive components are modeled through their equivalent circuits and the corresponding n-port Y matrices. The values of the equivalent circuit elements are derived from material and geometrical parameters. Since the MMICs are manufactured on a common semi-insulating substrate these equivalent models are grounded, e.g., a "two terminal component" is represented by a two-port. From these equivalent circuits we calculate the corresponding Y matrices. In general,

$$I = Y(\phi) V \tag{75}$$

where ϕ stands for physical parameters, and I and V are port current and voltage vectors.

For MIM capacitors ϕ includes the geometrical dimensions of the metal plate, the permittivity and the thickness of the dielectric film. For spiral inductors, ϕ includes the substrate height, the conductor width and spacing, and the number of turns. The configurations and schematics of spiral inductors, MIM capacitors and planar resistors are shown in Fig. 15. For instance, the value of capacitance C in the equivalent circuit for an MIM capacitor can be evaluated by [162]

$$C = \frac{10^{-3} \epsilon_{rd} wl}{36\pi d} \tag{76}$$

where C is in pF, ϵ_{rd} is the relative permittivity of the dielectric film, w and l are the width and length of the metal plate in μm, respectively, and d is the thickness of the dielectric film in μm.

In this way all the passive components, as well as active devices (with the exception of the extrinsic parasitics), can be simulated and optimized in terms of physical parameters.

C. Quadratic Approximation of Responses and Gradients

Yield optimization requires substantial computational effort for circuit simulations and, if gradient optimization is used, for gradient evaluations. Quadratic approximation is an efficient approach for speeding up the optimization process [163], [118], [164].

In quadratic approximation the circuit response $R(\phi)$ is approximated by a multidimensional quadratic polynomial of the form

$$R(\phi) \approx a_0 + \sum_{i=1}^{n} a_i(\phi_i - r_i) + \sum_{\substack{j,i=1 \\ j \geq i}}^{n} b_{ij}(\phi_i - r_i)(\phi_j - r_j) \tag{77}$$

where

$$r = [r_1 \quad r_2 \quad \cdots \quad r_n]^T \tag{78}$$

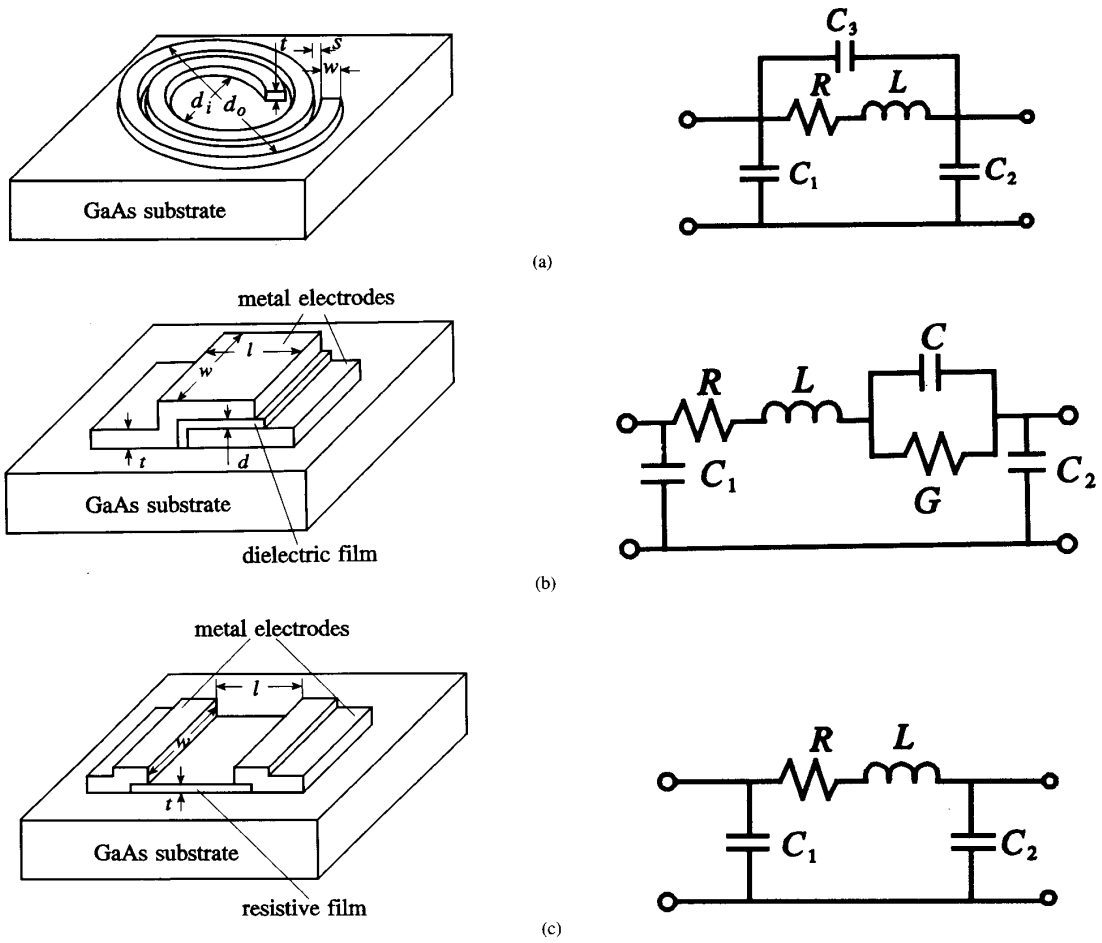

Fig. 15. Configuration of passive devices and their corresponding two port equivalent circuits [160]: (a) spiral inductor, (b) MIM capacitor and (c) planar resistor.

is a known reference point and

$$\boldsymbol{a} = [a_0 \quad a_1 \quad \cdots \quad a_n]^T \tag{79a}$$

$$\boldsymbol{b} = [b_{11} \quad b_{22} \quad \cdots \quad b_{nn} \quad b_{12} \quad b_{13} \quad \cdots \quad b_{n-1,n}]^T \tag{79b}$$

are the quadratic model parameters to be determined. According to [118], [164], $\boldsymbol{a}$ and $\boldsymbol{b}$ can be extremely efficiently determined using k, $n + 1 \leq k \leq 2n + 1$, function values calculated at k predetermined base points.

The gradient of $R(\boldsymbol{\phi})$ is a vector of functions, each function being the partial derivative of $R(\boldsymbol{\phi})$ w.r.t. one designable variable. In yield optimization we typically deal with four types of parameters, namely, n_{DS} designable variables $\boldsymbol{\phi}_{DS}$ with statistics, n_D designable variables $\boldsymbol{\phi}_D$ without statistics, n_{FS} non-designable variables $\boldsymbol{\phi}_{FS}$ with statistical variations, and n_F fixed parameters $\boldsymbol{\phi}_F$. The gradients of $R(\boldsymbol{\phi})$ with respect to the designable variables can be written as

$$\nabla R = \left[\left(\frac{\partial R}{\partial \boldsymbol{\phi}_{\mathrm{DS}}^0}\right)^T \left(\frac{\partial R}{\partial \boldsymbol{\phi}_D^0}\right)^T\right]^T. \tag{80}$$

The dimension of ∇R is $(n_{DS} + n_D)$. Each element in ∇R can also be approximated by its quadratic model of the form of (77).

For yield optimization we need to calculate all the responses of interest and their gradients at a number of statistical outcomes. Each statistical outcome is generated in a $(n_{DS} + n_{FS})$-dimensional space from the corresponding distributions of the statistical variables $\boldsymbol{\phi}_{DS}$ and $\boldsymbol{\phi}_{FS}$. Following (65), the statistical variables can be expressed as

$$\begin{aligned}\boldsymbol{\phi}_S &= [\boldsymbol{\phi}_{DS}^T \quad \boldsymbol{\phi}_{FS}^T]^T \\ &= [(\boldsymbol{\phi}_{DS}^0)^T \quad (\boldsymbol{\phi}_{FS}^0)^T]^T + [(\Delta\boldsymbol{\phi}_{DS})^T \quad (\Delta\boldsymbol{\phi}_{FS})^T]^T.\end{aligned} \tag{81}$$

For efficiency, we build the models of the circuit responses and their gradients in the $(n_{DS} + n_{FS})$-dimensional space using $\boldsymbol{\phi}_{DS}$ and $\boldsymbol{\phi}_{FS}$ as the variables in the quadratic models (77). The models are built at each optimization iteration for the updated nominal point and utilized for as many statistical outcomes as desired.

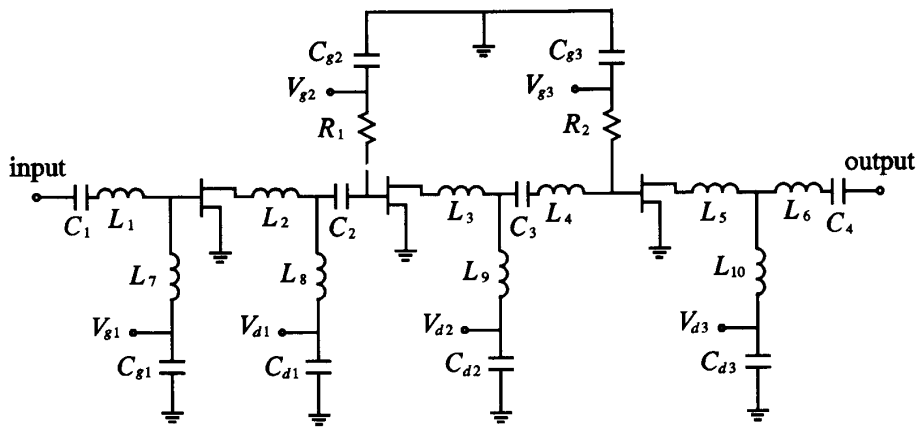

Fig. 16. Circuit diagram of an *X*-band amplifier [165].

D. FAST Gradient-Based Yield Optimization

Gradient-based yield optimization involves repeated simulation of a large number of statistical outcomes and requires sensitivity analysis to estimate the gradients of the error functions. Therefore, an effective and efficient approach to gradient calculation is very important. Two gradient estimation techniques IGAT and FAST, as discussed in Section IV, have been used in yield optimization of nonlinear circuits [63]. Here, we use FAST for physics-based yield optimization.

In order to solve the yield optimization problem (74), we need to calculate the gradients of the objective function U w.r.t. the designable variables. Let ϕ_k^0 be a generic designable variable out of ϕ^0. Differentiating (68) w.r.t. ϕ_k^0 we obtain, if $J(\phi^i) \neq \varnothing$,

$$\frac{\partial v(\phi^i)}{\partial \phi_k^0} = \left(\sum_{j \in J(\phi^i)} [e_j(\phi^i)]^p \right)^{(1/p)-1} \sum_{j \in J(\phi^i)} [e_j(\phi^i)]^{p-1} \cdot \left[\frac{\partial e_j(\phi^i)}{\partial \phi^i} \right]^T \frac{\partial \phi^i}{\partial \phi_k^0}. \tag{82}$$

From (65) we have $\partial \phi^i / \partial \phi_k^0 = \boldsymbol{u}_k$, unless a different than (65) relationship exists between ϕ^i and ϕ^0 (e.g., a relative perturbation). Following (66a) and (66b) the computation of $\partial e_j(\phi^i)/\partial \phi^i$ can be converted to the calculation of the gradients of circuit responses by expressing the gradient of $e_j(\phi^i)$ w.r.t. the lth element ϕ_l^i in ϕ^i as

$$\frac{\partial e_j(\phi^i)}{\partial \phi_l^i} = \pm \frac{\partial R_j(\phi^i)}{\partial \phi_l^i} \tag{83}$$

where the sign depends on the type of the specification S_j. If S_j is an upper (lower) specification, the positive (negative) sign is used. Finally, the FAST technique is used to evaluate $\partial R_j(\phi^i)/\partial \phi_l^i$.

E. Yield Optimization of A Three Stage X-band MMIC Amplifier

We consider a three stage small-signal *X*-band cascadable MMIC amplifier shown in Fig. 16. The design is based on the circuit topology and the fabrication layout described in [165], but with different parameter values. The amplifier contains three MESFETs using an interdigitated structure with two gate fingers of dimensions 150 μm $\times$ 1.0 μm. The matching circuits are composed of inductors and capacitors arranged in bandpass topology. All passive components are realized using lumped MMIC elements: spiral inductors, MIM capacitors and bulk resistors. The second and third MESFETs are biased through 1500 Ω GaAs bulk resistors. The drains and the first gate bias are bypassed by high value MIM capacitors. The input-output matching circuit includes a series capacitor to make the amplifier cascadable without additional components.

The amplifier is to meet the following specifications: in the passband (8 GHz–12 GHz) gain = 14 $\pm$ 1.5 dB, input and output VSWR $<$ 2.5; in the stopband (below 6 GHz or above 15 GHz) gain $<$ 2 dB.

We use the PBMs for both the MESFETs and the passive elements. Since all devices are made from the same material and on the same wafer, they share common parameters. All three MESFETs have the same values for the critical electric field, saturation velocity, relative permittivity, built-in potential, low-field mobility and high-field diffusion coefficient. All the MIM capacitors have the same dielectric film, and all bulk resistors have the same sheet resistance. The geometrical parameters can have different values for different devices, including the gate length, gate width, and channel thickness of the MESFETs, the metal plate area of the MIM capacitors, and the number of turns of the spiral inductors. The doping densities of the MESFETs are also considered as independent parameters.

First, a nominal design is performed using minimax optimization [166]. As in a traditional design, only the matching circuits are optimized. The parameters of the active devices (MESFETs) have fixed values. There are 14 design variables, namely, S_{C1}, S_{C2}, S_{C3}, S_{C4} (the area of the metal plate of MIM capacitors C_1, C_2, C_3 and C_4), n_{L1}, n_{L2}, $\cdots$, n_{L10} (the number of turns of the spiral

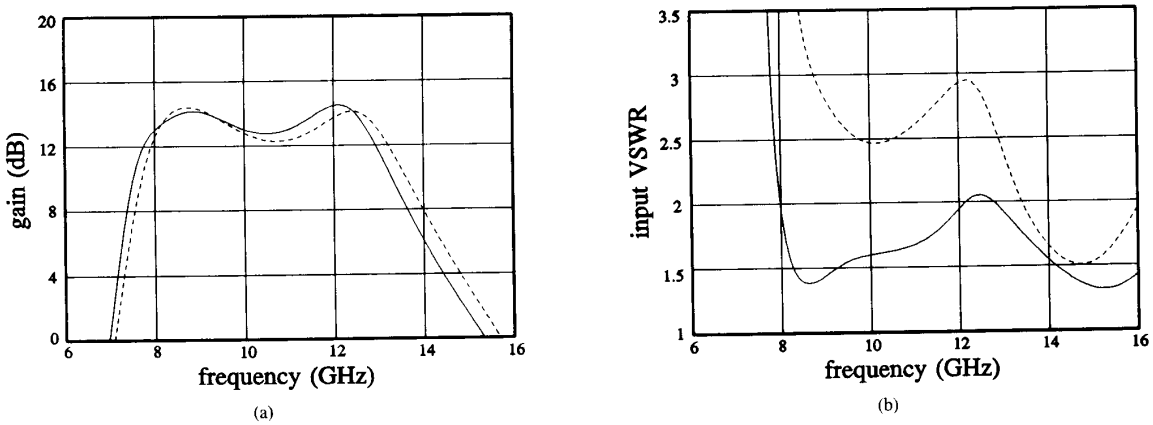

(a) (b)

Fig. 17. (a) Gain and (b) input VSWR versus frequency before (---) and after (——) nominal design optimization.

TABLE V
VARIABLES FOR NOMINAL DESIGN

Design Variable	Before Optimization	After Optimization	Design Variable	Before Optimization	After Optimization
S_{C1} (μm^2)	353.1	326.8	n_{L4}	3.68	3.63
S_{C2} (μm^2)	2014.4	2022.4	n_{L5}	2.13	2.17
S_{C3} (μm^2)	212.3	218.2	n_{L6}	2.61	2.58
S_{C4} (μm^2)	354.2	352.2	n_{L7}	2.42	2.62
n_{L1}	3.06	2.78	n_{L8}	2.45	2.43
n_{L2}	3.56	3.66	n_{L9}	2.88	2.78
n_{L3}	2.84	2.96	n_{L10}	3.09	3.01

S_{Ci} is the area of the metal plate of MIM capacitor C_i.
n_{Li} is the number of turns of the spiral inductor L_i.

TABLE VI
ASSUMED DISTRIBUTIONS FOR STATISTICAL VARIABLES

Variable	Mean	Deviation (%)	Variable	Mean	Deviation (%)
N_d ($1/m^3$)	1.0×10^{23}	7.0	d (μm)	0.1	4.0
L (μm)	1.0	3.5	S_{C1} (μm^2)	326.8	3.5
a (μm)	0.3	3.5	S_{C2} (μm^2)	2022.4	3.5
W (μm)	300	2.0	S_{C3} (μm^2)	218.2	3.5
W_L (μm)	20	3.0	S_{C4} (μm^2)	352.2	3.5
S_L (μm)	10	3.0			

The doping density N_d, gate length L, channel thickness a and gate width W of the three MESFETs have the same distribution. The conductor width W_L and spacing S_L of the 10 spiral inductors $L_1, L_2, \cdots, L_{10}$ have the same distribution. d is the thickness of the dielectric film for all MIM capacitors. S_{Ci} is the area of the metal plate of MIM capacitor C_i.

inductors $L_1, L_2, \cdots, L_{10}$). The values of the capacitors and inductors given in [165] were used to select the initial values for these variables. The nominal solution was achieved by minimax optimization after 15 iterations (about 5 minutes on a Sun SPARCstation 1). The gain and input VSWR before and after optimization are shown in Fig. 17. The values of the design variables before and after optimization are listed in Table V.

The minimax nominal design is then used as the starting point for yield optimization. A total of 37 parameters are considered as statistical variables. They include the gate length, gate width, channel thickness and doping density of the MESFETs, as well as the geometrical parameters of the passive elements. The extrinsic parasitic parameters of the MESFETs are assumed independent, nondesignable and without statistical variations. The mean values and standard deviations of the statistical variables are listed in Table VI. The correlation matrix used is given in Table VII. The most significant correlations are between the corresponding parameters for different devices. For instance, the gate lengths of the three MESFETs are strongly correlated. In addition to the number of turns of

TABLE VII
ASSUMED PARAMETER CORRELATIONS FOR THE THREE MESFETS

	a_{F1}	L_{F1}	W_{F1}	N_{dF1}	a_{F2}	L_{F2}	W_{F2}	N_{dF2}	a_{F3}	L_{F3}	W_{F3}	N_{dF3}
a_{F1}	1.00	0.00	0.00	−0.25	0.80	0.00	0.00	−0.20	0.78	0.00	0.00	−0.10
L_{F1}	0.00	1.00	0.00	−0.10	0.00	0.80	0.00	−0.05	0.00	0.78	0.00	−0.05
W_{F1}	0.00	0.00	1.00	0.00	0.00	0.00	0.80	0.00	0.00	0.00	0.78	0.00
N_{dF1}	−0.25	−0.10	0.00	1.00	−0.20	−0.05	0.00	0.80	−0.15	−0.05	0.00	0.78
a_{F2}	0.80	0.00	0.00	−0.20	1.00	0.00	0.00	−0.25	0.80	0.00	0.00	−0.20
L_{F2}	0.00	0.80	0.00	−0.05	0.00	1.00	0.00	−0.10	0.00	0.80	0.00	−0.10
W_{F2}	0.00	0.00	0.80	0.00	0.00	0.00	1.00	0.00	0.00	0.00	0.80	0.00
N_{dF2}	−0.20	−0.05	0.00	0.80	−0.25	−0.10	0.00	1.00	−0.20	−0.05	0.00	0.80
a_{F3}	0.78	0.00	0.00	−0.15	0.80	0.00	0.00	−0.20	1.00	0.00	0.00	−0.25
L_{F3}	0.00	0.78	0.00	−0.05	0.00	0.80	0.00	−0.05	0.00	1.00	0.00	−0.10
W_{F3}	0.00	0.00	0.78	0.00	0.00	0.00	0.80	0.00	0.00	0.00	1.00	0.00
N_{dF3}	−0.10	−0.05	0.00	0.78	−0.20	−0.10	0.00	0.80	−0.25	−0.10	0.00	1.00

The subscripts $F1$, $F2$ and $F3$ are used to distinguish the parameters of three different FETs.

TABLE VIII
DESIGN VARIABLES FOR YIELD OPTIMIZATION

Design Variable	Before Optimization	After Optimization	Design Variable	Before Optimization	After Optimization
a (μm)	0.3	0.31	n_{L2}	3.66	3.66
L (μm)	1.0	0.99	n_{L3}	2.96	3.03
W (μm)	300	308	n_{L4}	3.63	3.65
N_d ($1/m^3$)	1.0×10^{23}	1.03×10^{23}	n_{L5}	2.17	2.23
S_{C1} (μm^2)	326.8	322.7	n_{L6}	2.58	2.51
S_{C2} (μm^2)	2022.4	2006.3	n_{L7}	2.62	2.62
S_{C3} (μm^2)	218.2	222.9	n_{L8}	2.43	2.44
S_{C4} (μm^2)	352.2	356.7	n_{L9}	2.78	2.78
n_{L1}	2.78	2.74	n_{L10}	3.01	3.09

the 10 spiral inductors and the metal plate area of the 4 MIM capacitors, the gate length, gate width, channel thickness and doping density of the MESFETs are chosen as the variables for yield optimization.

At the starting point (i.e., the minimax nominal design), the yield was 26% as estimated by Monte Carlo analysis with 200 statistical outcomes. The yield was improved to 69% at the solution of yield optimization (about 4 and a half hours CPU time on a Sun SPARCstation 1). The solution is given in Table VIII. The Monte Carlo sweeps of gain and input VSWR before and after yield optimization are shown in Figs. 18 and 19.

VII. TWO-DIMENSIONAL (2D) FIELD-BASED MESFET SIMULATION AND MODELING

Among PBMs, field-based numerical models are considered to be the most accurate in terms of the simulation results they provide. For MESFETs, a number of numerical models such as the 2D drift-diffusion model [130], [133] have been proposed. Although conventional microwave CAD programs may have difficulties accommodating field-based models, the new generation of CAD systems should be able to do so with an open architecture. The Datapipe™ feature of OSA90/hope [127] is designed to functionally integrate external simulators. In this section we demonstrate 2D field-based MESFET simulation and modeling utilizing the Datapipe feature.

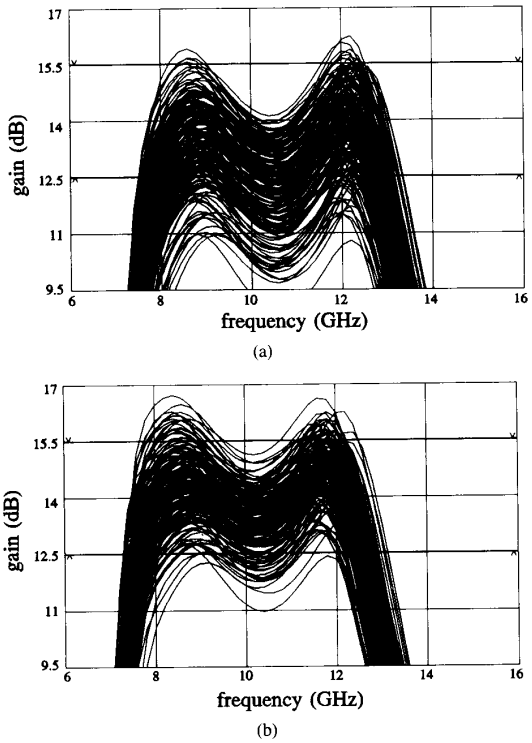

Fig. 18. Monte Carlo sweep of gain versus frequency: (a) before and (b) after yield optimization.

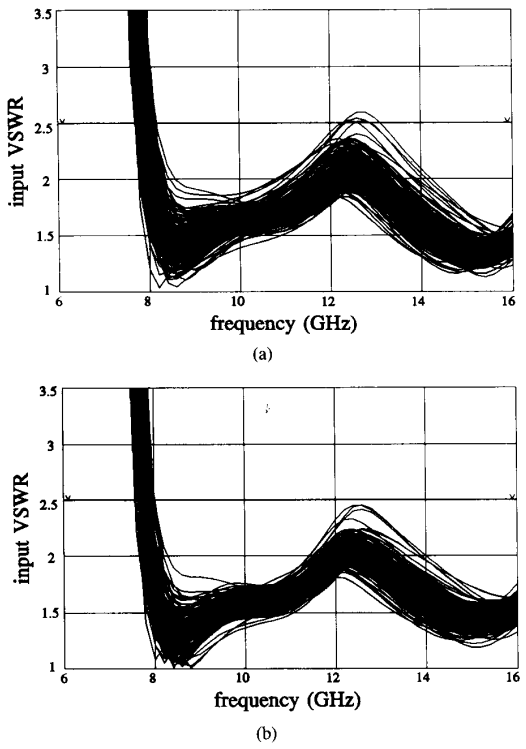

Fig. 19. Monte Carlo sweep of input VSWR versus frequency: (a) before and (b) after yield optimization.

A. 2D Drift-Diffusion MESFET Model

We use a 2D drift-diffusion MESFET model based on numerical techniques presented by Reiser [130] and Snowden *et al.* [133].

The model makes the following assumptions: (1) neglecting minority carriers, (2) neglecting thermal generation and recombination effects, and (3) describing the carrier flow by the diffusion equations. The basic model equations are described by (1)–(5) in Section II. The diffusion coefficient D is determined from the Einstein relation

$$D = \frac{kT}{q}\mu \tag{84}$$

with Boltzmann's constant k and the absolute temperature T. The electron mobility μ is calculated by (10).

Two-dimensional Poisson's equations and current continuity equations with the boundary conditions approximated according to the physical nature of the device are solved using the finite difference method to simulate the internal device physics.

B. Simulation Using Datapipe of OSA90/hope

The Datapipe feature of OSA90/hope [127] is designed to utilize UNIX interprocess pipes for high-speed data communication between OSA90/hope and external programs. Using Datapipe, external models and simulators

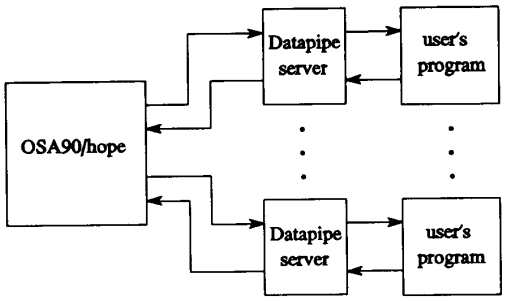

Fig. 20. Schematic diagram of Datapipe using inter-program pipe communication (IPPC), where user's programs may be user's in-house programs such as special purpose simulators, control programs, etc.

can be functionally integrated into the overall simulation, optimization and statistical environment. The basic Datapipe architecture is illustrated in Fig. 20.

We apply this concept to 2D field-based MESFET simulation. The 2D field simulator runs as an external program, concentrating on intensive number crunching operations such as solving Poisson's equations and current continuity equations. OSA90/hope interacts with the user, accepts and parses parameter values through its input file, organizes simulation (sweep) ranges, passes the necessary data to the external simulator, postprocesses the results returned from the external simulator, and provides graphical display capabilities.

We consider a 0.5 × 300 μm GaAs MESFET with the physical parameters listed in Table IX. The source and drain lengths are the equivalent ohmic contact lengths. Since the substrate has a very high resistivity and its effect on the results can almost be neglected in the finite difference simulation, a small value rather than the actual value of substrate thickness is considered in order to reduce computation time. The approximated doping profile is listed in Table X. We used the 2D model in dc simulation at 56 bias points, which took about 14 hours of CPU time on a Sun SPARCstation 1. The simulated dc results are indicated in Fig. 21 by circles.

C. The Plessey Model [167]

Field-based simulation provides accurate results but is very time-consuming. Often, field-based simulation is used to generate data for ECM modeling. We utilize a modified Statz model from Plessey [167] to match the results from our 2D field simulation. The Plessey model equation for the FET drain current is as follows

$$I_{ds} = \frac{I_{dss}(V_{gs} - V_t)^2}{1 + b(V_{gs} - V_t)}(1 + \lambda V_{ds})\tanh(\alpha V_{ds}) + \left(1 + \frac{V_{ds}}{V_{t1}}\right) G_{dst} V_{ds} \tanh(\alpha V_{ds}) \tag{85}$$

where

$$V_{t1} = V_t(1 - \beta V_{ds}). \tag{86}$$

TABLE IX
PARAMETERS FOR THE 0.5 μm GaAs MESFET

Source Length	0.15 μm
Source-Gate Gap	0.50 μm
Gate Length	0.50 μm
Drain-Gate Gap	0.60 μm
Drain Length	0.15 μm
Gate Width	300 μm
Channel Thickness	0.15 μm
Buffer Layer Thickness	0.20 μm
Substrate Thickness	0.05 μm
Schottky Barrier Height	0.80 V
Temperature	350°K
Doping of Active Layer	$1.5 \times 10^{23}/m^3$
Doping at Contacts	$3.7 \times 10^{23}/m^3$
Substrate Impurity Level	$1.0 \times 10^{10}/m^3$

TABLE X
DOPING PROFILE FOR THE 0.5 μm GaAs MESFET

Grid No.	Doping $(1/m^3)$	Grid No.	Doping $(1/m^3)$
0	1.5000×10^{23}	17	1.7705×10^{22}
1	1.5000×10^{23}	18	7.7109×10^{21}
2	1.5000×10^{23}	19	3.1290×10^{21}
3	1.5000×10^{23}	20	1.2247×10^{21}
4	1.5000×10^{23}	21	4.7939×10^{20}
5	1.5000×10^{23}	22	1.9453×10^{20}
6	1.5000×10^{23}	23	8.4721×10^{19}
7	1.5000×10^{23}	24	4.0886×10^{19}
8	1.5000×10^{23}	25	2.2485×10^{19}
9	1.5000×10^{23}	26	1.4419×10^{19}
10	1.5000×10^{23}	27	1.0967×10^{19}
11	1.5000×10^{23}	28	1.0000×10^{19}
12	1.5000×10^{23}	29	1.0000×10^{19}
13	1.3676×10^{23}	30	1.0000×10^{19}
14	1.0402×10^{23}	31	1.0000×10^{19}
15	6.6710×10^{22}	32	1.0000×10^{19}
16	3.6687×10^{22}		

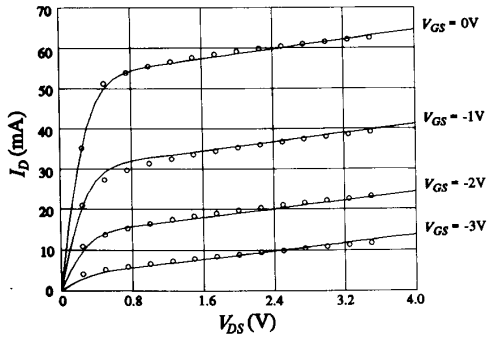

Fig. 21. Comparison of dc characteristics simulated by the 2D field-based simulator (○) and calculated by the Plessey model (——).

I_{dss}, V_t, G_{dst}, b, α, β and λ are the parameters to be determined. The model equation is implemented in the OSA90/hope input file using expressions.

The Plessey model parameters are extracted by ℓ_1 optimization of OSA90/hope, matching the dc data at 56 bias points. The extraction took about 3 minutes of CPU time on a Sun SPARCstation 1. The model parameter values before and after optimization are listed in Table XI.

TABLE XI
PARAMETERS FOR THE PLESSEY MODEL

Parameter	Before Optimization	After Optimization
I_{dss} (mA)	60	52.49
V_t (V)	−4.0	−4.10
b (V)	1.5×10^{-3}	2.23×10^{-6}
λ (1/Ω)	0.01	0.011
α (1/V)	14.5	3.316
G_{dst} (1/Ω)	3.0×10^{-3}	2.47×10^{-3}
β (1/V)	16.5	20.0

The dc drain currents calculated by the 2D field simulator and by the Plessey model are compared in Fig. 21.

VIII. CONCLUSIONS

We have presented our approach towards physics-oriented microwave circuit optimization. We have addressed device modeling, parameter extraction, nonlinear simulation, nominal design, statistical modeling and yield optimization.

Analytical large-signal physical models of MESFETs have been discussed and new developments presented. Nonlinear circuit analysis with PBMs integrated into the HB equations have been described.

PBMs provide flexibility for engineers to perform designs based on physical parameters and to foresee the characteristics of the circuits before fabrication. Although some phenomena of the FETs are not fully accommodated at present we believe that continuing research on and improvements of PBMs will address the unsolved problems in the near future.

FAST has been shown to be suitable for high speed gradient calculations for circuit optimization employing physical, geometrical and process-related parameters of devices as design variables. Hierarchical, nonlinear, yield-driven optimization has been demonstrated.

Statistical modeling of active devices with physics-based models has been explored. Our procedure has been illustrated through new implementations of the Ladbrooke model and the Khatibzadeh and Trew model. The results from the Ladbrooke model have demonstrated the feasibility of using PBMs for statistical modeling, though further investigation of the Khatibzadeh and Trew model for statistical purposes is needed.

Physics-based statistical models have been applied in physics-based yield-driven optimization suitable for MMICs. Both passive and active elements have been described in terms of material and geometrical statistical parameters.

Effective multidimensional quadratic functions have been employed to simultaneously approximate responses and gradients. Our novel theoretical developments have been incorporated into OSA90/hope and HarPE. They are thereby available to the microwave community. OSA90/hope's novel Datapipe structure constitutes the first microwave CAD product of its kind. The open architecture

feature enables device and circuit designers to solve a variety of relevant linear/nonlinear/statistical modeling, simulation and optimization problems with both circuit and physical parameters.

ACKNOWLEDGMENT

The authors would like to express their appreciation to Dr. Rolf H. Jansen of Jansen Microwave, Ratingen, Germany, Guest Co-Editor of this Special Issue, for several significantly inspiring discussions. The authors thank Dr. Robert J. Trew of North Carolina State University, Raleigh, NC, for useful discussions and providing essential data. The authors acknowledge some original work done by Dr. Jian Song which has been integrated into our presentation. Thanks are also due to Dr. D. Mike Brookbanks of GEC-Marconi Materials Research, Caswell, Northamptonshire, England, for technical discussions and generously providing measurement data. Thanks are also extended to his colleague Dr. Ron G. Arnold. Thanks are due to Dr. Peter H. Ladbrooke of GaAs Code Ltd., Cambridge, England, for helpful discussions and comments [168]. Thanks are given to Dr. Walter R. Curtice of W. R. Curtice Consulting, Princeton Junction, NJ, for helpful criticisms and discussions. Finally, thanks are extended to the reviewers for helpful comments, constructive criticisms and suggestions to improve this manuscript.

REFERENCES

[1] W. R. Curtice, "A MESFET model for use in the design of GaAs integrated circuits," *IEEE Trans. Microwave Theory Tech.*, vol. MTT-28, pp. 448-456, 1980.

[2] W. R. Curtice and M. Ettenberg, "A nonlinear GaAs FET model for use in the design of output circuits for power amplifiers," *IEEE Trans. Microwave Theory Tech.*, vol. MTT-33, pp. 1383-1394, 1985.

[3] A. Materka and T. Kacprzak, "Computer calculation of large-signal GaAs FET amplifier characteristics," *IEEE Trans. Microwave Theory Tech.*, vol. MTT-33, pp. 129-135, 1985.

[4] H. Statz, P. Newman, I. W. Smith, R. A. Pucel, and H. A. Haus, "GaAs FET device and circuit simulation in SPICE," *IEEE Trans. Electron Devices*, vol. ED-34, pp. 160-169, 1987.

[5] V. D. Hwang and T. Itoh, "An efficient approach for large-signal modeling and analysis of GaAs MESFET," *IEEE Trans. Microwave Theory Tech.*, vol. MTT-35, pp. 396-402, 1987.

[6] J. W. Bandler, S. H. Chen, S. Ye, and Q. J. Zhang, "Integrated model parameter extraction using large-scale optimization concepts," *IEEE Trans. Microwave Theory Tech.*, vol. 36, pp. 1629-1638, 1988.

[7] J. W. Bandler, Q. J. Zhang, S. Ye, and S. H. Chen, "Efficient large-signal FET parameter extraction using harmonics," *IEEE Trans. Microwave Theory Tech.*, vol. 37, pp. 2099-2108, 1989.

[8] J. W. Bandler, Q. J. Zhang, and Q. Cai, "Nonlinear circuit optimization with dynamically integrated physical device models," in *IEEE MTT-S Int. Microwave Symp. Dig.*, Dallas, TX, 1990, pp. 303-306.

[9] R. J. Gilmore and M. B. Steer, "Nonlinear circuit analysis using the method of harmonic balance—a review of the art. Part I. Introductory concepts," *Int. J. Microwave and Millimetre-Wave Computer-Aided Engineering*, vol. 1, pp. 22-37, 1991.

[10] L. O. Chua and P. Lin, *Computer-Aided Analysis of Electronic Circuits: Algorithms and Computational Techniques*. Englewood Cliffs, NJ: Prentice-Hall, 1975.

[11] S. Skelboe, "Computation of the periodic steady-state response of nonlinear networks by extrapolation methods," *IEEE Trans. Circuits Syst.*, vol. CAS-27, pp. 161-175, 1980.

[12] S. Skelboe, "Time-domain steady-state analysis of nonlinear electrical systems," *Proc. IEEE*, vol. 70, pp. 1210-1228, 1982.

[13] J. Vlach and K. Singhal, *Computer Methods for Circuit Analysis and Design*. New York: Van Nostrand Reinhold, 1983.

[14] A. K. Jastrzebski and M. I. Sobhy, "Analysis of microwave circuits using state-space approach," in *Proc. IEEE Int. Symp. Circuits Syst.*, Montreal, 1984, pp. 1119-1122.

[15] M. I. Sobhy and A. K. Jastrzebski, "Direct integration methods of nonlinear microwave circuits," in *Proc. 15th European Microwave Conf.*, Paris, 1985, pp. 1110-1118.

[16] L. W. Nagel and D. O. Pederson, SPICE (Simulation Program with Integrated Circuit Emphasis), Electronics Research Laboratory, University of California, Memo ERL-M382, Apr. 1973.

[17] S. W. Director, "A method for quick determination of the periodic steady-state in nonlinear networks," in *Proc. 9th Allerton Conf. Circuit Syst. Theory*, Urbana, IL, 1971, pp. 131-139.

[18] T. J. Aprille, Jr. and T. N. Trick, "Steady-state analysis of nonlinear circuits with periodic inputs," *Proc. IEEE*, vol. 60, pp. 108-114, 1972.

[19] T. J. Aprille, Jr. and T. N. Trick, "A computer algorithm to determine the steady-state response of nonlinear oscillators," *IEEE Trans. Circuit Theory*, vol. CT-19, pp. 354-360, 1972.

[20] F. R. Colon and T. N. Trick, "Fast periodic steady-state analysis for large-signal electronic circuits," *IEEE J. Solid-State Circuits*, vol. SC-8, pp. 260-269, 1973.

[21] S. W. Director and K. W. Current, "Optimization of forced nonlinear periodic circuits," *IEEE Trans. Circuits Syst.*, vol. CAS-23, pp. 329-335, 1976.

[22] M. S. Nakhla and F. H. Branin, Jr., "Determining the periodic response of nonlinear systems by a gradient method," *Int. J. Circuit Theory Appl.*, vol. 5, pp. 255-273, 1977.

[23] M. B. Steer, C. R. Chang, and G. W. Rhyne, "Computer-aided analysis of nonlinear microwave circuits using frequency-domain nonlinear analysis techniques: the state of the art," *Int. J. Microwave and Millimeter-Wave Computer-Aided Engineering*, vol. 1, pp. 181-200, 1991.

[24] R. G. Sea, "An algebraic formula for amplitudes of intermodulation products involving an arbitrary number of frequencies," *Proc. IEEE*, vol. 56, pp. 1388-1389, 1968.

[25] R. G. Sea and A. G. Vacroux, "On the computation of intermodulation products for a power series nonlinearity," *Proc. IEEE*, pp. 337-338, 1969.

[26] M. B. Steer and P. J. Khan, "An algebraic formula for the output of a system with large-signal multifrequency excitation," *Proc. IEEE*, pp. 177-179, 1983.

[27] G. W. Rhyne, M. B. Steer, and B. D. Bates, "Frequency-domain nonlinear circuit analysis using generalized power series," *IEEE Trans. Microwave Theory Tech.*, vol. 36, pp. 379-387, 1988.

[28] V. Volterra, *Theory of Functionals and of Integral and Integro-Differential Equations*. London: Blackie & Son, 1930.

[29] E. Bedrosian and S. O. Rice, "The output properties of Volterra systems (nonlinear systems with memory) driven by harmonic and Gaussian inputs," *Proc. IEEE*, vol. 59, pp. 1688-1707, 1971.

[30] J. J. Bussgang, L. Ehrman and J. W. Graham, "Analysis of nonlinear systems with multiple inputs," *Proc. IEEE*, vol. 62, pp. 1088-1119, 1974.

[31] D. D. Weiner and J. F. Spina, *Sinusoidal Analysis and Modeling of Weakly Nonlinear Circuits*. New York: Van Nostrand Reinhold, 1980.

[32] I. W. Sandberg, "Expansions for nonlinear systems," *Bell Syst. Tech. J.*, vol. 61, pp. 159-199, 1982.

[33] S. A. Maas, "A general-purpose computer program for the Volterra-series analysis of nonlinear microwave circuits," in *IEEE MTT-S Int. Microwave Symp. Dig.*, New York, 1988, pp. 311-314.

[34] A. Ushida and L. O. Chua, "Frequency-domain analysis of nonlinear circuits driven by multitone signals," *IEEE Trans. Circuits Syst.*, vol. CAS-31, pp. 766-779, 1984.

[35] J. H. Haywood and Y. L. Chow, "Intermodulation distortion analysis using a frequency-domain harmonic balance technique," *IEEE Trans. Microwave Theory Tech.*, vol. 36, pp. 1251-1257, 1988.

[36] C. R. Chang, M. B. Steer, and G. W. Rhyne, "Frequency-domain spectral balance using the arithmetic operator method," *IEEE Trans. Microwave Theory Tech.*, vol. 37, pp. 1681-1688, 1989.

[37] G. L. Heiter, "Characterization of nonlinearities in microwave devices and systems," *IEEE Trans. Microwave Theory Tech.*, vol. MTT-21, pp. 797-805, 1973.

[38] R. B. Swerdlow, "Analysis of intermodulation noise in frequency converters by Volterra series," *IEEE Trans. Microwave Theory Tech.*, vol. MTT-26, pp. 305-313, 1978.

[39] R. S. Tucker, "Third-order intermodulation distortion and gain compression in GaAs FET's," *IEEE Trans. Microwave Theory Tech.*, vol. MTT-27, pp. 400-408, 1979.
[40] R A. Minasian, "Intermodulation distortion analysis of MESFET amplifiers using Volterra series representation," *IEEE Trans. Microwave Theory Tech.*, vol. MTT-28, pp. 1-8, 1980.
[41] C. L. Law and C. S. Aitchison, "Prediction of wide-band power performance of MESFET distributed amplifiers using the Volterra series representation," *IEEE Trans. Microwave Theory Tech.*, vol. MTT-34, pp. 1308-1317, 1986.
[42] G. W. Rhyne and M. B. Steer, "Generalized power series analysis of intermodulation distortion in a MESFET amplifier: simulation and experiment," *IEEE Trans. Microwave Theory Tech.*, vol. MTT-35, pp. 1248-1255, 1987.
[43] Y. Hu, J. Obregon, and J. C. Mollier, "Nonlinear analysis of microwave FET oscillators using Volterra series," *IEEE Trans. Microwave Theory Tech.*, vol. 37, pp. 1689-1693, 1989.
[44] C. R. Chang and M. B. Steer, "Frequency-domain nonlinear microwave circuit simulation using the arithmetic operator method," *IEEE Trans. Microwave Theory Tech.*, vol. 38, pp. 1139-1143, 1990.
[45] W. J. Cunningham, *Introduction to Nonlinear Analysis*. New York: McGraw-Hill, 1958.
[46] J. C. Lindenlaub, "An approach for finding the sinusoidal steady-state response of nonlinear systems," in *Proc. 7th Allerton Conf. Circuit Syst. Theory*, Chicago, 1969, pp. 323-327.
[47] M. S. Nakhla and J. Vlach, "A piecewise harmonic-balance technique for determination of periodic response of nonlinear systems," *IEEE Trans. Circuits Syst.*, vol. CAS-23, pp. 85-91, 1976.
[48] A. I. Mees, *Dynamics of Feedback Systems*. New York: Wiley, 1981.
[49] V. Rizzoli, A. Lipparini, and E. Marazzi, "A general-purpose program for nonlinear microwave circuit design," *IEEE Trans. Microwave Theory Tech.*, vol. 31, pp. 762-770, 1983.
[50] K. S. Kundert and A. Sangiovanni-Vincentelli, "Simulation of nonlinear circuits in the frequency domain," *IEEE Trans. Computer-Aided Design*, vol. CAD-5, pp. 521-535, 1986.
[51] V. Rizzoli, C. Cecchetti, A. Lipparini, and F. Mastri, "General-purpose harmonic balance analysis of nonlinear microwave circuits under multitone excitation," *IEEE Trans. Microwave Theory Tech.*, vol. 36, pp. 1650-1660, 1988.
[52] R. J. Gilmore and M. B. Steer, "Nonlinear circuit analysis using the method of harmonic balance—a review of the art. Part II. Advanced concepts," *Int. J. Microwave and Millimeter-Wave Computer-Aided Engineering*, vol. 1, pp. 159-180, 1991.
[53] F. Filicori, V. A. Monaco and C. Naldi, "Simulation and design of microwave class-C amplifiers through harmonic analysis," *IEEE Trans. Microwave Theory Tech.*, vol. MTT-27, pp. 1043-1051, 1979.
[54] R. G. Hicks and P. J. Khan, "Numerical analysis of subharmonic mixers using accurate and approximate models," *IEEE Trans. Microwave Theory Tech.*, vol. MTT-30, pp. 2113-2120, 1982.
[55] W. R. Curtice, "Nonlinear analysis of GaAs MESFET amplifiers, mixers, and distributed amplifiers using harmonic balance technique," *IEEE Trans. Microwave Theory Tech.*, vol. 35, pp. 441-447, 1987.
[56] P. W. Van Der Walt, "Efficient technique for solving nonlinear mixer pumping problem," *Electronics Lett.*, vol. 21, pp. 899-900, 1985.
[57] S. El-Rabaie, J. A. C. Stewart, V. F. Fusco, and J. J. McKeown, "A novel approach for the large signal analysis and optimisation of microwave frequency doublers," in *IEEE MTT-S Int. Microwave Symp. Dig.*, New York, 1988, pp. 1119-1122.
[58] J. W. Bandler, R. M. Biernacki, S. H. Chen, J. Song, S. Ye, and Q. J. Zhang, "Analytically unified DC/small-signal/large-signal circuit design," *IEEE Trans. Microwave Theory Tech.*, vol. 39, pp. 1076-1082, 1991.
[59] V. D. Hwang, Y-C. Shih, H. M. Le, and T. Itoh, "Nonlinear modeling and verification of MMIC amplifiers using the waveform-balance method," *IEEE Trans. Microwave Theory Tech.*, vol. 37, pp. 2125-2133, 1989.
[60] R. Gilmore, "Nonlinear circuit design using the modified harmonic balance algorithm," *IEEE Trans. Microwave Theory Tech.*, vol. MTT-34, pp. 1294-1307, 1986.
[61] A. Lipparini, E. Marazzi, and V. Rizzoli, "A new approach to the computer-aided design of nonlinear networks and its application to microwave parametric frequency dividers," *IEEE Trans. Microwave Theory Tech.*, vol. MTT-30, pp. 1050-1058, 1982.
[62] V. Rizzoli and A. Neri, "State of the art and present trends in nonlinear microwave CAD techniques," *IEEE Trans. Microwave Theory Tech.*, vol. 36, pp. 343-365, 1988.
[63] J. W. Bandler, Q. J. Zhang, J. Song, and R. M. Biernacki, "FAST gradient based yield optimization of nonlinear circuits," *IEEE Trans. Microwave Theory Tech.*, vol. 38, pp. 1701-1710, 1990.
[64] R. H. Jansen, R. G. Arnold, and I. G. Eddison, "A comprehensive CAD approach to the design of MMICs up to mm-wave frequencies," *IEEE Trans. Microwave Theory Tech.*, vol. 36, pp. 208-219, 1988.
[65] R. H. Jansen, I. G. Eddison, and R. G. Arnold, "Recent developments in CAD of high packing density MMICs," in *Proc. MIOP 1989*, Sindelfingen, Germany, 1989, Paper 1.3.
[66] R. H. Jansen, "Progress in passive and active MMIC device modeling," in *Workshop on Progress in Microwave CAD and in CAD Applications Dig.*, Ratingen, Germany, 1989, pp. 173-196.
[67] F. A. Myers, "Advanced GaAs MMIC elements and circuits," in *Workshop on Progress in Microwave CAD and in CAD Applications Dig.*, Ratingen, Germany, 1989, pp. 197-203.
[68] R. Goyal, M. Golio, and W. Thomann, "Device Modeling," in *Monolithic Microwave Integrated Circuits: Technology & Design*, R. Goyal Ed. Boston: Artech House, 1989, ch. 4.
[69] E. D. Cohen, "MIMIC from the Department of Defense perspective," *IEEE Trans. Microwave Theory Tech.*, vol. 38, pp. 1171-1174, 1990.
[70] C. M. Snowden, "Microwave and millimeter-wave device and circuit design based on physical modeling," *Int. J. on Microwave and Millimeter-Wave Computer-Aided Engineering*, vol. 1, pp. 4-21, 1991.
[71] R. J. Trew, "MESFET models for microwave CAD applications," *Int. J. on Microwave and Millimeter-Wave Computer-Aided Engineering*, vol. 1, pp. 143-158, 1991.
[72] J. W. Bandler and S. H. Chen, "Circuit optimization: the state of the art," *IEEE Trans. Microwave Theory Tech.*, vol. 36, pp. 424-443, 1988.
[73] J. Purviance, D. Criss, and D. Monteith, "FET model statistics and their effects on design centering and yield prediction for microwave amplifiers," in *IEEE MTT-S Int. Microwave Symp. Dig.*, New York, 1988, pp. 315-318.
[74] R. W. Dutton, D. A. Divekar, A. G. Gonzalez, S. E. Hansen, and D. A. Antoniadis, "Correlation of fabrication process and electrical device parameter variations," *IEEE J. Solid-State Circuits*, vol. SC-12, pp. 349-355, 1977.
[75] D. A. Divekar, R. W. Dutton and W. J. McCalla, "Experimental study of Gummel-Poon model parameter correlations for bipolar junction transistors," *IEEE J. Solid-State Circuits*, vol. SC-12, pp. 552-559, 1977.
[76] M. A. Styblinski, "Factor analysis model of resistor correlations for monolithic integrated circuits," in *Proc. IEEE Symp. Circuits Syst.*, Tokyo, 1977, pp. 776-777.
[77] P. J. Rankin, "Statistical modeling for integrated circuits," *IEE Proc.*, vol. 129, pt. G, no. 4, pp. 186-191, 1982.
[78] S. Freeman, "Statistical techniques for calibrating simulation models of analog circuits and devices," in *Proc. IEEE Int. Symp. Circuits Syst.*, Montreal, 1984, pp. 684-688.
[79] S. Liu and K. Singhal, "A statistical model for MOSFETs," in *Proc. IEEE Int. Conf. Computer-Aided Design*, Santa Clara, CA, 1985, pp. 78-80.
[80] P. Cox, P. Yang, S. S. Mahant-Shetti and P. Chatterjee, "Statistical modeling for efficient parametric yield estimation of MOS VLSI circuits," *IEEE Trans. Electron Devices*, vol. ED-32, pp. 471-478, 1985.
[81] N. Herr and J. J. Barnes, "Statistical circuit simulation modeling of CMOS VLSI," *IEEE Trans. Computer-Aided Design*, vol. CAD-5, pp. 15-22, 1986.
[82] C. J. B. Spanos and S. W. Director, "Parameter extraction for statistical IC process characterization," *IEEE Trans. Computer-Aided Design*, vol. CAD-5, pp. 66-78, 1986.
[83] J. E. Purviance, M. C. Petzold, and C. Potratz, "A linear statistical FET model using principal component analysis," *IEEE Trans. Microwave Theory Tech.*, vol. 37, pp. 1389-1394, 1989.
[84] J. W. Bandler, R. M. Biernacki, S. H. Chen, J. Loman, M. Renault, and Q. J. Zhang, "Combined discrete/normal statistical modeling of microwave devices," in *Proc. European Microwave Conf.*, Wembley, England, 1989, pp. 205-210.
[85] J. Purviance, M. Meehan, and D. Collins, "Properties of FET parameter statistical data bases," in *IEEE MTT-S Int. Microwave Symp. Dig.*, Dallas, TX, 1990, pp. 567-570.

[86] J. W. Bandler, R. M. Biernacki, S. H. Chen, J. Song, S. Ye and Q. J. Zhang, "Statistical modeling of GaAs MESFETs," in *IEEE MTT-S Int. Microwave Symp. Dig.*, Boston, 1991, pp. 87-90.
[87] A. R. Jha, R. Goyal and B. Manz, "Introduction," in *Monolithic Microwave Integrated Circuits: Technology & Design*, R. Goyal, Ed. Boston: Artech House, 1989, ch. 1.
[88] B. J. Karafin, "The optimum assignment of component tolerances for electrical networks," *Bell Syst. Tech. J.*, vol. 50, pp. 1225-1242, 1971.
[89] J. F. Pinel and K. A. Roberts, "Tolerance assignment in linear networks using nonlinear programming," *IEEE Trans. Circuit Theory*, vol. CT-19, pp. 475-479, 1972.
[90] J. W. Bandler, "Optimization of design tolerances using nonlinear programming," in *Proc. 6th Princeton Conf. on Information Science and Systems*, Princeton, NJ, 1972, pp. 655-659. Also in *Computer-Aided Filter Design*, G. Szentirmai, Ed. New York: IEEE Press, 1973.
[91] ——, "The tolerance problem in optimal design," in *Proc. European Microwave Conf.*, Brussels, 1973, Paper A.13.1.(I).
[92] ——, "Optimization of design tolerances using nonlinear programming," *J. Optimization Theory and Applications*, vol. 14, pp. 99-114, 1974.
[93] J. W. Bandler, P. C. Liu, and H. Tromp, "A nonlinear programming approach to optimal design centering, tolerancing and tuning," *IEEE Trans. Circuits Syst.*, vol. CAS-23, pp. 155-165, 1976.
[94] ——, "Integrated approach to microwave design," *IEEE Trans. Microwave Theory Tech.*, vol. MTT-24, pp. 584-591, 1976.
[95] S. W. Director and G. D. Hachtel, "The simplicial approximation approach to design centering," *IEEE Trans. Circuits Syst.*, vol. CAS-24, pp. 363-372, 1977.
[96] J. W. Bandler and H. L. Abdel-Malek, "Optimal centering, tolerancing, and yield determination via updated approximations and cuts," *IEEE Trans. Circuits Syst.*, vol. CAS-25, pp. 853-871, 1978.
[97] E. Polak and A. Sangiovanni-Vincentelli, "Theoretical and computational aspects of the optimal design centering, tolerancing, and tuning problem," *IEEE Trans. Circuits Syst.*, vol. CAS-26, pp. 795-813, 1979.
[98] H. L. Abdel-Malek, and J. W. Bandler, "Yield optimization for arbitrary statistical distributions: Part I—Theory," *IEEE Trans. Circuits Syst.*, vol. CAS-27, pp. 245-253, 1980.
[99] R. S. Soin and R. Spence, "Statistical exploration approach to design centering," *Proc. IEE*, vol. 127, pt. G., pp. 260-269, 1980.
[100] M. A. Styblinski and A. Ruszczynski, "Stochastic approximation approach to statistical circuit design," *Electronics Lett.*, vol. 19, pp. 300-302, 1983.
[101] K. Singhal and J. F. Pinel, "Statistical design centering and tolerancing using parametric sampling," *IEEE Trans. Circuits Syst.*, vol. CAS-28, pp. 692-702, 1981.
[102] T. Downs, A. S. Cook, and G. Rogers, "A partitioning approach to yield estimation for large circuits and systems," *IEEE Trans. Circuits Syst.*, vol. CAS-31, pp. 472-485, 1984.
[103] J. W. Bandler and A. E. Salama, "Functional approach to microwave postproduction tuning," *IEEE Trans. Microwave Theory Tech.*, vol. MTT-33, pp. 302-310, 1985.
[104] A. J. Strojwas and A. Sangiovanni-Vincentelli, Eds., *IEEE Trans. Computer-Aided Design*, Special Issue on Statistical Design of VLSI Circuits, vol. CAD-5, pp. 5-169, 1986.
[105] P. Yang, D. E. Hocevar, P. F. Cox, C. Machala, and P. K. Chatterjee, "An integrated and efficient approach for MOS VLSI statistical circuit design," *IEEE Trans. Computer-Aided Design*, vol. CAD-5, pp. 5-14, 1986.
[106] M. L. Stein, "An efficient method of sampling for statistical circuit design," *IEEE Trans. Computer-Aided Design*, vol. CAD-5, pp. 23-29, 1986.
[107] M. A. Styblinski, "Problems of yield gradient estimation for truncated probability density functions," *IEEE Trans. Computer-Aided Design*, vol. CAD-5, pp. 30-38, 1986.
[108] M. A. Styblinski and L. J. Opalski, "Algorithms and software tools for IC yield optimization based on fundamental fabrication parameters," *IEEE Trans. Computer-Aided Design*, vol. CAD-5, pp. 79-89, 1986.
[109] J. P. Spoto, W. T. Coston, and C. P. Hernandez, "Statistical integrated circuit design and characterization," *IEEE Trans. Computer-Aided Design*, vol. CAD-5, pp. 90-103, 1986.
[110] S. R. Nassif, A. J. Strojwas, and S. W. Director, "A methodology for worst-case analysis of integrated circuits," *IEEE Trans. Computer-Aided Design.*, vol. CAD-5, pp. 104-113, 1986.
[111] W. Maly, A. J. Strojwas, and S. W. Director, "VLSI yield prediction and estimation: a unified framework," *IEEE Trans. Computer-Aided Design*, vol. CAD-5, pp. 114-130, 1986.
[112] D. Riley and A. Sangiovanni-Vincentelli, "Models for a new profit-based methodology for statistical design of integrated circuits," *IEEE Trans. Computer-Aided Design*, vol. CAD-5, pp. 131-169, 1986.
[113] L. J. Opalski and M. A. Styblinski, "Generalization of yield optimization problem: maximum income approach," *IEEE Trans. Computer-Aided Design*, vol. CAD-5, pp. 346-360, 1986.
[114] Y. Aoki, H. Masuda, S. Shimada and S. Sato, "A new design-centering methodology for VLSI device development," *IEEE Trans. Computer-Aided Design*, vol. CAD-6, pp. 452-461, 1987.
[115] T. K. Yu, S. M. Kang, I. N. Hajj, and T. N. Trick, "Statistical performance modeling and parametric yield estimation of MOS VLSI," *IEEE Trans. Computer-Aided Design*, vol. CAD-6, pp. 1013-1022, 1987.
[116] D. E. Hocevar, P. F. Cox and P. Yang, "Parametric yield optimization for MOS circuit blocks," *IEEE Trans. Computer-Aided Design*, vol. CAD-7, pp. 645-658, 1988.
[117] J. W. Bandler, R. M. Biernacki, S. H. Chen, M. Renault, J. Song, and Q. J. Zhang, "Yield optimization of large scale microwave circuits," in *Proc. European Microwave Conf.*, Stockholm, Sweden, 1988, pp. 255-260.
[118] R. M. Biernacki, J. W. Bandler, J. Song and Q. J. Zhang, "Efficient quadratic approximation for statistical design," *IEEE Trans. Circuits Syst.*, vol. 36, pp. 1449-1454, 1989.
[119] J. W. Bandler, Q. J. Zhang, J. Song, and R. M. Biernacki, "Yield optimization of nonlinear circuits with statistically characterized devices," in *IEEE MTT-S Int. Microwave Symp. Dig.*, Long Beach, CA, 1989, pp. 649-652.
[120] M. D. Meehan, T. Wandinger and D. A. Fisher, "Accurate design centering and yield prediction using the 'truth model'," in *IEEE MTT-S Int. Microwave Symp. Dig.*, Boston, 1991, pp. 1201-1204.
[121] J. Purviance and M. Meehan, "CAD for statistical analysis and design of microwave circuits," *Int. J. Microwave and Millimeter-Wave Computer-Aided Engineering*, vol. 1, pp. 59-76, 1991.
[122] R. J. Gilmore, M. Eron and T. Zhang, "Yield optimization of a MMIC distributed amplifier using physically-based device models," in *IEEE MTT-S Int. Microwave Symp. Dig.*, Boston, 1991, pp. 1205-1208.
[123] J. W. Bandler, Q. Cai, R. M. Biernacki, S. H. Chen and Q. J. Zhang, "Physics-based design and yield optimization of MMICs," in *Proc. European Microwave Conf.*, Stuttgart, 1991, pp. 1515-1520.
[124] C. H. Corbex, A. F. Gerodolle, S. P. Martin, and A. R. Poncet, "Data structuring for process and device simulations," *IEEE Trans. Computer-Aided Design*, vol. 7, pp. 489-500, 1988.
[125] J. R. F. McMacken and S. G. Chamberlain, "CHORD: a modular semiconductor device simulation development tool incorporating external network models," *IEEE Trans. Computer-Aided Design*, vol. 8, pp. 826-836, 1989.
[126] P. Lloyd, H. K. Dirks, E. J. Prendergast and K. Singhal, "Technology CAD for competitive products," *IEEE Trans. Computer-Aided Design*, vol. 9, pp. 1209-1216, 1990.
[127] *OSA90/hope™*, Optimization Systems Associates Inc., P.O. Box 8083, Dundas, ON, Canada L9H 5E7, 1991.
[128] *HarPE™*, Optimization Systems Associates Inc., P.O. Box 8083, Dundas, ON, Canada L9H 5E7, 1991.
[129] D. P. Kennedy and R. R. O'Brien, "Computer aided two dimensional analysis of the junction field-effect transistor," *IBM J. Res. Devel.*, vol. 14, pp. 95-116, 1970.
[130] M. Reiser, "A two-dimensional numerical FET model for dc, ac and large-signal analysis," *IEEE Trans. Electron Devices*, vol. ED-20, pp. 35-45, 1973.
[131] T. Wada and J. Frey, "Physical basis of short-channel MESFET operation," *IEEE Trans. Electron Devices*, vol. ED-26, pp. 476-490, 1979.
[132] W. R. Curtice and Y. H. Yun, "A temperature model for the GaAs MESFET," *IEEE Trans. Electron Devices*, vol. ED-28, pp. 954-962, 1981.
[133] C. M. Snowden, M. J. Hawes and D. V. Morgan, "Large-signal modeling of GaAs MESFET operation," *IEEE Trans. Electron Devices*, vol. ED-30, pp. 1817-1824, 1983.
[134] C. M. Snowden and D. Loret, "Two-dimensional hot-electron

models for short-gate-length GaAs MESFETs," *IEEE Trans. Electron Devices*, vol. ED-34, pp. 212-223, 1987.
[135] W. Shockley, "A unipolar 'field-effect' transistor," *Proc. IRE*, vol. 40, pp. 1365-1376, 1952.
[136] J. A. Turner and B. L. H. Wilson, "Implications of carrier velocity saturation in a gallium arsenide field-effect transistor," in *Proc. Symp. Gallium Arsenide*, 1968, pp. 195-204.
[137] A. B. Grebene and S. K. Ghandhi, "General theory for pinched operation of the junction-gate FET," *Solid-State Electron.*, vol. 12, pp. 573-589, 1969.
[138] K. Lehovec and R. Zuleeg, "Voltage-current characteristics of GaAs J-FETs in the hot electron range," *Solid-State Electron.*, vol. 13, pp. 1415-1426, 1970.
[139] A. Pucel, A. Haus and H. Statz, "Signal and noise properties of gallium arsenide microwave field-effect transistors," in *Advances in Electronics and Electron Physics*, vol. 38. New York: Academic Press, 1975, pp. 195-265.
[140] T. H. Chen and M. S. Shur, "Analytic models for ion-implanted GaAs FET's," *IEEE Trans. Electron Devices*, vol. ED-32, pp. 18-28, 1985.
[141] T. H. Chen and M. S. Shur, "A capacitance model for GaAs MESFETs," *IEEE Trans. Electron Devices*, vol. ED-32, pp. 883-891, 1985.
[142] K. Yamaguchi and H. Kodera, "Drain conductance of junction gate FET's in the hot electron range," *IEEE Trans. Electron Devices*, vol. ED-23, pp. 545-553, 1976.
[143] A. Madjar and F. J. Rosenbaum, "A large-signal model for the GaAs MESFET," *IEEE Trans. Microwave Theory Tech.*, vol. MTT-29, pp. 781-788, 1981.
[144] M. A. Khatibzadeh and R. J. Trew, "A large-signal, analytic model for the GaAs MESFET," *IEEE Trans. Microwave Theory Tech.*, vol. 36, pp. 231-238, 1988.
[145] C. S. Chang and D. Y. S. Day, "Analytic theory for current-voltage characteristics and field distribution of GaAs MESFET's," *IEEE Trans. Electron Devices*, vol. 36, pp. 269-280, 1989.
[146] J. G. Ruch and G. S. Kino, "Measurement of the velocity-field characteristic of gallium arsenide," *Appl. Phys. Lett.*, vol. 10, pp. 40-42, 1967.
[147] P. A. Houston and A. G. R. Evans, "Electron drift velocity in n-GaAs at high electric fields," *Solid-State Electron.*, vol. 20, pp. 197-204, 1977.
[148] M. A. Khatibzadeh, "Large-signal modeling of gallium-arsenide field-effect transistors," Ph.D. dissertation, North Carolina State University, Raleigh, NC, 1987.
[149] H. Fukui, "Determination of the basic device parameters of a GaAs MESFET," *Bell Syst. Tech. J.*, vol. 58, pp. 771-797, 1979.
[150] W. R. Curtice, "GaAs MESFET modeling and nonlinear CAD," *IEEE Trans. Microwave Theory Tech.*, vol. 36, pp. 220-230, 1988.
[151] Measurement data provided by Plessey Research Caswell Ltd., Caswell, Towcester, Northamptonshire, England NN12 8EQ, 1990.
[152] J. W. Bandler, S. H. Chen, and M. L. Renault, "KMOS-a fortran library for nonlinear optimization," Department of Electrical and Computer Engineering, McMaster University, Hamilton, ON, Canada, Report SOS-87-1-R, 1987.
[153] J. W. Bandler, S. H. Chen, S. Daijavad and K. Madsen, "Efficient optimization with integrated gradient approximations," *IEEE Trans. Microwave Theory Tech.*, vol. 36, pp. 444-455, 1988.
[154] C. G. Broyden, "A class of methods for solving nonlinear simultaneous equations," *Mathematics of Computation*, vol. 19, pp. 577-593, 1965.
[155] M. J. D. Powell, "A Fortran subroutine for unconstrained minimization, requiring first derivatives of the objective functions," Atomic Energy Research Establishment, Harwell, Berkshire, England, Rep. AERE-R. 6469, pp. 20-27, 1970.
[156] J. W. Bandler, Q. J. Zhang and R. M. Biernacki, "A unified theory for frequency domain simulation and sensitivity analysis of linear and nonlinear circuits," *IEEE Trans. Microwave Theory Tech.*, vol. 36, pp. 1661-1669, 1988.
[157] ——, "Practical, high-speed gradient computation for harmonic balance simulators," in *IEEE MTT-S Int. Microwave Symp. Dig.*, Long Beach, CA, 1989, pp. 363-366.
[158] H. L. Abdel-Malek and J. W. Bandler, "Yield optimization for arbitrary statistical distributions: Part II—implementation," *IEEE Trans. Circuits Syst.*, vol. CAS-27, pp. 253-262, 1980.
[159] P. H. Ladbrooke, *MMIC Design: GaAs FETs and HEMTs*. Norwood, MA: Artech House, 1989.
[160] J. W. Bandler, S. Ye, Q. Cai, R. M. Biernacki, and S. H. Chen, "Predictable yield-driven circuit optimization," in *IEEE MTT-S Int. Microwave Symp. Dig.*, Albuquerque, NM, 1992, pp. 837-840.
[161] J. W. Bandler, S. H. Chen, and R. M. Biernacki, "A new formulation for yield optimization," in *IEEE MTT-S Int. Microwave Symp. Dig.*, Albuquerque, NM, 1992, pp. 1465-1468.
[162] I. J. Bahl, "Transmission lines and lumped elements," in *Microwave Solid State Circuit Design*, I. J. Bahl and P. Bhartia, Eds. New York: Wiley, 1988, ch. 2.
[163] R. M. Biernacki and M. A. Styblinski, "Statistical circuit design with a dynamic constraint approximation scheme," in *Proc. IEEE Int. Symp. Circuits Syst.*, San Jose, CA, 1986, pp. 976-979.
[164] J. W. Bandler, R. M. Biernacki, S. H. Chen, J. Song, S. Ye, and Q. J. Zhang, "Gradient quadratic approximation scheme for yield-driven design," in *IEEE MTT-S Int. Microwave Symp. Dig.*, Boston, MA, 1991, pp. 1197-1200.
[165] C. Kermarrec and C. Rumelhard, "Microwave monolithic integrated circuits," in *GaAs MESFET Circuit Design*, R. Soares, Ed. Boston: Artech House, 1988, ch. 9.
[166] J. W. Bandler, W. Kellermann and K. Madsen, "A superlinearly convergent minimax algorithm for microwave circuit design," *IEEE Trans. Microwave Theory Tech.*, vol. MTT-33, pp. 1519-1530, 1985.
[167] D. M. Brookbanks, Plessey Research Caswell Ltd., Caswell, Towcester, Northamptonshire, England NN12 8EQ, Private Communication, 1990.
[168] P. H. Ladbrooke, GaAs Code Ltd., St. John's Innovation Centre, Cowley, Cambridge CB4 4WS, England, Private Communication, July 15, 1991.

John W. Bandler (S'66-M'66-SM'74-F'78), for a photograph and biography, see this issue, p. 1331.

Radoslaw M. Biernacki (M'85-SM'86) was born in Warsaw, Poland. He received the Ph.D. degree from the Technical University of Warsaw, Warsaw, Poland, in 1976.

He became a Research and Teaching Assistant in 1969 and an Assistant Professor in 1976 at the Institute of Electronics Fundamentals, Technical University of Warsaw, Warsaw, Poland. From 1978 to 1980 he was on leave with the Research Group on Simulation, Optimization and Control and with the Department of Electrical and Computer Engineering, McMaster University, Hamilton, Canada, as a Post-Doctorate Fellow. From 1984 to 1986 he was a Visiting Associate Professor at Texas A&M University, College Station, TX. He joined Optimization Systems Associates Inc., Dundas, Ontario, Canada, in 1986 as Senior Research Engineer. At OSA he has been involved in the development of commercial CAE software systems HarPE™, OSA90™ and OSA90/hope™ and related research on parameter extraction, statistical device modeling, simulation and optimization, including yield-driven design of linear and nonlinear microwave circuits. In 1988 he also became a Professor (part time) in the Department of Electrical and Computer Engineering, McMaster University, Hamilton, ON, Canada. His research interests include system theory, optimization and numerical methods, computer-aided design of integrated circuits and control systems.

Dr. Biernacki has more than 70 publications and has been the recipient of several prizes for his research and teaching activities.

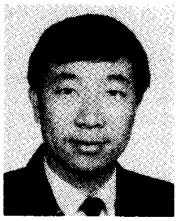

Qian Cai (S'90) was born in Zhanjiang, Guangdong, China, on October 16, 1957. He received the M.S.(Eng.) degree from the South China Institute of Technology, Guangzhou, China, in 1986.

From June 1986 to August 1988, he was with the Department of Electrical Engineering, Guangdong Institute of Technology, Guangzhou, China. He was awarded a Chinese Government Graduate Scholarship and joined the Simulation Optimization Systems Research Laboratory and the Department of Electrical and Computer Engineering, McMaster University, Hamilton, ON, Canada, in September 1988, where he is currently a teaching assistant and graduate student working towards the Ph.D. degree. He has been awarded a Clifton W. Sherman Graduate Scholarship for the academic year 1990–1991. His research interests are in circuit CAD, including device physics and modeling, circuit simulation and optimization, statistical modeling and design, sensitivity analysis and yield optimization.

Shao Hua Chen (S'84–M'88) was born in Swatow, Guangdong, China, on September 27, 1957. He received the B.S.(Eng.) degree from the South China Institute of Technology, Guangzhou, China, in 1982 and the Ph.D. degree in electrical engineering from McMaster University, Hamilton, ON, Canada, in 1987.

From July 1982 to August 1983, he was a teaching assistant in the Department of Automation at the South China Institute of Technology. He was a graduate student in the Department of Electrical and Computer Engineering at McMaster University from 1983 to 1987, during which time he was awarded an Ontario Graduate Scholarship for two academic years. He joined Optimization Systems Associates Inc., Dundas, ON, Canada, in 1987 and engaged in commercial CAD software development. Currently he is working as a Research Engineer in the Simulation Optimization Systems Research Laboratory at McMaster University. His professional interests include optimization theory and implementation, CAD software architecture, device modeling, statistical simulation, circuit design centering, sensitivity analysis, computer graphics and user interfaces.

Shen Ye (S'88–M'92) was born in Shanghai, China, in 1957. He received the B.Eng. and M.Eng. degrees from Shanghai University of Technology, Shanghai, China, in 1982 and 1984, respectively, and the Ph.D. degree from McMaster University, Hamilton, Canada, in 1991, all in electrical engineering.

From 1984 to 1986, he was a teaching and research assistant in the Department of Electrical Engineering, Shanghai University of Technology. He joined the Simulation Optimization Systems Research Laboratory and the Department of Electrical and Computer Engineering, McMaster University as a graduate student in 1986. He held an Ontario Graduate Scholarship for the academic year 1989/90. He was awarded a NSERC Industrial Research Fellowship in 1991 and has been a research engineer with Optimization Systems Associates Inc., Dundas, ON, Canada, since then. His research interests include circuit CAD software design, simulation and optimization techniques, active and passive device modeling and parameter extraction and statistical circuit design.

Qi-Jun Zhang (S'84–M'87) was born in Xianyan, Shanxi, China on October 8, 1959. He received the B.Eng. degree from the East China Engineering Institute, Nanjing, China in 1982, and the Ph.D. degree from McMaster University, Hamilton, ON, Canada, in 1987, both in electrical engineering.

He was with the Institute of Systems Engineering, Tianjin University, Tianjin, China, from 1982 to 1983. He was a postdoctorate fellow in the Department of Electrical and Computer Engineering, McMaster University, in 1987 and 1988. He was a research engineer with Optimization Systems Associates Inc., Dundas, On, Canada from 1988 to 1990. During 1989 and 1990 he was also an Assistant Professor (part-time) of Electrical and Computer Engineering in McMaster University. He joined the Department of Electronics, Carleton University, Ottawa, ON, Canada in 1990 where he is presently an Assistant Professor. His professional interests include all aspects of circuit CAD with emphasis on large scale simulation and optimization, statistical design and modelling, parameter extraction, sensitivity analysis, and optimization of microwave circuits and high-speed VLSI interconnects.

Dr. Zhang is a contributor to *Analog Methods for Computer-Aided Analysis and Diagnosis*, (Marcel Dekker, 1988). Currently he is the holder of the Junior Industrial Chair in CAE established at Carleton University by Bell-Northern Research and the Natural Sciences and Engineering Research Council of Canada.

Reprint 11

Yield-Driven Electromagnetic Optimization via Multilevel Multidimensional Models

Yield-Driven Electromagnetic Optimization via Multilevel Multidimensional Models

John W. Bandler, *Fellow, IEEE*, Radoslaw M. Biernacki, *Senior Member, IEEE*, Shao Hua Chen, *Member, IEEE*, Piotr A. Grobelny, and Shen Ye, *Member, IEEE*

Abstract—**We present the foundation of a sophisticated hierarchical multidimensional response surface modeling system for efficient yield-driven design. Our scheme dynamically integrates models and database updating in real optimization time. The method facilitates a seamless, smart optimization-ready interface. It has been specially designed to handle circuits containing complex subcircuits or components whose simulation requires significant computational effort. This approach makes it possible, for the first time, to perform direct gradient-based yield optimization of circuits with components or subcircuits simulated by an electromagnetic simulator. The efficiency and accuracy of our technique are demonstrated by yield optimization of a three-stage microstrip transformer and a small-signal microwave amplifier. We also perform yield sensitivity analysis for the three-stage microstrip transformer.**

I. Introduction

A NEW multilevel multidimensional response surface modeling technique is presented for effective and efficient yield-driven design. This approach makes it possible, for the first time, to perform yield optimization as well as yield sensitivity analysis of circuits with microstrip structures simulated by an electromagnetic (EM) simulator.

Yield-driven design is now recognized as effective, not only for massively manufactured circuits but also to ensure first-pass success in any design where the prototype development is lengthy and expensive. The complexity of calculations involved in yield optimization requires special numerical techniques, e.g., [1]–[4]. In this paper we extend our previously published [2], [4], highly efficient quadratic interpolation technique to dynamic multilevel response surface modeling. It has been specially designed to handle circuits containing complex subcircuits or components whose simulation requires significant computational effort.

With the increasing availability of EM simulators [5]–[7] it is very tempting to include them into performance-driven and even yield-driven circuit optimization. However, direct utilization of EM simulation for yield optimization or sensitivity analysis might seem to be computationally prohibitive. By constructing what we call local Q-models for each component simulated by an EM simulator we effectively overcome the computational burden of repeated EM simulations, which would otherwise be invoked for many statistical circuit outcomes throughout all yield optimization iterations. To maintain high accuracy, the Q-models are automatically updated whenever an outcome leaves the validity region of the current Q-model.

We show that when the proposed multilevel Q-modeling technique is used together with expensive, but more accurate simulations at the component level, the results are more reliable than those obtained from traditional analytical/empirical component simulations.

Efficiency and accuracy of our technique are demonstrated by yield optimization of a three-stage microstrip transformer and a small-signal amplifier. For the three-stage microstrip transformer we additionally perform yield sensitivity analyses and investigate different sets of optimization variables. Optimization was performed within the OSA90/hope™ [8] simulation-optimization environment with Empipe™ [9] driving ***em***™ [7] on a Sun SPARCstation 1+. We used the OSA90/hope one-sided ℓ_1 optimizer [10] for yield optimization.

Manuscript received March 29, 1993; revised June 16, 1993. This work was supported in part by Optimization Systems Associates Inc., and in part by the Natural Sciences and Engineering Research Council of Canada under Grants OGP0007239, OGP0042444, and STR0117819. Additional support was provided through a Natural Sciences and Engineering Research Council of Canada Industrial Research Fellowship granted to S. Ye.

J. W. Bandler, R. M. Biernacki, and S. H. Chen are with the Simulation Optimization Systems Research Laboratory, Department of Electrical and Computer Engineering, McMaster University, Hamilton, Ont., Canada L8S 4L7 and Optimization Systems Associates Inc., P.O. Box 8083, Dundas, Ont., Canada L9H 5E7.

P. A. Grobelny is with the Simulation Optimization Systems Research Laboratory, Department of Electrical and Computer Engineering, McMaster University, Hamilton, Ont., Canada L8S 4L7.

S. Ye was with Optimization Systems Associates Inc., P.O. Box 8083, Dundas, Ont., Canada L9H 5E7. He is now with Com Dev Ltd., Cambridge, Ont., Canada N1R 7H6.

IEEE Log Number 9212999.

II. Efficient Q-Modeling

A. Formulation of the Method

The Q-model of a generic response $f(\boldsymbol{x})$, i.e., any response or gradient function for which we want to build and utilize the model, is a multidimensional quadratic polynomial of the form

$$q(\boldsymbol{x}) = a_0 + \sum_{i=1}^{n} a_i(x_i - r_i) + \sum_{\substack{i=1 \\ j \geq i}}^{n} a_{ij}(x_i - r_i)(x_j - r_j) \quad (1)$$

0018-9480/93$03.00 © 1993 IEEE

where $\boldsymbol{x} = [x_1 \;\; x_2 \;\cdots\; x_n]^T$ is the vector of generic parameters in terms of which the response is defined, and $\boldsymbol{r} = [r_1 \;\; r_2 \;\cdots\; r_n]^T$ is a chosen reference point in the parameter space.

To build the Q-model we use $n + 1 \le m \le 2n + 1$ base points at which the function $f(\boldsymbol{x})$ is evaluated. The reference point $\boldsymbol{r}$ is selected as the first base point $\boldsymbol{x}^1$. The remaining $m - 1$ base points are selected by perturbing one variable at a time around $\boldsymbol{r}$, namely,

$$\boldsymbol{x}^{i+1} = \boldsymbol{r} + [0 \;\cdots\; 0 \;\; \beta_i \;\; 0 \;\cdots\; 0]^T, \quad i = 1, 2, \cdots, n \tag{2}$$

$$\boldsymbol{x}^{n+1+i} = \boldsymbol{r} + [0 \;\cdots\; 0 \;\; -\beta_i \;\; 0 \;\cdots\; 0]^T, \quad i = 1, 2, \cdots, m - (n + 1) \tag{3}$$

where β_i is a predetermined perturbation. If a variable is perturbed twice the second perturbation is located symmetrically w.r.t. $\boldsymbol{r}$. We have applied the maximally flat quadratic interpolation (MFQI) technique [2] to such a set of base points (see [3], [4] for details). MFQI builds the Q-model by minimizing in the least-squares sense all the second-order term coefficients in (1). It is intuitively equivalent to constructing an interpolation that has the smallest deviation from the linear interpolation.

B. Implementation

Applying MFQI to the base points defined by $\boldsymbol{r}$, (2), and (3) and reordering the variables such that the first $m - (n + 1)$ variables are perturbed twice yields the following formulas for the coefficients in (1):

$$a_{ii} = \frac{1}{2\beta_i^2}[f(\boldsymbol{x}^{n+1+i}) + f(\boldsymbol{x}^{i+1}) - 2f(\boldsymbol{r})], \quad i = 1, 2, \cdots, m - (n + 1) \tag{4a}$$

$$a_{ii} = 0, \quad i = m - n, \cdots, n, \; m \ne 2n + 1 \tag{4b}$$

and

$$a_{ij} = 0, \quad i, j = 1, 2, \cdots, n, \; i \ne j. \tag{4c}$$

The coefficients a_0 and a_i are given by

$$a_0 = f(\boldsymbol{r}) \tag{5}$$

$$a_i = \frac{1}{2\beta_i}[-f(\boldsymbol{x}^{n+1+i}) + f(\boldsymbol{x}^{i+1})], \quad i = 1, 2, \cdots, m - (n + 1) \tag{6a}$$

and

$$a_i = \frac{1}{\beta_i}[f(\boldsymbol{x}^{i+1}) - f(\boldsymbol{r})], \quad i = m - n, \cdots, n, \; m \ne 2n + 1. \tag{6b}$$

Substituting (4), (5) and (6) into (1) results in the following formula for the Q-model $q(\boldsymbol{x})$

$$\begin{aligned} q(\boldsymbol{x}) = f(\boldsymbol{r}) + \sum_{i=1}^{m-(n+1)} \{[f(\boldsymbol{x}^{i+1}) - f(\boldsymbol{x}^{n+1+i}) \\ + (f(\boldsymbol{x}^{i+1}) + f(\boldsymbol{x}^{n+1+i}) \\ - 2f(\boldsymbol{r}))(x_i - r_i)/\beta_i](x_i - r_i)/(2\beta_i)\} \\ + \sum_{i=m-n}^{n} \{[f(\boldsymbol{x}^{i+1}) - f(\boldsymbol{r})](x_i - r_i)/\beta_i\}. \end{aligned} \tag{7}$$

It is important to realize that the variable number of base points m offers a trade-off between the accuracy and cost of circuit analysis. Reducing the number of base points decreases the number of function evaluations. However, perturbing a variable only once results in a linear rather than quadratic interpolation w.r.t. that variable. This provides a spectrum of available models from a linear model (L-model), for $m = n + 1$, to a quadratic model w.r.t. all variables for $m = 2n + 1$.

The simplicity of (7) results in high efficiency of the approach. It should be noted that the computational effort increases only linearly with the number of variables n.

To apply a gradient-based optimizer we need to provide the gradients of functions $q(\boldsymbol{x})$ that are actually used by the optimizer. Differentiating (7) w.r.t. x_i results in

$$\begin{aligned} \partial q(\boldsymbol{x})/\partial x_i = [(f(\boldsymbol{x}^{i+1}) - f(\boldsymbol{x}^{n+1+i}))/2 + (f(\boldsymbol{x}^{i+1}) \\ + f(\boldsymbol{x}^{n+1+i}) - 2f(\boldsymbol{r}))(x_i - r_i)/\beta_i]/\beta_i \\ i = 1, \cdots, m - (n + 1) \end{aligned} \tag{8a}$$

and

$$\partial q(\boldsymbol{x})/\partial x_i = [f(\boldsymbol{x}^{i+1}) - f(\boldsymbol{r})]/\beta_i, \quad i = m - n, \cdots, n, \; m \ne 2n + 1 \tag{8b}$$

which again is very efficient.

C. Linear Versus Quadratic Modeling

We use a simple example in which we approximate the response of a microstrip line simulated as a two-port network by the ***em*** [7] simulator.

We fix the width of the microstrip line and sweep its length l with a step Δl. First, we simulate the circuit at each point in the sweep. This provides us with the response reference data. Subsequently, we use both L- and Q-models to approximate responses at *every other* sweep point using adjacent sweep points as the model base points. Fig. 1 summarizes the results. It shows the real part of S_{11} with l swept from 3.2 to 3.8 mm and $\Delta l = 0.1$ mm. The responses for $l = 3.3$, 3.5, and 3.7 mm are modeled. The L-model uses responses at two adjacent points to model the response at the point in between, e.g., responses at points 3.2 and 3.4 mm are used to model the

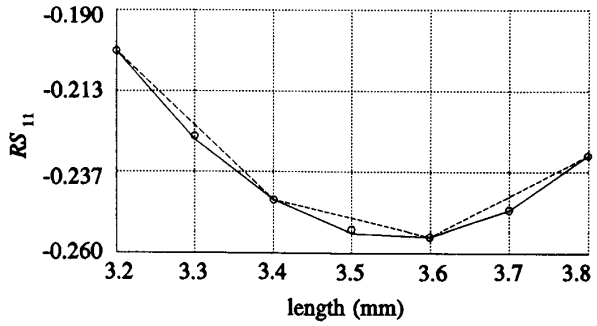

Fig. 1. Comparison between linear (dashed line) and quadratic (solid line) approximations of the real part of S_{11} of a microstrip line simulated by the *em* [7] simulator (circles).

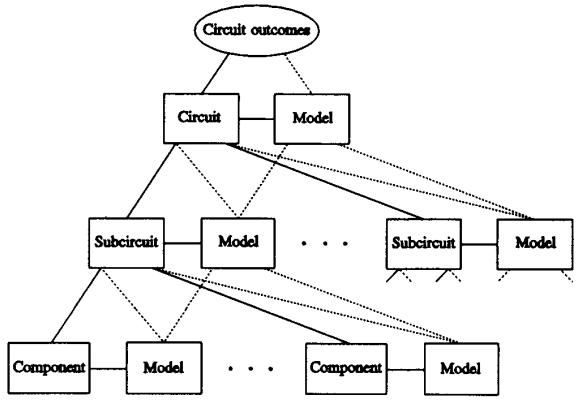

Fig. 2. Schematic diagram illustrating multilevel modeling for yield-driven optimization. Solid and dotted lines distinguish between simulated and modeled responses, respectively.

response at 3.3 mm. The Q-model uses three points, e.g., responses at points 3.4, 3.6, and 3.8 mm are used to model the response at 3.7 mm. It can be seen that the Q-model is more accurate than the L-model.

III. Multilevel Simulation and Modeling

A. Multilevel Modeling

Multilevel modeling is depicted schematically in Fig. 2. The circuit under consideration is divided into subcircuits, possibly in a hierarchical manner. At the lowest level we have circuit components, e.g., a lumped capacitor or a microstrip structure.

Defining f_c, f_s and f_e as circuit, subcircuit and component responses, respectively, we can express the response of the circuit as a function of the subcircuit responses that are in turn functions of component responses. This hierarchy can be expressed formally as

$$f_c = f_c(f_{s1}, f_{s2}, \cdots, f_{sn_s}) \tag{9}$$

$$f_{si} = f_{si}(f_{ei1}, f_{ei2}, \cdots, f_{ein_{ei}}), \qquad i = 1, 2, \cdots, n_s \tag{10}$$

and

$$f_{eij} = f_{eij}(\boldsymbol{x}), \qquad i = 1, 2, \cdots, n_s, \quad j = 1, 2, \cdots, n_{ei} \tag{11}$$

where n_s is the number of subcircuits and n_{ei} is the number of components in the ith subcircuit. $\boldsymbol{x}$ is the vector of circuit parameters. The responses are typically frequency-domain functions of multiport responses.

We can create a single Q-model for the overall circuit. We can also create a hierarchy of Q-models to represent some or all of the subcircuits and components, as illustrated in Fig. 2.

If the base points of a Q-model are given as $\boldsymbol{x}^1$, $\boldsymbol{x}^2$, $\cdots$, $\boldsymbol{x}^m$, where $\boldsymbol{x}^1$ is treated as the reference point $\boldsymbol{r}$ [see (2) and (3)] and $n + 1 \le m \le 2n + 1$, with n being the number of model parameters, then we can express the simulation results at these base points as

$$[\boldsymbol{f}(\boldsymbol{x}^1) \quad \boldsymbol{f}(\boldsymbol{x}^2) \quad \cdots \quad \boldsymbol{f}(\boldsymbol{x}^m)] \tag{12}$$

with

$$\boldsymbol{f}(\boldsymbol{x}^i) = [f_1(\boldsymbol{x}^i) \quad f_2(\boldsymbol{x}^i) \quad \cdots \quad f_k(\boldsymbol{x}^i)]^T, \qquad i = 1, 2, \cdots, m \tag{13}$$

where k is the total number of different responses. $\boldsymbol{f}$ can include a response of either circuit, subcircuit, or a component. Then

$$\boldsymbol{f}(\boldsymbol{x}) \approx \boldsymbol{q}(\boldsymbol{x}) = [q_1(\boldsymbol{x}) \quad q_2(\boldsymbol{x}) \quad \cdots \quad q_k(\boldsymbol{x})]^T. \tag{14}$$

The Q-models in (14) approximate $\boldsymbol{f}(\boldsymbol{x})$ for $\boldsymbol{x}$ belonging to the Q-model validity region centered around the reference point $\boldsymbol{r} = \boldsymbol{x}^1$.

B. Implementation

During optimization the design center moves, and so does the set of associated statistical outcomes. This may result in moving some or even all of the statistical outcomes out of the validity region of the current Q-models. In the present implementation the validity region $\boldsymbol{V}$ is defined as

$$\boldsymbol{V} = \{\boldsymbol{x} \mid -\beta_i/2 < (x_i - r_i) \le \beta_i/2, \quad i = 1, 2, \cdots, n\} \tag{15}$$

where β_i is the perturbation used in (2) and (3) to compute the model base points. To use the model for a point outside the current $\boldsymbol{V}$ requires that the Q-models in (14), and hence $\boldsymbol{V}$, be appropriately updated. We have developed

an updating scheme in which the Q-models are updated automatically in real optimization time. If a statistical outcome is outside the current $\boldsymbol{V}$, a new set of base points is generated and the responses at these base points are simulated *but only if they have not been simulated previously*. Updated Q-models follow immediately from recomputing (7). Our Q-model updating scheme is based on a database system storing results for newly simulated base points and providing extremely fast access to the results for already simulated base points. The database and Q-models are updated whenever new results become available.

If all components, subcircuits, and the overall circuit were to be simulated rather than modeled the evaluation of the circuit response $\boldsymbol{f}_c$ could proceed as follows.

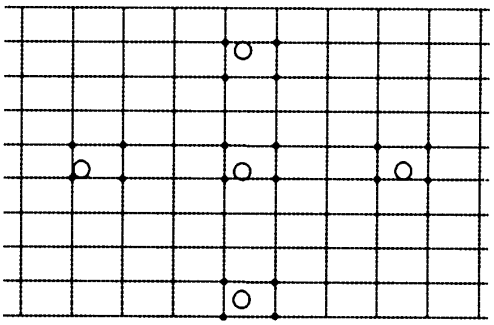

Fig. 3. Illustration of base points and discrete points. The large circles represent possible locations of base points w.r.t. a grid. The solid dots indicate discrete simulation points on the grid. If the base points are snapped to the grid, the number of simulations can be significantly reduced.

```
for the ith subcircuit, i = 1, 2, · · · , n_s {
        for the jth component in the ith subcircuit, j = 1, 2, · · · , n_ei {
                find f_eij by simulating the component according to (11);
        }
        find f_si according to (10);
}
find f_c according to (9);
```

Applying this algorithm to yield estimation or optimization may become prohibitive, especially if an EM simulator is to be used. Replacing costly circuit simulations with model evaluations yields an alternative algorithm.

```
if circuit model q_c exists
        evaluate q_c;
else {
        for the ith subcircuit, i = 1, 2, · · · , n_s {
                if subcircuit model q_si exists {
                        evaluate q_si;
                }
                else {
                        for the jth component in the ith subcircuit, j = 1, 2, · · · , n_ei {
                                if component model q_eij exists {
                                        evaluate q_eij;
                                }
                                else {
                                        find f_eij by simulating the component according to (11);
                                }
                        }
                        find f_si according to (10);
                }
        }
        find f_c according to (9);
}
```

Here, some of the responses $\boldsymbol{f}_{eij}$, $\boldsymbol{f}_{si}$ or $\boldsymbol{f}_c$ are replaced by the corresponding models $\boldsymbol{q}_{eij}$, $\boldsymbol{q}_{si}$, or $\boldsymbol{q}_c$.

C. Discrete Parameters

The circuit, subcircuits, and components may contain discrete parameters. For discrete parameters simulation can only be performed at discrete values located on the grid, as illustrated in Fig. 3. Normally, the reference vector $\boldsymbol{r}$ is taken as the nominal point $\boldsymbol{x}^1$. This is likely to be off-the-grid. Similarly, the other base points $\boldsymbol{x}^{i+1}$ and $\boldsymbol{x}^{n+1+i}$ are likely to be off-the-grid. Local interpolation involving several simulations on the grid in the vicinity of each of the base points must then be performed. In order to avoid these excessive simulations those base points are modified to snap to the grid.

IV. Yield Optimization of a Three-Section Microstrip Transformer

A. The Transformer

A three-section 3:1 microstrip impedance transformer is shown in Fig. 4. The source and load impedances are 50 and 150 ohms, respectively. The design specification is set for input reflection coefficient as

$$|S_{11}| \leq 0.12 \text{ from 5 to 15 GHz.}$$

The error functions for yield optimization are calculated for frequencies from 5 to 15 GHz with a 0.5 GHz step. The transformer is built on a 0.635 mm thick substrate with relative dielectric constant 9.7.

For EM simulators, the circuit is typically partitioned into components that are defined to encompass parts of the structure that can be isolated from the other parts. This can significantly increase the efficiency of EM simulation.

The transformer was decomposed into three components, each corresponding to a different section of the transformer. In order to account for the discontinuity effects the first two sections were simulated as step discontinuities and the last section as a microstrip line. Each of the components is simulated as a two-port network.

As a verification, we also simulated the entire transformer structure as one piece. The results of simulating the circuit at the nominal minimax solution using the two methods are virtually the same.

B. Yield Optimization with Six Optimization Variables

We start yield optimization from the solution of a nominal design with W_1, W_2, W_3, L_1, L_2, and L_3 as variables. Normal distributions with 2 percent standard deviations were assumed for W_1, W_2, and W_3 and 1 percent standard deviations for L_1, L_2, and L_3. Three component-level Q-models were established for each section of the transformer at the nominal point using ***em*** [7]. The Q-models were updated during the optimization process whenever necessary.

Utilizing these Q-models we conducted two experiments to demonstrate multilevel Q-modeling: 1) yield optimization using single-level (component) modeling and 2) yield optimization using two-level (component and circuit response) modeling. 100 statistical outcomes were used for yield optimization. The solutions in both cases are almost identical: yield (estimated by 250 outcomes) is increased from 71 to 86 percent using single-level modeling and to 85 percent using two-level modeling. Fig. 5(a) illustrates the Monte Carlo sweep before optimization and Fig. 5(b) shows the corresponding sweep after yield optimization using single-level (component) modeling. The values of the optimization variables before and after yield optimization for both single- and two-level modeling are given in Table I. The solution of design centering is quite close to the nominal minimax design. This is expected, taking into account the small tolerances on the parameters.

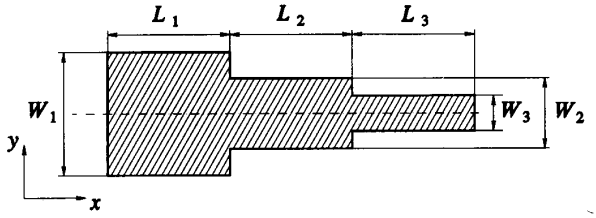

Fig. 4. The three-section 3:1 microstrip impedance transformer. The thickness and dielectric constant of the substrate are 0.635 mm and 9.7, respectively.

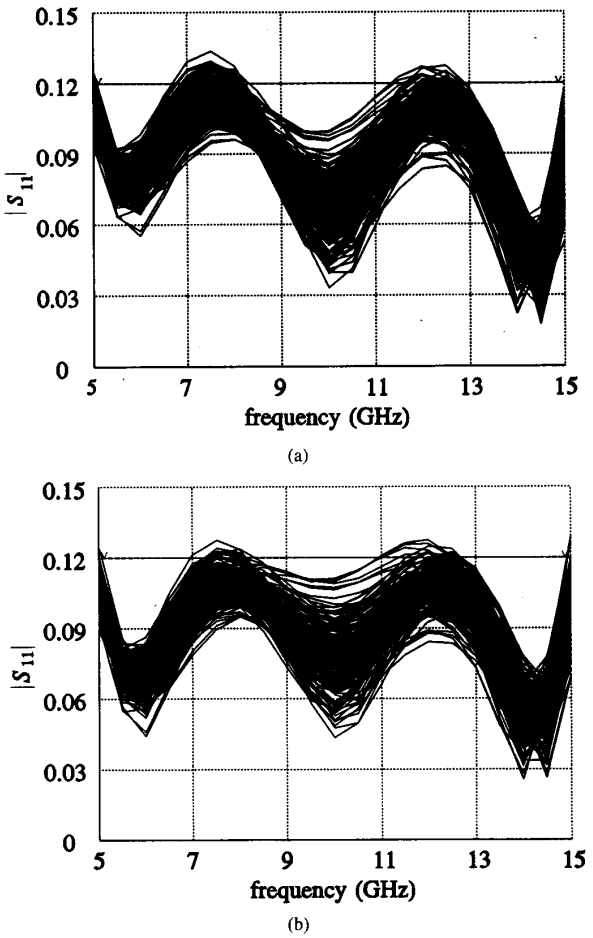

Fig. 5. Modulus of the reflection coefficient of the three-section microstrip impedance transformer versus frequency: (a) before and (b) after yield optimization. Yield is increased from 71 to 86 percent after optimization using single-level (component) Q-models.

CPU time for yield optimization, performed on a Sun SPARCstation 1+, was 16 min for single-level modeling and 3 min when two-level Q-models were used. Elapsed time for the ***em*** [7] simulations using single-level modeling was about 100 h. The two-level modeling approach exploited the database created during single-level optimization and did not require any additional ***em*** [7] simulations.

TABLE I
MICROSTRIP PARAMETERS OF THE THREE-SECTION MICROSTRIP TRANSFORMER (SIX VARIABLES)

Parameters[a]	Nominal design	Centered design[b]	Centered design[c]
W_1	0.4294	0.4363	0.4377
W_2	0.2080	0.2055	0.2053
W_3	0.07	0.07	0.07
L_1	3.0	2.951	2.8875
L_2	3.0	2.998	3.0007
L_3	3.0	3.046	3.058
Yield[d]	71 percent	86 percent	85 percent

[a]Parameters are in millimeters.
[b]Single-level modeling.
[c]Two-level modeling.
[d]100 outcomes were used in yield optimization and 250 outcomes for yield verification.

TABLE II
MICROSTRIP PARAMETERS OF THE THREE-SECTION MICROSTRIP TRANSFORMER (THREE VARIABLES)

Parameters[a]	Nominal design	Centered design[b]	Centered design[c]
W_1	0.4294	0.4339	0.4333
W_2	0.2080	0.2081	0.2079
W_3	0.07	0.07	0.07
L_1	3.0[d]	3.0[d]	3.0[d]
L_2	3.0[d]	3.0[d]	3.0[d]
L_3	3.0[d]	3.0[d]	3.0[d]
Yield[e]	71 percent	79 percent	78 percent

[a]Parameters are in millimeters.
[b]Single-level modeling.
[c]Two-level modeling.
[d]Not optimized.
[e]100 outcomes were used in yield optimization and 250 outcomes for yield verification.

C. Yield Optimization with Three Optimization Variables

We investigated yield optimization with W_1, W_2, and W_3 as variables. L_1, L_2, and L_3 were not optimized. The solutions obtained using component and both component and circuit modeling are again very similar. Yield is increased to 79 percent with component-level Q-models and to 78 percent with component- and circuit-level Q-models. Parameter values for both solutions are listed in Table II. The CPU time was 5 min for component-level and 41 s for two-level Q-modeling. The previously established database was sufficient for this experiment, so that no additional ***em*** [7] simulations were required.

D. Yield Sensitivity Analysis

We performed the yield sensitivity analysis at the centered solution obtained using six optimization variables.

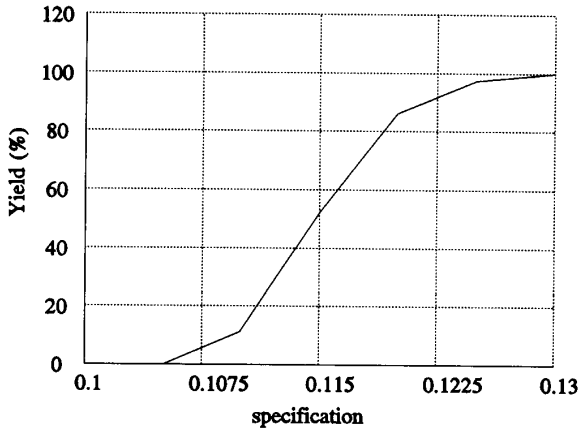

Fig. 6. Yield of the three-section microstrip transformer as a function of the specification imposed on $|S_{11}|$. High sensitivity of yield w.r.t. the specification can be observed. Yield is estimated with 250 Monte Carlo outcomes.

Fig. 6 shows yield as a function of the specification. The specification is swept from 0.10 to 0.13 with a 0.005 step. 250 Monte Carlo outcomes were used. The diagram confirms high sensitivity of yield w.r.t. the specification. The yield varies from 0 to 100 percent over a very small range of the specification.

We performed sensitivity analysis w.r.t. all six optimization variables using 250 statistical outcomes. As expected, the yield is very sensitive to the widths of all the sections and it is insensitive to the lengths of the sections. We also observed that the yield exhibits the highest sensitivity w.r.t. the width of the third section W_3. The analysis required very little additional computational effort. See Fig. 7 for the results.

V. YIELD OPTIMIZATION OF A SMALL-SIGNAL AMPLIFIER

The specification for a typical single-stage 6-18 GHz small-signal amplifier shown in Fig. 8 is

$$7 \text{ dB} \leq |S_{21}| \leq 8 \text{ dB from 6 to 18 GHz.}$$

The error functions for yield optimization are calculated at frequencies from 6 to 18 GHz with a 1 GHz step. The gate and drain circuit microstrip T-structures and the feedback microstrip line are built on a 10 mil thick substrate with relative dielectric constant 9.9.

First, we performed nominal minimax optimization using analytical/empirical microstrip component models. W_{g1}, L_{g1}, W_{g2}, L_{g2} of the gate circuit T-structure and W_{d1}, L_{d1}, W_{d2}, L_{d2} of the drain circuit T-structure were selected as optimization variables. W_{g3}, L_{g3}, W_{d3}, and L_{d3} of the T-structures, W and L of the feedback microstrip line, as

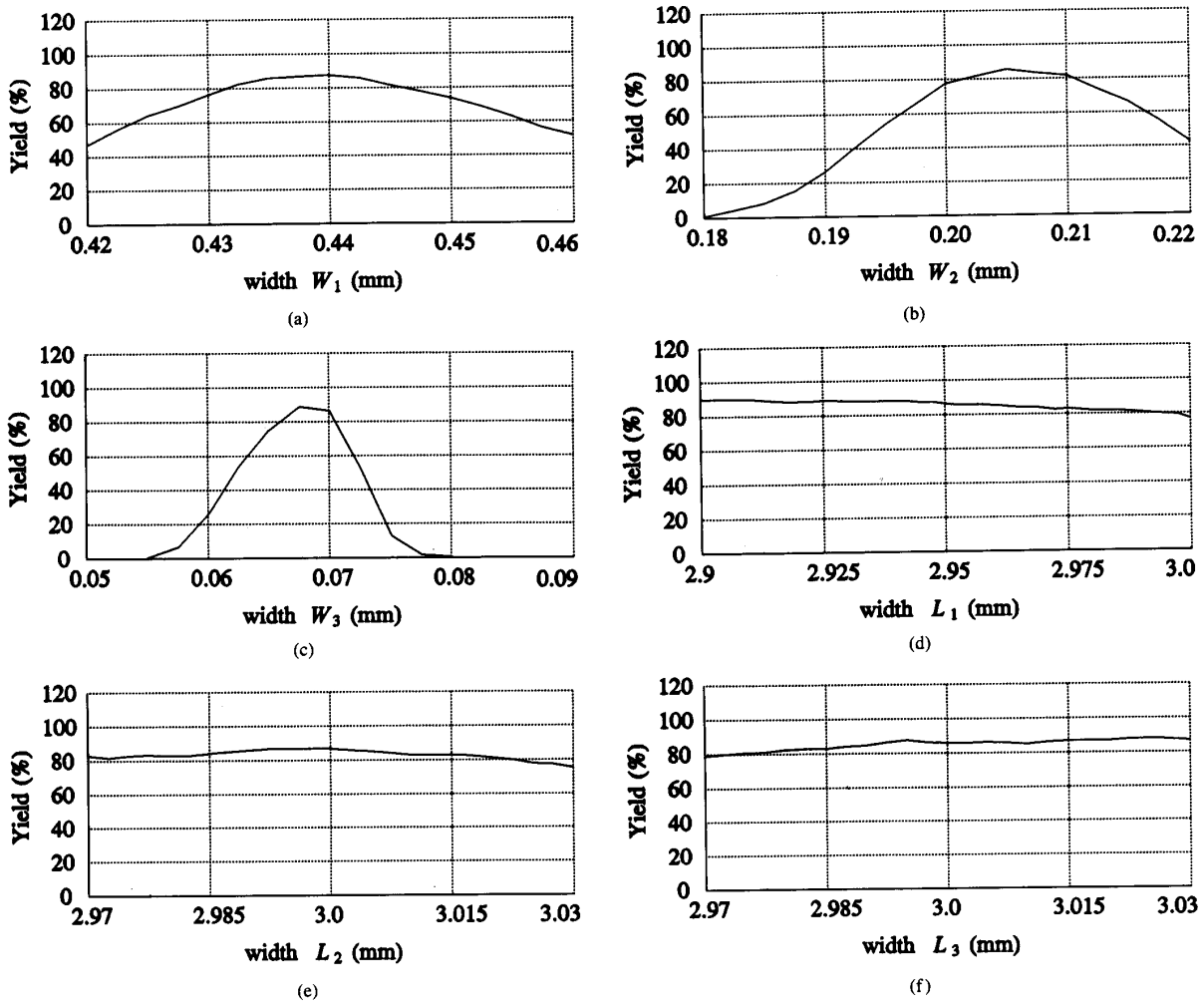

Fig. 7. Yield sensitivity analysis for the three-stage microstrip transformer at the centered solution. 250 Monte Carlo outcomes were used for yield estimation. The results are obtained with little additional computational effort. Yield as a function of (a) W_1, (b) W_2, (c) W_3, (d) L_1, (e) L_2, and (f) L_3.

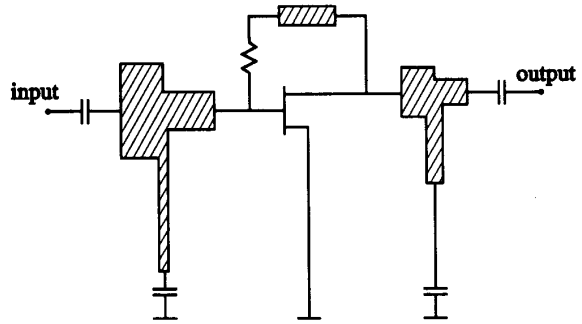

Fig. 8. Circuit diagram of the 6–18 GHz small-signal amplifier. We use *em* [7] to model the two *T*-structures and the microstrip line.

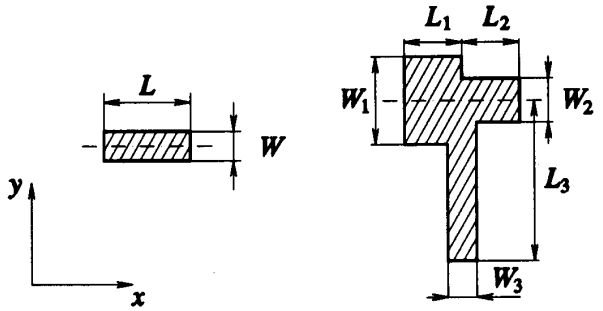

Fig. 9. Parameters of the feedback microstrip line and the microstrip *T*-structures.

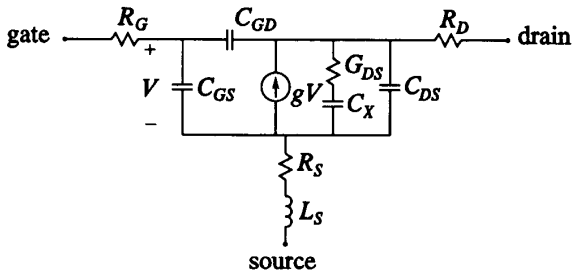

Fig. 10. Schematic diagram of the small-signal FET model. The value of the capacitor C_x is 2.0 pF. The transadmittance g is evaluated as $g = g_m e^{-2j\pi f\tau}$, where g_m and τ are given in Table III and f is the frequency.

TABLE III
EXTRACTED STATISTICAL DISTRIBUTIONS FOR THE FET PARAMETERS (FIG. 10)

FET parameter	Mean value	Standard deviation (percent)
R_G (Ω)	2.035	3
R_D (Ω)	3.421	8
R_S (Ω)	3.754	6
L_S (nH)	0.0811	7
$G_{DS}(1/\Omega)$	0.00598	1
C_{DS}(pF)	0.06978	1
g_m	−0.0713	2
τ(ps)	1.9093	2
C_{GD}(pF)	0.02606	2
C_{GS}(pF)	0.30319	1.5

TABLE IV
EXTRACTED FET MODEL PARAMETER CORRELATIONS

	R_G	R_D	R_S	L_S	G_{DS}	C_{DS}	g_m	τ	C_{GD}	C_{GS}
R_G	1	−0.3121	−0.5869	0.5244	0.1914	−0.1805	−0.4473	−0.0567	−0.0971	−0.2548
R_D	−0.3121	1	0.7279	−0.7479	0.07056	0.411	0.3914	−0.047	−0.206	0.2474
R_S	−0.5869	0.7279	1	−0.8461	−0.0663	0.4825	0.6637	−0.2376	−0.1262	0.1974
L_S	0.5244	−0.7479	−0.8461	1	0.0162	−0.7326	−0.5204	0.02553	0.3676	−0.3084
G_{DS}	0.1914	0.07056	−0.0663	0.0162	1	0.1504	−0.5752	−0.2991	−0.171	0.3561
C_{DS}	−0.1805	0.411	0.4825	−0.7326	0.1504	1	0.1765	0.0295	−0.6786	0.1946
g_m	−0.4473	0.3914	0.6637	−0.5204	−0.5752	0.1765	1	−0.1781	0.0863	−0.3412
τ	−0.0567	−0.047	−0.2376	0.02553	−0.2991	0.0295	−0.1781	1	−0.2122	0.2624
C_{GD}	−0.0971	−0.206	−0.1262	0.3676	−0.171	−0.6786	0.0863	−0.2122	1	−0.2904
C_{GS}	−0.2548	0.2474	0.1974	−0.3084	0.3561	0.1946	−0.3412	0.2624	−0.2904	1

well as the FET parameters were not optimized. Fig. 9 shows the parameters of the T-structures and the microstrip line. Fig. 10 shows the small-signal FET model.

We assumed a 0.5 mil tolerance and uniform distribution for all geometrical parameters of the microstrip components. The statistics of the small-signal FET model were extracted from measurement data [11] and are given in Table III. The correlations among the FET model parameters are listed in Table IV. The value of the feedback resistor was 1600 Ω.

Monte Carlo simulation with 250 outcomes performed at the nominal solution with analytical/empirical microstrip component models reported 91 percent yield. To obtain a more accurate estimate, we used component level Q-models built from ***em*** [7] simulations for the microstrip components. The yield dropped to 55 percent. Fig. 11(a) and (b) show the Monte Carlo sweeps obtained using analytical/empirical and our ***em*** [7] based Q-models, respectively. Close similarities can be observed for lower frequencies, while discrepancies become larger for higher frequencies.

Utilizing the component-level quadratic Q-models built from ***em*** simulations, we further performed yield optimization of this amplifier. Yield estimated by 250 Monte Carlo simulations was increased to 82 percent. The corresponding Monte Carlo sweep diagram is shown in Fig. 12. Yield and the values of the optimization variables before and after optimization are given in Table V.

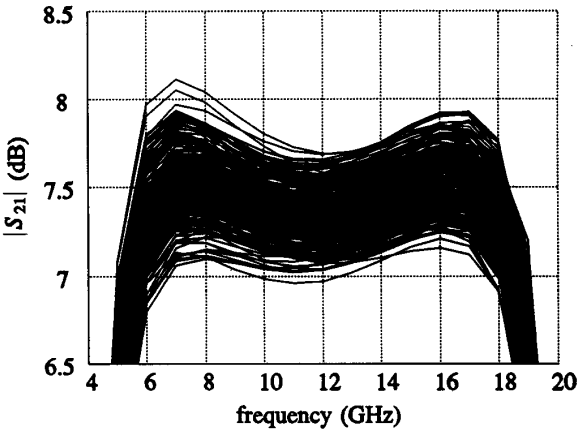

(a)

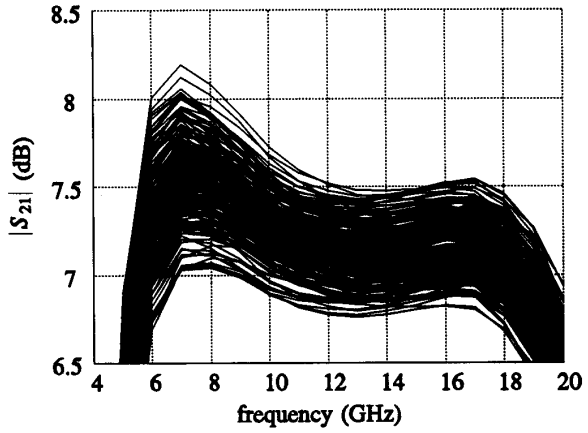

(b)

Fig. 11. $|S_{21}|$ of the small-signal amplifier for 250 statistical outcomes at the nominal minimax solution: (a) using analytical/empirical microstrip component models and (b) using ***em*** [7] based Q-models.

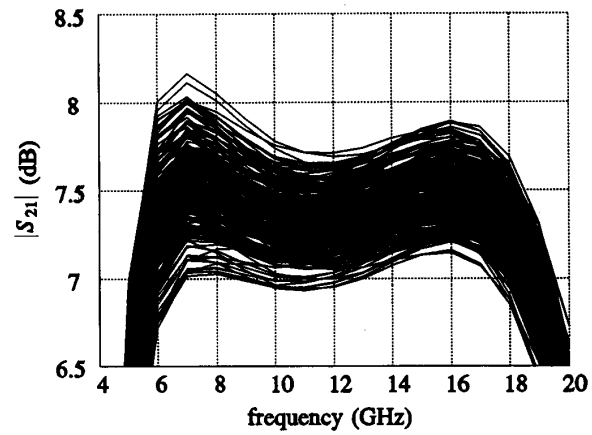

Fig. 12. $|S_{21}|$ of the small-signal amplifier for 250 statistical outcomes after yield optimization using ***em*** [7] based Q-models. Yield is increased from 55 to 82 percent.

TABLE V
MICROSTRIP PARAMETERS FOR THE AMPLIFIER

Parameters[a]	Nominal design	Centered design
W_{g1}	17.45	19
L_{g1}	35.54	34.53
W_{g2}	9.01	8.611
L_{g2}	30.97	32
W_{g3}	3[b]	3[b]
L_{g3}	107[b]	107[b]
W_{d1}	8.562	7
L_{d1}	4.668	6
W_{d2}	3.926	3.628
L_{d2}	9.902	11
W_{d3}	3.5[b]	3.5[b]
L_{d3}	50[b]	50[b]
W	2[b]	2[b]
L	10[b]	10[b]
Yield[c]	55 percent	82 percent

[a]Parameters are in mils. 0.5 mil tolerance and uniform distribution were assumed for all the parameters.
[b]Not optimized.
[c]50 outcomes were used in yield optimization and 250 outcomes for yield verification.

VI. CONCLUSIONS

We have presented a new multilevel quadratic modeling technique suitable for effective and efficient yield-driven design optimization. The method dynamically integrates the Q-models with database generation and updating, increasing both speed of processing and accuracy of the results. The approach is particularly useful for circuits containing complex subcircuits or components whose simulation requires significant computational effort. The efficiency of this technique allowed us to perform yield-driven design and analyze yield sensitivity for circuits containing microstrip structures accurately simulated by ***em*** [7]. We used a three-stage microstrip transformer and a small-signal amplifier to demonstrate the efficiency and accuracy of the method. Our approach significantly extends the microwave CAD applicability of yield optimization techniques.

ACKNOWLEDGMENT

The authors wish to thank Dr. J. C. Rautio of Sonnet Software, Inc., Liverpool, NY, for his initiatives and making ***em*** available for this work.

REFERENCES

[1] J. W. Bandler and S. H. Chen, "Circuit optimization: The state of the art," *IEEE Trans. Microwave Theory Tech.*, vol. 36, pp. 424–443, 1988.
[2] R. M. Biernacki and M. A. Styblinski, "Efficient performance function interpolation scheme and its application to statistical circuit design," *Int. J. Circuit Theory Appl.*, vol. 19, pp. 403–422, 1991.
[3] R. M. Biernacki, J. W. Bandler, J. Song, and Q. J. Zhang, "Efficient quadratic approximation for statistical design," *IEEE Trans. Circuits Syst.*, vol. 36, pp. 1449–1454, 1989.
[4] J. W. Bandler, R. M. Biernacki, S. H. Chen, J. Song, S. Ye, and Q. J. Zhang, "Gradient quadratic approximation scheme for yield-driven design," *IEEE MTT-S Int. Microwave Symp. Dig.*, Boston, MA, 1991, pp. 1197–1200.
[5] T. Itoh, Ed., *Numerical Techniques for Microwave and Millimeter-Wave Passive Structures*. New York: Wiley, 1989.
[6] R. H. Jansen and P. Pogatzki, "A hierarchically structured, compre-

hensive CAD system for field theory-based linear and nonlinear MIC/MMIC design," in *1992 2nd Int. Workshop German IEEE MTT/AP Joint Chapter Integrated Nonlinear Microwave and Millimeterwave Circuits Dig.*, Duisburg, Germany, 1992, pp. 333-341.
[7] *Em User's Manual* and *Xgeom User's Manual*. Sonnet Software, Inc., 135 Old Cove Road, Suite 203, Liverpool, NY, May 1992.
[8] *OSA90/hope™*, Optimization Systems Associates Inc., P.O. Box 8083, Dundas, Ont., Canada L9H 5E7, 1993.
[9] *Empipe™*, Optimization Systems Associates Inc., P.O. Box 8083, Dundas, Ont., Canada L9H 5E7, 1993.
[10] J. W. Bandler, S. H. Chen, and K. Madsen, "An algorithm for one-sided ℓ_1 optimization with application to circuit design centering," in *Proc. IEEE Int. Symp. Circuits Syst.*, Espoo, Finland, 1988, pp. 1795-1798.
[11] Measurement data provided by Plessey Research Caswell Ltd., Caswell, Towcester, Northamptonshire, England, 1990.

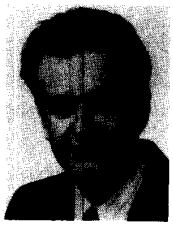

John W. Bandler (S'66-M'66-SM'74-F'78) was born in Jerusalem, on November 9, 1941. He studied at Imperial College of Science and Technology, London, England, from 1960 to 1966. He received the B.Sc. (Eng.), Ph.D. and D.Sc. (Eng.) degrees from the University of London, London, England, in 1963, 1967, and 1976, respectively.

He joined Mullard Research Laboratories, Redhill, Surrey, England in 1966. From 1967 to 1969 he was a Postdoctorate Fellow and Sessional Lecturer at the University of Manitoba, Winnipeg, Canada. He joined McMaster University, Hamilton, Canada, in 1969, where he is currently Professor of Electrical and Computer Engineering. He has served as Chairman of the Department of Electrical Engineering and Dean of the Faculty of Engineering. He currently directs research in the Simulation Optimization Systems Research Laboratory. He is President of Optimization Systems Associates Inc. (OSA), which he founded in 1983. OSA introduced the CAE systems RoMPE™ in 1988, HarPE™ in 1989, OSA90™ and OSA90/hope™ in 1991 and Empipe™ in 1992. He is also President of Bandler Research Inc., which he founded in 1989.

Dr. Bandler is a Fellow of the Royal Society of Canada, a Fellow of the Institution of Electrical Engineers (Great Britain), a member of the Association of Professional Engineers of the Province of Ontario (Canada), and a Member of the Electromagnetics Academy. He contributed to *Modern Filter Theory and Design*, Wiley-Interscience, 1973 and to *Analog Methods for Computer-Aided Analysis and Diagnosis*, Marcel Dekker, Inc., 1988. He has published more than 250 papers, four of which appear in *Computer-Aided Filter Design*, IEEE Press, 1973, one in each of *Microwave Integrated Circuits*, Artech House, 1975, *Low-Noise Microwave Transistors and Amplifiers*, IEEE Press, 1981, *Microwave Integrated Circuits*, 2nd ed., Artech House, 1985, *Statistical Design of Integrated Circuits*, IEEE Press, 1987, and *Analog Fault Diagnosis*, IEEE Press, 1987. He was an Associate Editor of the IEEE TRANSACTIONS ON MICROWAVE THEORY AND TECHNIQUES (1969-1974), Guest Editor of the IEEE TRANSACTIONS ON MICROWAVE THEORY AND TECHNIQUES Special Issue on Computer-Oriented Microwave Practices (March 1974) and Co-Guest Editor with R. H. Jansen of the IEEE TRANSACTIONS ON MICROWAVE THEORY AND TECHNIQUES Special Issue on Process-Oriented Microwave CAD and Modeling (July 1992). He joined the Editorial Boards of the *International Journal of Numerical Modelling* in 1987, and the *International Journal of Microwave and Millimeterwave Computer-Aided Engineering* in 1989.

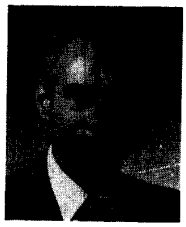

Radoslaw M. Biernacki (M'85-SM'86) was born in Warsaw, Poland. He received the Ph.D. degree from the Technical University of Warsaw, Warsaw, Poland, in 1976.

He became a Research and Teaching Assistant in 1969 and an Assistant Professor in 1976 at the Institute of Electronics Fundamentals, Technical University of Warsaw. From 1978 to 1980 he was on leave with the Research Group on Simulation, Optimization and Control and with the Department of Electrical and Computer Engineering, McMaster University, Hamilton, Ont., Canada, as a Postdoctorate Fellow. From 1984 to 1986 he was a Visiting Associate Professor at Texas A&M University, College Station. He joined Optimization Systems Associates Inc., Dundas, Ont., Canada, in 1986 as Senior Research Engineer. At OSA he has been involved in the development of commercial CAE software systems HarPE™, OSA90™, and OSA90/hope™ and related research on parameter extraction, statistical device modeling, simulation, and optimization, including yield-driven design of linear and nonlinear microwave circuits. In 1988 he also became a Professor (part-time) with the Department of Electrical and Computer Engineering, McMaster University. His research interests include system theory, optimization and numerical methods, and computer-aided design of integrated circuits and control systems.

Dr. Biernacki has authored or coauthored more than 80 publications and has been the recipient of several prizes for his research and teaching activities.

Shao Hua Chen (S'84-M'88) was born in Swatow, Guangdong, China, on September 27, 1957. He received the B.S. (Eng.) degree from the South China Institute of Technology, Guangzhou, China, in 1982, and the Ph.D. degree in electrical engineering from McMaster University, Hamilton, Ont., Canada, in 1987.

From July 1982 to August 1983, he was a teaching assistant with the Department of Automation, South China Institute of Technology. He was a graduate student with the Department of Electrical and Computer Engineering, McMaster University, from 1983 to 1987, during which time he was awarded an Ontario Graduate Scholarship for two academic years. He joined Optimization Systems Associates Inc., Dundas, Ont., Canada, in 1987 and engaged in commercial CAD software development. He has made major contributions to the development of the CAE systems HarPE™ and OSA90/hope™. Currently he is working as a Research Engineer in the Simulation Optimization Systems Laboratory, McMaster University. His professional research interests include optimization theory and implementation, CAD software architecture, device modeling, statistical simulation, circuit design centering, sensitivity analysis, computer graphics, and user interfaces.

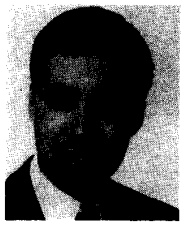

Piotr A. Grobelny was born in Zielona Gora, Poland, on September 18, 1962. He received the M.S. (Eng.) degree from the Technical University of Wroclaw, Wroclaw, Poland, in 1987.

From 1987 to 1990 he worked as a Research Assistant in the Machine Building Institute, Technical University of Wroclaw, where he was involved in the development of CAD and CAE software systems. In September 1990 he joined the Simulation Optimization Systems Research Laboratory and the Department of Electrical and Computer Engineering, McMaster University, Hamilton, Canada, where he is currently a teaching assistant and graduate student working towards the Ph.D. degree. He held an Ontario Differential Fee Waiver Award for the academic year 1990-1991. He has been awarded an Ontario Graduate Scholarship for the academic year 1993-1994. His research interests are in circuit CAD software design, simulation and optimization techniques, response function modeling techniques, sensitivity analysis, and yield optimization.

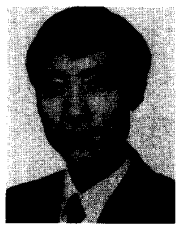

Shen Ye (S'88-M'92) was born in Shanghai, China, in 1957. He received the B.Eng. and M.Eng. degrees from Shanghai University of Technology, Shanghai, China, in 1982 and 1984, respectively, and the Ph.D. degree from McMaster University, Hamilton, Ont., Canada, in 1991, all in electrical engineering.

From 1984 to 1986, he was a teaching and research assistant with the Department of Electrical Engineering, Shanghai University of Technology. He joined the Simulation Optimization Systems Research Laboratory and the Department of Electrical and Computer Engineering, McMaster University as a graduate student in 1986. He held an Ontario Graduate Scholarship for the academic year 1989-1990. In 1991 he was awarded an Industrial Research Fellowship from the Natural Sciences and Engineering Research Council of Canada and was a research engineer with Optimization Systems Associates Inc., Dundas, Ont., Canada, from 1991 to 1993. He contributed substantially in the design and implementation of Empipe™. In 1993 he joined Com Dev Ltd., Cambridge, Ont., Canada, where he is a design engineer. His professional interests include general CAD software design, simulation and optimization techniques, design and optimization of microwave circuits, device modeling, parameter extraction, and statistical circuit design.

Reprint 12

Huber Optimization of Circuits: A Robust Approach

Huber Optimization of Circuits: A Robust Approach

John W. Bandler, *Fellow, IEEE*, Shao Hua Chen, *Member, IEEE*, Radoslaw M. Biernacki, *Senior Member, IEEE*, Li Gao, Kaj Madsen, and Huanyu Yu

***Abstract*—We introduce a novel approach to "robustizing" circuit optimization using Huber functions: both two-sided and one-sided. Advantages of the Huber functions for optimization in the presence of faults, large and small measurement errors, bad starting points, and statistical uncertainties are described. In this context, comparisons are made with optimization using ℓ_1, ℓ_2 and minimax objective functions. The gradients and Hessians of the Huber objective functions are formulated. We contribute a dedicated, efficient algorithm for Huber optimization and show, by comparison, that generic optimization methods are not adequate for Huber optimization. A wide range of significant applications is illustrated, including FET statistical modeling, multiplexer optimization, analog fault location, and data fitting. The Huber concept, with its simplicity and far-reaching applicability, will have a profound impact on analog circuit CAD.**

I. Introduction

ENGINEERING designers are often concerned with the robustness of numerical optimization techniques, and rightly so, knowing that engineering data is, with few exceptions, contaminated by model/measurement/statistical errors.

The classical least-squares (ℓ_2) method is well known for its vulnerability to gross errors: a few wild data points can alter the least-squares solution significantly. The ℓ_1 method is robust against gross errors [1], [2]. We will show, however, that when the data contains many small errors (such as statistical variations), the ℓ_1 solution can be undesirably biased toward a subset of the data points. This indicates that ℓ_1 is not suitable, in general, as a statistical estimator.

Neither the ℓ_2 nor the ℓ_1 method has flexible discriminatory power to recognize and treat differently large (catastrophic) errors and small (soft) errors. We introduce the Huber function [3]–[5], which appears to be a hybrid of the ℓ_1 and ℓ_2 measures. Compared with ℓ_2, the Huber solution is more robust w.r.t. large errors. Compared with ℓ_1, the Huber solution can provide a smoother, less biased estimate from data that contains many small deterministic or statistical variations. We demonstrate the benefits of this novel approach in FET statistical modeling, analog fault location, and data fitting.

We extend the Huber concept by introducing a "one-sided" Huber function for large-scale optimization. For large-scale problems, systematic decomposition techniques have been proposed (e.g., [6], [7]) to reduce computational time and prevent potential convergence problems. In practice, the designer often attempts, by intuition, a "preliminary" optimization with a small number of dominant variables. The full-scale optimization is performed if and when a reasonably good point is obtained.

With a reduced number of variables, the optimizer may not be able to reduce all the error functions at the same time. For instance, the specification may be violated more severely at some sample points (such as frequencies) than at the others. In such situations, the minimax method is preoccupied with the worst-case errors and therefore becomes ineffective or inefficient. We demonstrate, through microwave multiplexer optimization, that the one-sided Huber function can be more effective and efficient than minimax in overcoming a bad starting point.

We present a dedicated, efficient, gradient-based algorithm for Huber optimization and show, by comparison, that generic optimization methods, such as quasi-Newton, conjugate gradient, and simplex algorithms, are not adequate when directly applied to minimizing the Huber objective functions. The gradients and Hessians of the Huber objective functions are derived and their significance is discussed.

II. Theoretical Formulation of Huber Functions

The Huber optimization problem is defined as [3], [4]

$$\underset{x}{\text{minimize}}\ F(x) \triangleq \sum_{j=1}^{m} \rho_k(f_j(x)) \tag{1}$$

where $x = [x_1 \ \ x_2 \ \cdots \ x_n]^T$ is the set of variables and ρ_k is the Huber function defined as

$$\rho_k(f) = \begin{cases} f^2/2 & \text{if } |f| \le k \\ k|f| - k^2/2 & \text{if } |f| > k \end{cases} \tag{2}$$

where k is a positive constant and f_j, $j = 1, 2, \cdots, m$, are error functions.

The Huber function ρ_k is a hybrid of the least-squares

Manuscript received March 29, 1993; revised June 16, 1993. This work was supported in part by Optimization Systems Associates Inc., and in part by the Natural Sciences and Engineering Research Council of Canada under Grants OGP0007239, OGP0042444, and STR0117819.

J. W. Bandler, S. H. Chen, and R. M. Biernacki are with Optimization Systems Associates Inc., P.O. Box 8083, Dundas, Ont., Canada L9H 5E7, and the Simulation Optimization Systems Research Laboratory, Department of Electrical and Computer Engineering, McMaster University, Hamilton, Canada L8S 4L7.

L. Gao is with the Department of Mathematics and Institute of Mathematics, Peking University, Beijing 100871, China.

K. Madsen is with the Institute for Numerical Analysis, The Technical University of Denmark, DK-2800 Lyngby, Denmark.

H. Yu is with the Simulation Optimization Systems Research Laboratory, Department of Electrical and Computer Engineering, McMaster University, Hamilton, Canada L8S 4L7.

IEEE Log Number 9213017.

0018-9480/93$03.00 © 1993 IEEE

(ℓ_2) (when $|f| \leq k$) and the ℓ_1 (when $|f| > k$) functions. As illustrated in Figs. 1 and 2, the definition of ρ_k ensures a smooth transition between ℓ_2 and ℓ_1 at $|f| = k$. This means that the first derivative of ρ_k w.r.t. f is continuous.

The ℓ_1 is robust against gross errors in the data [1], [2]. Since the Huber function treats errors above the threshold (i.e., $|f| > k$) in the ℓ_1 sense, it is robust against those errors, i.e., the solution is not sensitive to those errors. The choice of k defines the threshold between "large" and "small" errors. By varying k, we can alter the proportion of error functions to be treated in the ℓ_1 or ℓ_2 sense. Huber gave a look-up table [3] from which k can be determined according to the percentage of gross errors in the data. If k is set to a sufficiently large value, the optimization problem (1) becomes least squares. On the other hand, as k approaches zero, ρ_k/k will approach the ℓ_1 function.

A. Gradient and Hessian

To further our insight into the properties of the Huber formulation, we derive the gradient and Hessian of the Huber objective function as follows.

The gradient vector of the Huber objective function F w.r.t. $\boldsymbol{x}$ is given by

$$\nabla F = \sum_{j=1}^{m} v_j \boldsymbol{f}_j' \tag{3}$$

where

$$v_j \triangleq \frac{\partial \rho_k(f_j(\boldsymbol{x}))}{\partial f_j(\boldsymbol{x})} = \begin{cases} f_j(\boldsymbol{x}) & \text{if } |f_j(\boldsymbol{x})| \leq k \\ \pm k & \text{if } |f_j(\boldsymbol{x})| > k \end{cases} \tag{4}$$

$$\boldsymbol{f}_j' \triangleq \left[\frac{\partial f_j(\boldsymbol{x})}{\partial x_1} \quad \frac{\partial f_j(\boldsymbol{x})}{\partial x_2} \quad \cdots \quad \frac{\partial f_j(\boldsymbol{x})}{\partial x_n}\right]^T. \tag{5}$$

The structure of (3) is very similar to the gradient of ℓ_2 (least squares), which is

$$\nabla F_{\ell_2} = \sum_{j=1}^{m} f_j \boldsymbol{f}_j'. \tag{6}$$

By comparing (3) with (6), we can see that v_j, namely the first derivative of ρ_k w.r.t. f_j, serves as a weighting factor in the Huber gradient. For $|f_j| \leq k$, v_j is defined in (4) as f_j, which is the same as in the ℓ_2 gradient given by (6). For $|f_j| > k$, v_j is held constant at the value of f_j at the threshold. In other words, the Huber gradient can be thought of as a modified ℓ_2 gradient, where the gross errors are reduced to the threshold value.

The Hessian matrix of the Huber objective function F w.r.t. $\boldsymbol{x}$ can be expressed as

$$\boldsymbol{H} = \sum_{j=1}^{m} (d_j \boldsymbol{f}_j' \boldsymbol{f}_j'^T + v_j \boldsymbol{f}_j'') \tag{7}$$

where

$$d_j \triangleq \frac{\partial^2 \rho_k(f_j(\boldsymbol{x}))}{\partial f_j^2(\boldsymbol{x})} = \begin{cases} 1 & \text{if } |f_j(\boldsymbol{x})| \leq k \\ 0 & \text{if } |f_j(\boldsymbol{x})| > k \end{cases} \tag{8}$$

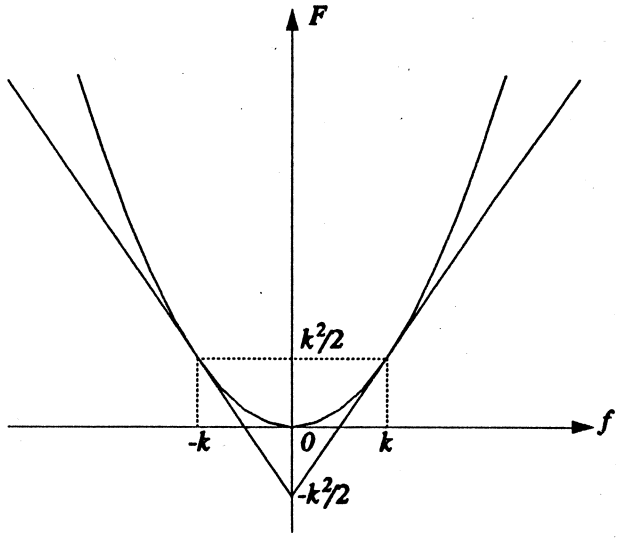

Fig. 1. The ℓ_1 and ℓ_2 objective functions in the one-dimensional case. The ℓ_1 function is rescaled and shifted in accordance with the corresponding part in the Huber function. It has the form $F = k|f| - k^2/2$. The ℓ_2 function has the form $F = f^2/2$.

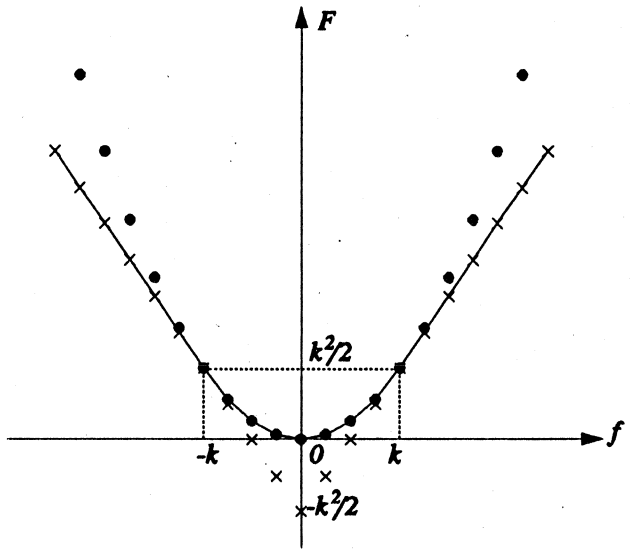

Fig. 2. The Huber, ℓ_1 and ℓ_2 objective functions in the one-dimensional case. The strikes and dots represent the discrete points on the ℓ_1 and ℓ_2 curves, respectively, in Fig. 1. The continuous curve indicates the Huber objective function.

$$\boldsymbol{f}_j'' \triangleq \frac{\partial \boldsymbol{f}_j'^T}{\partial \boldsymbol{x}}. \tag{9}$$

Comparing (7) with the ℓ_2 Hessian matrix given by

$$\boldsymbol{H}_{\ell_2} = \sum_{j=1}^{m} (\boldsymbol{f}_j' \boldsymbol{f}_j'^T + f_j \boldsymbol{f}_j'') \tag{10}$$

we can see that v_j serves as a weighting factor to reduce the contribution of gross errors in the data to the Hessian matrix.

B. One-Sided Huber Function

We present an extension of the Huber concept by introducing the "one-sided" Huber optimization defined as

$$\underset{x}{\text{minimize}}\ F(x) \triangleq \sum_{j=1}^{m} \rho_k^+(f_j(x)) \tag{11}$$

where

$$\rho_k^+(f) = \begin{cases} 0 & \text{if } f \le 0 \\ f^2/2 & \text{if } 0 < f \le k \\ kf - k^2/2 & \text{if } f > k. \end{cases} \tag{12}$$

This one-sided Huber function is tailored for design optimization with upper and/or lower specifications. f is truncated when negative because the corresponding design specification is satisfied.

The gradient vector of the one-sided Huber objective function F w.r.t. x is given by

$$\nabla F = \sum_{j=1}^{m} \nu_j^+ f_j' \tag{13}$$

where

$$\nu_j^+ \triangleq \frac{\partial \rho_k^+}{\partial f_j} = \begin{cases} 0 & \text{if } f_j \le 0 \\ f_j & \text{if } 0 < f_j \le k \\ k & \text{if } f_j > k. \end{cases} \tag{14}$$

The Hessian matrix of the one-sided Huber objective function is given by

$$H = \sum_{j=1}^{m} (d_j^+ f_j' f_j'^T + \nu_j^+ f_j'') \tag{15}$$

where

$$d_j^+ = \frac{\partial^2 \rho_k^+}{\partial f_j^2} = \begin{cases} 0 & \text{if } f_j \le 0 \\ 1 & \text{if } 0 < f_j \le k \\ 0 & \text{if } f_j > k. \end{cases} \tag{16}$$

III. A Dedicated Algorithm for Huber Optimization

We present a dedicated, efficient algorithm for minimizing the Huber objective functions, both one- and two-sided. We have implemented this algorithm in the CAD system OSA90/hope™ [8] as a new standard feature and used it to generate the numerical results presented in this paper.

The numerical algorithms proposed for solving (1) are of the trust region type. We calculate a sequence of points $\{x_p\}$ intended to converge to a local minimum of F. At each iterate x_p, a linear function l_j is used to approximate the nonlinear function f_j, $j = 1, 2, \cdots, m$, and thus a linearized model L_p of F is constructed. This model is a good approximation to F within a specified neighborhood N_p of the pth iterate x_p. This neighborhood N_p is intended to reflect the domain in which the l_j approximations of the f_j are valid.

Assume a tentative step h is being searched at the pth iterate x_p. If the search is successful, we go on to the next iteration, i.e., $x_{p+1} = x_p + h$. The problem is formulated as

$$\underset{h}{\text{minimize}}\ L_p(h) \triangleq L(h, x_p) = \sum_{j=1}^{m} \rho_k(l_j(h, x_p)) \tag{17}$$

where

$$l_j(h, x_p) \triangleq f_j(x_p) + [f_j'(x_p)]^T h \tag{18}$$

subject to the constraint $h \in N_p$, where

$$N_p \triangleq \{x \mid \|x - x_p\| \le \delta_p\} \tag{19}$$

and where $\|\cdot\|$ denotes the Euclidean norm.

The difference between the Hessians of the true Huber objective function (7) and this linearized model is the term

$$\sum_{j=1}^{m} \nu_j f_j''.$$

This error in approximating the true Hessian (7) is smaller than in the ℓ_2 case, namely,

$$\sum_{j=1}^{m} f_j f_j''.$$

We solve the foregoing problem (17) using an algorithm similar to that of Madsen and Nielsen for the linear Huber problem [9]. This method is based on the fact that L_p is a combination of quadratic functions which are linked together in a smooth manner. Therefore, a Newton iteration is very efficient, and can be proved to find the solution after a finite number of steps. The solution to this linear problem is denoted by h_p.

The trust region radius δ_p is updated in each iteration. We propose the usual updating scheme for trust region methods (e.g., see Moré [10]). This is based on the ratio

$$r_p = \frac{F(x_p) - F(x_p + h_p)}{L_p(0) - L_p(h_p)} \tag{20}$$

i.e., the ratio between the decrease in the nonlinear function and the decrease in the local approximation. If r_p is close to 1 then we can afford a larger trust region in the next iteration. On the other hand, if r_p is too small, the the trust region must be decreased.

The new point $x_p + h_p$ is only accepted if the objective function F decreases by a factor no less than s_1. Otherwise, another tentative step is calculated from x_p using a decreased trust region. A more precise step-by-step description of the algorithm follows.

Step 1: Given x_0 and $\delta_0 > 0$. Let $0 < s_2 < 1 < s_3$. (These constants are chosen according to our experience. The algorithm is not sensitive to small changes in these constants.) Set the iteration count $p = 1$.

Step 2: Solve the trust region linearized subproblem to find the minimizer h_p of (17) subject to (19).

Step 3: If $F(x_p + h_p) < (1 - s_1)F(x_p)$, let $x_{p+1} = x_p + h_p$; otherwise let $x_{p+1} = x_p$.

Step 4: If $r_p \le 0.25$, reduce the size of the trust region

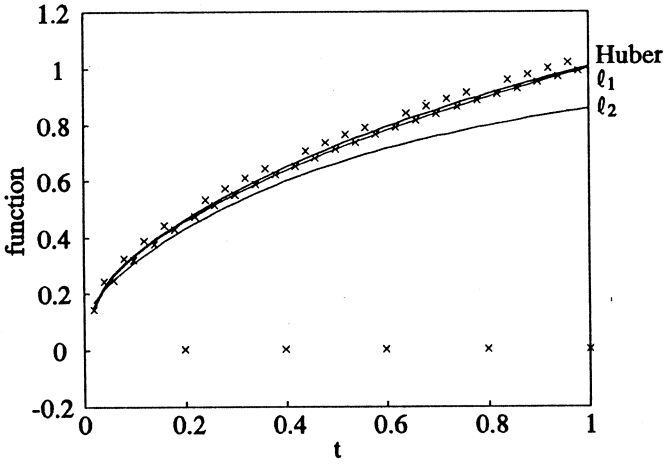

Fig. 3. ℓ_1, ℓ_2 and Huber solutions for data fitting in the presence of errors.

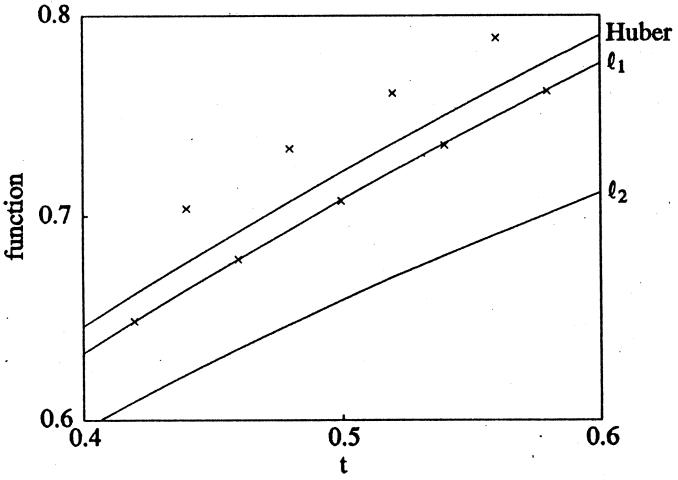

Fig. 4. An enlarged portion of Fig. 3.

by letting $\delta_{p+1} = \delta_p s_2$; or if $r_p \geq 0.75$, increase the size of the trust region by letting $\delta_{p+1} = \delta_p s_3$; otherwise keep the trust region size unchanged by letting $\delta_{p+1} = \delta_p$.

Step 5: If the convergence criteria are satisfied, stop; otherwise update the iteration count by letting $p = p + 1$ and repeat from Step 2.

It has been proved in [4] that this algorithm obeys the usual convergence theory for trust region methods.

IV. Comparison of ℓ_1, ℓ_2 and Huber Methods in Data Fitting

To illustrate the characteristics of the ℓ_1, ℓ_2 and Huber solutions for data fitting problems in the presence of large and small errors, we consider the approximation of $\sqrt{t}$ by the rational function

$$F(x, t) = \frac{x_1 t + x_2 t^2}{1 + x_3 t + x_4 t^2} \tag{21}$$

for $0 \leq t \leq 1$ [2]. $\sqrt{t}$ is uniformly sampled at 0.02, 0.04, $\cdots$, 1. We deliberately introduced large errors at 5 of the sample points and small variations to the remaining data. The ℓ_1, ℓ_2 and Huber solutions are obtained by optimizing the coefficients x_1, x_2, x_3, and x_4 in (21) to match the sampled data using the respective objective functions. The results are shown in Fig. 3. A portion of Fig. 3 is enlarged in Fig. 4 for a clearer view of the details.

As expected, the least-squares solution suffers significantly from the presence of the five erroneous points. On the other hand, the ℓ_1 solution, according to the optimality condition, is dictated by a subset of residual functions which have zero values at the solution. In a sense, all the nonzero residuals are viewed as large errors. This tendency towards a biased ℓ_1 solution, as dramatized in our example, is undesirable if we wish to model the small variations in the data.

The Huber solution features a flexible combination of the robustness of the ℓ_1 and the unbiasedness of the ℓ_2. In fact, the Huber solution is equivalent to an ℓ_2 solution with the gross errors reduced to the threshold value k. In our example, k is chosen as 0.04 according to the magnitude of the small variations in the data.

V. Huber Estimator for Statistical Modeling of Devices

One approach to statistical modeling of devices [11]–[13] is to extract the model parameters from a sample of device measurements and then postprocessing the sample of model parameters to estimate their statistics (means, statistical deviations, and correlations).

To estimate the mean of a parameter by optimization, we define the error functions as

$$f_j(\bar{\phi}) = \bar{\phi} - \phi^j, \quad j = 1, 2, \cdots, N \tag{22}$$

where ϕ^j is the extracted parameter value for the jth device and N is the total number of devices. Similarly, to estimate the variances, we define

$$f_j(V_\phi) = V_\phi - (\phi^j - \bar{\phi})^2, \quad j = 1, 2, \cdots, N \tag{23}$$

where V_ϕ denotes the estimated variance from which we can calculate the standard deviation σ_ϕ. The model parameters we use are extracted from the measurements of 80 FETs [14].

When the postprocessing is done using a least-squares estimator, problems will arise if the measurements contain gross measurement errors and/or involve faulty devices. For example, consider the run chart shown in Fig. 5 of an extracted model parameter, namely the FET time-delay τ.

Most of the extracted values of τ are between 2 and 2.5 ps, but there are a few abnormal values due to faulty devices and/or gross measurement errors. These wild points will severely affect the ℓ_2 estimator. In fact, the other model parameters extracted from those faulty devices also have abnormal values. In our earlier work [11], [12] using the ℓ_2 estimator, the abnormal data sets were manually excluded from the statistical modeling process.

The Huber function can be used as an automatic robust statistical estimator. The threshold value k is chosen to reflect the normal spread of the parameter values (e.g., we chose $k = 0.25$ ps for τ).

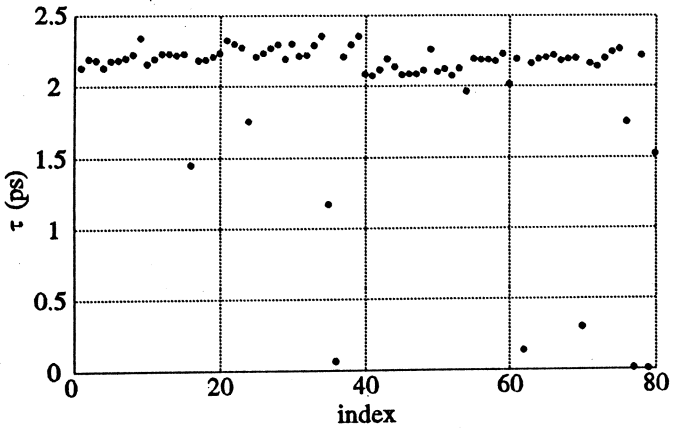

Fig. 5. Run chart of the extracted FET time-delay τ.

TABLE I
ESTIMATED STATISTICS OF SELECTED FET PARAMETERS

Parameter[a]	$\bar{\phi}$ (ℓ_2)	$\bar{\phi}$ (Huber)	$\bar{\phi}$ (ℓ_2^*)[b]	σ_ϕ (ℓ_2)	σ_ϕ (Huber)	σ_ϕ (ℓ_2^*)[b]
L_G (nH)	0.04387	0.03464	0.03429	94.6 percent	21.8 percent	17.4 percent
G_{DS} (1/KΩ)	1.840	1.820	1.839	28.6 percent	6.3 percent	4.9 percent
I_{DSS} (mA)	47.36	47.53	47.85	14.0 percent	12.7 percent	11.3 percent
τ (ps)	2.018	2.154	2.187	26.3 percent	5.8 percent	3.4 percent
C_{10} (pF)	0.3618	0.3658	0.3696	8.2 percent	4.6 percent	3.5 percent
K_1	1.2328	1.231	1.233	15.5 percent	10.8 percent	8.7 percent

[a] L_G represents the FET gate lead inductance, G_{DS} the drain-source conductance, I_{DSS} the drain saturation current, τ the time-delay, C_{10} and K_1 are parameters in the definition of the gate nonlinear capacitor.

[b] ℓ_2^* denotes ℓ_2 estimates after 11 abnormal sets are manually excluded [11].

Table I lists the means and standard deviations of a selected number of model parameters we have obtained using the ℓ_2 and the Huber estimators (the Materka and Kacprzak FET model [15] is used). For comparison, we also list the results obtained using the ℓ_2 estimator *after the abnormal data sets are manually excluded*.

The impact of the abnormal data points on the ℓ_2 estimates of the standard deviations is especially severe. Compared with ℓ_2^*, the Huber estimator does not require manual manipulation of the data and is more appropriate when there are data points that cannot be clearly classified as normal or abnormal.

It should also be noted that although ℓ_1 is effective for individual device parameter extraction, it is not, in general, suitable for statistical postprocessing. The ℓ_1 estimate (median) depends on the order rather than the actual values of the sample.

To illustrate the dependence of the Huber estimates on the threshold k, we list in Table II the estimated statistics of the parameter τ for different values of k. We can also define N_s as the number of "small errors," i.e., the cardinality of the set $\{f_j \mid |f_j| \leq k\}$, at the solution of Huber optimization for each value of k. Fig. 6 depicts N_s versus k, where N_s is expressed as a percentage of the total number of devices N. The "knee" on the curve corresponds to a solution that includes a majority of functions as "small errors." The value of k at the "knee" is consistent with our choice. Figs. 7 and 8 depict N_s for two other parameters, namely L_G and C_{10}, respectively.

TABLE II
ESTIMATED STATISTICS FOR DIFFERENT VALUES OF k

k	$\bar{\tau}$	σ_τ
0.15	2.168	4.4 percent
0.2	2.161	5.1 percent
0.225	2.157	5.4 percent
0.25	2.154	5.8 percent
0.275	2.150	6.2 percent
0.3	2.147	6.6 percent
0.5	2.122	9.6 percent
1	2.079	15.7 percent
∞	2.018	26.3 percent

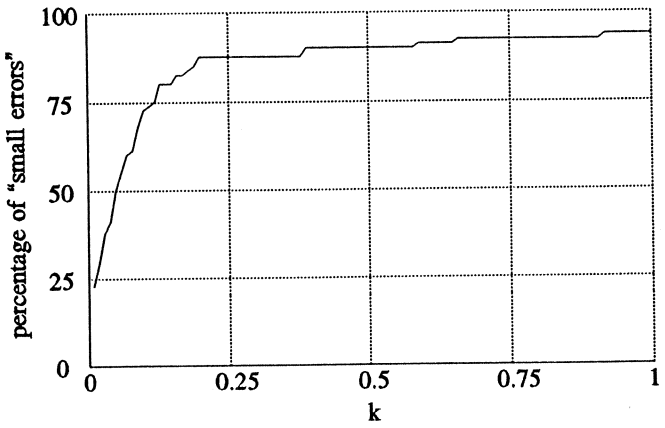

Fig. 6. Percentage of "small errors" for the FET time-delay τ versus the threshold k.

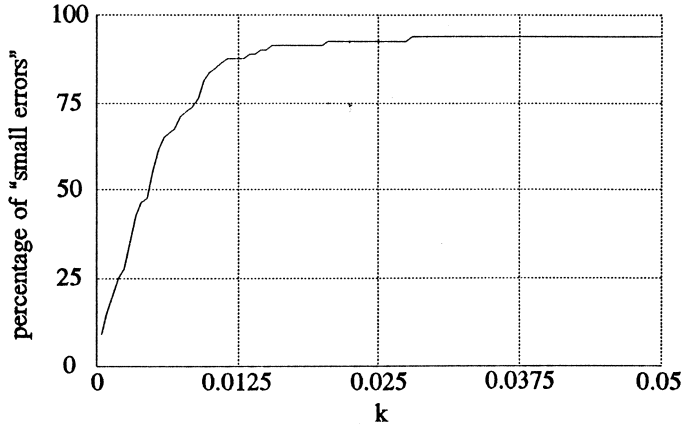

Fig. 7. Percentage of "small errors" for the FET gate lead inductance L_G versus the threshold k.

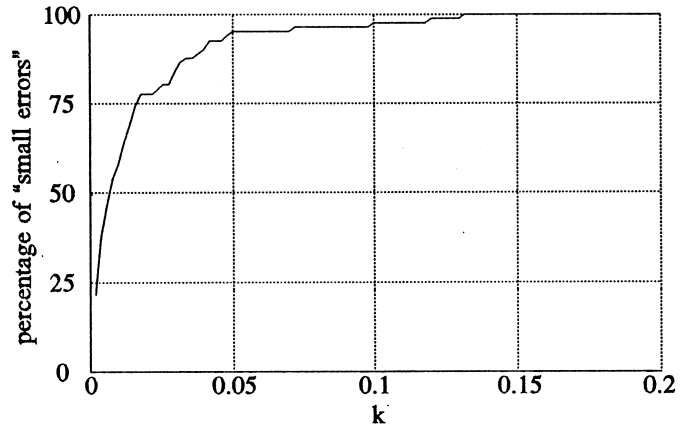

Fig. 8. Percentage of "small errors" for the FET model parameter C_{10} versus the threshold k.

VI. Application to Analog Fault Location

The ℓ_1 method has been applied successfully to the problem of fault location in analog circuits [1], [16], [17]. Typically, a faulty circuit contains only a few faults and possibly many small tolerances for the other elements. Also, the measurements taken on the faulty circuit are usually insufficient for complete parameter identification and, therefore, a robust optimization procedure is needed.

The fault location problem can be formulated as the ℓ_1 optimization [1]

$$\underset{x}{\text{minimize}} \sum_{i=1}^{n} |\Delta x_i / x_i^0| \tag{24}$$

subject to

$$V_1^c - V_1^m = 0$$

$$\vdots$$

$$V_K^c - V_K^m = 0$$

where $x = [x_1 \;\; x_2 \;\; \cdots \;\; x_n]^T$ is a vector of circuit parameters and x^0 represents the nominal parameter values. $\Delta x_i = x_i - x_i^0$ represents the deviation of the ith parameter from its nominal value. $V_1^m, \cdots, V_K^m$ are K measurements on the circuit under test (e.g., voltages measured at accessible nodes under one or more excitations). $V_1^c, \cdots, V_K^c$ are the calculated circuit responses.

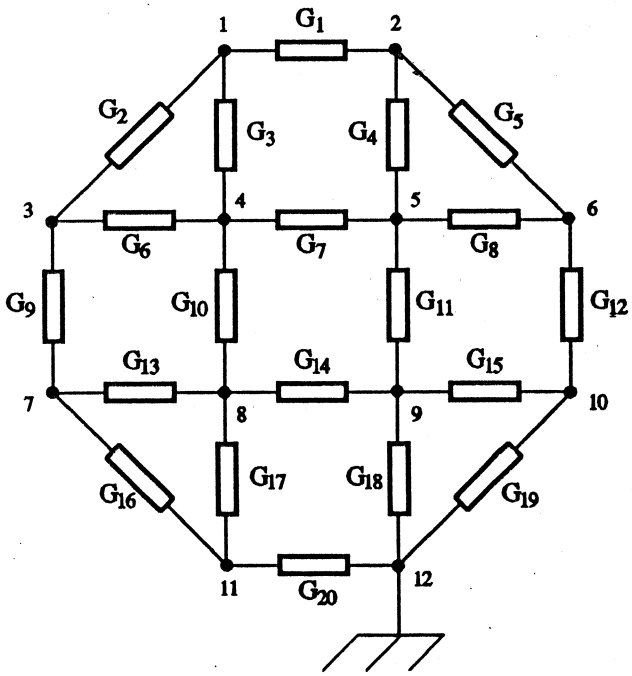

Fig. 9. The resistive mesh circuit.

Instead of the constrained optimization problem (24) we use the Huber method to minimize the following penalty function

$$\underset{x}{\text{minimize}} \sum_{j=1}^{n+K} \rho_k(f_j(x)) \tag{25}$$

where

$$f_i(x) = \Delta x_i / x_i^0, \qquad i = 1, 2, \cdots, n$$

$$f_{n+i}(x) = \beta_i (V_i^c - V_i^m), \qquad i = 1, 2, \cdots, K \tag{26}$$

and β_j, $i = 1, 2, \cdots, K$, are appropriate multipliers for the penalty terms.

Consider the resistive mesh network shown in Fig. 9 [1], [16]. The nominal element values are $G_i = 1.0$ with tolerances $\epsilon_i = \pm 0.05$, $i = 1, 2, \cdots, 20$. Node 12 is taken as the reference node, and nodes 4, 5, 8, and 9 are assumed to be internal and inaccessible for measurement. The voltage measurements at the other nodes are used for fault location.

The actual parameter values of a faulty network are listed in Table III. Two faults are assumed in the circuit, namely G_2 and G_{18}. A single excitation (a dc current source) is applied to node 1. Simulated voltage measurement data is obtained by circuit simulation using the actual parameter values. The nominal parameter values are used as the starting point for optimization. The results from the ℓ_1 optimization and Huber optimization are compared in Table III. The threshold k for the Huber function is chosen as 0.05, commensurate with the tolerances of

TABLE III
FAULT LOCATION OF THE RESISTIVE MESH CIRCUIT

Element	Nominal Value	Actual Value	Percentage Deviation		
			Actual	ℓ_1	Huber
G_1	1.0	0.98	−2.0	0.00	−0.11
G_2	1.0	0.50	−50.0[a]	−48.89	−47.28
G_3	1.0	1.04	4.0	0.00	−2.46
G_4	1.0	0.97	−3.0	0.00	−1.18
G_5	1.0	0.95	−5.0	−2.70	−3.16
G_6	1.0	0.99	−1.0	0.00	−0.06
G_7	1.0	1.02	2.0	0.00	−0.19
G_8	1.0	1.05	5.0	0.00	−0.41
G_9	1.0	1.02	2.0	2.41	3.75
G_{10}	1.0	0.98	−2.0	0.00	0.39
G_{11}	1.0	1.04	4.0	0.00	−0.37
G_{12}	1.0	1.01	1.0	2.73	1.32
G_{13}	1.0	0.99	−1.0	0.00	−0.26
G_{14}	1.0	0.98	−2.0	0.00	−0.50
G_{15}	1.0	1.02	2.0	0.00	−0.05
G_{16}	1.0	0.96	−4.0	−3.36	−2.67
G_{17}	1.0	1.02	2.0	0.00	−0.61
G_{18}	1.0	0.50	−50.0[a]	−50.09	−47.33
G_{19}	1.0	0.98	−2.0	−1.41	−3.81
G_{20}	1.0	0.96	−4.0	−4.40	−4.72

[a]Faults.

the elements. The penalty multipliers β_i in (26) are set to 1000, sufficiently large to ensure that the nonlinear constraints (circuit equations) are satisfied.

We tested this example for four other different starting points. The Huber approach correctly located the faults in all the cases. The ℓ_1 method was successful in three of the cases, but failed in one of the cases (trapped in a different local minimum).

VII. One-Sided Huber Optimization for Circuit Design

In a large-scale design problem, we often wish to optimize a small number of dominant variables in order to obtain a good starting point for the following full-scale optimization.

We consider a five-channel 12 GHz multiplexer with a total of 75 optimizable variables including waveguide manifold spacings, channel filter coefficients, and input/output couplings [18]. We know that the multiplexer responses are highly sensitive to the spacing lengths, which are initially set to half the wavelength corresponding to the channel center frequencies. The common port return loss and individual channel insertion loss responses at the starting point are shown in Fig. 10.

We first try to optimize a small number of dominant variables. We select the spacings and the channel input transformer ratios (10 variables) and consider a lower specification of 20 dB on the common port return loss. The minimax solution with these variables is shown in Fig. 11 and the one-sided Huber solution is shown in Fig. 12. The worst-case errors in these two figures are similar. Since the worst-case errors cannot be further reduced by changing the selected variables, the minimax optimizer gains nothing from directing effort elsewhere. Using one-sided Huber optimization, on the other hand, we were able

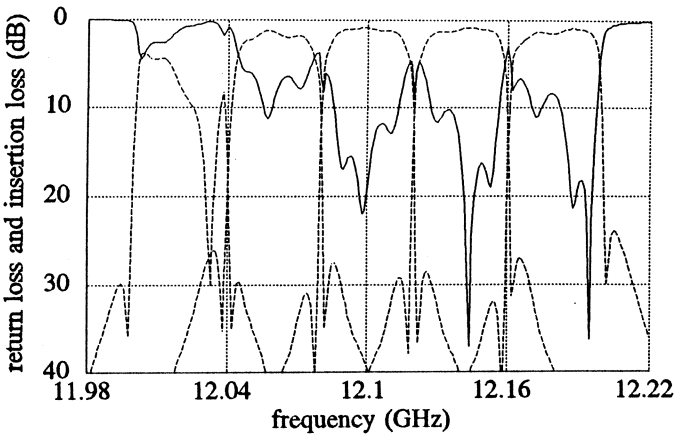

Fig. 10. Multiplexer responses at the starting point, showing the common port return loss (solid line) and the individual channel insertion losses (dashed line).

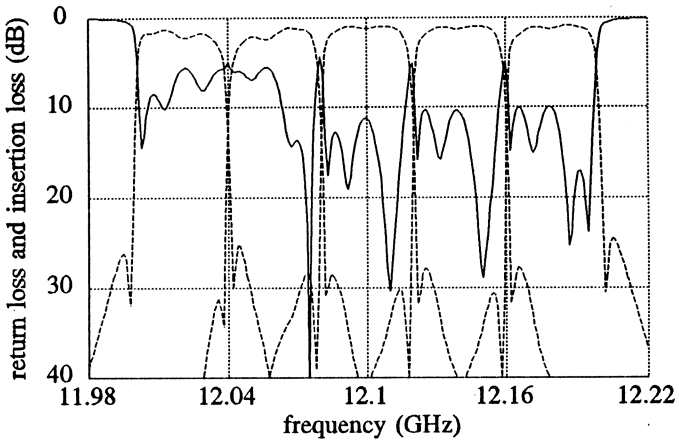

Fig. 11. Multiplexer responses after the minimax optimization with 10 variables: spacings and channel input transformer ratios; the common port return loss (solid line) and the individual channel insertion losses (dashed line). This result hardly improved upon the starting point shown in Fig. 10.

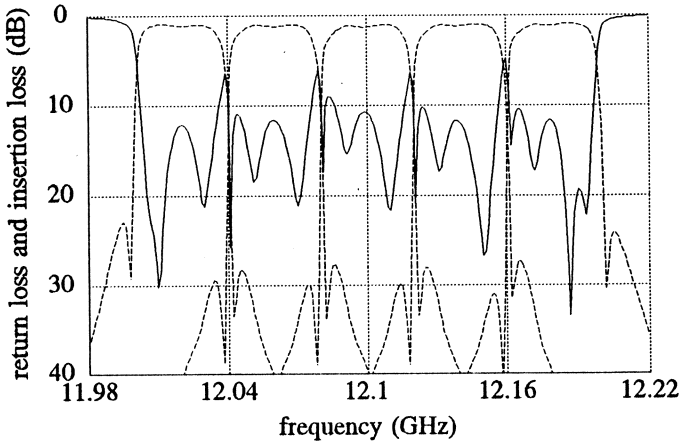

Fig. 12. Multiplexer responses after the one-sided Huber optimization with 10 variables: spacings and channel input transformer ratios; the common port return loss (solid line) and the individual channel insertion losses (dashed line). This result is significantly better than the minimax solution of Fig. 11.

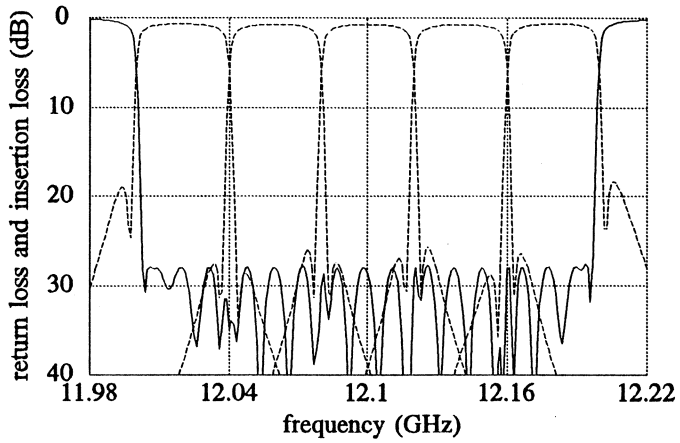

Fig. 13. Multiplexer responses after the minimax optimization with the full set of 75 variables, showing the common port return loss (solid line) and the individual channel insertion losses (dashed line).

to obtain a good starting point for subsequent optimization. The one-sided Huber optimization took 28 min on a Sun SPARCstation 1+.

From the solution shown in Fig. 12, we increase the number of variables from 10 to 45, include an upper specification of 2 dB on the channel insertion loss, and restart the one-sided Huber optimization. Then a minimax optimization with the full set of 75 variables is performed, resulting in the multiplexer responses shown in Fig. 13.

VIII. Comparison of Dedicated and Generic Algorithms

Since the Huber objective function is continuous and has a continuous gradient, it may be tempting to conclude that it is a straightforward matter to formulate the objective function and then minimize it by a generic algorithm, such as a quasi-Newton or direct search method.

We conducted a comparison between our dedicated algorithm (Section III) and three generic algorithms available in the OSA90/hope™ system: quasi-Newton, conjugate gradient, and simplex search.

The first test case is to estimate the mean value of the FET parameter τ as described in Section V. Only one variable is involved in this case, and all the algorithms under test converged to the correct solution. Table IV lists the number of function evaluations required by each algorithm from four different starting points. It shows that our dedicated Huber algorithm is more efficient than the generic ones.

We also attempted to apply the generic algorithms to the data fitting problem of Section IV, which involves four variables. None of them is able to find the correct solution unless starting very close to the solution. It attests to the need for the dedicated algorithm for solving multidimensional problems.

As derived in Section II, the Hessian of the Huber objective function is discontinuous wherever one of the error functions (f_j) crosses the threshold value. This may pose a serious problem for generic algorithms that explicitly rely on the continuity of the Hessian matrix.

TABLE IV
Number of Function Evaluations Required by Different Algorithms[a]

Algorithm	Starting Point 1.5	2	2.25	3
Dedicated Huber	4	4	4	4
Quasi-Newton	8	5	5	7
Conjugate-gradient	13	13	11	14
Simplex	26	16	16	24

[a]The optimization problem is to estimate the mean of FET parameter τ using the Huber objective function.

IX. Conclusions

We have introduced the unique Huber concept and presented novel results for analog circuit CAD. We have demonstrated that the Huber concept is consistent with practical engineering intuition. It should have a profound impact on modeling, design, fault diagnosis, and statistical processing of circuits and devices. We have exploited the robustness of Huber optimization, supported by strong numerical evidence. The similarities and differences between the Huber and ℓ_1, ℓ_2 and minimax objective functions have been discussed in a practical context. We have created the one-sided Huber function as an extension to accommodate upper and lower specifications in circuit optimization. A dedicated algorithm for Huber optimization has been presented. It has been shown by comparison to be more effective and efficient than generic minimization algorithms.

References

[1] J. W. Bandler, W. Kellermann, and K. Madsen, "A nonlinear ℓ_1 optimization algorithm for design, modeling and diagnosis of networks," *IEEE Trans. Circuits Syst.*, vol. CAS-34, pp. 174–181, 1987.

[2] J. W. Bandler, S. H. Chen, and S. Daijavad, "Microwave device modeling using efficient ℓ_1 optimization: A novel approach," *IEEE Trans. Microwave Theory Tech.*, vol. MTT-34, 1986, pp. 1282–1293, 1986.

[3] P. Huber, *Robust Statistics*. New York: Wiley, 1981.

[4] G. Li and K. Madsen, "Robust nonlinear data fitting," in *Numerical Analysis 1987*, D. F. Griffiths and G. A. Watson, Eds., Pitman Research Notes in Mathematics Series 170. Harlow, Essex, UK: Longman, 1988, pp. 176–191.

[5] H. Ekblom and K. Madsen, "Algorithms for nonlinear Huber estimation," *BIT*, vol. 29, pp. 60–76, 1989.

[6] J. W. Bandler and Q. J. Zhang, "An automatic decomposition approach to optimization of large microwave systems," *IEEE Trans. Microwave Theory Tech.*, vol. MTT-35, pp. 1231–1239, 1987.

[7] A. Sangiovanni-Vincentelli, L. K. Chen, and L. O. Chua, "An efficient heuristic cluster algorithm for tearing large-scale networks," *IEEE Trans. Circuits Syst.*, vol. CAS-24, pp. 709–717, 1977.

[8] *OSA90/hope™*, Optimization Systems Associates Inc., P.O. Box 8083, Dundas, Ont., Canada L9H 5E7, 1993.

[9] K. Madsen and H. B. Nielsen, "Finite algorithms for robust linear regression," *BIT*, vol. 30, pp. 682–699, 1990.

[10] J. J. Moré, "Recent developments in algorithms and software for trust region methods," in *Mathematical Programming, the State of the Art*. Bonn, West Germany: Springer-Verlag, 1982, pp. 258–287.

[11] J. W. Bandler, R. M. Biernacki, S. H. Chen, J. Song, S. Ye, and Q. J. Zhang, "Statistical modeling of GaAs MESFETs," in *IEEE MTT-S Int. Microwave Symp. Dig.*, Boston, MA, 1991, pp. 87–90.

[12] J. W. Bandler, R. M. Biernacki, Q. Cai, S. H. Chen, S. Ye, and Q. J. Zhang, "Integrated physics-oriented statistical modeling, simula-

tion and optimization," *IEEE Trans. Microwave Theory Tech.*, vol. 40, pp. 1374–1400, 1992.
[13] *HarPE™*, Optimization Systems Associates Inc., P.O. Box 8083, Dundas, Ont., Canada L9H 5E7, 1993.
[14] Measurement data provided by Plessey Research Caswell Ltd., Caswell, Towcester, Northamptonshire, England NN12 8EQ, 1990.
[15] A. Materka and T. Kacprzak, "Computer calculation of large-signal GaAs FET amplifier characteristics," *IEEE Trans. Microwave Theory Tech.*, vol. MTT-33, pp. 129–135, 1985.
[16] J. W. Bandler, R. M. Biernacki, A. E. Salama, and J. A. Starzyk, "Fault isolation in linear analog circuits using the ℓ_1 norm," in *Proc. IEEE Int. Symp. Circuits Syst.*, Rome, Italy, 1982, pp. 1140–1143.
[17] J. W. Bandler and A. E. Salama, "Fault diagnosis of analog circuits," *Proc. IEEE*, vol. 73, pp. 1279–1325, 1985.
[18] R. M. Biernacki, J. W. Bandler, J. Song, and Q. J. Zhang, "Efficient quadratic approximation for statistical design," *IEEE Trans. Circuits Syst.*, vol. 36, pp. 1449–1454, 1989.

John W. Bandler (S'66–M'66–SM'74–F'78), for a photograph and biography, see this issue, p. 2278.

Shao Hua Chen (S'84–M'88), for a photograph and biography, see this issue, p. 2278.

Radoslaw M. Biernacki (M'85–SM'86), for a photograph and biography, see this issue, p. 2278.

Li Gao was born in China in 1955. She received the B.S. degree in mathematics from Shandong University, China, in 1982 and the Ph.D. degree from the Institute for Numerical Analysis, Technical University of Denmark, Lyngby, Denmark, in 1988.

From 1988 to 1989, she carried out postdoctoral work in the Department of Mathematics, Peking University, China. Since 1989, she has been working as an Associate Professor at Peking University. Her research interests include optimization methods, robust parameter estimation and interval analysis.

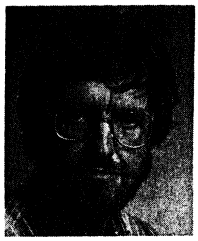

Kaj Madsen was born in Denmark in 1943. He received the Cand.Sci. degree in mathematics from the University of Aarhus in 1968 and the Dr.Techn. degree from the Technical University of Denmark in 1986.

From 1968 to 1988 he was a Lecturer in Numerical Analysis, apart from the academic year 1973 to 1974, when he was with AERE Harwell, Didcot, England. Much of his career has been spent with the Institute for Numerical Analysis, Technical University of Denmark, but during the years 1981–1983 he was with the Computer Science Department, Copenhagen University. During the summer of 1978, he visited McMaster University, Hamilton, Ont., Canada. He has been a frequent visitor since that time. In 1988 he became Professor with the Institute for Numerical Analysis, Technical University of Denmark. His fields of interest in teaching and research are programming languages, optimization, and interval analysis.

Huanyu Yu was born in Beijing, China, on May 27, 1966. He received the B.Eng. degree in electronic engineering from Tsinghua University, Beijing, China, in 1990, and completed the M.Eng. degree program in electrical and computer engineering from McMaster University, Hamilton, Ont., Canada in 1993.

From July 1990 to May 1991, he was a research associate with the Information System and Computer Application Group, Department of Electronic Engineering, Tsinghua University. He joined the Simulation Optimization Systems Research Laboratory and the Department of Electrical and Computer Engineering, McMaster University, Hamilton, Ont., Canada, in September 1991, where he is currently a teaching assistant and graduate student working toward the Ph.D. degree. He has been awarded an Ontario Graduate Scholarship for the academic year 1993–1994. His research interests include optimization theory and its circuit design application, computer graphics and user interfaces for CAD software.

Reprint 13

A Robust Physics-Oriented Statistical GaAs MESFET Model

Proceedings of the 1994 Gallium Arsenide Application Symposium, Turin, Italy, April, 1994

A ROBUST PHYSICS-ORIENTED STATISTICAL GaAs MESFET MODEL

J.W. Bandler,* R.M. Biernacki,* Q. Cai and S.H. Chen*

Optimization Systems Associates Inc.
P.O. Box 8083, Dundas, Ontario, Canada L9H 5E7

Abstract

In this paper we present a robust physics-oriented statistical GaAs MESFET model. Our model integrates the DC Khatibzadeh and Trew model for DC simulation with the Ladbrooke formulas for small-signal analysis (KTL). Accuracy of the statistical KTL model is verified by Monte Carlo simulations using device measurements. Statistical extraction and postprocessing of device physical parameters are carried out by HarPE.

Introduction

In IC manufacturing fabricated device parameter values deviate randomly from their nominal (or designed) values. These random variations result in complicated distributions and correlations of device responses, and affect production yield. Statistical modeling is needed to characterize the device statistics to provide accurate response prediction for statistical analysis and yield optimization.

Statistical models can be based on equivalent circuit models (ECMs), abstract models, data bases and physics-based models (PBMs). The advantages of PBMs for statistical modeling and yield optimization have been discussed by a number of researchers, e.g., [1-7]. The Ladbrooke model [8], in particular, has been used by Bandler *et al.* [1-3] and by Bastida *et al.* [6] for GaAs MESFET statistical modeling and yield optimization. Very promising results have been reported.

In this paper we present a novel robust GaAs MESFET statistical PBM for small-signal applications which we call the KTL (Khatibzadeh-Trew-Ladbrooke) statistical model. It combines the advantages of the Khatibzadeh and Trew model [9] and the small-signal Ladbrooke model [8] while overcoming their respective shortcomings. The KTL model has been implemented in the CAD systems HarPE [10] and OSA90/hope [11].

We also discuss the concept of data alignment to adjust the measured data to meet the requirement of consistent measurement conditions for statistical modeling. Deterministic models are extracted for individual manufactured outcomes from the corresponding measured data. These models are used to generate "pseudo measurements" at some other bias conditions. We apply the Materka and Kacprzak model [12] to this end.

Using HarPE [10] we illustrate the benefit of the KTL model by statistical characterization of a GaAs MESFET from wafer measurements [13]. Model accuracy is demonstrated by good agreement between Monte Carlo simulations using the KTL model and the statistical data.

The KTL Model for GaAs MESFETs

The Ladbrooke model [8] is a small-signal model which includes element values derived from device physical/geometrical parameters and intrinsic voltages at the DC operating point. Its attractive statistical properties have already been noticed [1,2,6]. However, the intrinsic voltages at the DC operating point must be determined separately.

On the other hand the Khatibzadeh and Trew model [9] is a large-signal (or global) model which is capable of providing accurate DC solutions. However, for small-signal applications, in particular statistical modeling, it is not as accurate as the Ladbrooke model [2].

For complete and accurate DC/small-signal device simulation we create the KTL model by combining the Ladbrooke model with the Khatibzadeh and Trew model. The latter is employed to solve for the DC operating point needed in establishing the former. Both models share the same physical

* J.W. Bandler, R.M. Biernacki and S.H. Chen are also with the Simulation Optimization Systems Research Laboratory, Department of Electrical and Computer Engineering, McMaster University, Hamilton, Canada L8S 4L7.

parameters, therefore the resulting combined, or integrated, model is consistently defined.

The KTL small-signal equivalent circuit follows the Ladbrooke model and is shown in Fig. 1. The model includes the intrinsic FET parameters, L, Z, a, N_d, V_{b0}, v_{sat}, μ_0, ε, L_{G0}, a_0, r_{01}, r_{02}, r_{03}, and the linear extrinsic elements, L_g, R_g, L_d, R_d, L_s, R_s, G_{ds}, C_{ds}, C_{ge}, C_{de}, where L is the gate length, Z the gate width, a the channel thickness, N_d the doping density, V_{b0} the zero-bias barrier potential, v_{sat} the saturation value of electron drift velocity, E_c the critical electric field, μ_0 the low-field mobility of GaAs, ε the dielectric constant, L_{G0} the inductance from gate bond wires and pads, a_0 the proportionality coefficient, and r_{01}, r_{02} and r_{03} the fitting coefficients [1].

The bias-dependent small-signal parameters, namely, g_m, C_{gs}, C_{gd}, R_i, L_g, r_0 and τ, as shown in Fig. 1, are derived using the modified Ladbrooke formulas once the DC operating point is solved for. For instance,

$$\begin{aligned} g_m &= \varepsilon v_{sat} Z/d, \\ \tau &= [0.5X - 2dL/(L+2X)]/v_{sat}, \\ R_i &= L/[Z\mu_0 qN_d(a-d)], \\ C_{gd} &= 2\varepsilon Z/(1+2X/L), \\ r_0 &= r_{01}V_{D'S'}(r_{02} - V_{G'S'}) + r_{03} \end{aligned} \tag{1}$$

where $V_{D'S'}$ and $V_{G'S'}$ are DC intrinsic voltages from D' to S' and from G' to S', respectively, as shown in Fig. 1.

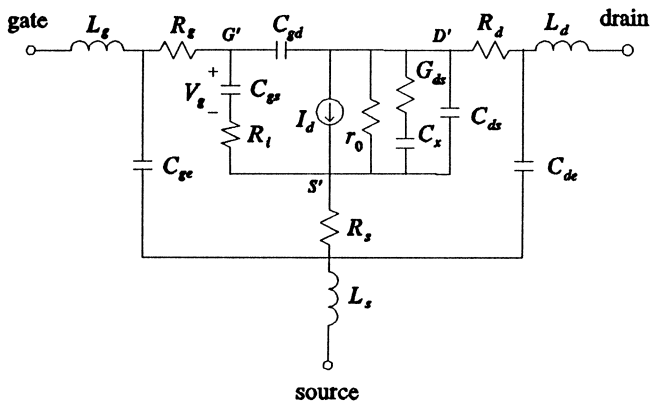

Fig. 1 Small-signal equivalent circuit, where $I_d = g_m V_g e^{-j\omega\tau}$.

The equivalent depletion depth d and the space-charge layer extension X are defined by

$$\begin{aligned} d &= [2\varepsilon(-V_{G'S'}+V_{b0})/(qN_d)]^{0.5}, \\ X &= a_0\{2\varepsilon/[qN_d(-V_{G'S'}+V_{b0})]\}^{0.5}(V_{D'G'}+V_{b0}). \end{aligned} \tag{2}$$

Measurement Data Alignment

Statistical modeling requires data for different, but supposedly identical, devices to be taken under identical measurement conditions. However, the measurement conditions (e.g., the bias conditions) of different devices may not be identical. We preprocess the data to achieve bias condition alignment.

Measurements on 0.5 μm GaAs MESFETs were chosen from the Plessey data [13]. We selected 34 individual devices from Wafer B and 35 individual devices from Wafer D for statistical modeling. Each data set contains small-signal S parameters measured at frequencies from 1 GHz to 21 GHz with 0.4 GHz step under three bias conditions with a fixed drain bias V_{DS} = 5 V. DC drain bias currents are also included in the measurements.

Due to the variations of the measurement conditions the gate bias voltages vary slightly from device to device except for V_{GS} = 0 V. For Wafer B V_{GS} for the other two bias conditions varies between -0.79 V and -0.59 V (mean value -0.6818 V and standard deviation 6.73 %) and between -1.38 V and -1.09 V (mean values -1.232 V and standard deviation 6.07 %), respectively. For Wafer D V_{GS} for the other two bias conditions varies between -0.89 V and -0.74 V (mean values -0.8039 V and standard deviation 5.83 %) and between -1.64 V and -1.25 V (mean values -1.347 V and standard deviation 5.93 %), respectively. Therefore, we need to align the different data sets to provide consistent bias points for statistical modeling. It is also desirable to interpolate measured data at other bias points. The Materka and Kacprzak model is a suitable interpolator for this purpose, because of its excellent single device fitting accuracy for these devices.

For each individual device we fitted the Materka and Kacprzak model to its corresponding data set. The resulting models were used to interpolate data for each device at two bias points (gate bias voltages -0.5 V and -0.7 V, drain bias voltage 5 V). In this way we generated 34 data sets for Wafer B

and 35 data sets for Wafer D, including DC responses and S parameters from 1 GHz to 21 GHz with 2 GHz step under the two bias conditions.

Statistical Modeling and Verification

Our statistical modeling technique consists of two stages: multi-device parameter extraction and postprocessing. The two stages, leading to a concise model described by the means, standard deviations, correlation matrix and discrete distribution functions (DDFs), were carried out by HarPE [10]. After alignment of the measurement data, the KTL model parameters were extracted for each device by fitting the model responses to the corresponding S-parameter data and drain bias currents at gate bias -0.5 V and -0.7 V and drain bias 5 V. The 34 (deterministic) models of Wafer B and the 35 models of Wafer D were then postprocessed to obtain the parameter statistics, respectively. The resulting mean values and the standard deviations for Wafer B and Wafer D are listed in Table I and Table II, respectively. Histograms of channel thickness for Wafer B and Wafer D are shown in Fig. 2 and Fig. 3, respectively.

TABLE I
KTL MODEL PARAMETERS FOR WAFER B

Parameter	Mean	Std. Dev. (%)
$L(\mu m)$	0.5237	2.84
$a(\mu m)$	0.1438	2.37
$N_d(m^{-3})$	2.1857×10^{23}	1.88
$v_{sat}(m/s)$	10.6416×10^{4}	2.85
$\mu_0(m^2/Vns)$	5.8309×10^{-10}	2.26
$L_{G0}(nH)$	0.0355	15.0
$r_{01}(\Omega/V^2)$	0.3525	0.277
$r_{02}(\Omega)$	2014.5	0.276
a_0	0.9978	1.19
$R_d(\Omega)$	1.0169	1.27
$R_s(\Omega)$	3.5209	3.46
$R_g(\Omega)$	6.5181	0.22
$L_d(nH)$	0.0766	9.58
$L_s(nH)$	0.0382	3.75
$G_{ds}(1/\Omega)$	3.7406×10^{-3}	1.63
$C_{ds}(pF)$	0.0505	1.57
$C_{gc}(pF)$	0.0669	5.84
$C_{dc}(pF)$	0.0104	2.16
$C_x(pF)$	3.2699	1.69

$Z = 300\ \mu m$, $\varepsilon = 12.9$, $V_{b0} = 0.6$ V and $r_{03} = 7.0$ V are fixed (non-statistical) parameters.

The bias-dependent linear extrinsic element L_g is computed using the Ladbrooke formula [8].

TABLE II
KTL MODEL PARAMETERS FOR WAFER D

Parameter	Mean	Std. Dev. (%)
$L(\mu m)$	0.5055	3.93
$a(\mu m)$	0.1337	2.49
$N_d(m^{-3})$	2.2885×10^{23}	2.19
$v_{sat}(m/s)$	9.8251×10^{4}	5.22
$L_{G0}(nH)$	0.0375	15.4
$r_{01}(\Omega/V^2)$	0.3463	2.15
$r_{02}(\Omega)$	1979.0	2.15
a_0	0.9337	5.71
$R_d(\Omega)$	1.0416	1.70
$R_s(\Omega)$	3.8814	4.77
$R_g(\Omega)$	6.5256	0.41
$L_d(nH)$	0.0499	12.7
$L_s(nH)$	0.0359	8.10
$G_{ds}(1/\Omega)$	3.6315×10^{-3}	3.71
$C_{ds}(pF)$	0.0517	1.92
$C_{gc}(pF)$	0.0733	7.74
$C_{dc}(pF)$	0.0106	2.75
$C_x(pF)$	3.7355	12.1

$Z = 300\ \mu m$, $\varepsilon = 12.9$, $V_{b0} = 0.6$ V, $r_{03} = 7.0$ V and $\mu_0 = 6.0\times10^{-10}\ m^2/Vns$ are fixed parameters.

The bias-dependent linear extrinsic element L_g is computed using the Ladbrooke formula [8].

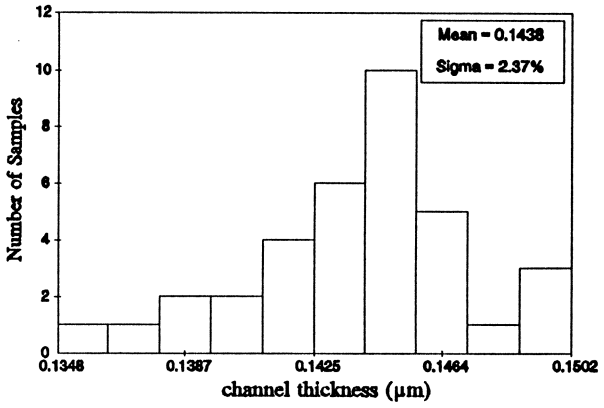

Fig. 2 Histograms of channel thickness for Wafer B.

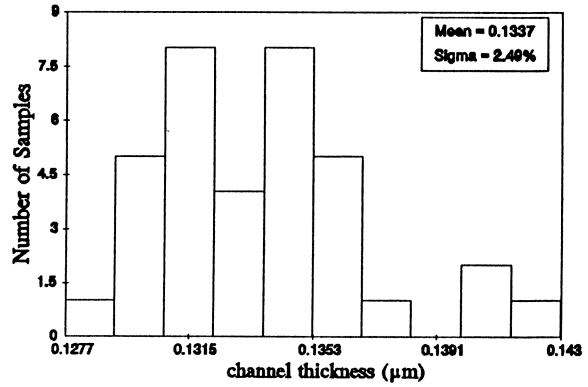

Fig. 3 Histograms of channel thickness for Wafer D.

For verification, 400 Monte Carlo outcomes were generated using the statistical KTL model. The statistics of the simulated S parameters and DC drain currents for those 400 outcomes were compared with the statistics of the data. The mean values and standard deviations from the data and the KTL model including S parameters at frequency 11 GHz and the DC drain currents at both bias points for Wafer B and Wafer D are listed in Table III and Table IV, respectively. Note that the statistics of the data and the KTL model responses are consistent.

TABLE III
MEAN VALUES AND STANDARD DEVIATIONS OF DATA AND KTL MODEL RESPONSES FOR WAFER B

	Bias 1				Bias 2			
	Data		KTL		Data		KTL	
	Mean	Dev. (%)	Mean	Dev. (%)	Mean	Dev. (%)	Mean	Dev. (%)
$\lvert S_{11}\rvert$	0.777	0.83	0.778	0.63	0.780	0.81	0.788	0.61
$\angle S_{11}$	-104.7	1.32	-105.8	1.00	-101.3	1.38	-102.7	1.07
$\lvert S_{21}\rvert$	1.793	1.17	1.739	1.44	1.703	1.61	1.700	1.47
$\angle S_{21}$	96.80	0.61	96.82	0.56	97.78	0.60	98.54	0.57
$\lvert S_{12}\rvert$	0.090	2.46	0.092	1.28	0.095	2.49	0.096	1.22
$\angle S_{12}$	35.30	1.35	35.64	1.58	35.95	1.30	34.80	1.59
$\lvert S_{22}\rvert$	0.571	0.90	0.574	0.72	0.572	0.91	0.576	0.71
$\angle S_{22}$	-39.58	1.23	-40.03	1.21	-39.91	1.21	-40.53	1.20
I_d(A)	0.040	8.16	0.0398	7.71	0.033	9.51	0.033	8.76

Bias 1: V_{GS} = -0.5 V, V_{DS} = 5 V.
Bias 2: V_{GS} = -0.7 V, V_{DS} = 5 V.
Frequency is 11 GHz for S parameters.

TABLE IV
MEAN VALUES AND STANDARD DEVIATIONS OF DATA AND KTL MODEL RESPONSES FOR WAFER D

	Bias 1				Bias 2			
	Data		KTL		Data		KTL	
	Mean	Dev. (%)	Mean	Dev. (%)	Mean	Dev. (%)	Mean	Dev. (%)
$\lvert S_{11}\rvert$	0.784	0.44	0.785	0.59	0.787	0.45	0.794	0.59
$\angle S_{11}$	-103.9	2.24	-105.8	1.81	-100.4	2.37	-102.7	1.91
$\lvert S_{21}\rvert$	1.725	2.14	1.648	2.88	1.612	3.0	1.608	2.95
$\angle S_{21}$	97.06	0.99	96.96	0.82	97.91	0.94	98.69	0.84
$\lvert S_{12}\rvert$	0.096	3.35	0.095	3.11	0.102	3.45	0.100	3.07
$\angle S_{12}$	34.51	1.78	33.97	1.99	35.25	1.76	34.19	2.08
$\lvert S_{22}\rvert$	0.583	1.18	0.591	1.01	0.588	1.09	0.593	1.00
$\angle S_{22}$	-40.51	0.97	-40.40	0.92	-40.47	0.84	-40.88	0.92
I_d(A)	0.031	9.54	0.031	9.73	0.025	11.2	0.025	11.0

Bias 1: V_{GS} = -0.5 V, V_{DS} = 5 V.
Bias 2: V_{GS} = -0.7 V, V_{DS} = 5 V.
Frequency is 11 GHz for S parameters.

Conclusions

We have presented the KTL model: a physics-oriented model for GaAs MESFETs particularly suitable for robust statistical device characterization. Our experiments demonstrate its ability to accurately represent the statistical properties of MESFETs. KTL has been implemented in HarPE and OSA90/hope and is suitable for both nominal design and yield optimization of small-signal circuits. Using KTL, exciting results have been achieved in yield-driven amplifier design [3].

References

[1] J.W. Bandler, R.M. Biernacki, S.H. Chen, J. Song, S. Ye and Q.J. Zhang, "Statistical modeling of GaAs MESFETs," *IEEE Int. Microwave Symp. Dig.* (Boston, MA), 1991, pp. 87-90.

[2] J.W. Bandler, R.M. Biernacki, Q. Cai, S.H. Chen, S. Ye and Q.J. Zhang, "Integrated physics-oriented statistical modeling, simulation and optimization," *IEEE Trans. Microwave Theory Tech.* vol. 40, 1992, pp. 1374-1400.

[3] J.W. Bandler, S. Ye, Q. Cai, R.M. Biernacki and S.H. Chen, "Predictable yield-driven circuit optimization," *IEEE Int. Microwave Symp. Dig.* (Albuquerque, NM), 1992, pp. 837-840.

[4] F. Filicori, G.Ghione and C.U. Naldi, "Physics-based electron device modelling and computer-aided MMIC design," *IEEE Trans. Microwave Theory and Tech.* vol. 40, 1992, pp. 1333-1352.

[5] D.E. Stoneking, G.L. Bilbro, P.A. Gilmore, R.J. Trew and C.T. Kelley, "Yield optimization using a GaAs process simulator coupled to a physical device model," *IEEE Trans. Microwave Theory and Tech.* vol. 40, 1992, pp. 1353-1363.

[6] E.M. Bastida, G.P. Donzelli and M. Pagani, "Efficient development of mass producible MMIC circuits," *IEEE Trans. Microwave Theory and Tech.* vol. 40, 1992, pp. 1364-1373.

[7] E.M. Bastida, G.P. Donzelli, F. Magistradi and M. Pagani, "Design yield and reliability issues in mass producible MMICs," *Proc. 23rd European Microwave Conf.* (Madrid, Spain), 1993, pp. 19-25.

[8] P.H. Ladbrooke, *MMIC Design: GaAs FETs and HEMTs.* Norwood, MA: Artech House, 1989.

[9] M.A. Khatibzadeh and R.J. Trew, "A large-signal, analytic model for the GaAs MESFET," *IEEE Trans. Microwave Theory Tech.*, vol. 36, 1988, pp. 231-238.

[10] *HarPE™*, Optimization Systems Associates Inc., P.O. Box 8083, Dundas, Ontario, Canada L9H 5E7, 1993.

[11] *OSA90/hope™*, Optimization Systems Associates Inc., P.O. Box 8083, Dundas, Ontario, Canada L9H 5E7, 1993.

[12] A. Materka and T. Kacprzak, "Computer calculation of large-signal GaAs FET amplifier characteristics," *IEEE Trans. Microwave Theory Tech.*, vol. MTT-33, 1985, pp. 129-135.

[13] Measurement data provided by Plessey Research Caswell Ltd., Caswell, Towcester, Northamptonshire, England NN12 8EQ, 1990.

Reprint 14

Exploitation of Coarse Grid for Electromagnetic Optimization

1994 IEEE International Microwave Symposium Digest, San Diego, CA, May 1994

EXPLOITATION OF COARSE GRID FOR ELECTROMAGNETIC OPTIMIZATION

J.W. Bandler, R.M. Biernacki, S.H. Chen, P.A. Grobelny and R.H. Hemmers

Optimization Systems Associates Inc.
P.O. Box 8083, Dundas, Ontario
Canada L9H 5E7

ABSTRACT

Direct, optimization-driven electromagnetic design is studied. Focusing upon a double folded stub microstrip filter, we explore design characteristics for coarse grids. EM models: coarse grid (EMC) for fast computations and the corresponding fine grid (EMF) for more accurate simulations are compared. The EMC model, useful when circuit-theoretic models may not be readily available, permits rapid exploration of different starting points, solution robustness, local minima, parameter sensitivities, yield-driven design, and other design characteristics within a practical time frame.

INTRODUCTION

We present new results of microwave filter design with accurate electromagnetic (EM) simulations driven by powerful gradient-based optimizers. We go far beyond the prevailing use of stand alone EM simulators, namely, validation of designs obtained using empirical circuit models. Feasibility of performance-driven and yield-driven circuit optimization employing EM simulations has already been shown in previous pioneering work [1, 2].

Simulation time using EM simulators can be significantly decreased if the grid used for numerical EM modeling is coarse (EMC). A coarse grid decreases the accuracy of EM analysis but qualitative, and often quite accurate quantitative, information about the behaviour of the circuit may be exploited. The EMC model allows us to explore different optimization starting points, solution robustness, local minima, parameter sensitivities and statistics, and other design characteristics within a practical time frame. As design data accumulates we can correlate the EMC model with the more accurate fine grid EM simulation model (EMF). The bulk of CPU intensive optimizations can then be carried out on the inexpensive EMC model. The final solution is always verified and fine tuned, if necessary, by an EMF model.

This work was supported in part by Optimization Systems Associates Inc. and in part by the Natural Sciences and Engineering Research Council of Canada under Grants OGP0042444, OGP0007239 and STR0117819.

J.W. Bandler, R.M. Biernacki and S.H. Chen are also with and P.A. Grobelny and R.H. Hemmers are with the Simulation Optimization Systems Research Laboratory and Department of Electrical and Computer Engineering, McMaster University, Hamilton, Ontario, Canada L8S 4L7.

We perform nominal and yield optimizations of the double folded stub filter [3] using an EMC model and verify the results with an EMF model. Encouraged by good consistency of both results we use the EMC model to perform the otherwise very CPU demanding analysis of robustness of our optimized solution.

In our work we utilize the OSA90/hope optimization environment [4] with the Empipe [5] interface to the *em* field simulator from Sonnet Software [6]. This interface addresses challenges of efficiency, discretization of geometrical dimensions, and continuity of optimization variables through efficient on-line response interpolation w.r.t. geometrical dimensions of microstrip structures simulated with fixed grid sizes, smooth gradient evaluation for use in conjunction with the interpolation, and storing the results of expensive EM simulations in a dynamically updated data base.

EMC OPTIMIZATION OF THE DOUBLE FOLDED STUB FILTER

We optimized the double folded stub filter of Fig. 1. The x and y grid sizes for EMC simulation are chosen as $\Delta x_C = \Delta y_C$ = 4.8 mil. The EMF simulation used to verify the EMC results uses a grid size of $\Delta x_F = \Delta y_F$ = 1.6 mil. The three designable geometrical parameters are L_1, L_2 and S, while W_1 and W_2 are fixed at 4.8 mil each. The design specifications are as follows.

$$|S_{21}| \geq -3 \text{ dB} \quad \text{for} \quad f \leq 9.5 \text{ GHz and } f \geq 16.5 \text{ GHz}$$

$$|S_{21}| \leq -30 \text{ dB} \quad \text{for} \quad 12 \text{ GHz} \leq f \leq 14 \text{ GHz}.$$

For the EMC case the time needed to simulate the filter at a single frequency and an arbitrary point is about 5 CPU seconds. This includes automatic response interpolation carried out to accommodate off-the-grid geometries. The corresponding time for EMF is approximately 70 seconds on a Sun SPARCstation 10.

To further refine the EMF solution we applied our new space mapping (SM) optimization technique [7]. The SM technique is based on parameter space transformation and aims at finding the image of the EMC optimal solution in the EMF parameter space. The main advantage of the SM method is that it requires very few EMF simulations. The optimized EMC and refined SM results are listed in Table I. Fig. 2 shows the $|S_{21}|$ response before and after minimax optimization using the EMC model. Fig. 3 shows the corresponding EMF and refined SM $|S_{21}|$ responses.

Comparing the responses in Figs. 2 and 3 shows that the EMC model can very closely approximate responses obtained using the much more CPU intensive EMF model. Design using

the EMF model can then be followed, if necessary, by applying the space mapping [7], or direct EMF optimization, to further refine the EMF solution.

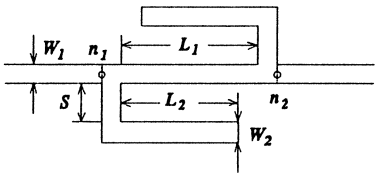

Fig. 1. Microstrip double folded stub bandstop filter [3].

TABLE I
NOMINAL DESIGN OPTIMIZATION

Parameter (mil)	Before Optimization	Coarse Grid Solution	SM Refined Solution
L_1	90.0	91.5	93.7
L_2	80.0	85.7	85.3
S	4.8	4.1	4.6

W_1 and W_2 are kept fixed at 4.8 mil.

YIELD OPTIMIZATION OF THE DOUBLE FOLDED STUB FILTER

For Monte Carlo estimation we assumed a uniform distribution and 0.25 mil tolerance on all five geometrical parameters. An efficient yield optimization technique is used [2]. The optimizable parameters are L_1, L_2 and S, with W_1 and W_2 fixed at 4.8 mil each.

The yield estimated from 250 statistical outcomes using the 4.8 mil EMC model at the coarse grid nominal minimax

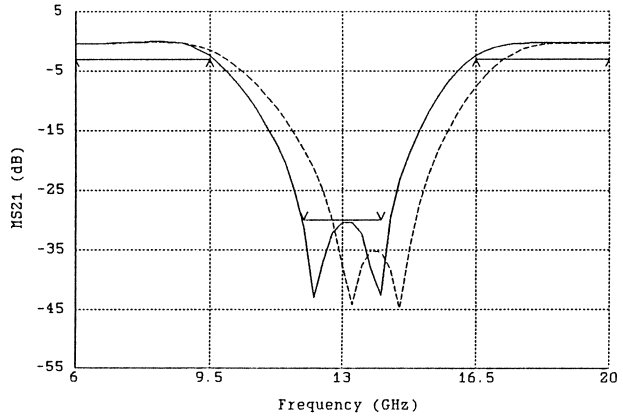

Fig. 2. EMC design of the double folded stub filter: the $|S_{21}|$ response of the filter before (dashed line) and after (solid line) minimax optimization.

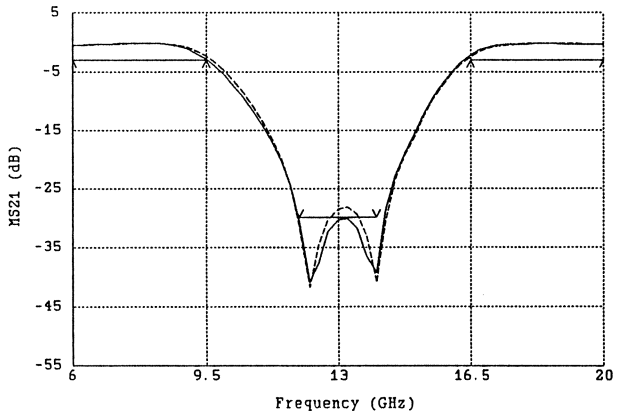

Fig. 3. EMF design of the double folded stub filter: the fine grid $|S_{21}|$ response at the EMC minimax solution (dashed line) and the $|S_{21}|$ response for the SM refined solution simulated using the fine grid (solid line).

solution is 71%. After yield optimization using 200 outcomes, the estimated yield increased to 81%. Subsequently, we performed yield estimation utilizing the 1.6 mil EMF model at the coarse grid nominal and centered solutions. The fine grid estimated yields are both 0%. This shows the potential pitfalls of relying on EMC-only design. Fig. 4(a) shows the fine grid $|S_{21}|$ response from Monte Carlo simulation after EMC yield optimization.

The yield estimated from 250 statistical outcomes using the 1.6 mil EMF model at the SM nominal solution is 9%. After carrying out yield optimization for 200 outcomes, utilizing the SM model, the yield increased to 24%. This result is compared with a fine grid yield optimization, which produced a comparable centered yield of 30%. Fig. 4(b) shows the fine grid $|S_{21}|$ response from Monte Carlo simulation after SM yield optimization. The centered solutions are listed in Table II.

TABLE II
YIELD OPTIMIZATION

Parameter (mil)	Before Yield Optimization	SM Yield Optimization	EMF Yield Optimization
L_1	93.7	92.0	91.8
L_2	85.3	85.0	85.1
S	4.6	5.0	4.9
EMF Yield	9%	24%	30%

Uniform tolerances of 0.25 mil on all five geometrical parameters.

Subsequently, we performed Monte Carlo analyses utilizing the 1.6 mil EMF model at the SM nominal and centered solutions using relaxed specifications. For case (a), both the upper and lower specifications were relaxed by 0.5 dB. For case (b), both were relaxed by 1 dB. The new SM and EMF centered yields show remarkable similarity as shown in Table III.

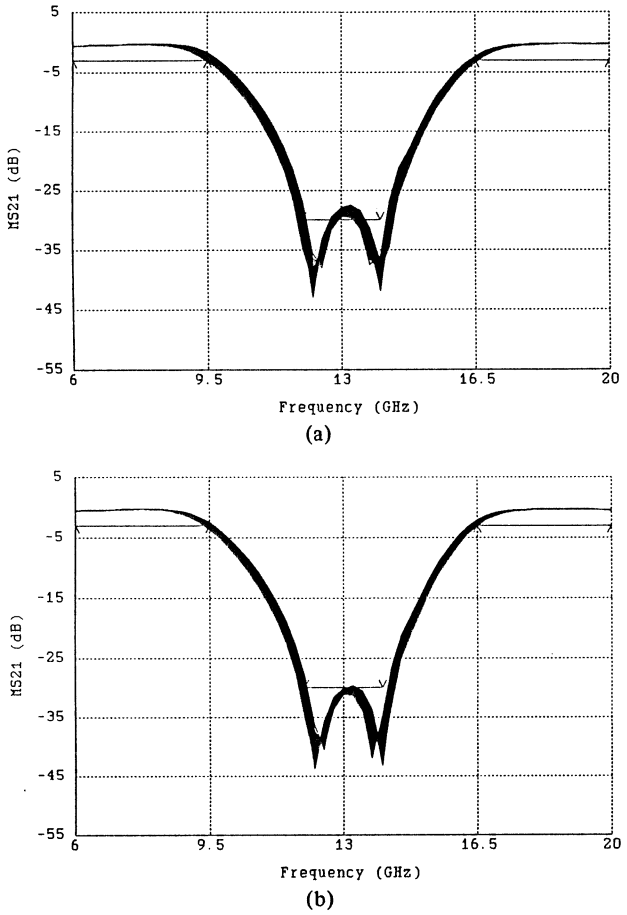

Fig. 4. The $|S_{21}|$ Monte Carlo sweep using the EMF model after (a) EMC yield optimization and (b) SM yield optimization. 250 outcomes are used for yield estimation and 200 outcomes for yield optimization.

TABLE III
FINE GRID YIELD ESTIMATION
FOR RELAXED CONSTRAINTS

Case	SM Nominal Yield	SM Centered Yield	EMF Centered Yield
(a)	63%	87%	88%
(b)	81%	97%	96%

Case (a): the lower specification is S_l = -3.5 dB and the upper specification S_u = -29.5 dB. Case (b): S_l = -4 dB and S_u = -29 dB.

ROBUSTNESS ANALYSIS OF THE NOMINAL SOLUTION

We investigated the robustness of EMC optimization for the double folded stub filter. The filter was optimized with L_1, L_2 and S selected as the designable parameters. W_1 and W_2 were fixed. Subsequently, we performed a number of EMC minimax optimizations, each starting from a different random starting point. We used 30 different starting points uniformly spread around the minimax solution within a ±20% deviation.

Fig. 5(a) plots the $|S_{21}|$ responses for all 30 starting points. Bars in Fig. 5(b) represent the Euclidian distances between the minimax solution and the perturbed starting points. Fig. 6 shows the corresponding diagrams after optimization. In Fig. 7, we visualize the optimization trajectories taken by the minimax optimizer by showing lines identifying corresponding starting points with optimized solutions for each optimization. These lines are shown for different pairs of designable parameters.

We can observe that nearly all of the optimizations converged to the reference minimax solution. This shows that the optimized solution is robust and that EMC optimization provides consistent results even if started from different starting points. This study has been confirmed from other families of starting points and with other gradient optimizers.

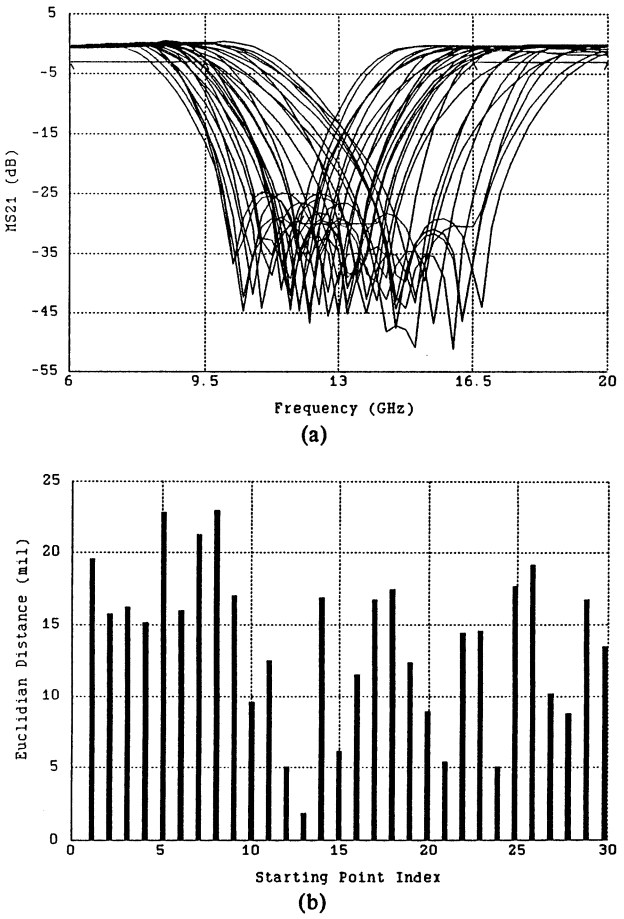

Fig. 5. (a) Simulated $|S_{21}|$ at 30 points randomly generated around the reference minimax solution, and (b) the Euclidian distances between the random starting points and the reference minimax solution.

CONCLUSIONS

We have exploited low-cost EM simulation utilizing a coarse grid for numerical field solutions. We have presented novel results involving coarse grid simulation, optimization and design centering of a double folded stub filter. Fine grid verification of the optimized solution has demonstrated that coarse grid models can provide useful qualitative and quantitative

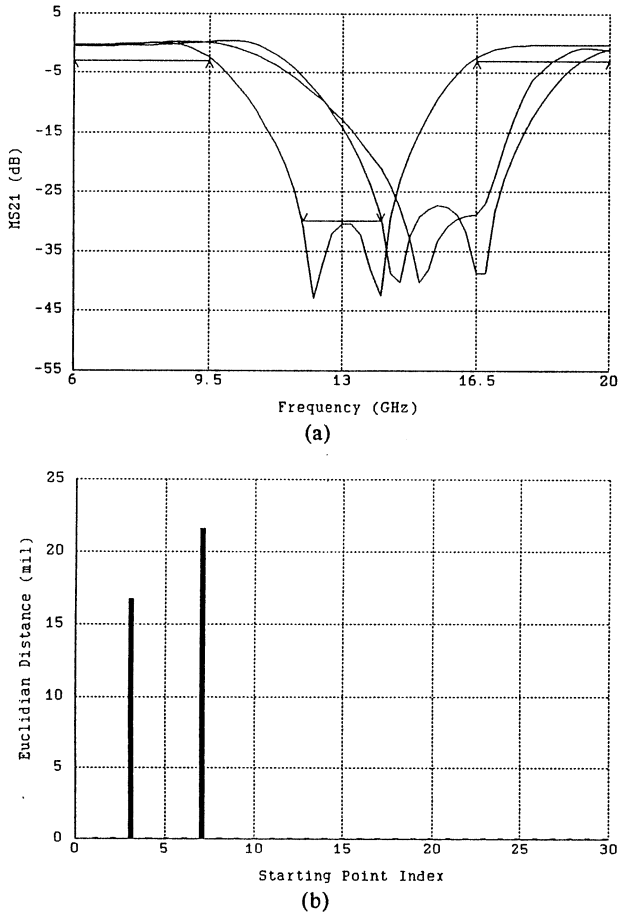

Fig. 6. (a) Simulated $|S_{21}|$ at the optimized solutions from the 30 randomly generated starting points shown in Fig. 5, (b) the Euclidian distances between the optimized points and the reference minimax solution.

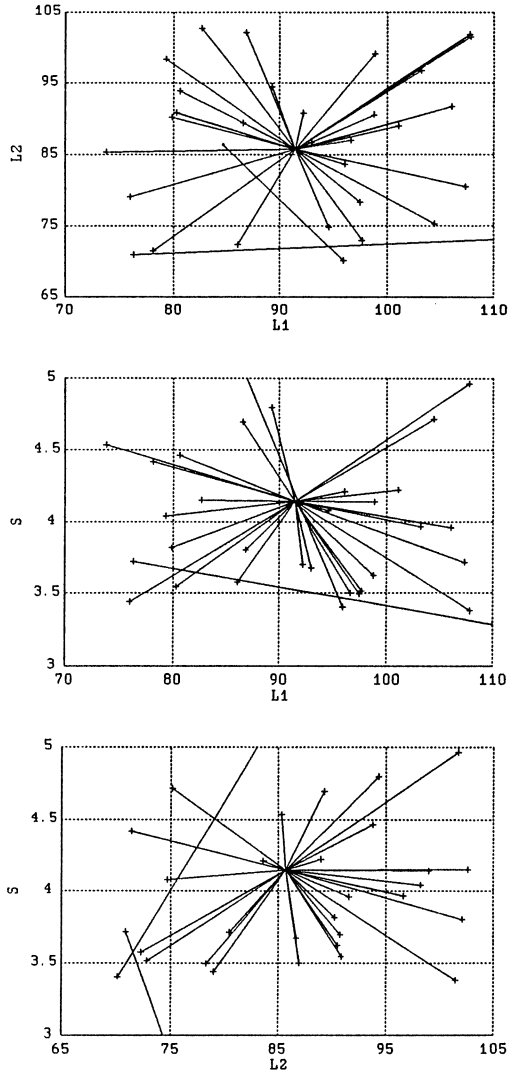

Fig. 7. Visualization of the trajectories taken by the minimax optimizer for each of the randomly generated starting points. Lines identifying corresponding starting points (+) with optimized solutions (·) for each optimization are shown in two-dimensional subspaces of the designable parameters: L_1, L_2 and S.

information about the performance of a circuit within a more practical time frame. We have studied the robustness of the coarse grid solution using the Monte Carlo method. Coarse grid EM simulation is especially attractive for structures for which analytical/empirical or theoretical circuit models are not readily obtainable.

REFERENCES

[1] J.W. Bandler, S. Ye, R.M. Biernacki, S.H. Chen and D.G. Swanson, Jr., "Minimax microstrip filter design using direct EM field simulation," *IEEE MTT-S Int. Microwave Symp. Dig.* (Atlanta, GA), 1993, pp. 889-892.

[2] J.W. Bandler, R.M. Biernacki, S.H. Chen, P.A. Grobelny and S. Ye, "Yield-driven electromagnetic optimization via multilevel multidimensional models," *IEEE Trans. Microwave Theory Tech.*, vol. 41, December 1993.

[3] J.C. Rautio, Sonnet Software, Inc., 135 Old Cove Road, Suite 203, Liverpool, NY 13090-3774, Private communication, 1992.

[4] *OSA90/hope™*, Optimization Systems Associates Inc., P.O. Box 8083, Dundas, Ontario, Canada L9H 5E7, 1993.

[5] *Empipe™*, Optimization Systems Associates Inc., P.O. Box 8083, Dundas, Ontario, Canada L9H 5E7, 1993.

[6] *Em User's Manual*, Sonnet Software, Inc., 135 Old Cove Road, Suite 203, Liverpool, NY 13090-3774, 1992.

[7] J.W. Bandler, R.M. Biernacki, S.H. Chen, P.A. Grobelny, C. Moskowitz and S.H. Talisa, "Electromagnetic design of high-temperature superconducting microwave filters," *IEEE MTT-S Int. Microwave Symp.* (San Diego, CA), 1994.

Reprint 15

A Novel Approach to Statistical Modeling Using Cumulative Probability Distribution Fitting

1994 IEEE International Microwave Symposium Digest, San Diego, CA, May 1994

A NOVEL APPROACH TO STATISTICAL MODELING USING CUMULATIVE PROBABILITY DISTRIBUTION FITTING

J.W. Bandler, R.M. Biernacki, Q. Cai and S.H. Chen

Simulation Optimization Systems Research Laboratory
and Department of Electrical and Computer Engineering
McMaster University, Hamilton, Ontario, Canada L8S 4L7

ABSTRACT

A novel approach to statistical modeling is presented. The statistical model is directly extracted by fitting the cumulative probability distributions (CPDs) of the model responses to those of the measured data. This new technique is based on a solid mathematical foundation and, therefore, should prove more reliable and robust than the existing methods. The approach is illustrated by statistical MESFET modeling based on a physics-oriented model which combines the modified Khatibzadeh and Trew model and the Ladbrooke model (KTL). The approach is compared with the established parameter extraction/postprocessing approach (PEP) in the context of yield verification.

INTRODUCTION

Yield analysis and optimization which take into account the manufacturing tolerances and model uncertainties have been recently addressed in microwave CAD, e.g., [1-4]. Accurate and reliable statistical modeling is a prerequisite for accurate yield analysis and optimization [1].

In our previous work [5], we established the parameter extraction/postprocessing approach (PEP) to statistical modeling. Optimization is applied to extract parameters of individual devices by fitting the simulated responses to the corresponding measured data. The parameter statistics, i.e., the mean values, standard deviations, discrete distribution functions and the correlation matrix, are then obtained by postprocessing the resulting models. That approach strongly relies on the uniqueness of the parameter extraction process and, therefore, the resulting statistical models may not reflect the actual distribution of measurement data, even if the fit of the simulated responses to the corresponding measurements for individual device models is excellent.

In this paper we propose a novel approach to statistical modeling. The statistical model is determined by fitting the cumulative probability distributions (CPDs) [6] of the model responses to those of the measured data. Efficient ℓ_1 optimization [7] is used for CPD fitting. The optimization variables include the mean values and standard deviations of the statistical parameters. Thus, the model parameter statistics are obtained directly instead of from postprocessing a set of individually extracted models.

The new technique was applied to statistical modeling of a MESFET. The statistical model used is based on a physics-oriented model which combines the modified Khatibzadeh and Trew model and the Ladbrooke model (KTL) [8].

The resulting model was tested using the yield verification technique presented in [2]. Monte Carlo simulation of a broadband small-signal amplifier was performed and compared using the new model and the data for several different specifications.

HarPE [9] and OSA90/hope [10] were used to implement the new technique and to carry out the calculations presented in this paper.

DEFINITION OF CPD AND MATCHING ERROR

Given a sample of data $S = [X_1\ X_2\ \ldots\ X_n]^T$, the measured CPD of S, denoted by $C(x)$, is defined as

$$C(x) = \frac{n_x}{n} \tag{1}$$

where n_x is the number of data points in S which are smaller than or equal to x. When n is adequately large $C(x)$ provides a very good approximation to the theoretical probability distribution from which the sample was drawn. Therefore, we can test whether two samples of data come from the same probability distribution by comparing their measured CPDs.

Consider two samples of data $S_a = [X_{a1}\ X_{a2}\ \ldots\ X_{an_a}]^T$ and $S_b = [X_{b1}\ X_{b2}\ \ldots\ X_{bn_b}]^T$. We can calculate their corresponding CPDs $C_a(x)$ and $C_b(x)$ using (1). The distance between the two CPDs at the point x is

$$D_{ab}(x) = |\ C_a(x) - C_b(x)\ | \tag{2}$$

The matching error between the two CPDs can be defined as

$$e_{ab} = \int_{-\infty}^{\infty} D_{ab}(x)\,dx \tag{3}$$

If we merge S_a and S_b to form $S_c = [X_{c1}\ X_{c2}\ \ldots\ X_{cn_c}]^T$, $n_c = n_a + n_b$, with all the points sorted in ascending order, the calculation of e_{ab} becomes

This work was supported in part by Optimization Systems Associates Inc. and in part by the Natural Sciences and Engineering Research Council of Canada under Grants OGP0042444, OGP0007239 and STR0117819.

The authors are also with Optimization Systems Associates Inc., P.O. Box 8083, Dundas, Ontario, Canada L9H 5E7.

$$e_{ab} = \sum_{i=1}^{n_c-1} D_{ab}(X_{ci})\ (X_{c(i+1)} - X_{ci}) \tag{4}$$

which is the absolute value of the area between the two CPDs, as shown in Fig. 1.

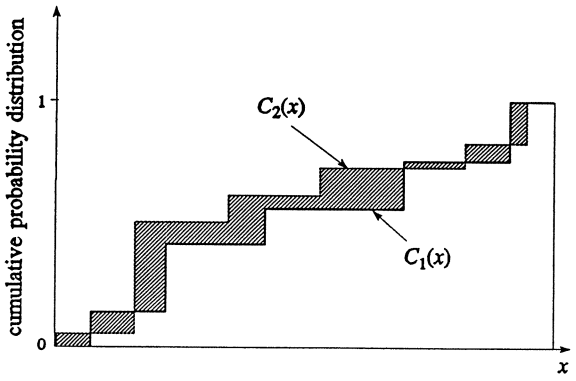

Fig. 1 Two cumulative probability distributions and their matching error (shaded area).

FORMULATION OF CPD FITTING FOR STATISTICAL MODELING

Suppose that the measurement data contains n_r measured responses for n_{mo} manufactured outcomes. For each measured response we thus have the sample

$$S_i = [X_{i1}\ X_{i2}\ \ldots\ X_{in_{mo}}]^T, \quad i = 1, 2, \ldots, n_r \tag{5}$$

The statistical model is simulated by Monte Carlo analysis with n_{so} outcomes and for each simulated response corresponding to S_i we have the sample

$$R_i(\phi) = [R_{i1}(\phi)\ R_{i2}(\phi)\ \ldots\ R_{in_{so}}(\phi)]^T \tag{6}$$

where $\phi = [\phi_1\ \phi_2\ \ldots\ \phi_{n_\phi}]^T$ is the set of optimization variables such as the mean values and standard deviations of a normal distribution, the nominal values and tolerances of a uniform distribution. For each pair S_i and R_i we calculate their CPDs using (1), the difference between these two CPDs using (2), and finally the matching error $e_i(\phi)$ using (4). Let

$$e(\phi) = [e_1(\phi)\ e_2(\phi)\ \ldots\ e_{n_r}(\phi)]^T \tag{7}$$

then the optimization problem of CPD fitting for statistical modeling can be defined as

$$\underset{\phi}{minimize}\ \ U(\phi) \triangleq H[e(\phi)] \tag{8}$$

where $H[e(\phi)]$ represents a norm of $e(\phi)$ such as the ℓ_1, ℓ_2 or the Huber norm. In our CPD fitting we have used the ℓ_1 norm, which can be written as

$$H[e(\phi)] = \sum_{i=1}^{n_r} |\ e_i(\phi)\ | \tag{9}$$

STATISTICAL MODEL EXTRACTION

The proposed statistical modeling technique of CPD fitting was applied to a sample of GaAs MESFET data which was obtained by aligning the Plessey wafer measurements to a consistent bias condition [8]. There were 35 data sets (devices) containing the small-signal S parameters measured at the frequencies from 1 to 21 GHz with 2 GHz step under the bias condition of V_{gs} = -0.7 V and V_{ds} = 5 V.

The KTL model [8] was selected for statistical modeling. The attractive statistical characteristics of the KTL model have been presented by Bandler *et al.* [2,8] using the method of multi-device parameter extraction and statistical postprocessing. That method was also used here for finding the starting point for optimization.

We considered 16 statistical parameters assuming normal distributions. This resulted in 32 optimization variables, namely all mean values and standard deviations. The initial values for the means and standard deviations were estimated from multi-device parameter extraction and statistical postprocessing based on 15 devices. The resulting correlation matrix was used to represent the correlations between the statistical parameters. By applying CPD fitting we obtained the KTL model parameter values listed in Table I. The CPDs of the real part of S_{21}, $\mathrm{Re}\{S_{21}\}$, at 11 GHz from the data and from the statistical KTL model before and after optimization are shown in Fig. 2. The mean values and the standard deviations of $\mathrm{Re}\{S_{21}\}$ versus frequency from the data and from the model before and after optimization are depicted in Figs. 3 and 4, respectively. From Fig. 2 we can see that after optimization the CPD matching between the data and the KTL model is significantly improved. The mean values and standard deviations of model responses after optimization are also closer to those of the data, as indicated in Figs. 3 and 4.

TABLE I
CPD OPTIMIZED KTL MODEL PARAMETERS

Parameter	Mean	σ(%)	Parameter	Mean	σ(%)
$L(\mu m)$	0.4685	3.57	C_{ds}(pF)	0.0547	1.58
$a(\mu m)$	0.1308	5.19	C_{ge}(pF)	0.0807	5.92
$N_d(m^{-3})$	2.3×10^{23}	3.25	C_{de}(pF)	0.0098	6.22
v_{sat}(m/s)	10.5×10^{4}	2.27	C_x(pF)	2.4231	4.03
$\mu_0(m^2/Vns)$	6.5×10^{-10}	2.16	$Z(\mu m)$	300	*
L_{G0}(nH)	0.0396	10.9	ε	12.9	*
$R_d(\Omega)$	1.2867	4.32	V_{b0}(V)	0.6	*
$R_s(\Omega)$	3.9119	1.91	$r_{01}(\Omega/V^2)$	0.35	*
$R_g(\Omega)$	8.1718	0.77	$r_{02}(\Omega)$	2003	*
L_d(nH)	0.0659	5.74	$r_{03}(\Omega)$	7.0	*
L_s(nH)	0.0409	5.49	a_0	1.0	*
$G_{ds}(1/\Omega)$	3.9×10^{-3}	1.78			

L is the gate length, a the channel thickness, N_d the doping density, v_{sat} the saturation electron drift velocity, μ_0 the low-field mobility of GaAs, L_{g0} the inductance from gate bond wires and pads, Z the gate width, ε the dielectric constant and V_{b0} the zero-bias barrier potential. r_{01}, r_{02}, r_{03} and a_0 are fitting coefficients. R_d, R_s, R_g, L_d, L_s, G_{ds}, C_{ds}, C_{ge}, C_{de} and C_x are extrinsic parameters.

σ denotes standard deviation.

* Assumed fixed (non-statistical) parameters.

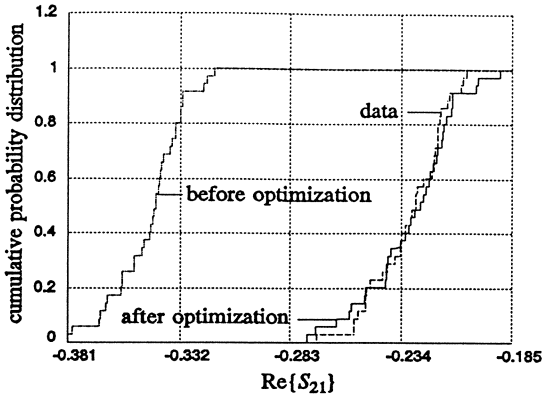

Fig. 2 CPDs of Re{S_{21}} at 11 GHz from data (---) and from the statistical KTL model before (-•-) and after (——) CPD matching.

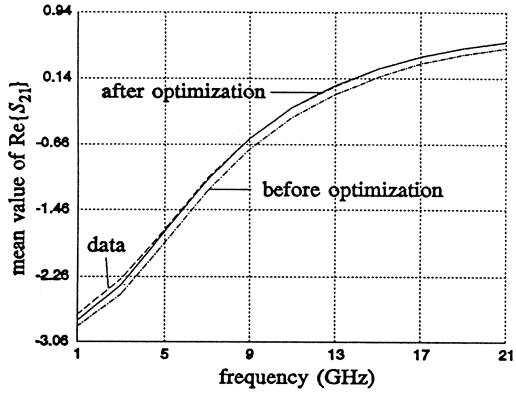

Fig. 3 Mean values of Re{S_{21}} versus frequency from data (---) and from the statistical KTL model before (-•-) and after (——) CPD matching.

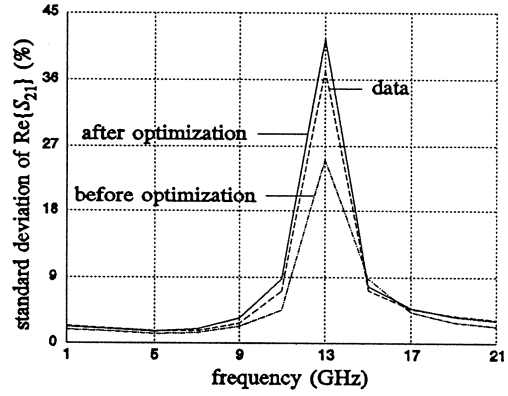

Fig. 4 Standard deviations of Re{S_{21}} versus frequency from data (---) and from the statistical KTL model before (-•-) and after (——) CPD matching.

In order to compare these results with the PEP method we also performed statistical modeling using multi-device parameter extraction and postprocessing based on the same 35 data sets. The KTL model parameter values obtained by the PEP method are listed in Table II. The CPDs of Re{S_{21}} at 11 GHz for both models are plotted in Fig. 5 together with the corresponding CPDs from the data. The mean values and the standard deviations of Re{S_{21}} versus frequency are shown in Figs. 6 and 7, respectively. From Fig. 5 we can observe that the CPD matching of Re{S_{21}} of the KTL model obtained by CPD fitting is better than that obtained by the PEP method. From Figs. 6 and 7 we see that our new approach gives better standard deviation match though the mean value matches of both models are similar.

TABLE II
PEP OPTIMIZED KTL MODEL PARAMETERS

Parameter	Mean	σ(%)	Parameter	Mean	σ(%)
$L(\mu m)$	0.5190	4.72	C_{ds}(pF)	0.0486	2.84
$a(\mu m)$	0.1584	8.20	C_{gs}(pF)	0.0698	9.72
$N_d(m^{-3})$	2.2×10^{23}	4.68	C_{dg}(pF)	0.0109	10.5
v_{sat}(m/s)	10.7×10^{4}	2.24	C_x(pF)	3.3046	3.69
$\mu_0(m^2/Vns)$	5.9×10^{-10}	1.89	$Z(\mu m)$	300	*
L_{G0}(nH)	0.0331	12.2	ε	12.9	*
$R_d(\Omega)$	1.1190	9.43	V_{b0}(V)	0.6	*
$R_s(\Omega)$	3.3226	2.69	$r_{01}(\Omega/V^2)$	0.35	*
$R_g(\Omega)$	6.6209	1.59	$r_{02}(\Omega)$	2003	*
L_d(nH)	0.0533	10.4	$r_{03}(\Omega)$	7.0	*
L_s(nH)	0.0407	9.75	a_0	1.0	*
$G_{ds}(1/\Omega)$	3.8×10^{-3}	2.51			

The parameter definitions are the same as in Table I.

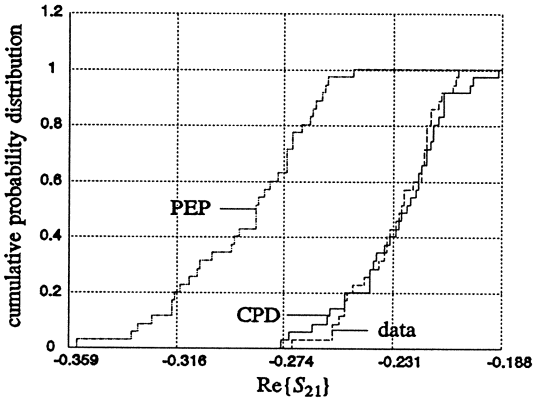

Fig. 5 CPDs of Re{S_{21}} at 11 GHz from data (---) and from the CPD (——) and PEP (-•-) statistical KTL models.

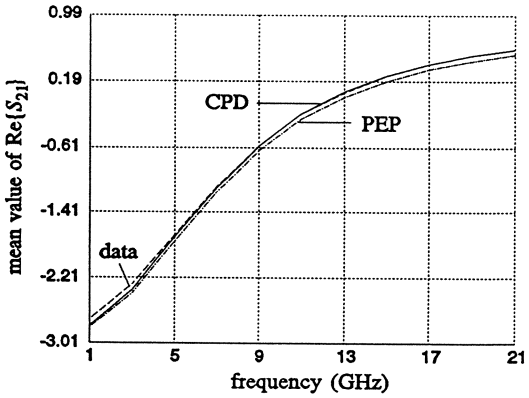

Fig. 6 Mean values of Re{S_{21}} versus frequency from data (---) and from the CPD (——) and PEP (-•-) statistical KTL models.

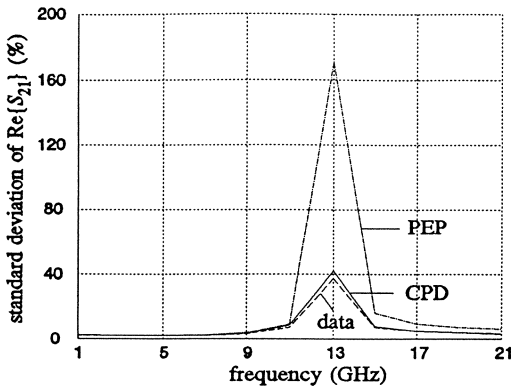

Fig. 7 Standard deviations of Re{S_{21}} versus frequency from data (---) and from the CPD (——) and PEP (-•-) statistical KTL models.

YIELD VERIFICATION

The ultimate goal of statistical modeling is to provide accurate statistical models for yield optimization. Therefore, the statistical model can be further verified by comparing the yield estimations by the model and data [2]. To this end we performed yield verification using Monte Carlo simulation.

We considered yield optimization of a small-signal broadband amplifier used in [2]. The design was carried out using OSA90/hope [10]. The passband of the amplifier is 8 GHz - 12 GHz. Three different specifications were considered. Yield optimization was performed using the two statistical KTL models (CPD and PEP). The yields predicted by Monte Carlo simulation from the data and from both models are listed in Tables III. We can see that the yields predicted by both models are in good agreement for every specification.

TABLE III
YIELD PREDICTED BY THE KTL MODELS AND VERIFIED BY DATA

	Yield Before Optimization			Yield After Optimization		
Spec.	CPD (%)	PEP (%)	Data (%)	CPD (%)	PEP (%)	Data (%)
Spec. 1	22	26	28.6	71	69.5	77.6
Spec. 2	30	38.5	37.1	76.5	78.5	90.9
Spec. 3	64.5	67.5	76.7	98.5	93.5	99.5

Spec. 1: 7.5 dB < $|S_{21}|$ < 8.5 dB, $|S_{11}|$ < 0.5, $|S_{22}|$ < 0.5.

Spec. 2: 6.5 dB < $|S_{21}|$ < 7.5 dB, $|S_{11}|$ < 0.5, $|S_{22}|$ < 0.5.

Spec. 3: 6.0 dB < $|S_{21}|$ < 8.0 dB, $|S_{11}|$ < 0.5, $|S_{22}|$ < 0.5.

200 outcomes are used for yield prediction by the statistical KTL model, 210 for yield verification using the device data.

CONCLUSIONS

We have presented a novel approach to statistical modeling. The parameter mean values and standard deviations are directly optimized to match the cumulative probability distributions of the model responses to those of the data. This approach avoids parameter extraction of individual devices and, therefore, is not affected by possible pitfalls of the parameter extraction process. Our investigations set the stage for further research, which could include determining parameter correlations in addition to mean values and standard deviations, as well as possible extensions to other than normal distributions. In principle, the proposed method is not limited to normal distributions. Finally, we point out that although the PEP technique normally provides adequate statistical models, the new CPD technique is based on a solid mathematical foundation and, therefore, should prove more reliable and robust.

REFERENCES

[1] J.W. Bandler, R.M. Biernacki, Q. Cai, S.H. Chen, S. Ye and Q.J. Zhang, "Integrated physics-oriented statistical modeling, simulation and optimization," *IEEE Trans. Microwave Theory Tech.*, vol. 40, 1992, pp. 1374-1400.

[2] J.W. Bandler, S. Ye, Q. Cai, R.M. Biernacki and S.H. Chen, "Predictable yield-driven circuit optimization," *IEEE Int. Microwave Symp. Digest* (Albuquerque, NM), 1992, pp. 837-840.

[3] F. Filicori, G. Ghione and C.U. Naldi, "Physics-based electron device modelling and computer-aided MMIC design," *IEEE Trans. Microwave Theory Tech.*, vol. 40, 1992, pp. 1333-1352.

[4] D.E. Stoneking, G.L. Bilbro, P.A. Gilmore, R.J. Trew and C.T. Kelley, "Yield optimization using a GaAs process simulator coupled to a physical device model," *IEEE Trans. Microwave Theory Tech.*, vol. 40, 1992, pp. 1353-1363.

[5] J.W. Bandler, R.M. Biernacki, S.H. Chen, J.F. Loman, M.L. Renault and Q.J. Zhang, "Combined discrete/normal statistical modeling of microwave devices," *Proc. 19th European Microwave Conf.* (London, England), 1989, pp. 205-210.

[6] W.H. Press, B.P. Flannery, S.A. Teukolsky and W.T. Vetterling, *Numerical Recipes. The Art of Scientific Computing*. Cambridge University Press: Cambridge, 1986.

[7] J.W. Bandler, S.H. Chen and S. Daijavad, "Microwave device modeling using efficient ℓ_1 optimization: a novel approach," *IEEE Trans. Microwave Theory Tech.*, vol. MTT-34, 1986, pp. 1282-1293.

[8] J.W. Bandler, R.M. Biernacki, Q. Cai and S.H. Chen, "A robust physics-oriented statistical GaAs MESFET model," *GAAS94* (Turin, Italy), 1994.

[9] *HarPE*™, Optimization Systems Associates Inc., P.O. Box 8083, Dundas, Ontario, Canada L9H 5E7, 1993.

[10] *OSA90/hope*™, Optimization Systems Associates Inc., P.O. Box 8083, Dundas, Ontario, Canada L9H 5E7, 1993.

Reprint 16

Electromagnetic Design of High-Temperature Superconducting Microwave Filters

1994 IEEE International Microwave Symposium Digest, San Diego, CA, May 1994

ELECTROMAGNETIC DESIGN OF HIGH-TEMPERATURE SUPERCONDUCTING MICROWAVE FILTERS

J.W. Bandler,* R.M. Biernacki,* S.H. Chen,* P.A. Grobelny,* C. Moskowitz** and S.H. Talisa***

Optimization Systems Associates Inc., P.O. Box 8083, Dundas, Ontario, Canada L9H 5E7

Westinghouse Science and Technology Center, 1310 Beulah Road, Pittsburgh, PA 15235, USA

ABSTRACT

We present novel approaches to electromagnetic design of high-temperature superconducting quarter-wave parallel coupled-line microstrip filters. The dielectric constant of substrate materials used in high-temperature superconductor technology is too large to be accurately treated by traditional microwave circuit design software packages with analytical/empirical models. We employ electromagnetic field simulation and develop a look-up table method and a powerful space mapping optimization technique, which dramatically reduce the CPU time for the design process.

INTRODUCTION

The recently discovered high-temperature superconductors (HTS) are of great potential for passive microwave military and commercial applications. Available low-loss and narrow-bandwidth (0.5 - 3%) filter banks are of very large size, which in some satellite and airborne applications is intolerable. Small conventional microstrip filters are too lossy for narrow-band applications. Using HTS technology [1, 2], however, low-loss, narrow-bandwidth microstrip filters, requiring relatively inexpensive cooling, can be made.

Advances in electromagnetic (EM) simulation provide designers the opportunity to accurately simulate passive microstrip circuits. We verified the usefulness of EM simulation in analyzing circuits built with the HTS technology by simulating two existing HTS microstrip filters. In both cases good correlation was observed between the EM simulated and measured responses of the filters.

In this paper we concentrate on the EM design of an HTS quarter-wave parallel coupled-line filter. The difficulty arising here is related to the large dielectric constant of the substrate materials ($\epsilon_r \approx 24$) used in the HTS technology and the inability of the traditional microwave circuit design techniques to analyze structures built of such materials. This is especially true for narrow-band, parallel coupled-line filters where loose coupling between sections is required. To overcome this problem we resort to EM field simulations. EM simulations can provide results that are in good agreement with experimental data. This, however, is at the expense of very high computational cost. This limitation shows up very clearly in analysis of narrow-bandwidth filters whose inherent high sensitivity calls for a very fine grid in the numerical EM simulation.

In order to decrease the CPU time required and overcome the high sensitivity of the filter we considered two approaches. The first approach is based on a table of coupling versus gap and frequency values and the second is based on space mapping (SM) circuit optimization. In the look-up table approach we analyze the couplings in different sections of the filter for different gaps in each of the sections swept over the frequency band of interest. The couplings are determined from EM simulations and the table is iteratively updated. In the SM approach an adaptive mapping between an OSA90/hope [3] simulation model and ***em*** [4, 5] simulation is established. Such a mapping, adaptively refined during optimization, allows us to benefit from the accuracy of EM simulation while using a much faster model for optimization. The SM method is a novel extension of our work on optimization-driven EM simulation [6, 7]. The method was tested using OSA90/hope interfaced to ***em*** through Empipe [8].

THE FILTER

We wish to design a four-pole quarter-wave parallel coupled-line microstrip filter. The geometry of the filter is shown in Fig. 1. L_1, L_2 and L_3 are the lengths of the parallel coupled-line sections and S_1, S_2 and S_3 are the gaps between the sections. The width W is the same for all the sections as well as for the input and output microstrip lines L_0. The thickness of the lanthanum aluminate substrate used is 20 mil and the dielectric constant is assumed to be 23.425. The design specifications are as follows.

$$|S_{21}| \le 0.05 \quad \text{for} \quad f \le 3.967 \text{ GHz and } f \ge 4.099 \text{ GHz}$$

$$|S_{21}| \ge 0.95 \quad \text{for} \quad 4.008 \text{ GHz} \le f \le 4.058 \text{ GHz}$$

This work was supported in part by Optimization Systems Associates Inc.; in part by the Natural Sciences and Engineering Research Council of Canada under Grants OGP0042444, OGP0007239 and STR0117819; and in part by the U.S. Navy under contracts N00014-92-C-2043 and N00014-91-C-0112.

* J.W. Bandler, R.M. Biernacki and S.H. Chen are with Optimization Systems Associates Inc. They are also with and P.A. Grobelny is with the Simulation Optimization Systems Research Laboratory and Department of Electrical and Computer Engineering, McMaster University, Hamilton, Ontario, Canada L8S 4L7.

** C. Moskowitz is with the Westinghouse Electronic Systems Group, Baltimore, MD 21203.

*** S.H. Talisa is with the Westinghouse Science and Technology Center, Pittsburgh, PA 15235.

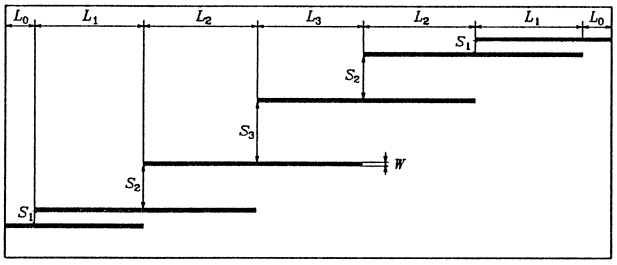

Fig. 1. The structure of the HTS quarter-wave parallel coupled-line microstrip filter (to scale). The dielectric constant and the substrate thickness are 23.425 and 20 mil, respectively. The geometrical dimensions are listed in Table I. The x and y grid sizes for *em* simulations are 1.0 and 1.75 mil. 100 elapsed minutes are needed for analysis at a single frequency on Sun SPARCstation 10.

This corresponds to a 1.25% bandwidth. L_1, L_2, L_3, S_1, S_2 and S_3 are the design parameters. L_0 and W are fixed.

FILTER DESIGN USING TRADITIONAL SIMULATORS

We started the design process by optimizing the filter using two commercial microwave CAD packages, namely, OSA90/hope and Touchstone [9]. The solutions are listed in the first two columns of Table I. Subsequently we performed *em* simulations at both solutions. The *em* simulation results differed from the circuit simulation results and did not satisfy the specifications. The responses are shown in Fig. 2. We set out to develop methods for adapting the traditional analytical/empirical models for the design process.

FILTER DESIGN USING THE LOOK-UP TABLE METHOD

Although the technique is general in nature, it has been applied only to the class of filters known as parallel coupled-line filters which are derivable from lowpass ladder networks. One starts with the normalized lowpass ladder network elements which satisfy some predetermined shape requirement and results in the lowpass prototype element values also known as the g values. An appropriate bandpass and impedance transformation is performed which leads to good approximations of the even and

TABLE I
HTS PARALLEL COUPLED-LINE MICROSTRIP FILTER DESIGN RESULTS

Parameter (mil)	OSA90/hope Optimization	Touchstone Optimization	Look-up Table Method	SM Method
L_1	191.00	188.70	188.70	190.00
S_1	21.74	22.52	20.88	19.25
L_2	195.58	188.11	188.10	192.00
S_2	96.00	93.19	76.02	75.25
L_3	191.00	188.58	188.59	189.00
S_3	114.68	109.13	85.07	91.00
W	7.00	6.93	6.93	7.00
L_0	50.00	50.00	50.00	50.00

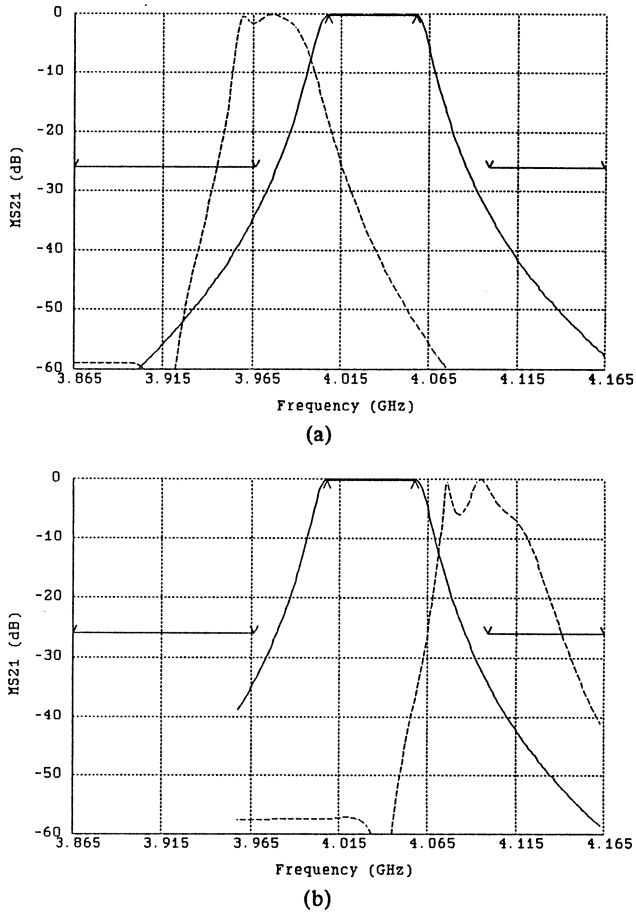

Fig. 2. The optimal solutions (solid lines) of $|S_{21}|$ obtained using (a) OSA90/hope and (b) Touchstone. The corresponding *em* simulation results are shown as dashed lines. V indicate upper and Λ indicate lower specifications.

odd mode impedances of the coupled-line sections which comprise the filter. The next step in the design process is to determine the geometry or conductor arrangement which realizes this set of even/odd mode impedances. The medium that we have chosen is microstrip on 20 mil lanthanum aluminate. In this medium, the coupled sections are characterized by three geometric parameters; line width, coupling length and coupling gap, which must be chosen to provide the required even and odd mode impedances. The ratio of these impedances depends only on the coupling coefficient of the coupler and the product depends on the impedance level.

The simulator aided design process consists of estimating the quarter wavelength in the medium at filter band center, and the gap required for the coupling. One then constructs a model for the field simulator which consists of a coupled-line with input and output ports on a diagonal with the other diagonal remaining as open circuits. Actually, several models are constructed over a range of gaps so that one can interpolate the *em* simulator's results to the required gap based upon the required coupling factor. This process is repeated for each coupled section of the filter. When a complete set of gaps has been determined by interpolation, the filter is modeled for analysis by the field simulator. The result usually has a shape that is close to the desired shape but is offset in center frequency. The amount of the frequency error and the original

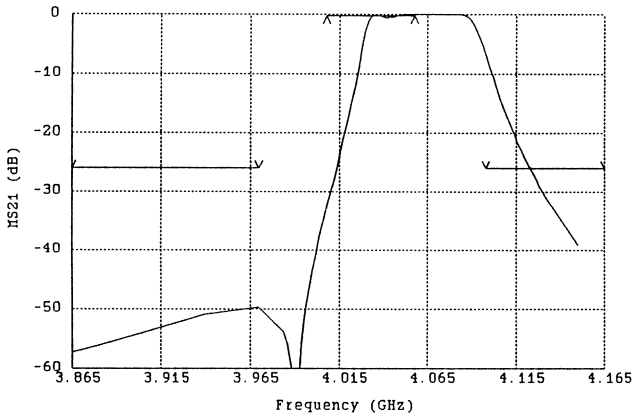

(a)

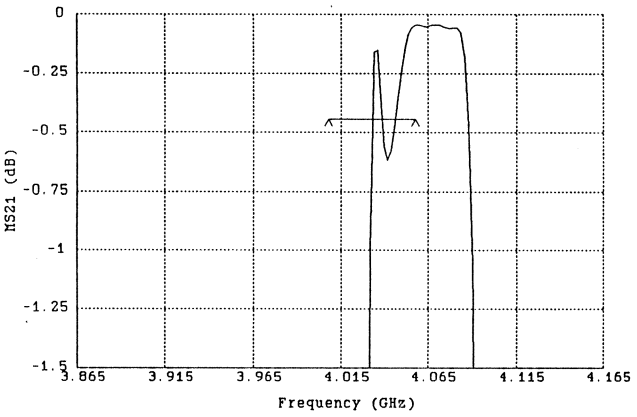

(b)

Fig. 3. The *em* simulated $|S_{21}|$ response of the HTS parallel coupled-line filter at the solution obtained using the look-up table method. (a) Response for the overall band. (b) Passband details of the response. V and Λ indicate upper and lower specifications, respectively. The response exhibits the desired shape with slightly shifted center frequency.

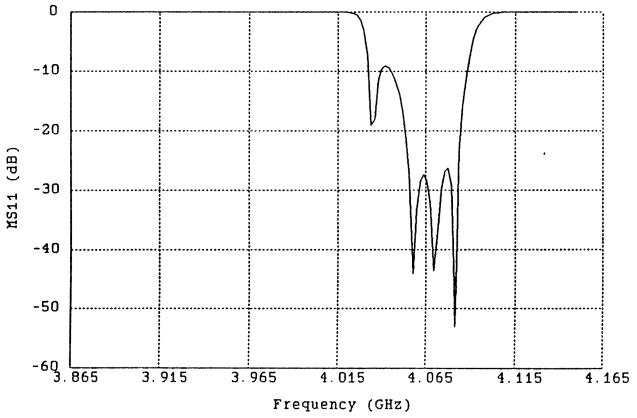

Fig. 4. The *em* simulated $|S_{11}|$ response of the HTS parallel coupled-line filter at the solution obtained using the look-up table method.

coupling length provide enough information to compute a length correction, i.e., the fractional change in frequency is proportional to the negative of the fractional change in length.

The process is then repeated using the new coupling length. We have found adequate convergence after three iterations.

The filter's $|S_{21}|$ and $|S_{11}|$ responses simulated by *em* at the look-up table method solution are shown in Figs. 3 and 4, respectively. The solution point is listed in the third column of Table I. The $|S_{21}|$ response has the desired shape but the center frequency is slightly shifted w.r.t. specifications. Also, a small ripple present in the passband, see Fig. 3(b), results in non-uniform $|S_{11}|$ in the passband.

FILTER DESIGN USING THE SPACE MAPPING METHOD

In the novel SM optimization technique we create and iteratively refine a mapping

$$x_{OS} = T(x_{EM}) \tag{1}$$

from the EM simulator input space $\{x_{EM}\}$ onto the optimization system (OS) parameter space $\{x_{OS}\}$. Though not necessary, it is desirable that T is invertible. If so, the inverse mapping T^{-1} is used to find the image of the optimal OS solution x^*_{OS}, namely,

$$\bar{x}_{EM} = T^{-1}(x^*_{OS}) \tag{2}$$

T is established through an iterative process. The initial mapping $T^{(0)}$ is found using a preselected set B_{EM} of k points in the EM input space and the set B_{OS} of corresponding points in the OS parameter space. The points in B_{OS} are determined such that

$$f_{OS}(x_{OS}^i) \approx f_{EM}(x_{EM}^i), \quad i = 1, 2, \ldots, k \tag{3}$$

where f_{OS} and f_{EM} are the circuit responses simulated by the OS and EM simulators, respectively. At the jth iteration B_{EM} is expanded by the new image of x^*_{OS} computed using $(T^{(j)})^{-1}$ and B_{OS} is expanded accordingly. The iterations continue until

$$f_{EM}(\bar{x}_{EM}) \approx f_{OS}(x^*_{OS}) \tag{4}$$

Applying the SM optimization technique to the design of our HTS filter we used the Empipe [8] interface interconnecting *em* to OSA90/hope. All the processing needed to establish the mapping was performed within the OSA90/hope environment.

A total of 13 *em* simulations was sufficient to establish the mapping T which satisfies (4). The point $\bar{x}_{EM}$ obtained as the $(T)^{-1}$ image of x^*_{OS} and listed in the fourth column of Table I gave us an excellent response of the filter, as simulated by *em*. The $|S_{21}|$ response, shown in Fig. 5, meets the design specifications well. The $|S_{11}|$ response, shown in Fig. 6, is also improved.

CONCLUSIONS

We have presented EM-based methods for CAD of narrow-band parallel coupled-line microstrip filters built using the HTS technology. The new space mapping optimization method is a general approach which can be applied to other design problems. It is especially attractive for designs involving CPU intensive simulators, where it substantially decreases the number of necessary simulations. Filters will be built according to the results obtained from both methods.

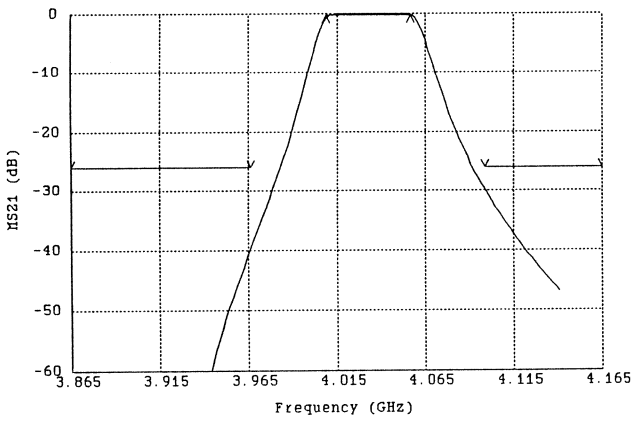

(a)

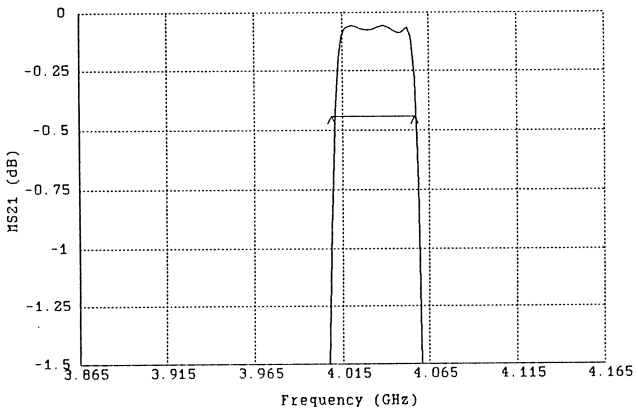

(b)

Fig. 5. The *em* simulated $|S_{21}|$ response of the HTS parallel coupled-line filter at the solution obtained using the SM optimization method. (a) Response for the overall band. (b) Passband details of the response. V and Λ indicate upper and lower specifications, respectively.

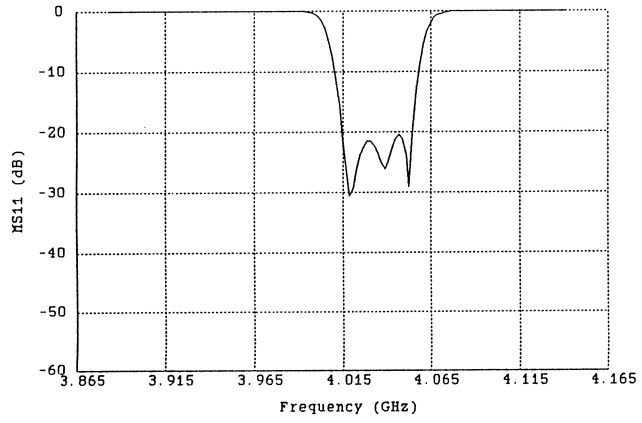

Fig. 6. The *em* simulated $|S_{11}|$ response of the HTS parallel coupled-line filter at the solution obtained using the SM optimization method.

REFERENCES

[1] S.H. Talisa, M.A. Janocko, C. Moskowitz, J. Talvacchio, J.F. Billing, R. Brown, D.C. Buck, C.K. Jones, B.R. McAvoy, G.R. Wagner and D.H. Watt, "Low- and high-temperature superconducting microwave filters," *IEEE Trans. Microwave Theory Tech.*, vol. 39, 1991, pp. 1448-1454.

[2] W.G. Lyons, R.R. Bonetti, A.E. Williams, P.M. Mankiewich, M.L. O'Malley, J.M. Hamm, A.C. Anderson, R.S. Withers, A. Meulenberg and R.E. Howard, "High-T_c superconductive microwave filters," *IEEE Trans. Magnetics*, vol. 27, 1991, pp. 2537-2539.

[3] *OSA90/hope*™, Optimization Systems Associates Inc., P.O. Box 8083, Dundas, Ontario, Canada L9H 5E7, 1993.

[4] *Em User's Manual* and *Xgeom User's Manual*, Sonnet Software, Inc., 135 Old Cove Road, Suite 203, Liverpool, NY 13090-3774, 1992.

[5] J.C. Rautio and R.F. Harrington, "An electromagnetic time-harmonic analysis of arbitrary microstrip circuits," *IEEE Trans. Microwave Theory Tech.*, vol. 35, 1987, pp. 726-730.

[6] J.W. Bandler, S. Ye, R.M. Biernacki, S.H. Chen and D.G. Swanson, Jr., "Minimax microstrip filter design using direct EM field simulation," in *IEEE MTT-S Int. Microwave Symp. Dig.* (Atlanta, GA), 1993, pp. 889-892.

[7] J.W. Bandler, R.M. Biernacki, S.H. Chen, P.A. Grobelny and S. Ye, "Yield-driven electromagnetic optimization via multilevel multidimensional models," *IEEE Trans. Microwave Theory Tech.*, vol. 41, December 1993.

[8] *Empipe*™, Optimization Systems Associates Inc., P.O. Box 8083, Dundas, Ontario, Canada L9H 5E7, 1993.

[9] *Touchstone® Reference Manual Version 3.0*, EEsof, Inc., 5601 Lindero Canyon Road, Westlake Village, CA 91362-4020, 1991.

Reprint 17

The Huber Concept in Device Modeling, Circuit Diagnosis and Design Centering

Proceedings of the 1994 International Symposium on Circuit and Systems, London, England, May 1994

The Huber Concept in Device Modeling, Circuit Diagnosis and Design Centering

J.W. Bandler, S.H. Chen, R.M. Biernacki

Simulation Optimization Systems Research Laboratory
Department of Electrical and Computer Engineering
McMaster University, Hamilton, Canada L8S 4L7
+1 905 525 9140 Ext. 24818
bandler@mcmail.cis.mcmaster.ca

K. Madsen

Institute of Mathematical Modelling
The Technical University of Denmark
DK-2800 Lyngby, Denmark
+45 4288 1433 Ext. 3075
numikm@vm.uni-c.dk

ABSTRACT

We present exciting applications of the Huber concept in circuit modeling and optimization. By combining the desirable properties of the ℓ_1 and ℓ_2 norms, the Huber function is robust against gross errors and smooth w.r.t. small variations in the data. We extend the Huber concept by introducing a one-sided Huber function tailored to design optimization with upper and lower specifications. We demonstrate the advantages of Huber optimization in the presence of faults, large and small measurement errors, bad starting points and statistical uncertainties. Circuit applications include parameter identification, design optimization, statistical modeling, analog fault location and yield optimization.

INTRODUCTION

Realistic circuit optimization must take into account model/measurement/statistical errors, variations and uncertainties. Least-squares (ℓ_2) solutions are notoriously susceptible to the influence of gross errors: just a few "wild" data points can alter the results significantly. The ℓ_1 method is robust against gross errors [1,2]. However, it inappropriately treats small variations in the data. In other words, neither the ℓ_1 nor ℓ_2 alone is capable of providing solutions which are robust against large errors *and* flexible w.r.t. small variations in the data.

The Huber function [3-5] is a hybrid of the ℓ_1 and ℓ_2 norms. The large errors are treated in the ℓ_1 sense and the small errors are measured in terms of least squares. Consequently, the Huber solution can provide a smooth model from data which contains many small variations and such a model is also robust against gross errors.

We extend the Huber concept by introducing a "one-sided" Huber function for design optimization with upper and/or lower specifications. The minimax objective is often chosen to achieve an equal-ripple design. However, from a "bad" starting point, a minimax optimizer can be trapped by the initial large errors. We have demonstrated [5] that the one-sided Huber function can be employed in a "preprocessing" optimization to overcome such a bad starting point. In this paper, we compare minimax optimization of multicavity filters with and without one-sided Huber preprocessing from randomly generated starting points.

Also, for the first time, we present a one-sided Huber approach to yield optimization of linear and nonlinear circuits.

Our approach is implemented in the CAD system OSA90/hope™ [6] which was used to produce the examples in this presentation.

THEORY

The Huber function is defined as [3-5]

$$\rho_k(f) = \begin{cases} f^2/2 & \text{if } |f| \le k \\ k|f| - k^2/2 & \text{if } |f| > k \end{cases} \qquad (1)$$

where k is a positive constant threshold value and f represents an error function.

J.W. Bandler, S.H. Chen and R.M. Biernacki are also with Optimization Systems Associates Inc., P.O. Box 8083, Dundas, Ontario, Canada L9H 5E7.

This work was supported in part by Optimization Systems Associates Inc. and in part by the Natural Sciences and Engineering Research Council of Canada under Grants OGP0007239, OGP0042444 and STR0117819.

The sum of ρ_k is a hybrid of the ℓ_2 (when $|f| \le k$) and the ℓ_1 (when $|f| > k$) norms. The definition of ρ_k ensures a smooth transition between ℓ_2 and ℓ_1 at $|f| = k$. The threshold k separates "large" and "small" errors. With a sufficiently large k, ρ_k becomes least squares. As k approaches zero, ρ_k approaches the ℓ_1 norm. By changing k, we can alter the proportion of error functions to be treated in the ℓ_1 or ℓ_2 sense.

We define the "one-sided" Huber function as

$$\rho_k^+(f) = \begin{cases} 0 & \text{if } f \le 0 \\ \rho_k(f) & \text{if } f > 0 \end{cases} \qquad (2)$$

This definition is tailored to one-sided (upper/lower) specifications. A negative value of f indicates that the corresponding specification is satisfied and is therefore truncated.

MULTICAVITY FILTER PARAMETER IDENTIFICATION

We consider a 6th-order multicavity filter [2]. The input reflection coefficient is used as simulated measurement. Two large errors are deliberately introduced into this data. The task is to identify the parameters from the contaminated data [2]. Our results obtained using the Huber function (1) are shown in Table I for selected couplings. The percentage entries represent the relative differences between the identified parameter values and the actual parameter values.

In Case A, the two large errors are the only errors contained in the data. The results in Table I show that the ℓ_2 solution is hopelessly corrupted by the gross errors, whereas the ℓ_1 and Huber solutions are equally robust.

In Case B, the data is truncated to the first two significant digits to emulate the limited accuracy of measurement equipment. The truncation errors are small relative to the two gross errors. We choose a threshold value commensurate with the magnitude of the truncation errors so that they are treated in the ℓ_2 sense by the Huber norm. Consequently, the Huber solution is less affected than the corresponding ℓ_1 solution (see Table I).

In Case C, we introduced into the data small errors randomly generated from the uniform distribution [-0.01 0.01]. Again, the Huber solution is better in comparison with the ℓ_1 solution, as shown in Table I.

TABLE I
PARAMETER IDENTIFICATION FOR MULTICAVITY FILTER

Couplings		M_{12}	M_{45}	M_{16}
Actual Values		0.859956	0.526602	0.087293
Starting Point		0.819006	0.511264	0.093863
Case A:	ℓ_2	-11%	7.3%	278%
	ℓ_1	0.05%	-0.06%	-0.01%
	Huber	0.02%	0.01%	-1.2%
Case B:	ℓ_1	0.51%	-2.9%	-14%
	Huber	0.15%	-0.01%	-8.3%
Case C:	ℓ_1	1.8%	-4.1%	-43%
	Huber	0.41%	0.04%	-27%

ANALOG FAULT LOCATION

Consider a resistive mesh network which has been used to demonstrate the ℓ_1 approach to analog fault location [2]. We have reported successful application of the Huber function to this problem [5]. In this paper, we present new results which take into account data truncation errors to represent the limited accuracy of measurement equipment.

Selected parameter values of the mesh network are listed in Table II. Two faults were assumed, namely G_2 and G_{18}. We generated simulated node voltage measurements at the accessible nodes. The voltages were then truncated to the first two significant digits.

TABLE II
FAULT LOCATION OF THE RESISTIVE MESH CIRCUIT

Element	Nominal Value	Actual Value	Percentage Deviation		
			Actual	ℓ_1	Huber
G_2	1.0	0.50	-50.0	-47.55	-54.40
G_3	1.0	1.05	5.0	-25.45	-3.68
G_{16}	1.0	0.95	-5.0	-20.24	-3.53
G_{17}	1.0	1.05	5.0	0.00	-0.81
G_{18}	1.0	0.50	-50.0	-8.90	-49.97
G_{19}	1.0	0.95	-5.0	-25.32	-4.74
G_{20}	1.0	0.95	-5.0	-20.73	-5.98

The nominal parameter values are used as the starting point for optimization. The results listed in Table II show that the ℓ_1 optimization failed to isolate the faults. The ℓ_1 optimization attempts to suppress as many parameter deviations as possible to exactly zero, which may lead to an incorrect solution, as demonstrated in this case.

ONE-SIDED HUBER PREPROCESSING OF ARBITRARY STARTING POINTS

We have exploited the potential of using one-sided Huber preprocessing to overcome bad starting points in large-scale multiplexer optimization [5]. In this paper, we expand our investigation by testing several starting points for optimization.

For the same 6th-order multicavity filter, 30 starting points were generated using uniform distribution centered at a "good" starting point with ±30% spread of the parameter values. The input return loss of the filter at these starting points is shown in Fig. 1(a). Clearly, some of the starting points are very bad.

From each starting point, we performed: (1) direct minimax optimization and (2) one-sided Huber optimization (preprocessing) followed by minimax optimization. The optimized responses are shown in Figs. 2(b) and 2(c), respectively. Although one-sided Huber preprocessing did not guarantee convergence to the optimal solution from all the starting points, it produced more focused results.

FET STATISTICAL MODELING

In our approach to statistical device modeling [7] we first extract model parameters for individual devices from device measurements and then postprocess the sample of model parameters to estimate the statistics (means, standard deviations and correlations). At the postprocessing stage we normally apply least-squares estimators using the error functions $f_j(\overline{\phi}) = \overline{\phi} - \phi^j$ to estimate mean values, or $f_j(V_\phi) = V_\phi - (\phi^j - \overline{\phi})^2$ to estimate standard deviations. ϕ^j is the extracted value of a parameter of the jth device, $j = 1, 2, ..., N$ and N is the total number of devices. V_ϕ denotes the estimated variance from which we can calculate the standard deviation σ_ϕ.

The Huber function (1) can be used as an automatic robust statistical estimator in place of least-squares estimators. If the sample of device measurements contains some wild points (e.g., due to faulty devices) they will severely degrade the least-squares estimates.

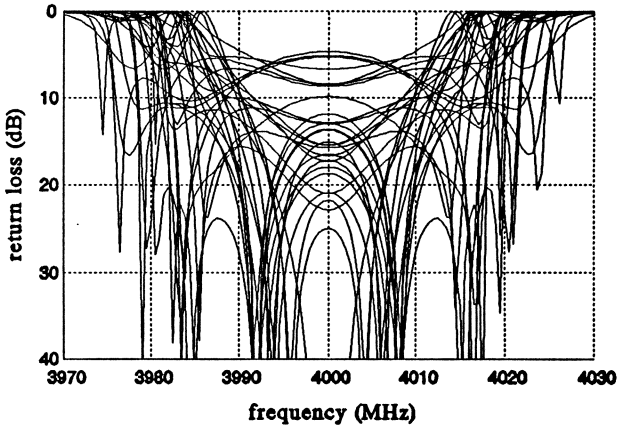

(a)

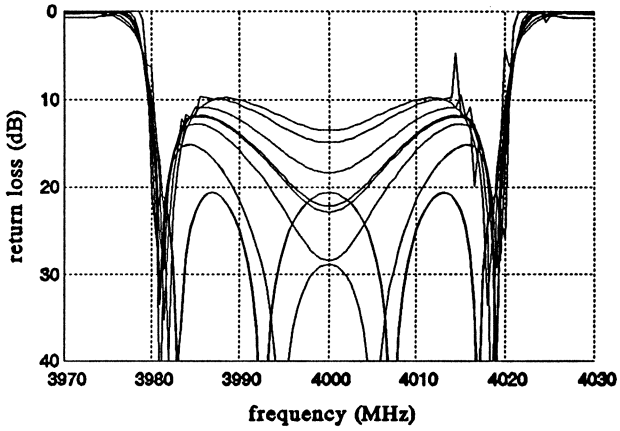

(b)

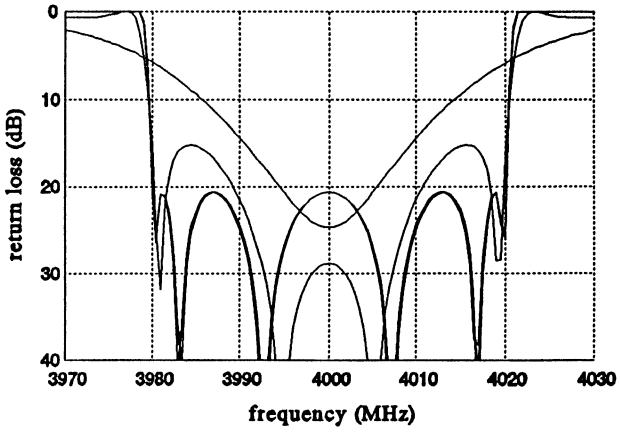

(c)

Figure 1

In our earlier work [7] using the ℓ_2 estimator, the wild points had to be manually excluded. Applying Huber estimators to the same data [5] we obtained similar results but without excluding any points.

ONE-SIDED HUBER FORMULATION FOR YIELD OPTIMIZATION

In Monte Carlo analysis, we consider a number of statistical outcomes of circuit parameters denoted by ϕ^i. Following the generalized ℓ_p centering approach [1], for each outcome we create a generalized ℓ_p function $\nu(\phi^i)$ which has a positive value if the outcome violates the design specifications or a zero or negative value if the specifications are satisfied.

In our earlier work [1,8], we have formulated yield optimization as a one-sided ℓ_1 problem. Here, we formulate yield optimization as a one-sided Huber problem in which the objective function is defined as

$$U(\phi^0) = \sum_{i=1}^{N} \rho_k^+(\alpha_i \nu(\phi^i)) \tag{3}$$

where ϕ^0 represents the nominal circuit parameters to be centered, α_i is a positive multiplier associated with the ith outcome, N the total number of outcomes and ρ_k^+ the one-sided Huber function defined in (2).

We considered a linear LC filter [9]. The one-sided ℓ_1 method needed 160 CPU seconds (11 iterations) on a Sun SPARCstation 10 while the one-sided Huber yield optimization with k=0.2 finished in 123 CPU seconds (9 iterations). Both produced 75% yield.

We also considered a nonlinear frequency doubler [10]. We assumed uniform tolerances for the linear matching subcircuits and normal distributions (with correlations) for the intrinsic FET parameters. At the nominal design (before yield optimization) yield was 28%. The centered designs were obtained after 17 iterations and 337 CPU seconds using one-sided ℓ_1 centering, and after 29 iterations and 574 CPU seconds using one-sided Huber technique, both on a Sun SPARCstation 10. The optimized yield values were 76% and 77%, respectively. Thus, the new one-sided Huber approach proved to be a competitive alternative to the one-sided ℓ_1 centering approach.

CONCLUSIONS

We have presented exciting developments in applying a novel Huber approach to parameter identification, preprocessing of arbitrary starting points, statistical modeling, analog fault location and design centering. Compared with ℓ_1, ℓ_2 and minimax techniques, the Huber approach has demonstrated robustness and consistency in the presence of large and small errors, deterministic and statistical variations, which are critical considerations for practical CAD in an engineering environment.

REFERENCES

[1] J.W. Bandler and S.H. Chen, "Circuit optimization: the state of the art," *IEEE Trans. Microwave Theory Tech.*, vol. 36, 1988, pp. 424-443.

[2] J.W. Bandler, W. Kellermann and K. Madsen, "A nonlinear ℓ_1 optimization algorithm for design, modeling and diagnosis of networks," *IEEE Trans. Circuits and Systems*, vol. CAS-34, 1987, pp. 174-181.

[3] P. Huber, *Robust Statistics*. New York: Wiley, 1981.

[4] G. Li and K. Madsen, "Robust nonlinear data fitting," in *Numerical Analysis*, D.F. Griffiths and G.A. Watson, Eds., Pitman Research Notes in Mathematics Series 170. UK: Longman, 1988, pp. 176-191.

[5] J.W. Bandler, S.H. Chen, R.M. Biernacki, L. Gao, K. Madsen and H. Yu, "Huber optimization of circuits: a robust approach," *IEEE Trans. Microwave Theory Tech.*, vol. 41, 1993, pp. 2279-2287.

[6] *OSA90/hope*™, Optimization Systems Associates Inc., P.O. Box 8083, Dundas, Ontario, Canada L9H 5E7, 1993.

[7] J.W. Bandler, R.M. Biernacki, Q. Cai, S.H. Chen, S. Ye and Q.J. Zhang, "Integrated physics-oriented statistical modeling, simulation and optimization," *IEEE Trans. Microwave Theory Tech.*, vol 40, 1992, pp.1374-1400.

[8] J.W. Bandler, S.H. Chen and K. Madsen, "An algorithm for one-sided ℓ_1 optimization with application to circuit design centering," *Proc. IEEE Int. Symp. Circuits and Systems* (Espoo, Finland), 1988, pp. 1795-1798.

[9] K. Singhal and J.F. Pinel, "Statistical design centering and tolerancing using parametric sampling," *IEEE Trans. Circuits and Systems*, vol. CAS-28, 1981, pp. 692-701.

[10] J.W. Bandler, Q.J. Zhang, J. Song and R.M. Biernacki, "FAST gradient based yield optimization of nonlinear circuits," *IEEE Trans. Microwave Theory Tech.*, vol. 38, 1990, pp. 1701-1710.

Reprint 18

A CAD Environment for Performance and Yield Driven Circuit Design Employing Electromagnetic Field Simulators

Proceedings of the 1994 International Symposium on Circuit and Systems, London, England, May 1994

A CAD Environment for Performance and Yield Driven Circuit Design Employing Electromagnetic Field Simulators

J.W. Bandler, R.M. Biernacki, S.H. Chen and P.A. Grobelny

Simulation Optimization Systems Research Laboratory
Department of Electrical and Computer Engineering
McMaster University, Hamilton, Canada L8S 4L7
+1 905 525 9140 Ext. 24818
bandler@mcmail.cis.mcmaster.ca

ABSTRACT

In this paper we describe a CAD environment for performance and yield driven circuit design with electromagnetic (EM) field simulations employed within the optimization loop. Microstrip structures are accurately simulated and their responses are incorporated into the overall circuit analysis. We unify the component level interpolation technique, devised to handle discretization of geometrical parameters, and the modeling technique used to lighten the computational burden of statistical design centering. We discuss the organization and utilization of our data base system integrated with the modeling technique. We demonstrate the feasibility and benefits of performance and yield optimization with EM simulations.

INTRODUCTION

Electromagnetic (EM) field simulators, though computationally intensive, are regarded as highly accurate at microwave frequencies. With the increasing availability of EM simulators it is very tempting to include them in performance-driven and even in yield-driven circuit optimization. Feasibility of such optimization has already been shown in our pioneering work [1,2].

J.W. Bandler, R.M. Biernacki and S.H. Chen are also with Optimization Systems Associates Inc., P.O. Box 8083, Dundas, Ontario, Canada L9H 5E7.

This work was supported in part by Optimization Systems Associates Inc. and in part by the Natural Sciences and Engineering Research Council of Canada under Grants OGP0007239, OGP0042444 and STR0117819.

We unify our interpolation technique, devised to reconcile inherent discretization of geometrical parameters with continuously varying optimization variables, and our modeling technique used for computationally intensive statistical design centering.

We report new results on circuit design employing EM simulators. Simulation of a microstrip line demonstrates the flexibility of our interpolation and modeling technique. With a 3-section microstrip impedance transformer we illustrate nominal and yield-driven design optimization. These results were obtained using the CAD system OSA90/hope [3] interfaced to the *em* field simulator from Sonnet Software [4] through Empipe [3].

EFFICIENT INTERPOLATION/MODELING

Numerical EM simulation requires discretized, or on-the-grid, values of geometrical parameters. Gradient based optimizers, on the other hand, assume continuously varying parameters. To this end we interpolate responses for off-the-grid points. Our efficient quadratic modeling technique [2,5,6] is extended and unified to handle this geometrical interpolation.

The quadratic model (or the Q-model) of a generic response $f(\boldsymbol{x})$ is a quadratic polynomial of the form [5,6]

$$q(\boldsymbol{x}) = a_0 + \sum_{i=1}^{n} a_i (x_i - r_i) + \sum_{\substack{i=1 \\ j \geq i}}^{n} a_{ij} (x_i - r_i)(x_j - r_j) \quad (1)$$

where $\boldsymbol{x} = [x_1 \; x_2 \; \ldots \; x_n]^T$ is the vector of generic parameters and $\boldsymbol{r} = [r_1 \; r_2 \; \ldots \; r_n]^T$ is a chosen reference point in the parameter space.

To build the Q-model we use $n + 1 \le m \le 2n + 1$ base points at which the function $f(x)$ is evaluated. The reference point r is selected as the first base point x^1. The remaining m - 1 base points are selected by perturbing one variable at a time around r with a predetermined perturbation β_i. If a variable is perturbed twice the second perturbation is located symmetrically w.r.t. r. Applying the Maximally Flat Quadratic Interpolation technique [5] to such a set of base points results in simple and efficient formulas for the Q-model $q(x)$ [2].

This formulation allows for a flexible choice of the number of base points starting at $m = n + 1$ which leads to the linear model (or the L-model), through linear/quadratic models w.r.t. selected variables, to the quadratic model w.r.t. all variables.

To discretize the model parameters we consider simulation and modeling grids. The first one is imposed by the EM simulator. Let the simulation grid δ_S be defined as

$$\delta_S = [\delta_{S1}\ \delta_{S2}\ \dots\ \delta_{Sn}]^T \tag{2}$$

The simulation grid sizes are floating point numbers and have the same units as the corresponding parameters. The modeling grid constitutes a subset of points defined by the simulation grid and is implied by the multipliers

$$\delta_M = [\delta_{M1}\ \delta_{M2}\ \dots\ \delta_{Mn}]^T \tag{3}$$

The modeling grid multipliers are dimensionless integers. Both δ_S and δ_M are positive. The first modeling grid point is aligned with the first nonzero simulation grid point. For the ith parameter the distance between adjacent modeling grid points is the δ_{Mi} multiple of the simulation grid δ_{Si}, i.e., $\delta_{Mi}\delta_{Si}$. In our approach, EM simulations are performed at the modeling grid points only.

To utilize the Q-modeling technique for geometrical interpolation we first generate a set of m base points called the interpolation base B. The reference point r is selected as the first base point x^1 by snapping $x = [x_1\ x_2\ \dots\ x_n]^T$ to the closest (in the ℓ_2 sense) modeling grid point. The vector

$$\theta = [\theta_1\ \theta_2\ \dots\ \theta_n]^T \tag{4}$$

defines the relative deviation of x from r and is calculated as

$$\theta_i = (x_i - r_i)/(\delta_{Si}\delta_{Mi}), \quad i = 1, 2, \dots, n \tag{5}$$

The other base points are created by perturbing one variable at a time around r. The magnitude of the perturbation β_i is $\delta_{Si}\delta_{Mi}$. These base points can then be expressed as

$$x^{i+1} = r + [0\dots0\ \ +\delta_{Si}\delta_{Mi}\ \ 0\dots0]^T,\ i = 1, \dots, n \tag{6a}$$

$$x^{n+1+i} = r + [0\dots0\ \ -\delta_{Si}\delta_{Mi}\ \ 0\dots0]^T,\ i = 1, \dots, m - (n + 1) \tag{6b}$$

For each Q-model we define a validity region V. If $x \in V$ than we assume that the model is valid and that $q(x) \approx f(x)$. If $x \notin V$ the model $q(x)$ must be updated. One possible choice for V is given by

$$V = \left\{x \mid \frac{-\delta_{Si}\delta_{Mi}}{2} < (x_i - r_i) \le \frac{\delta_{Si}\delta_{Mi}}{2}\right\},\ i = 1, 2, \dots, n \tag{7}$$

It is easy to see from (1) that if a certain x_i in x has the same value as the corresponding r_i in r then the contribution of x_i to $q(x)$ is zero. Therefore, the base points x^{i+1} and x^{n+1+i} need not be simulated and can be excluded from the interpolation base B.

MULTILEVEL MODELING

The circuit under consideration may be divided into subcircuits, possibly in a hierarchical manner. At the lowest level we have circuit components, e.g., a lumped capacitor or a microstrip structure.

We can express the response of the circuit as a function of the subcircuit responses which are in turn functions of component responses.

We can create a single Q-model for the overall circuit or a hierarchy of Q-models to represent some or all of the subcircuits and components. By applying the Q-modeling technique to geometrical interpolation outlined in the preceding section we effectively unify the overall multilevel modeling approach and address it in a consistent manner at all levels of hierarchy.

INTEGRATED DATA BASE/MODELING SYSTEM

Let the set of base points for a Q-model be defined by $[x^1\ x^2\ \dots\ x^m]^T$, where x^1 is the reference point r, $n + 1 \le m \le 2n + 1$, and n is the number of model parameters. Then we can express the simulation results at these base points as

$$[f(x^1)\ f(x^2)\ \dots\ f(x^m)] \tag{8}$$

with

$$f(x^i) = [f_1(x^i)\ \dots\ f_k(x^i)]^T,\ i = 1, 2, \dots, m \tag{9}$$

where k is the total number of different responses. f can be a response of the overall circuit, a subcircuit or a component. Then

$$f(x) \approx q(x) = [q_1(x)\ q_2(x)\ \ldots\ q_k(x)]^T \qquad (10)$$

The Q-models in (10) approximate $f(x)$ for x belonging to the Q-model validity region V centered around the reference point $r = x^1$.

The nominal point moves during optimization, and so does, in the case of yield optimization, the set of associated statistical outcomes. This may result in parameter values of the nominal point as well as of some or even all the statistical outcomes to be outside of the validity region V for the current Q-models. When this happens, the Q-models are automatically updated. That is, a new set of base points is formed, the responses at these base points are simulated *but only if they have not been simulated previously*, and the updated Q-models are generated.

In order to avoid repeated simulations, we maintain a data base of the already simulated base points together with the corresponding responses. These results are stored and accessed when necessary. Each time simulation is requested the corresponding interpolation base B is generated and checked against the existing data base. Actual simulation is invoked only for the base points not present in the data base. The data base and the Q-models are automatically updated whenever new simulation results become available.

A MICROSTRIP LINE EXAMPLE

To illustrate the benefits and flexibility of the Q-modeling technique we simulate a microstrip line with different simulation and modeling grids. The substrate is 25 mil thick and the relative dielectric constant is 9.8. The width of the line is 25 mil and the length is varied from 100 to 202.5 mils with a 2.5 mil step. There are two geometrical parameters: the line width W and length L.

To establish reference data we use a fine simulation grid set to 2.5 mil for both parameters. Setting the modeling grid multipliers to 1 and using the sweep step of 2.5 mil, all simulations are performed for on-the-grid points. No interpolation is needed.

We perform two experiments. In the first one we increase both simulation and modeling grids to a coarse 25 mil grid. In the second one we use the original fine simulation grid but change the modeling grid multiplier for the line length to 10. In both cases we build and examine the L-models as well as the Q-models. On a Sun SPARCstation 10 it takes 0.3 and 5 CPU seconds to simulate the line at a single frequency using the coarse and fine simulation grids, respectively.

All curves in Fig. 1 show the $|S_{11}|$ response vs. the line length L at 10 GHz for different grids and models. The curves form two groups. Each group contains responses of both the L- (solid lines) and the Q-models (dashed lines). Solid dots indicate EM simulations needed to build the models. The upper group of curves is formed by the reference data and by the responses of the models built using the fine simulation and coarse modeling grids. The lower group of curves is formed by the responses of the models built using the coarse simulation grid. Clearly, responses of the models built using the fine simulation grid are much closer to the reference data, even if the modeling grid is coarse. This is because the accuracy of the EM simulations and hence of the models is much better when the fine simulation grid is used.

YIELD OPTIMIZATION OF A 3-SECTION MICROSTRIP IMPEDANCE TRANSFORMER

We consider a 3-section microstrip impedance transformer [2]. The source and load impedances are 50 and 150 Ω, respectively. The design specification is set for input reflection coefficient as

$$|S_{11}| \le 0.11, \text{ from 5 GHz to 15 GHz}$$

The error functions for yield optimization are calculated at frequencies from 5 GHz to 15 GHz with a 0.5 GHz step. The substrate is 0.635 mm thick with relative dielectric constant of 9.7. The

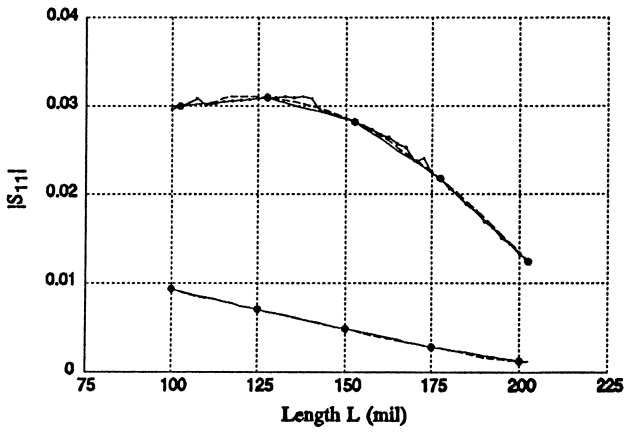

Figure 1

widths of the transformer sections, W_1, W_2 and W_3, are considered as optimization variables. The lengths, L_1, L_2 and L_3, are kept fixed. To obtain a good starting point for yield optimization we first perform minimax design. The maximum of $|S_{11}|$ is decreased from 0.28 to 0.09.

For all six geometrical parameters we assume normal distributions. Standard deviations are 0.005 mm and 2% for the lengths and widths, respectively. Yield estimated from 250 outcomes at the starting point (minimax solution) is 61%. It is increased to 77% after yield optimization. We used 100 outcomes in yield optimization. The Monte Carlo sweep at the centered design is shown in Fig. 2. The starting point, minimax and centered solutions are listed in Table I.

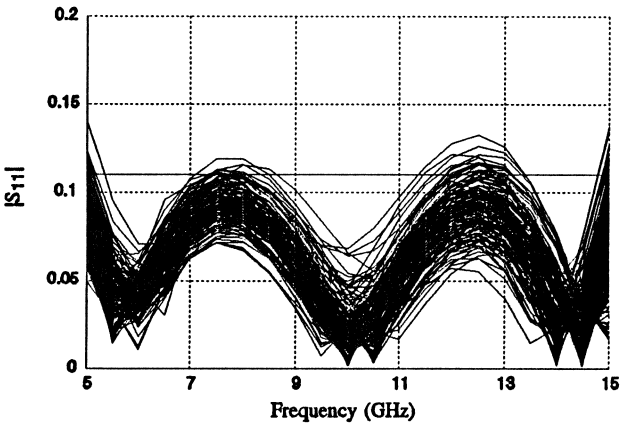

Figure 2

TABLE I
NOMINAL AND YIELD OPTIMIZATION OF A 3-SECTION MICROSTRIP TRANSFORMER

Parameter	Starting point (mm)	Minimax solution (mm)	Centered solution (mm)
W_1	0.65	0.349	0.373
W_2	0.35	0.139	0.165
W_3	0.15	0.039	0.049

L_1, L_2 and L_3 are fixed at 3 mm.

ACKNOWLEDGEMENT

The authors thank Dr. J.C. Rautio of Sonnet Software, Inc., Liverpool, NY, for his initiatives and making *em* available for this work.

CONCLUSIONS

In this paper we have described a CAD environment for performance and yield-driven design of circuits employing accurate EM field simulations. We have unified an efficient modeling technique used to decrease the computational burden of statistical design centering with geometrical interpolation needed to overcome problems related to the discrete nature of EM simulation. We have outlined the organization and utilization of our data base system integrated with the modeling technique. We have also outlined the concept of multilevel modeling. Simulation of a microstrip line demonstrates the flexibility of our unified interpolation/modeling technique. It also shows possible trade-offs between efficiency of EM simulations and accuracy of the models. We used a 3-section microstrip impedance transformer to exemplify the feasibility and benefits of both performance and yield-driven design with EM simulations invoked within the optimization loop.

REFERENCES

[1] J.W. Bandler, R.M. Biernacki, S.H. Chen, D.G. Swanson, Jr. and S. Ye, "Microstrip filter design using direct EM field simulation," *IEEE Trans. Microwave Theory Tech.*, vol. 42, July 1994.

[2] J.W. Bandler, R.M. Biernacki, S.H. Chen, P.A. Grobelny and S. Ye, "Yield-driven electromagnetic optimization via multilevel multidimensional models," *IEEE Trans. Microwave Theory Tech.*, vol. 41, 1993, pp. 2269-2278.

[3] *OSA90/hope*™ and *Empipe*™, Optimization Systems Associates Inc., P.O. Box 8083, Dundas, Ontario, Canada L9H 5E7, 1993.

[4] *Em User's Manual*, Sonnet Software, Inc., 135 Old Cove Road, Suite 203, Liverpool, NY 13090-3774, 1992.

[5] R.M. Biernacki and M.A. Styblinski, "Efficient performance function interpolation scheme and its application to statistical circuit design," *IEEE Int. J. Circuit Theory and Appl.*, vol. 19, 1991, pp. 403-422.

[6] R.M. Biernacki, J.W. Bandler, J. Song and Q.J. Zhang, "Efficient quadratic approximation for statistical design," *IEEE Trans. Circuits and Systems*, vol. 36, 1989, pp. 1449-1454.

Reprint 19

Compression Analysis of a High Power BJT Amplifier

3rd International Workshop on Integrated Nonlinear Microwave and Millimeterwave Circuits, Duisburg, Germany, October, 1994

COMPRESSION ANALYSIS OF A HIGH POWER BJT AMPLIFIER

J.W. Bandler, R.M. Biernacki, Q. Cai and S.H. Chen

Optimization Systems Associates Inc.
P.O. Box 8083, Dundas, Ontario, Canada L9H 5E7

ABSTRACT

In this paper we present the compression analysis of a BJT high power amplifier circuit. This circuit was chosen by Microwave Engineering Europe (MEE) as a challenge to CAD programs. The bipolar transistor is modeled by a SPICE model. Extraction of the model parameters was performed by fitting the model responses to vendor-published S-parameter data. In addition to compression analysis of the amplifier we carried out Monte Carlo statistical simulation and sensitivity analysis. All simulations and optimizations were performed by our CAD software system OSA90/hope, in particular by our nonlinear harmonic balance simulator.

INTRODUCTION

The harmonic balance (HB) technique is an efficient method for nonlinear steady-state circuit analysis [1-3]. It has been widely applied to nonlinear analysis and design of microwave circuits such as amplifiers, mixers and frequency doublers [4-7]. However, HB analysis of high power amplifiers may be a challenge to HB solvers [8] since the strong nonlinearity of the circuits may cause problems such as non-convergence. The success of the simulation depends on the accuracy of models and the intelligent use of nonlinear HB simulators.

In September 1993, Microwave Engineering Europe initiated a nonlinear CAD benchmark for the most popular microwave commercial HB simulators. The problem was the nonlinear simulation of a high power BJT amplifier.

The amplifier was designed by Jennings and Perry for communication applications around 2 GHz with less than 1 W output power [8]. The amplifier worked well in practice but proved very difficult to simulate using nonlinear HB simulators.

The difficulty came from the characteristics of the transistor. It is a classic power BJT with a poor S_{12} (i.e., the device must be regarded as bilateral), an electrically large package, and an emitter ballast resistor. Therefore, the success of analyzing this circuit depends largely on the accuracy of the model for the transistor.

We used OSA90/hope [9] to investigate the performance of this amplifier. In this paper we present compression analysis of the amplifier. This includes model parameter extraction for the transistor, nonlinear harmonic balance (HB) simulations, statistical analysis and sensitivity analysis.

CIRCUIT STRUCTURE AND CHARACTERISTICS [8]

The schematic of the amplifier is shown in Fig. 1. It consists of a power BJT (Avantek AT64023) and a number of distributed elements. The BJT is biased for a DC collector current of 100 mA and a DC collector emitter voltage of 16 V. The distributed elements for input and output matching circuits are realized in microstrip on standard 1.5 mm FR4 board. The amplifier was designed to provide a high power driver to saturate other high power devices being tested under nonlinear operation.

The configuration of the amplifier results in a very narrow band response centered at 2 GHz with the power characteristics having been somewhat sacrificed in favour of good impedance and gain characteristics [8].

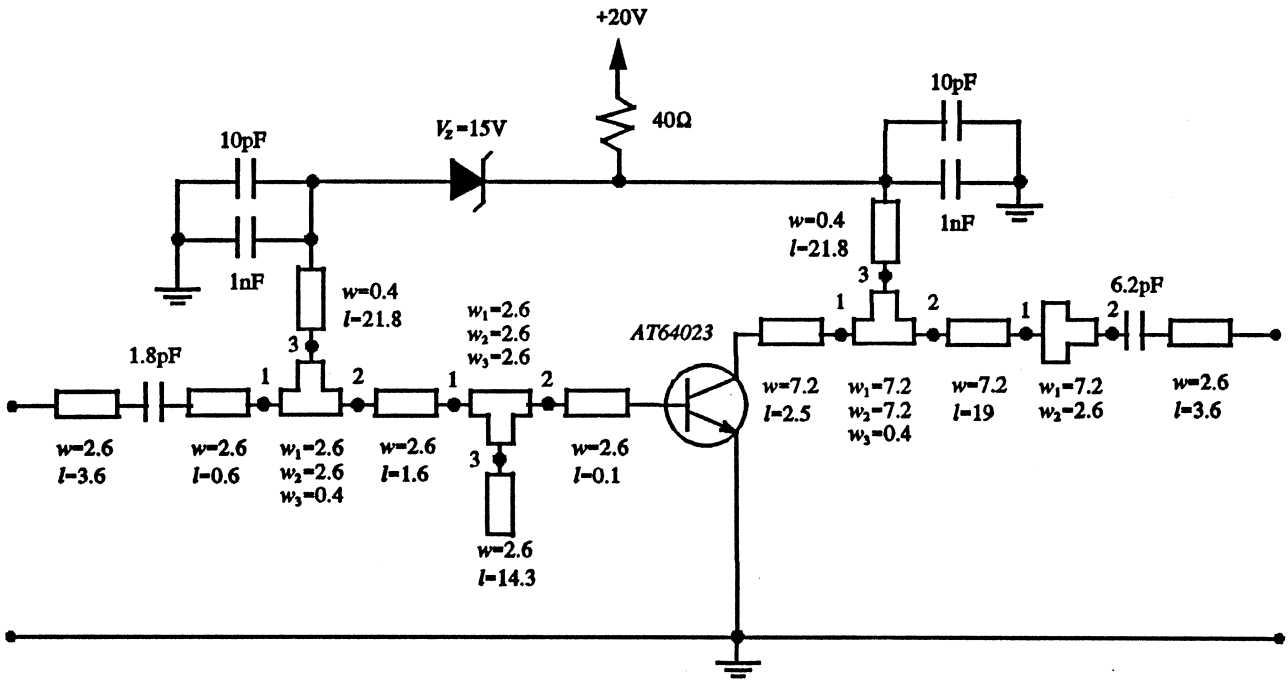

Fig. 1 The power amplifier circuit. Dimensions are in mm. The substrate thickness is 1.5 mm. The relative dielectric constant is 4.75. The metallization is 35 μm thick copper.

DEVICE MODELING

The model of the BJT used for simulation is the SPICE Gummel-Poon nonlinear model augmented by a diode circuit to model the distributed base capacitance and resistance, and a package model provided by Avantek [10]. OSA90/hope employs unified DC, small-signal and large-signal modeling. The small-signal model is derived, when necessary, from the nonlinear model. This ensures consistent responses from the DC, small-signal and HB analysis.

When the Gummel-Poon model with the parameters specified by Avantek [10] was applied to small-signal simulation, we noticed some discrepancies between the simulated *S* parameters and the average measured *S*-parameter data, also provided by Avantek [10]. The reason for such discrepancies can be attributed to the still fairly common "disjoint" modeling of small- and large-signal operation of the transistor.

Assuming that the *S*-parameter measurements are more reliable than the model provided by Avantek we performed model refinement for a better *S*-parameter fit. To this end we used the parameter extraction capabilities of OSA90/hope. Since the data represents the average values, the extracted model represents a typical device. If we wish to obtain the best model for the particular transistor used to build the amplifier, the *S*-parameter measurements for that transistor would be required.

Fig. 2 shows the match between the measured and simulated *S* parameters using the model provided by Avantek. Fig. 3 shows the much improved match using the optimized model.

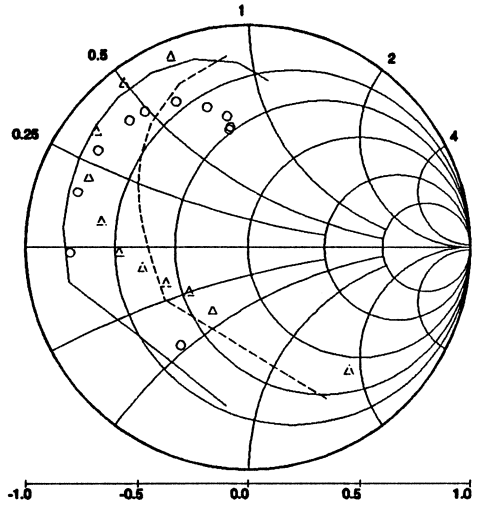

(a) S_{11} (model: ——, measured: o) and S_{22} (model: ---, measured: ▵).

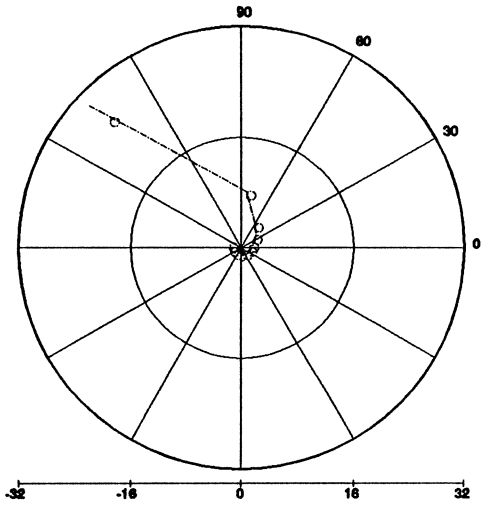

(b) S_{21} (model: -·-, measured: o).

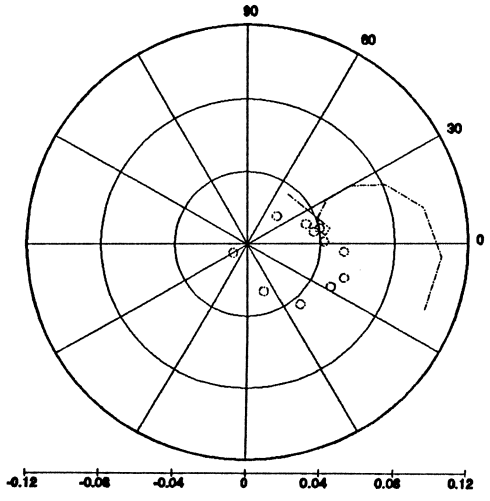

(c) S_{12} (model: -·-, measured: o).

Fig. 2 S-parameter match between the model provided by Avantek and the typical (average) S parameters [10].

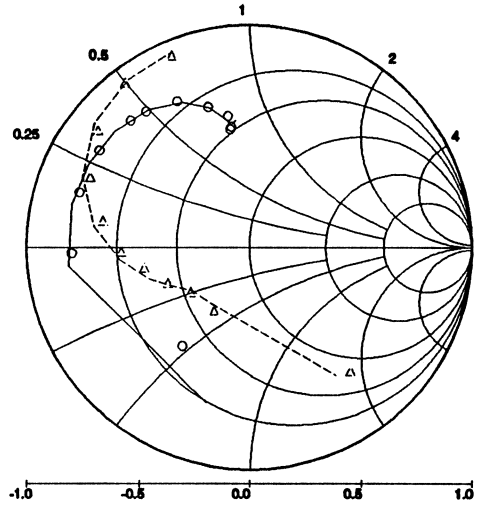

(a) S_{11} (model: ——, measured: o) and S_{22} (model: ---, measured: ▵).

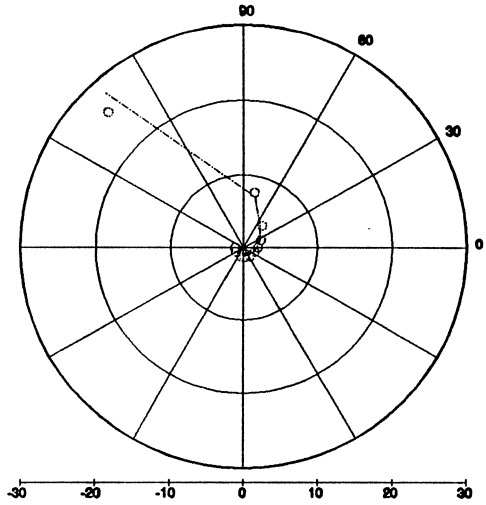

(b) S_{21} (model: -·-, measured: o).

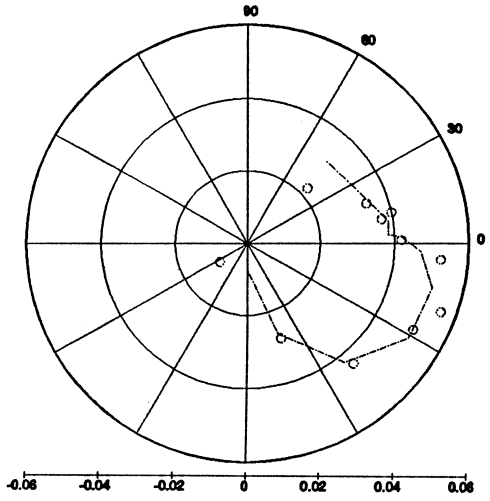

(c) S_{12} (model: -·-, measured: o).

Fig. 3 S-parameter match between the optimized model and the typical (average) S parameters [10].

SMALL- AND LARGE-SIGNAL SIMULATION

Using OSA90/hope, we performed both small-signal and large-signal HB simulations of the amplifier with the BJT model provided by Avantek and our optimized model extracted from the S-parameter data.

Small-signal gain of 16.3 dB and output power of 26.6 dBm at 1 dB gain compression, both at 2 GHz, were obtained using directly the model provided by Avantek. The corresponding results obtained using the optimized model were 10.7 dB small-signal gain and 23.4 dBm output power at 1 dB gain compression. The measured values at 2 GHz are: 12.2 dB small-signal gain and 23.0 dBm output power at 1 dB gain compression [8]. The simulation results using the optimized model are much closer to the measurements. The small-signal gain versus frequency and the output power versus input power of the amplifier are shown in Figs. 4 and 5, respectively.

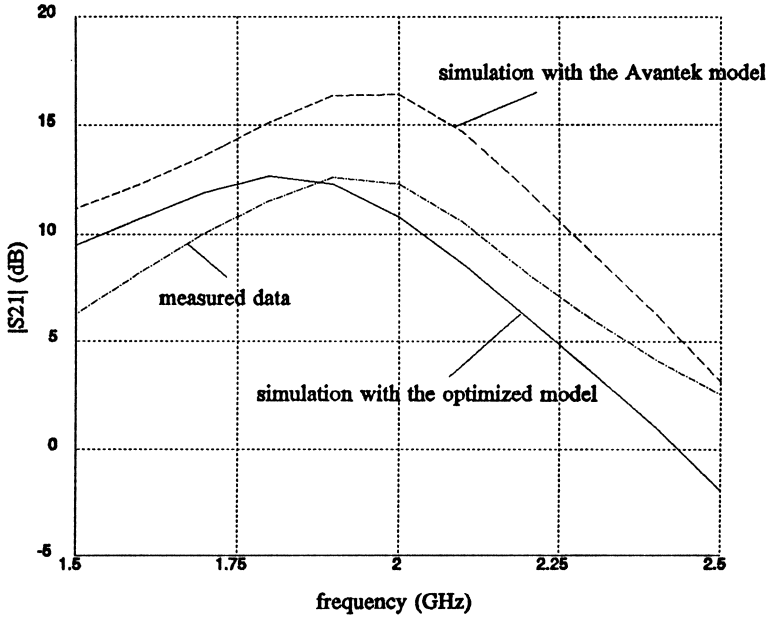

Fig. 4 Small-signal gain versus frequency of the amplifier.

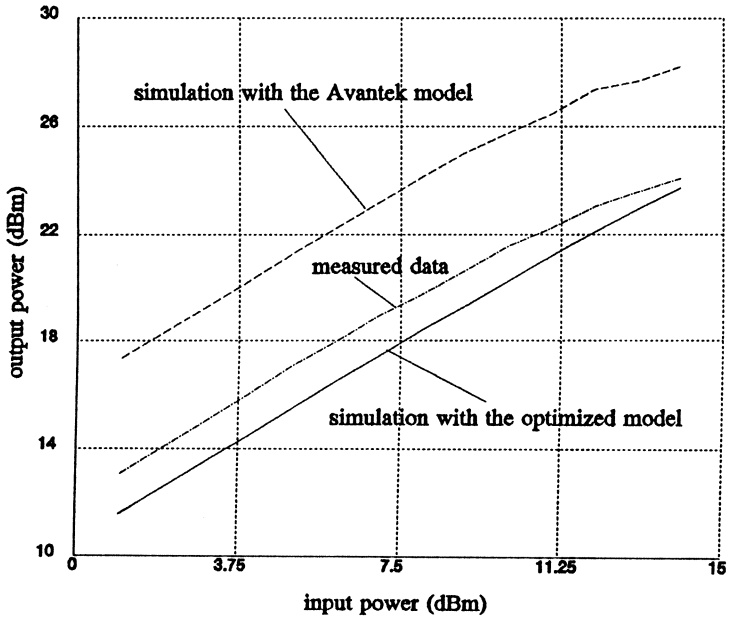

Fig. 5 Output power versus input power of the amplifier.

STATISTICAL ANALYSIS

The differences between the model provided by Avantek and the model obtained from the *S* parameters reveal the uncertainties associated with the device model. For an engineer to be confident with the design, a single simulation based on a single model may not be sufficient.

This motivated us to conduct statistical analysis of the amplifier to investigate the effect of parameter tolerances of the transistor model on the output power. The nominal parameter values were chosen as the average of the values provided by Avantek and the values of the optimized model. Tolerances were assigned to the model parameters according to the differences between the models. Monte Carlo simulation was carried out using 100 outcomes. The output power versus input power at 2 GHz is shown in Fig. 6.

The output power at 1 dB gain compression at 2 GHz are spread between 23.2 dBm and 27.2 dBm. This reflects the model uncertainty and is illustrated by the histogram shown in Fig. 7.

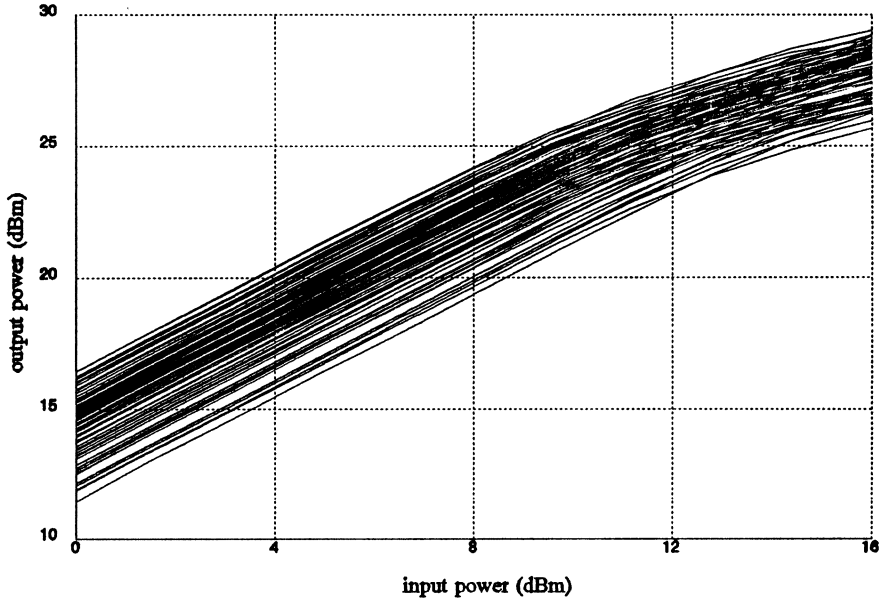

Fig. 6 Monte Carlo sweep of output power versus input power at 2 GHz.

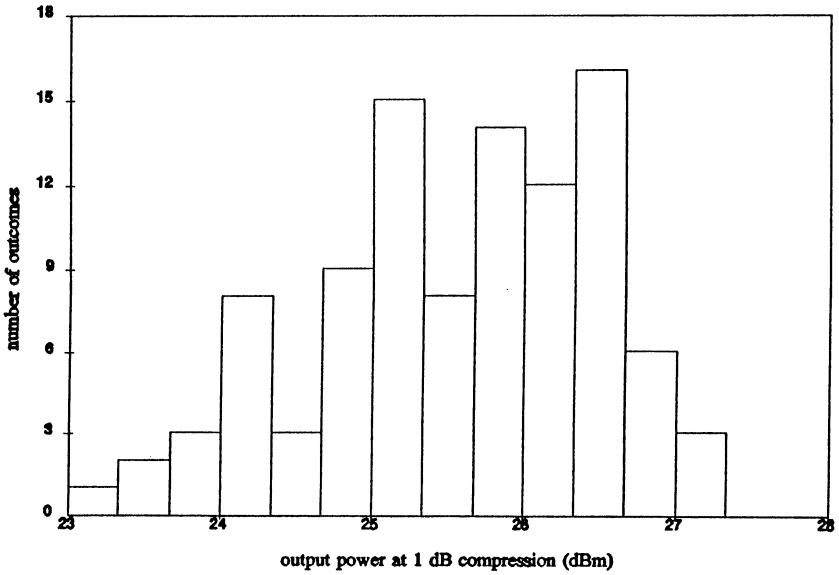

Fig. 7 Histogram of output power (dBm) at 1 dB gain compression at 2 GHz for assumed model uncertainty.

SENSITIVITY ANALYSIS

We have further investigated the sensitivity of the output power at 1 dB gain compression at 2 GHz w.r.t. the elements in the input and output matching circuits on a minimax design basis. The result shows that the response is more sensitive to the following parameters: the length of the open stub in the input matching circuit, the widths and lengths of the microstrip lines in the output matching circuits, than to the other parameters in the circuits.

CONCLUSIONS

We have presented the compression analysis of a high power BJT amplifier [8]. Parameter extraction was employed to refine the published Gummel-Poon model [10] of the transistor. Better agreement between our simulation results and the measurements of the amplifier has been obtained using the refined model rather than the Gummel-Poon model provided by Avantek. This exemplifies potential problems with vendor-supplied device models and a limited confidence the designer should have in such models. Different model implementations in different CAD packages and different parameter extraction procedures may contribute to this problem. It is more reliable to establish the model from measurements in a consistent manner within the same CAD environment. The statistical analysis by Monte Carlo simulation indicated that the BJT model accuracy is very important in the circuit simulation. Our sensitivity analysis identifies the circuit elements critical for the design.

REFERENCES

[1] V. Rizzoli, A. Lipparini and E. Marazzi, "A general-purpose program for nonlinear microwave circuit design," *IEEE Trans. Microwave Theory Tech.*, vol. 31, 1983, pp. 762-770.

[2] K.S. Kundert and A. Sangiovanni-Vincentelli, "Simulation of nonlinear circuits in the frequency domain," *IEEE Trans. Computer-Aided Design*, vol. CAD-5, 1986, pp. 521-535.

[3] V. Rizzoli and A. Neri, "State of the art and present trends in nonlinear microwave CAD techniques," *IEEE Trans. Microwave Theory Tech.*, vol. 36, 1988, pp. 343-365.

[4] F. Filicori, V.A. Monaco and C. Naldi, "Simulation and design of microwave class-C amplifiers through harmonic analysis," *IEEE Trans. Microwave Theory Tech.*, vol. MTT-27, 1979, pp. 1043-1051.

[5] W.R. Curtice, "Nonlinear analysis of GaAs MESFET amplifiers, mixers, and distributed amplifiers using harmonic balance technique," *IEEE Trans. Microwave Theory Tech.*, vol. 35, 1987, pp. 441-447.

[6] S. El-Rabaie, J.A.C. Stewart, V.F. Fusco and J.J. McKeown, "A novel approach for the large-signal analysis and optimisation of microwave frequency doublers", *IEEE MTT-S Int. Microwave Symp. Dig.* (New York, NY), 1988, pp. 1119-1122.

[7] J.W. Bandler, R.M. Biernacki, S.H. Chen, J. Song, S. Ye and Q.J. Zhang, "Analytically unified DC/small-signal/large-signal circuit design," *IEEE Trans. Microwave Theory Tech.*, vol. 39, 1991, pp. 1076-1082.

[8] "Non-linear CAD benchmark," *Microwave Engineering Europe*, November 1993, pp. 11-15.

[9] *OSA90/hope*™, Optimization Systems Associates Inc., P.O. Box 8083, Dundas, Ontario, Canada L9H 5E7, 1993.

[10] *Microwave Semiconductors GaAs and Silicon Products Data Book*, Avantek Inc., 3175 Bowers Ave., Santa Clara, CA 95054, USA, 1989.

Reprint 20

Microstrip Filter Design Using Direct EM Field Simulation

Microstrip Filter Design Using Direct EM Field Simulation

John W. Bandler, *Fellow, IEEE,* Radoslaw M. Biernacki, *Senior Member, IEEE,* Shao Hua Chen, *Member, IEEE,* Daniel G. Swanson, Jr., *Senior Member, IEEE,* and Shen Ye, *Member, IEEE*

***Abstract*— For the first time, we present minimax filter design with electromagnetic (EM) simulations driven directly by a gradient-based optimizer. Challenges of efficiency, discretization of geometrical dimensions, and continuity of optimization variables are overcome by a three-stage attack: 1) efficient on-line response interpolation with respect to geometrical dimensions of microstrip structures simulated with fixed grid sizes; 2) smooth and accurate gradient evaluation for use in conjunction with the proposed interpolation; and 3) storing the results of expensive EM simulations in a dynamically updated database. Simulation of a lowpass microstrip filter illustrates the conventional use of EM simulation for design validation. Design optimization of a double folded stub bandstop filter and of a millimeter-wave 26–40 GHz interdigital capacitor bandpass microstrip filter illustrates the new technique.**

I. Introduction

We present results of microwave filter design with accurate electromagnetic (EM) simulations driven by a minimax gradient-based optimizer. We exploit recent advances [1]–[5] in EM simulation which give the designer the opportunity to accurately simulate passive circuit components, in particular microstrip structures [2]. However, we go far beyond the prevailing use of stand-alone EM simulators, namely, validation of designs obtained through less accurate techniques.

EM simulators, although computationally intensive, are regarded as accurate at microwave frequencies, extending the validity of the models to higher frequencies, including millimeter-wave frequencies, and they cover wider parameter ranges [2]. EM simulators, whether stand-alone or incorporated into software frameworks, will not realize their full potential to the designer (whose task is to obtain the best parameter values satisfying design specifications) unless they are optimizer-driven to automatically adjust designable parameters.

Manuscript received July 27, 1993; revised January 12, 1994. This work was supported in part by Optimization Systems Associates Inc. and in part by the Natural Sciences and Engineering Research Council of Canada under Grants OGP0007239, OGP0042444, and STR0117819 and through an Industrial Research Fellowship to S. Ye.

J. W. Bandler, R. M. Biernacki, and S. H. Chen are with Optimization Systems Associates Inc., Dundas, Ont., Canada L9H 5E7, and the Simulation Optimization Systems Research Laboratory, Department of Electrical and Computer Engineering, McMaster University, Hamilton, Ont., Canada L8S 4L7.

D. G. Swanson, Jr., is with Watkins-Johnson Company, Palo Alto, CA 94304-1204 USA.

S. Ye was with Optimization Systems Associates Inc., Dundas, Ont., Canada L9H 5E7. He is now with Com Dev Ltd., Cambridge, Ont., Canada N1R 7H6.

IEEE Log Number 9402409.

Design optimization tools are widely available (e.g., [6]), typically in conjunction with analytical, heuristic models of microstrip structures developed in recent years. Consequently, designers, using such tools, try to generate designs in the form of either equivalent circuits, or physical parameters based on approximate models. Using an EM simulator, designers currently validate and improve their designs by manual adjustments. The need for direct design optimization with accurate field simulation is clear.

The feasibility of optimizing passive structures using EM simulation has already been shown in [3], [4]. Our paper addresses several challenges arising when EM simulations are to be put directly into the optimization loop. We consider the advantages of on-line EM simulations (performed on request) as opposed to up-front simulations, as in Jansen's look-up table approach. The requirement of circuit responses for continuously varying optimization variables must be reconciled with inherent discretization of geometrical parameters present in numerical EM simulations. Finally, the requirement of providing the optimizer with smooth and accurate gradient information must be given serious attention. We effectively deal with all these problems, contributing a new dimension to this subject.

The results presented in this paper have been obtained using Empipe^{TM} [7], an interface between OSA90/hope^{TM} [8] and *em*^{TM} [5]. On-line interpolation is applied to geometrical dimensions of microstrip structures to provide for continuity of optimization variables in the presence of fixed grid sizes in the EM simulations. The results of the EM simulations are stored in a database and can be retrieved if, during optimization, the same on-the-grid points need to be resimulated.

The proposed geometrical interpolation has been tested on a number of microstrip structures. The conventional use of EM simulation for design validation is illustrated by comparing the results of *em* [5] simulation and the corresponding measurements of a lowpass microstrip filter. Design optimization of a double folded stub filter for bandstop applications and of a millimeter-wave 26–40 GHz interdigital capacitor microstrip bandpass filter demonstrates the new technique.

Minimax design optimization is briefly reviewed in Section II. Section III includes our theory of geometrical interpolation, and Section IV contains a derivation of gradient expressions for use in conjunction with geometrical interpolation. Storing the results of expensive EM simulations in a database and issues of updating the database are discussed in Section V. Finally, Sections VI–VIII describe our experiments.

0018–9480/94$04.00 © 1994 IEEE

II. Minimax Design Optimization

Frequency-domain design of microwave filters involves design specifications imposed on the responses (S parameters, return loss, insertion loss, etc.). In order to formulate an objective function for design optimization, the filter is simulated at a given point (vector) of designable (optimization) variables $\boldsymbol{\phi}$ and at the same frequency points at which the upper (S_{uj}) and/or lower (S_{lj}) specifications are given. The corresponding responses, denoted by $R_j(\boldsymbol{\phi})$, determine the error vector $\boldsymbol{e}(\boldsymbol{\phi})$ as

$$\boldsymbol{e}(\boldsymbol{\phi}) = [e_1(\boldsymbol{\phi}) \quad e_2(\boldsymbol{\phi}) \cdots e_M(\boldsymbol{\phi})]^T \tag{1}$$

where the individual errors $e_j(\boldsymbol{\phi})$ are of the form

$$e_j(\boldsymbol{\phi}) = R_j(\boldsymbol{\phi}) - S_{uj} \tag{2}$$

or

$$e_j(\boldsymbol{\phi}) = S_{lj} - R_j(\boldsymbol{\phi}) \tag{3}$$

and M is the total number of errors. A negative error value indicates that the corresponding specification is satisfied. For positive error values, the corresponding specifications are violated. All the errors $e_j(\boldsymbol{\phi})$ are combined into a single objective function to be minimized. Minimax design optimization is defined as

$$\underset{\boldsymbol{\phi}}{\text{minimize}} \left(\max_j (e_j(\boldsymbol{\phi})) \right). \tag{4}$$

Effective minimax optimization requires a dedicated optimizer, such as [9], and accurate gradients of individual errors with respect to the optimization variables $\boldsymbol{\phi}$.

III. Geometrical Interpolation

The vector $\boldsymbol{\psi}$ of all geometrical parameters (structure lengths, widths, spacings, etc.) of a planar microstrip structure can be written as

$$\boldsymbol{\psi} = [\boldsymbol{\psi}_{opt}^T(\boldsymbol{\phi}) \quad \boldsymbol{\psi}_{fix}^T]^T \tag{5}$$

where the vector $\boldsymbol{\psi}_{opt}(\boldsymbol{\phi})$ contains designable geometrical parameters which are either directly the optimization variables or are functions of the optimization variables $\boldsymbol{\phi}$, and the vector $\boldsymbol{\psi}_{fix}$ contains fixed geometrical parameters. It is important to realize that each component of $\boldsymbol{\psi}$ belongs to one of the three physical orientations (x, y, or z) and, therefore, the vector $\boldsymbol{\psi}$ can be rearranged as

$$\boldsymbol{\psi} = [\boldsymbol{\psi}^{xT} \quad \boldsymbol{\psi}^{yT} \quad \boldsymbol{\psi}^{zT}]^T. \tag{6}$$

Numerical EM simulation is performed for discretized values of the geometrical parameters $\boldsymbol{\psi}$. Let the discretization matrix $\boldsymbol{\delta}$ be defined by the grid sizes Δx_i, Δy_i, and Δz_i as

$$\begin{aligned}\boldsymbol{\delta} &= \text{diag}\,\{\delta_i\} \\ &= \text{diag}\,\{\Delta x_1, \Delta x_2, \cdots, \Delta y_1, \Delta y_2, \cdots, \Delta z_1, \Delta z_2, \cdots\}.\end{aligned} \tag{7}$$

A specific EM simulator may allow only one grid size for each orientation while others may provide the flexibility of independent Δx_i, Δy_i, and Δz_i for different parameters of the same x, y, or z orientation. For uniform discretization in each direction $\Delta x_i = \Delta x$, $\Delta y_i = \Delta y$, and $\Delta z_i = \Delta z$.

Before invoking EM simulation for a given $\boldsymbol{\psi}$, it is necessary to find "the nearest" point (vector) on the grid, denoted by $\boldsymbol{\psi}^c$, which we call the *center base point*. We define it by the equation

$$\boldsymbol{\psi} = \boldsymbol{\psi}^c + \boldsymbol{\delta\theta} \tag{8}$$

subject to suitable conditions imposed on $\boldsymbol{\theta}$ to precisely define the term "the nearest." For example, the conditions on $\boldsymbol{\theta}$ can be chosen as

$$-0.5 \le \theta_i < 0.5, \qquad i = 1, 2, \cdots, n \tag{9}$$

or as

$$0 \le \theta_i < 1, \qquad i = 1, 2, \cdots, n \tag{10}$$

where n is the total number of geometrical parameters and $\boldsymbol{\theta}$ is the relative deviation of $\boldsymbol{\psi}$ from the center base point. $\boldsymbol{\psi}^c$ and $\boldsymbol{\theta}$ can be easily determined using the "floor" function as

$$\psi_i^c = |[\psi_i/\delta_i + 0.5]|\delta_i \quad \text{or} \quad \psi_i^c = |[\psi_i/\delta_i]|\delta_i \tag{11}$$

for (9) or (10), respectively, and

$$\theta_i = (\psi_i - \psi_i^c)/\delta_i. \tag{12}$$

If $\boldsymbol{\theta} \neq \boldsymbol{0}$, the point is off-the-grid and we use interpolation to determine each response $R(\boldsymbol{\psi})$. We drop the subscript j and take (5) into account in expressing $R_j(\boldsymbol{\phi})$. We consider the class of interpolation problems where the interpolating function can be expressed as a linear combination of some *fundamental interpolating functions* in terms of deviations with respect to the center base point. Let $\boldsymbol{f}(\boldsymbol{\delta\theta})$ be the vector of fundamental interpolating functions

$$\boldsymbol{f}(\boldsymbol{\delta\theta}) = [f_1(\boldsymbol{\delta\theta}) \quad f_2(\boldsymbol{\delta\theta}) \cdots f_K(\boldsymbol{\delta\theta})]^T. \tag{13}$$

We want to find a vector

$$\boldsymbol{a} = [a_1 \quad a_2 \cdots a_K]^T \tag{14}$$

such that

$$R(\boldsymbol{\psi}) - R(\boldsymbol{\psi}^c) = \boldsymbol{f}^T(\boldsymbol{\delta\theta})\boldsymbol{a} \tag{15}$$

holds exactly at K selected *base points*. Once $\boldsymbol{a}$ is determined, (15) will be used to interpolate the response elsewhere in a suitably defined *interpolation region* around the center base point $\boldsymbol{\psi}^c$. The *interpolation base* B in the space of geometrical parameters is a set of grid points defined as

$$B = \{\boldsymbol{\psi}^c\} \cup \{\boldsymbol{\psi} | \boldsymbol{\psi} = \boldsymbol{\psi}^c + \boldsymbol{S\delta\eta}, \boldsymbol{\eta} \in B^\eta\} \tag{16}$$

where

$$B^\eta = \{\boldsymbol{\eta}^j | \boldsymbol{\eta}^j \in I^n, \boldsymbol{\eta}^j \neq \boldsymbol{0}, \boldsymbol{\eta}^i \neq \boldsymbol{\eta}^j, i, j = 1, 2, \cdots, K\} \tag{17}$$

is a set of predefined integer vectors called *relative interpolation base*, and

$$\boldsymbol{S} = \text{diag}\,\{s_i\},$$

where

$$s_i = \begin{cases} 1 & \text{if } \psi_i \text{ is a nonsymmetric parameter} \\ 2 & \text{if } \psi_i \text{ is a symmetric parameter.} \end{cases} \quad (18)$$

The symmetry matrix $\boldsymbol{S}$ accounts for double grid size increments for parameters whose dimensions are modified by extending or contracting both ends simultaneously.

The interpolation base B is used as the set of base points $\boldsymbol{\psi}^c$ and $\boldsymbol{\psi}^{bj}$, $j = 1, 2, \cdots, K$, at which EM simulation is invoked to evaluate the corresponding set of responses $R_{EM}(\boldsymbol{\psi}^c)$, $R_{EM}(\boldsymbol{\psi}^{b_1}), \cdots, R_{EM}(\boldsymbol{\psi}^{bK})$. From (15), we formulate a set of K linear equations

$$[\Delta R_{EM}(\boldsymbol{\psi}^{b_1})\, \Delta R_{EM}(\boldsymbol{\psi}^{b_2}) \cdots \Delta R_{EM}(\boldsymbol{\psi}^{bK})]^T = [\boldsymbol{f}(\boldsymbol{S\delta\eta}^1)\, \boldsymbol{f}(\boldsymbol{S\delta\eta}^2) \cdots \boldsymbol{f}(\boldsymbol{S\delta\eta}^K)]^T \boldsymbol{a} \quad (19)$$

where $\Delta R_{EM}(\boldsymbol{\psi}^{bj}) = R_{EM}(\boldsymbol{\psi}^{bj}) - R_{EM}(\boldsymbol{\psi}^c)$. More concisely,

$$\Delta \boldsymbol{R}_{EM}(B) = \boldsymbol{F}(\boldsymbol{S\delta}, B^\eta)\boldsymbol{a}. \quad (20)$$

By solving (20), we determine the vector $\boldsymbol{a}$ of interpolation coefficients as

$$\boldsymbol{a} = \boldsymbol{F}^{-1}(\boldsymbol{S\delta}, B^\eta)\Delta \boldsymbol{R}_{EM}(B) \quad (21)$$

which, after substituting into (15), gives

$$R(\boldsymbol{\psi}) = R_{EM}(\boldsymbol{\psi}^c) + \boldsymbol{f}^T(\boldsymbol{\delta\theta})\boldsymbol{F}^{-1}(\boldsymbol{S\delta}, B^\eta)\Delta \boldsymbol{R}_{EM}(B). \quad (22)$$

Equation (22) provides the response values for the off-the-grid points. Note that the matrix $\boldsymbol{F}(\boldsymbol{S\delta}, B^\eta)$ in (20) must be invertible. This, however, depends only on the selection of the fundamental interpolating functions and the relative interpolation base B^η and can be determined prior to all calculations. It is also independent of the center base point, so the same formulas are involved as the variables move during optimization.

IV. Gradient Estimation

To facilitate the use of an efficient and robust dedicated gradient minimax optimizer, we need to provide the gradients of the errors (2) and (3), or the gradients of $R_j(\boldsymbol{\phi})$. From (5), we can determine

$$\nabla_\phi R_j(\boldsymbol{\phi}) = \nabla_\phi \boldsymbol{\psi}^T(\boldsymbol{\phi}) \nabla_\psi R(\boldsymbol{\psi}). \quad (23)$$

The first factor on the right-hand side of (23) is readily available since the mapping (5), as an integral part of the problem formulation, is known. The second factor on the right-hand side of (23) must be determined using EM simulations.

During optimization, it is very likely that the gradient will be requested at off-the-grid points. As discussed in Section III, the responses at off-the-grid points are determined by interpolation. It is, therefore, most appropriate from the optimizer's point of view to provide the gradient of the interpolating function, i.e., the function that is actually returned to the optimizer. This is fortunate since that gradient can be analytically derived from the fundamental interpolating functions. From (22), we get

$$\nabla_\psi R(\boldsymbol{\psi}) = \nabla_{\delta\theta} \boldsymbol{f}^T(\boldsymbol{\delta\theta})\boldsymbol{F}^{-1}(\boldsymbol{S\delta}, B^\eta)\Delta \boldsymbol{R}_{EM}(B). \quad (24)$$

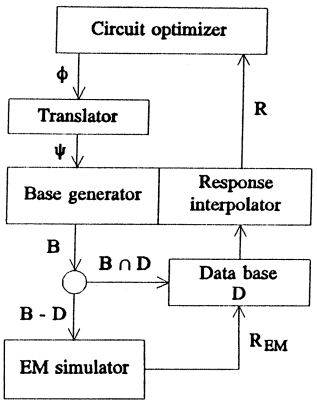

Fig. 1. Flow diagram illustrating the interconnection between a circuit optimizer and a numerical EM simulator.

Equation (24) gives accurate gradient information for the optimizer in a simple, straightforward, and efficient manner. Note that $\boldsymbol{F}^{-1}(\boldsymbol{S\delta}, B^\eta)$ and $\Delta \boldsymbol{R}(B)$ are already available from response interpolation.

Some optimizers may request perturbed simulation in the vicinity of the nominal point $\boldsymbol{\phi}^0$, say at $\boldsymbol{\phi}^{pert}$, in order to estimate the gradient by perturbation, instead of using the gradient at $\boldsymbol{\phi}^0$ directly. In such cases, using (22) at $\boldsymbol{\phi}^{pert}$ may provide a different result from (24) unless the fundamental interpolating functions are linear. As the exact gradient (24) is available, a modified response at $\boldsymbol{\phi}^{pert}$ can be easily evaluated from the linearized interpolating function at $\boldsymbol{\phi}^0$ as

$$R(\boldsymbol{\psi}^{pert}) = R_{EM}(\boldsymbol{\psi}^c) + [\boldsymbol{f}^T(\boldsymbol{\delta\theta}^0) + (\boldsymbol{\psi}^{pert} - \boldsymbol{\psi}^0)^T \nabla_{\delta\theta} \boldsymbol{f}^T(\boldsymbol{\delta\theta}^0)] \cdot \boldsymbol{F}^{-1}(\boldsymbol{S\delta}, B^\eta)\Delta \boldsymbol{R}_{EM}(B) \quad (25)$$

where $\boldsymbol{\psi}^0$, $\boldsymbol{\theta}^0$, and $\boldsymbol{\psi}^{pert}$ are determined from $\boldsymbol{\phi}^0$ and $\boldsymbol{\phi}^{pert}$, respectively. This formula, when used in gradient estimation by perturbation, will produce the same result as (24).

V. Updating the Database of Simulated Results

In order to efficiently utilize the results of EM simulations and to reduce their number, we have considered two levels of control. First, interpolation is invoked only when necessary, i.e., if a specific θ_i is zero we exclude the corresponding base point from the interpolation base. To be able to implement such a scheme, the fundamental interpolating functions must be appropriately devised. Second, a database D of base points and the corresponding responses obtained from exact EM simulations is stored and accessed when necessary (see Fig. 1). Each time EM simulation is requested, the corresponding interpolation base B is generated and checked against the existing database. Actual EM simulation is invoked only for the base points not present in the database $(B - D)$. Results for the base points already present in the database $(B \cap D)$ are simply retrieved from D and used for interpolation.

Updating the database D is a separate issue. Between the two extremes: 1) all simulated results are saved, and 2) only results for the latest interpolation base are saved, many schemes can be adopted depending on such factors as required

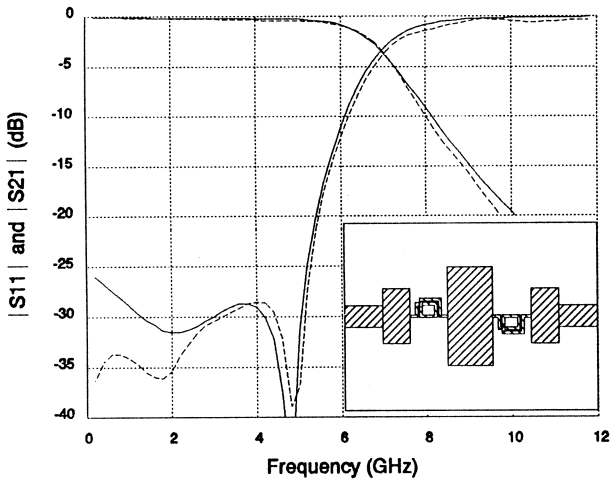

Fig. 2. EM simulation and measurements of the lowpass filter shown in the insert: simulated (——) and measured (- - -) $|S_{11}|$ and $|S_{21}|$. The thickness and dielectric constant of the substrate are 25 mils and 9.8, respectively.

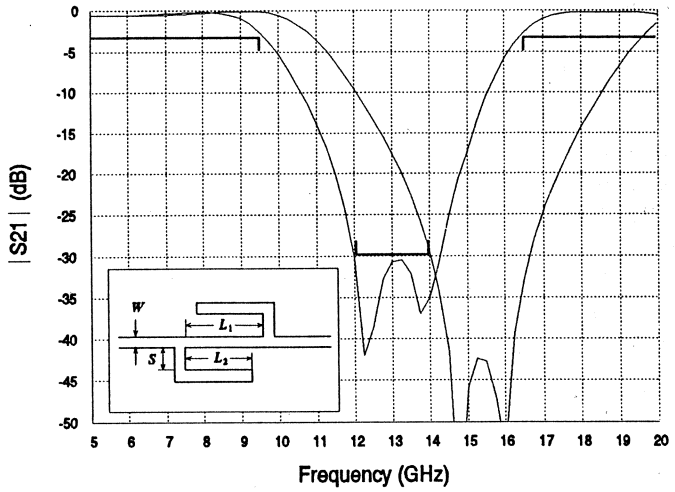

Fig. 3. $|S_{21}|$ before and after optimization for the double folded stub bandstop filter structure shown in the insert.

memory, access time, repeated simulations, etc. In any case, however, it is worthwhile to remember the current (active) interpolation base. This is particularly useful in (25), even if the perturbed point falls outside the interpolation region.

VI. Experimental Validation of a Microstrip Filter Design

A conventional, and until now state-of-the-art, use of EM simulation for design validation is illustrated by comparing measurements and EM simulation of the lowpass microstrip filter shown in the insert in Fig. 2. The filter was designed by first synthesizing an LC prototype, and then designing the corresponding microstrip components to match those of the prototype.

The filter was built on a 25-mil-thick alumina substrate with a relative dielectric constant of 9.8. The rectangular inductors, utilizing air bridges with vias, were made of 2-mil-wide lines with 1-mil gaps and occupied a total area of 19 × 16 mils. The center capacitor had dimensions of 50 × 115 mils and the end capacitors 35 × 74 mils (the value of 75 mils was used for simulation). The measurements on the filter were taken at frequencies from 0.2 to 11.8 GHz with a step of 0.2 GHz. The measured $|S_{11}|$ and $|S_{21}|$ versus frequency are shown in Fig. 2, together with the corresponding plots obtained by electromagnetic simulation using ***em*** [5].

On a Sun SPARCstation 2, simulation was carried out for the same frequency range from 0.2 to 11.8 GHz with a step of 0.2 GHz. For simulation, the whole structure was partitioned into individual components—capacitors and inductors—the latter including the connecting transmission lines. Because of symmetry, only one inductor and one end capacitor were simulated. Additional pieces of transmission lines were added for each component and de-embedded for better accuracy and to account for discontinuities at both sides of each capacitor.

The simulation times were approximately 100 s for the inductor, 10 s for the center capacitor, and 8 s for the end capacitor, all per one frequency point. The resulting S parameters of the individual components were then combined to determine the S parameters of the overall filter. The results give a very good approximation of filter behavior in all critical areas, in particular around the cutoff frequency. The discrepancies between measured and simulated $|S_{11}|$ at very low frequencies may be due to numerical problems in the EM simulation that becomes apparent when vias are electrically very short.

VII. Design of Double Folded Stub Microstrip Structure

A double folded stub microstrip structure for bandstop filter applications, shown in the insert in Fig. 3, may substantially reduce the filter area while achieving the same goal as the conventional double stub structure [10]. The symmetrical double folded stub can be described by 4 parameters: width (W), spacing (S), and two lengths (L_1 and L_2). The input and output reference planes are located at the stubs.

We used minimax optimization to move the center frequency of the stopband from 15 to 13 GHz. W was fixed at 4.8 mils, and L_1, L_2, and S were optimization variables with the starting values given by [10]. Design specifications were taken as

$$|S_{21}| > -3\,\text{dB} \qquad \text{for } f < 9.5 \text{ GHz and } f > 16.5 \text{ GHz}$$

$$|S_{21}| < -30\ \text{dB} \qquad \text{for } 12 \text{ GHz} < f < 14 \text{ GHz}.$$

The substrate thickness and the relative dielectric constant were 5 mils and 9.9, respectively.

Optimization was carried out in two steps. First, we applied identical $\Delta x = \Delta y = 2.4$ mils grid size in both x and y directions. Then the grid size was reduced to $\Delta x = \Delta y = 1.6$ mils for fine resolution. The values of the optimization variables before and after optimization are reported in Table I. Fig. 3 shows $|S_{21}|$ in decibels versus frequency before and after optimization, with the center frequency clearly moved to 13 GHz as desired.

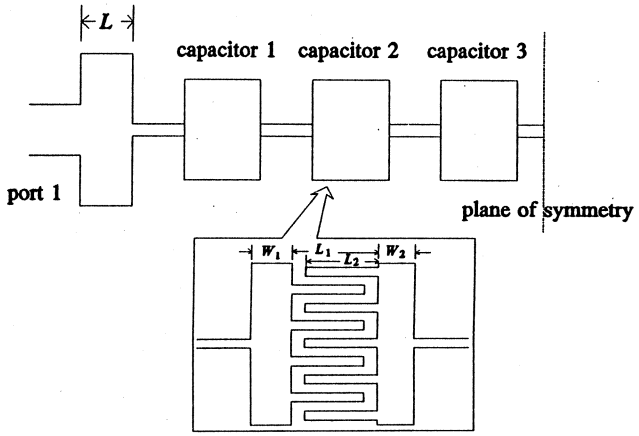

Fig. 4. The 26–40 GHz millimeter-wave bandpass filter. The dielectric constant is 2.25. Substrate thickness and shielding height are 10 and 120 mils, respectively. The optimization variables include L, and L_1, L_2, W_1, W_2 for each capacitor, totaling 13.

TABLE I
PARAMETER VALUES FOR THE DOUBLE FOLDED STUB BEFORE AND AFTER OPTIMIZATION

Parameter	Before optimization (mil)	After optimization (mil)
L_1	74.0	91.82
L_2	62.0	84.71
S	13.0	4.80

VIII. DESIGN OF A MILLIMETER-WAVE MICROSTRIP FILTER

A 26–40 GHz millimeter-wave bandpass filter [11] was built on a 10-mil-thick substrate with relative dielectric constant of 2.25. The filter, shown in Fig. 4, utilized high impedance microstrip lines and interdigital capacitors to realize inductances and capacitances of a synthesized lumped ladder circuit. The filter was designed to satisfy the specifications

$$|S_{11}| < -20 \text{ dB}$$

$$|S_{21}| > -0.04 \text{ dB}$$

for 26 GHz $< f <$ 40 GHz. The original microstrip design was determined by manually matching each element of the lumped prototype at the center frequency using ***em*** [5]. However, when the filter was simulated by ***em*** in the whole frequency range, the results exhibited significant discrepancies with respect to the prototype. It necessitated a tedious series of manual interpolations and made a satisfactory design very difficult to achieve. The filter was then built and measured [11].

The redesign of the bandpass filter was carried out using ***em*** [5] driven by our minimax gradient optimizer. There was a total of 13 designable parameters including the distance between the patches L_1, the finger length L_2, and two patch widths W_1 and W_2 for each of the three interdigital capacitors, and the length L of the end capacitor, as shown in Fig. 4. The finger width and spacing for all capacitors were held constant at 2.0 mils. The transmission lines between the capacitors were fixed at the originally designed values. The second half of the circuit, to the right of the plane of symmetry, is assumed identical to the first half, so it contains no additional variables.

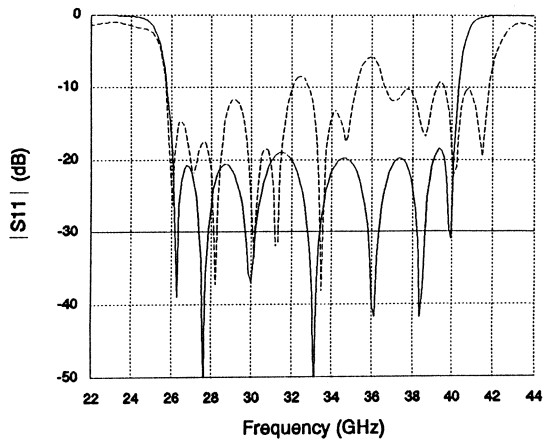

(a)

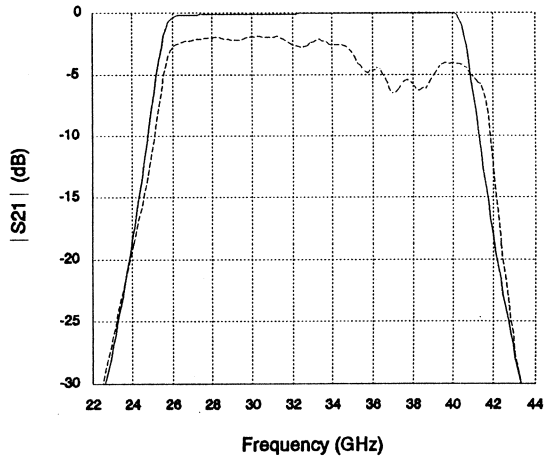

(b)

Fig. 5. The 26–40 GHz millimeter-wave bandpass filter after minimax optimization and fabrication. All the optimization variables have been rounded to 0.1 mil resolution. Simulated (——) and measured (- - -): (a) $|S_{11}|$, and (b) $|S_{21}|$.

A typical minimax equal-ripple response of the filter was achieved after a series of consecutive optimizations with different subsets of optimization variables and frequency points [12]. The filter was then built with the resulting geometrical dimensions rounded to 0.1 mil resolution. Fig. 5 shows the corresponding simulated and measured filter responses: $|S_{11}|$ and $|S_{21}|$. The larger error in the measured results appears to be in the bandwidth which points to analysis of the series capacitors. A grid size of 1.0 mil in both x and y directions was used for the interdigital capacitor simulation. More recent

error analysis studies [13] indicate that 6–10 cells across the width of the finger may be needed to reduce the error in computed capacitance to below 1.0%. This filter is also surprisingly sensitive to the impedance and phase velocity of the series transmission lines. The same convergence issues discussed for the interdigital capacitors also apply to the series transmission lines. Experimentally, we found it very difficult to hold ±0.1 mil tolerances in the 0.23-mil-thick metallization.

IX. Conclusions

For the first time, we have presented a comprehensive approach to microwave filter design which exploits accurate electromagnetic field simulations driven directly by a powerful gradient-based minimax optimizer. The benefits of electromagnetic simulations are thus significantly extended. Our approach, illustrated by simulation of two microstrip structures and the minimax design of two filters, paves the way for direct use of field theory-based simulation in practical optimization-driven microwave circuit design.

Acknowledgment

The authors thank Dr. J. C. Rautio of Sonnet Software, Inc., Liverpool, NY. His initiatives, encouragement, and help substantially facilitated this timely and important work.

References

[1] J. C. Rautio and R. F. Harrington, "An electromagnetic time-harmonic analysis of arbitrary microstrip circuits," *IEEE Trans. Microwave Theory Tech.*, vol. 35, pp. 726–730, 1987.

[2] T. Itoh, Ed., *Numerical Techniques for Microwave and Millimeter-Wave Passive Structures.* New York: Wiley, 1989.

[3] R. H. Jansen and P. Pogatzki, "A hierarchically structured, comprehensive CAD system for field theory-based linear and nonlinear MIC/MMIC design," in *1992 2nd Int. Workshop German IEEE MTT/AP Joint Chapter Integrated Nonlinear Microwave Millimeterwave Circuits Dig.*, Duisburg, Germany, 1992, pp. 333–341.

[4] *LINMIC + /N Version 3.0*, Jansen Microwave, Bürohaus am See, Am Brüll 17, D-4030 Ratingen 1, Germany, 1992.

[5] *Em User's Manual*, Sonnet Software, Inc., 135 Old Cove Road, Suite 203, Liverpool, NY 13090-3774, May 1992.

[6] J. W. Bandler and S. H. Chen, "Circuit optimization: the state of the art," *IEEE Trans. Microwave Theory Tech.*, vol. 36, pp. 424–443, 1988.

[7] *Empipe*^{TM} *Version 1.1 User's Manual*, Optimization Systems Associates Inc., P.O. Box 8083, Dundas, Ont., Canada L9H 5E7, 1993.

[8] *OSA90/hope*^{TM} *Version 2.5 User's Manual*, Optimization Systems Associates Inc., P.O. Box 8083, Dundas, Ont., Canada L9H 5E7, 1993.

[9] J. W. Bandler, W. Kellermann, and K. Madsen, "A superlinearly convergent minimax algorithm for microwave circuit design," *IEEE Trans. Microwave Theory Tech.*, vol. MTT-33, pp. 1519–1530, 1985.

[10] J. C. Rautio, Sonnet Software, Inc., 135 Old Cove Road, Suite 203, Liverpool, NY 13090-3774, private communication, 1992.

[11] D. G. Swanson, Jr., Watkins-Johnson Company, 3333 Hillview Avenue, Stanford Research Park, Palo Alto, CA 94304-1204, private communication, 1992.

[12] J. W. Bandler, S. Ye, R. M. Biernacki, S. H. Chen, and D. G. Swanson, Jr., "Minimax microstrip filter design using direct EM field simulation," in *IEEE MTT-S Int. Microwave Symp. Dig.*, Atlanta, GA, 1993, pp. 889–892.

[13] J. C. Rautio *et al.*, "Critical issues in experimental validation," presented at the Workshop WSMK, IEEE MTT-S Int. Microwave Symp., Atlanta, GA, 1993.

John W. Bandler (S'66–M'66–SM'74–F'78) was born in Jerusalem, on November 9, 1941. He studied at Imperial College of Science and Technology, London, England, from 1960 to 1966. He received the B.Sc.(Eng.), Ph.D., and D.Sc.(Eng.) degrees from the University of London, London, England, in 1963, 1967, and 1976, respectively.

He joined Mullard Research Laboratories, Redhill, Surrey, England, in 1966. From 1967 to 1969 he was a Postdoctorate Fellow and Sessional Lecturer at the University of Manitoba, Winnipeg, Canada. He joined McMaster University, Hamilton, Canada, in 1969, where he is currently Professor of Electrical and Computer Engineering. He has served as Chairman of the Department of Electrical Engineering and Dean of the Faculty of Engineering. He currently directs research in the Simulation Optimization Systems Research Laboratory. He is President of Optimization Systems Associates Inc. (OSA), which he founded in 1983. OSA introduced the CAE systems RoMPE^{TM} in 1988, HarPE^{TM} in 1989, OSA90^{TM} and OSA90/hope^{TM} in 1991, and Empipe^{TM} in 1992. He is President of Bandler Research Inc., which he founded in 1989. He contributed to *Modern Filter Theory and Design* (New York: Wiley-Interscience, 1973) and to *Analog Methods for Computer-Aided Analysis and Diagnosis* (New York: Marcel Dekker, 1988). He has published more than 260 papers, four of which appear in *Computer-Aided Filter Design* (New York: IEEE Press, 1973), one in each of *Microwave Integrated Circuits* (Norwood, MA: Artech House, 1975), *Low-Noise Microwave Transistors and Amplifiers* (New York: IEEE Press, 1981), *Microwave Integrated Circuits*, 2nd ed. (Norwood, MA: Artech House, 1985), *Statistical Design of Integrated Circuits* (New York: IEEE Press, 1987), and *Analog Fault Diagnosis* (New York: IEEE Press, 1987).

Dr. Bandler was an Associate Editor of the IEEE TRANSACTIONS ON MICROWAVE THEORY AND TECHNIQUES (1969–1974), Guest Editor of the Special Issue of the IEEE TRANSACTIONS ON MICROWAVE THEORY AND TECHNIQUES on Computer-Oriented Microwave Practices (March 1974), and Guest Co-Editor with R. H. Jansen of the Special Issue of the IEEE TRANSACTIONS ON MICROWAVE THEORY AND TECHNIQUES on Process-Oriented Microwave CAD and Modeling (July 1992). He joined the Editorial Boards of the *International Journal of Numerical Modelling* in 1987, and the *International Journal of Microwave and Millimeterwave Computer-Aided Engineering* in 1989. He is a Fellow of the Royal Society of Canada, a Fellow of the Institution of Electrical Engineers (Great Britain), a member of the Association of Professional Engineers of the Province of Ontario (Canada), and a Member of the Electromagnetics Academy.

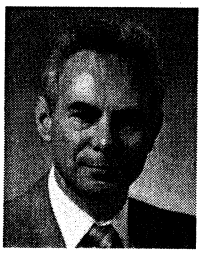

Radoslaw M. Biernacki (M'85–SM'86) was born in Warsaw, Poland. He received the Ph.D. degree from the Technical University of Warsaw, Warsaw, Poland, in 1976.

He became a Research and Teaching Assistant in 1969 and an Assistant Professor in 1976 at the Institute of Electronics Fundamentals, Technical University of Warsaw, Warsaw, Poland. From 1978 to 1980 he was on leave with the Research Group on Simulation, Optimization and Control and with the Department of Electrical and Computer Engineering, McMaster University, Hamilton, Canada, as a Postdoctorate Fellow. From 1984 to 1986 he was a Visiting Associate Professor at Texas A&M University, College Station, TX. He joined Optimization Systems Associates Inc., Dundas, Ont., Canada, in 1986, where he is currently Vice President Research and Development. At OSA he has been involved in the development of commercial CAE software systems HarPE^{TM}, OSA90^{TM}, and OSA90/hope^{TM}, and related research on parameter extraction, statistical device modeling, simulation and optimization, including yield-driven design, of linear and nonlinear microwave circuits. Since 1988 he has been a Professor (part time) in the Department of Electrical and Computer Engineering, McMaster University, Hamilton, Canada. His research interests include system theory, optimization and numerical methods, computer-aided design of integrated circuits and control systems. He has more than 80 publications.

Dr. Biernacki has been the recipient of several prizes for his research and teaching activities.

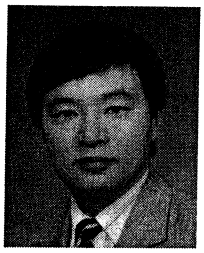

Shao Hua Chen (S'84–M'88) was born in Swatow, Guangdong, China, on September 27, 1957. He received the B.S.(Eng.) degree from the South China Institute of Technology, Guangzhou, China, in 1982 and the Ph.D. degree in electrical engineering from McMaster University, Hamilton, Canada in 1987.

From July 1982 to August 1983, he was a Teaching Assistant in the Department of Automation at the South China Institute of Technology. He was a graduate student in the Department of Electrical and Computer Engineering at McMaster University from 1983 to 1987, during which time he was awarded an Ontario Graduate Scholarship for two academic years. He joined Optimization Systems Associates Inc., Dundas, Ont., Canada, in 1987 and engaged in commercial CAD software development. He has made major contributions to the development of the CAE systems HarPE^{TM} and OSA90/hope^{TM}. Currently he is working as a Research Engineer in the Simulation Optimization Systems ResearchLaboratory at McMaster University. His professional interests include optimization theory and implementation, CAD software architecture, device modeling, statistical simulation, circuit design centering, sensitivity analysis, computer graphics, and user interfaces.

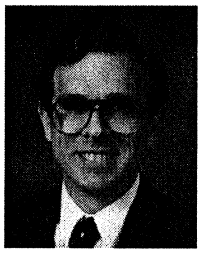

Daniel G. Swanson, Jr. (S'74–M'78–SM'91) received the B.S.E.E. degree from the University of Illinois in 1976 and the M.S.E.E. degree from the University of Michigan in 1978.

In 1978 he joined Narda Microwave, where he developed a 6–18 GHz low-noise amplifier, an 8–10 GHz low-noise amplifier, and a de-embedding system for S-parameter device characterization. In 1980 he was with the Wiltron Company designing YIG tuned oscillators for use in microwave sweepers. He also developed a broad-band load-pull system for optimization of output power. In 1983 he joined a startup company, Iridian Microwave, where he was responsible for the dielectric resonator oscillator product line. In 1984 he joined Avantek Inc., where he developed thin-film microwave filters, software for filter design, and a low-frequency broad-band GaAs MMIC amplifier. In 1989 he joined Watkins-Johnson Company where he is Staff Scientist. His current work includes thin-film filter design and the application of electromagnetic field solvers to microwave component design.

Mr. Swanson served as an officer in the Santa Clara Valley Chapter of the MTT-S from 1985 to 1989. He is presently serving as MTT-S AdCom Treasurer. He is a member of Eta Kappa Nu.

Shen Ye (S'88–M'92) was born in Shanghai, China, in 1957. He received the B.Eng. and M.Eng. degrees from Shanghai University of Technology, Shanghai, China, in 1982 and 1984, respectively, and the Ph.D. degree from McMaster University, Hamilton, Canada, in 1991, all in electrical engineering.

From 1984 to 1986 he was a Teaching and Research Assistant in the Department of Electrical Engineering, Shanghai University of Technology. He joined the Simulation Optimization Systems Research Laboratory and the Department of Electrical and Computer Engineering, McMaster University as a graduate student in 1986. He held an Ontario Graduate Scholarship for the academic year 1989–1990. In 1991 he was awarded an Industrial Research Fellowship from the Natural Sciences and Engineering Research Council of Canada and was a Research Engineer with Optimization Systems Associates Inc., Dundas, Ont., Canada, from 1991 to 1993. He contributed substantially to the design and implementation of Empipe^{TM}. In 1993 he joined Com Dev Ltd., Cambridge, Ont., Canada, where he is a Design Engineer. His professional interests include general CAD software design, simulation and optimization techniques, design and optimization of microwave circuits, device modeling, parameter extraction, and statistical circuit design.

Technical Briefs

HarPE™
Version 1.8 Technical Brief

INTRODUCTION

HarPE™ is a powerful CAD software system dedicated to complete nonlinear device characterization including advanced statistical modeling and parameter extraction. HarPE provides you with simulation and design optimization capabilities for single nonlinear device circuits.

DEVICE MODELS

The circuit topology for HarPE consists of an intrinsic nonlinear device encompassed by an extrinsic linear environment representing the parasitic, packaging and bias circuits. The overall circuit configuration can be either a one-port or a two-port.

The built-in intrinsic nonlinear device models include:

- the semiconductor diode model
- the Curtice and Ettenberg FET model
- the Materka and Kacprzak FET model
- the Raytheon (Statz *et al.*) FET model
- the Khatibzadeh and Trew FET model
- the modified Trew FET model for uniform doping
- the KTL (Trew/Ladbrooke) FET model
- the Gummel and Poon model of bipolar NPN and PNP transistors
- HEMT models (HOBD, DP, Curtice) provided by Golio, Motorola
- custom device models created using HarPE's unique Expression Block

The linear environment can be represented by built-in extrinsic super-components for the fastest simulation speed. It can also be constructed from linear library elements or supplied as *S*, *Y* or *Z* data.

The linear library elements includes the typical lumped elements, a comprehensive set of microstrip structures and controlled sources.

CIRCUIT SIMULATION

At AC, HarPE calculates the RF input and output voltages and currents, output power, and small-signal *S* parameters. At DC, HarPE calculates the DC currents and voltages at the bias ports. Frequency, bias, power and arbitrary parameter sweeps can be defined for simulation.

Built-in responses include:

- power, voltage and current spectra
- voltage and current waveforms
- DC IV curves
- small-signal parameters linearized from nonlinear models
- Smith chart and polar plots of S parameters
- insertion loss, maximum available gain and stability factor

HarPE offers a comprehensive approach to seamlessly integrated large- and small-signal frequency-domain simulations of nonlinear devices. Using a unified circuit description the small-signal parameters of nonlinear devices, when needed, are automatically derived from nonlinear models.

OPTIMIZATION

The power of HarPE lies in its implementation of state-of-the-art techniques. The gradient-based minimax, ℓ_1 and least-squares optimizers have proven track records in circuit optimization. A novel Huber optimizer enhances Version 1.8.

Combining the optimizers with OSA's unique nonlinear FAST™ adjoint sensitivity analysis, HarPE provides solutions to your design and modeling problems with unparalleled speed, accuracy, consistency and robustness.

PARAMETER EXTRACTION

HarPE was introduced as the world's first software system for parameter extraction from harmonic data. It offers a truly nonlinear device parameter extraction procedure which utilizes spectrum measurements, including DC bias information and output power at different harmonics measured under RF large-signal excitations.

If large-signal measurements are not available HarPE can extract the nonlinear model parameters from small-signal S-parameter data taken over a number of bias conditions, or even just from DC data (which alone is not sufficient to determine some parameters such as nonlinear capacitors). In general, HarPE accepts and fully utilizes all information from any combination of the three types of measurement data.

CUSTOMIZING MODELS AND RESPONSES

Using typical mathematical expressions, you can create your own device models or modify the built-in models directly in the circuit file. Preprogrammed user-defined models include both the symmetric and asymmetric Curtice models, the Materka model, the Plessey model and TriQuint's Own Model (TOM), all suitable for both DC and AC simulations.

You can also define your own response functions, as well as goals and specifications for optimization. User-defined models and response functions enjoy the power of HarPE in simulation and optimization just like the built-in models and responses.

Combinations of algebraic operations and standard mathematical functions are available in formulating an expression. Conditional expressions (nested IF ELSE structures) are also supported.

A set of predefined labels allows you to refer to the program's internal variables and built-in responses, such as the frequency, bias voltages, intrinsic voltages, input power, output power spectrum components, DC current and *S* parameters.

The flexibility of customizing device models and responses has been instrumental for many HarPE users in developing new and/or proprietary FET, bipolar, HEMT and HBT models, including modeling device thermal characteristics.

STATISTICAL MODELING AND ANALYSIS

Statistical modeling, as a prerequisite for meaningful statistical analysis and yield optimization, is one of the most significant features of HarPE.

Any of the built-in or user defined models can be used for statistical modeling. Based on a large set of measurement data from multiple devices, a multi-device parameter extraction procedure provides a sample of device models. This can be further postprocessed automatically in order to create a consolidated statistical model, immediately ready for statistical Monte Carlo analysis.

Another novel offering of OSA's technology in Version 1.8 is statistical modeling by cumulative probability distribution (CPD) fitting. Model parameter statistics are directly extracted by matching the model and measured response statistics. An alternative option available is fitting the model and measured response histograms (based on Chi-square test).

The result of Monte Carlo analysis can be displayed as sweep plots, histograms, run charts, yield, scattering diagrams and cumulative probability distribution plots. If statistical measurement data is supplied, the data can be superimposed on the corresponding model responses.

USER INTERFACE

The sophisticated capabilities of HarPE are presented through a polished and friendly user interface in the industry-standard X-Windows environment. It is menu-driven and features an integrated full screen editor, on-line help and on-line User's Manual.

Text macro definitions allow you to introduce your own keywords, circuit description, etc. The color map, key map and "hot keys" are user-definable. The flexible data format is especially favored by HarPE users.

COMPATIBILITY WITH OTHER CAD SOFTWARE

HarPE's parameter extraction capabilities can help you use other CAD software most effectively by supplying model parameters that truly characterize the devices in your design. All library models in HarPE are fully compatible with those in OSA90/hope™ - a general CAD software system from OSA.

HarPE's expression processor allows you to modify the built-in models or create user-defined models to easily adapt to any new developments or modifications introduced by other vendors. This ensures that HarPE models are always compatible with other software you use.

HarPE supports linear subcircuits described by "black box" *S*, *Y* or *Z* data imported from external simulators.

In addition to its flexible data format, HarPE directly accepts measured data from Cascade Microtech's MicroCAT™ Test Executive system and data in the MDIF (Measurement Data Interchange Format) format.

WARRANTY AND SUPPORT

With your acquisition of HarPE you are entitled to a 90 day limited warranty. A software support option which includes software upgrades is also available.

As a user of HarPE, you can rely on professional and timely support from our technical experts, including authors of the program.

PLATFORMS AND AVAILABILITY

HarPE runs under X windows on Hewlett-Packard and Sun workstations. For further information contact

Optimization Systems Associates Inc.
P.O. Box 8083, Dundas, Ontario
Canada L9H 5E7

Tel 905 628 8228
Fax 905 628 8225

HarPE, OSA90/hope and FAST are trademarks of Optimization Systems Associates Inc.
Sun Workstation and MicroCAT are trademarks of respective organizations.

OSA90/hope™
Version 3.0 Technical Brief

INTRODUCTION

OSA90/hope™ is a general CAD software system offering simulation, modeling, statistical analysis, nominal and yield optimization, and data visualization for linear and nonlinear analog circuits. Its open architecture allows you to create fully optimizable interconnections of components, subcircuits, simulators and mathematical functions.

CIRCUIT SIMULATION

OSA90 simulates linear and nonlinear circuits of general n-port topology. Multiple nonlinear devices and sources, both DC and AC, are allowed. Built-in simulators handle DC, small-signal AC, large-signal harmonic balance and two-tone spectral analyses. **OSA90** supports oscillator analysis and design.

The DC, small-signal and large-signal simulations are analytically unified through a consistent circuit description. Small-signal circuits, when needed, are automatically derived from nonlinear models.

Available built-in responses include DC and AC voltages, currents and output powers at all external ports, voltages at designated nodes and currents in designated branches. Small-signal analysis produces *S*, *Y* and *Z* parameters, and group delay. For 2-ports, **OSA90** calculates insertion loss, stability factor and maximum available gain. Frequency, power and arbitrary multi-parameter sweeps can be defined for simulation.

EXPRESSION COMPOSITION

OSA90 supports expression composition directly in the input file. You can define constants, variables, vectors and matrices. You define expressions using typical algebraic operations and a rich set of built-in mathematical functions, including array operations. You can define interdependent variables, describe model equations, postprocess responses and create user-defined functions. All user-defined variables and functions can be used for optimization.

Even complicated operations such as solving a set of linear equations, finding eigenvalues, the Discrete Fourier Transform, cubic spline interpolation, and estimating data statistics are available as built-in functions. Conditional expressions (IF ELSE structures) are also supported.

DATAPIPE™ TECHNOLOGY

OSA90 is equipped with several Datapipe protocols for connecting external programs through UNIX interprocess pipes. This facilitates high-speed data connections to external *executable* programs, even across networks. It is especially suitable for sensitive software since you do not need to reveal the source code.

Datapipes are flexibly defined in the input file. You specify a set of inputs from **OSA90** to the external program and define outputs to be returned. **OSA90** starts the external programs in separate processes, and communicates with them in a manner similar to subroutine calls. You can invoke **OSA90** itself through Datapipe to create a simulation/optimization hierarchy of virtually unlimited depth.

You can enhance your own software with **OSA90**'s friendly user interface, graphics, expression parser, optimization and statistical features. You can link several separate programs through **OSA90** to design a functionally integrated system as your own "total CAE solution".

DRIVE SPICE AND *em*™ THROUGH DATAPIPE

Specialized Datapipe interfaces are available for the popular analog circuit simulator SPICE and the electromagnetic simulator ***em*** from Sonnet Software, Inc. An extensive library of parameterized microstrip components and user-parameterized arbitrary structures allow you to employ ***em*** in design optimization. Refer to the **Empipe™ Technical Brief** for complete details.

The interfaces can be modified to suit your particular needs, or can be used as templates for connections to other software systems you may be interested in.

POWERFUL OPTIMIZERS

OSA90 features powerful and robust gradient-based optimizers: ℓ_1, ℓ_2, Huber, minimax, quasi-Newton, conjugate gradient, as well as non-gradient simplex and random optimizers. These optimizers offer unrivalled accuracy and efficiency.

Optimization variables can include circuit parameters, bias voltages, input power levels, inputs to Datapipe external programs and abstract variables. You can optimize built-in and user-defined circuit responses, Datapipe outputs and abstract error functions. You can define upper, lower and equality specifications. You can also assign weighting factors.

ELEMENT LIBRARY

The linear element library includes the typical lumped elements, a comprehensive set of microstrip components and controlled sources. You can also import linear subcircuit *S*, *Y* and *Z* matrices through data files, arrays and Datapipes.

The nonlinear device model library includes built-in and user-definable models for diodes, FETs, bipolar transistors and HEMTs, including the Curtice FET (both symmetrical and asymmetrical), the Statz FET, the Materka and Kacprzak FET, the Khatibzadeh and Trew physics-based FET, the physics-based KTL (Trew/Ladbrooke) FET, the Gummel and Poon bipolar model, and HEMT models (HOBD, DP, Curtice) provided by Golio (Motorola).

FLEXIBLE MODELING

One of **OSA90**'s most widely acclaimed features is its modeling flexibility. Linear subcircuits, *with user-definable parameters*, can be created and reused.

Nonlinear controlled current and charge sources with arbitrary controlling voltages/currents allow you to create models with unrestricted topology and model equations. A number of models, including TriQuint's Own Model (TOM) and the Plessey model, are supplied. **OSA90** has been widely used to create, test, verify and optimize new and/or proprietary models, such as HEMT models, temperature-dependent HBT models, and CNN-based models.

YIELD SIMULATION AND OPTIMIZATION

OSA90's statistical Monte Carlo analysis and yield optimization features can help you to greatly improve first-pass design success. Parameters can be subject to uniform, normal, exponential and lognormal distributions with absolute or relative tolerances. Hierarchical, correlated and sample distributions are supported. Monte Carlo analysis estimates the yield and displays histograms, run charts, scattering diagrams, parameter sweeps and yield sensitivities.

OSA90 employs sophisticated one-sided ℓ_1 and one-sided Huber design centering algorithms for yield optimization. Advanced quadratic approximation is an integrated option to reduce the computer time required for large-scale yield optimization.

3D VISUALIZATION

Responses and functions can be plotted versus any two variables as 3D surfaces and contours. The 3D images can be zoomed, rotated, smoothed and colored. It is a great visual aid for revealing and illustrating function-variable dependence, clarifying design strategy and verifying optimization solutions.

SPACE MAPPING

Space Mapping™ is a fundamental new theory exclusive to **OSA90** for linking "coarse" and "fine" models, such as empirical and EM models. Coarse models are used for fast optimization, and the optimal solution is mapped to the fine model space. When applied to direct EM optimization, the results can be astounding!

USER INTERFACE

OSA90 operates through a polished and friendly user interface in the industry-standard X-Windows environment. It is menu-driven, features an integrated full screen editor and offers on-line help and an on-line User's Manual. The syntax and menus are logical and intuitive.

Graphical views can be created to customize the displays. For documentation, **OSA90** can generate report, HPGL and PostScript files.

You can define macros to automate repetitive operations, and customize keywords and styles. You can run **OSA90** in macro and background modes.

WARRANTY AND SUPPORT

With your acquisition of **OSA90** you are entitled to a 90 day limited warranty. A software support option which includes software upgrades is also available.

As a user of **OSA90**, you can rely on professional and timely support from our technical experts, including authors of the program.

OTHER PRODUCTS FROM OSA

HarPE™ is the world's best commercial software system for device parameter extraction, simulation, optimization and statistical modeling.

Optimization Systems Associates Inc. offers consulting and customization services, to create software solutions to your specific needs.

PLATFORMS AND AVAILABILITY

OSA90 runs under X-Windows on Hewlett-Packard, and Sun workstations. For further information contact

Optimization Systems Associates Inc.
P.O. Box 8083, Dundas, Ontario
Canada L9H 5E7

Tel 905 628 8228
Fax 905 628 8225

OSA90, OSA90/hope, Datapipe, HarPE, Empipe and Space Mapping are trademarks of Optimization Systems Associates Inc. Sun Workstation, UNIX, *em* and PostScript are trademarks of respective organizations.

Empipe™ Version 2.0 Technical Brief

INTRODUCTION

Empipe™ is a smart software interface connecting **OSA90/hope**™ of Optimization Systems Associates Inc. of Dundas, Ontario, Canada, and ***em***™ of Sonnet Software, Inc. of Liverpool, New York.

Empipe provides RF and microwave designers with the exciting new dimension of direct EM optimization, even for structures with arbitrary geometries!

OSA90/hope is a general CAD software system for simulation, modeling, statistical analysis, and nominal and yield optimization (design centering) for linear and nonlinear analog circuits. Its open architecture allows external programs to be integrated into a design optimization framework. See the **OSA90/hope Technical Brief** for complete details.

em is an efficient full-wave EM simulator for predominantly planar circuits. With full accuracy up to millimeter-wave frequencies, ***em*** simulates arbitrary geometries accounting for dispersion, coupling, surface waves, radiation, metallization and dielectric losses, etc. It is recommended whenever high simulation accuracy is needed in the design process.

INTERFACE BETWEEN OSA90/hope AND *em*

Empipe incorporates our exclusive **Datapipe**™ technology to facilitate high-speed data communications between **OSA90/hope** and ***em***, even across networks.

Empipe reads the geometrical parameter values from **OSA90/hope** and then converts them to the format required by ***em***. In **OSA90/hope**'s user-friendly environment you can define optimizable variables, statistical tolerances, and interdependent parameters linked by mathematical expressions.

Discretization of the geometrical parameters for on-grid ***em*** simulation is automatically handled by **Empipe**. For off-grid points, user-selectable linear or quadratic interpolation is employed. The computational savings realized by the interpolation are particularly valuable for EM-based statistical analysis and yield optimization. An intelligent database system is built into **Empipe** to ensure efficient retrieval of ***em*** analysis results.

BUILT-IN COMPONENT LIBRARY

Empipe provides a built-in library of parameterized microstrip components. These components are ***em***-ready and optimizable. The library includes

- asymmetrical gap
- bend
- mitered microstrip bend
- cross junction
- interdigital capacitor (two models)
- double patch capacitor
- double stub (two models)
- folded double stub (two models)
- symmetrical gap
- microstrip line
- overlay double patch capacitor (four models)
- open stub
- rectangular structure
- spiral inductor
- step junction
- T-junction

OPTIMIZATION OF ARBITRARY STRUCTURES

In addition to the built-in library components, **Empipe** Version 2.0 supports user-defined EM-optimizable arbitrary structures. Using our unique Pattern Sensor technology, user-defined optimizable **Empipe** components can be created, with user-definable parameter names, from "geo" files describing an arbitrary structures. Any structures that you can simulate using ***em*** you can now optimize using **Empipe**!

EM AND CIRCUIT MODELS

The ***em*** simulation results are directly incorporated into the overall circuit defined in **OSA90/hope**. You can seamlessly integrate any number of ***em***-simulated structures with elements represented by conventional empirical models in the same circuit for linear and nonlinear simulation and optimization. This also allows you to decompose a large structure into several substructures, individually simulated by ***em*** and then connected via circuit theory, for a less accurate but faster analysis.

Empipe SYNTAX

The syntax is illustrated by the built-in **Empipe** component EM_TEE (microstrip T-junction).

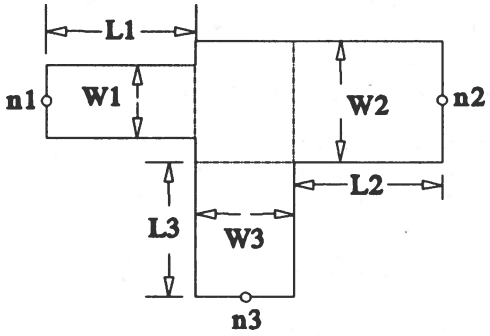

Keywords

INDEX	database index
W1	line width at node n1 (symmetrical)
W2	line width at node n2 (symmetrical)
W3	line width at node n3
L1	line length at node n1
L2	line length at node n2
L3	line length at node n3
H	substrate thickness
H2	shielding height
EPSR	substrate dielectric constant
UR	substrate relative permeability
TAND	dielectric loss tangent
MTAND	magnetic loss tangent
T	conducting metal strip thickness
RHO	conducting metal strip resistivity
SR	surface reactance in Ω/square
XCELL	cell size along the X-axis
YCELL	cell size along the Y-axis
FMIN	lower limit of the frequency range
FMAX	upper limit of the frequency range
FSTEP	increments in the frequency range

Example

```
EM_TEE  1 2 3 0   INDEX=1    W1=2mil
        W2=4mil   W3=3mil    L1=8mil
        L2=4mil   L3=0       H=5mil
        H2=120mil EPSR=1.9   T=3um
        TAND=0.001
        XCELL=1mil   YCELL=1mil
        FMIN=1GHZ    FMAX=10GHZ
        FSTEP=1GHZ;
```

ARBITRARY GEOMETRY

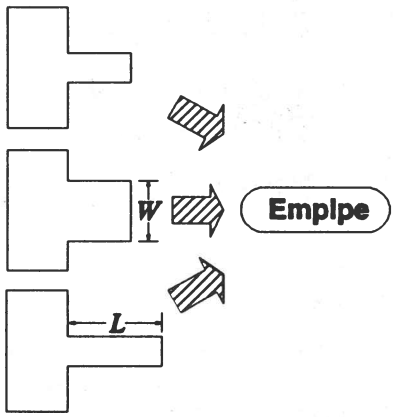

DESIGN EXAMPLE

A 26-40 GHz microstrip interdigital capacitor filter was optimized by **OSA90/hope** with **Empipe** and ***em***. After minimax, or equal-ripple, optimization and rounding the optimization variables to 0.1mil resolution, the resulting filter gain and return loss are shown in the accompanying diagram.

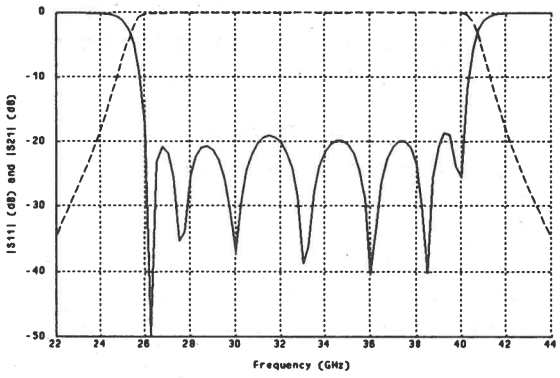

AVAILABILITY

Empipe is available on Hewlett-Packard and Sun workstations. For further information contact

Optimization Systems Associates Inc.
P.O. Box 8083, Dundas, Ontario
Canada L9H 5E7

Tel 905 628 8228 Fax 905 628 8225

OSA90/hope, OSA90, Datapipe and Empipe are trademarks of Optimization Systems Associates Inc. UNIX and em are trademarks of respective organizations.